Reinforced Concrete Beam-Column Connection Behaviour

PhD Thesis

May 2000

Stephen J Hamil

School of Engineering, University of Durham

South Road, Durham DH1 3LE

Abstract

This thesis describes an investigation into reinforced concrete beam-column connection behaviour. This behaviour is governed by mechanisms such as shear, bond and confinement. These are not fully understood in themselves. Seventy external beam-column connection specimens were manufactured and tested. Forty nine of these were subjected to monotonic (gravity) loading and twenty one to simulated seismic loading.

The monotonic tests investigated the influence of the following parameters on specimen performance :

1. Beam steel anchorage
2. Concrete strength
3. Joint ties and their positioning
4. Joint aspect ratio
5. Steel fibre and steel plate reinforced concrete

Non-linear finite element analyses of these tests were conducted using the computer package SBETA. Following a considerable learning period a standard finite element mesh was proposed for reinforced concrete beam-column connection design. This was validated using the experimental results and used to conduct a parametric study.

The experimental work, in addition to this finite element modelling, allowed a comprehensive analysis of monotonic beam-column connection behaviour to be made. Within this thesis, conclusions are made on the prediction of joint strength and the subsequent methods of joint enhancement. Guidelines are developed to be considered in the design of reinforced concrete external beam-column connections.

The twenty one specimens tested to investigate the cyclic strength of monotonically designed connections were subjected to load cycles of increasingly large beam rotations. This allowed cyclic performance to be analysed. An attempt was also made to shift the beam's plastic hinge away from the column face in order to improve this performance.

The cyclic tests gave an insight into how monotonically designed connections would perform if subjected to earthquake motions, very high winds or blast effects. Recommendations are made for the design of such structures.

Acknowledgements

I would like to thank my supervisor Dr. Richard Scott for his expert help and guidance over the last three years.

I would like to thank Dr. Paul Baglin for his experimental work on the specimens investigating tie positioning and the specimens investigating the influence of joint shear plates. I would like to extend my thanks to Dr. Baglin for his support with the finite element modelling.

I am grateful to Cervenka Consulting, in particular Dr. Jana Margoldova, for their support and assistance with the finite element package, SBETA.

I would like to thank the Engineering and Physical Sciences Research Council for funding the work.

The project required considerable technical assistance. Special thanks must go to Neil Clarey for his work on strain gauge installation.

Thanks also go to Steve Richardson and Bernie M^{c}Eleavey in the Civils Laboratory; Brian Blackburn, Brian Wallace and Ian Glassford in the Mechanical Workshop; and Trevor Nancarrow and Michael Wilson in I.T.

I would like to thank the four undergraduate students who worked on the investigation, under my supervision, as part of their 4H projects. Paul Brayshaw, Richard Nixon, Graham Lunn and Brian Leach.

Finally I would like to thank my girlfriend, Dionne Martens, and my family for their support over the last three years.

Publications

Publications by the author arising from this research :

1. Hamil S.J. and Scott R.H. : 'Connection zone strains in reinforced concrete beam-column connections', Proceedings of the 11th International Conference on Experimental Mechanics, Oxford, UK, 24-28 August 1998, pp 65-69

   ISBN 90 5809 014 0

2. Hamil S.J., Baglin P.S. and Scott R.H. : 'Finite element modelling of reinforced concrete beam-column connections', Proceedings of the 7th Annual Conference of the Association for Computational Mechanics in Engineering, Durham, UK, 29-30 March 1999, pp 7-10

   ISBN 0 9530967 6 9

3. Scott R.H., Hamil S.J. and Baglin P.S. : 'Behaviour of high strength concrete beam-column connections', Proceedings of the CANMET/ACI International Conference on High Performance Concrete, Gramado, Brazil, 1-4 June 1999, pp 699-713

   ACI Special Publication SP-186

4. Hamil S.J. and Scott R.H. : 'Developments in high strength concrete beam-column connection design', Proceedings of the International Conference held at the University of Dundee, Innovation in Concrete Structures: Design and Construction, 8-10 September 1999, pp 157-166

   ISBN 0 7277 2824 5

Other publications quoting results from this research :

1. Vollum R.L. : 'Design and analysis of reinforced concrete beam-column joints', PhD thesis, Imperial College, London, 1998

2. Vollum R.L. and Newman J.B. : 'The design of external, reinforced concrete beam-column joints', The Structural Engineer, Volume 77, Numbers 23 & 24, 7 December 1999, pp 21-27

Author's Note

Over the period of nine months, September 1997 to May 1998, Dr. Paul Baglin worked closely with the author, during his period in Durham as a Research Associate. During this time the author and Dr. Baglin worked on related elements of this project. Dr. Baglin's main responsibility was for the eleven specimens investigating joint tie positioning and the three specimens using joint plates.

In addition to this Dr. Baglin provided the author with some much appreciated support with the development of the finite element model. Dr. Baglin had past experience using finite element methods from his doctorate, which involved the finite element modelling of plate reinforced concrete beams.

Towards the end of his time at Durham, Dr. Baglin wrote two internal reports : *"The Experimental Programme"* and *"The Finite Element Programme"*.

Copies of publications by the author may be found on the website:

http://www.webgeordie.co.uk/stephenhamil/research.htm

Contents

Figures

Tables

Notation

Symbol	Description
α	Beam tension steel reduction factor
β	Joint aspect ratio reduction factor
β_1	Beam redistribution factor
ε	Strain
γ	Column load reduction factor
γ_{ACI}	Joint classification reduction factor
γ_m	Partial safety factor
σ	Stress
σ_b	Bearing stress
$\sigma_{b\,lim}$	Limiting value of bearing stress
ρ_s	Ratio of joint reinforcement to joint area
τ_{rd}	Basic shear strength
ϕ	Diameter of rebar
a_b	Concrete cover to rebar
A	Overall beam section area
A_{bar}	Rebar cross sectional area
A_g	Gross cross sectional area of the column
A_s	Beam tension steel cross sectional area
A_{sc}	Column steel cross sectional area
b_b	Beam breadth
b_c	Column breadth
b_e	Effective beam width
b_w	Minimum beam width
c	Concrete (cracked) strength factor
c_3	Concrete tension softening strain
c_d	Concrete compression softening factor
d_b	Effective depth of beam
d_c	Effective depth of column
e	Distance from centre of column to beam load point
e_c	Concrete crushing strain
e_{face}	Distance from column face to beam load point
E_c	Concrete Young's modulus
E_s	Steel Young's modulus
E_{sh}	Steel post-yield modulus
f_{ab}	Bond stress between two points (a and b)
f_c	Stress in the joint due to column load
f_{cd}	Design concrete compressive strength

f_{ck}	Concrete compressive cylinder strength
f_{cu}	Concrete compressive cube strength
f_s	Axial force in steel
f_t	Concrete tensile strength
f_y	Characteristic strength of steel
f_{yv}	Characteristic strength of joint steel
F_{bt}	Rebar tensile force
h	Overall beam section depth
h_c	Column section height
L_{col}	Column height
M	Beam moment
M_{ult}	Beam's ultimate moment of resistance
N	Column load
n_u	Poisson's ratio
P	Beam load
P	Column load
P_{bar}	Rebar perimeter
P_{crack}	Beam load at initial shear cracking of joint
P_{fail}	Beam load at joint failure
r	Radius of rebar bend
R_c	Concrete uniaxial compressive cylinder strength
R_s	Steel yield strength
R_t	Concrete uniaxial tensile strength
s_v	Centre to centre spacing of shear reinforcement
T	Force in the beam tension reinforcement
v_c	Joint shear stress
v_c'	Design concrete shear stress
v_{cr}	Joint cracking strength
v_u	Ultimate joint shear strength
v_{umr}	Joint shear stress at beam ultimate moment of resistance
V_{col}	Shear force in upper column
V_{crack}	Joint shear force at initial shear cracking
V_j	Joint shear force
V_{umr}	Joint shear force at beam ultimate moment of resistance
x	Neutral axis depth
z_b	Lever arm depth of beam
z_c	Lever arm depth of column

Introduction

The structural behaviour of reinforced concrete beams and columns has been the subject of extensive research. As a result, accurate predictions can be made of their behaviour under load. However, the behaviour of the joints in a framed structure, connecting the beams and columns, is less well understood. Previous research has shown that the joints in a framed structure may be less strong than their intersecting members. This is undesirable as premature cracking of the joint may occur under working loads and joint failure may occur under extreme loading.

Previous research has indicated that the following parameters have an influence on joint performance :

1. Concrete strength
2. The detailing arrangement of the beam tension steel
3. The presence of ties within the joint
4. The position of ties within the joint
5. Joint aspect ratio
6. Column axial load

In addition to the above, further uncertainties exist due to the behaviour of the joint being governed by a number of mechanisms such as shear, bond and confinement which are not fully understood in themselves.

Figure 1 shows a photograph of a typical reinforced concrete external beam-column connection and Figure 2 displays a diagrammatic representation of this.

Throughout this thesis the whole beam-column assemblage is referred to as the **connection** whereas the interface between the beam and column is referred to as the **joint**. The longitudinal reinforcement within the beam or the column is defined as the **main reinforcement**. Shear links in the joint and column are referred to as **ties** whilst shear links in the beam are termed **stirrups** (the notation used in the USA was chosen to provide an easy distinction between the two link positions).

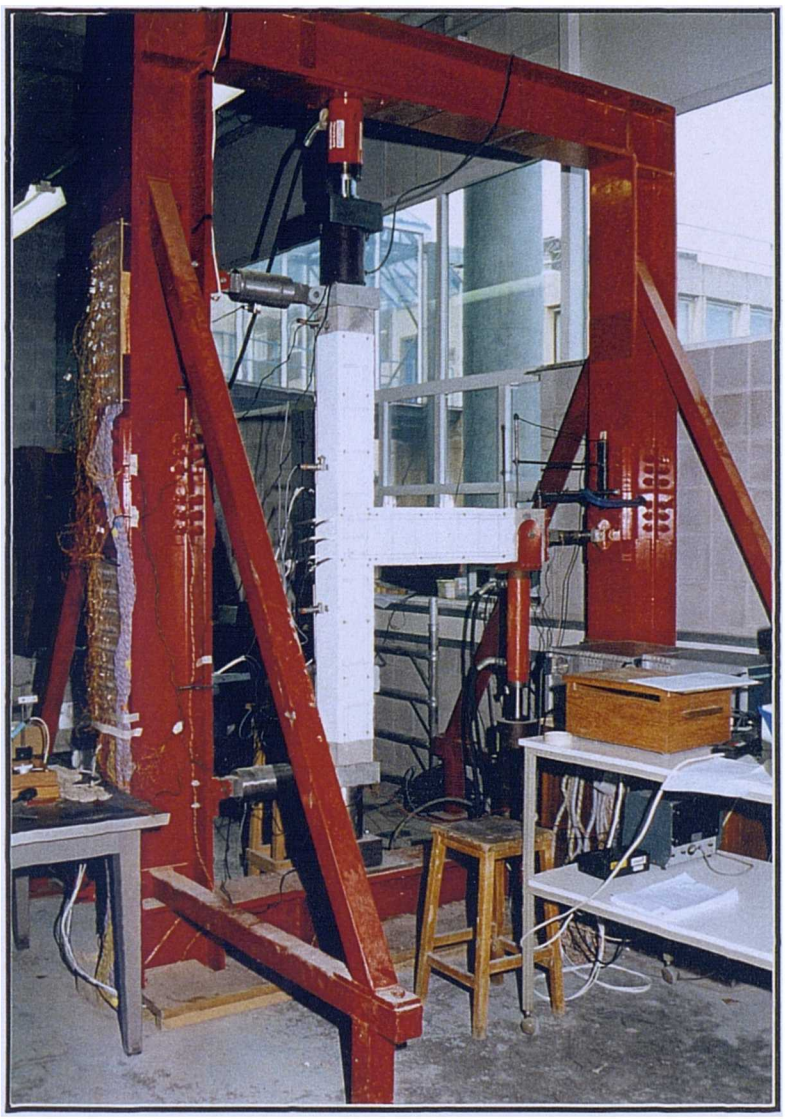

Figure 1 Typical beam-column connection - photograph

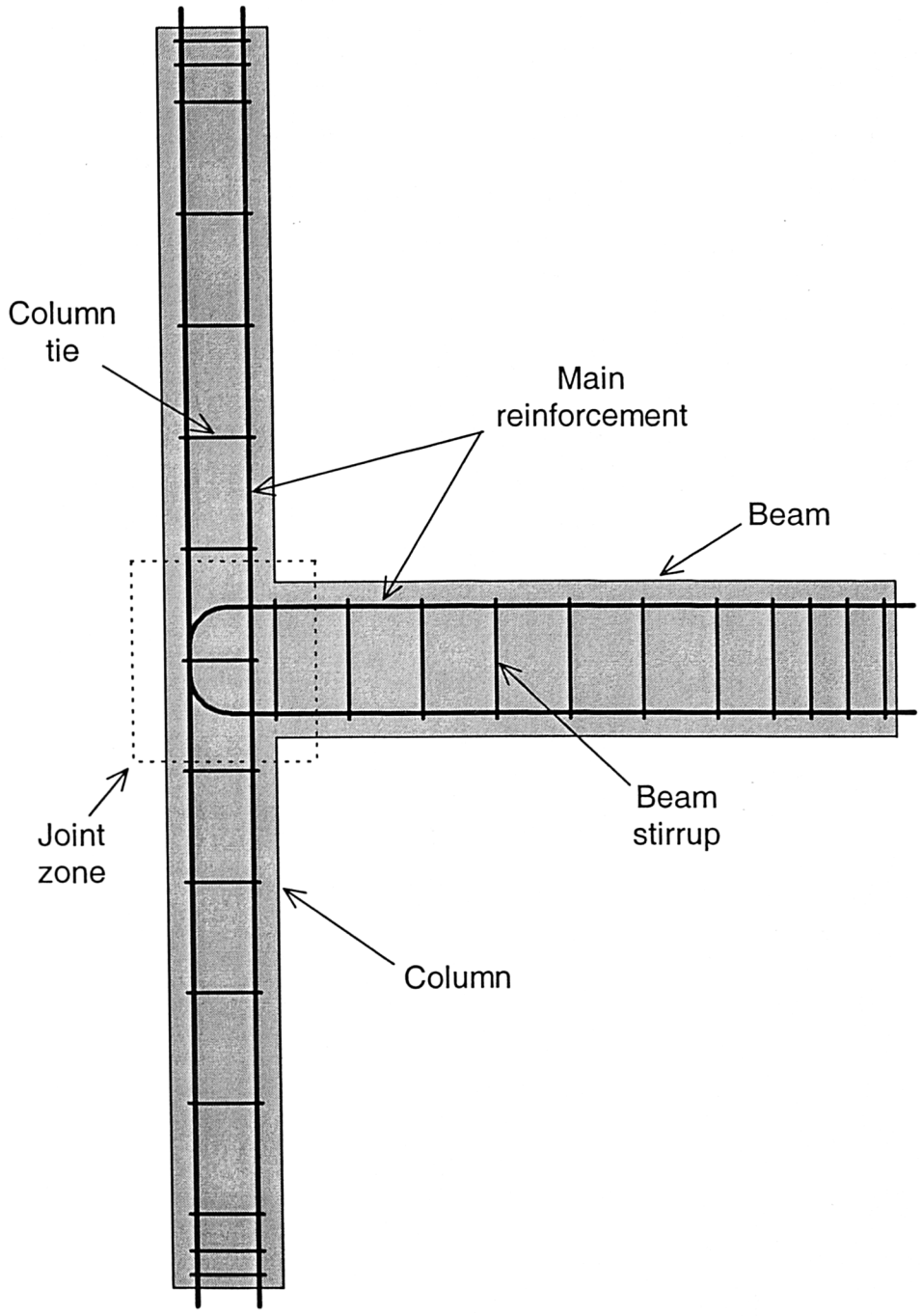

Figure 2 Typical beam-column connection - diagrammatic representation

Examples of shear cracks within beam-column joints in a *real* structure are shown in Figures 3(a) and 3(b). These are photographs of external beam-column connections within a reinforced concrete multi-story car park in Newcastle upon Tyne. The author noted that the majority of the joints within this structure contained similar cracks. The fact that major structures in service contain visible shear cracks within their joints was a powerful incentive for this research.

The focus of this research was to investigate the influence of various parameters on joint zone behaviour. The parameters to be investigated were :

1. The influence of ties within the joint
2. The strength of the concrete
3. The detailing arrangement of the beam tension steel

Detailed reinforcement strains were measured using the technique of internally strain gauging the reinforcement. Electric resistance strain gauges were mounted in a central duct running longitudinally through the centre of the reinforcement bars, thus avoiding the disruption of the bond between the bars and the surrounding concrete. This technique has received extensive development at the University of Durham.

The author originally set out to test a series of sixteen beam-column connection specimens designed for monotonic loading. After the testing of these initial sixteen specimens, the investigation developed further. Thirty three additional specimens were manufactured and tested to investigate methods of enhancing the joint zone's strength. The following parameters were investigated :

1. Joint tie positioning
2. Joint aspect ratio
3. Fibre reinforced concrete
4. The use of steel shear plates

Figure 3(a) Cracking within an external beam-column joint - photograph

Figure 3(b) Cracking within an external beam-column joint - photograph

The monotonic investigation was supported by a non-linear finite element study using the computer package SBETA. Following a considerable learning period a standard finite element mesh design was proposed for reinforced concrete beam-column connection design. This was validated using the experimental results and then used to conduct a parametric study.

When the monotonic study was completed, twenty one further specimens were manufactured and tested to investigate the cyclic performance of monotonically designed reinforced concrete beam-column connections. Subjecting these specimens to load cycles of increasing amplitudes allowed this performance to be analysed. An attempt was also made to shift the beam's plastic hinge away from the column face in order to reduce joint deterioration.

This thesis consists of the following chapters :

Chapter 1. Literature Review :

A detailed review of the previous literature on reinforced concrete beam-column connections is presented.

Chapter 2. Experimental Programme :

The details of the experimental specimens and the monotonic loading technique are given.

Chapter 3. Monotonic Results and Discussion (Overview) :

An overview of the results from the monotonic test programme is given.

Chapter 4. Monotonic Results and Discussion (Detailed) :

A discussion of the results, in detail, from each individual test series within the monotonic test programme is presented.

Chapter 5. Finite Element Analysis :

A finite element model for reinforced concrete beam-column connections is presented. The performance of the model is compared with the monotonic experimental results and the model is used to conduct a parametric study.

Chapter 6. Monotonic Design Guidelines :

This summarises the experimental and analytical results from Chapters 4 and 5. Guidelines for the monotonic design of reinforced concrete external beam-column connections are presented.

Chapter 7. Cyclic Testing (Background) :

A review of the cyclic methods of testing reinforced concrete beam-column connections is given. Specimen details and the loading technique used within this investigation are also outlined.

Chapter 8. Cyclic Results and Discussion (Overview) :

An overview of the results from the cyclic test programme is given.

Chapter 9. Cyclic Results and Discussion (Detailed) :

A discussion of the results, in detail, from each individual test series within the cyclic test programme is presented.

Chapter 10. Conclusions :

The conclusions from this investigation are presented.

Chapter 11. Recommendations for Further Work :

Within this chapter, the author presents his recommendations for further research which should take place.

1. Literature Review

Over the last 40 years much work has taken place researching reinforced concrete beam-column connection behaviour. A suprisingly small amount of this has been concerned with the strength of beam-column connections subjected to monotonic (gravity) loading, whereas extensive world-wide research has been directed at the problem of seismic (cyclic) loading.

Although there are significant differences in the behaviour and design of monotonic and seismic joints some of the principles, such as the influence of concrete strength, joint reinforcement and column axial load, are relevant to both. A monotonically designed connection should have sufficient joint strength to resist the applied beam and column loads at the ultimate limit state. A seismically designed connection should ensure that under forced displacements (such as those exerted on a building during an earthquake) the joint is strong enough to allow the beam's flexural strength to govern the connection's behaviour. As a result, seismically designed joints must be detailed to be both stronger and more ductile than monotonically designed joints.

The work presented within this thesis investigates the performance of exterior beam-column connections (a single beam framing into a column). In a framed structure the exterior beam-column joints are subjected to the greatest shear force. Internal beam-column joints (two or more beams framing into a column) are subjected to a smaller shear force as the shear effects from the beams on opposite sides of the joint *detract* from each other. This effect is demonstrated by considering the internal equilibrium forces as shown in Figures 1.1 and 1.2. The joint shear force, V_j, is evaluated from the equations 1.1 and 1.2 for each load case.

External monotonic joint : $V_j = T - V_{col}$ .....(eq. 1.1)

Internal monotonic joint : $V_j = T_1 - T_2 \pm V_{col}$ .....(eq. 1.2)

where T is the force in the beam tension reinforcement,

V_{col} is the shear force in the upper column.

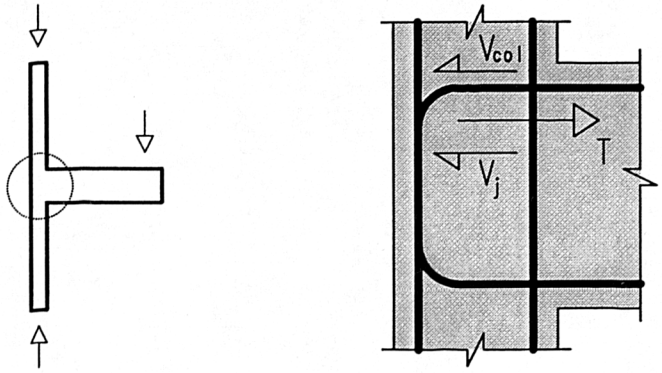

Figure 1.1 Force equilibrium within an external monotonic joint

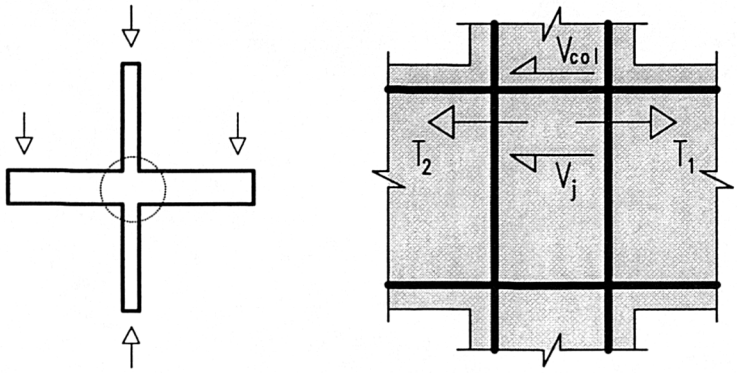

Figure 1.2 Force equilibrium within an internal monotonic joint

The majority of previous seismic work has investigated the performance of interior beam-column connections. This is because under seismic loading conditions a beam on one side of the joint may be forced downwards whilst a beam on the opposite side is forced upwards - this would give the most extreme seismic load case as the two effects would *add* to the shear force within the joint. This effect is demonstrated by considering the equilibrium forces within the joint as shown in Figure 1.3. The shear force, V_j, is evaluated from the equation 1.3 :

Internal seismic joint : $V_j = T_1 + T_2 - V_{col}$ .....(eq. 1.3)

This literature review gives a detailed analysis of the previous research regarding the monotonic testing of beam-column connections. Seismic literature is considered in Chapter 7 (*Cyclic Testing (Background)*).

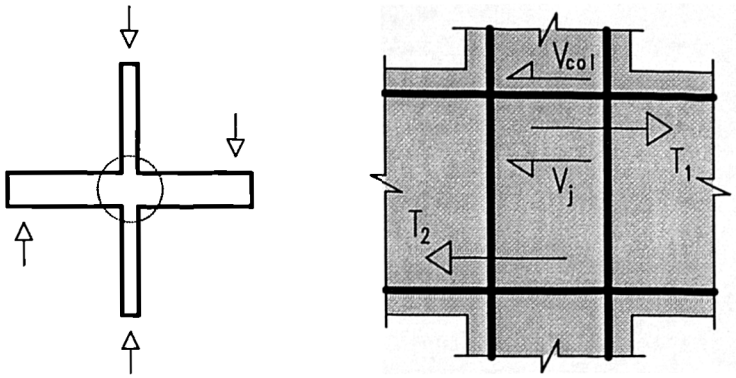

Figure 1.3 Force equilibrium within an internal seismic joint

1.1 Monotonic Beam-Column Connection Failure Modes

Before discussing the research from previous investigations in Section 1.2 it is necessary to outline the failure modes that can occur within a beam-column connection.

All previous investigations have tested beam-column connections using a similar method. Firstly an axial load, which is kept constant throughout the test, is applied to the column. The beam is then loaded by applying a series of downward load increments until failure occurs. A variety of failure modes can take place which may be grouped into the following three categories :

Flexural Failure : If the joint is strong enough then the strength of the connection will be governed by the flexural behaviour of its intersecting members. It is desirable for the column to have a higher ultimate capacity than the beam, thus avoiding column failure. Sufficient stirrups should ensure that the beam fails in flexure and not in shear. Figure 1.1.1 gives a diagrammatic representation of a beam flexural failure, typified by large cracks in the beam near the column face where the beam reinforcement yields.

Joint Failure : If the strength of the joint is less than the shear force required for beam failure then joint failure will occur at this lower load. Figure 1.1.2 gives a diagrammatic representation of a joint failure, typified by extensive diagonal shear

cracking within the joint. The ultimate shear capacity of a joint should not be confused with the shear strength at initial joint cracking. Previous research has shown that a joint can withstand a further significant increase in load after initial shear cracking.

Anchorage Failure : If the beam tension rebars are not anchored correctly within the joint then anchorage failure may occur. The beam tension rebars may be pulled out of the joint at an applied beam load significantly lower than that required to develop either the beam's flexural strength or the joint's shear strength.

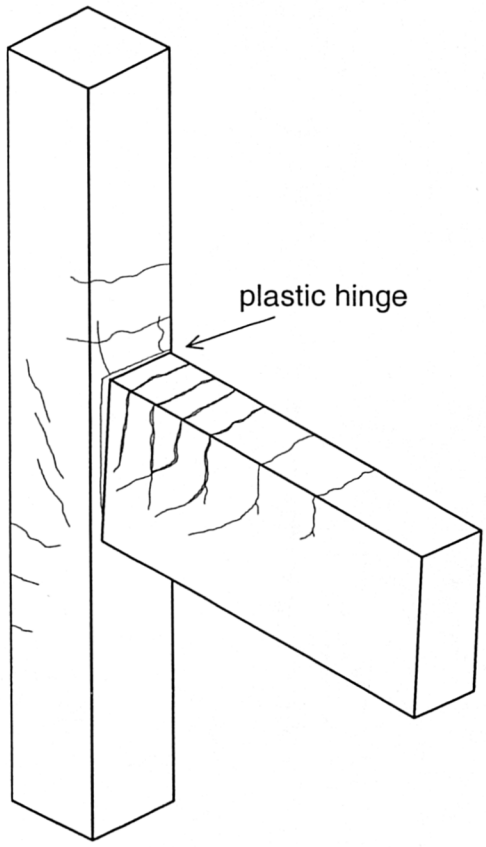

Fig 1.1.1 Diagrammatic representation of a beam flexural failure

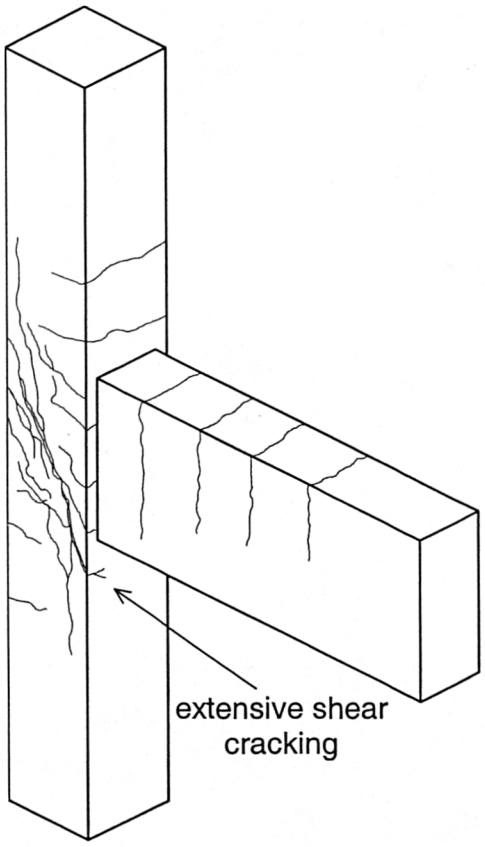

Fig 1.1.2 Diagrammatic representation of a joint failure

1.2 Previous Monotonic Research

1.2.1 Taylor [1]

In 1974 Taylor reported on the manufacturing and testing of twenty six reinforced concrete exterior beam-column connections. Dimensions are given in Figure 1.2.1 and further details are given in Table 1.2.1.

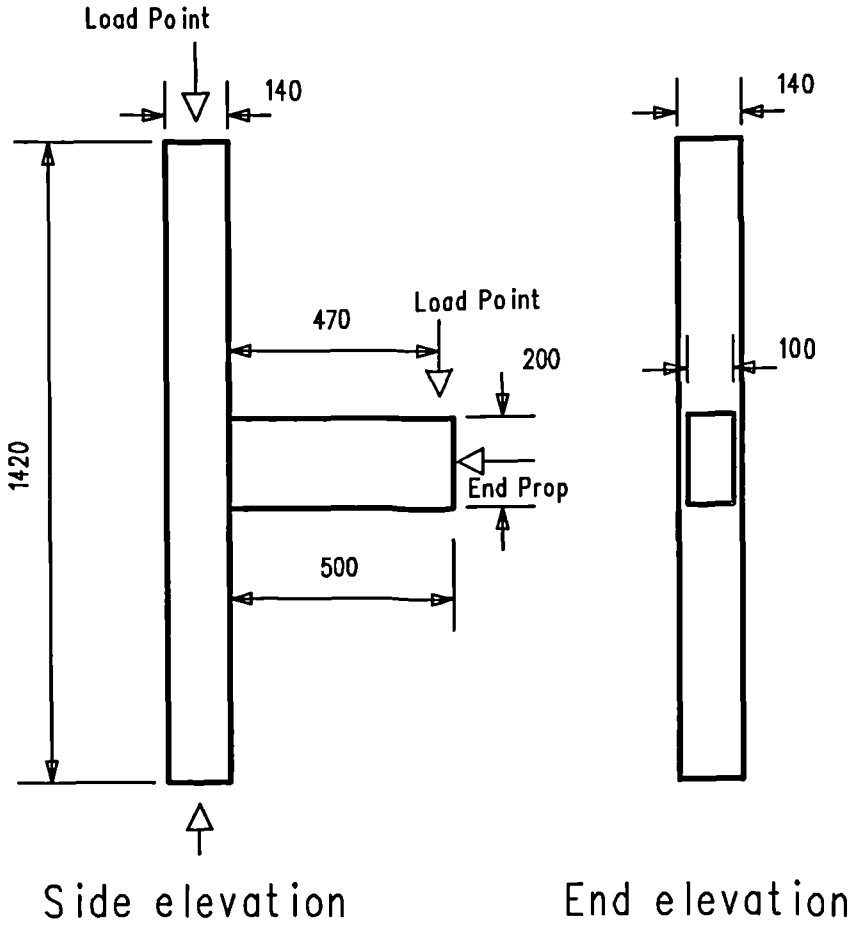

Figure 1.2.1 Specimen layout (dimensions in mm) - Taylor [1]

A prop was provided at the end of the beam as indicated in Figure 1.2.1. Taylor found in a preliminary test without a prop that the full moment capacity of the lower column was not utilised after initial joint cracking. The inclusion of the prop was believed to allow the joint to reach its full capacity by allowing the upper column to carry its correct proportion of the moment throughout the test.

Table 1.2.1 Specimen details - Taylor [1]

Specimen	Variable	Column Load (kN)	f_{cu} (MPa)	Cracking Load (kN)	Failure Load (kN)	Failure Type
P1/41/24	Preliminary	240	33	25.5	34.2	J
P2/41/24		240	29	21.3	34.2	J
P2/41/24A		240	47	29.9	45.9	J
P1/41/09		240	37	22.3	31.9	F
A3/41/24	Beam Steel	240	27	21.3	34.0	J
A3/41/13	Percentage	240	45	34.0	40.7	F
A3/41/09		240	44	21.3	23.5	F
A3/41/06		240	28	-	23.3	F
B3/41/24	Column ties	240	22	21.3	29.7	J
C3/41/24X	Beam steel	240	50	26.6	29.2	J
C3/41/24BY	detail	240	32	21.3	28.2	J
C3/41/13Y		240	28	26.2	26.2	J
C3/41/24Y		240	60	36.1	44.0	J
D3/41/24	Column load	60	53	29.8	49.0	J
D3/41/13		60	56	23.4	37.5	F
D3/41/09		60	43	25.5	29.0	F
D3/41/06		60	21	-	18.5	F
E3/41/24A	Beam thrust	240	43	21.3	26.2	J
E3/41/24B		240	45	29.8	29.8	J
E3/41/24C		240	42	34.0	39.4	J
F3/41/24A	Various with	240	37	18.1	18.2	F
F3/41/16A	reduced beam	240	21	-	15.0	F
F3/41/24B	height	240	34	13.8	17.9	F
F3/41/16B		240	24	13.3	14.1	F
F3/41/24C		60	34	-	18.4	F
F3/41/16C		60	38	-	14.5	F

Notes

1. The absence of a cracking load indicates that beam failure occurred prior to joint cracking,
2. J - indicates joint failure, F - indicates beam flexural failure.

Taylor conducted seven test series designated P and A to F. The first series was preliminary and was used to develop the method of testing and the test rig. The other test series were designed to look at the following variables :

A - Beam steel percentage,
B - Column ties within the joints,
C - Beam steel detail,
D - Column load,
E - Beam thrust,
F - The influence of some of these variables on beams of a height of 125 mm.

The system of specimen numbering was chosen so that the details of each test specimen could be recognised. The letter at the front of this number refers to the test series, P and A to F. This is followed by a digit indicating what kind of prop was used to simulate beam continuity. Number 1 implies that no prop was used, number 2 indicates that a prop of stiffness 0.11×10^3 kN/mm was used and number 3 indicates that a prop of stiffness 0.89×10^3 kN/mm was used. The next two digits refer to the percentage of steel in the column and the last two digits refer to the percentage of tension steel within the beam, this was either two 8 mm rebars (0.6%), two 10 mm rebars (0.9%), two 12 mm rebars (1.3%) or two 16 mm rebars (2.4%). Finally, in some of the tests letters A, B and C refer to repeats of similar specimens whilst X refers to beam steel bent up into the column and Y refers to the U-bar beam steel detail. All bends in the main beam steel had an internal radius of three times the bar diameter and at least one column tie was present within the centre of each joint. Four 16 mm bars were used for the column reinforcement.

Taylor made the following observations from his test results :

Initial Joint Cracking

Although the widths of the diagonal cracks first observed in the joint were not greater than the criteria given by the then British design code, CP 110 [2], Taylor

commented that, in his opinion, it was desirable to design these areas so that diagonal cracking was avoided at the working load.

Taylor used an approximate principle stress analysis approach to try and predict when diagonal cracking of the joint first occurred. The effect of the beam thrust on the joint was ignored as it was found to be very small, two orders of magnitude below the column load at the time of cracking. The shear stress within the joint at initial diagonal cracking was suggested to be equal to :

$$v_c = 0.67\sqrt{f_t^2 + f_c f_t} \quad \text{.....(eq. 1.2.1)}$$

where f_t is the concrete tensile strength and f_c is the stress in the joint due to the column load, where $f_c = N/b_c h_c$,

N is the column load,

b_c and h_c are the column breadth and height respectively.

This is now equation 54 in the BS8110 design code [3].

Bending moment within the column

Taylor calculated the bending moment carried by the column above and below the joint for each test. He concluded that the beam moment is not necessarily carried by the column in equal proportions but that the closing corner of the joint may be carrying as much as 75% of the beam moment at failure.

Taylor commented that designing columns to carry equal amounts of the beam moment above and below the joint may be dangerous. He suggested that it would be safer to design for 70% of the beam moment below the joint and 50% of the beam moment above the joint. It should be noted however that current BS 8110 design code [3] states that the upper and lower column should be designed to take an equal share of the beam's moment.

Ultimate Strength

Taylor suggested that to ensure the joint has sufficient strength at the ultimate limit state the following design equation should be used :

$$100\rho_b = 100\left(3+\frac{2d_c}{z_b}\right)\frac{b_c d_c}{b_b d_b}\frac{v_c \beta_1}{0.87 f_y} \quad \text{.....(eq. 1.2.2)}$$

where $100\rho_b$ is the limiting steel percentage of the beam,

v_c is the nominal shear stress for the column,

d_c is the effective depth of the column,

b_c is the column breadth,

d_b is the effective depth of the beam,

b_b is the beam breadth,

z_b is the lever arm of the beam at the column face,

f_y is the characteristic strength of the steel,

β_1 is a redistribution factor, equal to (100 - % redistribution)/100.

The detail of bending beam tension rebars up into the column was found to be unsatisfactory. The ultimate capacity of specimens using bent down and U-bar beam steel detail was found to be significantly greater.

Taylor commented that the test with three joint ties did not show any increase in ultimate strength. He suggested that joint behaviour may be compared with diagonal compression failure in over reinforced deep beams in which the presence of beam stirrups does not affect the ultimate shear capacity. Taylor suggested that additional column ties within the joint would similarly not enhance the ultimate strength of the joint.

The tests on specimens with a low column load were inconclusive although Taylor suspected that the U-bar detail may be enhanced when using a higher column load as the greater normal force would 'pinch' and anchor the bar in the joint.

1.2.2 Ryan [4]

In 1977 Ryan reported on the manufacturing and testing of twelve reinforced concrete beam-column connection specimens. In spite of strenuous efforts the author has located only one brief paper [4] that Ryan wrote. As a result full experimental details are not known.

Five different specimen details were tested :

Type H_A specimens investigated the performance of U-bar beam steel detail.
Type H_B specimens investigated the performance of bent down beam steel detail.
Type H_P specimens investigated the influence of additional joint reinforcement.
Type H_E specimens investigated the presence of transverse beams framing into the connection zone.
Type X specimens were interior beam-column connections - the two beams were loaded in opposite directions to simulate the force from a very strong wind.

The specimens were of a similar size to those tested by Taylor [1] but had a 200×150 mm beam. A pair of rebars ranging in size from 8 mm to 16 mm were used for the beam tension steel.

Ryan made the following observations from his test results :

Initial Joint Cracking

By considering the forces on the joint zone Ryan found that the occurrence of a diagonal crack could be predicted. The additional joint ties and diagonal joint reinforcement did not increase the load at which diagonal cracking first occurred. Additional joint reinforcement did however serve to limit the extent of the cracking.

Bending moment within the column

Similarly to Taylor [1], Ryan found that the closing corner of the joint took the greatest share of the beam moment. A maximum value of 66% was observed. After cracking, however this moment was seen to divide equally between the upper and lower column.

Ultimate Strength

Again Ryan, like Taylor [1], suggested that a limit on steel percentage in the beam was required to avoid the risk of joint failure.

Unlike Taylor [1], Ryan concluded that the U-bar detail was a more efficient steel detail than bending the steel down into the column.

There was a difference of opinion between Ryan and Taylor [1] over the influence of joint reinforcement. Ryan commented that additional column ties within the joint provided good restraint against failure whereas Taylor [1] suggested that additional ties did not influence the ultimate capacity of the joint. Unfortunately since Ryan's test results are not available, the author cannot present data to support these comments.

1.2.3 Meinheit and Jirsa [5]

In 1977 Meinheit reported on the manufacturing and testing of fourteen large scale reinforced concrete *interior* beam-column connection specimens, an example of which is given in Figure 1.2.2. The example shown displays the beams framing into the narrow side of the column. Specimens were also tested which had 410 mm wide beams which framed into the wider side of the column.

Although the author's investigation is concerned with the design of exterior beam-column connections, the behaviour of Meinheit's interior connections is considered

of interest. It is believed that the influence of certain parameters is relevant to both types of connection.

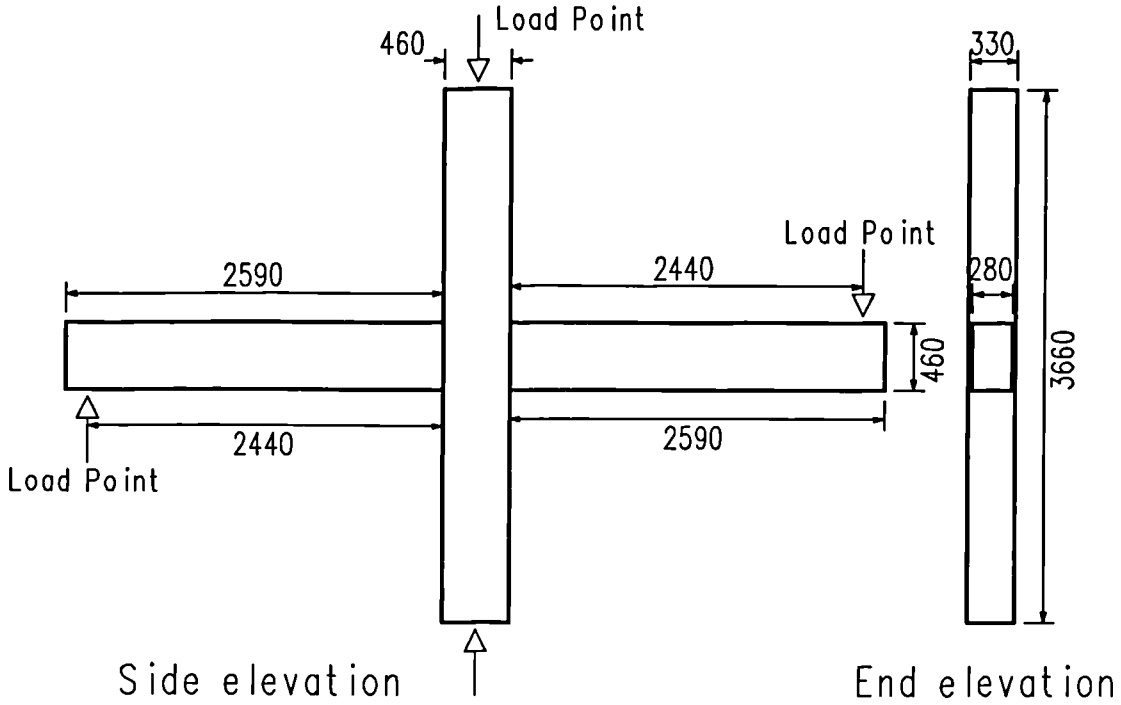

Figure 1.2.2 Specimen layout for strong column (dimensions in mm) Meinheit and Jirsa [5]

The details of Meinheit's fourteen specimens are given in Table 1.2.2. It can be seen that a number of parameters were investigated including the effect of column load, concrete strength and the quantity of reinforcement in both the joint and the column.

The method of testing used by Meinheit was slightly different from that used in other monotonic investigations. After the column load had been applied the beam was loaded downwards until joint cracking had taken place, the beam was then loaded upwards until joint cracking had occurred in the opposite direction before the specimen was loaded downwards to failure. This probably slightly reduced the ultimate strength of the specimens, but as this method of loading was considered for all specimens, comparisons within this test series are considered valid. After the ultimate capacity of the connections had been determined Meinheit continued the test to investigate the cyclic strength of the joint.

Table 1.2.2 Specimen details - Meinheit [5]

Specimen	Column Stiffness	Column Reinf %	Column Load (kN)	f_{ck} (MPa)	Joint Reinf	V_{crack} (kN)	V_{fail} (kN)	Failure Mode
I	S	2.0	1570	26	2 × 13	400	1090	J
II	S	4.3	1570	42	2 × 13	480	1600	J
III	S	6.7	1570	27	2 × 13	440	1230	J
IV	W	4.3	1570	36	2 × 13	620	1450	J
V	S	4.3	210	36	2 × 13	240	1530	J
VI	S	4.3	2620	37	2 × 13	750	1640	F
VII	W	4.3	2620	37	2 × 13	800	1470	J
VIII (tra)	S	4.3	1570	33	2 × 13	820	1690	F
IX (tra)	S	4.3	1570	31	2 × 13	450	1600	J
X (tra)	S	4.3	1570	30	2 × 13	460	1480	J
XI (tra)	W	4.3	1570	26	2 × 13	400	1280	J
XII	S	4.3	1570	35	6 × 16	600	1950	F
XIII	S	4.3	1570	41	6 × 13	720	1560	J
XIV	W	4.3	1570	33	6 × 13	550	1540	J

Notes

1. tra - indicates that transverse beams were present,
2. S - indicates strong column stiffness (the beams framed into the column's narrow face),
3. W- indicates weak column stiffness (the beams framed into the column's wider face),
4. The joint reinforcement notation is 'number of ties × tie diameter' (mm),
5. V is the shear force on the joint - the method of calculation of this from beam load is given in Section 1.3,
6. J - indicates joint failure, F - indicates beam flexural failure.

Meinheit made the following observations from his test results :

Initial Joint Cracking

The cracking strength of the joint was seen to be mainly dependent on the concrete strength and the magnitude of the column load. The following empirical equation to

calculate joint cracking strength was presented and was the result of a statistical regression analysis :

$$v_{cr} = 0.0124(f_{ck})^{0.85}(\frac{P}{A_g})^{0.485} \quad \text{.....(eq. 1.2.3)}$$

where f_{ck} is the concrete compressive cylinder strength (psi),

P is the column load (kip),

A_g is the gross area of the column (in^2).

Similarly to Taylor [1] and Ryan [4], Meinheit did not believe that the initial cracking strength was affected by the amount of joint reinforcement present.

Ultimate Strength

It was suggested that the ultimate strength of beam-column connections depended mainly on concrete strength and the quantity of joint reinforcement present. Interestingly, like Taylor [1], he suggested that the effect of column load was considered to be negligible.

Again after a statistical regression analysis on the test results the following empirical equation to calculate ultimate joint shear strength was presented:

$$v_u = 5.492(f_{ck})^{0.660}(1+\rho_s)^{0.5371} \quad \text{.....(eq. 1.2.4)}$$

where f_{ck} is the concrete compressive cylinder strength (psi),

ρ_s is the ratio of joint reinforcement to joint area.

1.2.4 Kordina [6]

In 1984 Kordina reported on the manufacturing and testing of nine reinforced concrete beam-column connection specimens. Dimensions of a typical specimen are

given in Figure 1.2.3 and the test results are given in Table 1.2.3. Over the nine tests the following parameters were varied :

1. Beam depth,
2. Method of anchorage,
3. Column load,
4. % and type of beam reinforcement,
5. % and type of joint reinforcement.

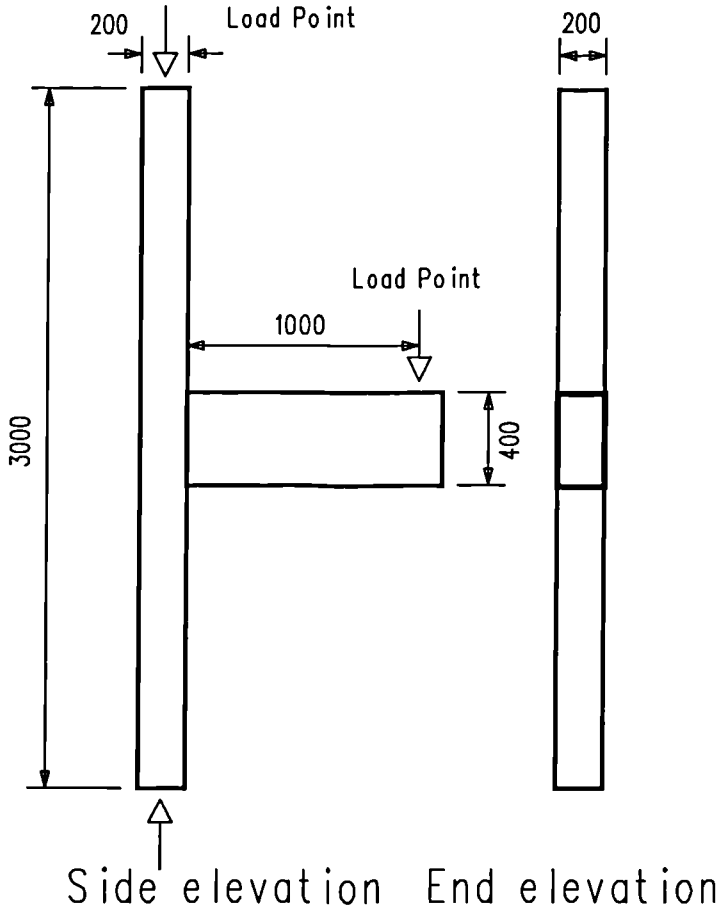

Figure 1.2.3 Specimen layout (dimensions in mm) - Kordina [6]

In the author's opinion it is hard to draw conclusions from Kordina's tests because so many parameters were varied in only a small number of tests. In addition novel joint strengthening methods such as diagonal ties and joint U-bars were used.

Table 1.2.3 Specimen details - Kordina [6]

Spec	Anch	d_b (mm)	f_{cu} (MPa)	Joint Steel (mm)	Beam Steel %	Diagonal Bar	Column Load (kN)	Failure Load (kN)
RE2	D	400	32	None	0.84	1T20	240	67
RE3	D	300	51	1T10 U-bar	1.14	1T20	400	80
RE4	D	300	40	1T8	1.14	-	51	51
RE5	P	300	37	None	0.37	-	46	46
RE6	P	300	40	3T8	1.14	1T20	213	66
RE7	D	350	32	4T8	1.26	2T18	650	117
RE8	U	350	35	4T8	1.26	2T18	525	105
RE9	U	350	36	4T8 U-bars	1.26	2T18	770	110
RE10	U	390	30	5T8 U-bars	1.12	2T16	551	100

Notes

1. d_b - is the depth of the beam,
2. Anch - indicates the beam steel anchorage detail,
3. D - indicates bent down anchorage, P - indicates the use of a plate at the outer face of the column for beam anchorage, U - indicates U-bar anchorage,
4. The additional U-bars for joint reinforcement were across the width of the beam,
5. The diagonal bar passed across the cracking diagonal of the joint.

1.2.5 Sarsam [7]

Sarsam reported on the testing of five reinforced concrete beam-column connection specimens in 1985. Dimensions of a typical specimen are given in Figure 1.2.4.

The method of anchoring the beam tension bars was by bending them down into the column. The specimens were grouped according to the different parameters. Specimen EX1 had three 8 mm diameter ties within the joint whereas the joint in Specimen EX2 was unreinforced. Specimens EX3 and EX4 had beams with shorter lengths (663 and 881 mm respectively) allowing different applied moments and shear forces to be compared. Specimens EX1 and EX5 were tested under different column loads, enabling the effect of axial compressive stress to be examined. Details of the results from these five tests are given in Table 1.2.4.

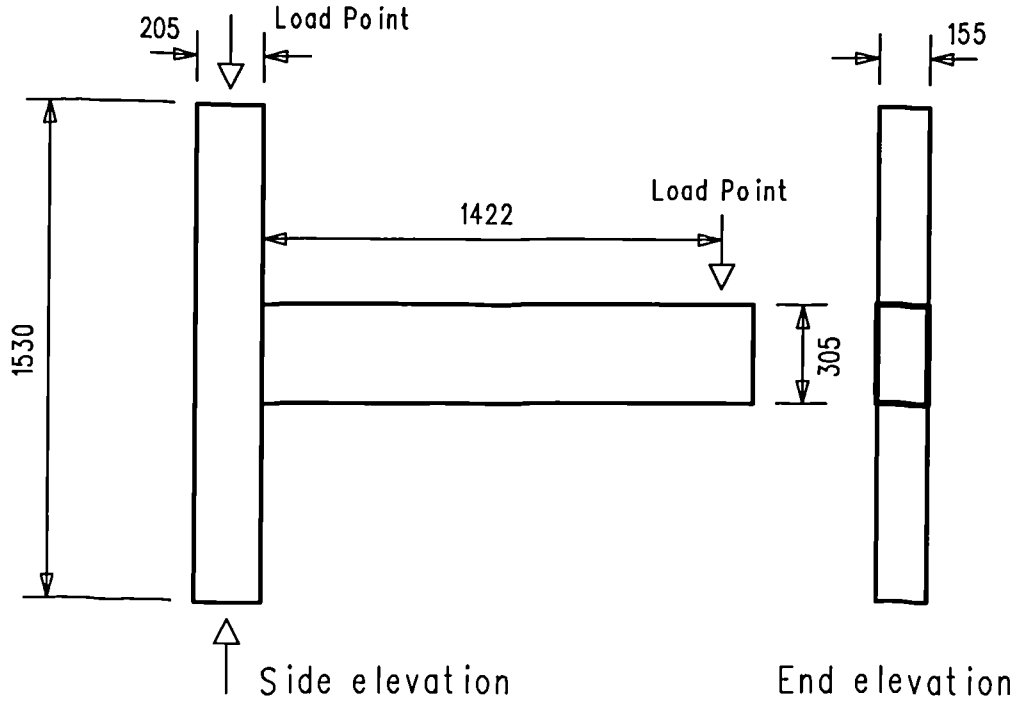

Figure 1.2.4 Specimen layout (dimensions in mm) - Sarsam [7]

Table 1.2.4 Specimen details - Sarsam [7]

Specimen	f_{cu} (MPa)	Column Load (kN)	V_{crack} (kN)	V_{ult} (kN)	Failure Modes
EX1	69	300	125	181	F
EX2	66	300	123	172	J
EX3	53	300	111	161	F
EX4	66	300	113	173	F
EX5	65	900	121	170	F

Notes

1. V is the shear force on the joint - the method of calculation of this from the beam load is given in Section 1.3,
2. F - indicates beam flexural failure, J - indicates joint shear failure.

Table 1.2.4 shows that four out of five specimens failed by beam flexural failure. EX2 was the only specimen that exhibited joint shear failure.

Sarsam commented that the presence of ties did not influence the load at which initial joint cracking occurred. An empirical equation was suggested to predict the shear stress within the joint at initial cracking :

$$v_{cr} = 2.03(f_{cu}\rho_c d_c / d_b)^{0.33}(1 + 0.29N / A_g)^{0.5} \quad \text{.....(eq. 1.2.3)}$$

where ρ_c is equal to $A_{sc}/b_c d_c$,

A_{sc} is the steel cross sectional area,

b_c is the column breadth,

d_c and d_b are the column and beam depths respectively,

N is the applied column load,

A_g is the column cross sectional gross area.

The enhancement factor, $(1+0.29N/A_g)^{0.5}$, was included in equation 1.2.3 to account for the effect of column load on the initial cracking strength. However Sarsam did not believe that the **ultimate** shear capacity of the joint was enhanced with increasing column load.

1.2.6 Scott [8, 9]

In 1994 Scott reported on the manufacturing and testing of fifteen external beam-column connection specimens, an example of which is given in Figure 1.2.5.

All specimens had four 16 mm bars for the column reinforcement and one tie was present, at mid-height, within each joint. The fifteen specimens were split into three test series; the first, (details C1 to C3), investigated the use of 2T12 beam bars for tension reinforcement; the second (details C4 - C6) investigated the use of using 2T16 beam tension bars; the final test series (details C7 - C9) investigated the performance of specimens using beams of depth 300 mm.

Specimens with the prefix C1, C4 and C7 had beam tension bars bent down into the column, C2, C5 and C8 had beam tension bars bent up into the column and C3, C6

and C9 used U-bar steel detail. A letter *A* indicated that a shorter anchorage leg was used for the beam bent down into the column. This length was the minimum allowed by BS 8110 [3]. The majority of tests used a column load of 275 kN, a letter *L* however indicated that a lower column load (50 kN) was used. Specimen details are shown in Table 1.2.5.

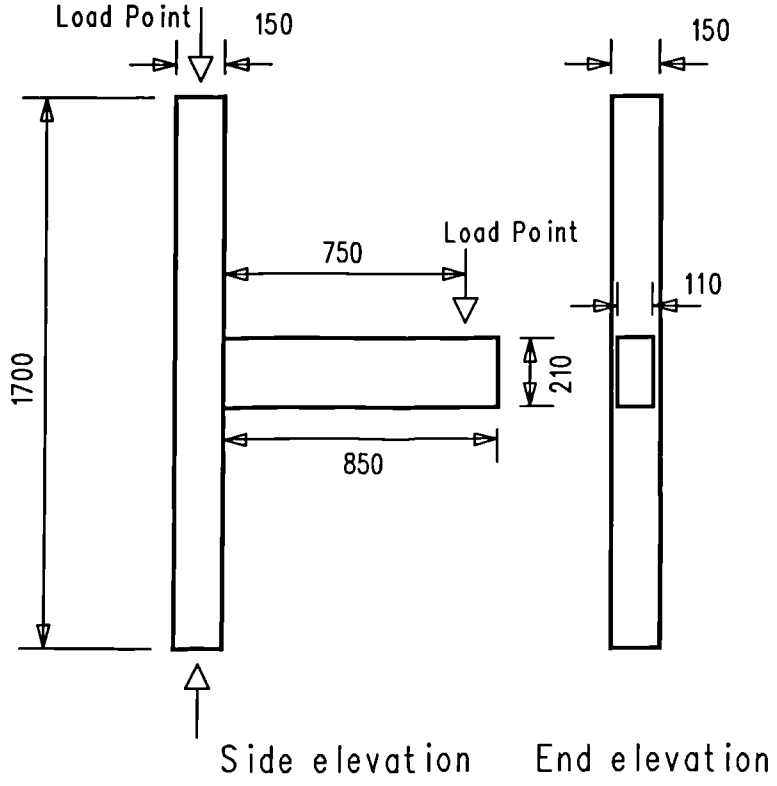

Figure 1.2.5 Specimen layout (dimensions in mm) - Scott [8]

Each specimen contained around 230 electric resistance strain gauges. These were positioned internally within the main column and beam steel. This was unique as never before had reinforcement strains been investigated in such detail (within this field of study). The technique of internally strain gauging the column and beam reinforcing bars (outlined further in Section 2.2.1) allowed very detailed measurements to be taken. The fact that the strain gauges were mounted internally meant that the complex bond behaviour between the steel and the concrete was not disturbed.

A prop was used at the end of the beam to simulate the effect of a continuous beam and to eliminate the risk of side sway. The purpose of this prop was not to induce an axial force into the beam throughout the tests (as was the case with a number of Taylor's [1] tests). Experimental results showed that the prop typically carried no load prior to joint cracking. After this the load carried by the prop was seen to rise to around 5 kN at failure.

Table 1.2.5 Specimen details - Scott [8]

Specimen	f_{cu} (MPa)	Anch	Column Load (kN)	P_{crack} (kN)	P_{fail} (kN)	Failure Mode
C1	50	A	275	17.1	26.2	F
C1A	60	A	275	19.0	26.8	F
C1AL	42	A	50	11.1	22.0	J
C2	62	B	275	18.9	21.5	J
C3	45	C	275	19.9	25.9	F
C3L	44	C	50	12.5	21.6	J
C4	52	A	275	18.8	29.7	J
C4A	55	A	275	18.8	31.8	J
C4AL	48	A	50	12.1	28.3	J
C5	41	B	275	9.7	13.8	J
C6	50	C	275	14.8	21.8	J
C6L	57	C	50	14.8	26.0	J
C7	44	A	275	22.2	32.0	J
C8	56	B	275	26.2	27.3	J
C9	45	C	275	22.9	27.9	J

Notes

1. A - indicates beam steel bent down into the column, B - indicates beam steel bent up into the column, C - indicates that U-bars were used,
2. F - indicates beam flexural failure, J indicates joint failure.

Scott made the following observations from his test results :

Initial Joint Cracking

The internal strain gauges within the beam rebars allowed detailed bond and bearing stress calculations to be made. Scott observed that up to joint cracking the load transfer from the beam into the joint was predominantly by bond stresses at the first bend of the beam tension rebar. After joint cracking, the bars bent down and the U-bars compensated for loss of bond at this bend by developing increasing bond stress over their anchorage length.

As a result of this research BS 8110 equation 6 [3] was split into equations 6(a) and 6(b). Scott *et al* [9] showed that equation 6(b) gave a good correlation with the test data for when the joint first cracked. They concluded that this equation should be used when it is necessary to avoid shear cracking in the joint prior to the ultimate limit state. Equation 6(b) is given below :

$$v_c' = v_c \sqrt{\left(1 + \frac{N}{b_c h_c v_c}\right)} \quad \text{.....(eq. 1.2.5)}$$

where v_c is the design concrete shear stress for a reinforced concrete section,

N is the column load,

b_c and h_c are the column breadth and height respectively.

This enhancement factor took into consideration the effect of column load as it was found that in the low column load tests joint cracking occurred at a lower applied beam load than in the corresponding high column load tests. Scott *et al* [9] also commented that Taylor's equation to predict initial joint cracking (eq. 1.2.1) gave a good correlation with the experimental results.

Ultimate Strength

Scott made similar comments to Taylor [1] regarding detailing of the beam steel. Overall, beam tension bars bent down and U-bar details performed significantly better than the bars bent up into the column. The data from the strain gauges within Scott's specimens showed that beam tension bars bent down and U-bar details accommodated changes as they occurred within a specimen, the bent up detail did not and its use would seem undesirable in practical connection design.

BS8110 [3] specifies an upper limit for maximum shear stress in concrete as $\sqrt{f_{cu}}$ (with the partial safety factor of 1.25 removed). This upper limit corresponds to a diagonal stress field crushing failure in the concrete, taken to be at 45°. Scott *et al* [9] suggested that it may be more realistic to assume a field which is parallel to the diagonal of the compression zone which gives:

$$v_{crsh} = \frac{2\sqrt{f_{cu}}}{\left[\frac{z_c}{z_b} + \frac{z_b}{z_c}\right]} \quad \text{.....(eq. 1.26)}$$

where z_c and z_b are the lever arms of the column and beam, *respectively, at failure.*

The method of internally strain gauging the reinforcement allowed accurate bearing stresses to be calculated at the bends of the beam steel. It was observed that bearing stresses within the specimens were higher than permitted by BS8110 [3]. Scott *et al* suggested that high bearing stresses could be tolerated by the provision of additional joint ties rather than having to resort to large radius bends.

1.2.7 Reys de Ortiz [10]

In 1993 Reys de Ortiz presented the results of seven exterior reinforced concrete beam-column connection specimens, an example of which is shown in Figure 1.2.7.

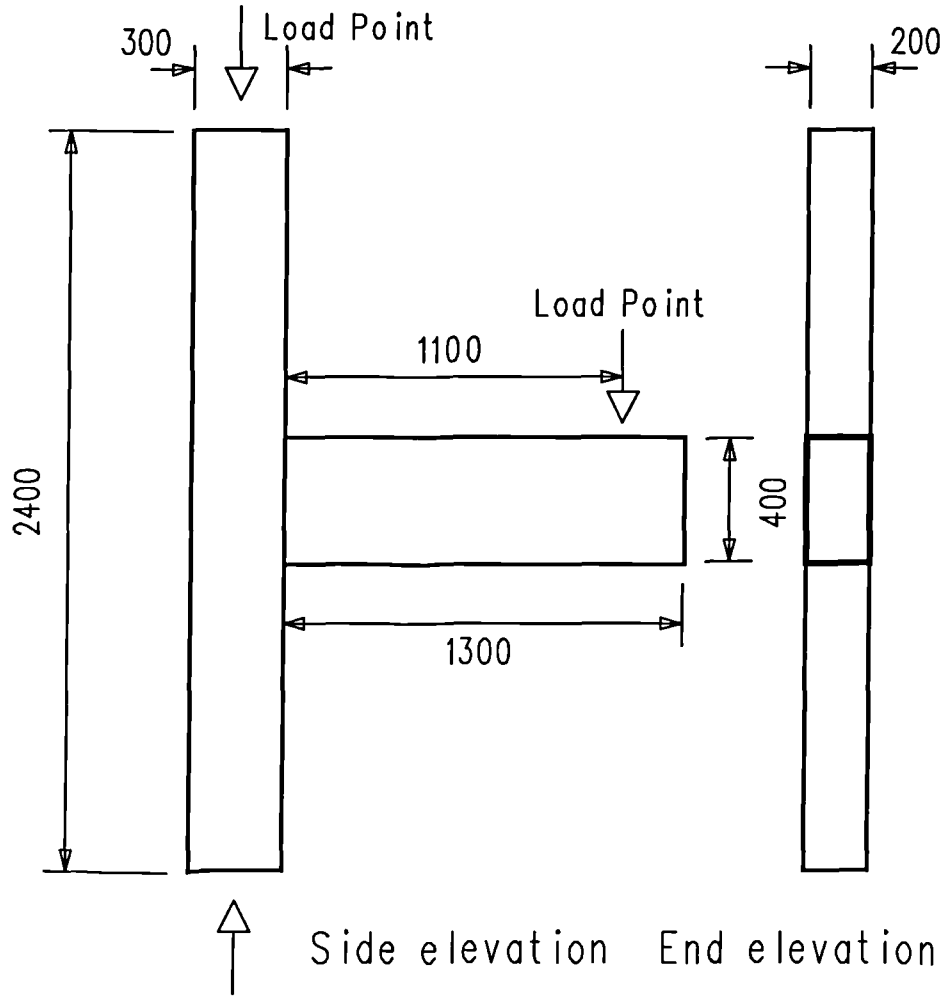

Figure 1.2.7 Specimen layout (dimensions in mm) - Reys de Ortiz [10]

Table 1.2.7 Specimen details - Reys de Ortiz [10]

Specimen	Column Steel %	Joint Reinf	Anchorage Radius (mm)	Column Load (kN)	P_{crack} (kN)	P_{fail} (kN)	Failure Mode
BC1	1.5	-	65	0	40	118	J
BC2	1.5	1T8	65	0	50	125	J
BC3	2.0	-	130	0	50	118	J
BC4	2.5	3T8	65	0	50	130	J
BC5	2.5	-	65	300	80	115	J
BC6	2.5	-	130	300	80	115	J
BC7	2.5	4T10	130	300	70	170	F

Notes

1. J - indicates joint failure, F - indicates beam flexural failure.

A number of parameters were varied by Reys de Ortiz, as shown in Table 1.2.7. All specimens used four 16 mm rebars for the beam tension reinforcement and the method of anchorage used in each case was bending the beam steel down into the column. Concrete strengths ranged from 41 to 47 MPa.

In the author's opinion Reys de Ortiz varied too many parameters for the number of tests which took place. When comparing certain results this leaves doubts as to exactly which variable accounted for which particular change in behaviour.

These results were used to form the basis for a strut-tie analysis, a review of which is given in Appendix A1.

Reys de Ortiz made the following observations from her test results :

Initial Joint Cracking

The load at which initial joint cracking occurred was dependent on the magnitude of the column axial load.

Ultimate Strength

The ultimate load appeared to be independent of the magnitude of the column load.

Reys de Ortiz argued that a greater number of small diameter rebars would be more effective in transferring the beam's force into the column than fewer large bars. (An example of this would be that 5T12 mm rebars may give a higher joint strength than 2T20 mm bars even though the actual area of reinforcement was slightly less in the first layout). She suggested that this applied for both beam anchorage detail and outer column bar detail.

1.2.8 Parker [11]

In 1997 Parker presented the results of 12 reinforced concrete external beam-column connection specimens with dimension shown in Figure 1.2.8.

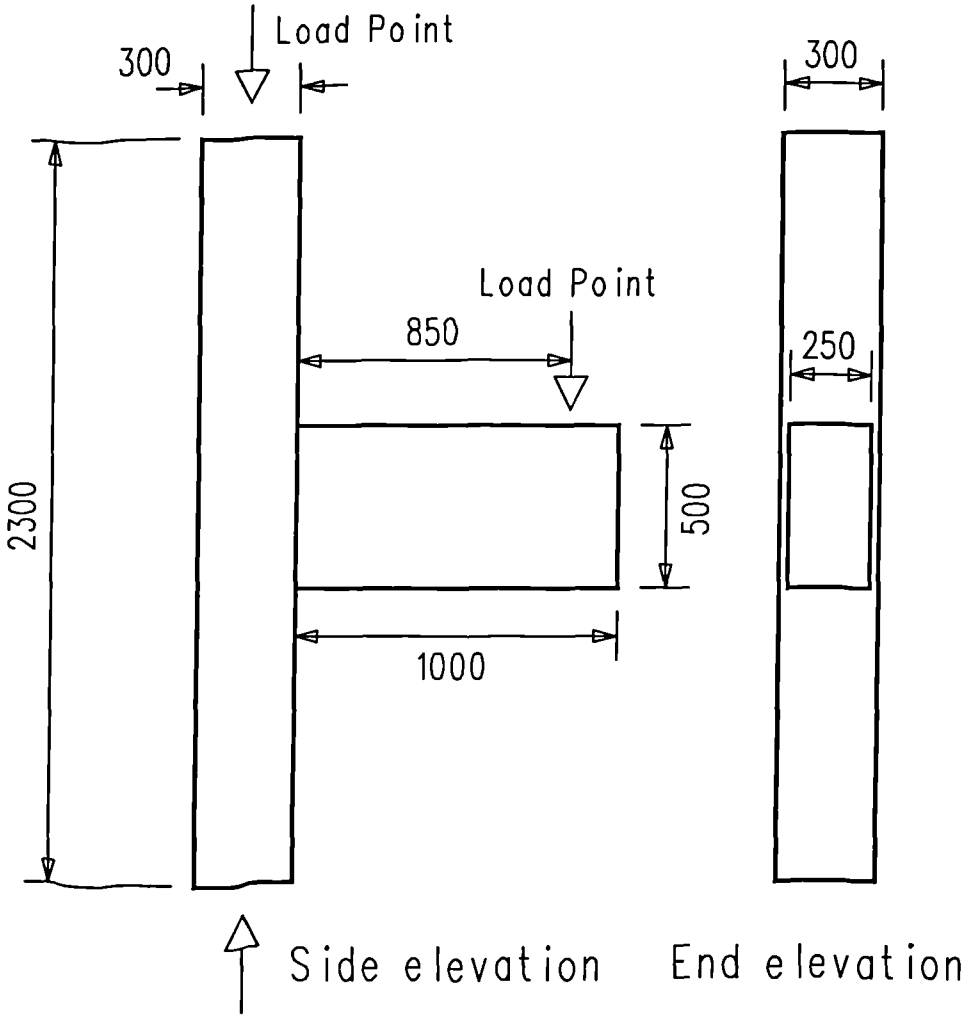

Figure 1.2.8 Specimen layout (dimensions in mm) - Parker [11]

Four test series were examined, as shown in Table 1.2.8, with the applied column load being varied in each case. Specimens 4a-4c were compared with specimens 4d-4f to examine the effect of increasing the percentage of column steel. Specimens 5a-5c were compared with specimens 5d-5f to examine the effects of increasing the number of joint ties and increasing the percentage of beam steel. Concrete cube

strengths ranged from 47 to 56 MPa. The applied load at initial diagonal cracking was not included in the results presented by Parker.

Similarly to Reys de Ortiz [10], Parker presented a strut-tie analysis of the results which is outlined in Appendix A2.

Table 1.2.8 Specimen details - Parker [11]

Specimen	Column Steel (%)	Beam Steel (%)	Joint Reinf	Column Load (kN)	P_{fail} (kN)	Failure Mode
4a	0.9	0.8	-	0	118	FC
4b	0.9	0.8	-	300	138	J
4c	0.9	0.8	-	570	170	J
4d	3.6	0.8	-	0	150	J
4e	3.6	0.8	-	300	160	J
4f	3.6	0.8	-	600	183	J
5a	2.2	0.8	3T12	0	213	FC
5b	2.2	0.8	3T12	300	236	J
5c	2.2	0.8	3T12	600	242	FB
5d	2.2	1.3	5T12	0	226	FC
5e	2.2	1.3	5T12	300	295	FC
5f	2.2	1.3	5T12	600	322	J

Notes

1. FC - indicates column flexural failure, FB - indicates beam flexural failure
2. J - indicates joint shear failure.

Parker made the following observations from his test results :

Ultimate Strength

The ultimate strength of the joint was dependent on both the column load and the amount of joint ties. The percentage of steel within the column was also thought to be a factor.

1.2.9 Vollum [12]

In 1998 Vollum presented the results from ten reinforced concrete ***eccentric*** beam column connection specimens. These tests are believed to be outside the scope of this investigation. However, Vollum also completed a thorough review of the previous monotonic research. The results from the tests by Reys de Ortiz [10], Parker [11], Kordina [6], Taylor [1], Sarsam [7], Scott [8] and some of the early tests from this research were all analysed. All of these results were used to develop his strut-tie analysis (outlined in Appendix A3). Of the three strut-tie models (Reys de Ortiz, Parker and Vollum) the author considers Vollum's to be the most thorough and to give the best performance.

Vollum commented that the available test data on the strength of monotonically loaded exterior beam-column connections was far from comprehensive and that there was a clear need for further tests. Vollum, like Sarsam [7], made the point that most of the world-wide research has been focused on seismically loaded connections which had resulted in a lack of knowledge concerning monotonically loaded connections.

There is a growing need for knowledge regarding monotonically designed joint behaviour under cyclic loading conditions. There are increasing concerns in the USA over the strength of buildings in regions which are considered non-seismic. **The behaviour of monotonically designed reinforced concrete joints subject to cyclic loads is considered from Chapter 7 onwards.**

Author's Note : One month before the submission of this thesis, Vollum and Newman published a review of all known literature on monotonically-loaded, external beam-column connections [13]. All of the research presented in Vollum and Newman's paper (excluding tests investigating floor slabs) has also been covered within this Literature Review.

1.3 Joint Shear Calculations

The observations made in previous research concerning **monotonically loaded beam-column connections** have been discussed in Sections 1.2.1 to 1.2.7. However direct comparisons are difficult to make between results from different size specimens. For example, a large joint would be considerably stronger than a smaller joint regardless of the design. However, the behaviour of different size specimens may be normalised by converting the applied beam load into firstly a joint **shear force** and then a joint **shear stress**. This section outlines the method used for joint shear calculations within this investigation. This method is then compared with those used in previous research.

Converting the loads into joint shear stresses helps eliminate size effects between specimens from different research programmes. However, the influence of variables such as steel anchorage length, cracking patterns and aggregate size all create complications. Abrams [14] reported on a series of tests on scale relations in 1987. Eighteen reinforced connection assemblies were manufactured and tested at small, medium or large scale (defined by Abram as approximately one-twelfth, one-quarter and three-quarter scales). Figure 1.3.1 displays the dimensions of a large scale specimen. The scale relationships were kept as constant as possible including the applied loads, the steel percentages and even the concrete aggregate size.

Although the specimens were designed and tested using seismic methods the findings are believed to be relevant to the simpler loading techniques used for monotonic testing.

Abrams concluded that scale relationships for reinforced concrete research, using stone aggregate and deformed bars should be limited to one-quarter scale and main rebar diameters limited to 10 mm. All test specimens reviewed in Sections 1.2.1 to 1.2.7 of this thesis were larger than one quarter scale. Therefore, on this basis, all of these tests may be considered valid.

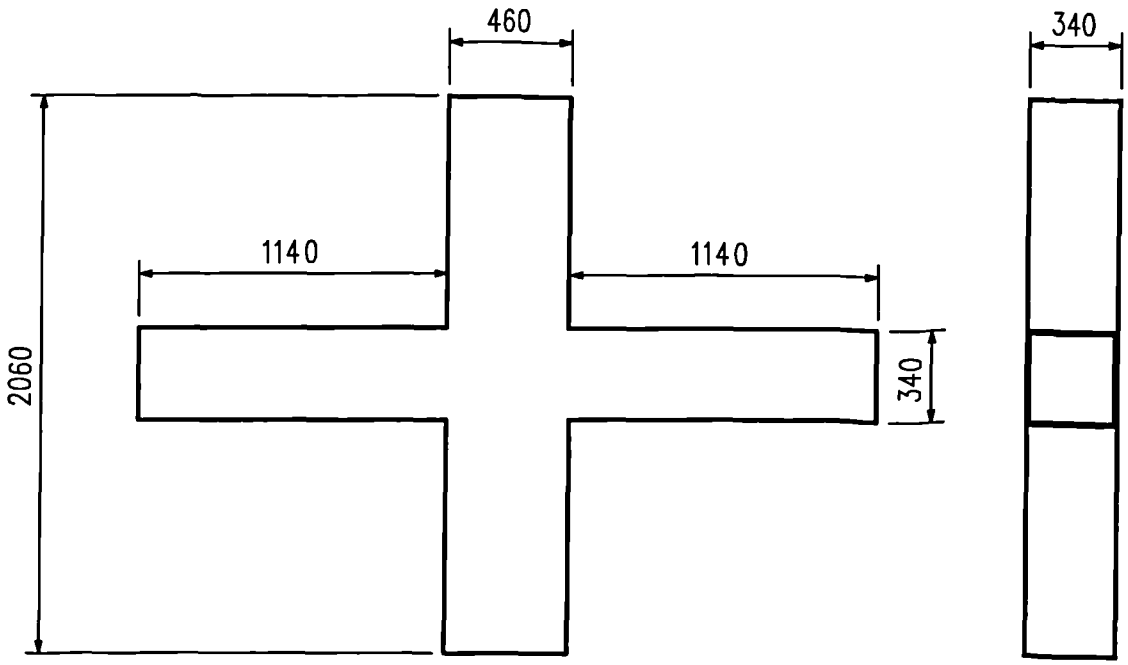

Figure 1.3.1 Dimensions of a large scale specimen as defined by Abrams [14] (dimensions in mm)

Joint shear calculations

The joint shear force, V_j, as shown in Figure 1.3.2, is evaluated by considering equilibrium within the joint :

$V_j = T - V_{col}$ .....(eq. 1.3.1)

where T is the force in the beam tension reinforcement,

V_{col} is the shear force in the upper column.

By balancing the moments about the compression face of the beam at the face of the column, the moment due to the tension reinforcement, $T \times z_{bm}$, is equal to the moment due to the applied beam load, $P \times e_{face}$, as shown in Figure 1.3.3. The effects of the beam compression reinforcement and the self weight of the specimen are assumed to be negligible.

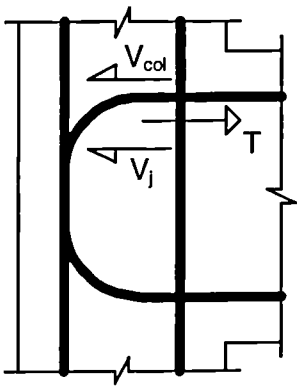

Figure 1.3.2 Horizontal joint forces

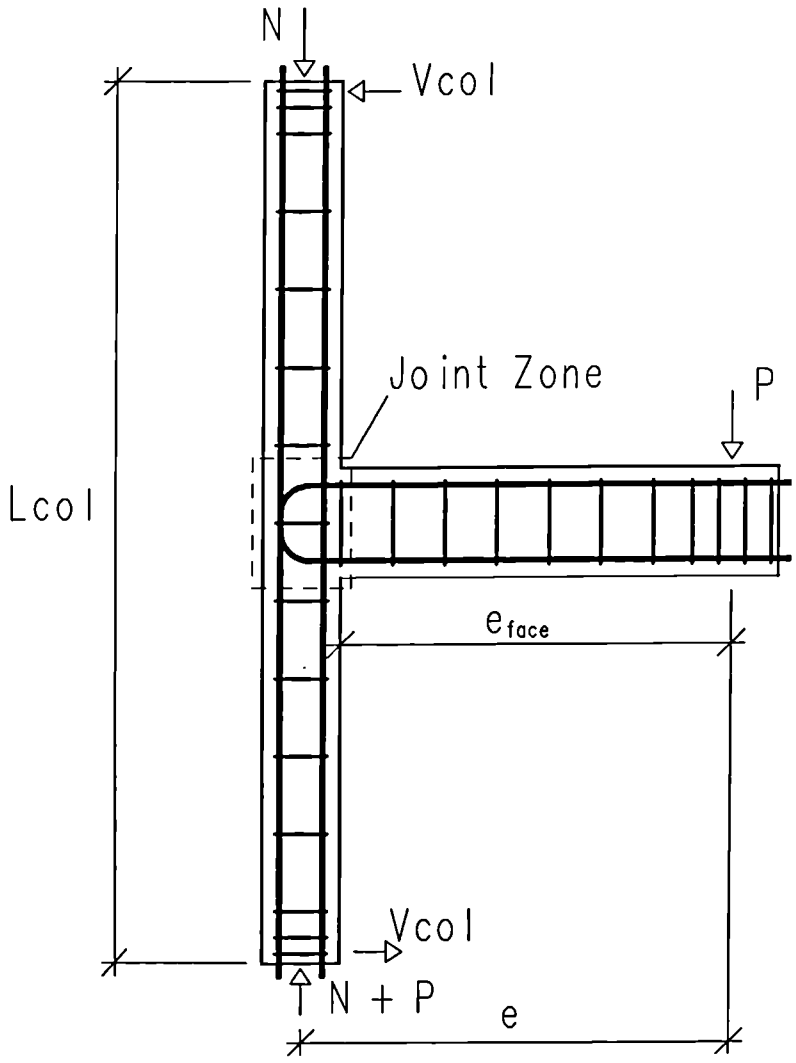

Figure 1.3.3 Exterior forces and dimensions

$$T = \frac{Pe_{face}}{z_{bm}} \quad \text{.....(eq. 1.3.2)}$$

where P is the applied beam load,

e_{face} is the distance between the column face and the load point,

z_{beam} is the lever arm depth of the beam.

The shear force in the upper column can be calculated by taking moments about the column mid-point at the base.

$$Pe = V_{col}L_{col} \quad \text{.....(eq. 1.3.3)}$$

where L_{col} is the distance between the restraints at the top and the base of the column.

$$V_{col} = \frac{Pe}{L_{col}} \quad \text{.....(eq. 1.3.4)}$$

where e is the distance between the column centre-line and the load point.

Substituting equations 1.3.2 and 1.3.4 into 1.3.1 gives the joint zone shear force :

$$V_j = \frac{Pe_{face}}{z_{bm}} - \frac{Pe}{L_{col}} \quad \text{.....(eq. 1.3.5)}$$

This is the general method used in both ACI-318 [15] (Section 1.6.2) and previous research to calculate the shear force within the joint zone. However, a number of section analysis methods have been used to calculate the beam's lever arm depth.

Scott *et al* [9] used an iterative computer program, using both experimental stress-strain data and taking into consideration the effect of compression steel. Their equation also involved the column's lever arm depth. This was approximated as the distance between the centres of the inner and outer column reinforcement.

Parker [11] significantly simplified the calculation of the lever arm by assuming that it was equal to $0.9d_{bm}$.

Vollum [12] calculated the beam lever arm depth using the design compressive stress-strain block method recommended by the CEB Model Code [16]. The contribution of the beam compression steel was ignored.

This investigation, like Vollum's [12], used a simplified method to calculate the lever arm depth of the beam, which assumed the contribution of the beam compression bars to be negligible. The method used the design compressive stress strain block recommended by BS8110 [3].

BS 8110 [3]

The area of the simplified stress block in Figure 1.3.4 has had the partial safety factor of 1.5 removed. The lever arm depth is calculated as follows :

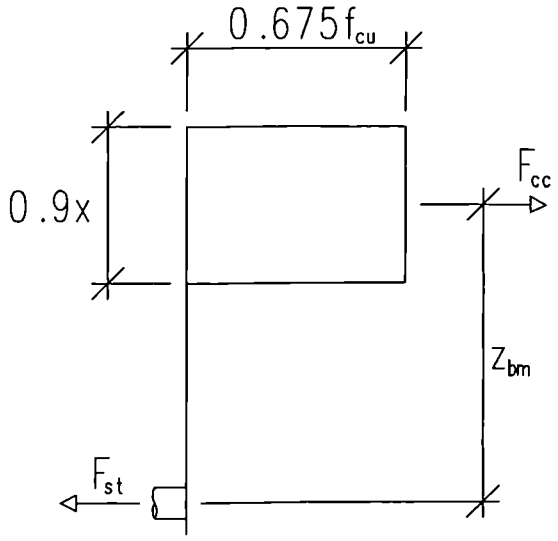

Figure 1.3.4 BS 8110 [3] simplified stress block

$M = 0.675f_{cu}b_{bm}0.9x \times z_{bm}$ .....(eq. 1.3.6)

$M = 0.675f_{cu}b_{bm}2(d_{bm}-z_{bm})z_{bm}$ .....(eq. 1.3.7)

where M is the beam moment,

x is the neutral axis depth,

b_{bm} is the beam depth,

d_{bm} is the effective depth of the beam.

and by arranging and then solving the subsequent quadratic equation :

$$k = \frac{M}{b_{bm} d_{bm}^{2} f_{cu}} \quad \text{.....(eq. 1.3.8)}$$

$$z_{bm} = d_{bm}\left\{0.5 + \sqrt{0.25 - \frac{k}{1.35}}\right\} \quad \text{.....(eq. 1.3.9)}$$

where k is a dimensionless constant.

The ability to represent the applied beam force as a joint shear stress allows comparisons to be made between the specimens from previous research. This joint shear force is converted into a shear stress using the following equation :

$$v_j = \frac{V_j}{b_e d_{col}} \quad \text{.....(eq. 1.3.10)}$$

where b_e is the effective width of the column,

d_{col} is the depth of the column.

Note

1. *When comparing results using compressive cylinder strengths, f_{ck}, with compressive cube strength, f_{cu}, the relationship defined in EC2 [17] is used :*

   $$f_{ck} = 0.8 \times f_{cu} \quad \text{.....(eq 1.3.11)}$$

2. *Within this investigation the effective width of the column, b_e, was used. This was defined as the average of the beam and column widths. This was consistent*

with the methods used by the ACI 318 Code [15] (discussed further in Section 1.6.2).

3. *The effective depth of the column was used. This was equal to the depth of the column minus the concrete cover (calculated to the centre of the rebar).*

1.4 Parametric Study of Previous Monotonic Research

This parametric study of the previous monotonic research considers the influence of the parameters outlined below and their influence on the specimen behaviour. For comparisons all applied beam loads have been converted into shear stresses using the method previously defined in Section 1.3. All steel reinforcement quantities have been converted into percentages of their respective member sections and all column loads have been converted into axial stresses.

The influences of the following parameters are considered in the following sections :

1.4.1 Concrete strength
1.4.2 Detailing arrangement for the beam tension steel
1.4.3 Column load
1.4.4 Presence of joint ties
1.4.5 Joint aspect ratio
1.4.6 Longitudinal column steel

Although the above list of parameters is clearly not exhaustive it does cover all relevant parameters for standard reinforced concrete design in the UK.

1.4.1 Influence of concrete strength

The BS8110 [3], and ACI-318 [15] design codes indicate that, for reinforced concrete, shear strength is proportional to the square root of the concrete compressive strength. (*A review of the code provisions for joint design is presented in Section 1.6*). Previous monotonic research on beam-column connection specimens [5, 8, 12], served to confirm this relationship.

$v_j \propto \sqrt{f_{cu}} \propto \sqrt{f_{ck}}$.....(eq. 1.4.1)

where f_{cu} is the concrete compressive cube strength,

f_{ck} is the concrete compressive cylinder strength.

Because of the large number of parameters varied in previous tests it is important to isolate the influence which each variable has on the strength of the joint. Thus, if the influence of concrete strength on joint strength is to be considered, then the influence of all other parameters must preferably be eliminated.

Table 1.4.1.1 shows the results of a selection of previous test results outlined in Section 1.2. The results displayed were chosen to minimise the effects of beam steel anchorage, column load, joint steel percentage and joint aspect ratio. Only specimens with bent down anchorage were considered. Previous research had indicated that specimens using U-bar beam steel detail failed at a lower load than corresponding specimens using bent down beam steel. Due to previous disagreement regarding the influence of column load, all specimens with column stresses greater than 10 MPa were excluded. Similarly only specimens with nominal joint reinforcement were considered; joint steel percentages greater than 0.5% were excluded. As a result of Vollum's [12] concerns regarding joint aspect ratio, specimens with joint aspect ratio over 1.4 were also excluded.

Parker's results were not included due to concerns that beam steel anchorage problems may have caused premature failure of the joints in his investigation. This was suggested by Vollum [12] and is discussed further in Section 1.4.2.

Table 1.4.1.1 therefore gives a good representation of joint behaviour in which all influences other than concrete strength were minimised. By eliminating test results in which other parameters were a major influence the remaining nine specimens clearly show the relationship between concrete compressive strength and ultimate joint capacity.

It should be noted that for the remainder of this thesis, the compressive cylinder strength, f_{ck}, is used in preference to the concrete cube strength, f_{cu}. This is due to the use of this in both the ACI 318 [15] and EC2 [17] Codes. All conversions from cube to cylinder strengths were made using equation 1.3.11.

Table 1.4.1.1 The effect of concrete strength on ultimate joint capacity

Investigation	Specimen	f_{ck} (MPa)	$\sqrt{f_{ck}}$ ($MPa^{0.5}$)	v_j (MPa)	$v_j/\sqrt{f_{ck}}$ ($MPa^{0.5}$)
Kordina [6]	**RE2**	31.6	5.6	5.08	0.90
Sarsam [7]	**EX2**	52.5	7.2	6.63	0.91
Scott [8]	**C1AL**	33.6	5.8	6.12	1.06
	C4AL	36.0	6.0	8.08	1.35
Reys de Ortiz [10]	**BCJ1**	33.8	5.8	5.62	0.97
	BCJ2	37.8	6.2	6.23	1.01
	BCJ3	33.0	5.7	5.94	1.03
	BCJ5	37.9	6.2	5.68	0.92
	BCJ6	35.0	5.9	5.73	0.97
			Mean of $v_j/\sqrt{f_{ck}}$ ($MPa^{0.5}$)		**1.01**
			Standard deviation		**0.14**
			Variation (s.d./mean)		**13%**

Table 1.4.1.1 shows that test results from four different investigations indicate that a joint under a low column load, with bent down beam steel detail and no significant joint reinforcement has a joint strength directly proportional to the square root of the concrete strength. Thus dividing the ultimate shear stress by $\sqrt{f_{ck}}$ gives us a **normalised** value of 1.0 for an unreinforced joint. This allows comparisons to be made between test specimens of different dimensions and different concrete strengths.

Specimens with an enhanced joint strength, (due to, for example, the presence of a joint reinforcement) have a normalised shear stress greater than 1.0.

Specimens with a weakened joint strength, (due to, for example, steel detail bent up into the column) have a normalised shear stress less than 1.0.

Table 1.4.1.2 shows the results from all 70 previous monotonic tests outlined in Section 1.2. The shear stress at joint cracking and specimen failure is normalised for all test results.

As outlined at the start of this chapter, only a small amount of research has been concerned with the monotonic loading of beam-column connections. Through strenuous efforts and communication with colleagues the author has been reliably informed that there is no further work to date on this subject. In addition to this, the work on beam-column connections in North America, Japan and New Zealand has been almost exclusively on earthquake design. The author believes that Table 1.4.1.2 contains the results of **all** previous monotonic test results relevant to this investigation.

1.4.2 Influence of beam steel anchorage

Previous research has shown a difference of opinion regarding the method of anchoring beam tension steel for exterior beam-column connection specimens. Taylor [1], Scott [8] and Vollum [12] recommended that beam steel should not be bent up into the column. Taylor [1] did not comment on the relative differences between U-bars and bent down bars but Scott [8] and Vollum [12] suggested that bars bent down into the column were a better anchorage detail than U-bars. Vollum suggested that specimens using U-bar beam steel detail have joint capacities 20% lower than specimens using steel bent down into the column. Kordina [6] shared Vollum's [12] concern about the use of U-bars and recommended that they should only be used if extra joint reinforcement was present. Alternatively Ryan [4] suggested that the U-bar detail was more efficient than the bent down detail.

Table 1.4.1.2 Normalised test data - previous research

Specimen	Anchorage type	Column steel %	Beam steel %	Joint steel %	Column load MPa	$v_{crack}/\sqrt{f_{ck}}$ $MPa^{0.5}$	$v_{fail}/\sqrt{f_{ck}}$ $MPa^{0.5}$	Failure mode
Taylor [1]								
P1/41/24	A	4.1	2.4	0.3	14.0	**1.15**	**1.50**	J
P2/41/24	A	4.1	2.4	0.3	14.0	**1.07**	**1.71**	J
P2/41/24A	A	4.1	2.4	0.3	14.0	**1.12**	**1.72**	J
P1/41/09	A	4.1	0.9	0.3	14.0	**0.89**	**1.27**	F
A3/41/24	A	4.1	2.4	0.3	14.0	**1.13**	**1.80**	J
A3/41/13	A	4.1	1.3	0.3	14.0	**1.26**	**1.51**	F
A3/41/09	A	4.1	0.9	0.3	14.0	**0.73**	**0.81**	F
A3/41/06	A	4.1	0.6	0.3	14.0	-	**1.04**	F
B3/41/24	A	4.1	2.4	0.9	14.0	**1.29**	**1.79**	J
C3/41/24X	B	4.1	2.4	0.3	14.0	**0.88**	**0.97**	J
C3/41/24BY	U	4.1	2.4	0.3	14.0	**0.95**	**1.25**	J
C3/41/13Y	U	4.1	1.3	0.3	14.0	**1.21**	**1.21**	J
C3/41/24Y	U	4.1	2.4	0.3	14.0	**1.14**	**1.39**	J
D3/41/24	A	4.1	2.4	0.3	3.1	**1.04**	**1.71**	J
D3/41/13	A	4.1	1.3	0.3	3.1	**0.74**	**1.19**	F
D3/41/09	A	4.1	0.9	0.3	3.1	**0.91**	**1.03**	F
D3/41/06	A	4.1	0.6	0.3	3.1	-	**0.96**	F
F3/41/24A	A	4.1	2.4	0.3	14.0	**1.67**	**1.68**	F
F3/41/16A	A	4.1	1.6	0.3	14.0	-	**2.33**	F
F3/41/24B	A	4.1	2.4	0.3	14.0	**1.39**	**1.80**	F
F3/41/16B	A	4.1	1.6	0.3	14.0	**1.65**	**1.76**	F
F3/41/24C	A	4.1	2.4	0.3	3.1	-	**1.90**	F
F3/41/16C	A	4.1	1.6	0.3	3.1	-	**1.15**	F
Kordina [6]								
RE2	A	2.0	0.8	0.0	6.0	-	**0.90**	J
RE3	A	2.0	1.1	0.3*	10.0	-	**1.25**	J
RE4	A	2.0	1.1	0.2	1.3	-	**0.87**	J
RE5	P	1.8	0.4	0.0	1.0	-	**0.74**	J
RE6	P	2.0	1.1	0.6	5.3	-	**1.16**	J
RE7	A	1.4	1.3	0.6	11.3	-	**1.30**	J
RE8	U	1.4	1.3	0.6	9.1	-	**1.09**	J
RE9	U	1.4	1.3	0.6*	13.4	-	**1.14**	J
RE10	U	1.4	1.1	0.6*	9.6	-	**0.98**	J
Sarsam [7]								
EX1	A	2.5	1.0	0.7	9.7	**0.63**	**0.92**	F
EX2	A	2.5	1.0	0.0	9.7	**0.64**	**0.89**	J
EX3	A	2.5	1.0	0.7	9.7	**0.64**	**0.93**	F
EX4	A	2.5	1.0	0.7	9.7	**0.59**	**0.90**	F
EX5	A	2.5	1.0	0.7	28.3	**0.63**	**0.89**	F

Table 1.4.1.2 Normalised test data - previous research (cont.)

Specimen	Anchorage type	Column steel %	Beam steel %	Joint steel %	Column load MPa	$v_{crack}/\sqrt{f_{ck}}$ $MPa^{0.5}$	$v_{fail}/\sqrt{f_{ck}}$ $MPa^{0.5}$	Failure mode
Scott [8]								
C1	A	3.6	1.2	0.3	12.2	**0.75**	**1.15**	F
C1A	A	3.6	1.2	0.3	12.2	**0.75**	**1.06**	F
C1AL	A	3.6	1.2	0.3	2.2	**0.53**	**1.06**	J
C2	B	3.6	1.2	0.3	12.2	**0.72**	**0.82**	J
C3	U	3.6	1.2	0.3	12.2	**0.93**	**1.22**	F
C3L	U	3.6	1.2	0.3	2.2	**0.58**	**1.00**	J
C4	A	3.6	2.1	0.3	12.2	**0.82**	**1.30**	J
C4A	A	3.6	2.1	0.3	12.2	**0.80**	**1.35**	J
C4AL	A	3.6	2.1	0.3	2.2	**0.58**	**1.35**	J
C5	B	3.6	2.1	0.3	12.2	**0.45**	**0.64**	J
C6	U	3.6	2.1	0.3	12.2	**0.64**	**0.94**	J
C6L	U	3.6	2.1	0.3	2.2	**0.60**	**1.05**	J
C7	A	3.6	1.4	0.2	12.2	**0.62**	**0.90**	J
C8	B	3.6	1.4	0.2	12.2	**0.64**	**0.66**	J
C9	U	3.6	1.4	0.2	12.2	**0.63**	**0.77**	J
Reys de Ortiz [10]								
BCJ1	A	1.5	1.1	0.0	0.0	**0.33**	**0.97**	J
BCJ2	A	1.5	1.1	0.1	0.0	**0.41**	**1.01**	J
BCJ3	A	2.0	1.1	0.0	0.0	**0.44**	**1.03**	J
BCJ4	A	2.5	1.1	0.4	0.0	**0.44**	**1.14**	J
BCJ5	A	2.5	1.1	0.0	3.8	**0.64**	**0.92**	J
BCJ6	A	2.5	1.1	0.0	3.8	**0.67**	**0.97**	J
BCJ7	A	2.5	1.1	0.8	3.8	**0.62**	**1.51**	F
Parker [11]								
4a	A	0.9	0.8	0.0	0.0	-	**0.43**	F
4b	A	0.9	0.8	0.0	3.3	-	**0.51**	J
4c	A	0.9	0.8	0.0	6.3	-	**0.66**	J
4d	A	3.6	0.8	0.0	0.0	-	**0.56**	J
4e	A	3.6	0.8	0.0	3.3	-	**0.59**	J
4f	A	3.6	0.8	0.0	6.7	-	**0.70**	J
5a	A	2.2	0.8	0.6	0.0	-	**0.77**	F
5b	A	2.2	0.8	0.6	3.3	-	**0.83**	J
5c	A	2.2	0.8	0.6	6.7	-	**0.85**	F
5d	A	2.2	1.3	1.0	0.0	-	**0.79**	F
5e	A	2.2	1.3	1.0	3.3	-	**1.07**	F
5f	A	2.2	1.3	1.0	6.7	-	**1.21**	J

Notes

1. A - indicates bent down steel, B - indicates bent up steel, U - indicates U-bars,
2. * - indicates that additional joint reinforcement was used,
3. J - indicates joint failure, F - indicates beam or column flexural failure.

Sarsam [7], Reys de Ortiz [10] and Parker [11] only tested specimens using steel bent down into the column. Kordina [6] tested three methods of anchoring the beam steel within the column, however other parameters were not kept constant and this made the isolation of beam anchorage difficult.

Table 1.4.2.1 gives the results of tests carried out by Taylor [1] and Scott [8] in which the influence of beam steel can be analysed. In order to eliminate the influence of different parameters only similar specimens are compared. The specimens are grouped by their percentage of beam steel. The average results from this selection are displayed in Table 1.4.2.2.

A number of Taylor's [1] tests involved applying an axial force to the *beam*, this was believed to have increased the joint capacity. Since no attempt was made to exert an end thrust on the beam within this research this was believed to be outside the scope of this thesis and is not discussed further.

Table 1.4.2.2 shows that initial joint cracking occurred at a similar load for both bent down and U-bar anchorage. Results however show that initial joint cracking occurred at a load around 20% lower for specimens with bent up steel detail compared to specimens with bent down or U-bar detail.

Beam bars bent-up into the column appeared to severely weaken the joint. Test results suggest a reduction in joint capacity as high as 40% for such an anchorage detail. Vollum's [12] suggestion that U-bar anchorage may be around 20% less efficient than bent down bars would appear reasonable.

Scott [8] varied the length of the bent down bar's anchor leg. Table 1.4.2.3 shows the results from these specimens. The anchorage length of specimens C1A and C4A was
the minimum required by BS 8110 [3]. Specimens C1 and C4 used beam steel with a longer anchorage length.

Table 1.4.2.1 Beam steel anchorage

Specimen	Method of Anchorage	$v_{crack}/\sqrt{f_{ck}}$ ($MPa^{0.5}$)	$v_{fail}/\sqrt{f_{ck}}$ ($MPa^{0.5}$)	Failure Mode
Scott [8]				
C2	Bent up	0.72	0.82	J
C3	U-bar	0.93	1.22	J
C1	Bent down	0.75	1.15	B
C5	Bent up	0.45	0.64	J
C6	U-bar	0.64	0.94	J
C4	Bent down	0.80	1.35	J
C8	Bent up	0.64	0.66	J
C9	U-bar	0.63	0.77	J
C7	Bent down	0.62	0.90	J
Taylor [1]				
C3/41/24X	Bent up	0.88	0.97	J
C3/41/24BY	U-bar	0.95	1.25	J
C3/41/24Y	U-bar	1.14	1.39	J
P1/41/24	Bent down	1.15	1.50	J
P2/41/24	Bent down	1.07	1.71	J
P2/41/24A	Bent down	1.12	1.72	J
A3/41/24	Bent down	1.13	1.80	J

Notes

1. Specimens which failed due to beam flexure did not reach their full joint capacities.

Table 1.4.2.2 Average results from Table 1.4.2.1

Detail	$v_{crack}/\sqrt{f_{ck}}$ ($MPa^{0.5}$)	$v_{fail}/\sqrt{f_{ck}}$ ($MPa^{0.5}$)
Scott [8]		
Bent up	0.60	0.71
U-bar	0.73	0.98
Bent down	0.72	1.13
Taylor [1]		
Bent up	0.88	0.97
U-bar	1.05	1.32
Bent down	1.12	1.68

Table 1.4.2.3 Anchor leg length (*Scott [8]*)

Specimen	Anchorage leg length (mm)	$v_{fail}/\sqrt{f_{ck}}$ ($MPa^{0.5}$)
C1	580	1.15
C1A	215	1.06
C4	710	1.30
C4A	320	1.35

Table 1.4.2.3 shows that the bent down bar's anchorage was not enhanced by using a longer anchor leg. It may be inferred that Scott's bent down specimens (containing one column tie) had sufficient anchorage to ensure that, even with minimum anchorage length, only minimal *bar slip* contributed to the joint's failure.

Table 1.4.1.2 shows that the specimens tested by Parker [11] failed at a significantly lower shear stress than similar sized specimens tested by Reys de Ortiz [10]. An example of this can be seen by comparing specimens BCJ5 and 4e. Both were almost identical yet Parker's [11] 4e failed at a joint capacity 36% lower than Reys de Ortiz's [10] BCJ5. Vollum [12] suggested the reason for this was maybe due to the different detailing of the beam bars. Reys de Ortiz [10] used 4T16 mm bars for the beam tension reinforcement and 10T16 mm bars within the column, whereas Parker [11] used 2T25 mm bars for the beam tension reinforcement and 4T32 mm bars for the column reinforcement. It was suggested that a large number of small diameter bars gave better anchorage than a small number of large diameter bars. This would give a smaller bar spacing and also increase the steel-concrete bond area. The author would agree with Vollum [12] and suggests the specimens failed prematurely for this reason.

1.4.3 Influence of column load

Most previous research is agreed that the initial joint cracking capacity depends on the magnitude of the column load. Table 1.4.3.1 shows a comparison of specimens which had different column loads but were otherwise identical.

Table 1.4.3.1 Column axial stress and initial cracking strength

Investigation	Specimen	Column stress (MPa)	$v_{crack}/\sqrt{f_{ck}}$ ($MPa^{0.5}$)	Enhance-ment
Scott [8]	C1AL	2.2	0.53	
	C1A	12.2	0.75	42%
	C3L	2.2	0.58	
	C3	12.2	0.93	60%
	C4AL	2.2	0.58	
	C4A	12.2	0.80	38%
	C6L	2.2	0.60	
	C6	12.2	0.64	7%
Reys de Ortiz [10]	BCJ3	0	0.44	
	BCJ6	3.8	0.67	52%
Taylor [1]	D3/41/24	3.1	1.04	
	A3/41/24	14.0	1.13	9%

Table 1.4.3.1 shows that, in every case, the joint's cracking strength was increased with greater column stress. This is consistent with the BS8110 [3], EC2 [17] and ACI-318 [15] code equations for the calculation of shear cracking strength under an axial load.

There has been a certain amount of disagreement in previous research on whether increasing the column load leads to an increase in **ultimate** joint strength. Taylor [1] suggested that U-bar detail may be enhanced when using a higher column load as the increased axial force would 'pinch' and anchor the bar within the joint. Meinheit [5] suggested that the column force may have a small enhancement effect but he considered this to be insignificant and excluded it from his recommended design equation. Vollum [12] concluded that there was no convincing evidence to suggest that the ultimate joint strength increases with increasing column load. However, Parker [11] suggested that an increased column load has a significant enhancement effect on the joint's strength regardless of the reinforcement detail.

Table 1.4.3.2 shows a comparison of the same specimens that were considered in Table 1.4.3.1 when considering initial diagonal cracking.

Table 1.4.3.2 Column axial stress and ultimate joint strength

Investigation	Specimen	Column stress (MPa)	$v_{fail}/\sqrt{f_{ck}}$ ($MPa^{0.5}$)	Enhance-ment
Scott [8]	C1AL	2.2	1.06	
	C1A	12.2	1.06	0%
	C3L	2.2	1.00	
	C3	12.2	1.22	22%
	C4AL	2.2	1.35	
	C4A	12.2	1.35	0%
	C6L	2.2	1.05	
	C6	12.2	0.94	-10%
Reys de Ortiz [10]	BCJ3	0	1.03	
	BCJ6	3.8	0.97	-6%
Taylor [1]	D3/41/24	3.1	1.71	
	A3/41/24	14.0	1.80	5%

Table 1.4.3.2 shows no convincing evidence that joint capacity increases with increased column stress. Parker's [11] test results, however, contradict this by suggesting that joint strength is significantly enhanced with increasing column stress, as shown in Table 1.4.3.3.

Table 1.4.3.3 Column axial stress - Parker's [11] specimens

Specimen	Column stress (MPa)	$v_{fail}/\sqrt{f_{ck}}$ ($MPa^{0.5}$)	Enhance-ment
4a	0	0.43	-
4b	3.3	0.51	19%
4c	6.3	0.66	53%
4d	0	0.56	-
4e	3.3	0.59	5%
4f	6.7	0.70	25%
5a	0	0.77	-
5b	3.3	0.83	8%
5c	6.7	0.85	10%
5d	0	0.79	-
5e	3.3	1.07	35%
5f	6.7	1.21	53%

The results in Table 1.4.3.3 clearly show that for Parker's test specimens an increase in column stress was accompanied by an increase in ultimate joint strength for all test series.

After considering these apparently contradictory test results it is suggested that an increased column load increases the ultimate joint strength of specimens only if the beam tension bars are not properly anchored. Taylor [1] suspected that certain beam tension steel details may be enhanced when using higher column loads as the greater normal force would 'pinch' the bar in the joint. The author suggests that for specimens with good beam tension steel anchorage there is no evidence that column load influences the ultimate joint strength, but for specimens in which anchorage is a problem an increase in column load does increase the ultimate joint strength. Although this was not investigated experimentally within this investigation it was considered within the numerical modelling. This is considered in Chapter 5 (*Finite Element Analysis*).

1.4.4 Presence of joint ties

Taylor [1] suspected that the presence of joint ties may not enhance the ultimate strength of the joint. Taylor [1], however, based his comments on only one specimen result (B3/41/24) and did not have the advantage of being able to examine results from previous investigations. Since Taylor's [1] work, however, there has been general agreement that the strength of the joint is enhanced by the use of additional joint reinforcement.

Table 1.4.4.1 shows a comparison of specimens which had different quantities of joint reinforcement but were otherwise identical.

Table 1.4.4.1 Additional joint reinforcement - Ultimate joint strength

Investigation	Specimen	Joint reinf. %	$v_{fail}/\sqrt{f_{ck}}$ ($MPa^{0.5}$)	Enhance-ment
Taylor [1]	A3/41/24	0.3	1.80	-
	B3/41/24	0.9	1.79	-1%
Kordina [6]	RE2	0	0.90	-
	RE3	0.3*	1.25	39%
Reys de Ortiz [10]	BCJ1	0	0.97	-
	BCJ4	0.4	1.14	18%
	BCJ6	0	0.97	-
	BCJ7	0.8	1.51	56%
Parker [12]	4f	0	0.70	-
	5f	1.0	1.21	73%

Notes

1. * - indicates that additional joint reinforcement was used.

Table 1.4.4.1 shows that, with the exception of Taylor's [1] test, there was a clear increase in ultimate joint strength with additional joint reinforcement.

As outlined previously in Section 1.2 there have been a number of empirical relationships suggested in previous research. There has also been some disagreement on the exact influence of joint ties and the role they play in carrying the joint shear force. However there is general agreement that the addition of joint ties enhances the joint capacity through a combination of two roles :

1. By providing the horizontal element to an equilibrium model; the joint shear force is carried by a combination of the core concrete and the joint ties.
2. By providing confinement to the concrete core; the shear capacity of the joint concrete is enhanced by the presence of joint ties.

The contribution of ties to both a specimen's joint strength and ductility is of special relevance to seismic research. Detailed discussion regarding the relative influences of both roles outlined above has been investigated elsewhere [18].

It must be noted that the joint ties in all previous investigations have been equally spaced. There has been no previous research investigating the influence of tie positioning within the joint. Scott [8] and Vollum [12] expressed views that positioning of ties within the joint may affect the ultimate strength. The work outlined in this thesis is partly a result of Scott's [8] suggestion that a better understanding of the role of joint ties is necessary to progress further the understanding of beam-column connection behaviour. Vollum [12] suggested that only ties in the top two-thirds of the joint and below the height of the beam tension steel had an influence on the ultimate strength.

Whereas it seems clear that additional joint reinforcement enhances the ultimate joint strength, Table 1.4.4.2 suggests that the initial cracking strength may be unaffected.

Taylor [1], Ryan [4], Meinheit [5], Sarsam [7] and Vollum [12] all commented that the magnitude of the load at initial cracking was unaffected by the presence of joint ties. The author suggests that because the column ties used in these investigations were smooth they do not achieve the necessary bond needed to give additional resistance to initial joint cracking.

Table 1.4.4.2 Additional joint reinforcement - Initial cracking strength

Investigation	Specimen	Joint reinf. %	$v_{crack}/\sqrt{f_{ck}}$ ($MPa^{0.5}$)	Enhance-ment
Taylor [1]	A3/41/24	0.3	1.13	-
	B3/41/24	0.9	1.29	14%
Sarsam [7]	EX2	0	0.64	-
	EX3	0.7	0.64	0%
Reys de Ortiz [9]	BCJ1	0	0.33	-
	BCJ4	0.4	0.44	33%
	BCJ6	0	0.67	-
	BCJ7	0.8	0.62	-7%

1.4.5 Influence of joint aspect ratio

Vollum [12] noted that Scott's [8] results indicated that joint shear strength reduced with increasing joint aspect ratio (h_{bm}/h_{col}).

Table 1.4.5.1 Joint aspect ratio and ultimate strength (*Scott [9]*)

Specimen	Aspect ratio (h_{bm}/h_{col})	$v_{fail}/\sqrt{f_{ck}}$ ($MPa^{0.5}$)	Strength reduction
C4	1.4	1.30	
C7	2.0	0.90	-31%
C5	1.4	0.64	
C8	2.0	0.66	+6%
C6	1.4	0.94	
C9	2.0	0.77	-18%

The results in Table 1.4.4.1 show that joint aspect ratio may affect the ultimate strength of the joint. More tests are required to confirm this.

As a result of his strut-tie analysis Vollum [12] suggested that the following enhancement factor should be used when calculating ultimate joint strength :

$1+(0.555(2-h_{bm}/h_{col}))$ .....(eq. 1.4.5.1)

Note

This is based only on specimens with joint aspect ratios of between 1.4 and 2.0.

1.4.6 Influence of column longitudinal steel

Results from previous research indicate that the load at which initial joint cracking occurred may be influenced by the percentage of longitudinal steel present within the column. Table 1.4.6.1 displays both the average normalised shear stress values at initial joint cracking and the percentage of column steel present.

Table 1.4.6.1 Percentage of column steel - Initial cracking strength

Investigation	% of column steel	$v_{crack}/\sqrt{f_{ck}}$ (MPa$^{0.5}$)	No. of specimens
Reys de Ortiz [10]	1.5	0.37	2
	2.0	0.44	1
	2.5	0.59	4
Sarsam [7]	2.5	0.63	6
Scott [8]	3.6	0.67	15
Taylor [1]	4.1	1.03	15

Notes

1. The shear stress is an average value calculated from the number of specimens tested.

Table 1.4.6.1 shows that there is a clear increase in joint capacity at initial diagonal cracking as the percentage of column steel increases.

1.5 Findings from Parametric Study

Initial Joint Cracking

1. Initial cracking capacity increases with the magnitude of the column load.

2. Initial joint cracking is not influenced by the presence of joint ties.

3. Initial cracking capacity increases with the percentage of longitudinal steel in the column.

Ultimate Strength

4. The joint shear strength of properly anchored specimens without joint ties is proportional to the square root of the compressive strength of the concrete.

5. The anchorage technique of bending beam tension bars up into the column should not be used in design as this may weaken the joint by as much as 40%.

6. The use of U-bars may weaken the joint by as much as 20%. If U-bars are to be used then the joint should be strengthened accordingly to account for this.

7. The ultimate shear strength of the joint does not appear to be significantly influenced by the magnitude of the column load.

8. Joint shear strength can be increased by the presence of joint ties.

9. Beam steel anchorage would appear to be improved by using a larger number of small diameter bars as opposed to a small number of large diameter bars.

As a result of this review of present knowledge it is clear that there is a substantial lack of knowledge on the following aspects of joint behaviour :

1. There have been no tests to investigate the positioning of ties within the joint zone. It is unclear whether there is an optimum position for a joint tie or whether a tie carries the same load regardless of its location in the joint.

2. Although certain investigations [5, 10] have published strain data from the reinforcement within the joint, more data is required. Detailed results from the main reinforcement and the ties are required if a better understanding of beam-column connection behaviour is to be achieved.

3. There is a lack of data concerning the influence of joint aspect ratio on the behaviour of beam-column connections.

4. As outlined in Appendix A1 to A3, three attempts at strut-tie modelling of beam-column connections have been made. However there has been no successful modelling of beam-column connections using finite element techniques. (Taylor [1] and Vollum [12] both made attempts at finite element modelling of joint behaviour; this is reviewed in Chapter 5).

1.6 Design Code Requirements

There are few recommendations for monotonic beam-column joints design within the various international design codes. BS 8110 [3] does not give any specific recommendations and as a result, within the UK, joint zones are rarely individually designed. Other international codes have detailed recommendations but only for joint requirements in seismic regions.

Within this section a summary of the following design code requirements are presented.

1.6.1 BS 8110 [3]
1.6.2 EC2 [17]
1.6.3 CEB-FIB [16]
1.6.4 ACI 318 [15]

1.6.1 BS 8110 [3]

BS 8110 includes design requirements for the shear resistance of reinforced concrete beam members. The data in BS 8110, Table 3.9, was derived using the following expression :

$$v_c = \frac{0.79}{\gamma_m}\left(\frac{100A_s}{b_v d}\right)^{\frac{1}{3}}\left(\frac{400}{d}\right)^{\frac{1}{4}} \quad \text{.....(eq. 1.6.1.1)}$$

where A_s is the quantity of beam steel,

b_v is the section width,

d is the section depth,

γ_m is the partial safety factor 1.25,

$\left(\frac{100A_s}{b_v d}\right)^{\frac{1}{3}}$ should be taken as no greater than 3,

$\left(\frac{400}{d}\right)^{\frac{1}{4}}$ should be taken as no less than 1,

Within this section, v, is the actual shear stress whereas v_c is the design concrete shear stress.

BS 8110 allows this basic value of concrete shear stress to be enhanced as follows :

Concrete strength

The value of design shear stress, v_c, may be multiplied by $(f_{cu}/25)^{1/3}$ where f_{cu} is the compressive cube strength, limited to 40 MPa (BS 8110 Table 3.9).

Angle of failure plane

BS 8110 clause 3.4.5.8 allows this basic value of shear stress to be multiplied by $(2d/a_v)$. Within this expression d is the section depth and a_v is the shear span.

Column load

As a result of research by Scott *et al* [9] BS 8110 equation 6 was split into equations 6(a) and 6(b). Scott *et al* recommended the use of equation 6(b) in joint design if shear cracking was to be avoided prior to the ultimate limit state.

$$v_c' = v_c + 0.6\frac{N}{A}\frac{Vh}{M} \quad \text{.....(BS 8110 eq. 6(a))}$$

$$v_c' = v_c\sqrt{\left(1+\left(\frac{N}{Av_c}\right)\right)} \quad \text{.....(BS 8110 eq. 6(b))}$$

where N is the column load,

A is the section area,

V is the design ultimate shear force,

h is the overall section depth,

M is the design ultimate bending moment,

the 0.6 coefficient in eq. 6a contains a partial safety factor of 1.33.

If the shear stress in the section, v, is greater than (v_c+0.4) then shear links (*stirrups*) should be provided where :

$$A_{sv} = \frac{b_v s_v (v - v_c)}{0.87 f_{yv}} \quad \text{.....(eq. 1.6.1.3)}$$

where s_v is the centre to centre spacing of the shear reinforcement,

f_{yv} is the strength of the shear reinforcement.

However, BS 8110 states that the value of shear stress within a section, v, may not exceed $0.8\sqrt{f_{cu}}$ or 5 MPa, whichever is less. (*These terms contain a partial safety factor of 1.25*). If a reinforced concrete section exceeds these values then that section should be redesigned to increase the product $b_v d$ (equation 1.6.1.2) to ensure that v does not exceed these limits.

It should be noted that these requirements within BS 8110 are intended for reinforced concrete **beam** sections and are not intended for beam-column joint design.

Relevant BS 8110 recommendations regarding column shear reinforcement are as follows :

1. All longitudinal bars should be enclosed by links (*ties*), which should be arranged such that every corner and alternate bar shall have lateral support provided by the corner of a link.
2. Links should have a minimum diameter of at least one-quarter of that of the largest longitudinal bar, and the maximum link spacing should not exceed 12 times the diameter of the smallest longitudinal bar.

BS 4466 [19] gives the anchorage requirement for reinforcement bars to develop their full design strength. In regions of the structure, such as beam-column joints, where it is impossible to provide the necessary *straight* anchorage length, the designer may use **hooks** and **bends**. These should meet the detailing requirements of BS 4466.

1.6.2 EC2 [17]

Standard EC2 design recommendations for the design of a reinforced concrete beam in shear are as follows :

The total shear resistance of the section, V_{Rd3}, is given by the following equation :

$V_{Rd3} = V_{Rd1} + V_{wd}$ .....(eq. 1.6.2.1)

where V_{Rd1} is the concrete shear resistance,
V_{wd} is the shear resistance provided by the stirrups.

The concrete shear resistance is given by the following empirical expression :

$V_{Rd1} = [\tau_{Rd}k(1.2 + 40\rho_1)]b_w d$ .....(eq. 1.6.2.2)

where τ_{Rd} is the basic shear strength $0.035f_{ck}^{2/3}$,
$k = (1.6 - d)$ (> 1),
$\rho_1 = A_{s1}/b_w d$ (< 0.02),
A_{s1} is the area of longitudinal tension reinforcement,
b_w is the minimum section width,
d is the effective depth of the section.

EC2 allows the value of concrete shear resistance to be enhanced by a factor, β, which takes into consideration a steeper angle of failure plane. $\beta = 2.5d/x$ where x is the neutral axis depth.

The shear resistance of the stirrups is given as :

$$V_{wd} = \frac{1}{1.28}\frac{A_{sw}}{s} df_{yk} \quad \text{.....(eq. 1.6.2.3)}$$

where A_{sw} is the cross-sectional area of the two legs of the stirrup,

s is the stirrup spacing,

f_{yk} is the characteristic strength of the stirrup reinforcement.

V_{Rd2} is defined as the maximum allowable shear force which a section can sustain irrespective of any shear reinforcement.

$V_{rd2} = 0.3vf_{ck}b_wd$ .....(eq. 1.6.2.4)

where v is an efficiency factor = $0.7 - f_{ck}/200$ (≥ 0.5).

The relevant recommendations regarding the placement and detailing of column ties are the same as previously outlined for BS 8110 [3] (in Section 1.6.1).

1.6.3 CEB-FIP Model Code [16]

Like the BS 8110 [3] and EC2 [17] Codes the CEB-FIP Model Code again does not make any specific design recommendations for the design of reinforced concrete beam-column joints.

The shear resistance for a reinforced concrete member however is given as :

$$V_{Rd(max)} = \frac{f_{cd2}}{2} b_w z(1+\cot\alpha) \quad \text{.....(eq. 1.6.3.1)}$$

where $f_{cd2} = 0.60\left[1-\frac{f_{ck}}{250}\right]f_{cd}$,

f_{cd} is the design concrete compressive strength,

b_w is the minimum section width,

z is the section lever arm,

α is the angle of inclination of the shear plane.

The transverse reinforcement (ties) in the columns should surround the longitudinal reinforcement. The diameter of these ties should not be less than 5 mm or one-quarter of the maximum diameter of the longitudinal bars. The spacing of these ties should be a minimum distance of 150 mm or so that they intersect at least one shear crack under the most adverse conditions.

The anchorage requirements for the column ties are considerably more restrictive than with the BS 8110 [3] or EC2 [17] codes. Plain ties should be anchored through a minimum angle of 150°.

1.6.4 ACI 318 [15]

ACI 318 is the American code which incorporates recommendations from the ACI-ASCE Committee 352 [20]. The ACI-ASCE Committee 352 was specifically set up to investigate reinforced concrete beam-column connection behaviour. A summary of the recommendations concerning monotonic design is included within this section.

Structural joints are classified into two categories, Type 1 and Type 2, based on the loading conditions and the anticipated deformations of the joint. A Type 1 joint connects members designed to satisfy strength requirements in which no significant inelastic deformations are anticipated. A typical joint within a frame designed to resist gravity and normal wind load would fall into this category. A Type 2 joint connects members designed to have sustained strength under deformation reversals into the inelastic range. A typical joint within a frame designed to resist earthquake motions, very high winds or blast effects would fall into this category.

The design recommendations of Type 1 (monotonic) joints are summarised as follows :

The shear force in the joint is evaluated on the assumption that at failure the steel in the beam (framing into the column) yields. *This is the theory presented previously in Section 1.3.*

$$V_j = T_{beam} - V_{col}$$
$$= A_s f_y - V_{col} \quad \text{.....(eq. 1.6.4.1)}$$

where T_{beam} is the force in the beam,

V_{col} is the shear force in the upper column,

A_s is the quantity of beam steel,

f_y is the yield strength of the beam steel.

The limiting value for the shear stress, v_j, is :

$$v_j = 0.083\gamma_{ACI}\sqrt{f_{ck}} \quad \text{.....(eq. 1.6.4.2)}$$

Where the value of γ depends on the joint classification as indicated in Table 1.6.4.1.

Table 1.6.4.1 Value of γ_{ACI} for Type 1 beam-column joints

Interior	Exterior	Corner
24	20	15

Note

External connection specimens without transverse beams, such as those considered within this thesis, are classified as ***Corner Joints.***

The recommendations for minimum amount of confinement are as follows :

1. At least two layers of confining reinforcement must be placed between the top and bottom layers of beam longitudinal reinforcement in the deepest member framing into the joint.
2. The centre to centre spacing of the confining reinforcement should not exceed 12 in. (305 mm). If the joint is part of the primary lateral load resisting system, the spacing is reduced to 6 in. (152 mm) unless the joint is confined by members framing into the joint opposite faces.
3. No transverse reinforcement is required in the joint, if members frame into all four sides of the joint and meet various geometric requirements.
4. Transverse reinforcement is only required in the direction unconfined by members if beams frame into opposite sides and meet various joint requirements.
5. Ties shall be arranged such that every corner and every alternate longitudinal bar shall have lateral support provided by the corner of a tie with an included angle of not more than 135° and no bar shall be further than 6 in. clear on each side along the tie from such a laterally supported bar.

For Type 2 beam-column joints stricter limits are placed on the limiting value of shear stress. An increased area of joint ties is also required for all Type 2 structures.

Other major international design codes used for the design of joints to resist earthquake motions are as follows :

1. The AIJ guidelines (Japan) [21]
2. NZS 3101 (New Zealand) [22]
3. Eurocode 8 [23]

As seismic design is not considered within this thesis these codes are highlighted for reference purposes only.

1.7 Further Methods of Concrete Strengthening

In addition to the parameters investigated in previous research and those presented in the design codes there are further methods of strengthening concrete. The use of high strength and steel fibre reinforced concrete is considered within this investigation :

Section 1.7.1 High strength concrete
Section 1.7.2 Steel fibre reinforced concrete

The use of both of these methods to strengthen concrete members is well documented. This section presents a brief overview of each of these methods and, where applicable, previous seismic beam-column connection research is reviewed.

It should be noted that neither of these methods has previously been used to investigate the **monotonic** strength of reinforced concrete beam-column connections.

1.7.1 High strength concrete

The use of microsilica in concrete has allowed compressive cylinder strengths well in excess of 100 MPa to be achieved. The microsilica contributes to the hydration reaction between the cement and the water to strengthen the *paste* which binds the aggregate together. The microsilica particles are also extremely fine which means that they can fill the air voids between the cement grains and reduce porosity. These factors, in addition to the very low water : cement ratio used, allow very high concrete strengths to be achieved.

By using high strength concrete, higher compressive, tensile and shear strengths are possible. Unfortunately the workability of the fresh concrete is considerably worse for high strength concrete compared with normal strength concrete. This means that both plasticisers and admixtures must be used and in construction care must be taken placing the concrete in areas of a structure where steel congestion may be a problem.

A further concern with high strength concrete is that the concrete material properties, including tensile and shear strength, do not increase in proportion to the compressive strength [24, 25, 26].

1.7.1.1 Previous high strength beam-column connection research

The research reviewed in this section was concerned with the **seismic design** of high strength reinforced beam-column connections. The author believes that the following findings are relative to the design of **monotonic** connections.

In 1985 the ACI-ASCE Committee 352 [20] concluded that further research was necessary on the behaviour of high strength concrete beam-column connections.

In 1991 Ehshani and Alameddine [27] reported on the manufacturing and testing of twelve beam-column connection specimens. Previously concerns had been expressed over high strength concrete tests indicating that the ultimate shear capacity was proportional to $\sqrt[3]{f_{ck}}$ and not $\sqrt{f_{ck}}$ [28, 29, 30]. As a result of these beam-column connection tests a refinement of the ACI-318 Code [15] was suggested. This took into consideration the increased brittleness of high strength concrete compared with normal strength concrete.

In 1992 Ha *et al* [31] reported on the manufacture and testing of eight high strength beam-column connection specimens. As a result of these tests it was suggested that Type 2 connections, designed to the ACI-318 Code [15], had comparatively low safety. It was found that the higher the strength of the concrete the worse the ductility became and the higher the stiffness.

These concerns highlighted from previous seismic tests confirm the clear need for similar tests on monotonically designed beam-column connections.

1.7.2 Fibre reinforced concrete

The use of fibres to improve the tensile strength of brittle materials is a well known technique and was believed to be first used in Roman times, where bricks with low tensile strengths were strengthened by including straw or animal hair in the mix.

From the early 1970's onwards the technique of using fibres to strengthen concrete has been the subject of much research [32, 33, 34]. A variety of materials with a tensile strength greater than concrete, such as steel, plastic and glass, can be used for the fibres. This investigation, however, is concerned with steel fibre reinforced concrete only.

The addition of steel fibres to concrete makes only a slight difference to the compressive strength. However a significant increase to the tensile and shear strength of the concrete allows crack growth to be controlled and the ultimate shear capacity to be increased.

The addition of steel fibres to concrete is also believed to improve the ductility which is of significant importance when designing beam-column connections for seismic loads. In addition previous research [35] has shown that even after the maximum load of a steel fibre reinforced member has been exceeded and deflections are increasing, the load bearing capacity of the concrete is by no way exhausted.

Adebar *et al* [36] reviewed the results from eighteen different investigations on fibre reinforced concrete beams between 1972 and 1994. The range of percentages, by volume, was from 0 to 3.0%. Adebar *et al* concluded that percentages higher than 3.0% made workability of fresh concrete a problem.

1.7.2.1 Previous fibre reinforced concrete beam-column connection research

The following research was concerned with the **seismic design** of fibre reinforced concrete beam-column connections. However, the author believes that the following findings are equally relative to the design of **monotonic** connections.

In 1988 Olariu *et al* [37] reported on the manufacture and testing of eight beam-column connection specimens, six of which contained steel fibres and two of which were conventionally designed connections. Improvements in both the ductility and the ultimate joint capacity were observed. An improvement in the bond between the steel tension bars and the fibre reinforced concrete was also seen.

In 1989 Gefken and Ramey [38] reported on the manufacture and testing of ten beam-column connections. Again improvements in the ductility and the ultimate joint capacity were observed. Gefken and Ramey commented that the necessary spacing of joint ties may be increased if steel fibre concrete is used within the joint.

In 1997 Henager [39] reported on the testing of two beam-column connection specimens. One specimen used fibre reinforced concrete whilst the other was conventionally reinforced using an equivalent amount (by volume) of joint ties. This seismic test programme found that the fibre reinforced specimen was stronger, more ductile and more damage tolerant than the conventional specimen. Henager commented that substantial savings were possible if fibre reinforced concrete was used for a whole building.

1.8 Conclusions

A comprehensive review of all previous research on the monotonic loading of reinforced concrete beam-column connections has been presented. A review of international design code recommendations and an overview of the use of high strength and fibre reinforced concrete has also been given.

In previous research Sarsam [7] and Vollum [12] commented that the available test data on the behaviour of monotonically loaded exterior beam-column connections was far from comprehensive and that there was a clear need for further tests.

This literature review has confirmed this. In particular the author believes that there is a clear lack of knowledge in the following specific areas :

1. The role of the joint tie in connection behaviour and the effect of the positioning of this tie within the joint.
2. The joint enhancement possible using high strength concrete and concrete strengthening techniques such as the addition of steel fibres and shear plates.
3. The influence of aspect ratio on the strength of the joint.

In addition, the review of the present design codes has clearly shown a lack of specific recommendations for monotonic joint design.

This research programme set out to conduct a comprehensive series of tests investigating, in particular, the influence of the parameters highlighted above. This experimental work was supported by the use of a non-linear finite element modelling programme. It was the object of this research programme to provide a greater understanding of joint behaviour and thus to develop concise rules for design.

2. Monotonic Experimental Programme

This investigation originally set out to investigate the behaviour of a series of sixteen monotonic beam-column connection specimens. The parameters to be investigated were the influence of ties within the joint, the strength of the concrete and the detailing arrangement of the beam tension steel. Figure 2.1 shows how this original test programme developed into the complete test programme of seventy specimens.

The original sixteen specimens were divided into two test series; eight normal strength specimens (defined as the *standard* test series) and eight high strength specimens. As this investigation developed further, additional specimens were manufactured and tested; eleven specimens investigating joint ties positioning, eight specimens investigating joint aspect ratio and nine specimens investigating fibre reinforced concrete. Five further specimens were manufactured and tested investigating parameters such as joint tie anchorage, beam steel plate anchorage and joint shear plates.

Precise specimen details, steel and strain gauge layouts are considered in detail in Section 2.1. Diagrammatic representations of the individual joint zones, which are recommended for referral throughout this thesis, are shown in the following figures :

Figure 2.2 Standard specimens
Figure 2.3 High strength specimens
Figure 2.4 Specimens investigating tie positioning
Figure 2.5 Specimens investigating joint aspect ratio
Figure 2.6 Steel fibre reinforced specimens
Figure 2.7 Additional specimens

Note

Figure 2.1 displays the complete test programme, however the specimens from the cyclic test programme are not considered until Chapter 7 of this thesis.

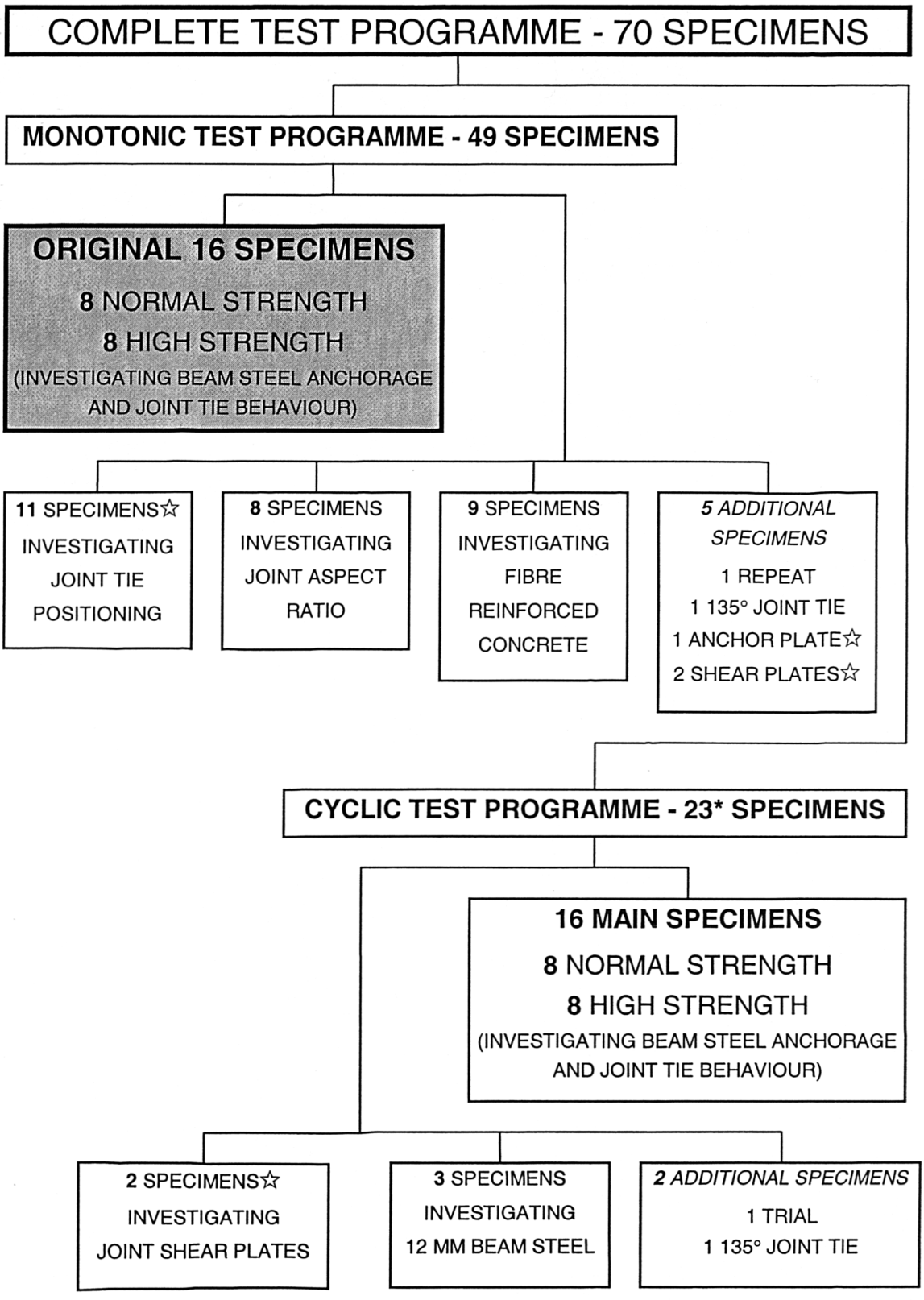

Figure 2.1 Breakdown of test programme

Notes 1 ☆ Baglin's specimens,

2 * the joint shear plate specimens were part of both test programmes.

Table 2.2 Standard specimens

Specimen	Joint Layout	Gauging	Beam steel anchorage	No. of joint ties
C4ALN0	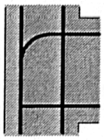	-	Bent down	0
C4ALN1	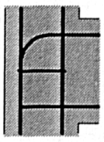	Full	Bent down	1
C4ALN3	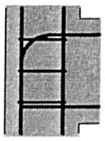	Full	Bent down	3
C4ALN5	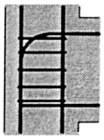	-	Bent down	5
C6LN0		-	U-bar	0
C6LN1	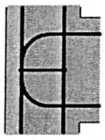	Full	U-bar	1
C6LN3	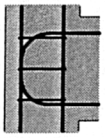	Full	U-bar	3
C6LN5	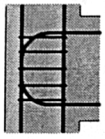	-	U-bar	5

Note

For gauging details see Section 2.2.1

Table 2.3 High strength specimens

Specimen	Joint Layout	Gauging	Beam steel anchorage	No. of joint ties
C4ALH0	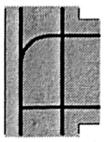	-	Bent down	0
C4ALH1	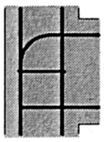	Full	Bent down	1
C4ALH3	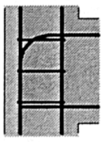	Full	Bent down	3
C4ALH5	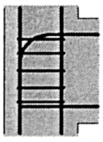	One tie (middle)	Bent down	5
C6LH0		-	U-bar	0
C6LH1		Full	U-bar	1
C6LH3	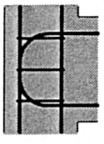	Full	U-bar	3
C6LH5	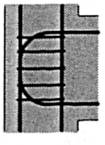	-	U-bar	5

Table 2.4 Specimens investigating tie positioning

Specimen	Joint Layout	Gauging	Anchorage	Joint ties
C4ALN1T	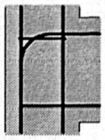	One tie	Bent down	1
C4ALN3C	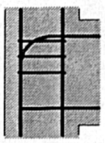	One tie (below beam tension steel height)	Bent down	3
C4ALN3D	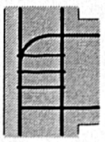	-	Bent down	3
C6LN1B		One tie	U-bar	1
C6LN1T	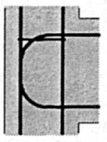	One tie	U-bar	1
C6LN1A	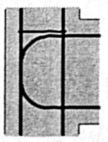	One tie	U-bar	1
C6LN2A	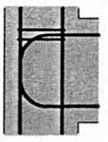	One tie (below beam tension steel height)	U-bar	2
C6LN2B	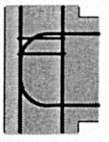	One tie (below beam tension steel height)	U-bar	2
C6LN3A	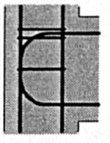	One tie (below beam tension steel height)	U-bar	3
C6LN3B	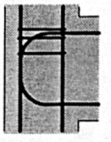	One tie (below beam tension steel height)	U-bar	3
C6LN3C	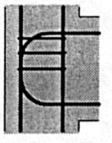	One tie (below beam tension steel height)	U-bar	3

Table 2.5 Specimens investigating joint aspect ratio

Specimen	Joint Layout	Gauging	Anchorage	Joint ties
C7LN0	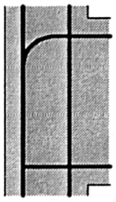	-	Bent down	0
C7LN1	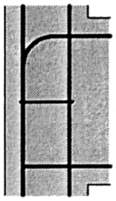	-	Bent down	1
C7LN3	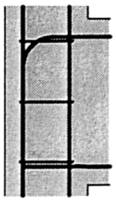	One tie (middle)	Bent down	3
C7LN5	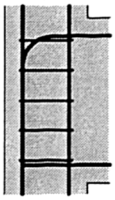	-	Bent down	5
C9LN0	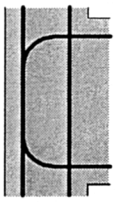	-	U-bar	0
C9LN1	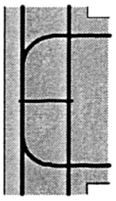	-	U-bar	1
C9LN3	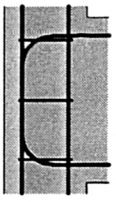	One tie (middle)	U-bar	3
C9LN5	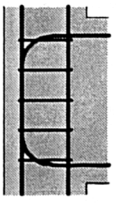	-	U-bar	5

Table 2.6 Steel fibre reinforced specimens

Specimen	Joint Layout	Fibre type	Anchorage	% fibres
C4AL04SF	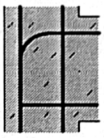	Short	Bent down	0.4
C4AL15SF	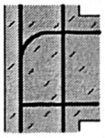	Short	Bent down	1.5
C4AL23SF	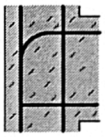	Short	Bent down	2.3
C4AL04LF	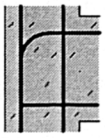	Long	Bent down	0.4
C4AL15LF	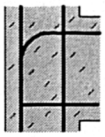	Long	Bent down	1.5
C4AL23LF	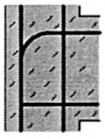	Long	Bent down	2.3
C4AL38LF	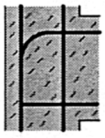	Long	Bent down	3.8
C6L04SF	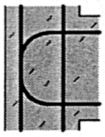	Short	U-bar	0.4
C6L04LF		Long	U-bar	0.4

Notes

1. No gauged reinforcing bars were used in the fibre programme.

Table 2.7 Additional specimens

Specimen	Joint Layout	Gauging	Beam steel anchorage	Joint reinforcement
C6LN1(r)	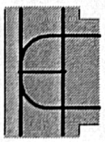	One tie	U-bar	1
C6LN1AE	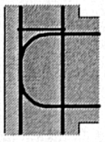	One tie	U-bar	1 (legs bent through 135°)
C4PLN0	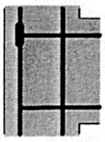	-	Bearing plate	-
C6LNP4	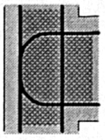	-	U-bar	Shear plate
C6PLNP4	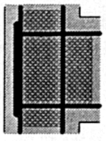	-	Bearing plate	Shear plate

2.1 Specimen Details

2.1.1 Specimen dimensions

With the exception of the eight specimens investigating joint aspect ratio all specimens had a column 1700 mm high and 150×150 mm square into which framed, at mid-height, a beam 840 mm long, 210 mm deep and 110 mm wide. These specimen details are shown in Figure 2.1.1.1. The eight specimens investigating joint aspect ratio had 300 mm deep beams, the details of this arrangement are given in Figure 2.1.1.2.

2.1.2 Steel properties

All main reinforcement was high yield steel and the concrete cover to the centre of the bars was 33 mm. Four 16 mm diameter rebars were used for the column reinforcement and a pair of 16 mm rebars for the beam tension steel. A pair of 12 mm rebars were used for the compression steel with the bent-down steel arrangement. The beam and column shear reinforcement was provided by 6 mm smooth stirrups / ties. The steel properties are given in Table 2.1.2 and the stress-strain curves are displayed in Figures 2.1.2.1 to 2.1.2.3

Table 2.1.2 Steel properties

Bar diameter (mm)	6	12	16
Yield strain (με)	2500	2500	2500
f_y (MPa)	500	500	500
E_s (GPa)	200	200	200

Note

1. These values were taken from an average of three typical bars and were rounded to two significant figures.
2. As the experimental response was almost perfectly elastic-plastic in characteristic the yield strain was taken at this elastic-plastic transition.

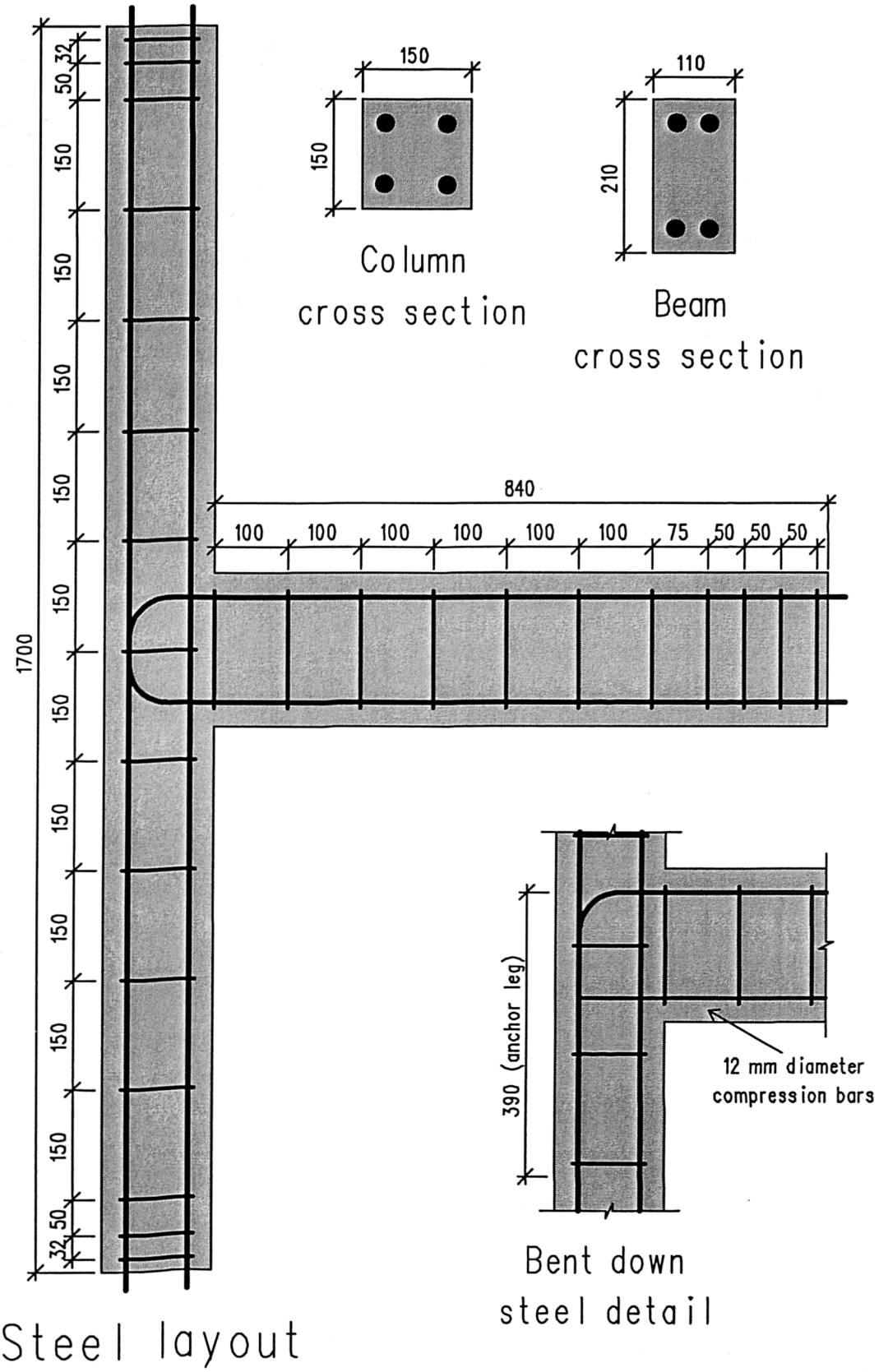

Figure 2.1.1.1 Specimen details - 210 mm deep beam

(all dimensions in mm)

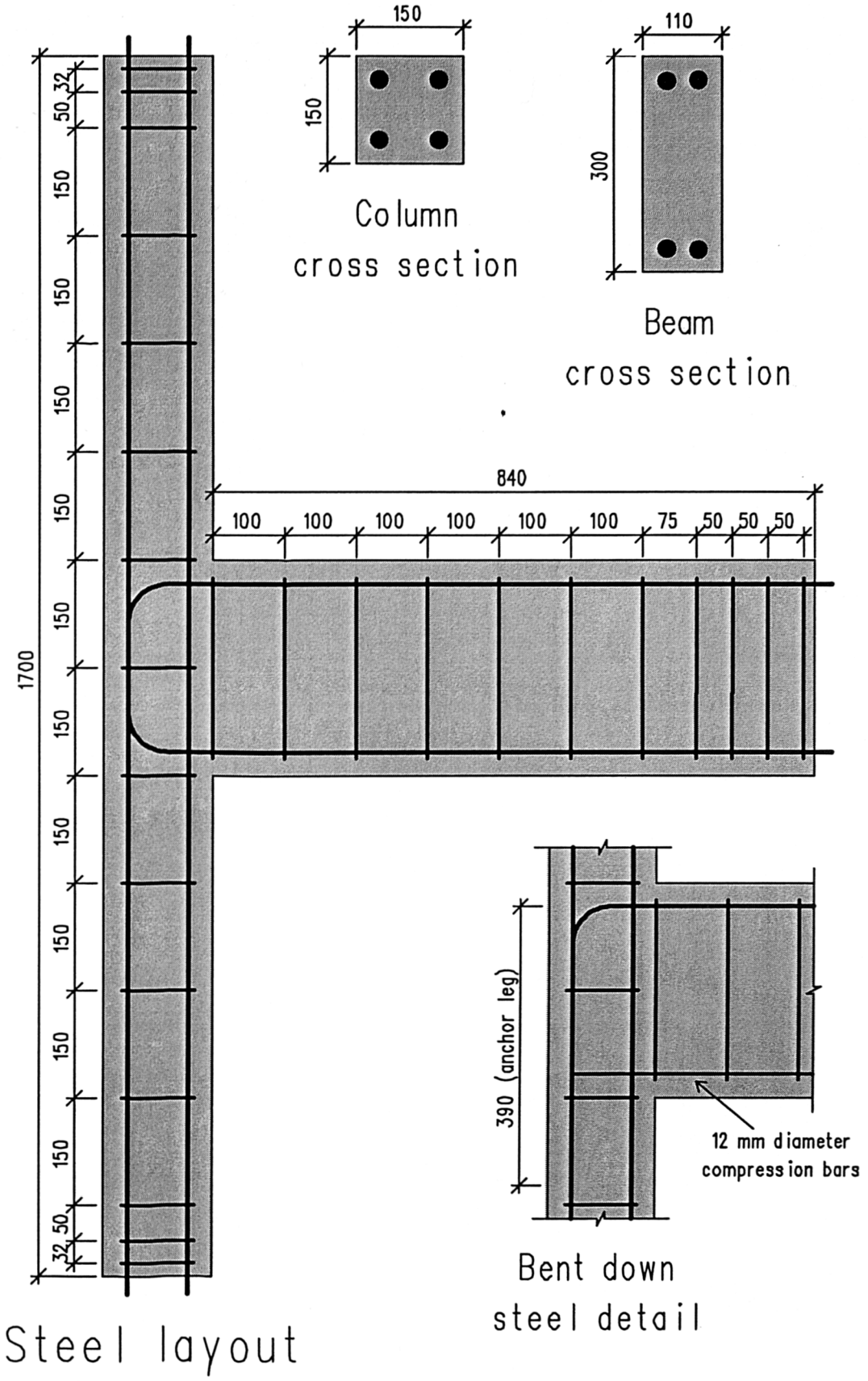

Figure 2.1.1.2 Specimen details - 300 mm deep beam

(all dimensions in mm)

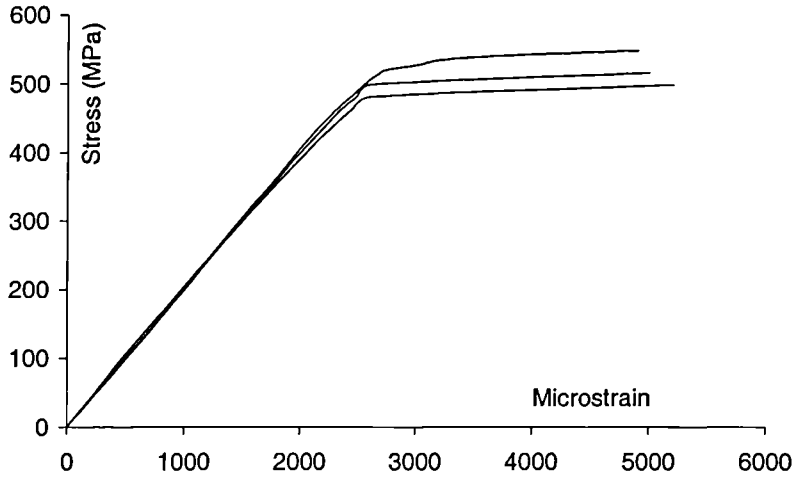

Figure 2.1.2.1 Stress-strain relationships - 6 mm diameter bars

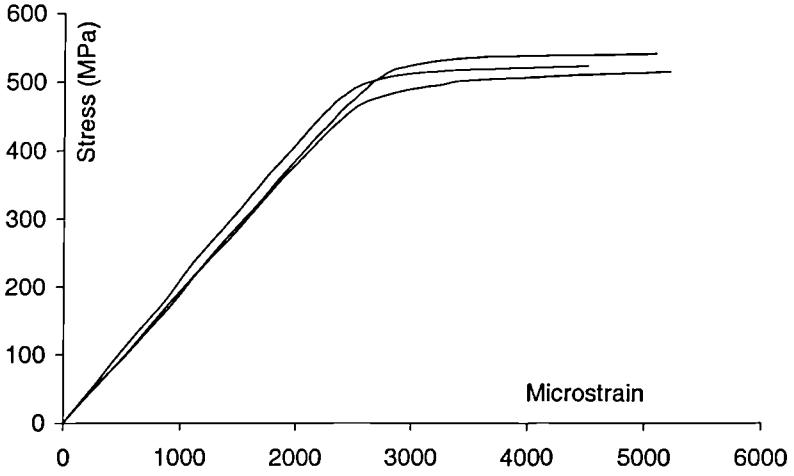

Figure 2.1.2.2 Stress-strain relationships - 12 mm diameter bars

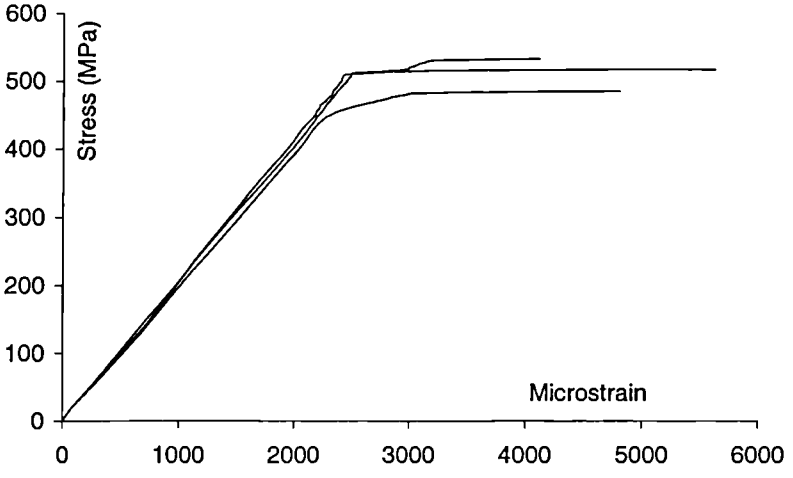

Figure 2.1.2.3 Stress-strain relationships - 16 mm diameter bars

2.1.3 Specimen notation

For consistency the specimen notation used previously by Scott [8] was used for this investigation :

Example notation -	**Part**	**1st**	**2nd**	**3rd**	**4th**
	Name	C6	L	N	1

The first part of the specimen notation referred to the beam tension steel detail :

C4A - Bent down beam steel within a 210 mm deep beam,
C6 - U-bar beam steel within a 210 mm deep beam,
C7 - Bent down beam steel within a 300 mm deep beam,
C9 - U-bar beam steel within a 300 mm deep beam.

The letter **L** in the second part of the notation indicated that a low column load was used. This was selected as 50 kN for the normal strength specimens and 100 kN for the high strength specimens. This column loading induced strains in the column steel of around 100 $\mu\varepsilon$ at the start of each test.

The third part of the notation referred to the concrete strength :

N - Normal strength concrete with a typical cube strength of 60 MPa,
H - High strength concrete with a typical cube strength of 120 MPa.

The fourth part of the notation referred to the quantity and type of joint reinforcement. A single digit signified the number of ties present within the joint, a letter after this referred to a specific positioning of the tie(s). However a double number implied that fibre reinforced concrete was used, this number indicated the percentage of steel fibres present in the mix design (i.e. 15 corresponded to 1.5% steel fibres). The letters after these digits referred to the type of fibre used, **SF** indicated short fibres and **LF** indicated long fibres.

Details of the additional specimens are as follows :

C6LN1AE

An attempt to eliminate tie anchorage effects from the joint behaviour was made with specimen C6LN1AE. This was a repeat of specimen C6LN1A, with the legs of the joint tie being bent through 135° as opposed to 90°, as shown in Figure 2.1.3.1. This is in accordance with recommendations from the ACI-ASCE Committee 352 [22] for the anchorage of ties (discussed previously in Section 1.6.4).

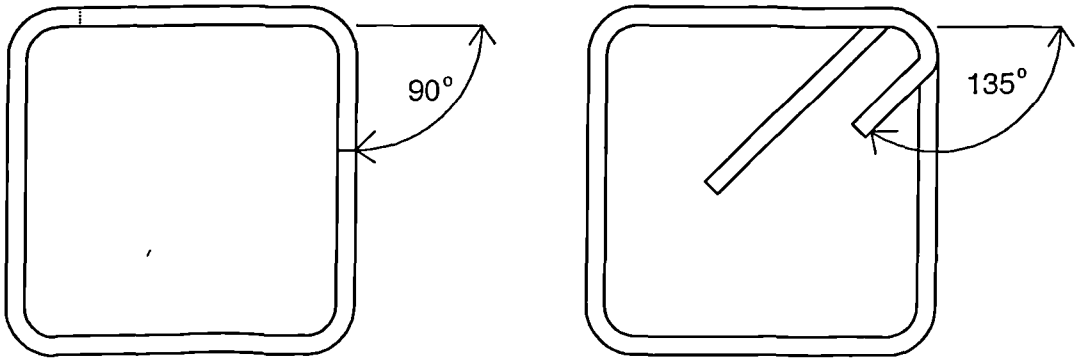

Figure 2.1.3.1 Joint tie anchorage

C4PLN0

An attempt to eliminate beam steel anchorage effects from the joint behaviour was made with specimen **C4PLN0**. The 16 mm beam tension bars were welded to a 4 mm thick, 100 × 100 mm bearing plate as shown in Figure 2.1.3.2. A pair of 12 mm bars provided the compression steel for the beam.

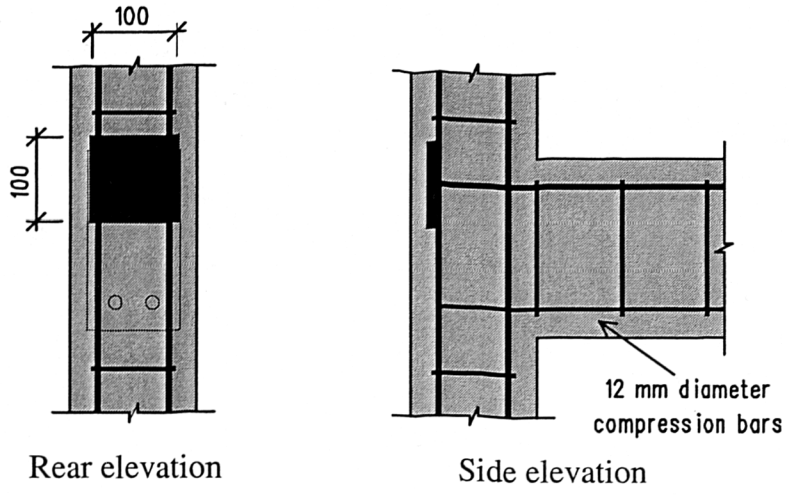

Figure 2.1.3.2 Specimen C4PLN0

One method of improving the shear resistance of reinforced concrete *beams* is to use deformed shear plates. **Dr Paul Baglin**, who worked closely with the author for nine months, had past experience using shear plates from his doctorate [40]. Similar shear plates were used within this investigation in an attempt to enhance the shear capacity of two specimens, C6LNP4 and C6PLNP4.

C6LNP4

A diagrammatic representation of the specimen C6LNP4 is shown in Figure 2.1.3.3(a). C6LNP4 contained a single 4 mm shear plate within the joint area. This was positioned on the centre-line of the specimen and had a cover of 25 mm from the edge of the plate. The main steel layout within the specimen was identical to the monotonic specimen C6LN0.

C6PLNP4

A diagrammatic representation of the specimen C6PLNP4 is shown in Figure 2.1.3.3(b). C6PLNP4 contained a similar single 4 mm shear plate within the joint area. This was again positioned on the centre-line of the specimen and had a cover of 25 mm from the edge of the plate. A pair of 16 mm rebars were provided in the upper and lower section of the beam. Beam steel anchorage was provided by a large bearing plate.

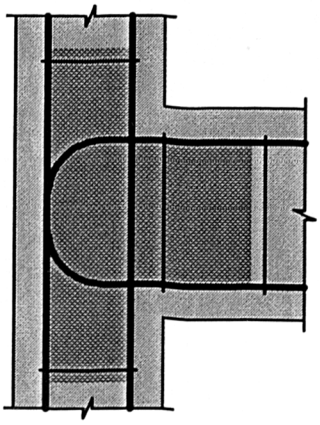

Figure 2.1.3.3(a)
Specimen C6LNP4

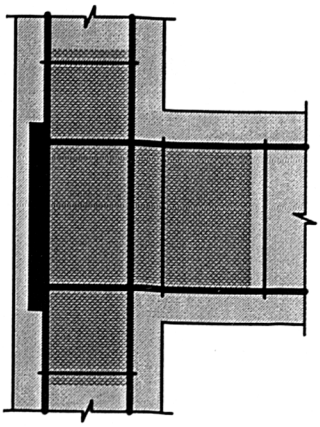

Figure 2.1.3.3(b)
Specimen C6PLNP4

The shear plates were produced by sandwiching a mild steel plate between two layers of Expamet expanded metal mesh and welding the layers together. These deformed plates were then welded to the two column ties and the beam stirrup outside of the joint. The specimens were cast with the column resting *flat* on the lab floor and the beam initially raised to an angle of around 45°. This allowed the fresh concrete to compact beneath the lower face of the plate.

C6LN1(r)

Specimen C6LN1, outlined previously, was tested early in the investigation. The column load used was 100 kN as opposed to 50 kN for the other normal strength specimens. Specimen C6LN1(**r**) was a repeat of C6LN1 using a column load of 50 kN.

2.2 Specimen Manufacture

2.2.1 Internally strain gauged reinforcement

For reinforced concrete members to perform correctly there must be bond between the steel reinforcement and the surrounding concrete. Within this investigation the technique of internally strain gauging the reinforcement was used. This allowed bond and bearing stress values to be calculated without effecting this concrete-steel bond.

2.2.1.1 Previous strain gauging techniques

Previously the most common method of measuring reinforcement strains has simply been to attach the strain gauges to the surface of the steel. However the presence of gauges, their associated waterproofing compounds and lead wires reduces the effectiveness of the concrete-steel bond.

The earliest attempt at overcoming this problem was by Bernander [41] who placed strain gauges on the side walls of a slot cut longitudinally along the bar. Mains [42], in 1951, developed an alternative technique which left the perimeter of the bar intact and was therefore more satisfactory for bond research. A rebar was cut into two axially and up to twenty gauges were mounted in a groove milled in one portion of the bar. The two pieces were then tack welded together to re-create a complete rebar. A number of researchers in the US [43, 44, 45] have used a similar technique since Mains. In the UK this technique has been considerably developed, as follows, by Scott and Gill [46, 47] at the University of Durham. As part of this investigation the technique was developed in order to install strain gauges within 6 mm ties.

The technique of internally strain gauging ties is believed to be unique and it is believed that it has not been previously attempted.

2.2.1.2 Strain gauging technique

Each strain gauged reinforcing bar was formed by milling a pair of rebars down to a half round and then machining a longitudinal groove in each to accommodate the strain gauges and their wiring. The two half bars were then glued together so that they had the appearance of a single reinforcing bar but with wiring from the gauges exiting from each end.

A foil gauge with a 3 mm gauge length and a strain limit of around 3% (30 000 με) was used for the 12 mm and 16 mm rebars. A gauge spacing of 12.5 mm was used for the region of the bar within or near the joint. This gauge spacing was increased to 25 mm and then 50 mm in other areas of the specimen considered less important. Gauges were staggered between the two sides of the duct so, for an effective spacing of 12.5 mm, the actual spacing on each half round was 25 mm. For the joint ties, a gauge length of 2 mm was used and the gauge spacing was 12.5 mm throughout. All gauge layout diagrams are given in the following figures :

Figure 2.2.1.2.1 Joint tie - strain gauge layout,
Figure 2.2.1.2.2 Column rebar - strain gauge layout A,
Figure 2.2.1.2.3 Column rebar - strain gauge layout B,
Figure 2.2.1.2.4 Column rebar - strain gauge layout C,
Figure 2.2.1.2.5 Beam U-bar - strain gauge layout A,
Figure 2.2.1.2.6 Beam U-bar - strain gauge layout B,
Figure 2.2.1.2.7 Beam bent down and compression rebars - strain gauge layout.

Gauges were attached to the steel using a cyanoacrylic adhesive and protected with a polyurethane varnish. Because the space available in the duct was extremely limited, very fine lead wires of only 0.2 mm diameter were used. The effects of electrical resistance were reduced through a three wire, common dummy installation, which effectively eliminated all lead wire resistance and minimised thermal drift problems.

A ***full*** gauged beam-column connection specimen, as indicated previously in Tables 2.1.2 to 2.1.7, had all of the rebars on one side of the specimen strain gauged in addition to the joint ties. A ***one tie*** gauged specimen had only the particular joint tie strain gauged and none of the main steel. The strain gauge layouts and number of gauges used for each of these specimens are displayed in Table 2.2.1.2.1.

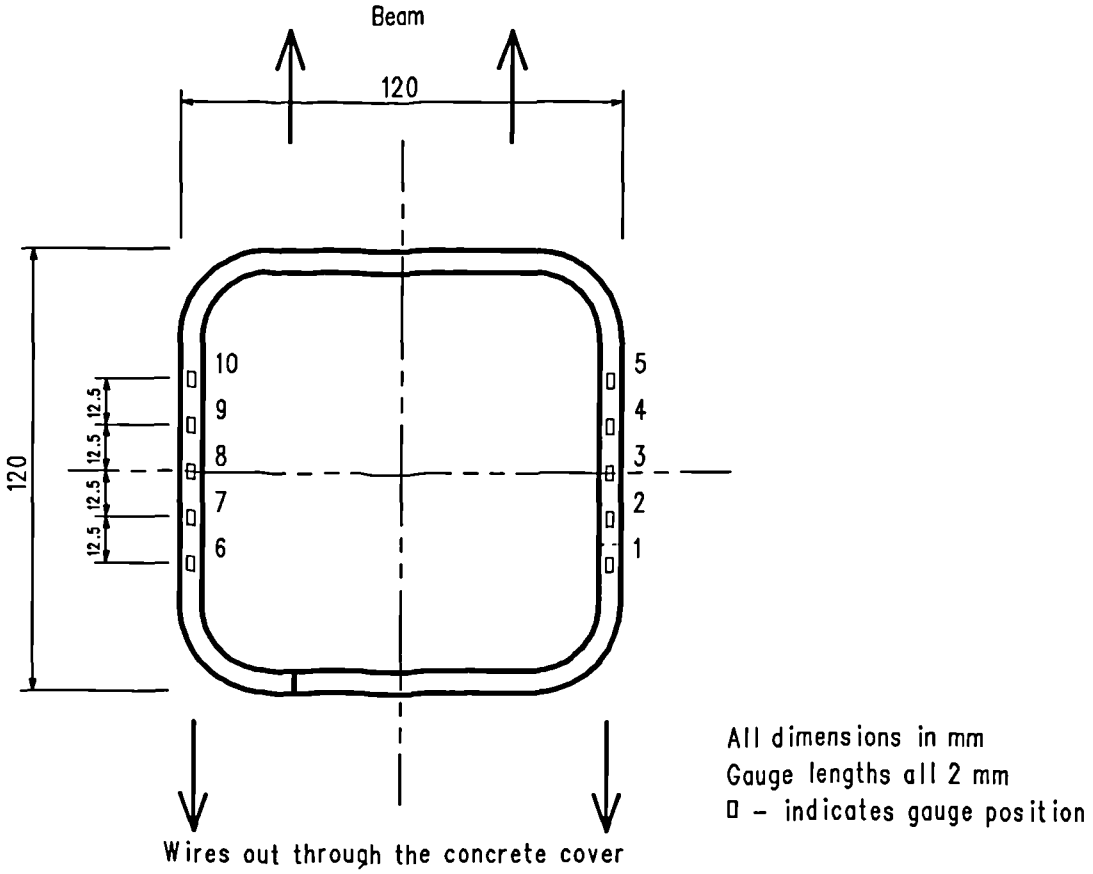

Figure 2.2.1.2.1 Joint tie - strain gauge layout

Note

Throughout this thesis the leg containing gauges 1-5 is referred to as **leg one**, the leg containing gauges 6-10 is referred to as **leg two**.

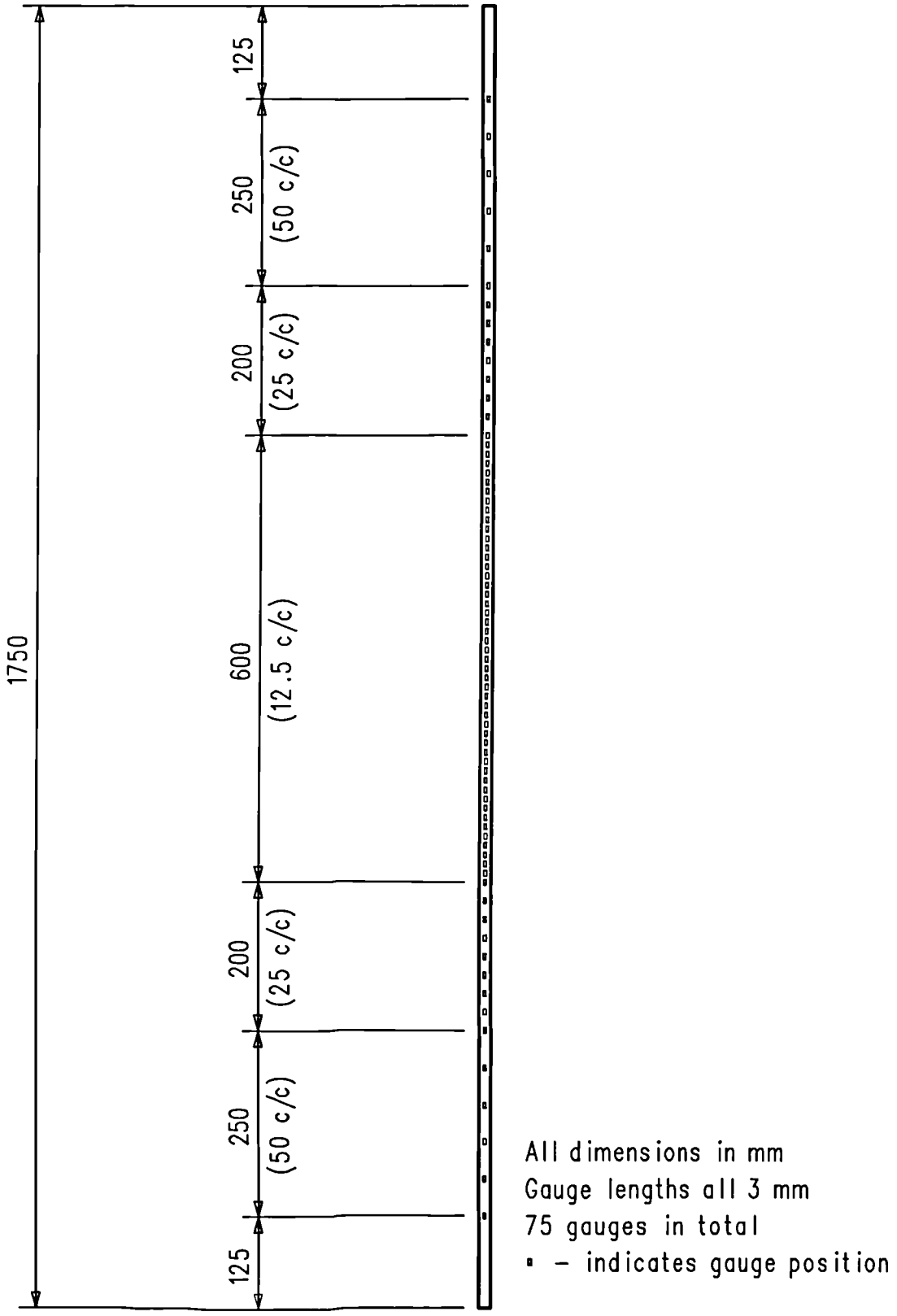

Figure 2.2.1.2.2 Column rebar - strain gauge layout A

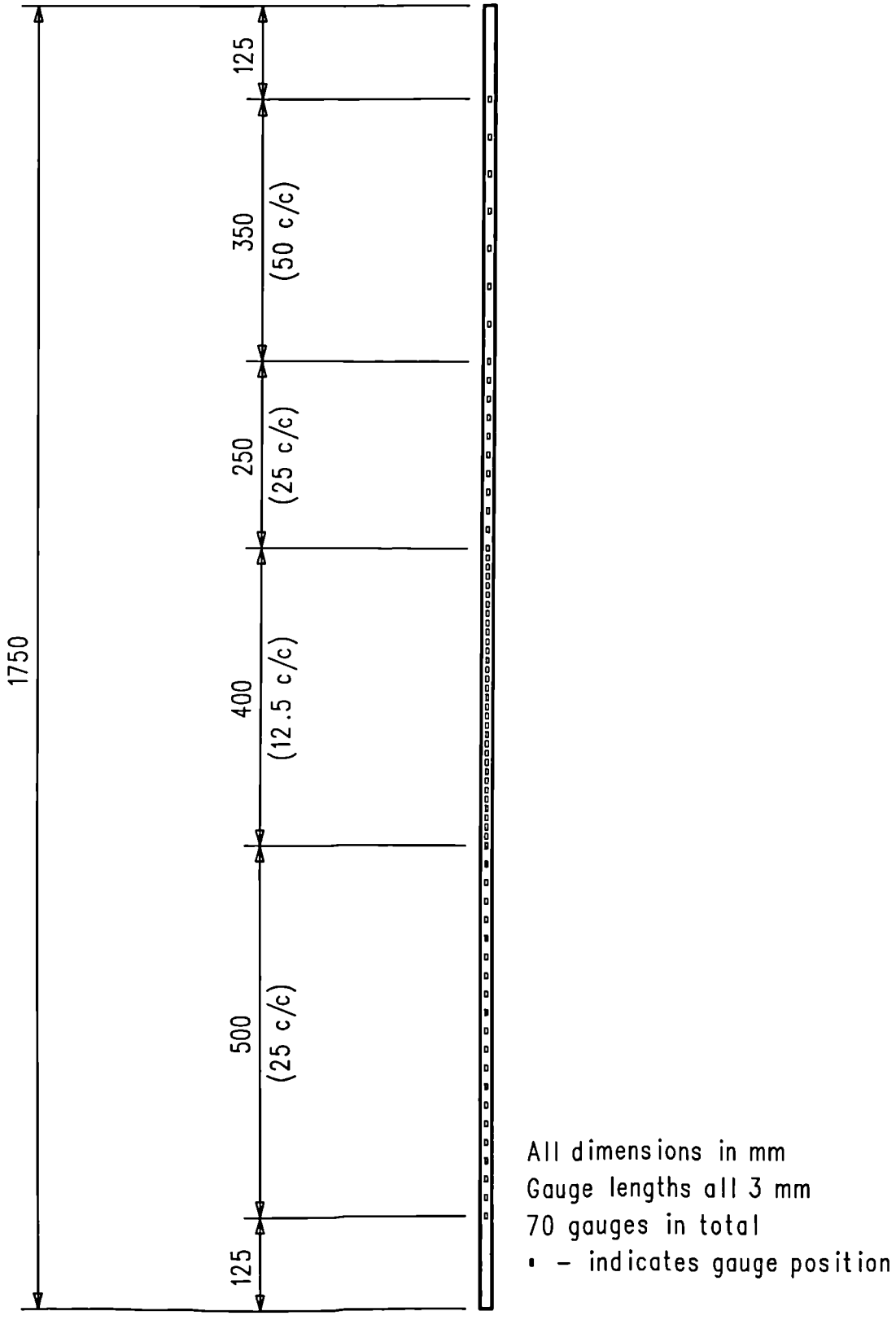

Figure 2.2.1.2.3 Column rebar - strain gauge layout B

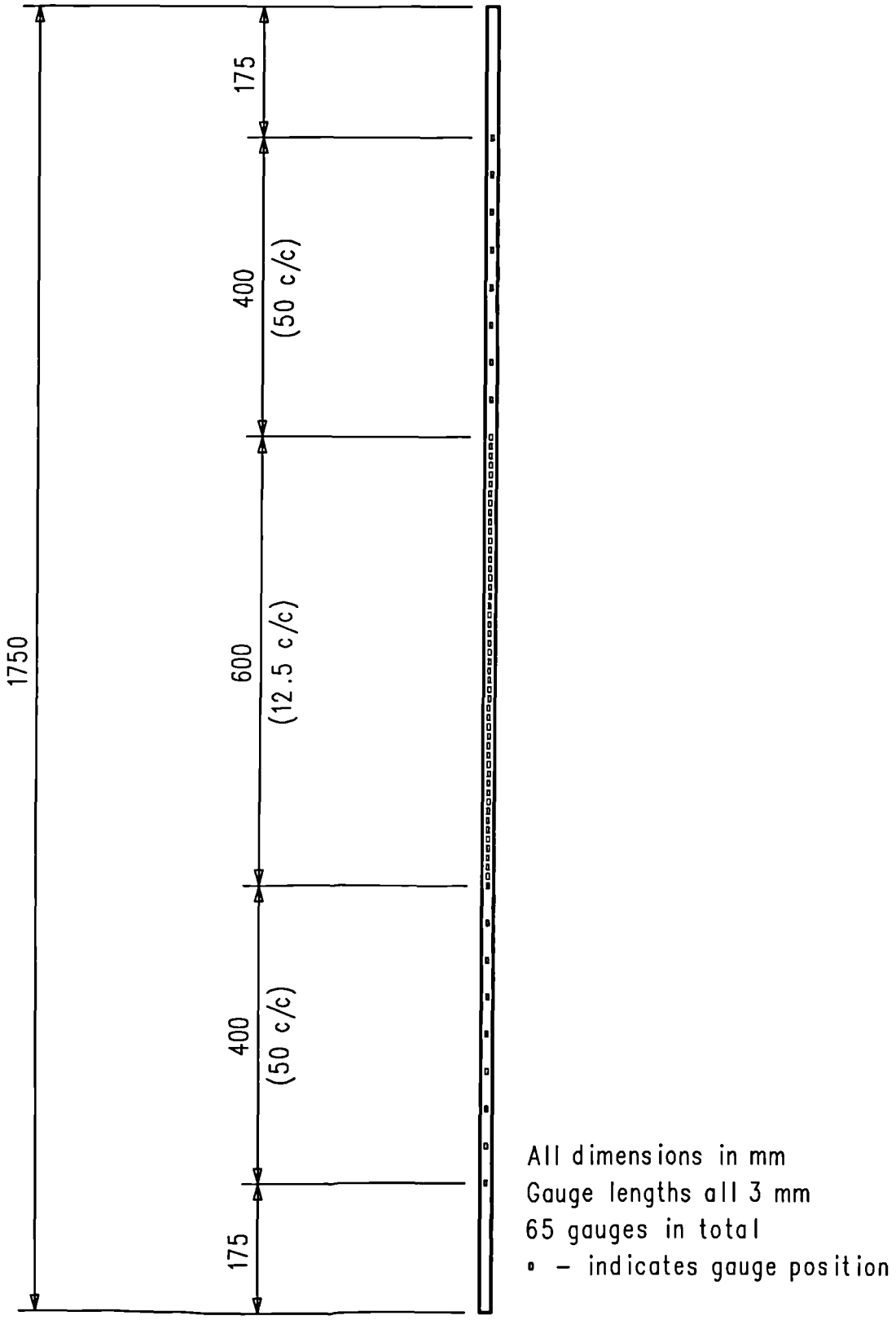

Figure 2.2.1.2.4 Column rebar - strain gauge layout C

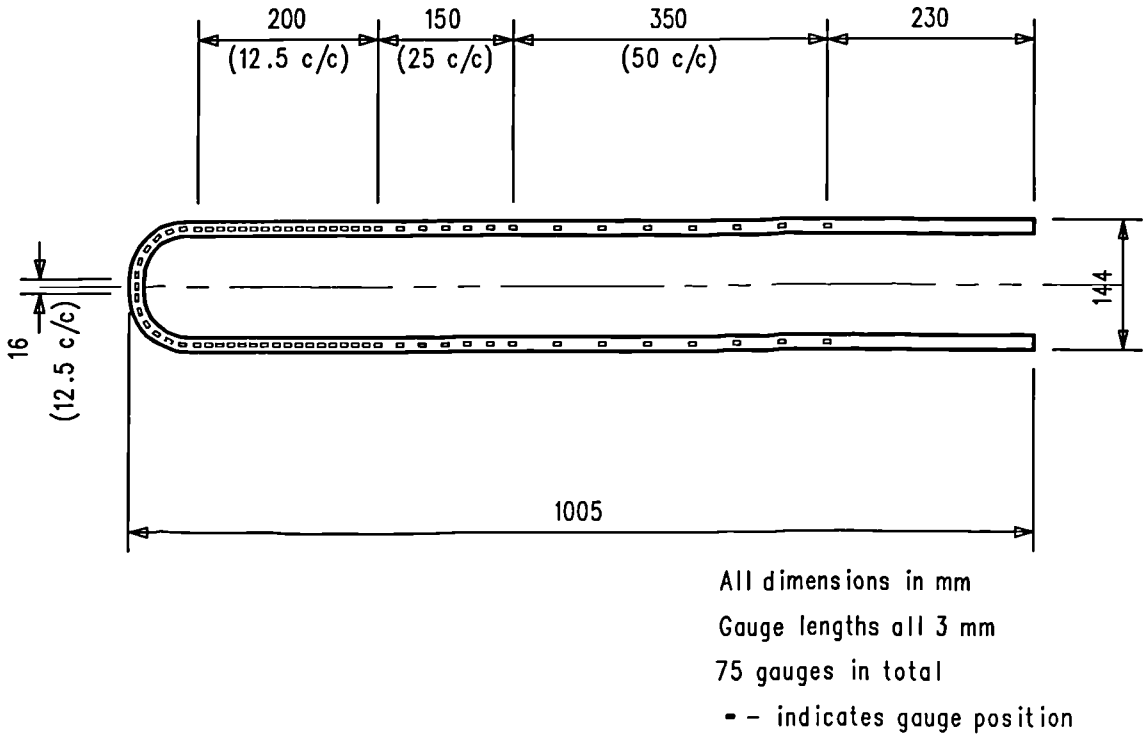

Figure 2.2.1.2.5 Beam U-bar - strain gauge layout A

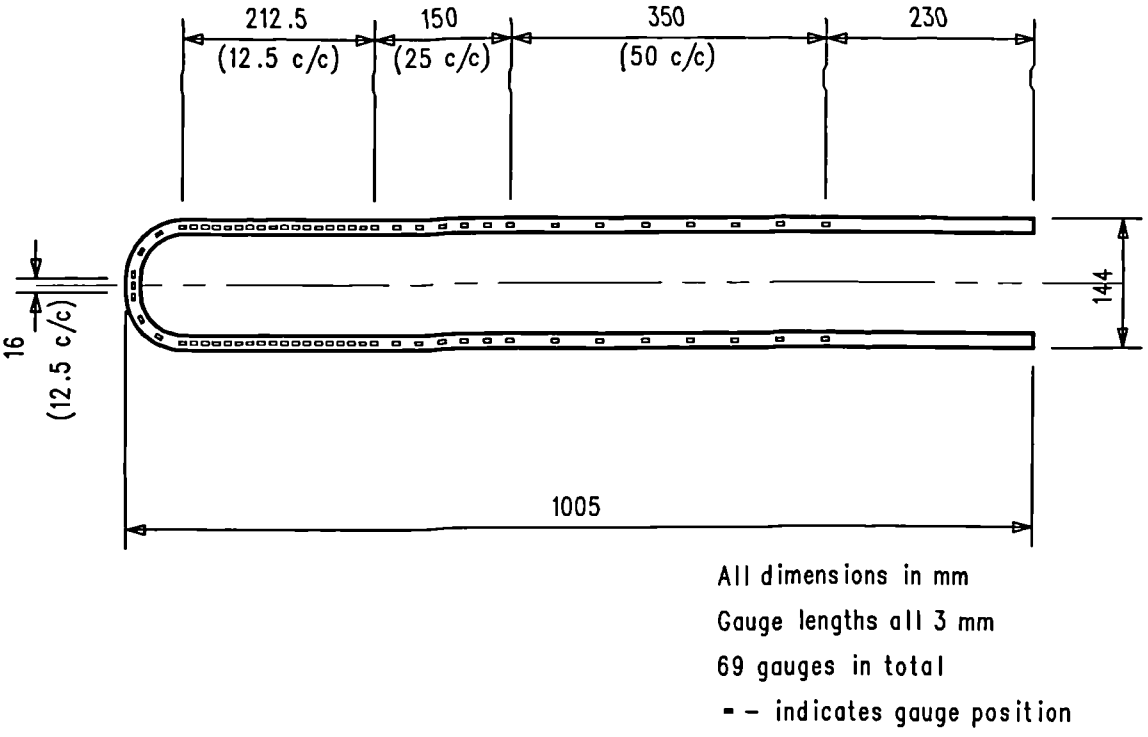

Figure 2.2.1.2.6 Beam U-bar - strain gauge layout B

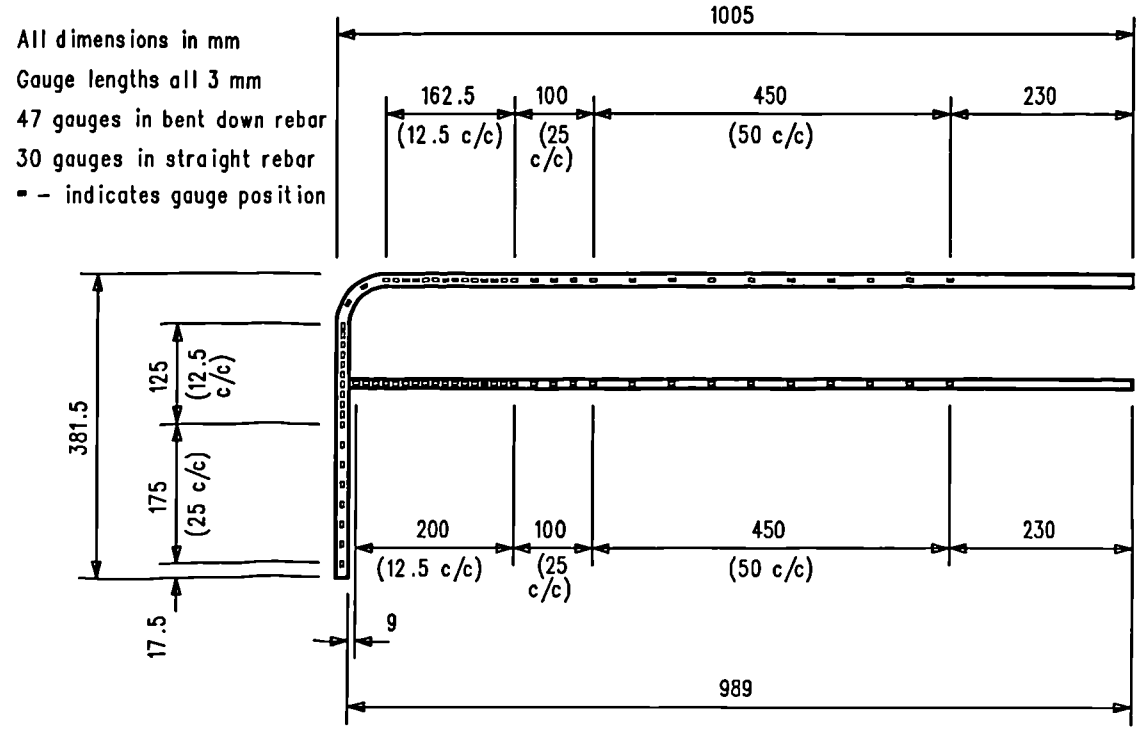

Figure 2.2.1.2.7 Beam bent down and compression rebars - strain gauge layout

Notes

1. For the U-bars and bent down bars the gauges within the bends are equally spaced between the defined straight sections,
2. The strain gauged bars were load cycled (where possible), within the elastic range, prior to being cast in the concrete. This was to minimise hysteresis and also acted as a check on strain gauge performance,
3. For a specimen containing around 230 strain gauges, typically between two and five gauges were damaged in the manufacturing process. **This gave a gauging success rate of around 98 to 99%.**

Table 2.2.1.2.1 Strain gauging within the monotonic test programme

Specimen	Outer column	Inner Column	Beam	Joint ties	Total
Standard specimens					
C4ALN1	70 (col B)	70 (col B)	77 (bent down)	10	227
C4ALN3	65 (col C)	65 (col C)	77 (bent down)	3 × 10	237
C6LN1	75 (col A)	75 (col A)	75 (U-bar A)	10	235
C6LN3	65 (col C)	65 (col C)	69 (U-bar B)	3 × 10	229
High strength specimens					
C4ALH1	70 (col B)	70 (col B)	77 (bent down)	10	227
C4ALH3	65 (col C)	65 (col C)	77 (bent down)	3 × 10	237
C4ALH5	-	-	-	10	10
C6LH1	75 (col A)	75 (col A)	75 (U-bar A)	10	235
C6LH3	65 (col C)	65 (col C)	69 (U-bar B)	3 × 10	229
Specimens investigating tie positioning					
C4ALN1T	-	-	-	10	10
C4ALN3C	-	-	-	10	10
C6LN1B	-	-	-	10	10
C6LN1T	-	-	-	10	10
C6LN1A	-	-	-	10	10
C6LN2A	-	-	-	10	10
C6LN2B	-	-	-	10	10
C6LN3A	-	-	-	10	10
C6LN3B	-	-	-	10	10
C6LN3C	-	-	-	10	10
Specimens investigating joint aspect ratio					
C7LN3	-	-	-	10	10
C9LN3	-	-	-	10	10
Additional specimens					
C6LN1(r)	-	-	-	10	10
C6LN1AE	-	-	-	10	10

Notes

1. col A, B and C refer to the gauge layouts in Figures 2.2.1.2, 2.2.1.3 and 2.2.1.4 respectively,
2. U-bar A and B refer to the gauge layouts in Figures 2.2.1.5 and 2.2.1.6 respectively.

2.2.2 Concrete mix design

The **normal strength** concrete had an aggregate-cement ratio of 5.5 (limestone and river sand aggregate) and a water-cement ratio of approximately 0.6. However, part way through the experimental programme it became necessary to increase the workability of the mix. The drive cable of the main vibrating poker failed and whilst this was under repair only a small, less powerful, poker was available. To increase the workability of the mix when using this small poker, superplasticiser was added. 500 ml of superplasticiser per 100 kg mix of concrete was required The effects of this are outlined in Section 4.3.

The **high strength** concrete had a reduced aggregate-cement ratio of 3.5 (granite and river sand aggregate) and a moisture-binder ratio of 0.22. The water content was carefully controlled by drying the aggregate in ovens prior to mixing. Admixtures were added to increase the workability of the concrete. The precise mix design was kindly supplied by Tarmac Topmix, UK.

The normal and high strength concrete mix designs are displayed in Table 2.2.2.

Table 2.2.2 Normal and high strength mix designs

	Normal strength (kg)	High strength (kg)
Coarse Aggregate	46.7	47.1
Fine Aggregate	30.8	24.3
Cement	14.2	20.3
Water	8.3	2.5
Microsilica	-	4.8
Admixtures	-	1.0
	100	100

For the **steel fibre** reinforced concrete two types of carbon steel fibres were used. Throughout this thesis they are referred to as *short* and *long*. The short fibres were 25 mm in length, crimped and made by the slit sheet method. The long fibres were cold drawn wire with end hooks, 50 mm in length. Fibre details are given in Figure 2.2.2.

Figure 2.2.2 Steel fibre details

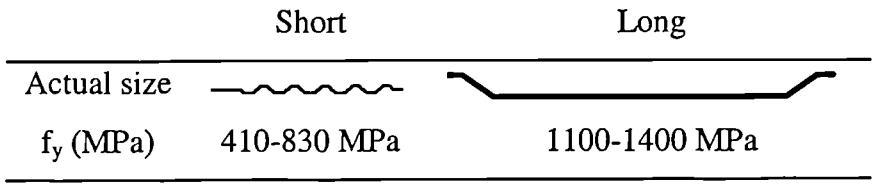

Fibre quantities used were 0.4, 1.5, 2.3 and 3.8 % by volume, (approximately 30, 110, 170 and 300 kg/m^3 respectively). Normal strength concrete was mixed and then the fibres were evenly sprinkled over the fresh concrete towards the end of the mixing process and blended in. Superplasticiser (500 ml per 100 kg of concrete) was used to increase the fresh concrete's workability.

Specimens were cast horizontally, the wooden formwork removed after twenty four hours and then the specimens were covered for fourteen days under damp hessian and plastic sheeting. Testing took place after six weeks for normal strength specimens and after eight weeks for the high strength specimens. This curing time before testing was found to give concrete of the desired compressive strength, 60MPa and 120MPa for normal and high strength concrete respectively.

On the day of a test concrete compressive strengths were determined from the average of three 100 mm cubes and tensile strengths were determined from the average of three cylinder splitting (Brazilian) tests.

2.3 Specimen Testing

2.3.1 Test rig and monitoring

Figure 1, previously displayed in the *Introduction*, shows a photograph of the test rig. Loads were measured at six locations as shown diagrammatically in Figure 2.3.1. The shear load cells at the top and the bottom of the column (load cells 4 and 5) and the beam load cell (load cell 2) were able to read loads in both directions. This was important for the monitoring of cyclic specimens tested later in the investigation using the same rig.

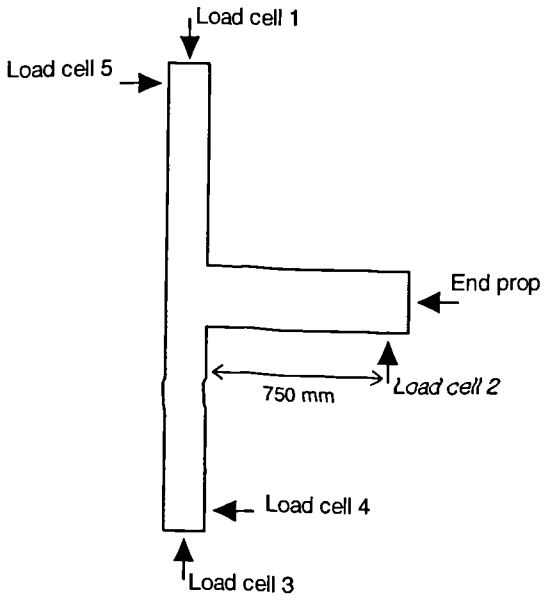

Figure 2.3.1 Load measurements (not to scale)

The load cells at the top and bottom of the column were pinned to steel plates and measured the horizontal and vertical loads at the column ends. The beam load cell (load cell 2) was located 750 mm from the face of the column, this was attached to the hydraulic ram used for loading the beam (more details regarding the loading technique are given in Section 2.3.2). The beam end prop was a 40 mm diameter steel rod, attached to this were four strain gauges in a half bridge arrangement, this was calibrated to measure axial load. Two gauges were arranged longitudinally and two gauges transversely in order to increase sensitivity.

Equilibrium checks for the vertical loads over the duration of test showed an accuracy of within 1.0%. Similar checks on the horizontal loads showed an accuracy of within 2.0%.

During this investigation, prior to the start of the cyclic tests, three tilt meters and six displacement transducers were purchased. However, the use of these devices within the monotonic test programme was for trial purposes only.

2.3.2 Loading technique

The test procedure was to load the column, in 25 kN increments to 50 kN for normal strength and fibre reinforced concrete and 100 kN for high strength concrete. (This relatively low column load was selected as a result of previous research [12] suggesting that this was a more critical load case). This column load was then maintained throughout the test while the beam was loaded incrementally, vertically downwards, at a point 750 mm from the column face. The specimen was judged to have failed when no further increase in beam load was possible.

2.4 Data Processing

Each test produced a large amount of output data. This data was logged as one long column of unformatted text. The size of a data file from a simple test specimen was around 30 kB. The size of a data file from a fully gauged test specimen (giving an additional 237 strain gauge readings per load step) was around 180 kB. The size of a data file from a fully gauged *cyclic* test specimen was around 460 kB.

The author wrote the following computer program to convert this data into a *user friendly* table to be used within Microsoft Excel :

RCBCC

The input data file was read by this program. All zero errors were removed and each data series was then multiplied by its corresponding conversion factor. This data was then tabulated and written to an output file. **RCBCC** was written using C and the coding is presented in Appendix B1.

As part of the analysis it was necessary to calculate the bond stress within the reinforcement. The author wrote the following computer program for this task :

AVBON

The input data file was read by this program. This input data was taken from a region of the reinforcement for the considered load stages. Average bond stresses were then calculated for this region at each load stage and then written to an output file. **AVBON** was written using C and the coding is presented in Appendix B2.

3. Monotonic Results and Discussion (Overview)

The Monotonic Results and Discussion section of this thesis is split into two chapters; **Chapter 3** provides an overview of the results from the entire monotonic test programme; **Chapter 4** is a discussion of the results, in detail, from each individual test series within the monotonic programme.

3.1 Specimen Behaviour

The first sign of distress in the test specimens was the appearance of flexural cracks in the beam near the column face. These cracks became visible at an applied load of around 25% of the beam's ultimate flexural capacity. As the loading increased similar flexural cracking was seen in the column, above and below the joint.

A diagonal shear crack within the joint was the first indication of weakness within the joint. Figure 3.1.1 shows how the internal forces within the joint led to this shear cracking. The force from the beam reinforcement, in addition to the complimentary forces in the column bars, set up a diagonal tension field. When the tensile capacity of the concrete was reached a diagonal shear crack appeared in the joint. Figure 3.1.2 shows a photograph of a specimen at initial joint cracking. The diagonal shear crack is clearly visible within the joint.

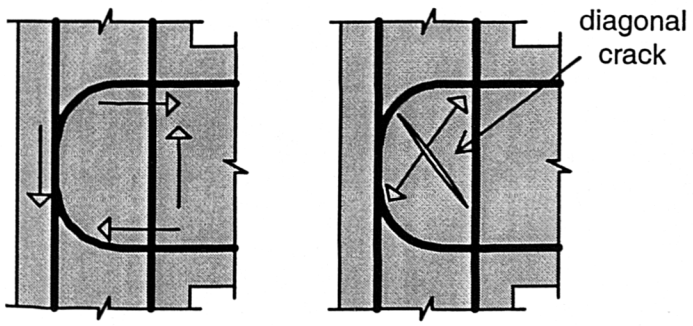

Figure 3.1.1 Simplified internal forces within the joint

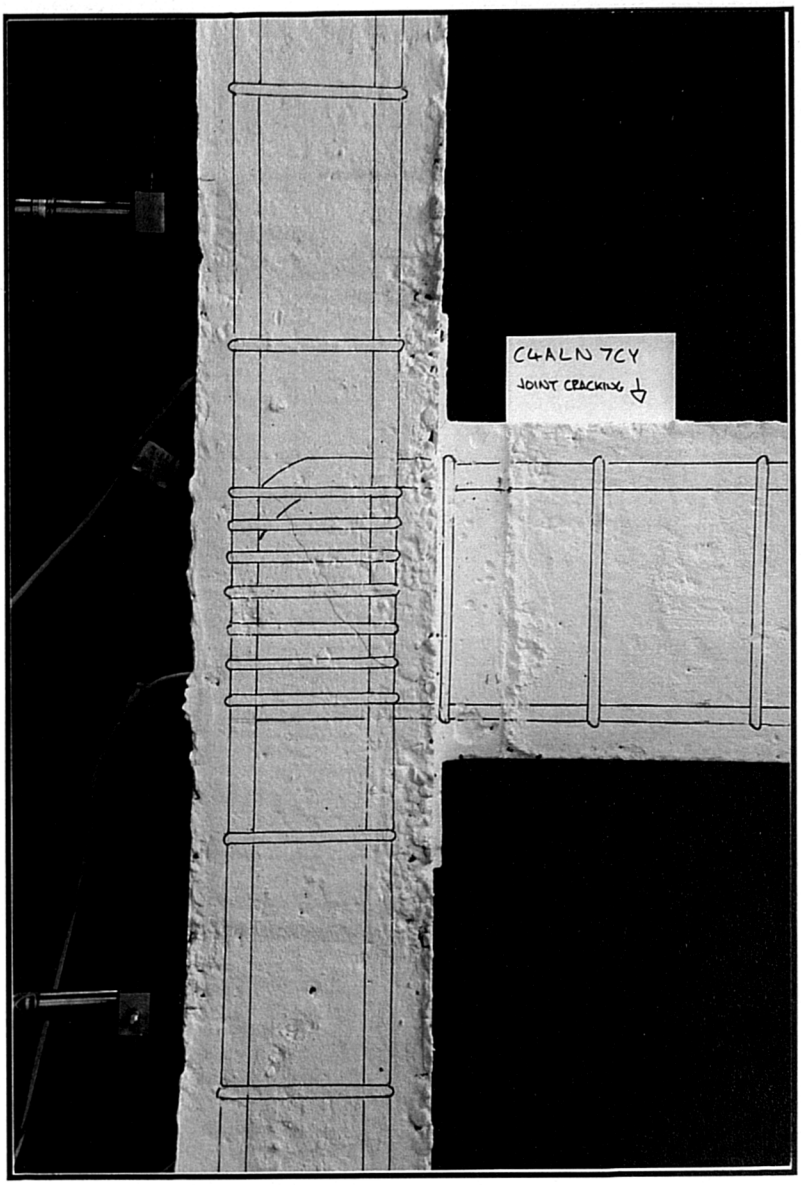

Figure 3.1.2 Initial joint cracking

Two types of failure modes were observed throughout the investigation; beam flexural failure and joint failure. Both of these failure modes were described previously in Section 1.1.

Beam flexural failure

If the ultimate shear capacity of the joint was greater than the beam's ultimate moment of resistance then a plastic hinge developed in the beam at the column face. Figure 3.1.3 shows a photograph of a specimen which exhibited beam failure. The extensive cracking in the beam corresponds to where gross yield of the beam tension steel occurred.

Joint failure

If the ultimate shear capacity of the joint was less than the beam's ultimate moment of resistance then joint failure occurred. Figure 3.1.4 shows a photograph of a specimen which exhibited joint failure. The initial shear cracking had developed extensively to a situation where the joint could withstand no further increase in the applied beam load.

3.2 Joint Cracking and Failure Loads

Table 3.2.1 displays the concrete compressive strengths, obtained from the average of three cube tests, and indirect tensile strengths, obtained from the average of three cylinder splitting (Brazilian) tests. The beam loads at which initial joint cracking and specimen failure occurred are also displayed. Although these loads are shown to one decimal place the author suggests that they should be taken as accurate to the nearest kN. The failure mode for each specimen is indicated in the final column of Table 3.2.1.

Due to the large number of monotonic specimens the author recommends referral to the plots of joint layout in Tables 2.2 to 2.7.

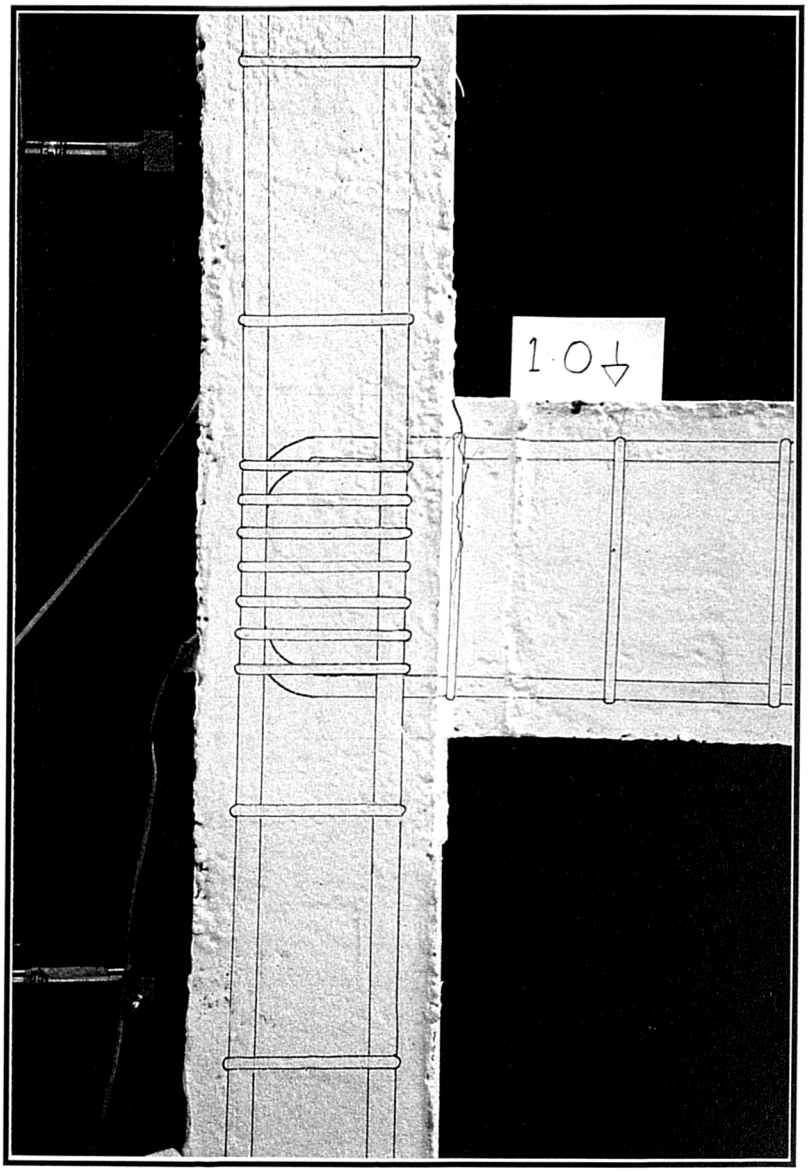

Figure 3.1.3 Beam flexural failure

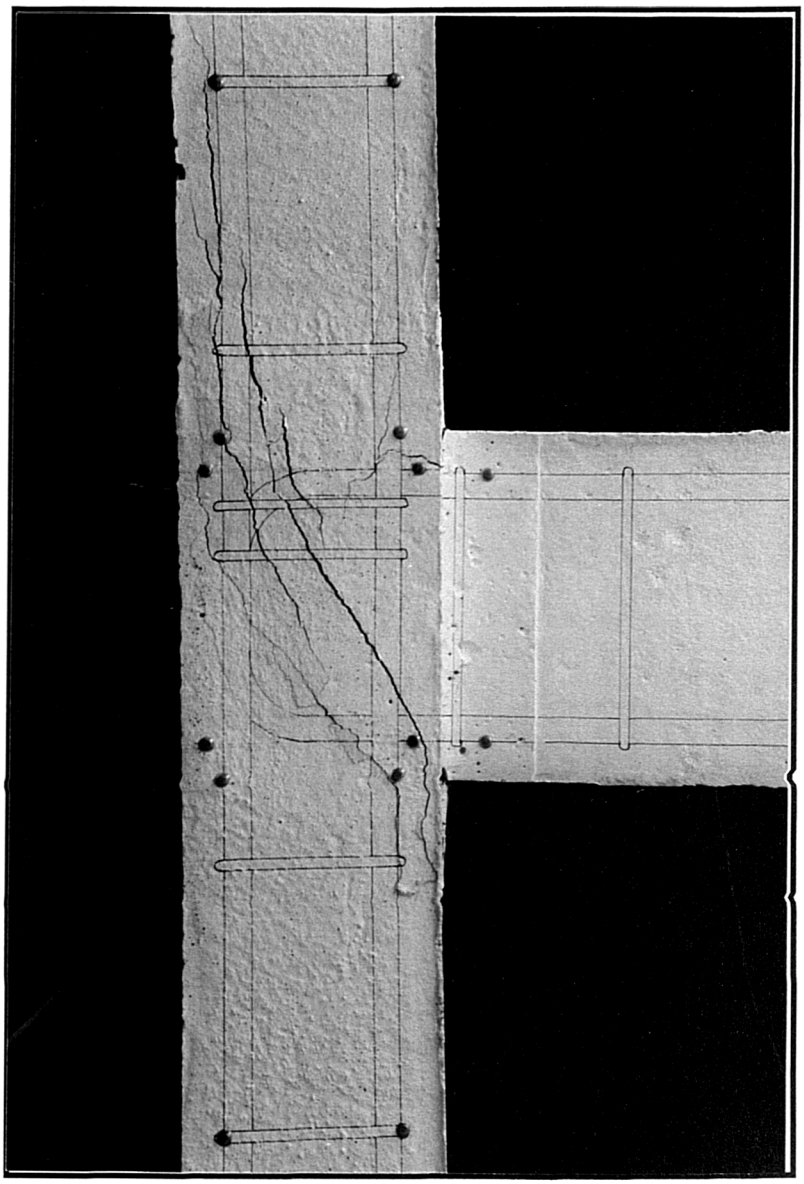

Figure 3.1.4 Joint failure

Table 3.2.1 Joint cracking and failure loads

Specimen	f_{cu} (MPa)	f_t (MPa)	P_{crack} (kN)	P_{fail} (kN)	Failure Mode
		Standard specimens			
C4ALN0	53	2.7	13.2	26.5	J
C4ALN1	57	3.4	18.7	33.5	J
C4ALN3	52	2.9	13.3	35.2	J
C4ALN5	63	3.2	14.1	39.5	J
C6LN0	64	3.4	18.5	23.9	J
C6LN1	64	3.3	18.1	24.6	J
C6LN3	61	3.2	17.8	28.7	J
C6LN5	46	2.7	14.7	33.9	J
		High strength specimens			
C4ALH0	130	4.9	20.6	43.2	F
C4ALH1	119	3.7	19.7	43.4	F
C4ALH3	132	5.5	24.8	45.6	F
C4ALH5	123	5	27.4	48.6	F
C6LH0	126	4.7	25.4	36.1	J
C6LH1	127	4.9	22.2	37.1	J
C6LH3	121	3.7	23.3	41.2	J
C6LH5	125	5.2	25.5	51.4	F
		Specimens investigating tie positioning			
C4ALN1T	50	3.3	14.7	30.8	J
C4ALN3C	56	3.2	17.0	41.0	F
C4ALN3D	59	3.4	16.8	41.2	F
C6LN1B	49	3.2	16.0	22.4	J
C6LN1T	50	3.2	16.6	26.9	J
C6LN1A	61	3.2	15.6	27.3	J
C6LN2A	64	3.4	18.8	30.5	J
C6LN2B	64	3.3	20.0	35.1	J
C6LN3A	58	3.1	14.9	30.8	J
C6LN3B	65	3.7	18.9	37.8	J
C6LN3C	60	3.3	16.7	34.3	J

(Table 3.2.1 continued on next page)

Table 3.2.1 Joint cracking and failure loads (cont.)

Specimen	f_{cu} (MPa)	f_t (MPa)	P_{crack} (kN)	P_{fail} (kN)	Failure Mode
Specimens investigating joint aspect ratio					
C7LN0	48	2.6	23.5	35.7	J
C7LN1	47	2.7	30.0	39.7	J
C7LN3	50	3.4	22.5	47.5	J
C7LN5	50	3.3	27.5	54.0	J
C9LN0	51	3.3	19.6	33.3	J
C9LN1	48	3.4	18.9	33.2	J
C9LN3	46	3.0	19.7	37.9	J
C9LN5	44	3.4	18.6	45.9	J
Steel fibre reinforced specimens					
C4AL04SF	45	4.5	18.2	31.2	J
C4AL15SF	47	3.8	17.6	33.2	J
C4AL23SF	55	4.7	23.9	42.0	F
C4AL04LF	42	4.2	15.6	34.7	J
C4AL15LF	50	4.6	23.0	35.6	J
C4AL23LF	56	4.2	21.9	42.9	F
C4AL38LF	52	4.7	24.9	44.8	F
C6L04SF	54	3.2	17.1	23.9	J
C6L04LF	42	4.5	18.1	23.4	J
Additional specimens					
C6LN1(r)	61	3.2	18.3	27.6	J
C6LN1AE	55	3.1	15.7	28.8	J
C4PLN0	54	3.1	19.4	32.0	J
C6LNP4	58	3.0	19.8	38.2	J
C6PLNP4	51	3.2	17.6	47.8	J

Notes

1. J - indicates joint failure, F - indicates flexural *beam* failure.

3.3 Joint Cracking and Failure Stresses

To allow the comparison of specimens of different sizes, the joint cracking and failure loads were converted into shear stresses. The method used for these calculations has been outlined in detail in Section 1.3.

Table 3.3.1 displays the values of shear stress in the joint at both initial cracking and specimen failure. These values were normalised by dividing by the square root of the concrete compressive cylinder strength (as outlined in Section 1.4). The failure modes for each specimen are indicated in the final column of Table 3.3.1.

It should be noted that, for the specimens that failed due to beam flexure, the shear stress values **do not** represent the ultimate shear capacity of the joint. They represent the shear stress value developed in the joint at beam flexural failure. For these values the tensile force within the beam steel was taken to be equal to the bar's yield strength (for the steel stress-strain relationships see Section 2.1).

Table 3.3.1 Joint cracking and failure stresses

Specimen	$v_{crack}/\sqrt{f_{ck}}$ ($MPa^{0.5}$)	$v_{fail}/\sqrt{f_{ck}}$ ($MPa^{0.5}$)	Failure Mode
Standard specimens			
C4ALN0	0.52	1.11	J
C4ALN1	0.73	1.39	J
C4ALN3	0.53	1.56	J
C4ALN5	0.51	1.57	J
C6LN0	0.67	0.89	J
C6LN1	0.66	0.92	J
C6LN3	0.67	1.12	J
C6LN5	0.64	1.63	J
High strength specimens			
C4ALH0	0.51	1.12	F
C4ALH1	0.51	1.18	F
C4ALH3	0.62	*1.14*	F
C4ALH5	0.71	*1.18*	F
C6LH0	0.65	0.94	J
C6LH1	0.56	0.96	J
C6LH3	0.61	1.11	J
C6LH5	0.65	*1.16*	F
Specimens investigating tie positioning			
C4ALN1T	0.61	1.37	J
C4ALN3C	0.67	*1.78*	F
C4ALN3D	0.64	1.73	F
C6LN1B	0.67	0.97	J
C6LN1T	0.69	1.17	J
C6LN1A	0.58	1.06	J
C6LN2A	0.69	1.16	J
C6LN2B	0.73	1.36	J
C6LN3A	0.57	1.25	J
C6LN3B	0.68	1.46	J
C6LN3C	0.63	1.38	J

(Table 3.3.1 continued on next page)

Table 3.3.1 Joint cracking and failure stresses (cont.)

Specimen	$v_{crack}/\sqrt{f_{ck}}$ ($MPa^{0.5}$)	$v_{fail}/\sqrt{f_{ck}}$ ($MPa^{0.5}$)	Failure Mode
Specimens investigating joint aspect ratio			
C7LN0	0.61	0.94	J
C7LN1	0.79	1.07	J
C7LN3	0.57	1.26	J
C7LN5	0.70	1.45	J
C9LN0	0.49	0.85	J
C9LN1	0.48	0.87	J
C9LN3	0.52	1.03	J
C9LN5	0.50	1.31	J
Steel fibre reinforced specimens			
C4AL04SF	0.81	1.50	J
C4AL15SF	0.76	1.56	J
C4AL23SF	0.97	*1.79*	F
C4AL04LF	0.72	1.79	J
C4AL15LF	0.99	1.63	J
C4AL23LF	0.87	*1.77*	F
C4AL38LF	1.05	*1.83*	F
C6L04SF	0.68	0.98	J
C6L04LF	0.84	1.12	J
Additional specimens			
C6LN1(r)	0.69	1.07	J
C6LN1AE	0.62	1.20	J
C4PLN0	0.78	1.36	J
C6LNP4	0.77	1.60	J
C6PLNP4	0.73	2.32	J

Notes

1. J - indicates joint failure, F - indicates flexural *beam* failure.

4. Monotonic Results and Discussion (Detailed)

As outlined previously in Tables 2.2 to 2.7, the monotonic test programme was divided into six test series. The results from these test series are reviewed in detail within this chapter.

Each test series is considered in terms of initial joint cracking and specimen failure. For the gauged specimens the strains from the main beam steel are shown at two stages; prior to joint cracking and approaching specimen failure. Due to the unique nature of the strain gauged ties, complete tie strain readings are displayed. A bond and bearing stress analysis of the main reinforcement is also conducted for appropriate regions of the main beam steel.

4.1 Standard Specimens

This section considers the results from the eight *standard* specimens. These are the eight specimens which were used as the standard for all other test comparisons. The parameters investigated were the **number of joint ties** and the **beam tension steel anchorage detail**. The specimen details are given below in Table 4.1.

Table 4.1 *Standard* specimen details

Specimen	Gauging	Beam steel anchorage	No. of joint ties
C4ALN0	-	Bent down	0
C4ALN1	Full	Bent down	1
C4ALN3	Full	Bent down	3
C4ALN5	-	Bent down	5
C6LN0	-	U-bar	0
C6LN1	Full	U-bar	1
C6LN3	Full	U-bar	3
C6LN5	-	U-bar	5

4.1.1 Initial joint cracking

Figure 4.1.1 shows the normalised shear stress values for the eight standard specimens at initial joint cracking. These results were previously displayed in Table 3.2.2.

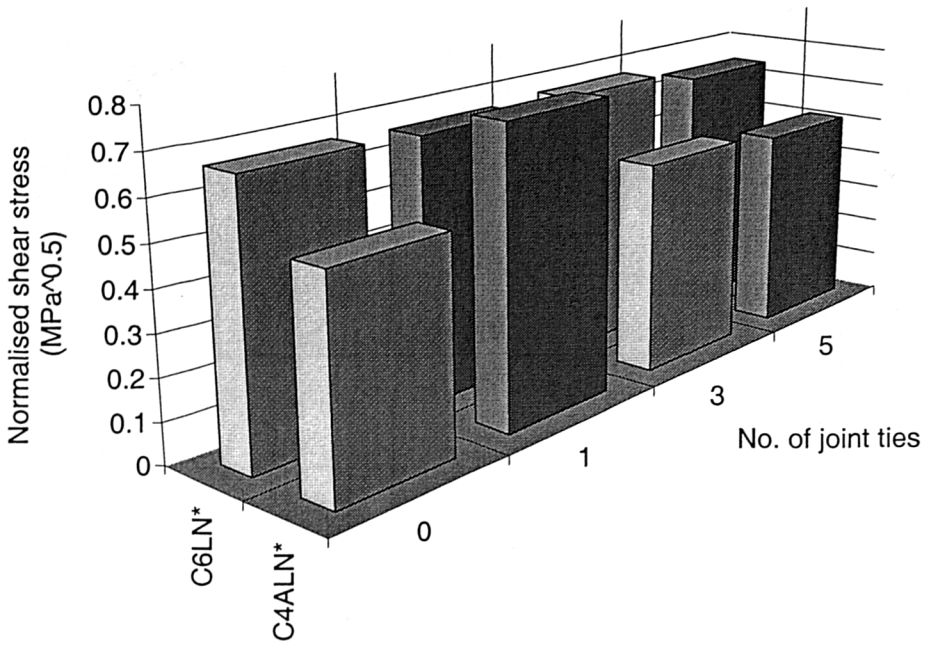

Figure 4.1.1 Shear stress at initial joint cracking - standard specimens

Figure 4.1.1 displays no evidence to suggest that the joint cracking capacity was influenced by the number of ties present within the joint. Even with the maximum number of five joint ties there was still insufficient additional volumetric steel to provide an increased resistance to initial joint cracking.

Initial joint cracking occurred at an average normalised shear stress value of 0.57 $MPa^{0.5}$ for specimens with bent down beam steel detail compared with 0.66 $MPa^{0.5}$ for specimens with U-bar beam steel detail. Although these values are based on only eight specimens first indications are that specimens with U-bar beam steel detail have a greater resistance to initial joint cracking than specimens with bent down beam steel detail.

4.1.2 Specimen failure

Figure 4.1.2 shows the shear stress values for the eight standard specimens at failure. These results were previously displayed in Table 3.2.2. All specimens exhibited joint failure.

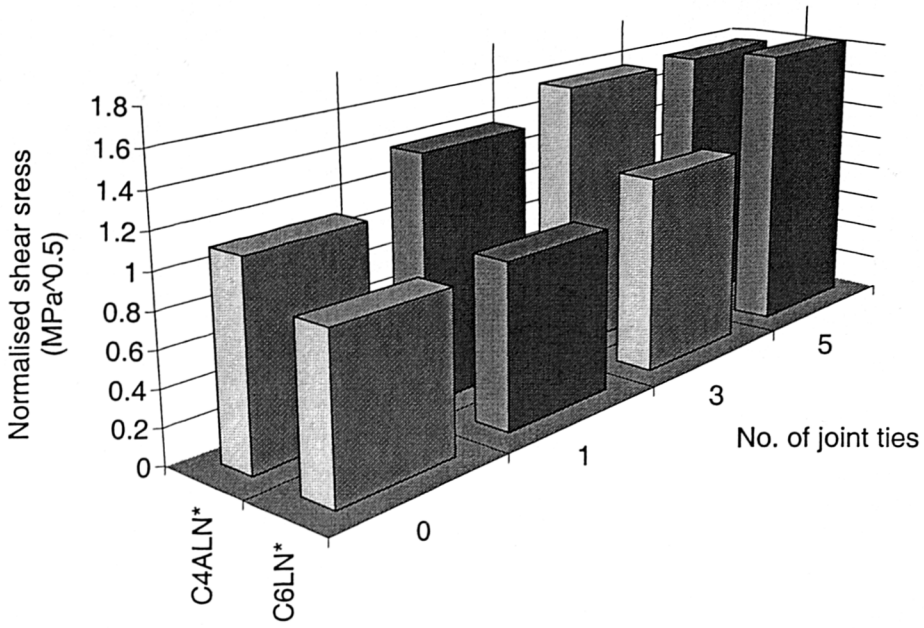

Figure 4.1.2 Shear stress at failure - standard specimens

Figure 4.1.2 clearly shows that a significant enhancement of joint shear strength was possible through the provision of ties within the joint zone. The presence of ties gave an enhancement to the joint capacity by providing extra resistance across the crack width and increased confinement to the core concrete.

Figure 4.1.2 shows that specimens with bent down beam steel detail performed better than specimens with U-bar beam steel detail. The individual performance of both beam steel anchorage methods is considered further in Section 4.1.4 (*Bond Stress Analysis*).

4.1.3 Reinforcement strains

Reinforcement strains are presented for the four fully strain gauged specimens. Throughout this thesis the sign convention used for strain distributions is **tension positive.**

Specimen C6LN1 was tested at a column load of 100 kN, as opposed to the other normal strength specimens which were tested at a column load of 50 kN. As a result of this the strain in the column reinforcement of specimen C6LN1 was more compressive than for other similar specimens. The author estimates that this difference was of a value of around -50 με.

The number of gauges present within each specimen is shown below in Table 4.1.3. The gauge layouts for each bar were shown previously in Figures 2.2.1.2.1 to 2.2.1.2.7.

For all reinforcement strain plots within this thesis beam loads are rounded to the nearest kN.

Table 4.1.3 Strain gauge distribution

	Outer column bar	Inner column bar	Beam steel	Joint ties
C4ALN1	70	70	47 (*T*) / 30 (*C*)	10
C4ALN3	65	65	47 (*T*) / 30 (*C*)	30
C6LN1	75	75	75 (U-bar)	10
C6LN3	65	65	69 (U-bar)	30

Notes

1. For the specimens using bent down beam steel detail, *T* indicates the tension steel and *C* indicates the compression steel.

4.1.3.1 Outer column bars

Figure 4.1.3.1.1 displays the reinforcement strains present in the outer column bars at a beam load of 12 kN. At this stage all of the specimens were essentially elastic in behaviour.

Figure 4.1.3.1.1 shows that at the top and base of the column the reinforcement was in compression with strains of around -50 με. The shape of the strain distributions was very similar for all four specimens. The force transmitted from the beam into the joint pulled the region of the bar in the lower column into tension. Consequently the strain in the upper part of the column was forced into further compression. The magnitude of the strains at this stage, however, was reasonably small with a maximum of around -300 με in the upper column and 200 με in the lower column.

Figure 4.1.3.1.2 displays the reinforcement strains present in the same bars at specimen failure. All four specimens exhibited joint failure and thus had extensive cracking throughout the level of the beam depth. The strain distribution was similar to that seen previously in Figure 4.1.3.1.1. The main difference was the magnitude of the tensile strains within the lower column. Strains approaching 1000 με were recorded in the lower column at specimen failure.

Interestingly, the region of tensile strain in the outer column bar advanced above the joint for the specimens with the U-bar beam steel detail (C6LN1 and C6LN3). However the region of tensile strain remained below the mid-height of the column bar for the specimens with bent down beam steel detail.

The author believes that the bent down beam steel's anchor leg allowed the majority of force transfer to occur below the level of the joint. This reduced the force transfer requirements within the joint giving a greater ultimate capacity. More evidence of this is presented in Section 4.2.3.1 from the similar strain results for high strength specimens.

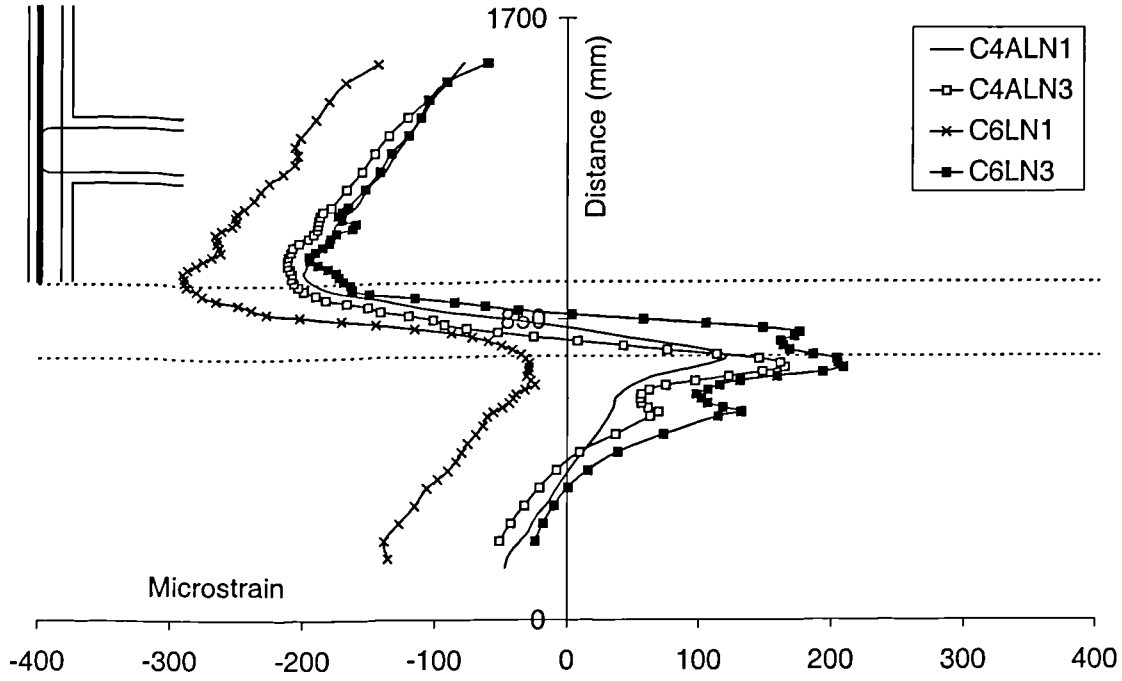

Figure 4.1.3.1.1 Outer column strains - 12 kN beam load

1. The dashed line indicates the beam level for all column rebar plots,
2. Throughout this thesis a data series is expressed as a single line, with no data points, if clarity is a concern. Specimen C4ALN1 is an example of this.

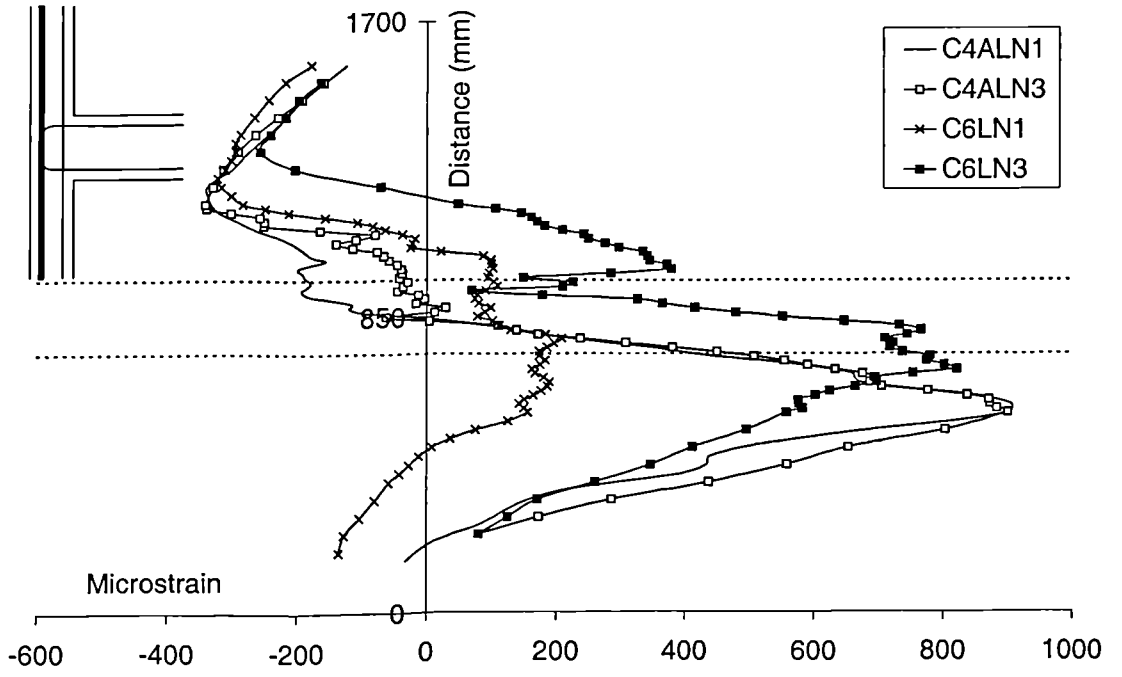

Figure 4.1.3.1.2 Outer column strains - specimen failure

4.1.3.2 Inner column bars

Figure 4.1.3.2.1 displays the reinforcement strains present in the inner column bars at a beam load of 12 kN.

The inner bars, like the outer bars, were in compression at the top and base of the column and strains of around -50 με were recorded. As expected, the shape of the strain distributions were complementary to those seen in the outer column bars. The force transmitted from the beam into the joint region pulled the upper column into tension. As a result, the lower column was forced into further compression. As the specimen was still essentially elastic at this stage the magnitude of the strains in the inner column bar was similar to that seen for the outer column bar with numerical maximums of around 300 με.

Figure 4.1.3.2.2 displays the reinforcement strains present in these inner column bars at specimen failure. The shape of the distributions remained similar but the magnitude of the tensile strain considerably increased. These strain values ranged from around 1000 με to yield and beyond. The maximum strain recorded was 3060 με within specimen C6LN3.

Even though its failure load was lower, the inner column bar of C6LN3 yielded whereas the inner column bars of C4ALN1 and C4ALN3 did not. This again suggests that the method of load transfer for the U-bar beam steel detail was not the same as for the bent down beam steel detail. Further evidence of this is presented in Section 4.2.3.2 from the similar high strength strain results.

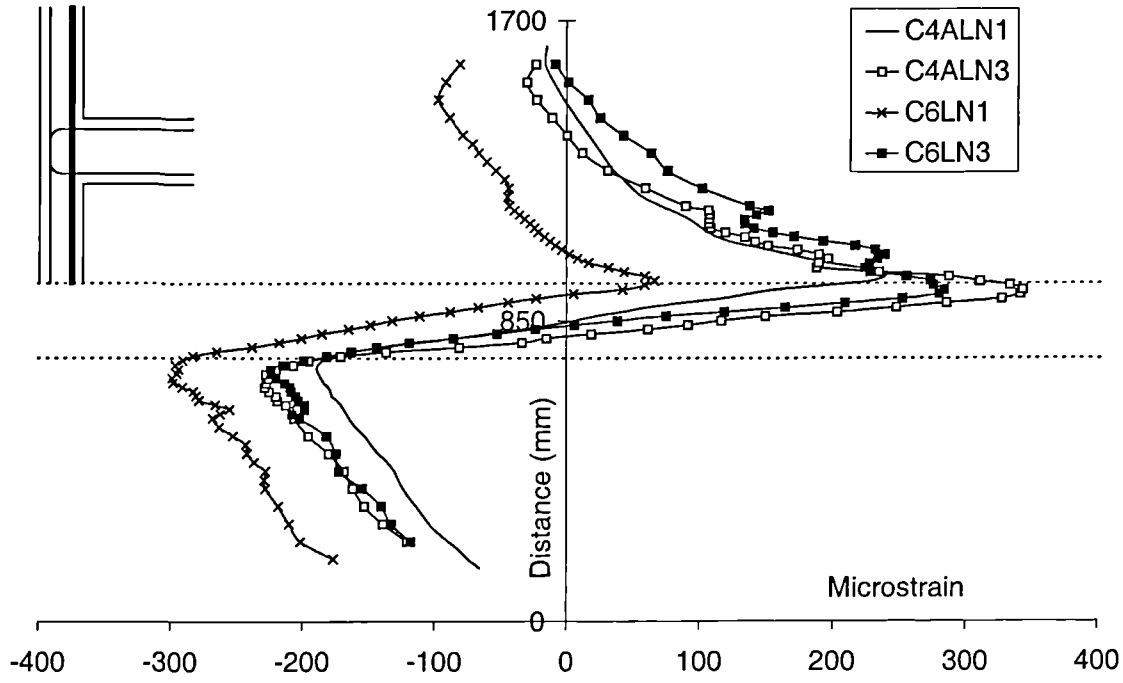

Figure 4.1.3.2.1 Inner column strains - 12 kN beam load

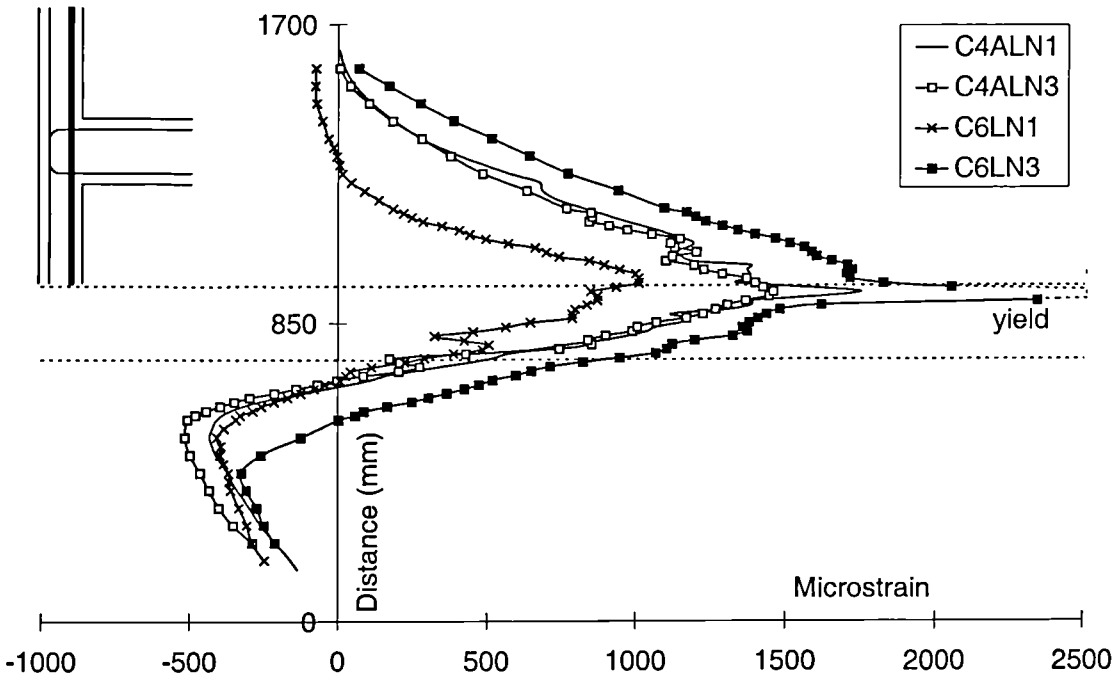

Figure 4.1.3.2.2 Inner column strains - specimen failure

(*Note* - Bar yield (2500 με) is indicated by the strain distribution line being dashed)

4.1.3.3 Beam bars

To allow simple representation of the strain distributions from the beam steel, the rebars were divided into defined regions. Figure 4.1.3.3.1 and 4.1.3.3.2 show these regions for the bent down and U-bars respectively. Throughout this thesis the beam steel is considered in this way.

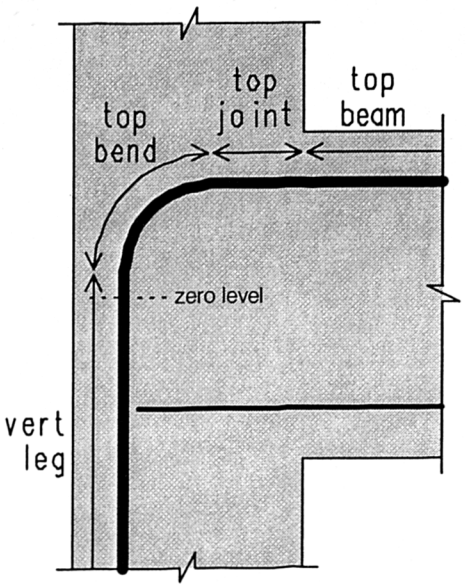

Figure 4.1.3.3.1 Defined regions along the bent down bar

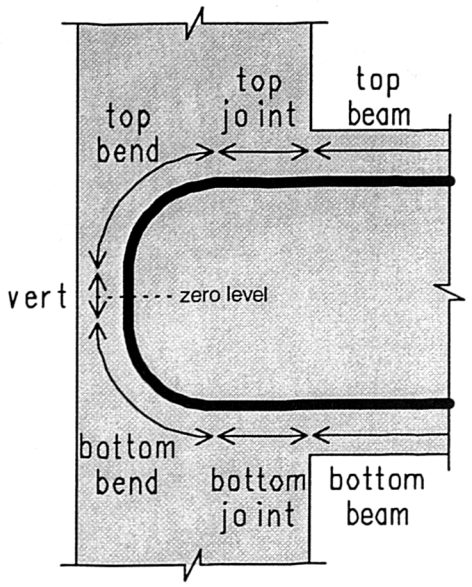

Figure 4.1.3.3.2 Defined regions along the U-bar

Bar distances were measured positively along the top of the beam from the zero level indicated in Figures 4.1.3.3.1 and 4.1.3.3.2. For clarity, strain distributions only up to a distance of 400 mm from this zero level are shown in the strain plots. Strains further than this distance were sufficiently far from the joint to ensure that the strain gradients were essentially linear to the point of loading.

Strain distributions were considered separately for the bent down and the U-bar beam steel detail.

Bent down beam steel

Figure 4.1.3.3.3 displays the reinforcement strains present in the bent down tension bars and straight compression bars within specimens C4ALN1 and C4ALN3 at a beam load of 12 kN.

The strain in both tension bars peaked at the column face, at a value of around 800 με. The strain then rapidly reduced along the *top joint* region and around the *top bend.* The *vertical leg* section of both specimens was under slight tension along its full length.

The compression beam steel was under a maximum strain of around -400 με. This value reduced to zero within the joint.

Figure 4.1.3.3.4 displays the reinforcement strains present within these bars at specimen failure.

Both specimens exhibited joint failure. This extensive cracking within the joint was believed to have reduced the beam lever arm at the column face and caused yielding of the steel. Yielding occurred in both tension bars in the *top joint* region and the start of the *top bend.* Maximum recorded strains were 3580 με for specimen C4ALN1 and 4230 με for specimen C4ALN3.

Notably both *vertical legs* were under significant tension at specimen failure. The strain decayed reasonably linearly along both legs. An anchorage length of around 300 mm was required for this load transfer process.

The strain within the compression steel was at a maximum of around -800 με at a distance of around 200 mm from the column face. This compressive strain rapidly reduced over the region of the bar approaching the joint. Tensile strains were actually recorded for the region of this bar inside the joint zone.

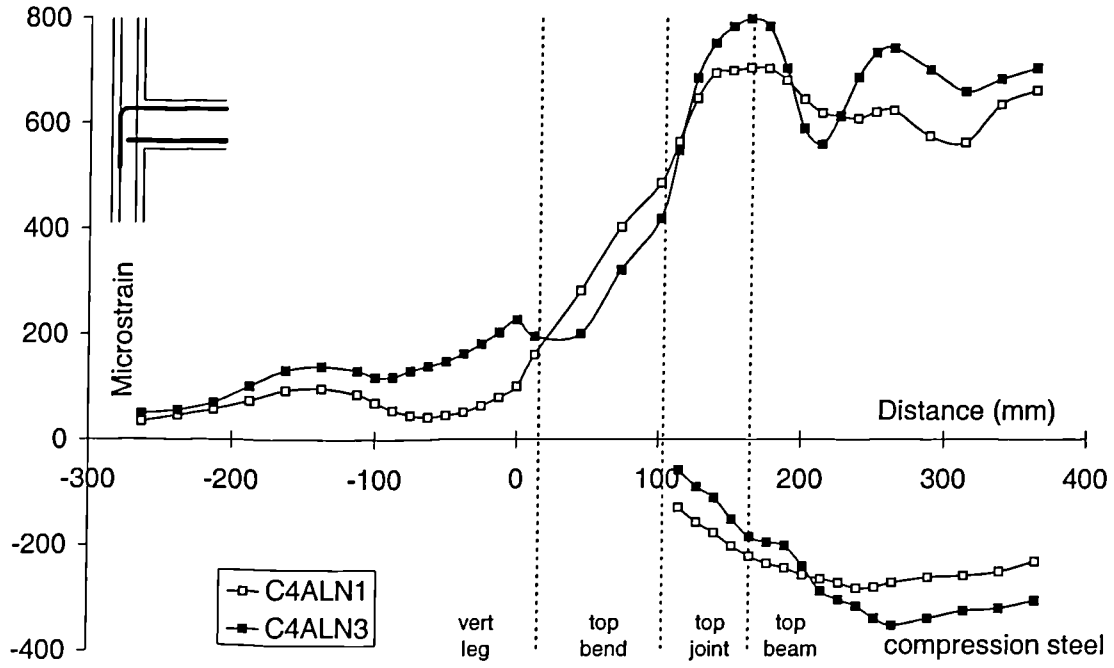

Figure 4.1.3.3.3 Bent down bar strains - 12 kN beam load

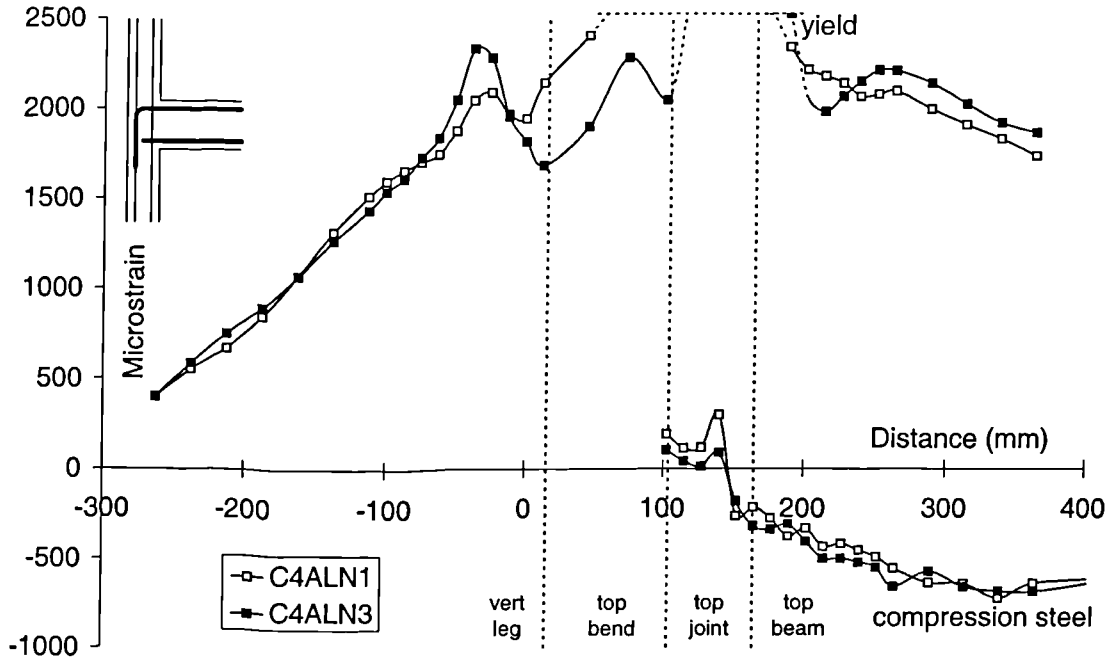

Figure 4.1.3.3.4 Bent down bar strains - specimen failure

U-bar beam steel

Figure 4.1.3.3.5 displays the reinforcement strains present within the U-bars within specimens C6LN1 and C6LN3 at a beam load of 12 kN.

The peak strain within both U-bars was around 800 με at the beam-column interface. This strain then rapidly deteriorated along the *top joint* region and around the *top bend.* This behaviour was very similar to that observed with the bent down beam steel detail at this load stage.

The strain distribution reduced reasonably linearly to around -400 με at the beam-column interface at the base of the beam. This compressive value was also comparable to that observed with the bent down beam steel detail.

Figure 4.1.3.3.6 displays the reinforcement strains present within these bars at specimen failure.

The peak strain in specimen C6LN1, which failed at a beam load of 25 kN, was around 1500 με. This tensile strain peaked at the column face and reduced most significantly around the *top bend* of the U-bar.

The beam steel within specimen C6LN3 had shown signs of yielding along the top joint region of the U-bar recording a maximum value of 3130 με. This yielding was believed to be as a result of extensive cracking within the joint.

By the end of the test tensile strains had progressed around the bends of both U-bars and into their nominally compressive regions. Again, as for the specimens with bent down steel detail, the maximum compressive strain occurred at a distance approaching 200 mm from the beam-column interface. This strain was around -400 με for specimen C6LN1 and -600 με for specimen C6LN3.

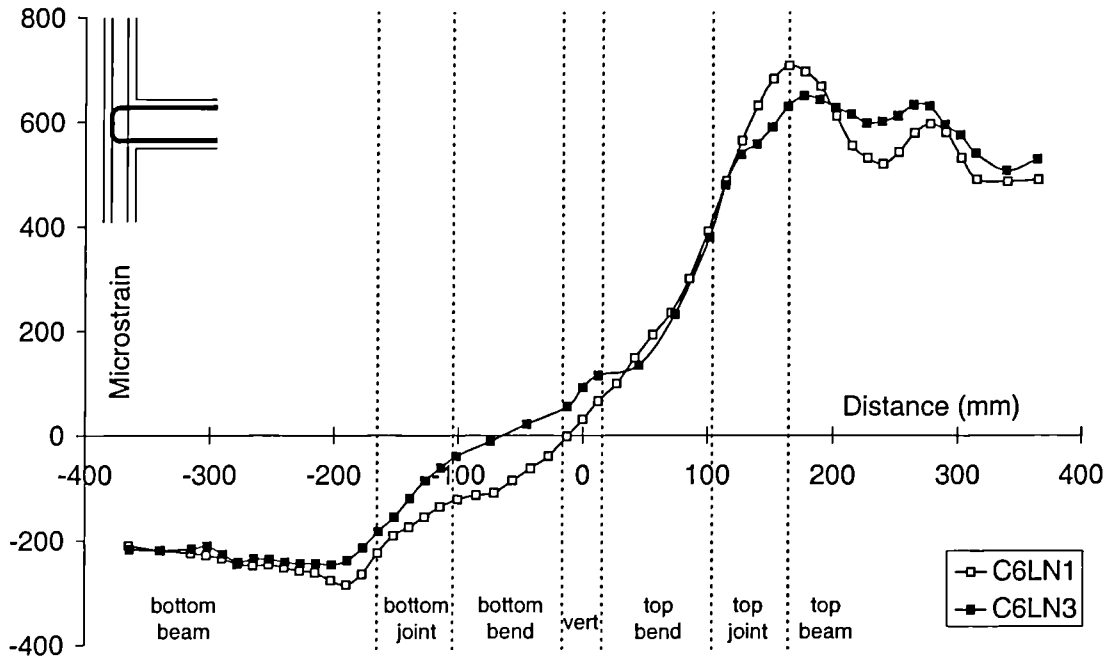

Figure 4.1.3.3.5 U-bar strains - 12 kN beam load

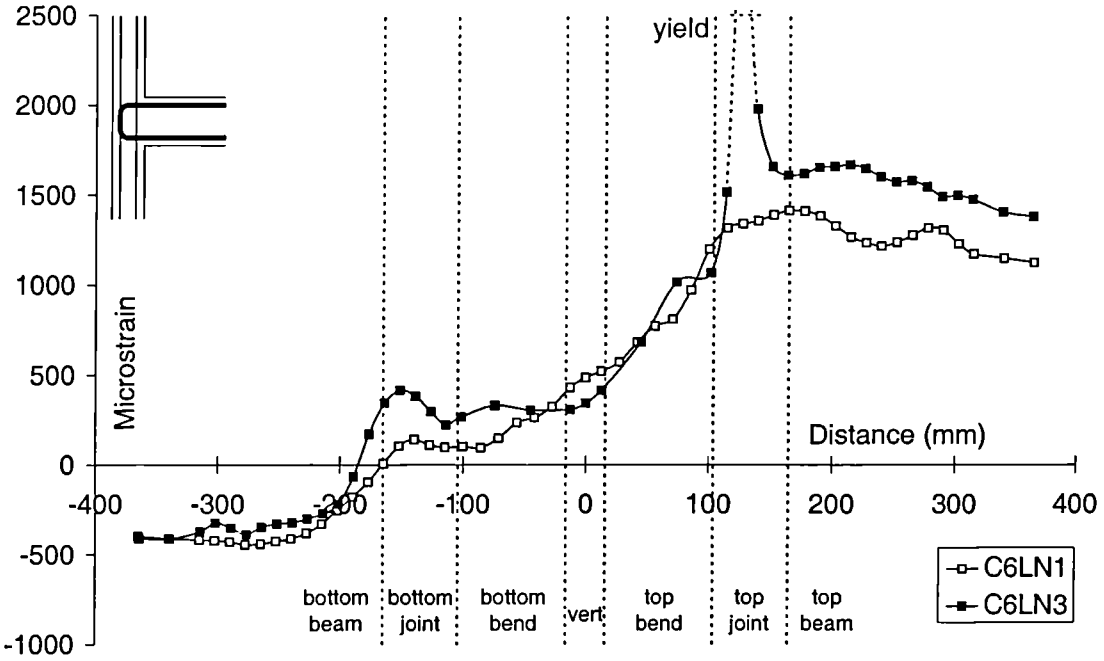

Figure 4.1.3.3.6 U-bar strains - failure

4.1.3.4 Joint ties

Only Reys de Ortiz [10] previously attempted to measure tie strains within a monotonic joint. Three of her specimens contained strain gauged joint ties. The technique of externally mounting a single strain gauge on the tie's surface was used, with the wiring from the gauge passing out through the concrete.

Within the author's investigation the more advanced technique of **internally** gauging joint ties was used (as outlined in Section 2.2.1). This technique had the advantage of allowing strain values to be recorded without disrupting the concrete-steel bond. Within this investigation twenty three of the forty nine monotonic specimens contained internally strain gauged ties. A gauged tie contained ten strain gauges, five in each of its main legs. Due to the unique nature of these readings all of the tie strain readings are presented within this thesis.

As it is joint behaviour that is under consideration, all applied beam loads have been converted to normalised shear stresses.

C4ALN1

Figure 4.1.3.4.1 displays the strains from the joint tie within specimen C4ALN1. Up to a normalised shear stress of around 0.6 $MPa^{0.5}$, the tie was under very little strain. Just prior to visible joint cracking these strains began to increase. At joint cracking the strain readings in the tie ranged from around 200 to 400 με. Most gauges recorded steadily increasing strains until specimen failure at around 1.4 $MPa^{0.5}$. By the end of the test the spread of strain readings was from around 1000 to 2000 με.

C6LN1

Figure 4.1.3.4.2 displays the strains from the joint tie within specimen C6LN1. The strain results displayed a similar distribution to those seen within C4ALN1. Again until a shear stress of around 0.6 $MPa^{0.5}$, the tie was under very little strain. Just prior

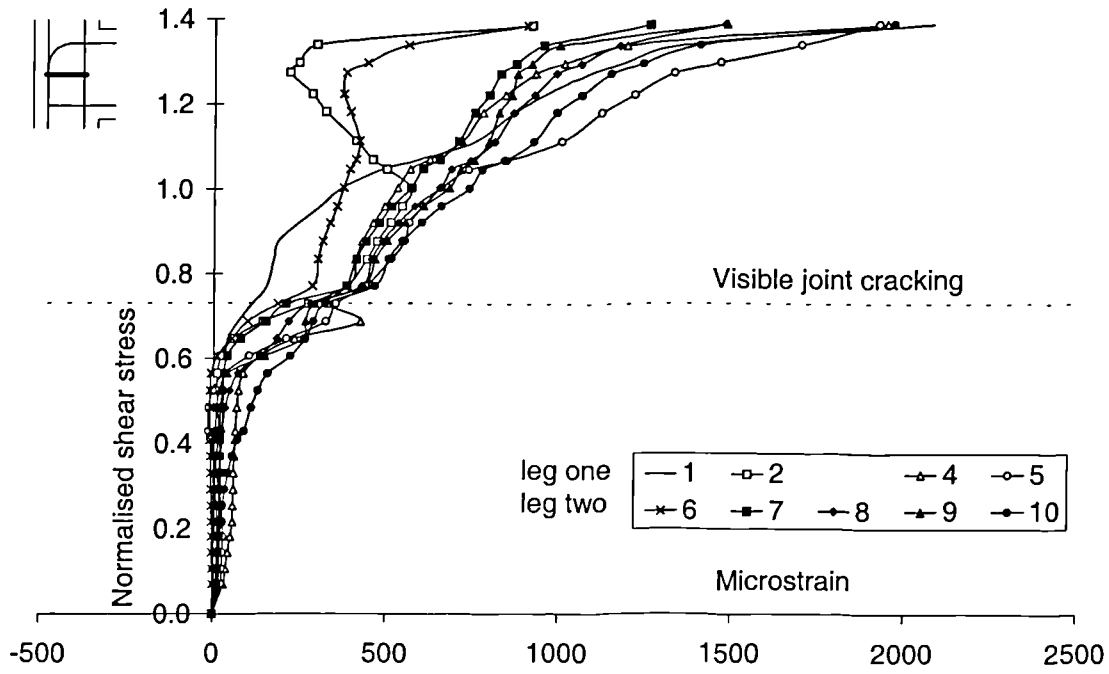

4.1.3.4.1 Tie strains - specimen C4ALN1

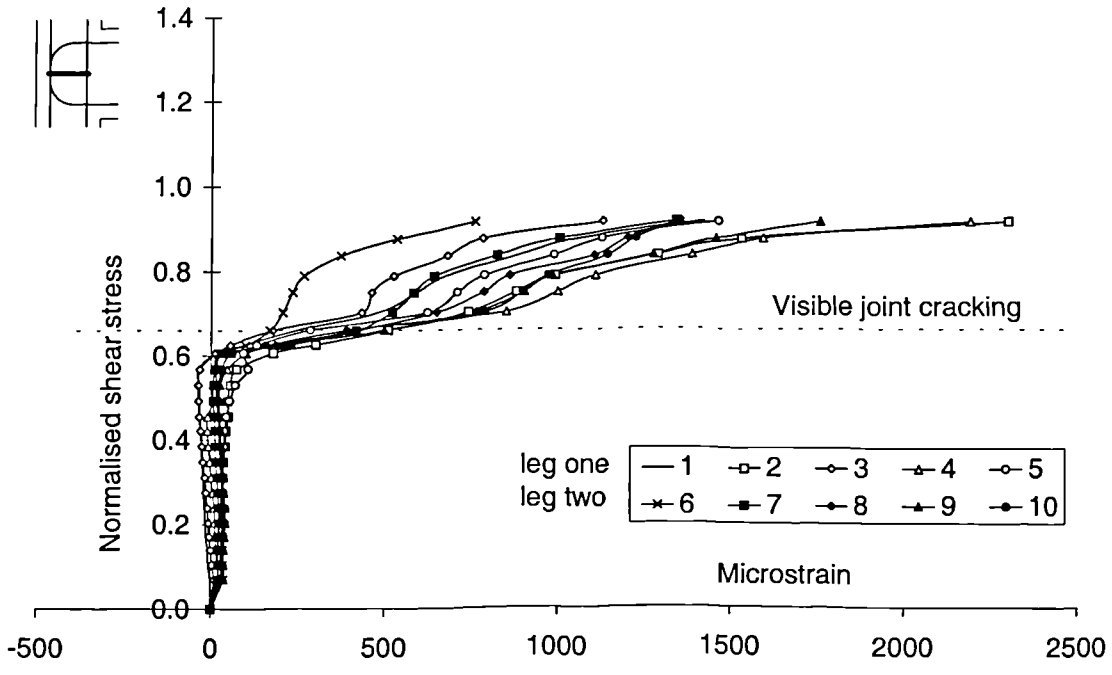

4.1.3.4.2 Tie strains - specimen C6LN1

to visible joint cracking the strains started to steadily increase. By the end of the test the spread of strain readings was large, from around 700 to 2200 με.

C4ALN3

Figure 4.1.3.4.3(a) displays the strains from the upper joint tie within specimen C4ALN3. A significant increase in strain occurred quite early in the load history and this increased throughout the test. There was evidence of slippage of gauges six to ten (*leg two*) at a normalised shear stress of around 1.3 $MPa^{0.5}$. The tie legs were smooth and were only bent through 90°. As a result of this, anchorage failure of these legs was a concern and was apparent when the strain values reduced despite the joint shear force increasing. The problem of slippage and the method of correction is considered in Section 4.5. Strains of over 2000 με were recorded in the gauges of *leg one.*

Figure 4.1.3.4.3(b) displays the strains from the middle joint tie within specimen C4ALN3. Very little strain was present within the tie prior to visible joint cracking. At joint cracking there was a significant development of strain of up to 500 με. The spread of strain at the end of the test ranged from 1000 με to yield and beyond (2900 με).

Figure 4.1.3.4.3(c) displays the strains from the lower joint tie within specimen C4ALN3. Again there was very little strain development until visible joint cracking. At specimen failure the strain values were generally around only 1000 με. This was significantly less than the values recorded within the two other ties. A strain of around 2500 με was recorded for gauge five. It is suggested that this gauge was coincident with a large crack as this resulted in the large jump of around 500 με at joint cracking.

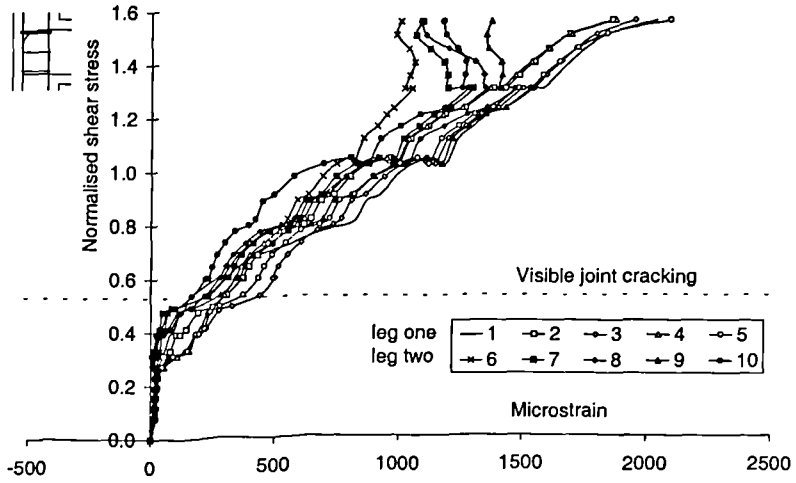

Figure 4.1.3.4.3(a) Tie strains - upper tie - C4ALN3

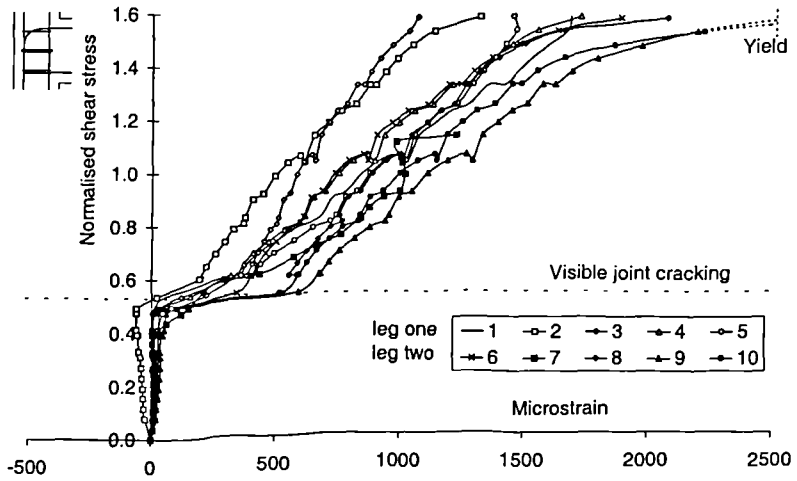

Figure 4.1.3.4.3(b) Tie strains - middle tie - C4ALN3

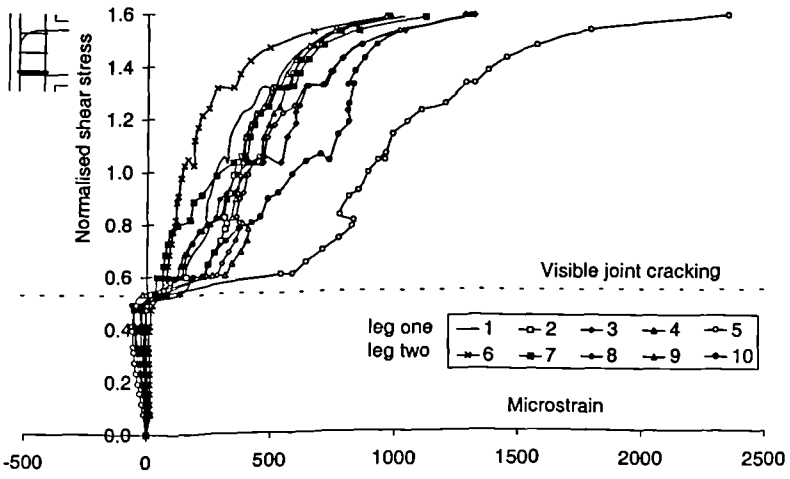

Figure 4.1.3.4.3(c) Tie strains - lower tie - C4ALN3

C6LN3

Figure 4.1.3.4.4(a) displays the strains from the upper joint tie within specimen C6LN3. Prior to visible joint cracking a significant amount of strain had already been developed. This strain continued to increase until yielding of *leg one* was recorded at failure (a maximum value of 5930 με). Slippage, as previously observed with specimen C4ALN3, was apparent in *leg two*. Quite a significant drop in strain was recorded with this leg at specimen failure.

Figure 4.1.3.4.4(b) displays the strains from the middle joint tie within specimen C6LN3. Again the strain development began prior to visible joint cracking. *Leg one* rapidly developed an increasing strain and had yielded prior to specimen failure (a maximum value of 4470 με). A very pronounced slip was recorded at the same load for *leg two*.

Figure 4.1.3.4.4(c) displays the strains from the lower joint tie within specimen C6LN3. Gauges eight and ten were damaged in the manufacturing process and thus are not displayed on the chart. The strain developed within this lower tie peaked at around 1200 με, this value was less than 50% of the strain developed in the upper and middle ties.

The strain results from specimens C4ALN3 and C6LN3 suggest that **a tie positioned in the middle or upper joint provides more enhancement to the joint capacity than a tie positioned in the lower joint**. Section 4.3.3 provides more detailed results regarding the positioning of joint ties.

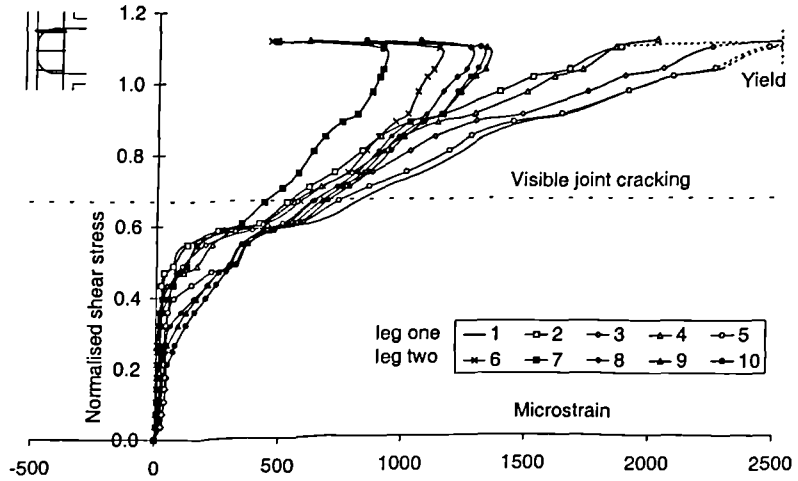

Figure 4.1.3.4.4(a) Tie strains - upper tie - C6LN3

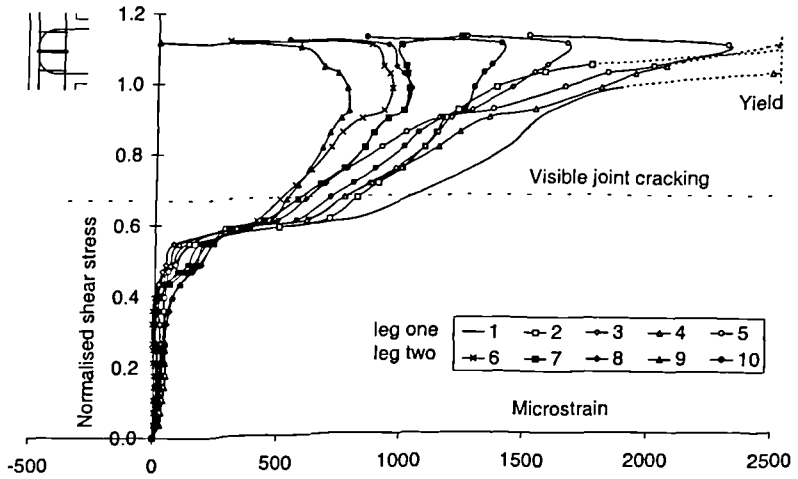

Figure 4.1.3.4.4(b) Tie strains - middle tie - C6LN3

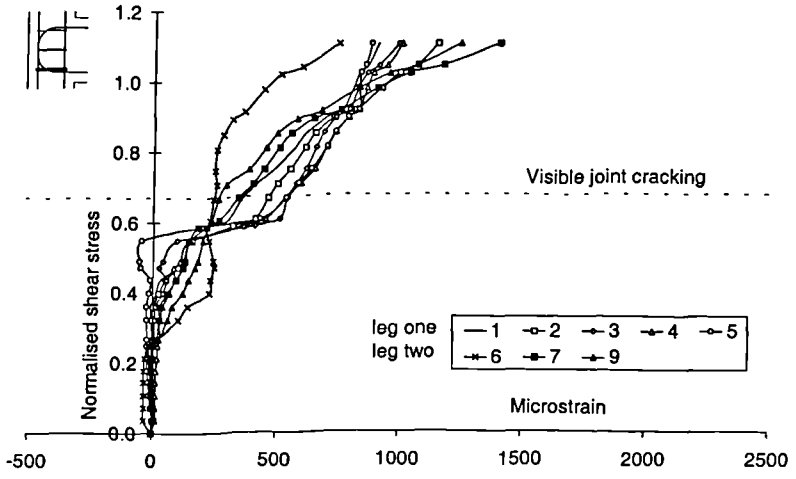

Figure 4.1.3.4.4(c) Tie strains - lower tie - C6LN3

4.1.4 Bond stress analysis

The force within a steel bar is transmitted into the surrounding concrete by the development of bond stresses around its perimeter. For deformed steel bars the majority of bond stresses are developed as a result of the effects of the ribs bearing on the concrete; friction and adhesion also contribute, but to a lesser extent. By considering bond stresses it is possible to achieve an improved insight into the behaviour of beam-column connections, in particular how load transfer by bond is influenced by beam reinforcement detail.

The bond stress between two points, a distance l apart, assuming a linear stress gradient is :

$$f_{ab} = \left(\frac{f_{s2} - f_{s1}}{l} \right) \frac{A_{bar}}{P_{bar}} \quad \text{.....(eq. 4.1.4.1)}$$

where f_{s1} is the axial force in the steel at the start of the considered stress gradient,

f_{s2} is the axial force in the steel at the end of the considered stress gradient,

A_{bar} is the cross sectional area of the bar,

P_{bar} is the perimeter of the bar.

In 1992 Scott [8] presented a detailed bond stress analysis from the results of his test programme of fifteen specimens. The additional results from the author's investigation enable further development of these initial findings.

Within this and Scott's investigation detailed assessments of bond stress distributions were made using the data obtained from the internally strain gauged main beam steel. This gave a unique understanding of the bar force transfer mechanisms within the joint of a reinforced concrete beam-column connection.

Within this investigation the bond stress analysis was conducted at two stages :

1. ***Prior to joint cracking*** - at an applied beam load of 12 kN, this corresponded to a peak strain of around 800 με in the main tension steel.
2. ***Approaching failure*** - at the load stage which corresponded to specimen failure or at a peak strain approaching 2500 με (yield).

This allowed comparisons between the method of load transfer for elastic specimen behaviour with the method of load transfer approaching failure.

The computer program AVBON (outlined in Section 2.4) was used to determine the stress gradient between each and every pair of strain gauges. However care was necessary when interpreting these results as the process considerably magnified even small perturbations in the stress data. More usefully, average bond stresses were determined. Average bond stresses were considered over regions where the strain gradients were elastic and essentially linear.

The strain gradient was calculated for these zones by minimising the square of the deviation from the y data values (a *least squares* fit). Bent down and U-bar steel details were considered separately. The considered steel regions were as defined in Figures 4.1.3.3.1 and 4.1.3.3.2. All axial stresses were evaluated from the bar strains using the stress-strain data from Section 2.1.2.

Bent down beam steel detail

Figure 4.1.4.1 displays the strains present within the beam tension steel, prior to joint cracking, for the specimens C4ALN1 and C4ALN3. As mentioned previously in Section 4.1.3.3 the strain distribution reached a peak at the beam-column interface, which then reduced almost to zero along the *top joint* and *top bend* regions. This region was where the beam's force was transmitted into the joint. The corresponding average bond stress, calculated as the average for both specimens, was 3.2 MPa.
Figure 4.1.4.2 displays the strains present within the beam tension steel, approaching failure, for the specimens C4ALN1 and C4ALN3. The strain distribution was

essentially linear from the top bend to a distance 300 mm down the anchor leg. Although the beam steel had almost yielded the average bond stress was still only 3.5 MPa.

Notably the steel along the *top joint* region had lost its ability to develop any useful anchorage. The cracking of the specimen in this region is visible in the photographs in Figure 3.1.3.and 3.1.4.

U-bar beam steel detail

Figure 4.1.4.3 displays the strains present within the beam tension steel, prior to joint cracking, for the specimens C6LN1 and C6LN3. At this stage of the load history the behaviour of the U-bar beam steel detail was very similar to that of the bent down beam steel detail. The load transfer from the beam into the joint again occurred along the *top joint* and *top bend* regions of the steel. The average bond stress developed over this region was 3.2 MPa which was the same value as for the specimens using bent down beam steel detail.

Figure 4.1.4.4 displays the strains present within the beam tension steel, approaching failure, for the specimens C6LN1 and C6LN3. The majority of the beam load was transferred into the joint around the *top bend* region. The very steep strain gradient over this region which corresponded to an average bond stress of 7.8 MPa is apparent. A smaller amount of the load transfer was possible around the *vertical leg* and *bottom bend* regions which developed an average bond stress of 1.9 MPa.

Again, as for the bent down beam steel detail, the U-bar lost its ability to develop bond stress along its top joint region.

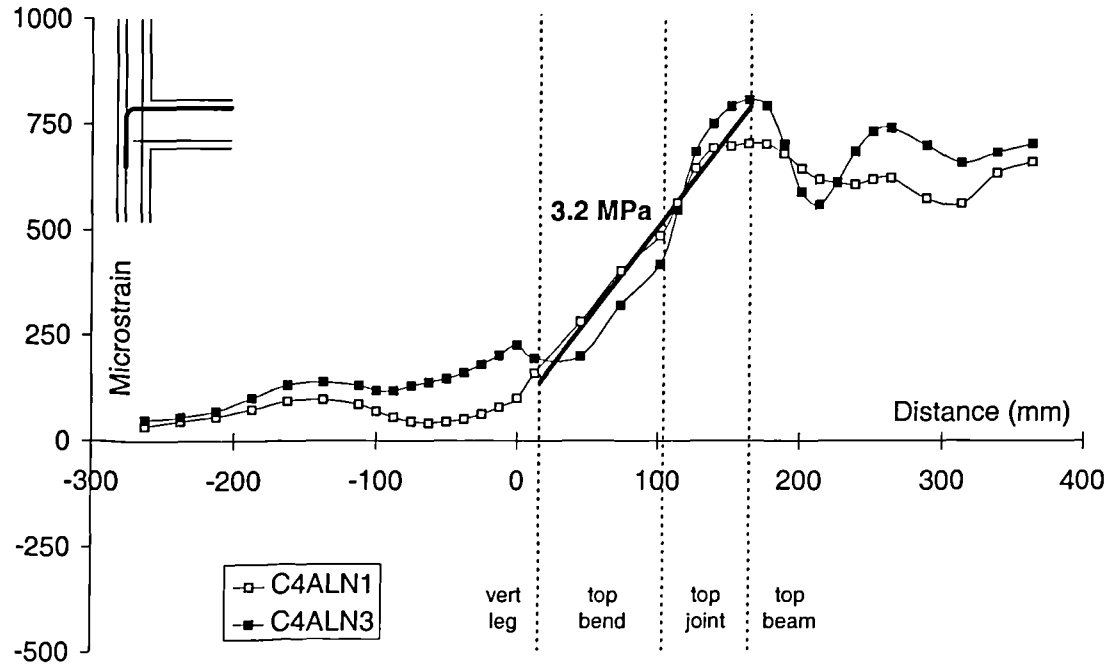

Figure 4.1.4.1 Bent down bar - average bond stresses - prior to joint cracking

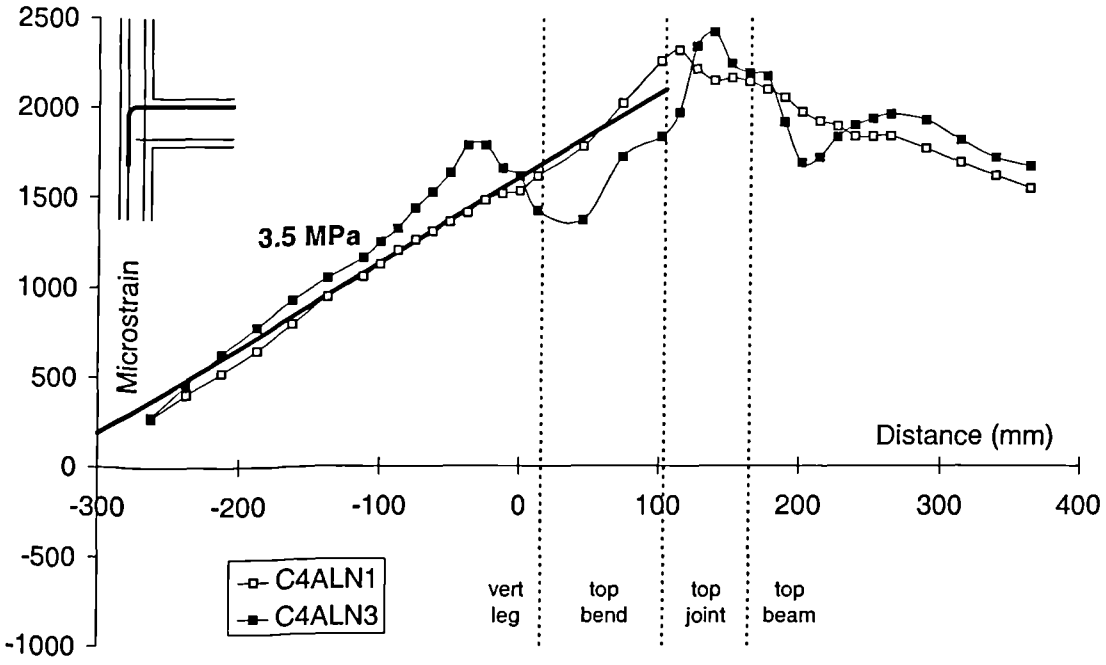

Figure 4.1.4.2 Bent down bar - average bond stresses - approaching failure

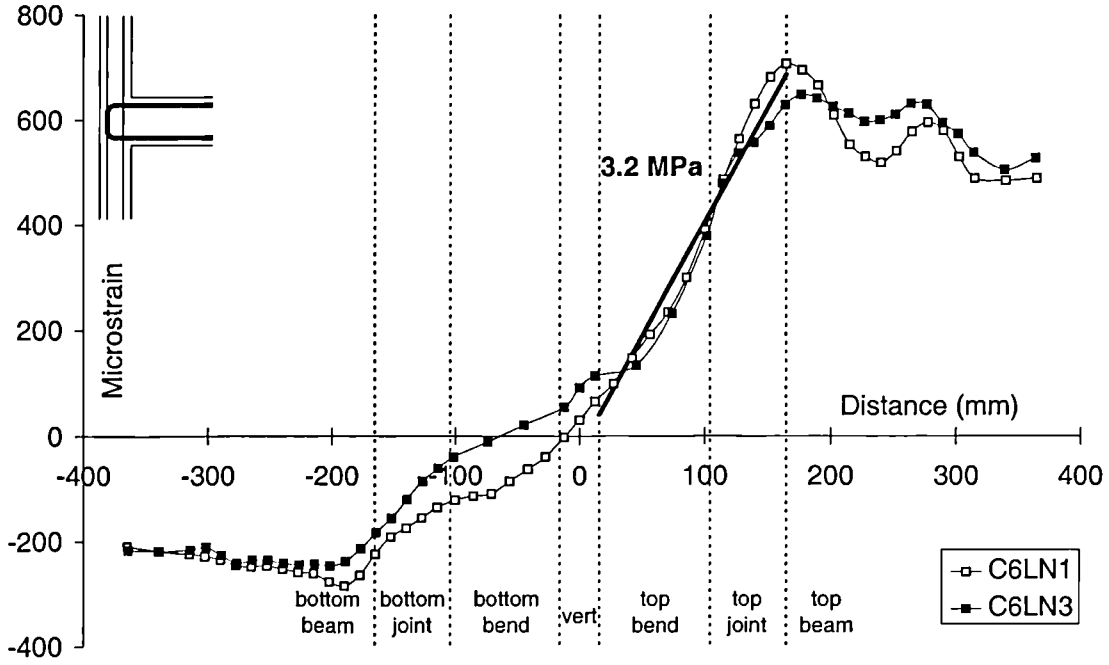

Figure 4.1.4.3 U-bar - average bond stresses - prior to joint cracking

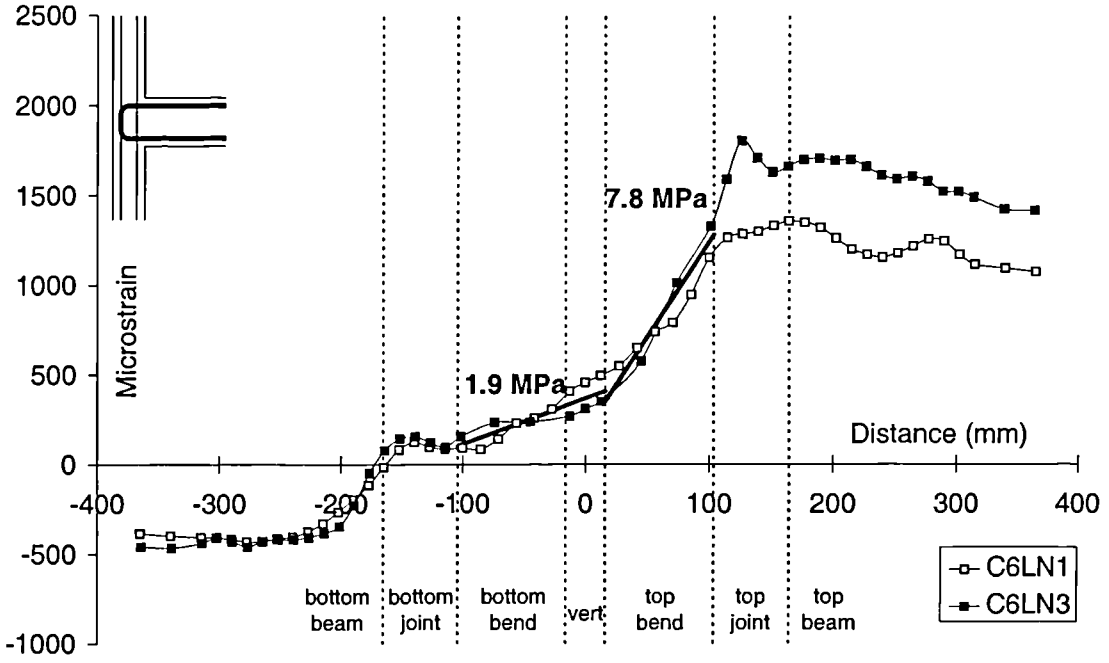

Figure 4.1.4.4 U-bar - average bond stresses - approaching failure

Both beam steel details behaved similarly over the initial load stages. However, after joint cracking the bent down beam steel detail utilised its vertical leg to transfer the beam's force into the lower column. The U-bar beam steel detail transferred all of the beam's force into the joint region and the majority of this load transfer took place around its top bend. This would suggest why specimens with U-bar beam steel had a lower joint capacity than specimens with bent down beam steel.

For this standard test series, using U-bar beam steel anchorage reduced the ultimate shear capacity of the joint by an average of 18%.

4.1.5 Bearing stress analysis

Values of bearing stress around the top bend of the beam rebar were evaluated for the fully strain gauged specimens. The value of bearing stress was calculated using the following equation :

$$\sigma_b = \frac{F_{bt}}{r\phi} \quad \text{.....(eq. 4.1.5.1)}$$

where F_{bt} is the tensile force in the bar,

r is the radius of the bend (which was equal to 3ϕ for this investigation),

ϕ is the bar diameter.

Equation (50) of BS 8110 [3] states an upper limit of bearing stress of :

$$\sigma_{b(lim)} = \frac{2f_{cu}}{\left[1+2\left(\phi / a_b\right)\right]} \quad \text{.....(eq. 4.1.5.2)}$$

where a_b is the cover to the reinforcement plus ϕ,

this expression contains a factor of safety, however doubts exist regarding the magnitude of this.

Table 4.1.5 displays the values of bearing stress under the top bend of the beam rebar at failure. Values were calculated at the start (σ_{b1}) and the end (σ_{b2}) of each bend.

Table 4.1.5 Bearing stresses within the top bend of the beam rebar

Specimen	σ_{b1} (MPa)	σ_{b2} (MPa)	$\sigma_{b(lim)}$ (MPa)	$\sigma_{b(max)}/\sigma_{b(lim)}$
C6LN1	60	29	84	0.72
C6LN3	54	18	80	0.67
C4ALN1	127 (Y)	105	75	1.66
C4ALN3	67	94	68	1.38

Notes

1. The stress values were evaluated from the experimental strain readings using the stress-strain data displayed in Section 2.1,
2. Y - indicates that the steel had yielded.

Table 4.1.5 shows that the two specimens with U-bar beam steel detail had bearing stress values well below that permitted by BS 8110 equation (50) at failure.

Specimen C4ALN1 exhibited yield at the start of its top bend. The bearing stress value which corresponded to yield, even taking into consideration the factor of safety, was higher than permitted by BS 8110 equation (50).

This suggests that higher bearing stresses than permitted by BS 8110 may be tolerated by the provision of ties rather than large radius bends.

4.1.6 Stresses within the joint ties

As the joint ties were smooth and did not have ribs, it was believed that less significant bond was possible between them and the concrete. The majority of the tensile force within the tie was transferred through bearing of its legs on the column rebars. As previously shown in Section 4.1.3.4 slippage of these legs was possible and in certain cases the value of strain in all five gauges within a leg reduced.

Although there was only a small amount of bond developed between the tie legs and the concrete the strain within each leg of the tie was not constant. Fluctuations as large as 1000 to 2300 με were observed within tie legs at specimen failure. It is believed that these fluctuations were due to bending stresses induced by dowel behaviour of the tie as demonstrated in Figure 4.1.6.

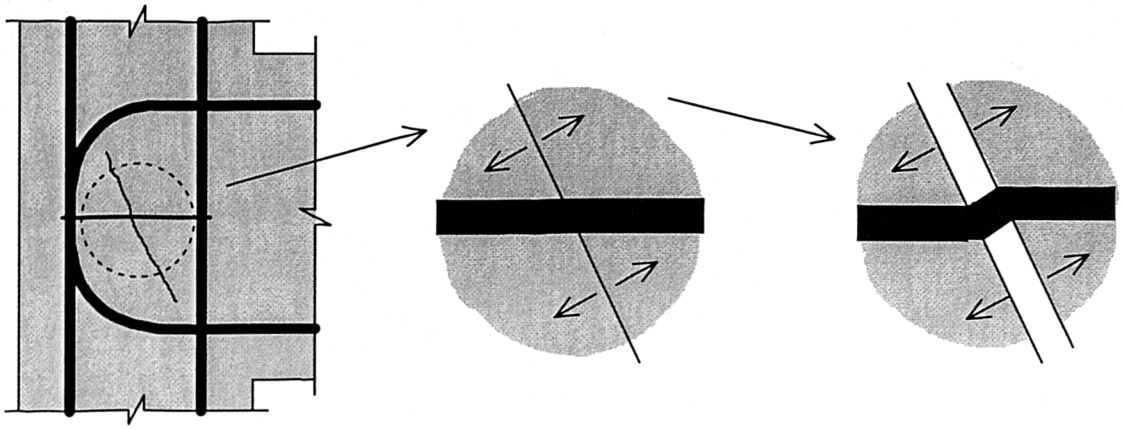

Fig 4.1.6 Dowel action of the joint ties

Figure 4.1.6 shows that after a crack forms, the crack faces attempt to pull apart causing bending (*kinking*) of the tie. When the crack is first formed this effect is small due to resistance from aggregate interlock. However, as the crack widens the influence of aggregate interlock reduces and the tie is subjected to increased bending stresses. Depending on the positioning of a strain gauge within the tie the value of strain will increase or decrease. A strain gauge located at the position of a crack may give a value of strain significantly larger than other gauges in the same leg. **Similarly it may be possible for a gauge to record a compressive value even though the tie leg is in overall tension.**

4.2 High Strength Specimens

This section considers the results from the eight **high strength** specimens. The parameters investigated were the **number of joint ties** and the **beam tension steel anchorage detail**. The only difference between the specimens in this test series and the *standard* test series was the strength of the concrete. The high strength concrete had a compressive cube strength of around 120 MPa, twice that of the normal strength concrete. The specimen details are given below in Table 4.2.

Table 4.2 *High strength* specimen details

Specimen	Gauging	Beam steel anchorage	No. of joint ties	f_{cu} (MPa)
C4ALH0	-	Bent down	0	130
C4ALH1	Full	Bent down	1	119
C4ALH3	Full	Bent down	3	132
C4ALH5	Middle tie	Bent down	5	123
C6LH0	-	U-bar	0	126
C6LH1	Full	U-bar	1	127
C6LH3	Full	U-bar	3	121
C6LH5	-	U-bar	5	125

4.2.1 Initial joint cracking

Figure 4.2.1.1 shows the normalised shear stress values for the eight specimens at initial joint cracking. These results were previously displayed in Table 3.2.2.

Figure 4.2.1.1 displays no evidence to suggest that the joint cracking capacity was influenced by the number of ties present within the joint. Even with the maximum number of five joint ties there was still insufficient additional volumetric steel to provide an increased resistance to initial joint cracking. This is consistent with the results from the *standard* test series.

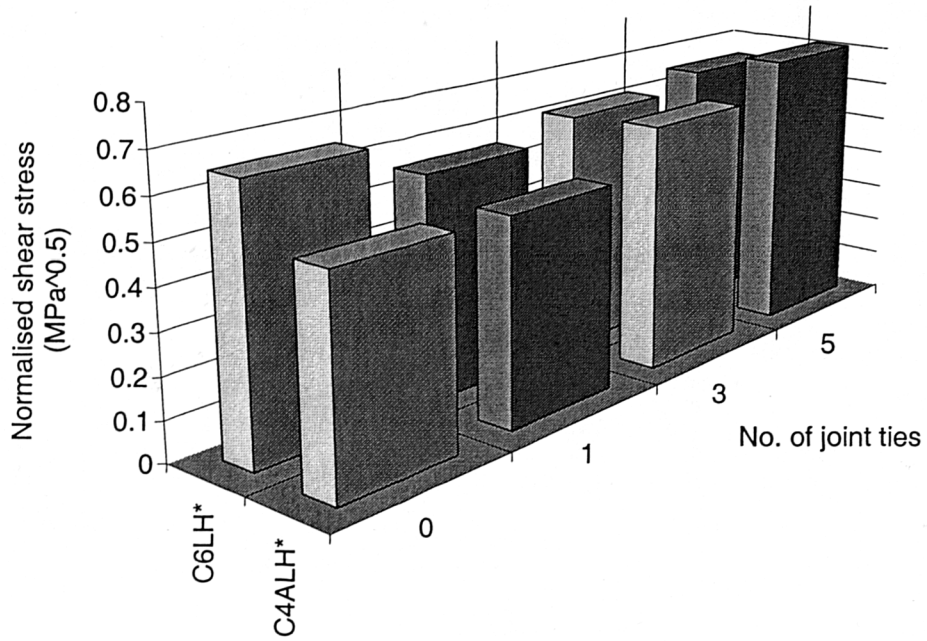

Figure 4.2.1.1 Shear stress at initial joint cracking - high strength specimens

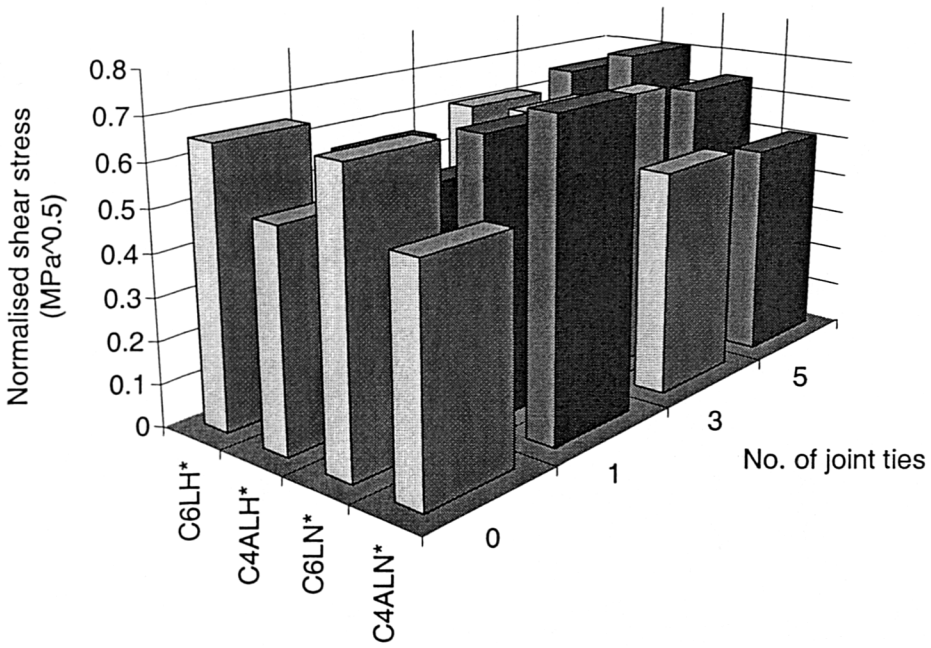

Figure 4.2.1.2 Joint cracking - standard / high strength comparisons

Figure 4.2.1.2 displays the shear stress values at initial joint cracking for both the *standard* specimens and the *high strength* specimens. There is no evidence from these results to indicate that specimens using high strength concrete behaved in a way different from specimens using normal strength concrete.

For the high strength specimens, initial joint cracking occurred at an average normalised shear stress value of 0.59 $MPa^{0.5}$ for specimens with bent down beam steel detail compared with 0.62 $MPa^{0.5}$ for specimens with U-bar beam steel detail. These values are similar to those from the *standard* test series.

Again it would appear that specimens with U-bar beam steel detail have a slightly higher resistance to initial joint cracking than specimens with bent down beam steel. The fact that specimens with U-bar beam steel had slightly more volumetric ribbed steel within the joint was perhaps the reason for this.

4.2.2 Specimen failure

Figure 4.2.2.1 shows the shear stress values for the eight high strength specimens at failure. These results were previously displayed in Table 3.2.2. Five out of the eight specimens had a sufficient joint capacity to exhibit beam flexural failure. This unfortunately meant that the joint strength of these five specimens was not established.

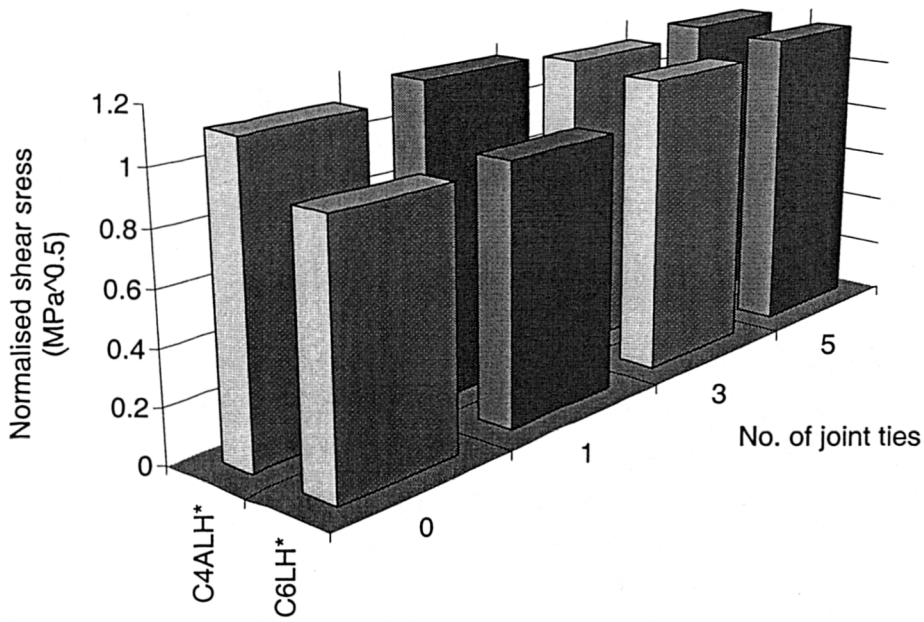

Figure 4.2.2.1 Shear stress at failure - high strength specimens

Figure 4.2.2.1 shows that specimens with bent down beam steel detail performed better than specimens with U-bar beam steel detail. This is consistent with the results from the *standard* test series. The performance of both beam steel anchorage methods is considered further in Section 4.2.4 (*Bond Stress Analysis*).

Figure 4.2.2.2 compares the three high strength specimens which exhibited joint failure with their corresponding *standard* specimens.

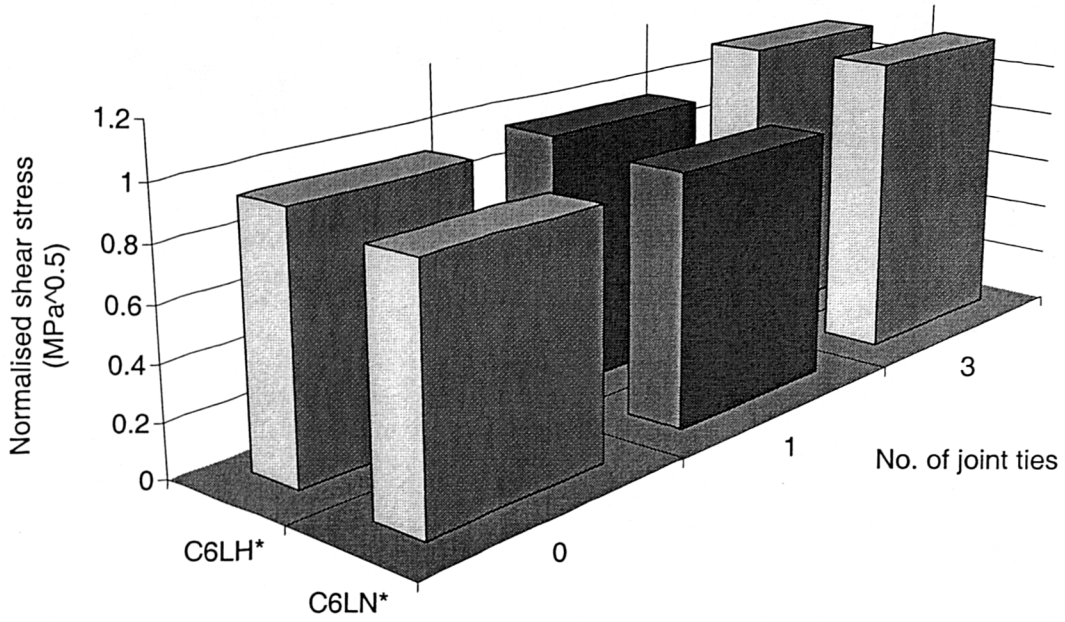

Figure 4.2.2.2 Shear stress at failure - standard / high strength comparisons

Again there is no evidence from these results to indicate that specimens using high strength concrete behaved in a way different from specimens using normal strength concrete.

4.2.3 Reinforcement strains

Reinforcement strains are presented for the four fully strain gauged specimens and for the gauged tie present within specimen C4ALH5.

The number of strain gauges present and their gauge layout were the same as for the corresponding specimens from the *standard* test series.

4.2.3.1 Outer column bars

Figure 4.2.3.1.1 displays the reinforcement strains present in the outer column bars at a beam load of 18 kN. At this stage the specimens were essentially elastic in behaviour.

Figure 4.2.3.1.1 shows that at the top and base of the column the reinforcement was in compression with strains of around -100 με. The shape of the strain distributions was very similar for all four specimens. The force transmitted from the beam into the joint pulled the region of the bar in the lower column into tension. Consequently the strain in the upper part of the column was forced into further compression. The magnitude of the strains at this stage however was reasonably small with maximums of around -400 με in the upper column and 200 με in the lower column.

Figure 4.2.3.1.2 displays the reinforcement strains present in the same bars at specimen failure. Strains approaching 1000 με were recorded in the lower column.

The region of tensile strain in the outer column bar advanced into the regions above the joint for the specimens with U-bar beam steel detail (C6LH1 and C6LH3). The region of tensile strain remained below the mid-height of the column bar for the specimens with bent down beam steel detail. This is the same trend seen for the outer column bars from the *standard* test series.

This confirms the previous suggestions in Section 4.1.3.1 that the bent down beam steel's anchor leg allowed the majority of force transfer to occur below the level of the joint. This contributed towards the specimens with bent down beam steel detail achieving a greater joint capacity.

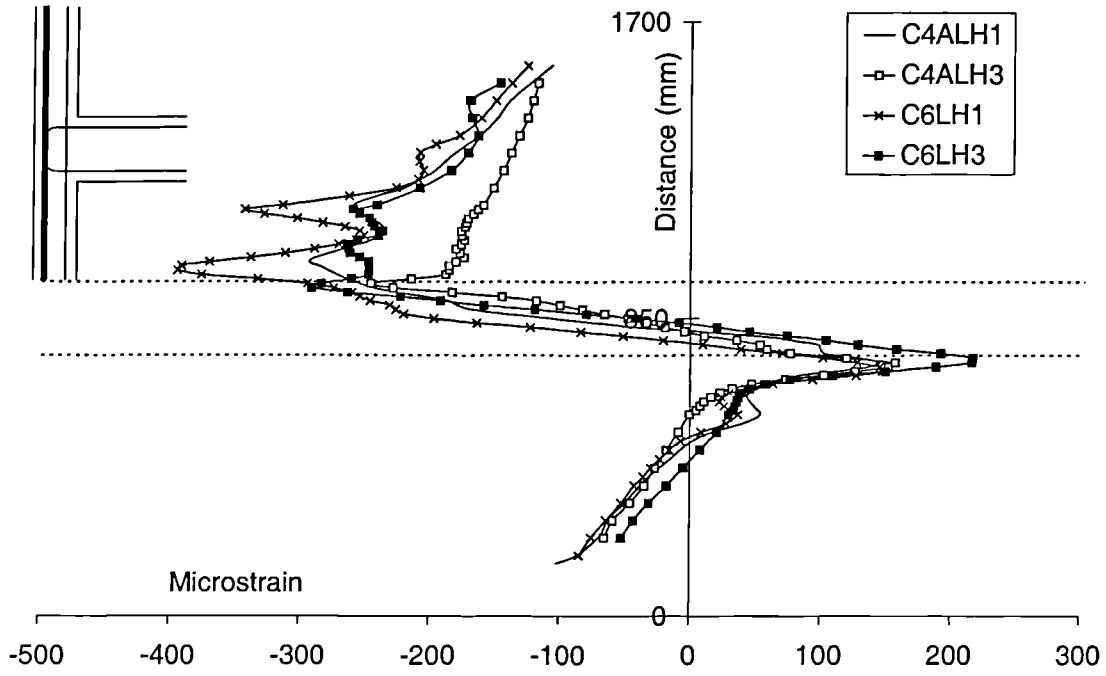

Figure 4.2.3.1.1 Outer column strains - 18 kN beam load

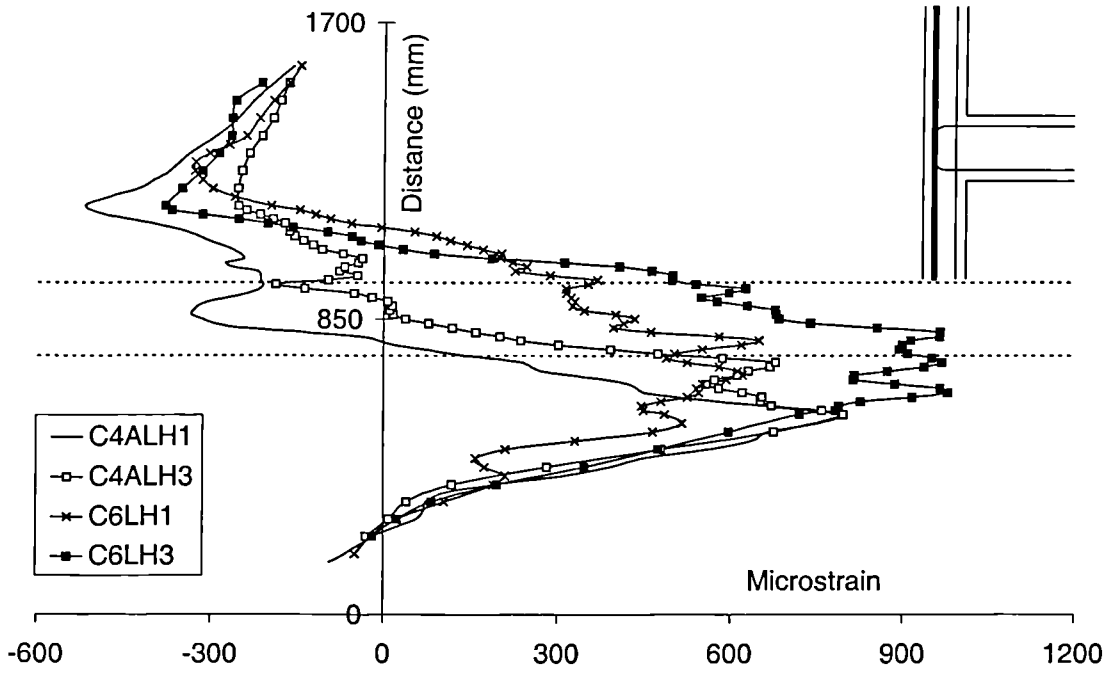

Figure 4.2.3.1.2 Outer column strains - specimen failure

4.2.3.2 Inner column bars

Figure 4.2.3.2.1 displays the reinforcement strains present in the inner column bars at a beam load of 18 kN.

The inner bars, like the outer bars, were in compression at the top and base of the column and strains of around -100 με were recorded. As expected, the strain distributions were complementary to those seen for the outer column bars. The force transmitted from the beam into the joint region had pulled the upper column into tension. Consequently, the lower column was forced into further compression. As the specimens were still reasonably elastic at this stage the magnitude of the strains in the inner column bar was similar to that seen for the outer column bar with numerical maximums of around 400 με.

Figure 4.2.3.2.2 displays the reinforcement strains present in these inner column bars at specimen failure. The shape of the distributions remained similar but the magnitude of the strain in tension considerably increased. The value of these strains ranged from around 1500 με to yield and beyond (3130 με).

The inner column bar of C6LH3 yielded whereas the inner column bar of C4ALH1 and C4ALH3 did not, even though their failure loads were lower. This was the same trend as for the corresponding *standard* specimens. This is more evidence to suggest that the vertical leg of the bent down beam steel transfers the applied load into the lower column and not just into the joint region.

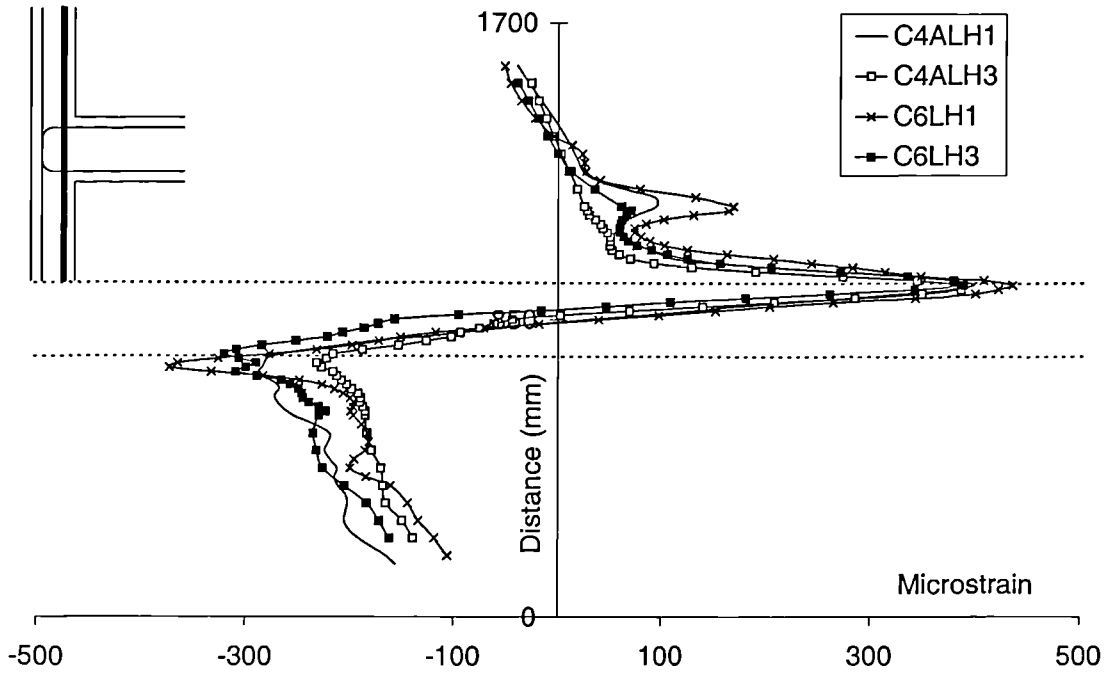

Figure 4.2.3.2.1 Inner column strains - 18 kN beam load

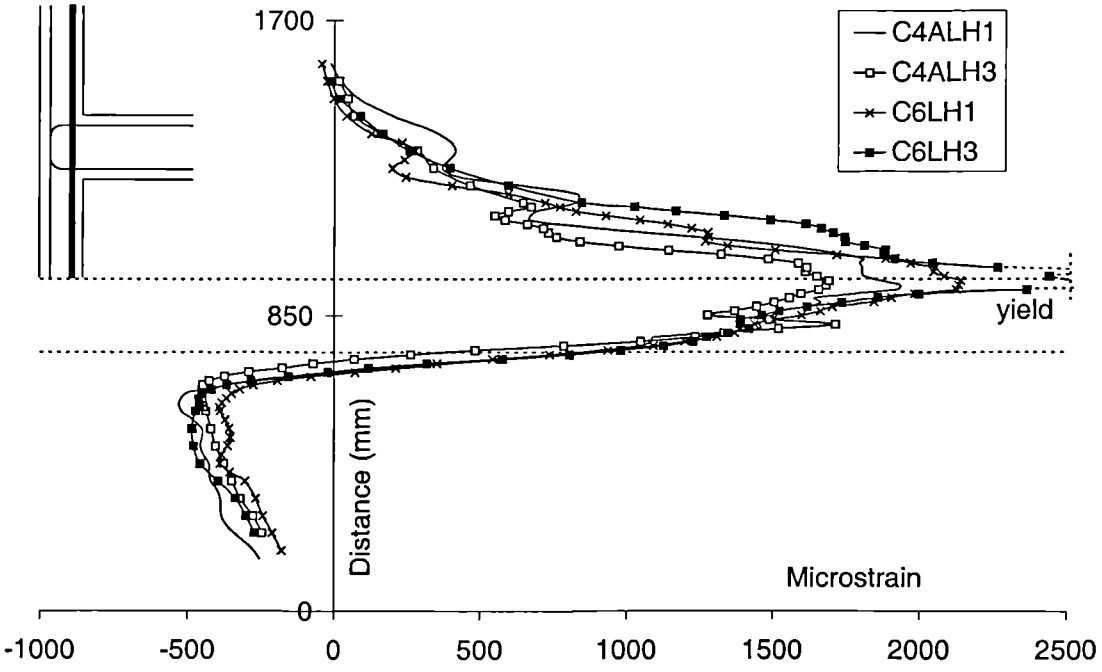

Figure 4.2.3.2.2 Inner column strains - specimen failure

4.2.3.3 Beam bars

The strain distributions from the beam steel reinforcement were considered in the same regions as previously defined in Figure 4.1.3.3.1 and 4.1.3.3.2.

Bent down beam steel

Figure 4.2.3.3.3 displays the reinforcement strains present in the bent down tension bars and the straight compression bars within specimens C4ALH1 and C4ALH3 at a beam load of 18 kN.

The strain in both tension bars peaked at the column face at a value of around 1200 με. The strain then rapidly reduced over the *top joint* region and around the *top bend.* The *vertical leg* section of both specimens was only under slight tension along its full length.

The compression beam steel was under a maximum strain of around -500 με. This value reduced to zero within the joint.

Figure 4.2.3.3.4 displays the reinforcement strains present within these bars at specimen failure.

Both specimens exhibited beam flexural failure. Gross yielding took place over the *top joint* region and extended to a distance around 200 mm from the column face. The maximum recorded strains were 17 100 με for C6LH1 and 7 200 με for C6LH3. Both vertical legs were under significant tension at specimen failure and an anchorage length of around 300 mm was required for the load transfer.

The strain within the compression steel was at a maximum of -1000 με at a distance around 200 mm from the column face. Fluctuations of tensile strains of around 500 με were recorded in the compression bar within the region of the beam at the column interface.

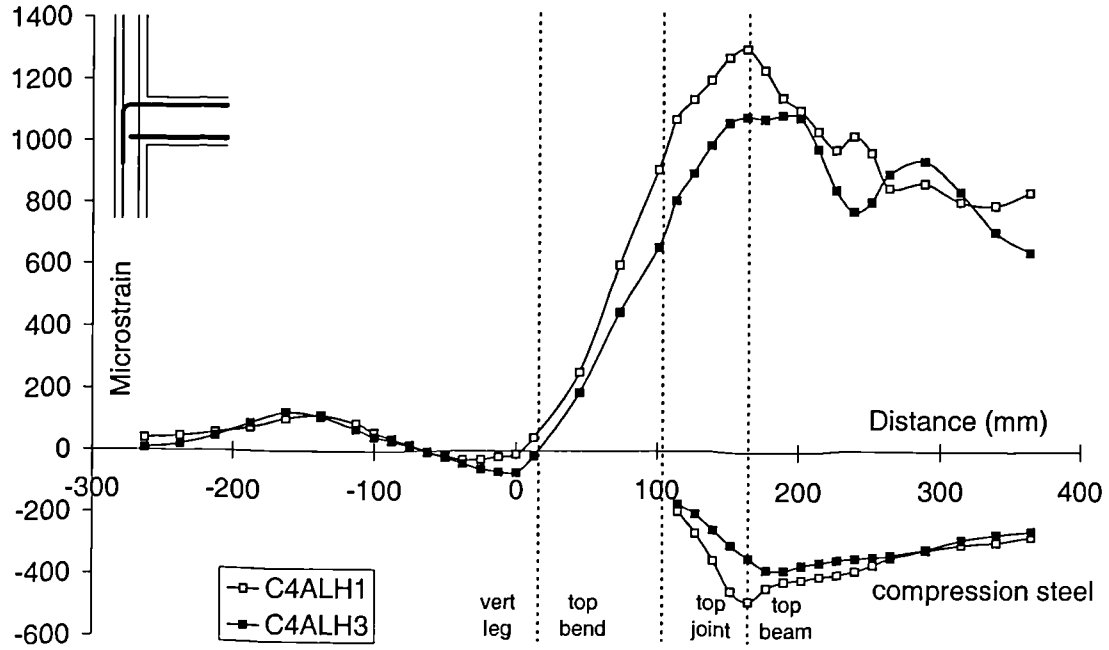

Figure 4.2.3.3.3 Bent down bar strains - 18 kN beam load

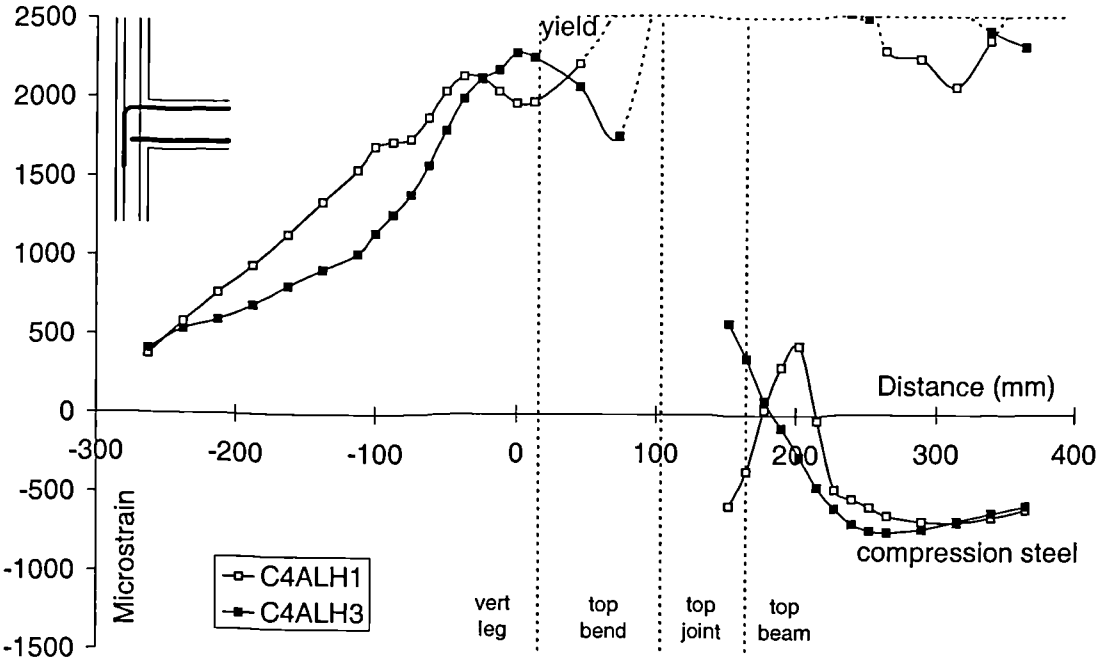

Figure 4.2.3.3.4 Bent down bar strains - specimen failure

U-bar beam steel

Figure 4.2.3.3.5 displays the reinforcement strains present within the U-bars within specimens C6LN1 and C6LN3 at a beam load of 18 kN.

The peak strain within both U-bars was around 1200 με at the beam-column interface. This strain then rapidly deteriorated along the *top joint* region and around the *top bend.* This behaviour was very similar to that observed with the bent down beam steel detail at this load stage.

The strain distribution reduced reasonably linearly to around -400 με at the beam-column interface at the base of the beam. This compressive value was also comparable with that observed with the bent down beam steel detail.

Figure 4.2.3.3.6 displays the reinforcement strains present within these bars at specimen failure.

Both U-bars had yielded along the *top joint* region, this strain reduced to around 500 με by the end of the *top bend* of the steel. Both specimens exhibited extensive joint cracking at failure. The maximum recorded strains were 6 590 με for C6LH1 and 8 280 με for C6LH3.

The strain within the lower region of the beam was at a maximum of around -500 με at a distance approaching 200 mm from the beam-column interface. Again the value of strain at the column interface was around zero.

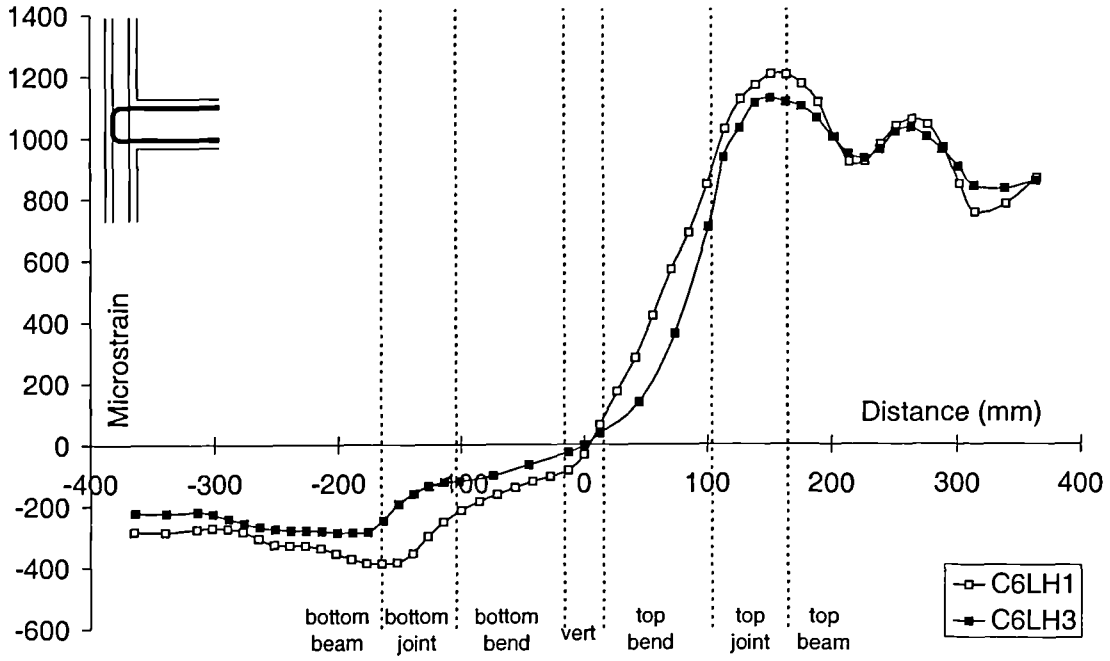

Figure 4.2.3.3.5 U-bar strains - 18 kN beam load

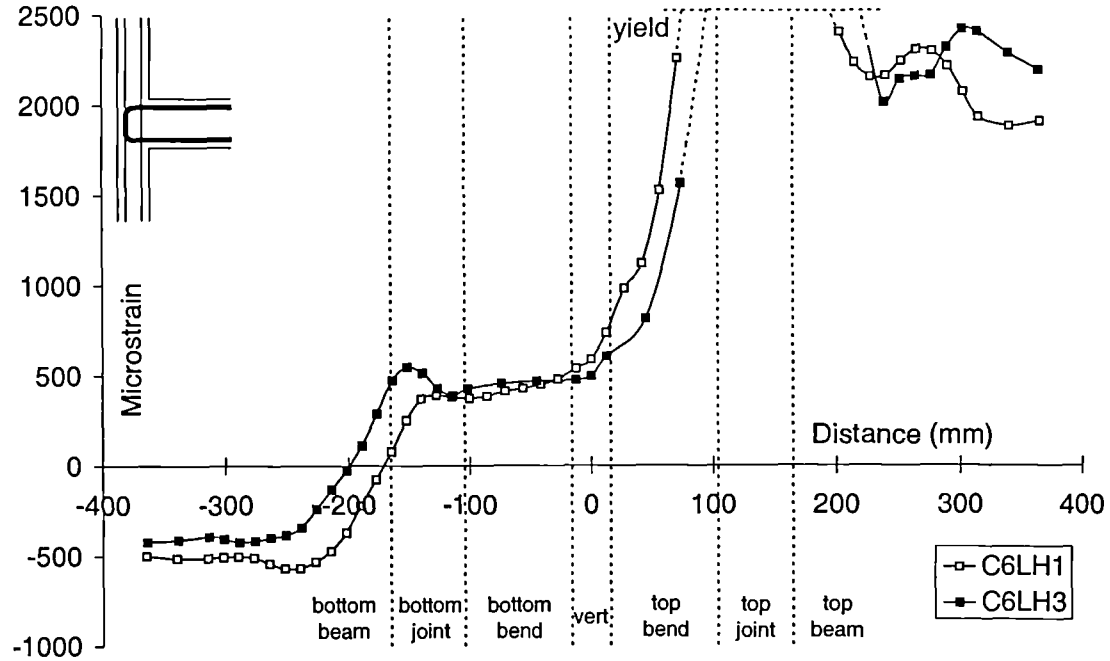

Figure 4.2.3.3.6 U-bar strains - specimen failure

4.2.3.4 Joint ties

C4ALH1

Figure 4.2.3.4.1 displays the strains from the joint tie within specimen C4ALH1. Up to a normalised shear stress of around 0.5 $MPa^{0.5}$ the tie was under very little strain. At visible joint cracking this strain suddenly began to increase. Most gauges recorded steadily increasing strains until specimen failure at around 1.2 $MPa^{0.5}$. By the end of the test the spread of strain readings ranged from around 1500 με to yield and beyond (2750 με).

C6LH1

Figure 4.2.3.4.2 displays the strains from the joint tie within specimen C6LH1. Again, up to visible joint cracking the tie was under very little strain. After joint cracking this strain rapidly increased. Yielding of both legs occurred at around 80% of the failure load. At specimen failure eight of the ten gauges had yielded. The highest recorded strain value was 16300 με.

C4ALH3

Figure 4.2.3.4.3(a) displays the strains from the upper joint tie within specimen C4ALH3. A significant increase in strain occurred quite early in the load history and this continued throughout the test. The spread of strain by the end of the test ranged from around 1500 με to yield and beyond (2610 με). Gauge six independently developed a compressive strain after joint cracking. It is believed that this behaviour was due to the cracking effects outlined previously in Section 4.1.6.

Figure 4.2.3.4.3(b) displays the strains from the middle joint tie within specimen C4ALH3. Very little strain was present within the tie prior to visible joint cracking. At joint cracking there was a significant development of strain by as much as 1200 με. At a normalised shear stress of around 0.9 $MPa^{0.5}$ both legs of the tie

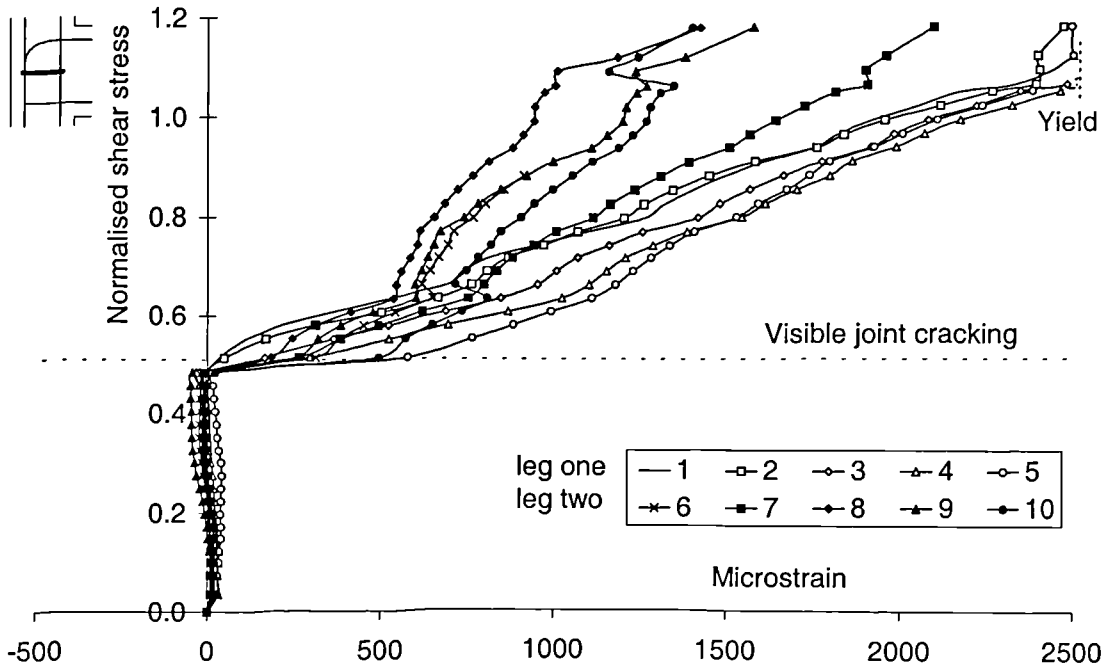

4.2.3.4.1 Tie strains - specimen C4ALH1

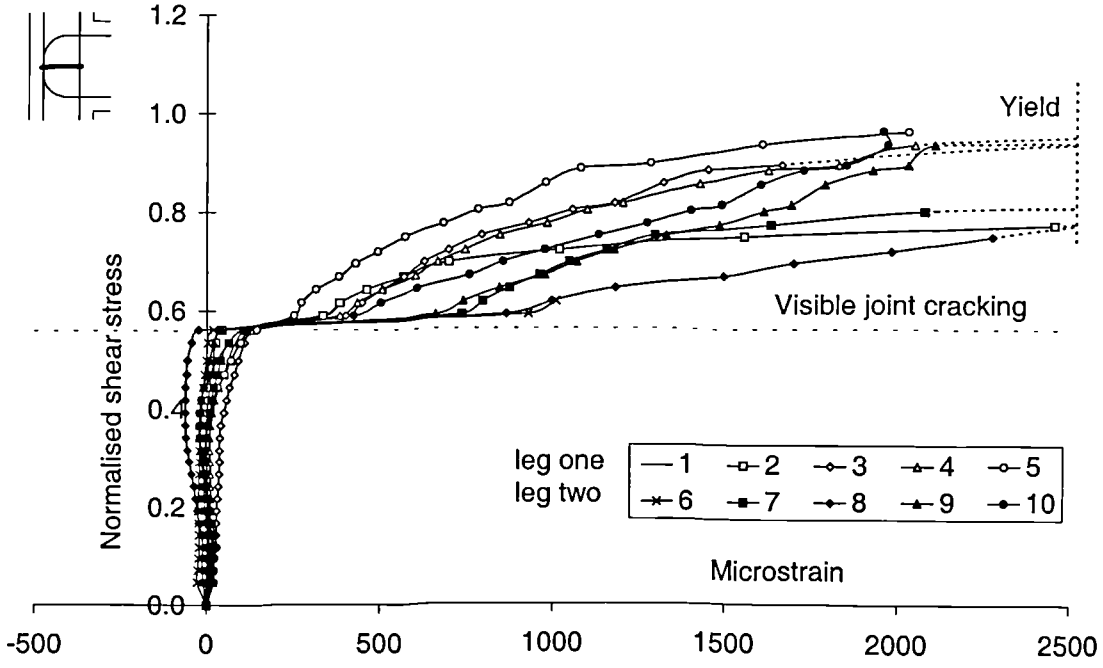

4.2.3.4.2 Tie strains - specimen C6LH1

displayed signs of major slippage. There was a large spread of strain values by the end of the test. Gauge one developed a compressive strain similar to that recorded by gauge six in the upper tie. As both gauges lay on the same plane this would appear reasonable and would suggest that there was not a fault with either gauge.

Figure 4.2.3.4.3(c) displays the strains from the lower joint tie within specimen C4ALH3. Again there was very little strain development until visible joint cracking. As with the *standard* specimens the strain developed within the lower tie was significantly less than that for ties in the middle or upper section of the joint. By the end of the test the spread of strains ranged from only 100 to 900 με. Gauge two, however, developed a strain of around 2000 με and it is suggested that this gauge was intercepted by a large crack.

C6LH3

Figure 4.2.3.4.4(a) displays the strains from the upper joint tie within specimen C6LH3. Prior to visible joint cracking a significant amount of strain had already developed within the tie. This strain continued to increase until yielding of *leg one* was recorded at failure. The maximum recorded strain was 4980 με in gauge one. Slight slippage was observed in *leg two* prior to failure.

Figure 4.2.3.4.4(b) displays the strains from the middle joint tie within specimen C6LH3. The strain development occurred just prior to visible joint cracking and steadily increased until failure. The spread of strains by the end of the test ranged from around 2000 με to yield (3560 με).

Figure 4.2.3.4.4(c) displays the strains from the lower joint tie within specimen C6LH3. As previously seen the strain developed by this tie in the lower section of the joint was significantly lower than for ties in the middle or top. By the end of the test the spread of strains ranged from around 500 to 2000 με. Certain gauges in both legs showed signs of slippage.

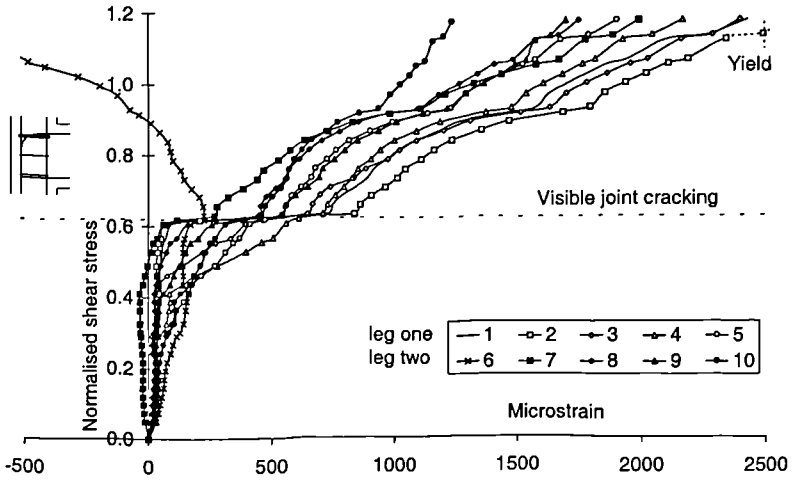

Figure 4.2.3.4.3(a) Tie strains - upper tie - C4ALH3

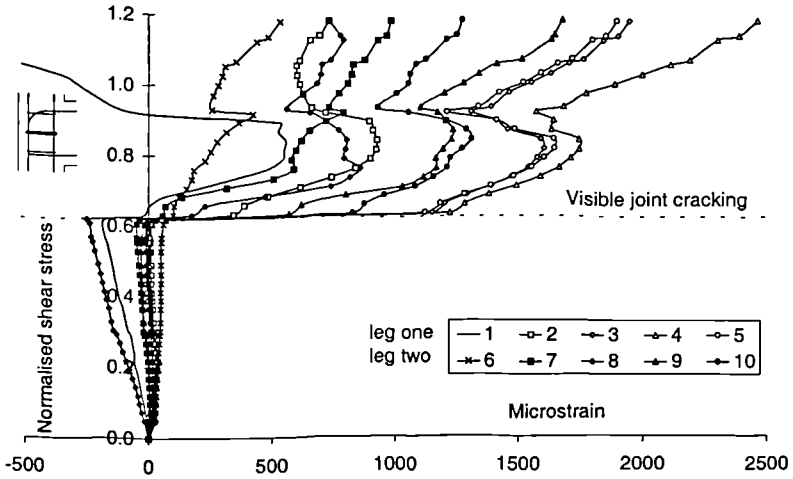

Figure 4.2.3.4.3(b) Tie strains - middle tie - C4ALH3

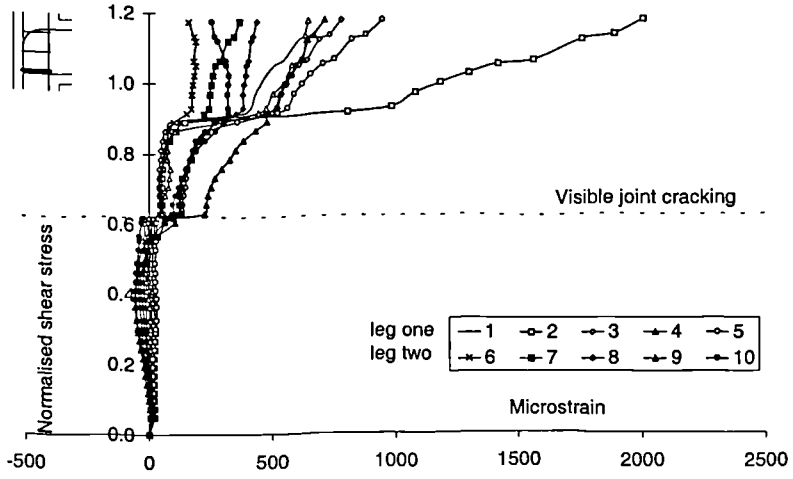

Figure 4.2.3.4.3(c) Tie strains - lower tie - C4ALH3

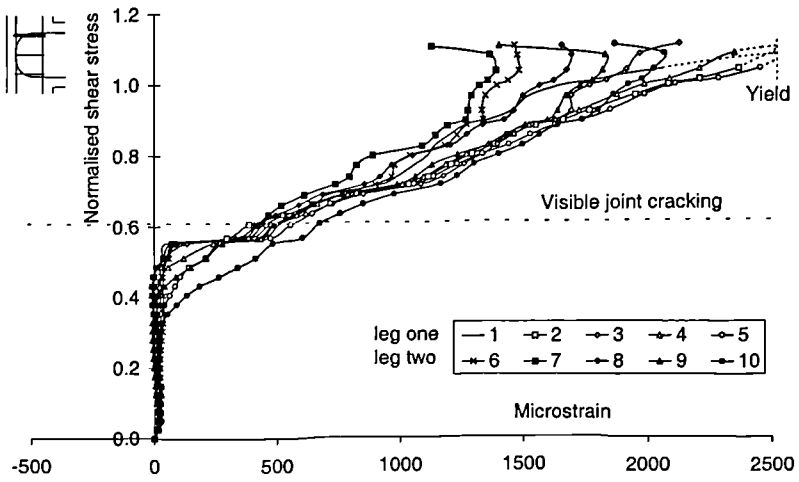

Figure 4.2.3.4.4(a) Tie strains - upper tie - C6LH3

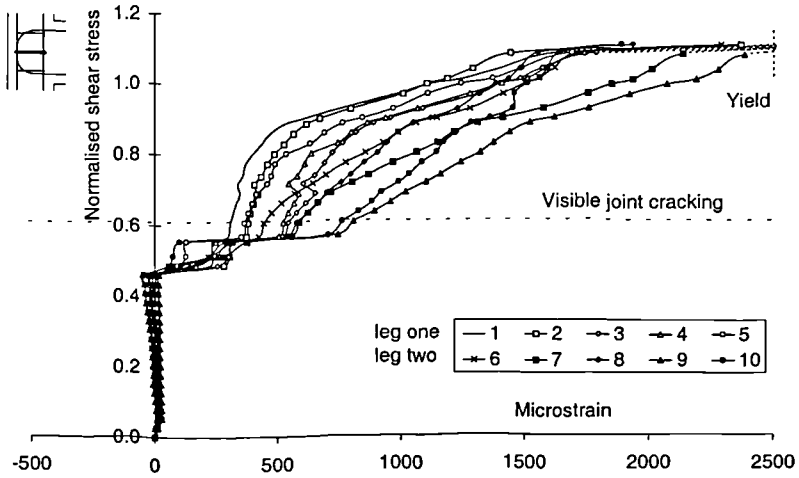

Figure 4.2.3.4.4(b) Tie strains - middle tie - C6LH3

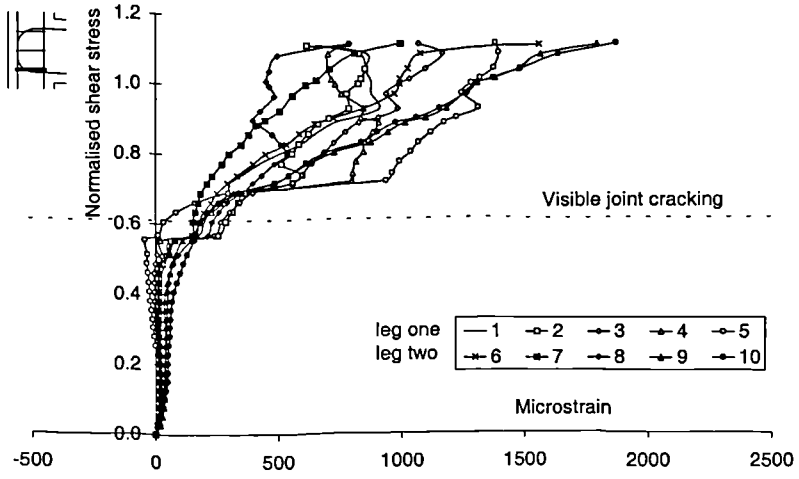

Figure 4.2.3.4.4(c) Tie strains - lower tie - C6LH3

The strain results from specimens C4ALH3 and C6LH3 again suggest that a tie positioned in the middle or upper joint provides more enhancement to the joint capacity than a tie positioned in the lower joint. Section 4.3.3 provides further results on the positioning of joint ties.

Figure 4.2.3.4.5 displays the strains from the middle tie within specimen C4ALH5. Prior to visible joint cracking very little strain was present in the tie. A significant increase of strain was achieved at joint cracking. The strain distribution at specimen failure ranged from 600 to 1500 με.

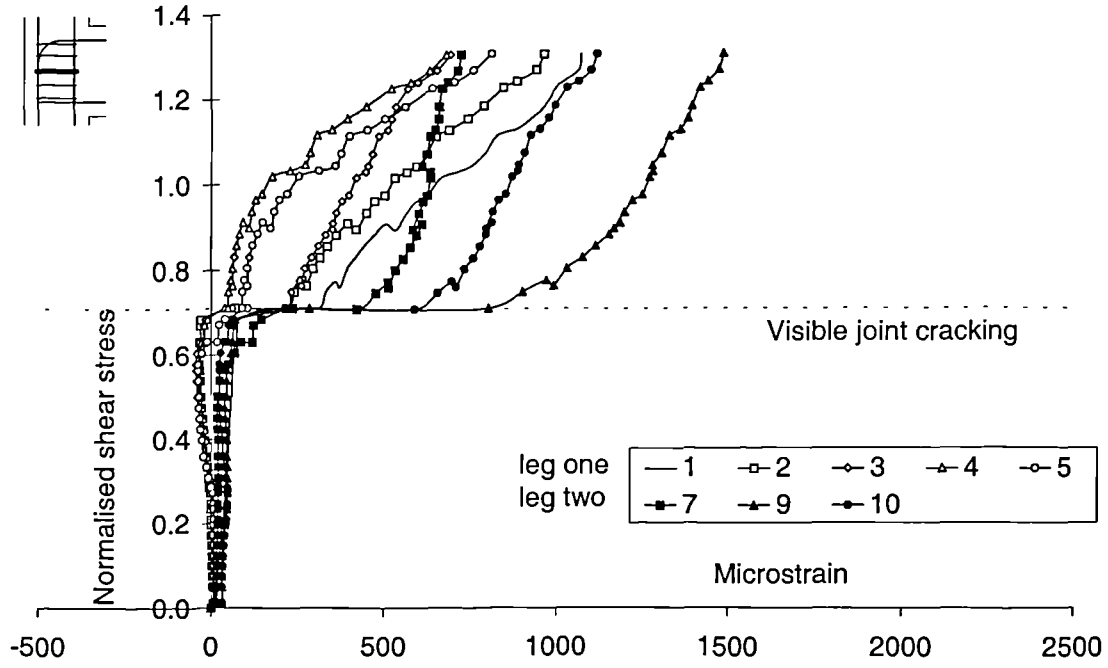

4.2.3.4.5 Tie strains - specimen C4ALH5

4.2.4 Bond stress analysis

As with the *standard* test specimens the bond stress analysis was conducted at two stages :

1. ***Prior to joint cracking*** - at an applied beam load of 18 kN, this corresponded to a peak strain of around 1200 με in the main tension steel.
2. ***Approaching failure*** - at the load stage which corresponded to a peak strain of almost 2500 με (yield) in the main tension steel.

Average bond stresses were considered using the same principles as defined previously in Section 4.1.4.

Bent down beam steel detail

Figure 4.2.4.1 displays the strains present within the beam tension steel, prior to joint cracking, for the specimens C4ALH1 and C4ALH3. As mentioned previously in Section 4.2.3.3 the strain distribution reached a peak at the beam-column interface which then reduced to almost zero over the *top joint* and *top bend* regions. This region was where the beam's force was transmitted into the joint.

Although this strain distribution pattern was the same as with the *standard* specimens the gradient was higher. Using equation 3.5.1 the average bond stress evaluated was 6.5 MPa. This was twice the value of the bond stress developed at joint cracking for the corresponding *standard* specimens.

Figure 4.2.4.2 displays the strains present within the beam tension steel, approaching failure, for the specimens C4ALH1 and C4ALH3. The strain gradient was essentially linear from the start of the *top bend* to a distance 300 mm down the anchor leg. Although the beam steel had almost yielded the average bond stress was still only 3.1 MPa.

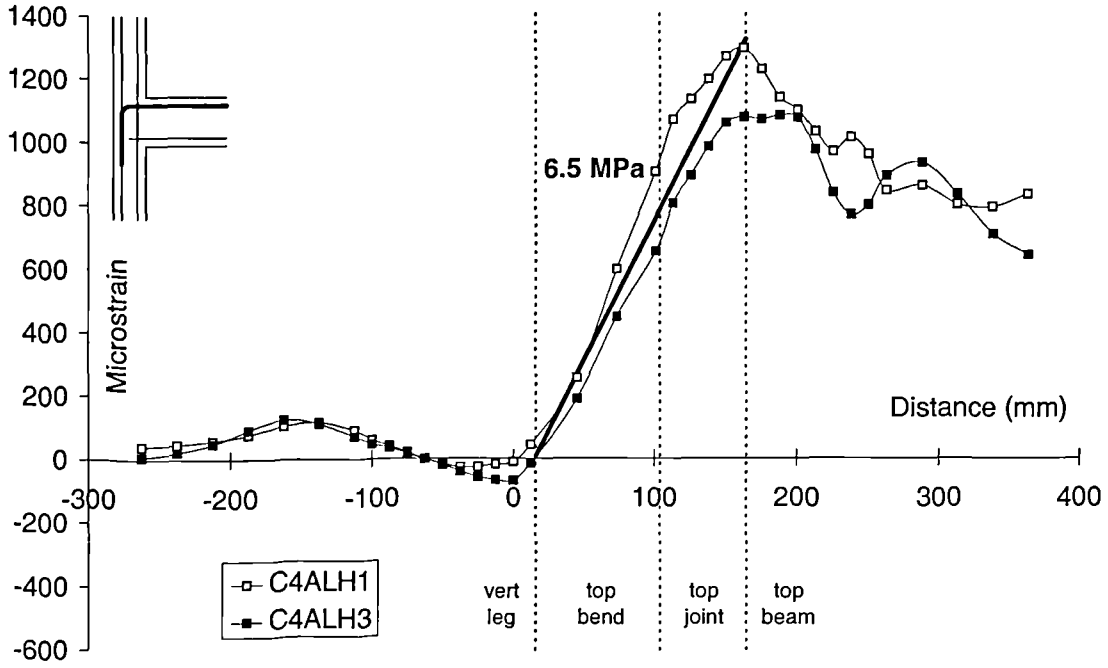

Figure 4.2.4.1 Bent down bar - average bond stresses - prior to joint cracking

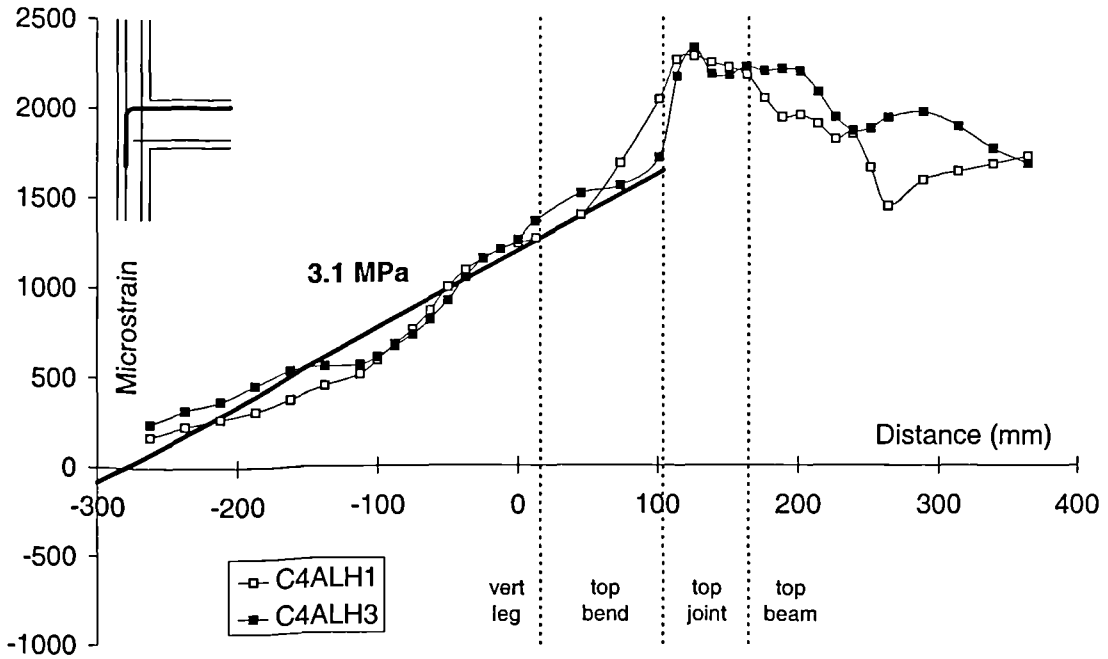

Figure 4.2.4.2 Bent down bar - average bond stresses - approaching failure

Notably the steel along the *top joint* region had lost its ability to develop any useful anchorage. This behaviour of the beam steel approaching failure was similar to corresponding *standard* specimens.

U-bar beam steel detail

Figure 4.2.4.3 displays the strains present within the beam tension steel, prior to joint cracking, for the specimens C6LH1 and C6LH3. At this stage of the load history the behaviour of the U-bar beam steel detail was very similar to that of the bent down beam steel detail. The load transfer from the beam into the joint again took place along the *top joint* and *top bend* regions of the steel. The average bond stress developed over this region was 6.4 MPa which was essentially the same value as for the specimens using bent down beam steel detail.

Figure 4.2.4.4 displays the strains present within the beam tension steel, approaching failure, for the specimens C6LH1 and C6LH3. The majority of the beam load was transferred into the joint along the *top bend* region. The very high strain gradient over this region corresponded to an average bond stress of 12.1 MPa. This was the largest average bond stress value recorded throughout the investigation. A smaller amount of the load transfer process was possible around the *vertical* and *bottom bend* regions which developed an average bond stress of 2.7 MPa.

These values were again significantly higher than the bond stress developed over the same regions for the corresponding *standard* specimens. Again, as for the bent down beam steel detail, the U-bar lost its ability to develop bond stress along the *top joint* region.

Both beam steel details behaved similarly over the initial load stages. However, after joint cracking the bent down beam steel detail utilised its vertical leg to transfer the beam's force into the lower column. The U-bar beam steel detail transferred all of the beam's force into the joint region and the majority of this load transfer took place

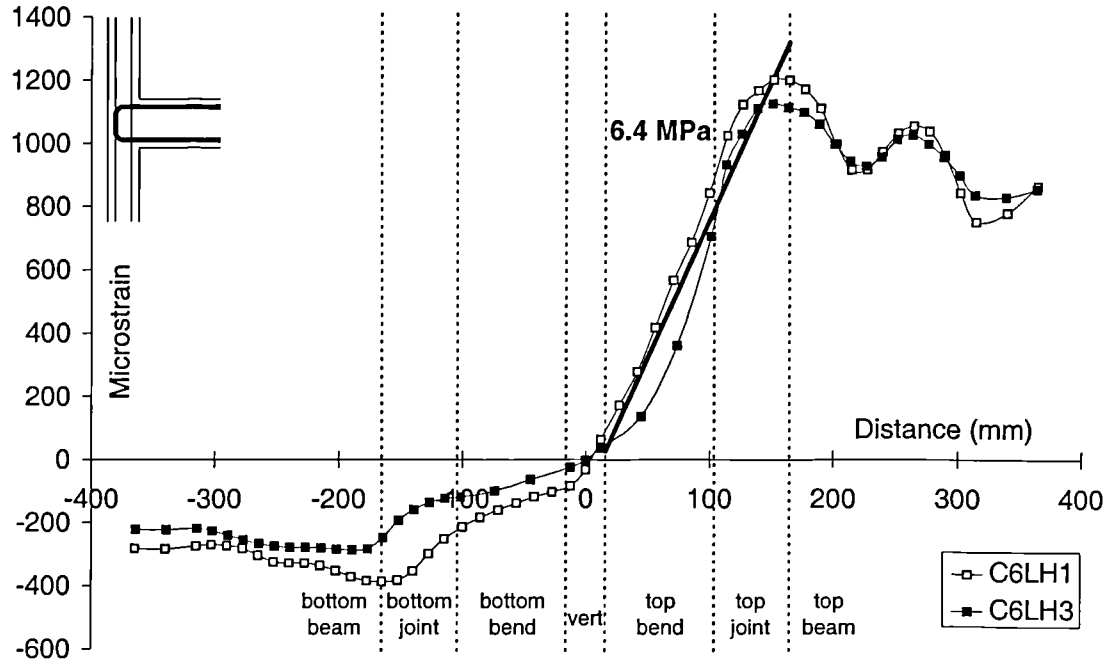

Figure 4.2.4.3 U-bar - average bond stresses - prior to joint cracking

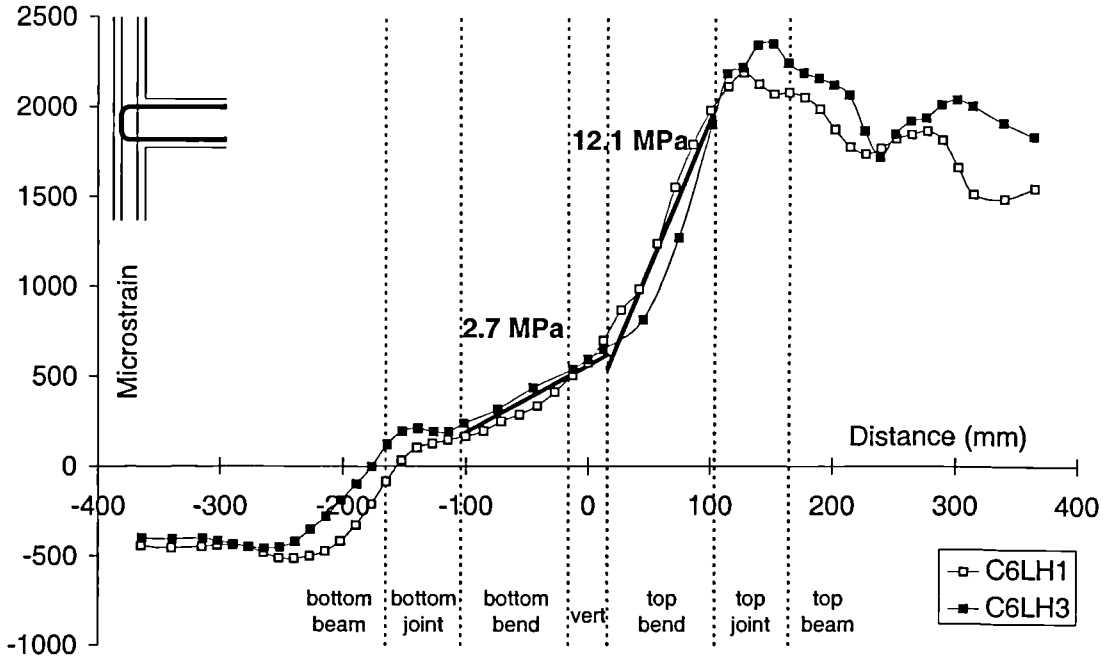

Figure 4.2.4.4 U-bar - average bond stresses - approaching failure

around its top bend. Again this would indicate why specimens with U-bar beam steel had a lower joint capacity than specimens with bent down beam steel.

The high strength specimens were able to sustain average bond stresses almost twice the magnitude of their corresponding normal strength (*standard*) specimens as shown in Table 4.2.4.

Table 4.2.4 Comparisons of average bond stresses at joint cracking and failure

	Initial joint cracking	Joint failure
C4ALN1 / C4ALN3	3.2 MPa (top bend/top joint)	-
C4ALH1 / C4ALH3	6.5 MPa (top bend/top joint)	-
C6LN1 / C6LN3	3.2 MPa (top bend/top joint)	7.8 MPa (top bend)
C6LH1 / C6LH3	6.4 MPa (top bend/top joint)	12.1 MPa (top bend)

Notes

1. Specimens C4ALH1 and C4ALH3 exhibited beam failure and thus their failure loads were mainly dependent on the flexural strength of the main beam tension steel.

4.2.5 Bearing stress analysis

Values of bearing stress around the top bend of the beam rebar were evaluated for the fully strain gauged specimens. The values of bearing stress were calculated using equation 4.1.5.1. Table 4.2.5 displays the values of bearing stress under the top bend of the beam rebar at failure. Values were calculated at the start (σ_{b1}) and the end (σ_{b2}) of each bend.

Table 4.2.5 shows that all specimens exhibited yielding in their beam rebar at the start of the first bend. The value of bearing stress at yield was around 75% of that

permitted by BS 8110 equation (50). This suggests that the behaviour of high strength specimens within this investigation was not influenced by bearing effects.

Table 4.2.5 Bearing stresses within the top bend of the beam rebar

Specimen	σ_{b1} (MPa)	σ_{b2} (MPa)	$\sigma_{b(lim)}$ (MPa)	$\sigma_{b(max)}/\sigma_{b(lim)}$
C6LH1	127 (Y)	26	166	0.77
C6LH3	127 (Y)	25	167	0.76
C4ALH1	127 (Y)	95	156	0.81
C4ALH3	127 (Y)	127 (Y)	173	0.73

Notes

1. The stress values were evaluated from the experimental strain readings using the stress-strain data displayed in Section 2.1,
2. The bearing stresses were evaluated using the true compressive cube strength values,
3. Y - indicates that the steel had yielded.

4.3 Specimens Investigating Tie Positioning

This section considers the results from the eleven specimens investigating **tie positioning**. The parameters investigated were the **quantity and position of the joint ties** and the **beam tension steel anchorage detail**. The specimen details are given below in Table 4.3. Specific joint layouts and gauged tie details were displayed previously in Table 2.4.

Table 4.3 Specimens investigating *tie positioning* - details

Specimen	Gauging	Beam steel anchorage	No. of joint ties	Super-plasticiser
C4ALN1T	One tie	Bent down	1	
C4ALN3C	One tie	Bent down	3	*
C4ALN3D	-	Bent down	3	*
C6LN1B	One tie	U-bar	1	
C6LN1T	One tie	U-bar	1	
C6LN1A	One tie	U-bar	1	*
C6LN2A	One tie	U-bar	2	*
C6LN2B	One tie	U-bar	2	*
C6LN3A	One tie	U-bar	3	
C6LN3B	One tie	U-bar	3	
C6LN3C	One tie	U-bar	3	

Note - Addition of Superplasticiser

As outlined previously in Section 2.2.2 superplasticiser was added to a number of normal strength concrete mixes which appeared to cause an increase in the specimen's ultimate joint capacity. This enhancement may have been as high as 15% compared with similar specimens. This was the test series mainly influenced by this problem and specific examples are highlighted within this section. Specimens which were cast using superplasticiser are indicated in Table 4.3 and throughout this section with an asterisk (*).

4.3.1 Initial joint cracking

Figure 4.3.1 shows the normalised shear stress values for the eleven specimens at initial joint cracking. These results were previously displayed in Table 3.2.2.

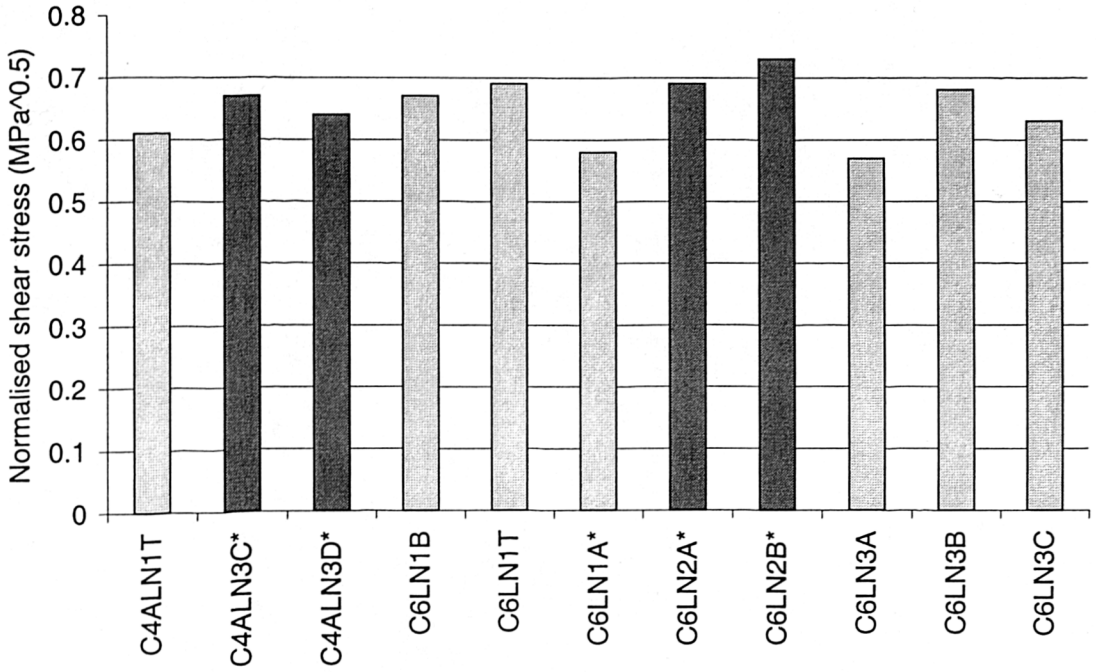

Figure 4.3.1 Shear stress at initial joint cracking - tie positioning specimens

Figure 4.3.1 shows that the number, or positioning, of joint ties had no influence over the load at which initial joint cracking occurred. The mean average value of normalised shear stress for this test series was 0.65 $MPa^{0.5}$ which was comparable with the results from previous test series.

4.3.2 Specimen Failure

This section considers specimens with U-bar and bent down bar beam steel detail separately. The majority of specimens tested used U-bar beam steel and are therefore considered first. The specimens from this test series are compared with specimens from the *standard* test series. To eliminate the influence of concrete strength the failure values are again considered as normalised shear stresses.

4.3.2.1 U-bar beam steel detail

One tie

Figure 4.3.2.1.1 displays the performance of the specimens with U-bar beam steel detail containing a single joint tie. Specimen C6LN0 is included to show the performance of an unreinforced joint.

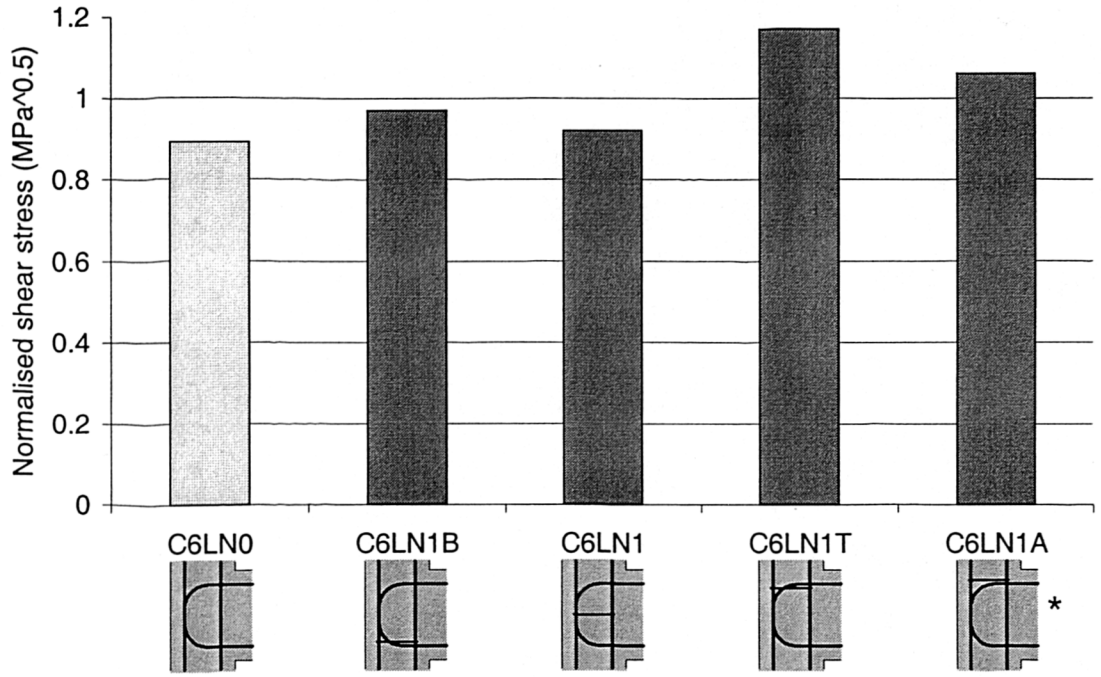

Figure 4.3.2.1.1 Joint capacity enhancement from a single tie

Figure 4.3.2.1.1 shows that specimen C6LN1T had the highest joint capacity. The single tie within C6LN1T was positioned in the upper joint below the level of beam tension steel. The increase in performance compared with C6LN0 was 31%.

The results from previous test series have indicated that the U-bar beam steel anchorage detail may have experienced slippage which induced premature joint failure. The single tie within C6LN1T not only gave added shear resistance to the joint but also gave increased confinement around the top bend of the rebar. This resulted in better anchorage of the beam steel and enhanced joint capacity.

Two ties

Figure 4.3.2.1.2 displays the performance of the specimens with U-bar beam steel detail containing two joint ties. Specimen C6LN0 is included to show the performance of an unreinforced joint.

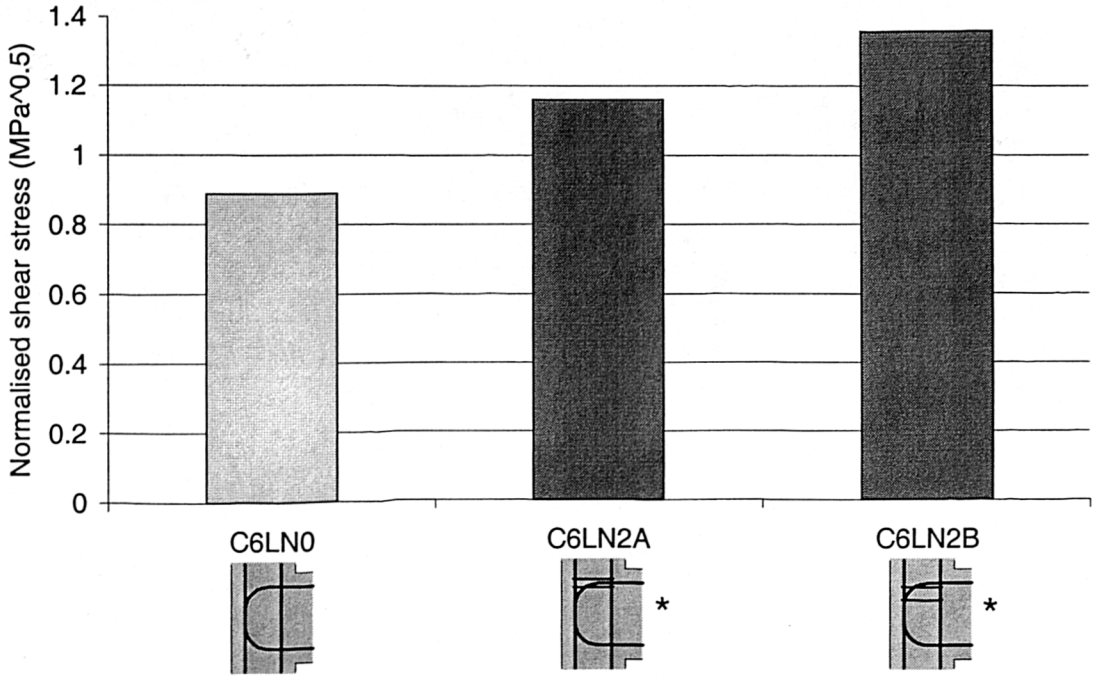

Figure 4.3.2.1.2 Joint capacity enhancement from two ties

Figure 4.3.2.1.2 shows that specimen C6LN2B had the highest joint capacity. The ties within C6LN2B were positioned in the upper joint below the level of beam tension steel. The increase in performance over C6LN0 was 53%. Specimen C6LN2B did however contain superplasticiser, but nevertheless the joint enhancement was still substantial, over and above any possible effects due to this additive.

It is believed that specimen C6LN2B performed better than C6LN2A as its ties were in a position within the joint which provided not only increased shear resistance to the joint core but also an improved anchorage of the beam tension steel.

Three ties

Figure 4.3.2.1.3 displays the performance of the specimens with U-bar beam steel detail containing three joint ties. Specimen C6LN0 is again included to show the performance of an unreinforced joint.

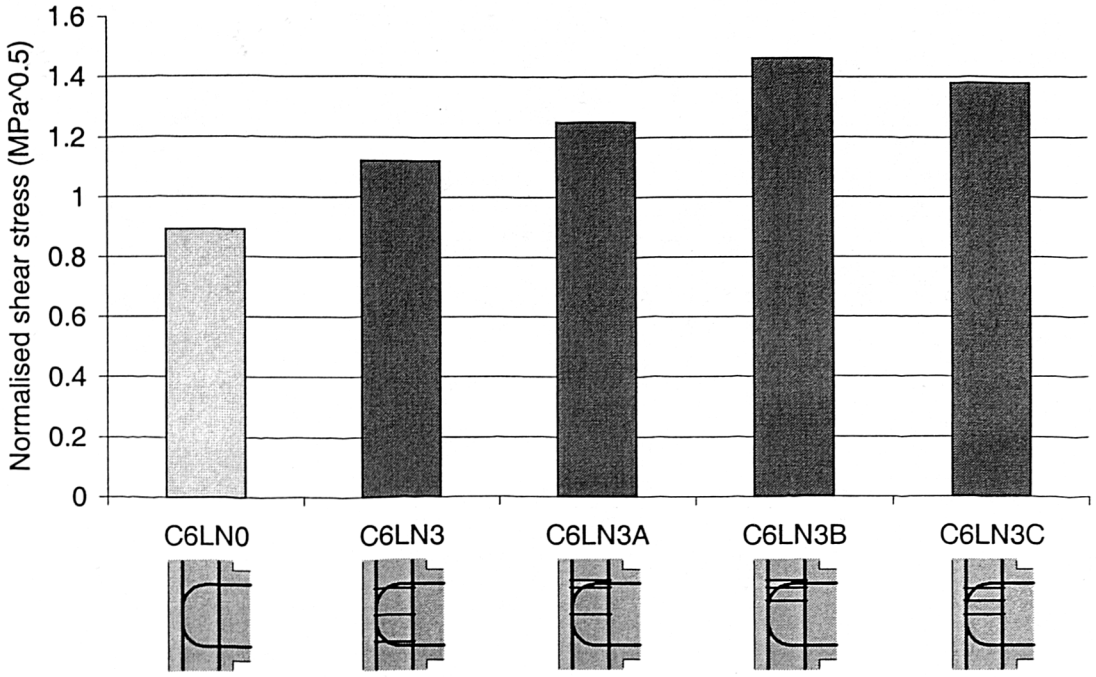

Figure 4.3.2.1.3 Joint capacity enhancement from three ties

Figure 4.3.2.1.2 shows that specimens C6LN3B and C6LN3C had the highest joint capacities. Two of their three ties were in the same position as the joint ties within C6LN2B. The third tie was positioned above the level of beam tension steel for specimen C6LN3B and at the joint mid-height for specimen C6LN3C. The increase in performance compared with C6LN0 was around 60% which was a true enhancement factor as neither specimen contained superplasticiser.

For specimens with U-bar beam steel detail the optimum position for joint ties would appear to be between the joint mid-height and the level of beam tension steel.

4.3.2.2 Bent down beam steel detail

One tie

Figure 4.3.2.2.1 displays the performance of the specimens with bent-down beam steel detail containing a single joint tie. Specimen C4ALN0 is included to show the performance of an unreinforced joint.

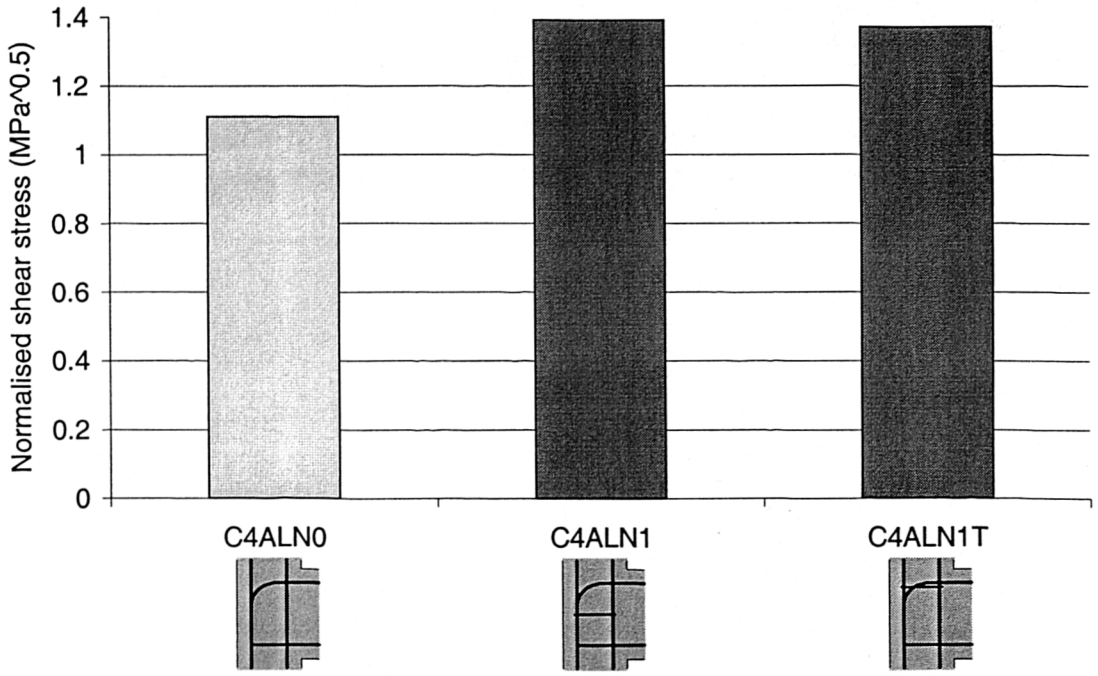

Figure 4.3.2.2.1 Joint capacity enhancement from a single tie

Figure 4.3.2.2.1 shows that both C4ALN1 and C4ALN1T achieved a similar joint capacity. The addition of one tie to the joint gave an enhancement of around 25% compared with specimen C4ALN0.

It is suggested that the anchorage detail of the bent down beam steel was already sufficient and joint failure was not induced by any slippage effects. The fact that no increase in performance was achieved by positioning the tie around the level of beam tension steel supports this.

Three ties

Figure 4.3.2.2.2 displays the performance of the specimens with bent-down beam steel detail containing three joint ties. Specimen C4ALN0 is again included to show the performance of an unreinforced joint.

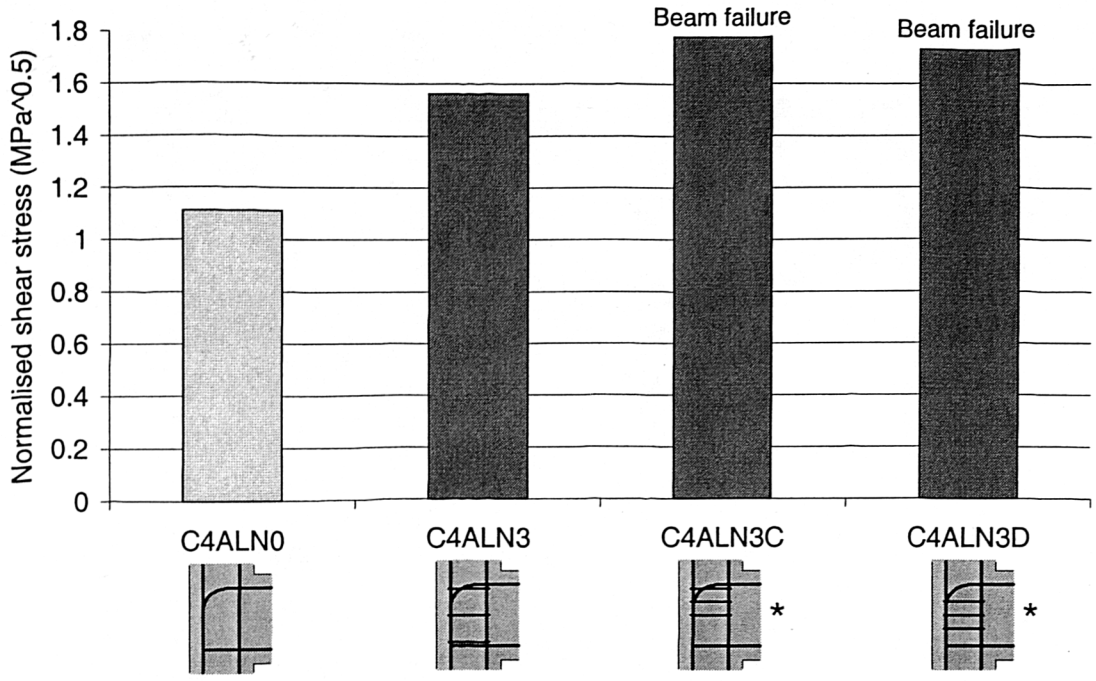

Figure 4.3.2.2.2 Joint capacity enhancement from three ties

Figure 4.3.2.2.2 shows that both C4ALN3C and C4ALN3D had sufficient joint strength to allow the beam's ultimate moment of resistance to be reached. The fact that the ultimate joint capacities were not achieved unfortunately means that the full enhancement cannot be established.

The number of tests investigating joint tie positioning for specimens using bent down beam steel was limited. **However, for specimens with bent down beam steel detail the optimum position for joint ties would appear to be around the joint mid-height level.** This would be the case for any beam steel detail in which anchorage detail was not a concern.

4.3.3 Reinforcement strains

Reinforcement strains are presented for all strain gauged joint ties within this test series. However, as tie strains have already been discussed in detail for the *standard* and *high strength* specimens only brief comments are made.

C6LN1B

Figure 4.3.3.1 displays the strains from the gauged joint tie within specimen C6LN1B. The tie strains were consistent with ties in the lower joint from the *standard* and *high strength* test series. The strain distribution at specimen failure ranged from around 800 to 2000 με.

C6LN1T

Figure 4.3.3.2 displays the strains from the gauged joint tie within specimen C6LN1T. The strain distribution at specimen failure ranged from around 1000 to 2200 με.

C6LN1A

Figure 4.3.3.3 displays the strains from the gauged joint tie within specimen C6LN1A. Prior to specimen failure *leg one* of the tie exhibited slippage. This specimen was repeated with the tie's legs bent through 135° to try and improve its anchorage. The results from this repeated specimen, C6LN1AE, are considered in Section 4.5.2.

C6LN2A

Figure 4.3.3.4 displays the strains from the gauged joint tie within specimen C6LN2A. Gauge six within *leg two* had yielded at specimen failure. The maximum strain recorded by this gauge was 2700 με. All of leg one had exhibited slippage by a normalised shear stress of around 1.0 $MPa^{0.5}$.

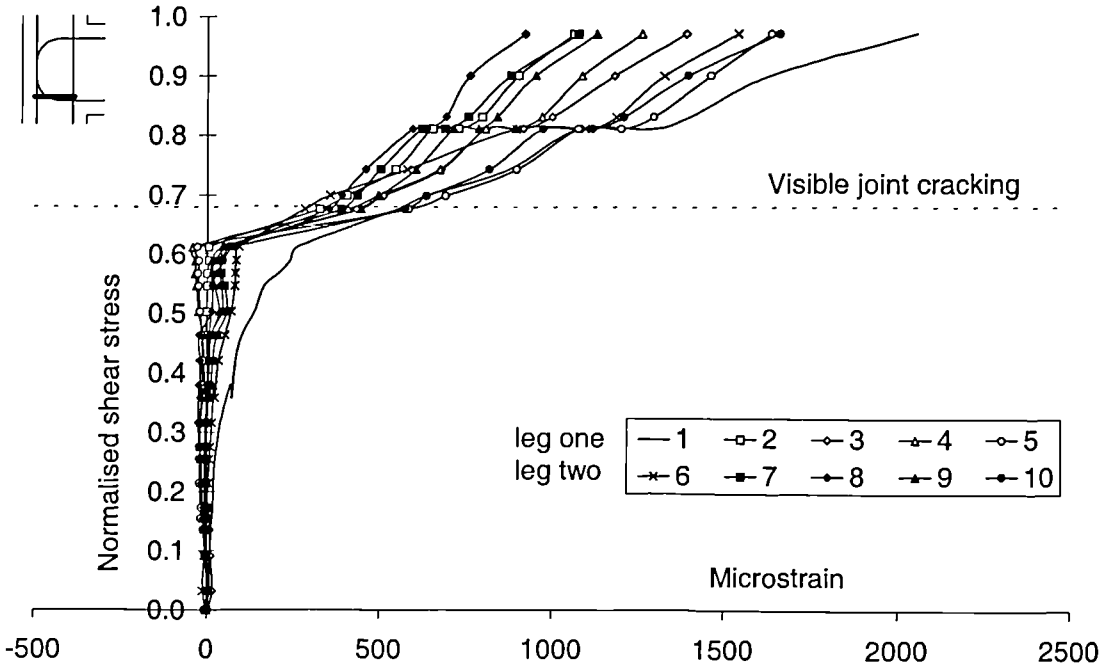

4.3.3.1 Tie strains - specimen C6LN1B

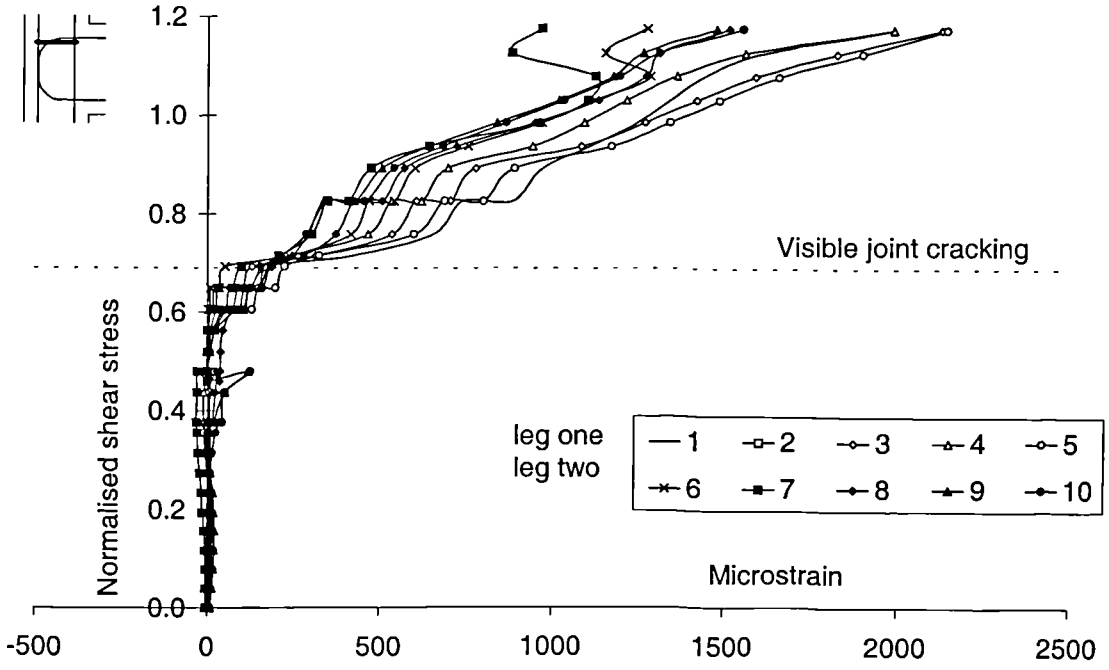

4.3.3.2 Tie strains - specimen C6LN1T

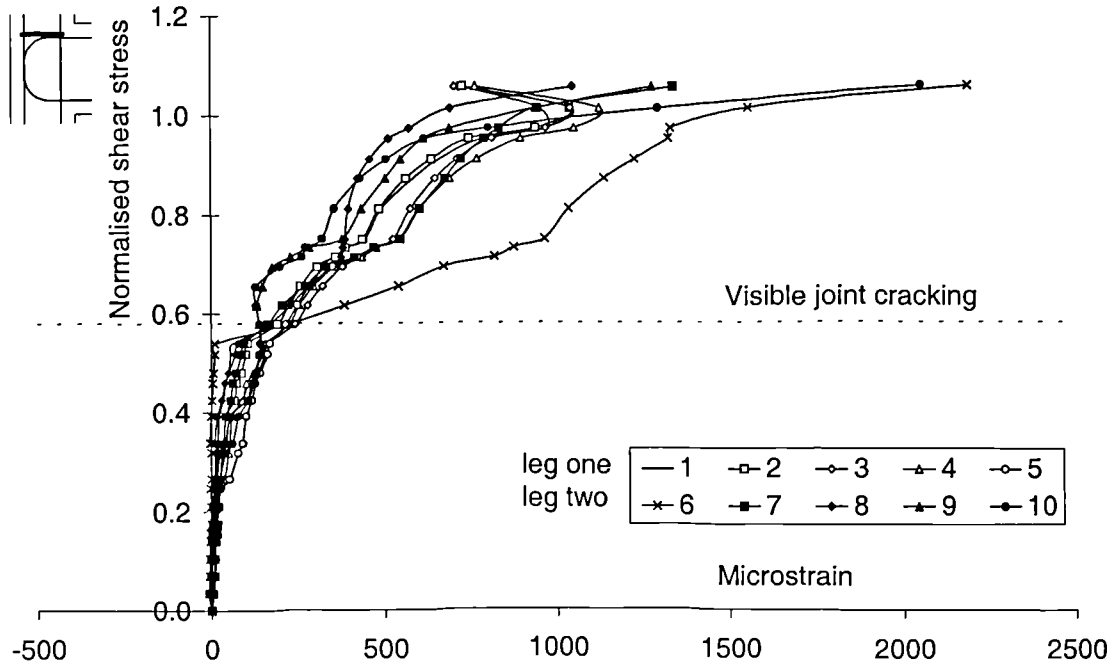

4.3.3.3 Tie strains - specimen C6LN1A

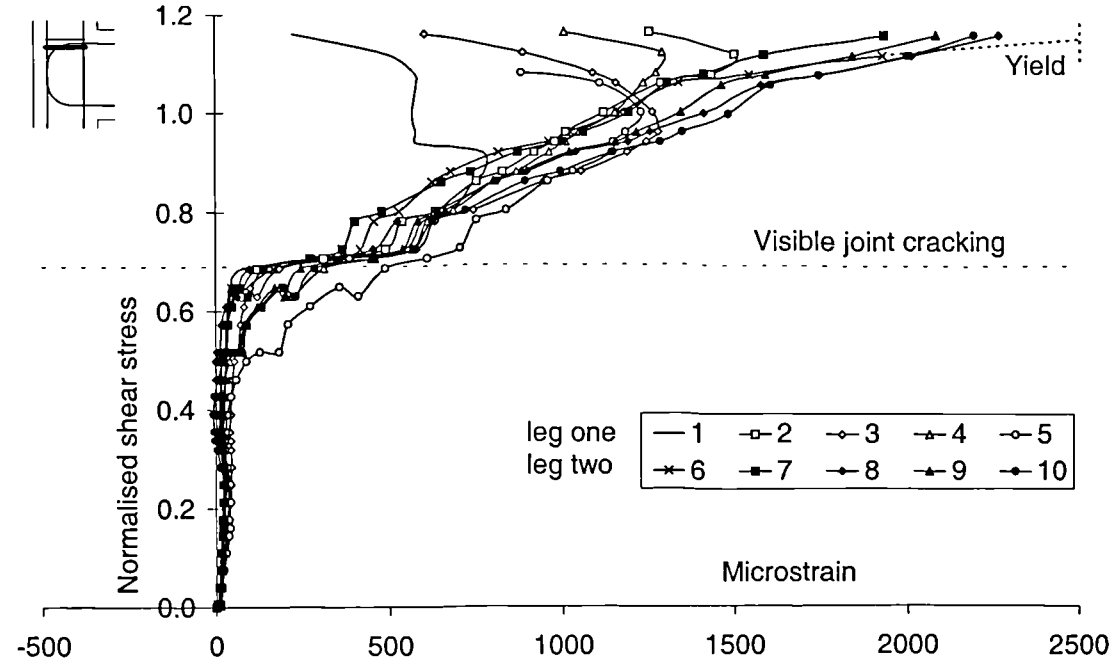

4.3.3.4 Tie strains - (tie below beam tension steel height) - specimen C6LN2A

C6LN2B

Figure 4.3.3.5 displays the strains from the gauged joint tie within specimen C6LN2B. All of the gauges showed a very similar strain development. The strain values at failure ranged from around 1300 to 2300 με.

C6LN3A

Figure 4.3.3.6 displays the strains from the gauged joint tie within specimen C6LN3A. All of the gauges again showed a similar strain development. The strains at the end of the test were low considering the position of the tie within the joint. The strain values at failure ranged from 700 to 1700 με.

C6LN3B

Figure 4.3.3.7 displays the strains from the gauged joint tie within specimen C6LN3B. A gauge in both *leg one* and *leg two* had yielded at specimen failure. There was a wide range of strain values from 1000 με to yield and beyond (3210 με).

C6LN3C

Figure 4.3.3.8 displays the strains from the gauged joint tie within specimen C6LN3C. *Leg one* showed signs of major slippage approaching specimen failure. The strains in *leg two* ranged from 1500 to 2300 με at failure.

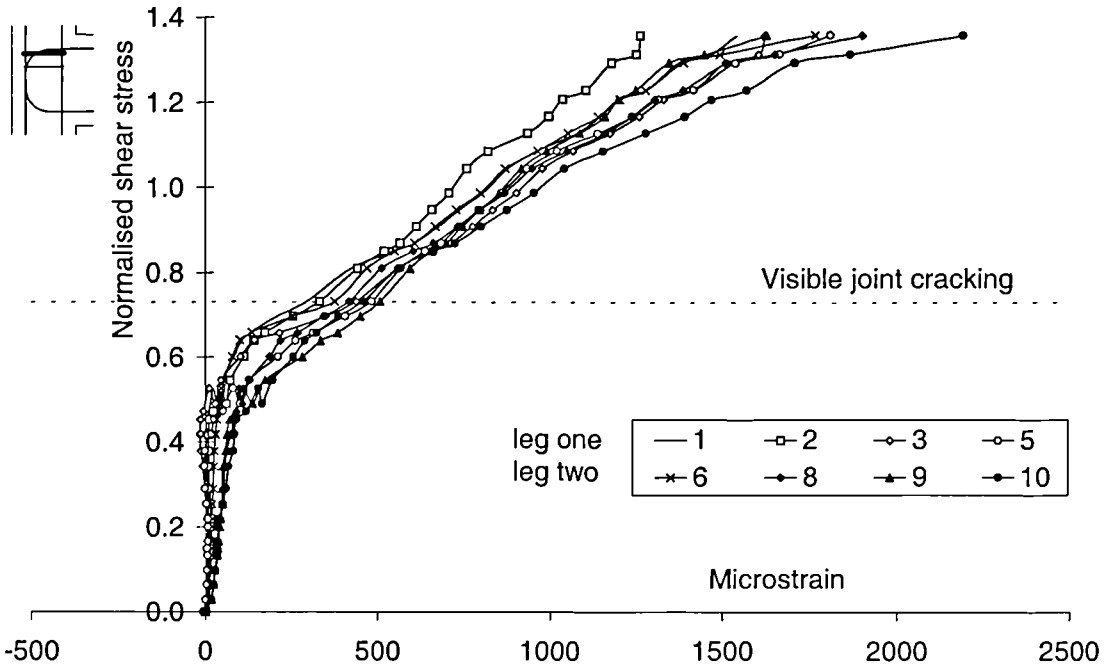

4.3.3.5 Tie strains - (tie below beam tension steel height) - specimen C6LN2B

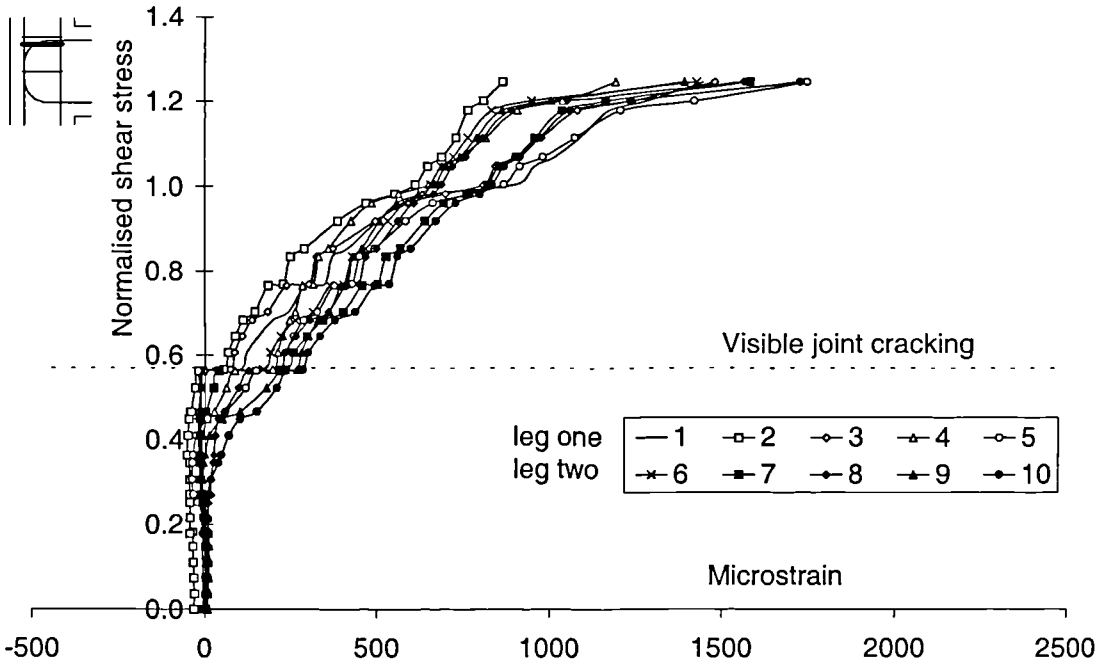

4.3.3.6 Tie strains - (tie below beam tension steel height) - specimen C6LN3A

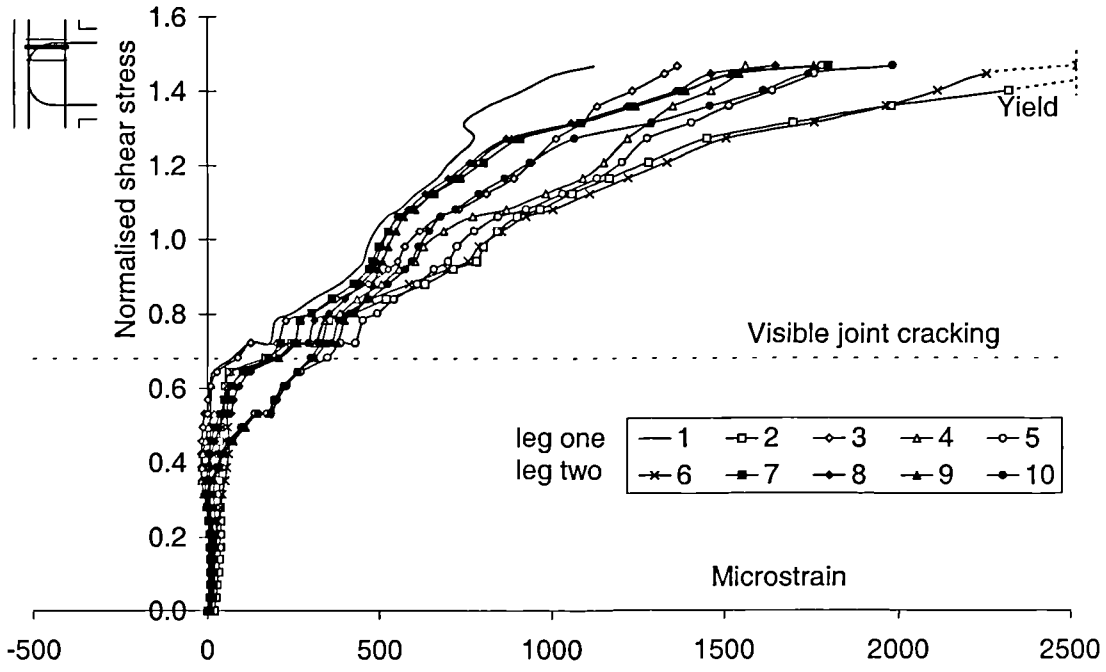

4.3.3.7 Tie strains - (tie below beam tension steel height) - specimen C6LN3B

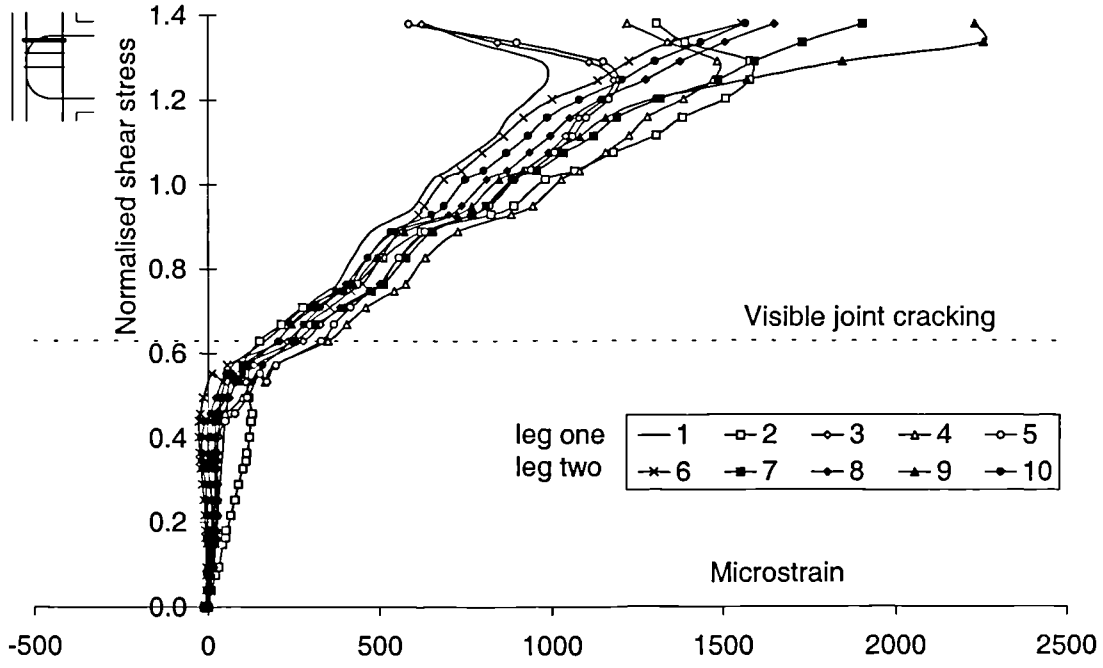

4.3.3.8 Tie strains - (tie below beam tension steel height) - specimen C6LN3C

C4ALN1T

Figure 4.3.3.9 displays the strains from the gauged joint tie within specimen C4ALN1T. The strain development was very similar for all of the gauges. Slight slippage of *leg one* was observed prior to specimen failure. The range of strains was from around 1000 to 2300 με.

C4ALN3C

Figure 4.3.3.10 displays the strains from the gauged joint tie within specimen C4ALN3C. The strain developed in the tie was reasonably low. At specimen failure the range of strains was from around 700 to 1700 με. Gauge three developed a compressive strain up to a normalised shear stress of 1.0 MPa. This was similar behaviour to gauges seen previously within specimen C4ALH3 (Section 4.2.3.4).

C4ALN3D

Specimen C4ALN3D did not contain any strain gauged ties.

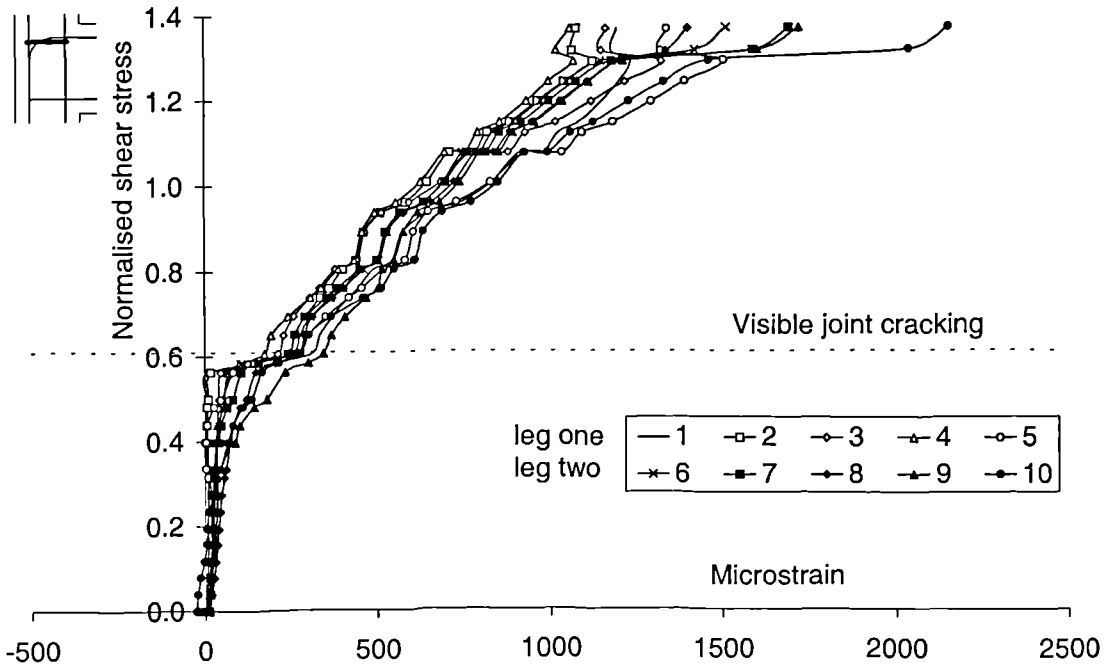

4.3.3.9 Tie strains - specimen C4ALN1T

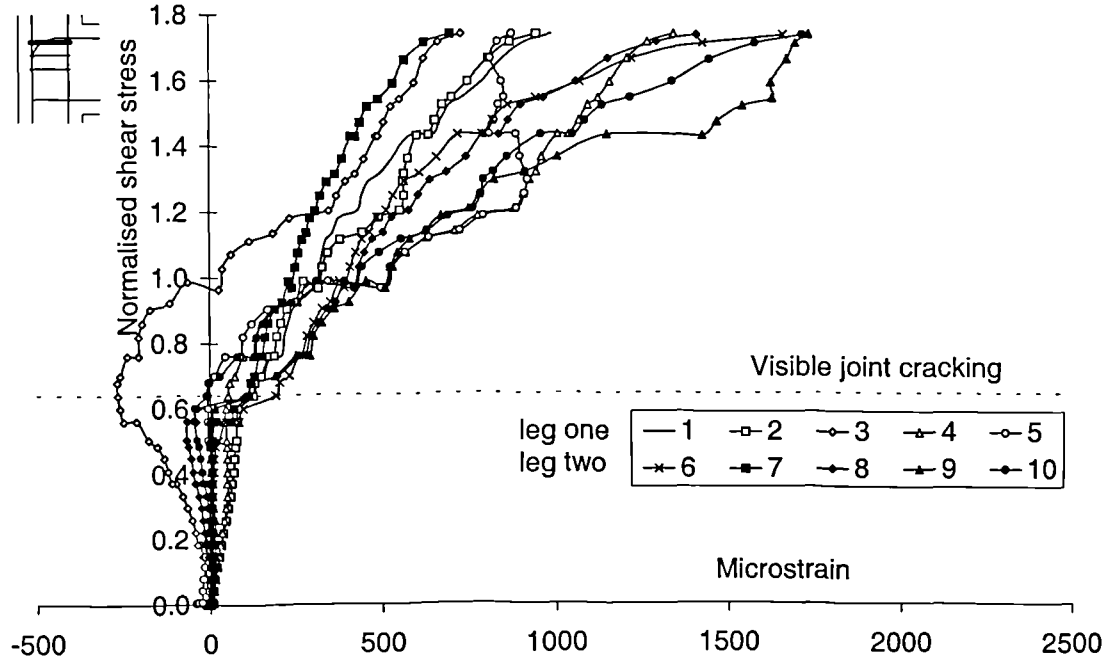

4.3.3.10 Tie strains - (upper joint tie) - specimen C4ALN3C

4.4 Specimens Investigating Joint Aspect Ratio

This section considers the results from the eight specimens investigating **joint aspect ratio**. The parameters investigated were the **number of joint ties** and the **beam tension steel anchorage detail** for specimens with 300 mm deep beams. The specimen details are given below in Table 4.4.

Table 4.4 Specimens investigating *joint aspect ratio* - details

Specimen	Gauging	Beam steel anchorage	No. of joint ties	Joint aspect ratio
C7LN0	-	Bent down	0	2.0
C7LN1	-	Bent down	1	2.0
C7LN3	One tie	Bent down	3	2.0
C7LN5	-	Bent down	5	2.0
C9LN0	-	U-bar	0	2.0
C9LN1	-	U-bar	1	2.0
C9LN3	One tie	U-bar	3	2.0
C9LN5	-	U-bar	5	2.0

4.4.1 Initial joint cracking

Figure 4.4.1 shows the normalised shear stress values for the eight specimens at initial joint cracking. These results were previously displayed in Table 3.2.2.

Again, as with previous test series, Figure 4.4.1 shows that the number of ties present within the joint had no influence over the initial joint cracking capacity. Notably the specimens with bent down steel detail (C7*) had a higher initial joint cracking capacity than specimens with U-bar beam steel (C9*). Previous test series indicated that specimens with U-bar beam steel had a higher initial capacity.

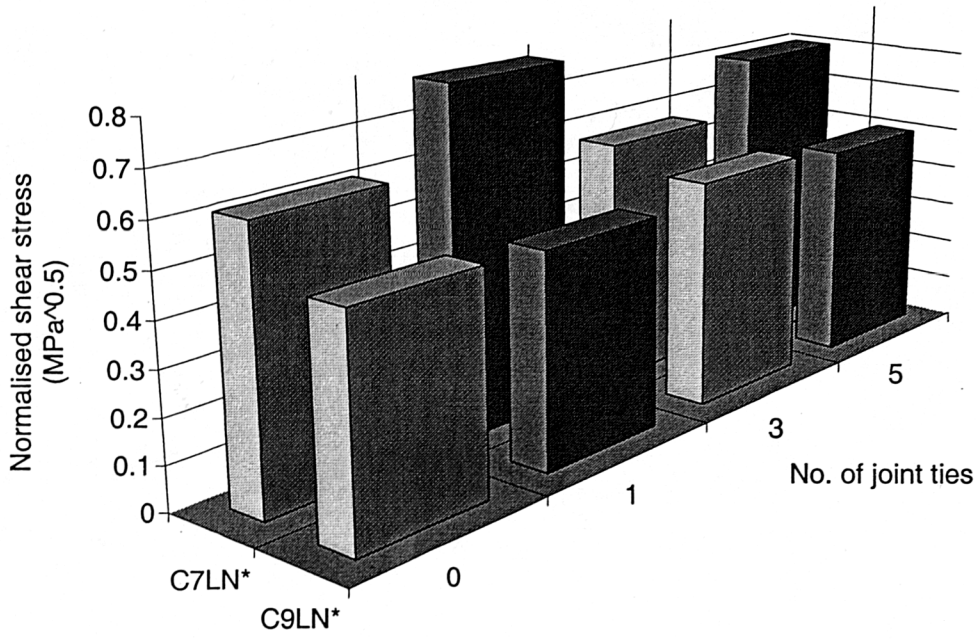

Figure 4.4.1 Shear stress at initial joint cracking - joint aspect ratio

The average normalised shear stress at which initial joint cracking occurred was 0.58 $MPa^{0.5}$. Table 4.4.1 shows the average joint cracking values for all the test series considered so far.

Table 4.4.1 Average shear stress at initial joint cracking

Test series	No. of specimens	$v_{crack}/\sqrt{f_{ck}}$ ($MPa^{0.5}$)
Standard	8	0.62
High strength	8	0.60
Tie positioning	11	0.65
Joint aspect ratio	8	0.58

Table 4.4.1 shows that initial joint cracking occurred at an average shear stress around 0.6 $MPa^{0.5}$ for all four test series.

4.4.2 Specimen failure

Figure 4.4.2.1 shows the normalised shear stress values for the eight specimens at failure. These results were previously displayed in Table 3.2.2.

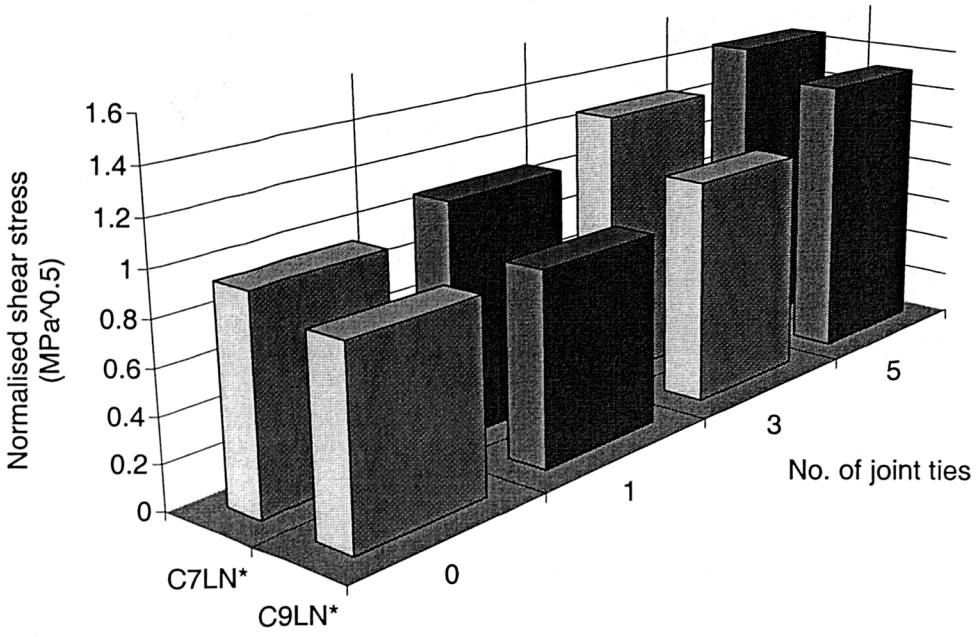

Figure 4.4.2.1 Shear stress at specimen failure - joint aspect ratio

Figure 4.4.2.1 confirms the following findings from previous test series.

1. Specimens with bent down beam steel detail have a greater ultimate capacity than specimens with U-bar beam steel detail.

2. The addition of ties to the joint zone increases the ultimate capacity.

The purpose of this test series was to investigate concerns expressed by Scott *et al* [9] and Vollum [12] that a specimen's joint shear strength reduced as the joint aspect ratio (h_b/h_c) increased. Vollum suggested that this reduction may be as high as 25% as the joint aspect ratio increased from 1.4 to 2.0.

Figure 4.4.2.2 displays comparisons between the *standard* specimens and the specimens investigating joint aspect ratio. The light and dark grey columns indicate specimens with bent down and U-bar beam steel detail respectively.

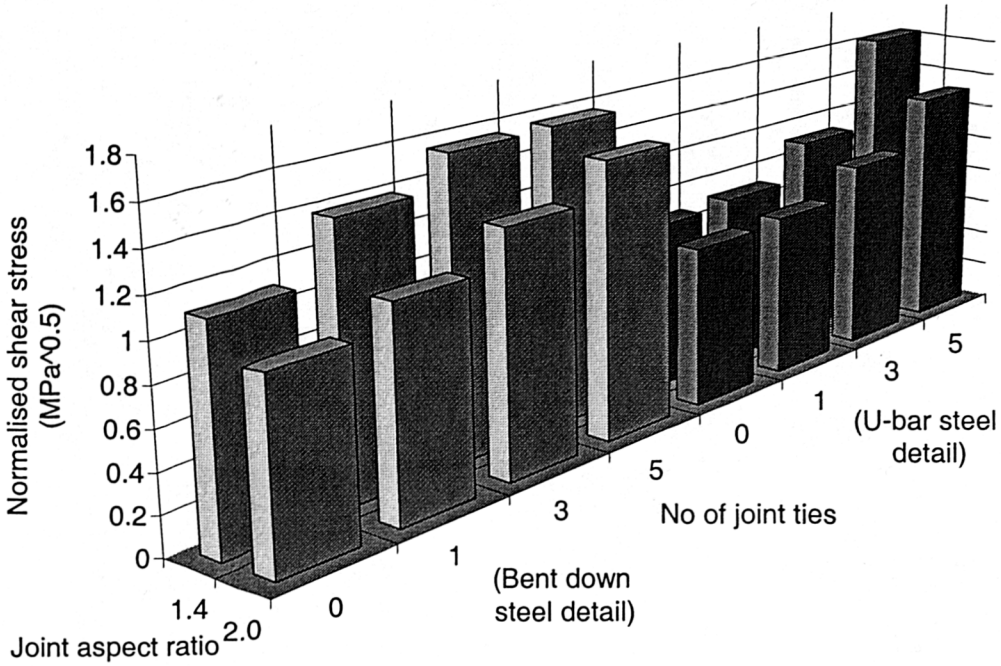

Figure 4.4.2.2 Shear stress at failure - joint aspect ratio comparisons

Figure 4.4.2.2 clearly shows that as the joint aspect ratio increased from 1.4 to 2.0 the joint shear strength reduced. The average reduction in joint shear strength was 16% for specimens with bent down beam steel detail and 11% for specimens with U-bar beam steel detail.

The author suggests the following reasons for the reduction in ultimate shear strength with increasing joint aspect ratio.

1. The slenderness increased and thus the capacity of the concrete strut decreased with increasing joint aspect ratio. This was suggested previously by Scott *et al* [9] and was considered previously in equation 1.26 within this thesis.

2. The ties within a more slender joint were a greater relative distance from the top bend of the beam steel. Thus any enhancement to the steel's anchorage capacity was less.

For this test series, using U-bar beam steel anchorage reduced the ultimate shear capacity of the joint by an average of 13%. Due to the increased anchorage length available in the joints with an aspect ratio of 2.0 this reduction factor was lower than previously seen with the *standard* specimens (this had previously been an average of 18%). Both of these values are lower than the upper value predicted by Vollum [12] of 25%.

4.4.3 Reinforcement strains

Reinforcement strains are presented for the strain gauged joint ties within specimens C7LN3 and C9LN3.

C7LN3

Figure 4.4.3.1 displays the reinforcement strains present in the middle tie within specimen C7LN3. Until visible joint cracking very little strain was developed in either of the tie's legs. After joint cracking the strains steadily increased and at specimen failure the range of strains was from around 1500 με to yield (8350 με).

C9LN3

Figure 4.4.3.2 displays the reinforcement strains present in the middle tie within specimen C9LN3. Again very little strain was developed in either of the tie's legs until initial joint cracking. After joint cracking both legs behaved differently; *leg one* steadily developed strain until all of its gauges were at a value of around 2000 με, *leg two* developed strain more slowly and showed clear signs of slippage towards the end of the test.

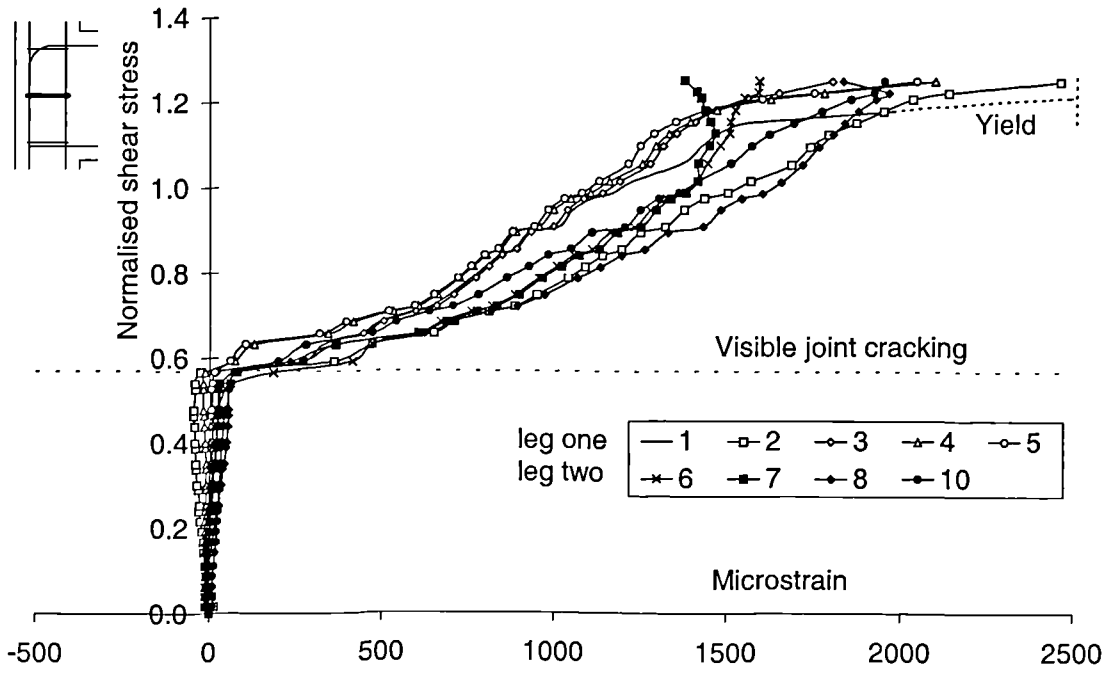

4.4.3.1 Tie strains - specimen C7LN3 - middle tie

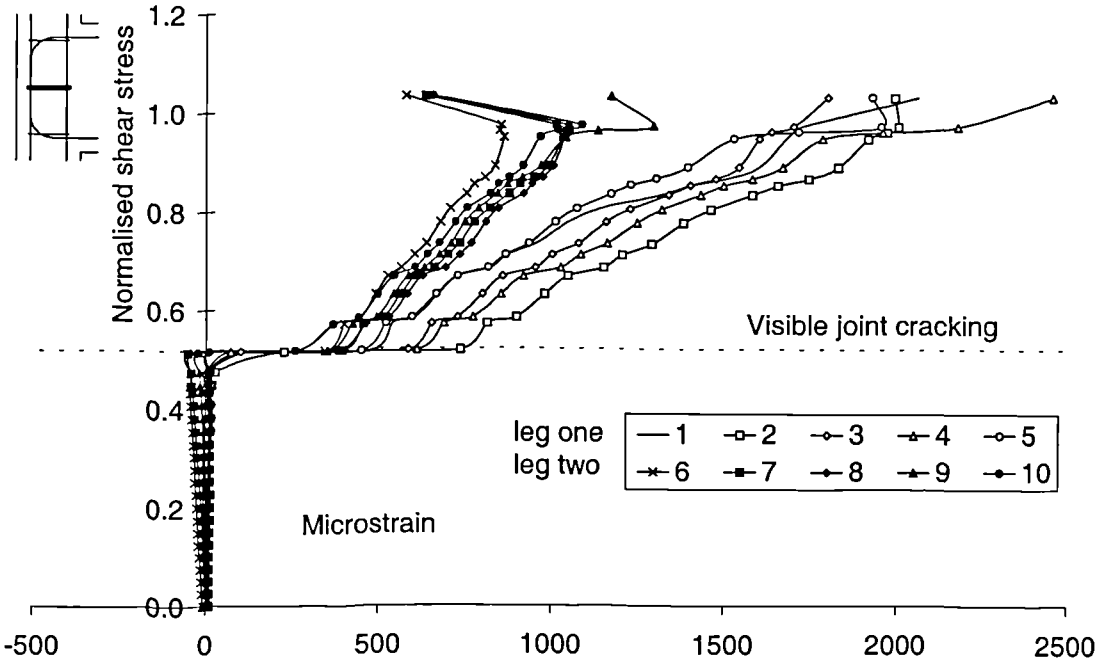

4.4.3.2 Tie strains - specimen C9LN3 - middle tie

4.5 Steel Fibre Reinforced Specimens

This section considers the results from the nine specimens investigating **steel fibre reinforced concrete**. The parameters investigated were the **type and quantity of steel fibres** and the **beam tension steel anchorage detail**. The specimen details are given below in Table 4.5.

Two types of steel fibre were used, short and long, as previously defined in Section 2.2.2.

Table 4.5 ***Steel fibre*** **reinforced specimens - details**

Specimen	Beam steel anchorage	Fibre type	Fibre %
C4AL04SF	Bent down	Short	0.4
C4AL15SF	Bent down	Short	1.5
C4AL23SF	Bent down	Short	2.3
C4AL04LF	Bent down	Long	0.4
C4AL15LF	Bent down	Long	1.5
C4AL23LF	Bent down	Long	2.3
C4AL38LF	Bent down	Long	3.8
C6L04SF	U-bar	Short	0.4
C6L04LF	U-bar	Long	0.4

The percentage of fibres was calculated by volume. Adebar *et al* [36] reviewed the results from eighteen different investigations, on fibre reinforced concrete beams, between 1972 and 1994. The range of percentages, by volume, was from 0 to 3.0%. Fibre Technology Ltd, UK, [48] recommend a percentage of 1.1% for *general use* and a percentage of 1.5% for *high performance* concrete. **The author suggests that the specimens within this investigation containing 2.3% fibres are at the maximum practical limit for fibre reinforced concrete.**

4.5.1 Initial joint cracking

Figure 4.5.1 shows the normalised shear stress values for the nine fibre reinforced specimens at initial joint cracking. These results were previously displayed in Table 3.2.2. The **average** value of 0.6 $MPa^{0.5}$ for initial joint cracking from previous test series is marked on the chart as a comparison.

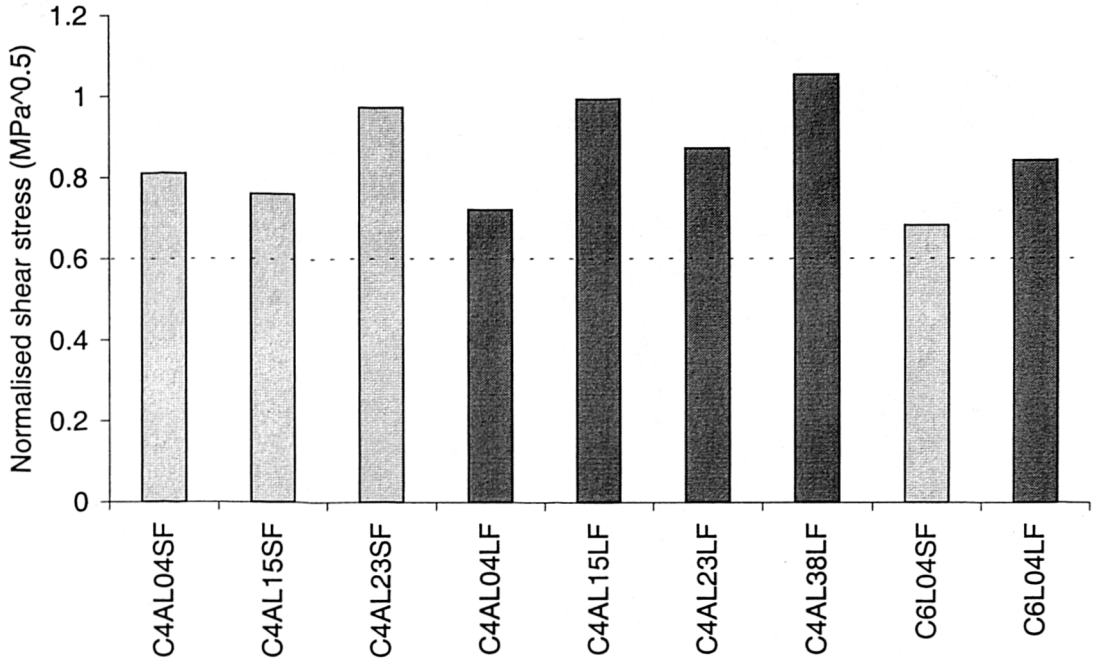

Figure 4.5.1 Shear stress at initial joint cracking - fibre reinforced specimens

Figure 4.5.1 clearly shows that an enhancement to initial joint cracking capacity was achieved by the addition of steel fibres. This was because the fibres increased the tensile strength of the concrete within the joint. The higher the percentages of fibres used the greater the initial joint cracking capacity.

The results from the nine test specimens show that both short and long fibres gave a similar performance. An enhancement to the joint capacity of around 50% was possible using 2.3% fibres. However, more tests are required to present firm conclusions.

4.5.2 Specimen failure

The specimens using bent down and U-bar beam steel detail are considered separately within this section.

Bent down beam steel detail

Figure 4.5.2.1 shows the shear stress values from the seven specimens with bent down beam steel detail at failure. Specimen C4ALN0 from the *standard* test series is included to allow comparisons with an unreinforced joint.

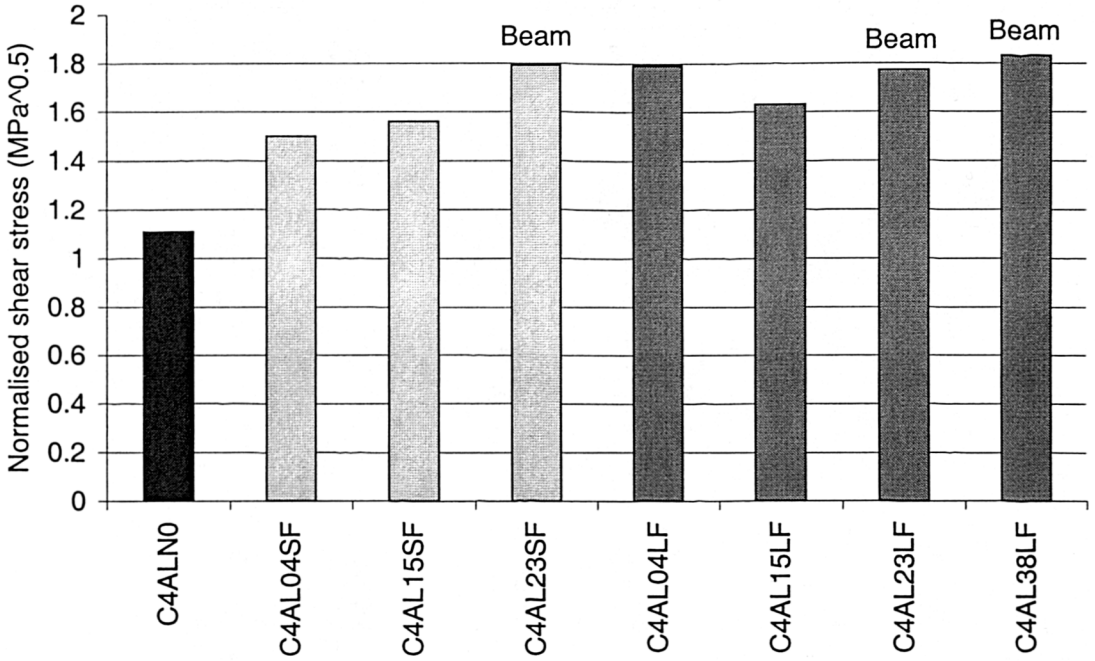

Figure 4.5.2.1 Shear stress at specimen failure - bent down beam steel detail

Figure 4.5.2.1 clearly shows that an enhancement to the ultimate joint capacity was achieved by the addition of steel fibres. The same percentage of long fibres were seen to give a greater joint enhancement than short fibres. More research is necessary to establish the ideal size and shape of steel fibre for the optimum joint enhancement. However, the use of 2.3% of either fibre type gave the joint sufficient strength to allow flexural failure of the beam.

U-bar beam steel detail

Figure 4.5.2.2 shows the shear stress values from both specimens with U-bar beam steel detail at failure. Specimen C6LN0 from the *standard* test series is included to allow comparisons with an unreinforced joint.

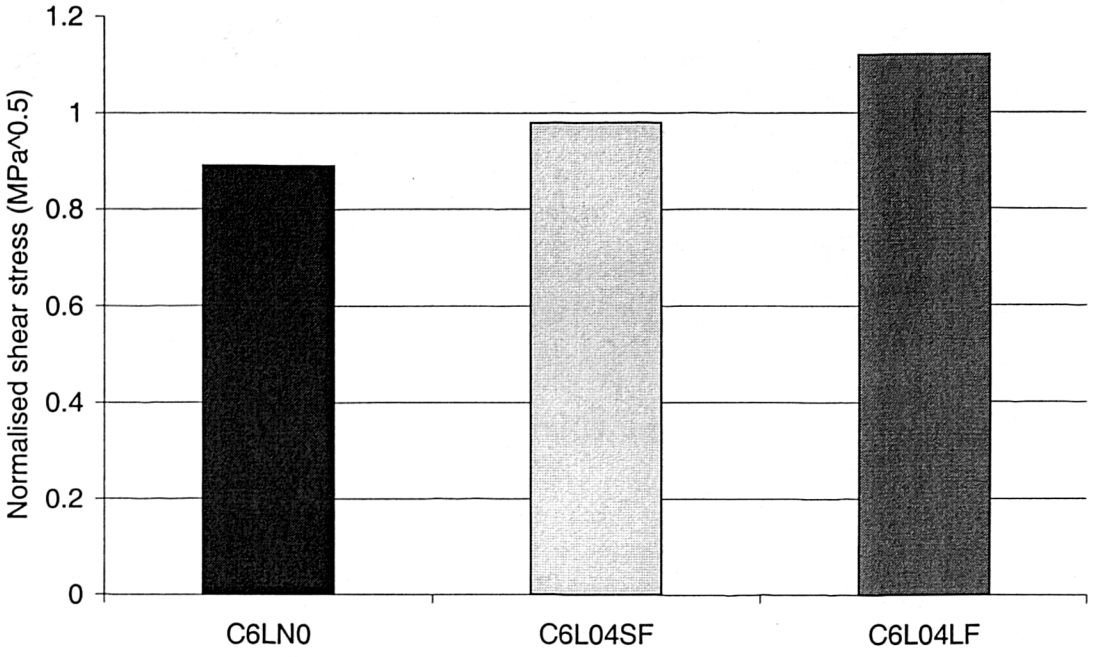

Figure 4.5.2.2 Shear stress at specimen failure - U-bar beam steel detail

Figure 4.5.2.2 shows that again only a small percentage of steel fibres was required to produce a significant joint enhancement. Using 0.4% of short fibres gave a joint enhancement of 10%. Using 0.4% of long fibres gave a larger enhancement of 25%.

Again, as with previous test series, the joint capacity of specimens with U-bar beam steel detail was lower than for specimens using bent down beam steel detail.

4.6 Additional Specimens

This section considers the results from the five additional specimens which were part of the monotonic test programme.

4.6.1 C6LN1(r)

The specimen **C6LN1** from the *standard* test series was tested early in the investigation. The column load used for C6LN1 was 100 kN as opposed to 50 kN for the other normal strength specimens. Specimen **C6LN1(r)**, considered here, was a repeat of C6LN1 using a column load of 50 kN. Specimen C6LN1(r) however contained superplasticiser.

4.6.1.1 Initial joint cracking and specimen failure

Figure 4.6.1.1 displays the normalised shear stress at joint cracking and specimen failure for specimens C6LN1 and C6LN1(r).

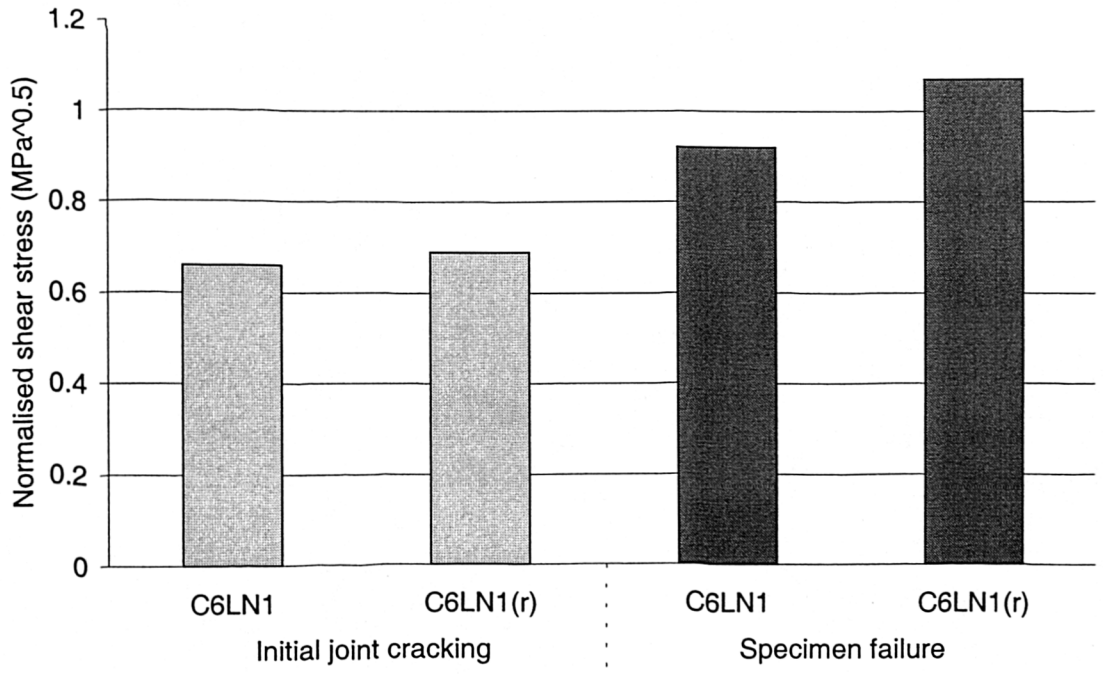

Figure 4.6.1.1 Shear stress comparisons C6LN1 / C6LN1(r)

Specimen C6LN1(r) was tested in an attempt to establish the effects of column load on joint strength. However, Figure 4.6.1.1 shows that the addition of the superplasticiser was a more significant factor. Both specimens exhibited initial joint cracking at similar values of shear stress. The superplasticiser gave an enhancement to the ultimate capacity of C6LN1(r) of around 15%. Clearly more research is required to investigate this influence of superplasticiser on the concrete-steel bond.

4.6.1.2 Reinforcement strains

Figure 4.6.1.2 displays the strains from the joint tie within specimen C6LN1(r). There is a pronounced increase in the strain within both legs of the tie at visible joint cracking. At specimen failure gauge five of *leg one* had yielded (3050 με). Generally however, the tie strain distributions were similar to those shown in Figure 4.1.3.4.2 for specimen C6LN1.

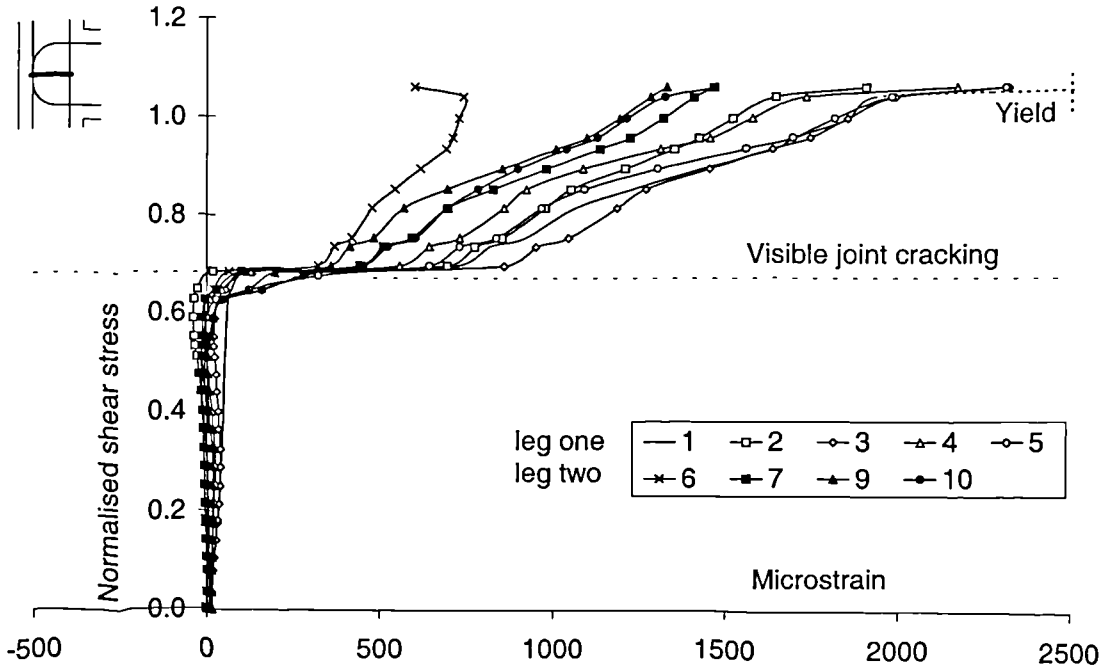

Figure 4.6.1.2 Tie strains - specimen C6LN1(r)

4.6.2 C6LN1AE

Specimen **C6LN1AE** was a repeat of specimen C6LN1A from the test series investigating *tie positioning*. The single joint tie present within C6LN1A had exhibited slippage of one of its legs. These strain distributions are displayed in Figure 4.6.2.1.1 for comparisons.

The single tie within specimen C6LN1AE had its legs fully restrained so that no slippage could occur. The legs were bent through 135° and as a result were embedded within the joint core. A diagrammatic representation of this was shown previously in Figure 2.1.6.

Within this section the tie strains are displayed first in order to establish the behaviour of the tie with its legs bent through 135°. Joint cracking and failure stresses are then considered to investigate whether any enhancement was achieved. Both specimens C6LN1A and C6LN1AE contained the same quantity of superplasticiser.

4.6.2.1 Reinforcement strains

Figure 4.6.2.1.1 displays the strains from the joint tie within specimen C6LN1A and Figure 4.6.2.1.2 displays the strains from the fully anchored joint tie within specimen C6LN1AE.

Figure 4.6.2.1.1 shows that after joint cracking, the strain development for specimen C6LN1A was slightly erratic. The strain readings from the ten gauges were not especially closely grouped and the gradient of the strain development was not steady. Clear slippage of *leg one* is apparent prior to failure.

Figure 4.6.2.1.2 shows the effect of using ties with 135° anchored legs. Nine out of the ten gauges exhibited very similar strains throughout the test. In addition the rate of strain development was reasonably constant until specimen failure. Gauge ten, within *leg two*, yielded by specimen failure (2860 με).

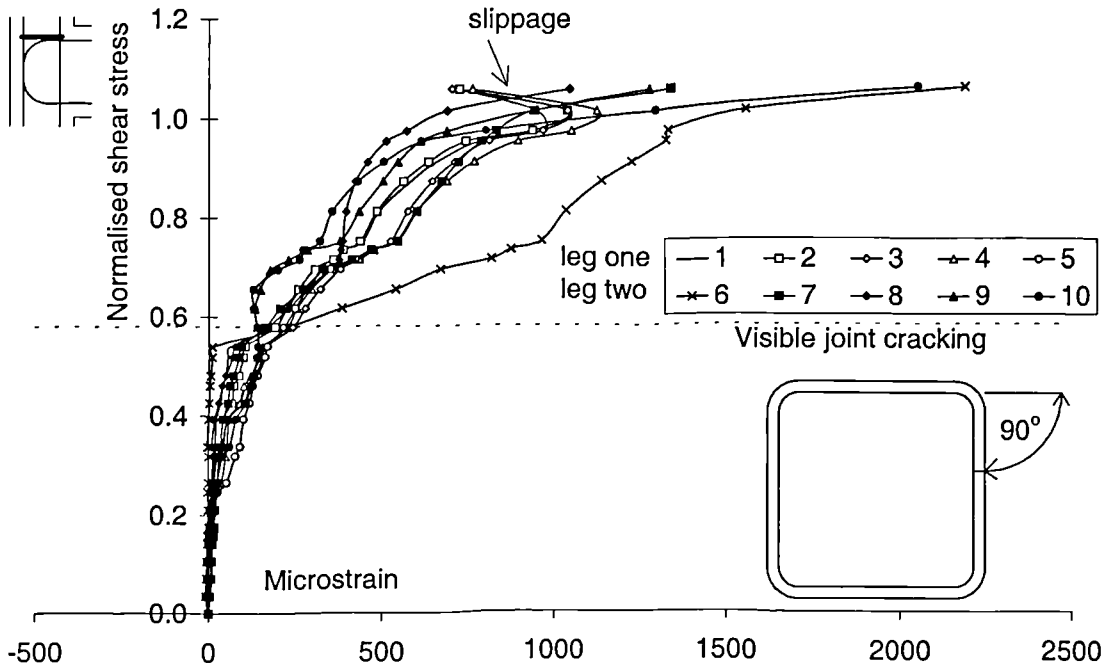

Figure 4.6.2.1.1 Tie strains - specimen C6LN1A

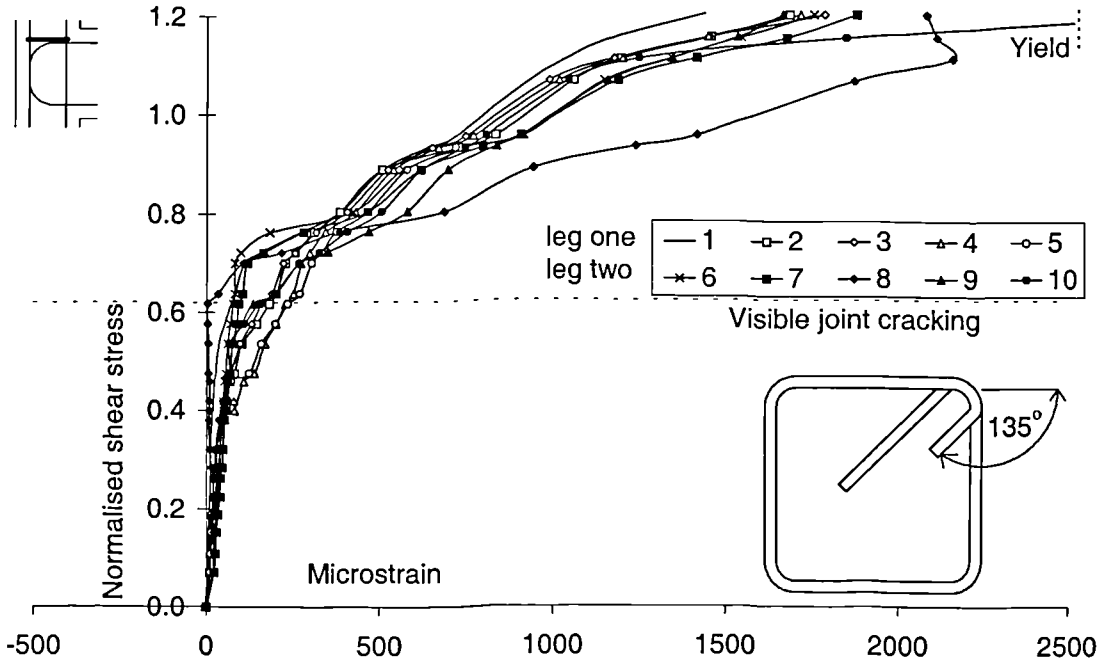

Figure 4.6.2.1.2 Tie strains - specimen C6LN1AE

4.6.2.2 Initial joint cracking and specimen failure

Figure 4.6.2.2 displays the normalised shear stress at joint cracking and specimen failure for specimens C6LN1A and C6LN1AE.

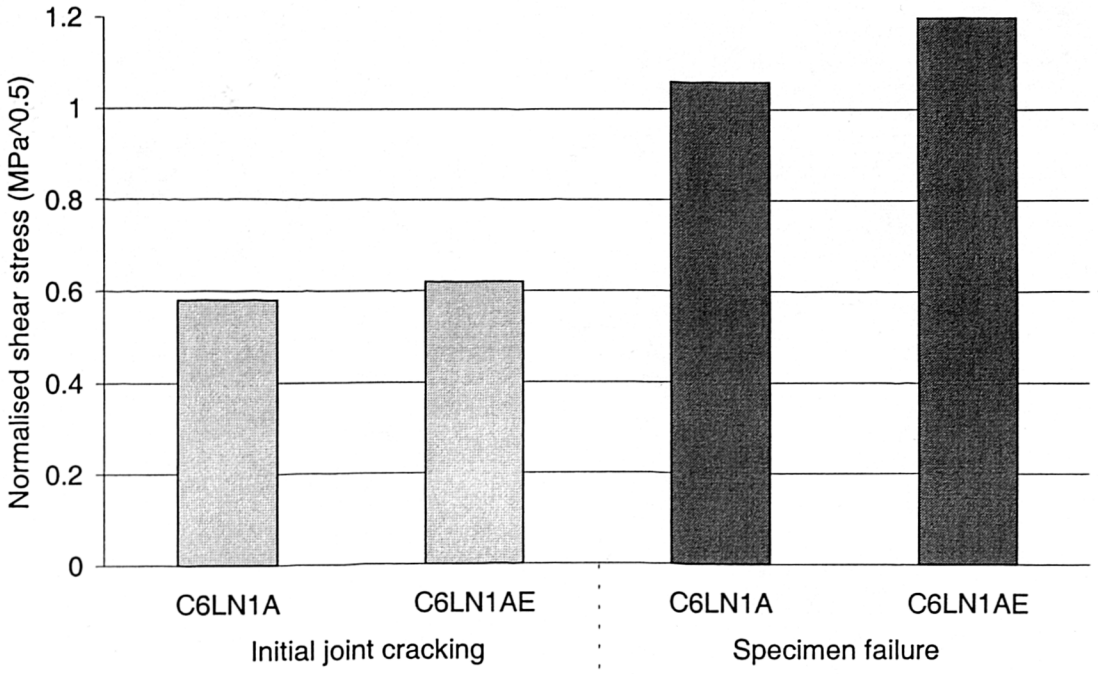

Figure 4.6.2.2 Shear stress comparisons C6LN1A / C6LN1AE

Figure 4.6.1.1 shows that specimen C6LN1AE exhibited initial joint cracking at a similar shear stress to specimen C6LN1A. As the single tie was positioned above the beam tension steel it was not considered to influence the initial cracking strength of the joint.

Specimen C6LN1AE achieved a joint capacity 13% higher than C6LN1A. The author believes that this is a significant enhancement considering this was achieved from only a single tie. It would appear that if a joint tie is to be utilised fully it should have its legs bent through at least 135°.

4.6.3 C4PLN0

An attempt to eliminate any beam steel anchorage effects from the joint behaviour was made with specimen **C4PLN0**. The elimination of any slippage consideration was believed to be achieved by attaching the 16 mm beam tension bars to a 4 mm thick, 100 × 100 mm bearing plate. A diagrammatic representation of this was shown previously in Figure 2.1.7.

Figure 4.6.3 displays the normalised shear stress at joint cracking and specimen failure for specimen C4PLN0, and specimen C4ALN0 from the *standard* test series.

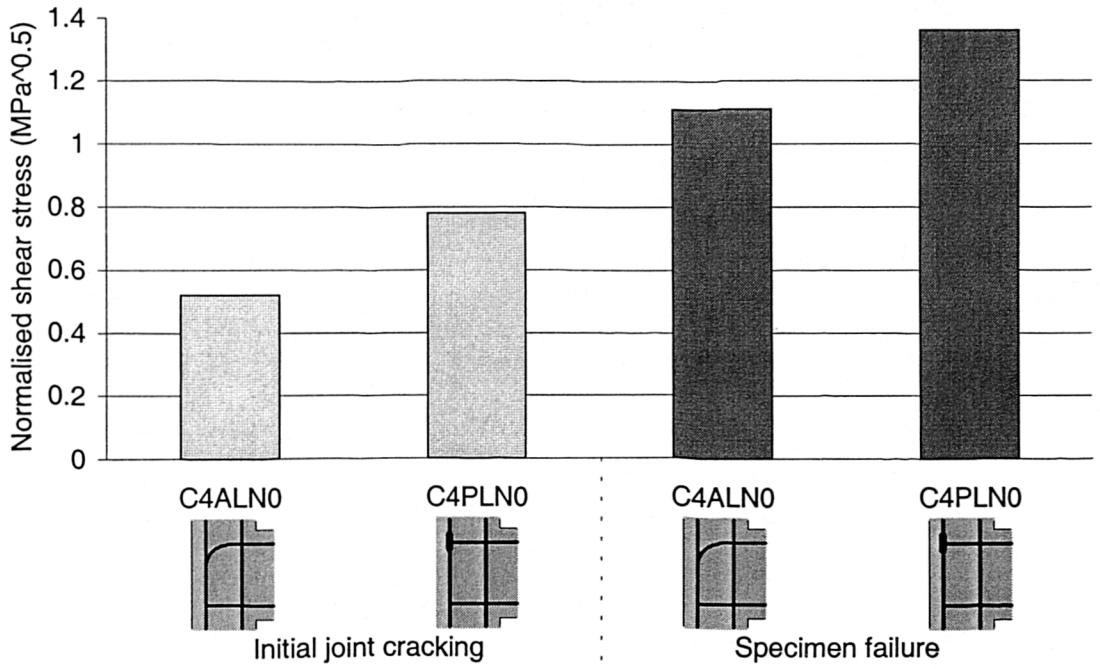

Figure 4.6.3 Shear stress comparisons C4ALN0/C4PLN0

Figure 4.6.3 shows that specimen C4PLN0 performed significantly better than specimen C4ALN0. C4PLN0 exhibited initial joint cracking at a normalised shear stress 30% higher than the average value from previous specimens of 0.6 $MPa^{0.5}$. C4PLN0 exhibited specimen failure at a normalised shear stress 23% higher than specimen C4ALN0.

However, these results may be misleading as specimen C4PLN0 contained superplasticiser which had previously contributed to a joint enhancement of around 15%. In addition to this the 4 mm thick, 100 × 100 mm bearing plate is believed to have provided additional confinement to the joint core.

Due to these concerns there is no evidence that suggests that using bent down beam steel caused any significant joint capacity reduction.

4.6.4 Plate reinforced specimens

Two specimens containing shear plates within their joints were tested. **C6LNP4** had a 4 mm shear plate within its joint area. The main steel layout within the specimen was identical to specimen C6LN0 from the *standard* test series.

C6PLNP4 had a similar 4 mm shear plate within its joint area. A pair of 16 mm rebars was provided in the upper and lower section of the beam. Beam steel anchorage was provided by a large bearing plate. Diagrammatic representations of both specimens were displayed previously in Figures 2.1.8(a)-(b).

C6LNP4

Figure 4.6.4.1 displays the normalised shear stress at joint cracking and specimen failure for C6LNP4. The performance is compared with specimens C6LN0 and C6LN5 from the *standard* test series.

Figure 4.6.4.1 shows that the presence of the shear plate increased the initial joint cracking capacity. C6PLN4 exhibited initial joint cracking at a normalised shear stress 28% higher than the average value from previous specimens of 0.6 $MPa^{0.5}$.

The shear plate also increased the ultimate capacity of the joint. The performance of specimen C6PLN4 was comparable to specimen C6LN5 which had five ties within the joint.

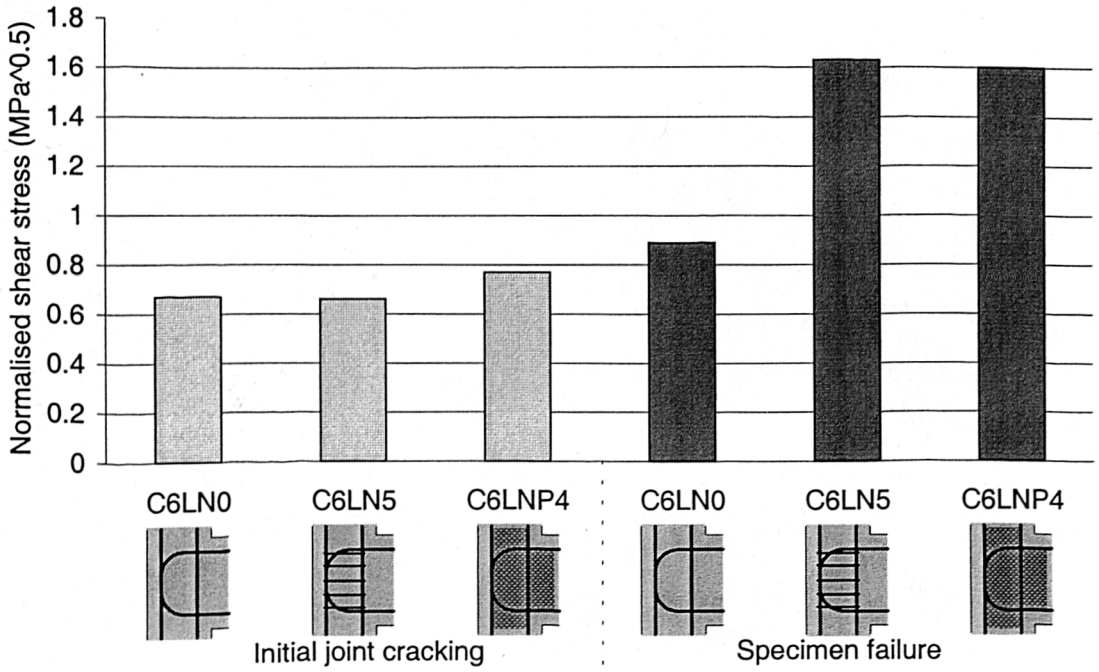

Figure 4.6.4.1 Shear stress comparisons - C6LN0, C6LN5 and C6LNP4

C6PLNP4

Figure 4.6.4.1 displays the normalised shear stress at joint cracking and specimen failure for C6PLNP4. The performance is compared with specimen C6LN5 from the *standard* test series and specimen C6LNP4.

Figure 4.6.4.1 shows that the initial joint capacity of specimen C6PLNP4 was similar to specimen C6LNP4. However, the ultimate joint capacity of C6PLNP4 was significantly higher than C6LNP4. The fully anchored main beam steel bars allowed C6PLNP4 to achieve a joint capacity almost 50% greater than C6LNP4.

After monotonic testing of both specimen C6LNP4 and C6PLNP4, they were loaded further to investigate their cyclic response. This is considered in Chapter 8.

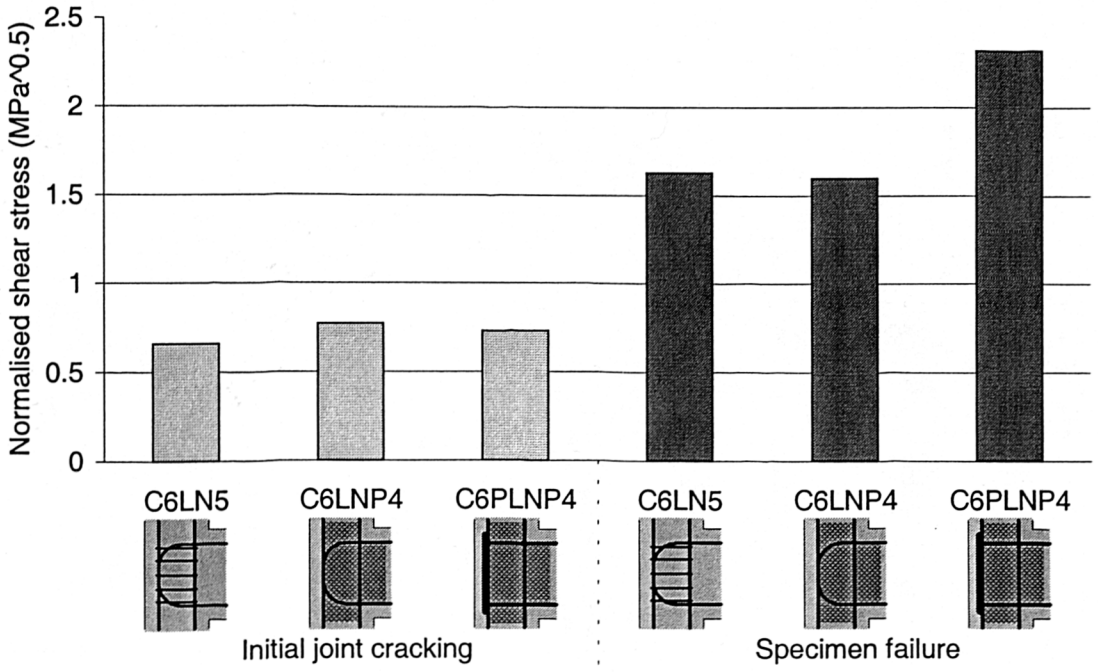

Figure 4.6.4.2 Shear stress comparisons - C6LN5, C6LNP4 and C6PLNP4

Neither specimen C6LNP4 or C6PLNP4 failed within the beam. The shear plates extended into the beam by a distance of 100 mm. The intention of this was to induce a plastic hinge 100 mm away from the column face. However, neither specimens could reach their increased ultimate moment of resistance. The author suggests that in any future designs the shear plate should extend a shorter distance into the beam.

4.7 Use of the Experimental Data

The next stage of this investigation was to use the data from the monotonic test program to calibrate a finite element model.

The aim was to develop a model which could be used as an aid for the design of any external beam-column connection. The user of this model would simply add the particular steel layout to the finite element mesh design.

The model was developed and calibrated using experimental data from this and previous investigations. Once verified, this model was then used to complete a comprehensive parametric study.

The following chapter of this thesis details this finite element study.

5. Finite Element Analysis

Within this investigation an attempt to model the monotonic experimental specimens, using finite element methods, was made. The results from this are presented within this chapter.

Previously, two attempts at finite element modelling of monotonic beam-column connections have been made. In 1974, Taylor [1] used an *elastic* finite element method to model his specimens at initial joint cracking. The aim of this was for the model to develop diagonal tensile stresses, similar to the tensile strength of the concrete, when initial joint cracking occurred. Taylor concluded that although the model gave good results, the modelling process was very time consuming. Further details of Taylor's elastic finite element model are presented in Appendix C1. (It should be noted, however, that to model post-cracking concrete behaviour a *non-linear* finite element model is required).

In 1998, Vollum [12] used a non-linear finite element package in an attempt to analyse experimental specimens similar to Reys de Ortiz's [10]. This, however, was presented in the Appendix of his thesis as his main concern had been to develop a successful strut-tie analytical method. Vollum concluded that his attempt at finite element modelling was not very successful as the specimen failure loads were under predicted due to premature, extensive cracking within the joint. The model did, however, demonstrate that the dominant mode of shear transfer through a beam-column joint was via an inclined strut.

As outlined in the Literature Review and in Appendix A1 to A3, three attempts at strut-tie modelling of beam-column connections have been made in previous research [10, 11, 12]. However, there has been no successful modelling of beam-column connections using finite element techniques.

Within this investigation it was originally anticipated that a programme of numerical modelling would be undertaken at Cornell University using the commercial finite

element package DIANA [49]. This modelling was to be of the experimental work outlined in this thesis. Unfortunately Cornell University was unable to obtain funding. Consequently, it was decided to undertake this work at the University of Durham at a stage when the experimental work was already well advanced.

After discussions with Ove Arup and Partners (Research and Development), the software package SBETA [50] was purchased from Cervenka Consulting, Prague. SBETA was cheaper than DIANA but was believed to be equally effective and suitable for practical design. This was believed to be the first purchase of this package in the UK although it had been used previously, for design purposes, in Germany, Norway and Switzerland [50]. The modelling originally took place on a 200 MHz personal computer (pc). This was considered fast at the time of purchase in 1997. Later two additional machines became available which were also dedicated to the project, a 133 MHz and a 50 MHz pc. A typical production run took around two and a half hours on the 200 MHz pc and the author estimates that over 300 such runs were completed.

The aims of this finite element analysis were :

1. To validate the SBETA package by analysing problems with known solutions.
2. To develop a standard mesh arrangement to model all reinforced concrete external beam-column connection specimens with the only variables being the material properties, the specimen dimensions and the steel layout. This would save time in future design as it would eliminate the problems associated with mesh development and refinement.
3. To validate this standard mesh arrangement by showing that it exhibited the correct failure mechanisms and loads.
4. To establish an acceptable balance between precision and time / computing costs.
5. To model experimental specimen response and failure loads from the author's test specimens, to a good level of accuracy.
6. To model experimental specimen response and failure loads from previous research, to a reasonable level of accuracy.

7. To conduct a parametric study to establish the influence of the main parameters on beam-column connection behaviour.

The method of finite element analysis [51] is so widely used in structural design today that a detailed description is not included within this thesis. An overview of the non-linear finite element computer package, SBETA, is given in the following section and a full description is given elsewhere [52].

5.1 The Non-Linear Finite Element Package, SBETA

SBETA, a non-linear finite element package, was used for the specimen modelling. SBETA has a user friendly, mesh generating pre-processor which allows pre-defined concrete and steel material properties to be used. Definitions for equilibrium control and maximum iteration limits are also user defined. First order quadrilateral elements are formed from a pair of triangular elements with nodes at each corner. These elements are automatically generated within larger, user defined *macroelements*.

A number of post-processing programs are available within SBETA and displacements and stress data from all of the concrete elements and steel bar sections are produced for each load step of the solution.

5.1.1 Pre-processing

SBPRE is the pre-processor within the SBETA package and Figure 5.1.1 displays an example *screen dump* from this program. SBPRE is reasonably user friendly with the design of the model layout possible using the *mouse* and *scroll-down* menu bars.

Using SBPRE, a finite element model is developed as follows :

1. The concrete and steel properties are defined (see Section 5.2.1).
2. The nodes, which form the corners of the macroelements, are positioned.
3. The lines connecting the nodes are added and the user defines how many sections

each line is divided into - the more sections the more complex the mesh.

4. The macroelements between the lines are generated defining the concrete's thickness, density and how the mesh is generated. If smeared reinforcement is to be used then this is specified and the reinforcement properties are *smeared* across the width of the macroelement.
5. Discreet steel reinforcement is added which is defined at starting and end points within the model and is given a cross sectional area. If the bar is curved then, in addition, the bar radius is defined. Within this investigation only discreet reinforcement was used due to it being more precise than smeared reinforcement.
6. The restraints and the loads are applied to the model.
7. The load history is defined which can be proportional or non-proportional.
8. The equilibrium control, maximum number of load steps, iteration limits and solution methods are all defined (see Section 5.4).

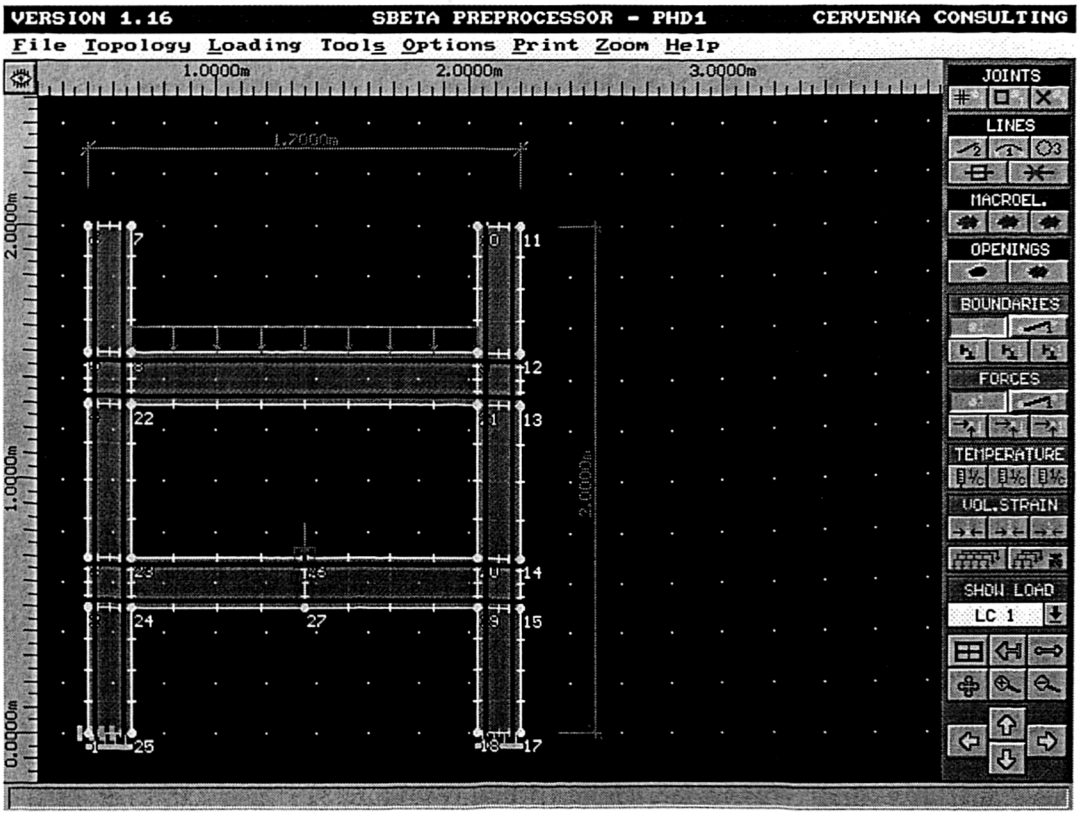

Figure 5.1.1 The pre-processor, SBPRE

The final part of the pre-processing is to run a program called GENES which takes the SBPRE input file and converts it into a format suitable for the main solution program SBETA.

5.1.2 Processing

Only first order quadrilateral elements are available. These have two degrees of freedom and a single integration point at the centre. First order elements have linear strain gradients which means that mesh refinement is necessary in areas of the structure where concrete crushing or complex stress behaviour is expected. Accurate results of complex problems are not possible if too coarse a mesh is used. Two solution methods are available, **Newton-Raphson** and **Arc-length** :

The **Newton-Raphson** method applies the user defined load in proportional steps and evaluates the required displacements to maintain equilibrium each time. This method should be used when an approximate failure load is known. Within this investigation specimen failure was defined when a pre-set displacement was reached.

The **Arc-length** method takes the magnitude of the displacement from the first applied load step and then continues the solution in steps equal to this first displacement. Equilibrium is maintained by evaluating the equivalent applied load. Specimen failure is defined as the stage at which the model can sustain no further increase in load. This method should be used when an approximate displacement at failure is known.

Ideally the Newton-Raphson method would be used over the initial load stages and the Arc-length method for the final load stages. This would allow the modelling to initially simulate the loading of the specimen but then detect the descending branch of the load-deflection curve at failure. Unfortunately, this option was not available with SBETA.

Both processes use input files from the GENES program to calculate their solution. Files are produced which include all of the output data. The user can view this continuous solution in a choice of three modes; *hidden*, *alpha-numeric* or *graphical*. Figure 5.1.2 shows a screen dump from the *graphical* mode.

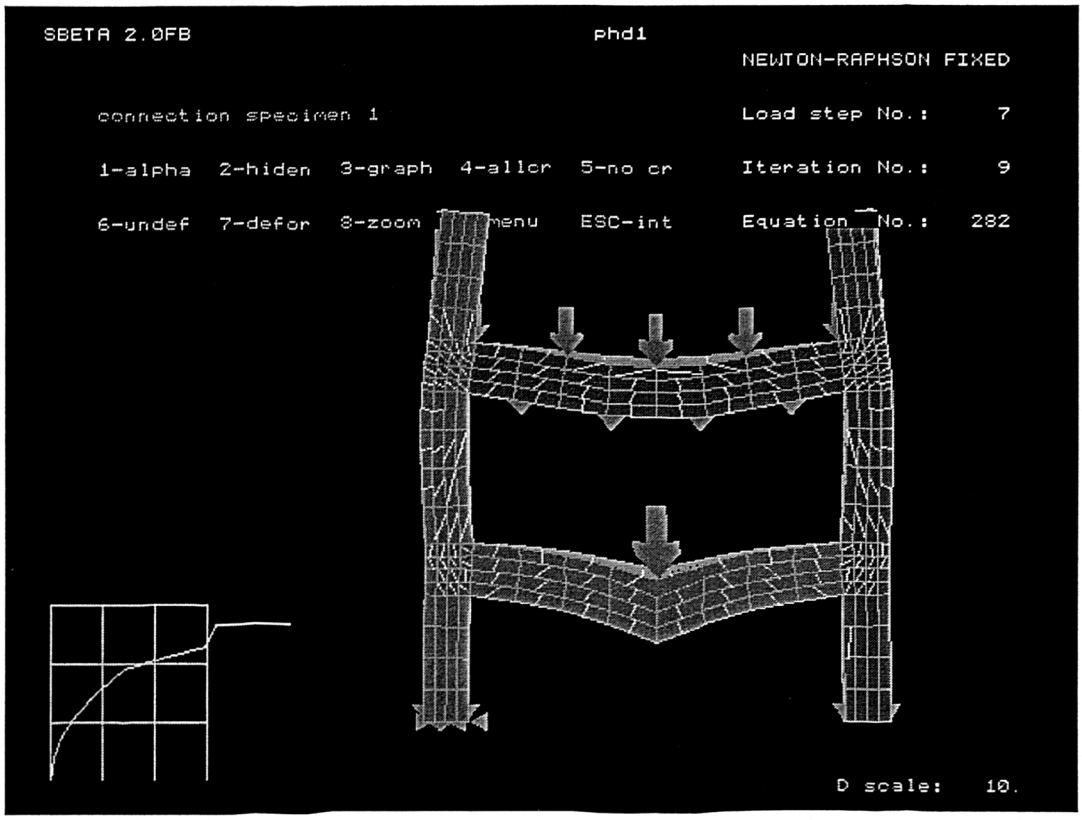

Figure 5.1.2 The solution program, SBETA - graphical display

5.1.3 Post-processing

The output data, from each load step, is produced in standard text files. The user may process these using independent programs. Alternatively a number of post-processing packages are available within SBETA, including :

SB-ISOLINE graphically displays stresses or strains within the model (lines),

SB-ISOAREA graphically displays stresses or strains within the model (areas),

SB-CROSS evaluates and plots moments and forces along a section's axis,

SB-ROD extracts and plots stresses along each reinforcing bar.

5.2 Development of the Model

Thanks must go to **Dr Paul Baglin** (see *Acknowledgements*) who provided the author with some much appreciated support with the development of the model. He worked as a Research Associate at the University of Durham for nine months on a parallel investigation alongside the author. He had past experience using finite element methods from his doctorate [40], which involved the finite element modelling of plate reinforced concrete beams.

Thanks must also go to **Cervenka Consulting**, in particular **Dr Jana Margoldova**, for their support and assistance with the package.

5.2.1 Material properties

5.2.1.1 Steel

The finite element package, SBETA, allows the steel stress-strain response to be user defined. Figure 5.2.1.1.1 and 5.2.1.1.2 show the two available options.

Figure 5.2.1.1.1
Bi-linear stress-strain relationship

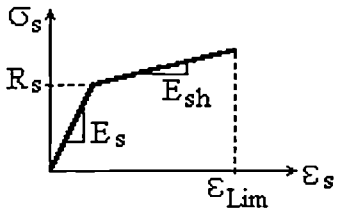

Figure 5.2.1.1.2
Multi-linear stress-strain relationship

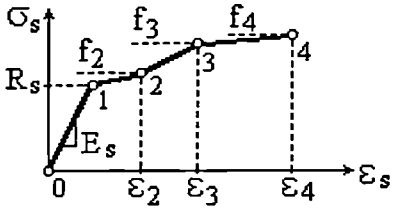

Within this investigation the experimental stress-strain curves for the steel (Section 2.1.2) were all seen to be reasonably similar. To model this steel behaviour the bi-linear stress-strain relationship, shown in Figure 5.2.1.1.1, was selected.

The steel properties chosen were as follows :

Yield strength, R_s = 500 MPa
Young's modulus, E_s = 200 kN/mm^2
Post-yield modulus, E_{sh} = 0

Figure 5.2.1.1.3 displays the bi-linear response generated from these values which is compared with the experimental curves from three 16 mm bars used in this investigation. Due to the experimental stress-strain response being almost perfectly *elastic-plastic* the correlation was very good.

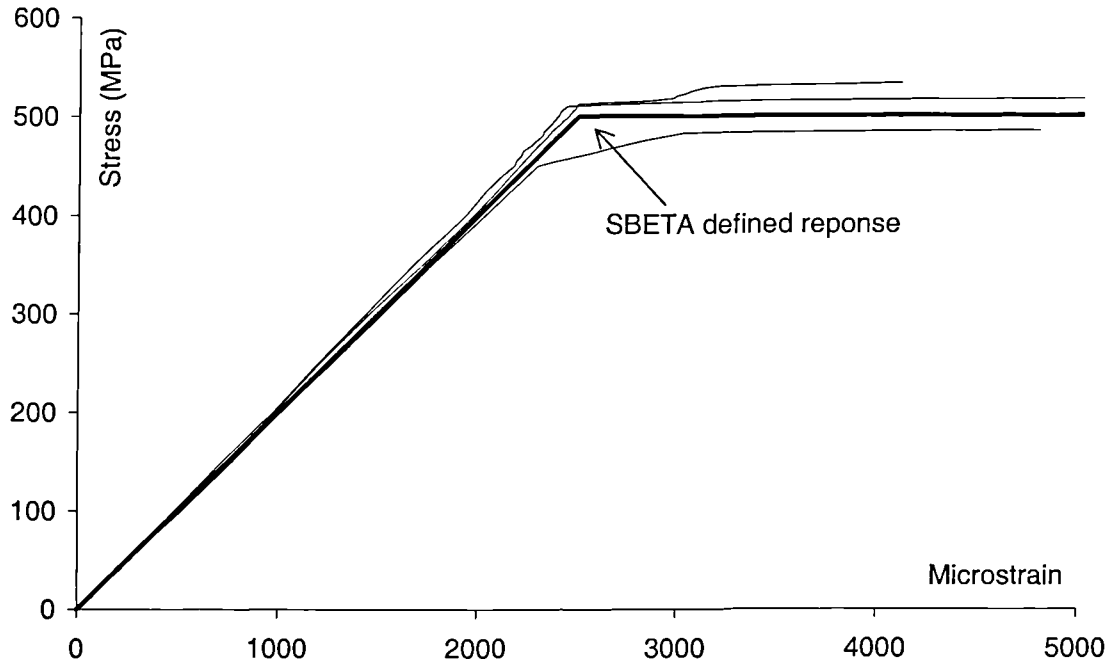

Figure 5.2.1.1.3 Modelled stress-strain response for the 16 mm bars

5.2.1.2 Concrete

SBETA allows a number of different concrete properties to be user defined. Figure 5.2.1.2.1 shows the stress-strain relationship; $\mathbf{R_c}$ is the uniaxial compressive cylinder strength of the concrete, $\mathbf{R_t}$ is the uniaxial tensile strength and $\mathbf{E_c}$ is the Young's Modulus.

Figure 5.2.1.2.1 shows the concrete as being in one of four states :

1. Tension prior to cracking of the concrete.
2. Tension softening after cracking of the concrete.
3. Compression prior to crushing of the concrete.
4. Compression softening after crushing of the concrete.

Figure 5.2.1.2.1
Stress-strain relationship

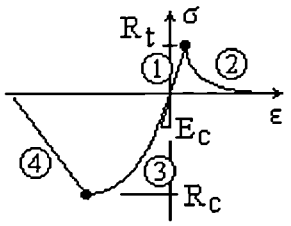

SBETA evaluates the stress(σ)-strain(ε) relationship for uncrushed concrete in compression (state 3) from the following equation :

$\sigma = R_c(2a-a^2)$ .....(eq. 5.1.2.1)

where $a = \varepsilon(E_c/2R_c)$.

Figure 5.2.1.2.2 shows the bi-axial failure relationship of the concrete; σ_1 and σ_2 are the principle stresses in the concrete.

Figure 5.2.1.2.2
Bi-axial failure
relationship

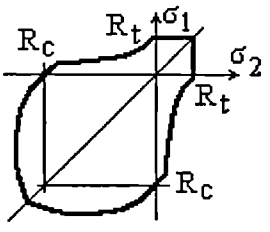

Figure 5.2.1.2.3 shows the tension softening decay line for the cracked concrete; $\mathbf{c_3}$ is the strain at which all tensile strength is lost.

Figure 5.2.1.2.3
Stress-strain relationship in tension

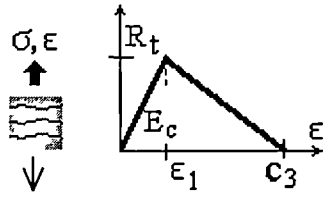

Figure 5.2.1.2.4 shows the compressive strength of the cracked concrete; the compressive strength of the cracked concrete is reduced by the factor **c**.

Figure 5.2.1.2.4
Compressive strength of cracked concrete

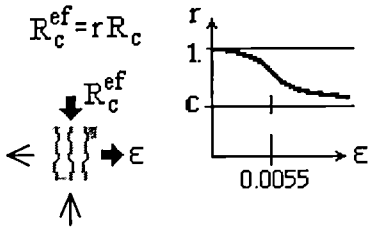

Figure 5.2.1.2.5 shows the compression softening decay line for the crushed concrete; the constant $\mathbf{c_d}$ defines the gradient of this line, ε_c is the crushing strain of the concrete.

Figure 5.2.1.2.5
Compression strain softening

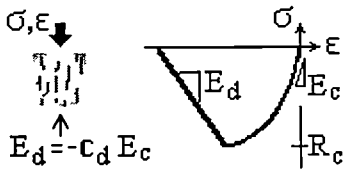

If required SBETA can generate default properties for the concrete but throughout this investigation the concrete properties were evaluated using the methods displayed in Table 5.2.1.2.

5.2.2 Validation of SBETA

Before SBETA could be used to model a structure as complex as a reinforced concrete beam-column connection it was important that the package could be shown to model simple problems, with known solutions, to a good level of accuracy.

The following reinforced concrete members were modelled :

1. A concrete cylinder (in compression and tension).
2. A simply supported reinforced concrete beam.
3. A reinforced concrete cantilever with similar dimensions to those used for the beam within this investigation.

Table 5.2.1.2 Concrete properties

Property		Value	Units
Uniaxial compressive cylinder strength	**Rc**	$0.8 \times f_{cu}$	MPa
Tensile strength	**Rt**	$0.4 \times f_{cu}^{0.5}$	MPa
Young's Modulus	**Ec**	$(22+(0.2 \times f_{cu})) \times 10^3$	MPa
Tension softening strain	$\mathbf{c_3}$	300×10^{-6}	-
Cracked strength factor	**c**	0.3	-
Crushing strain	$\mathbf{e_c}$	$(2550-(5 \times f_{cu})) \times 10^{-6}$	-
Compression softening factor	$\mathbf{c_d}$	0.33	-
Poisson's ratio	$\mathbf{n_u}$	0.16	-

Notes

1. All values are taken from either experimental data or from BS 8110 [3],
2. The compressive stress-strain relationship (eq 5.1.2.1) generates a different value for the crushing strain than that quoted in Table 5.1.2.1. In this situation the SBETA solution uses the prompted value as opposed to the default value.

5.2.2.1 Cylinder model

5.2.2.1.1 Uniaxial compression

Figure 5.2.2.1.1.1 shows the mesh design used to represent a simple concrete cylinder. The cylinder was represented as a square based prism due to limitations with the software. The *cylinder* dimensions were 300 × 100 × 100 mm and the mesh was kept as simple as possible using 50 mm square elements. The bottom face of the cylinder was fully restrained and the load was uniformly distributed over the top face of the cylinder. The solution method chosen was Newton-Raphson using load steps

of 1 kN. All concrete properties were calculated from a cube strength of 60 MPa using the methods shown in Table 5.2.1.2.

Figure 5.2.2.1.1.2 shows the comparison between the load-deflection response of the cylinder and the stress-strain input data for the concrete in compression (as previously defined in Section 5.2.1.2). As expected a good level of correlation was seen with the slight increase in stiffness exhibited by the model was believed to be due to bi-axial effects from the end restraints.

5.2.2.1.2 Uniaxial tension

To model the cylinder under uniaxial tension, the same mesh design was used as for the compressive model. Figure 5.2.2.1.2.1 shows the comparison between the load-deflection response of the modelled cylinder and the stress-strain input data for the concrete under uniaxial tension (as defined previously in Section 5.2.1.2). An almost perfect correlation of the results can be seen.

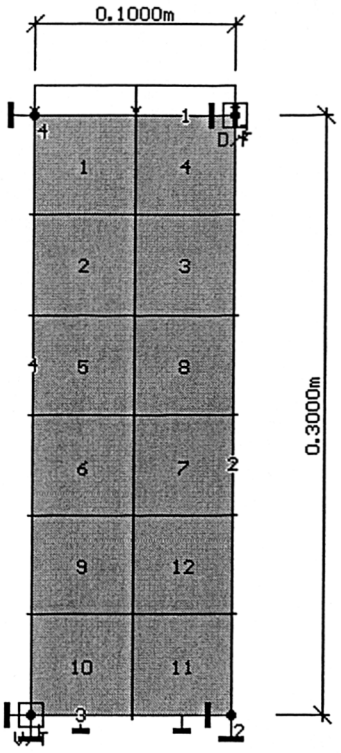

Figure 5.2.2.1.1.1 Cylinder model under uniaxial compression

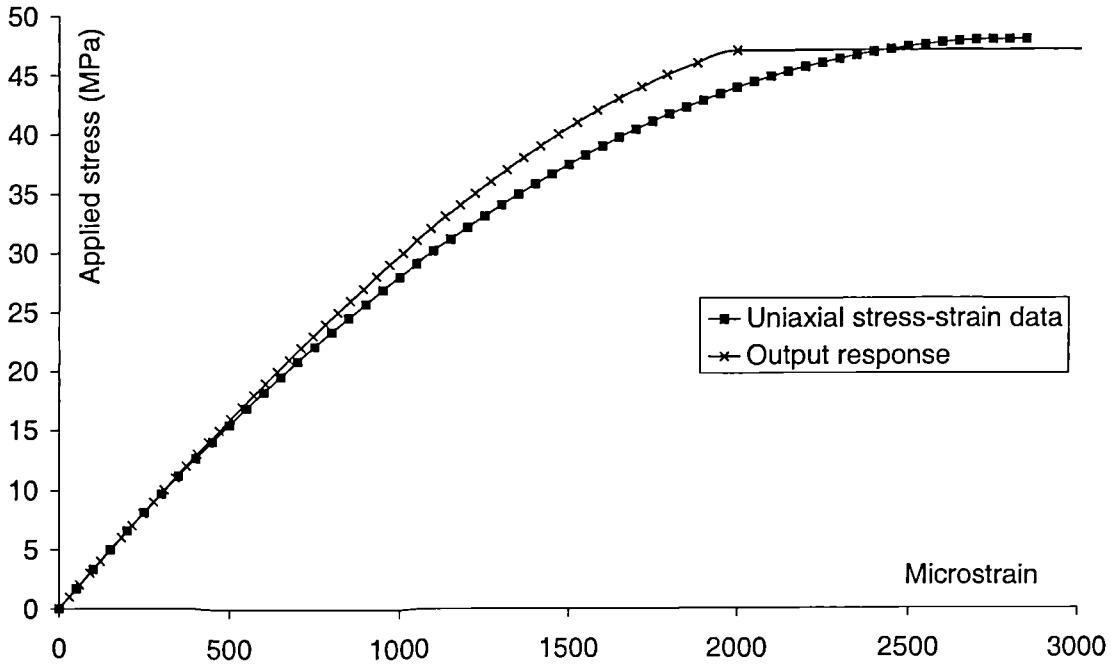

Figure 5.2.2.1.1.2 Cylinder in compression, load-strain response

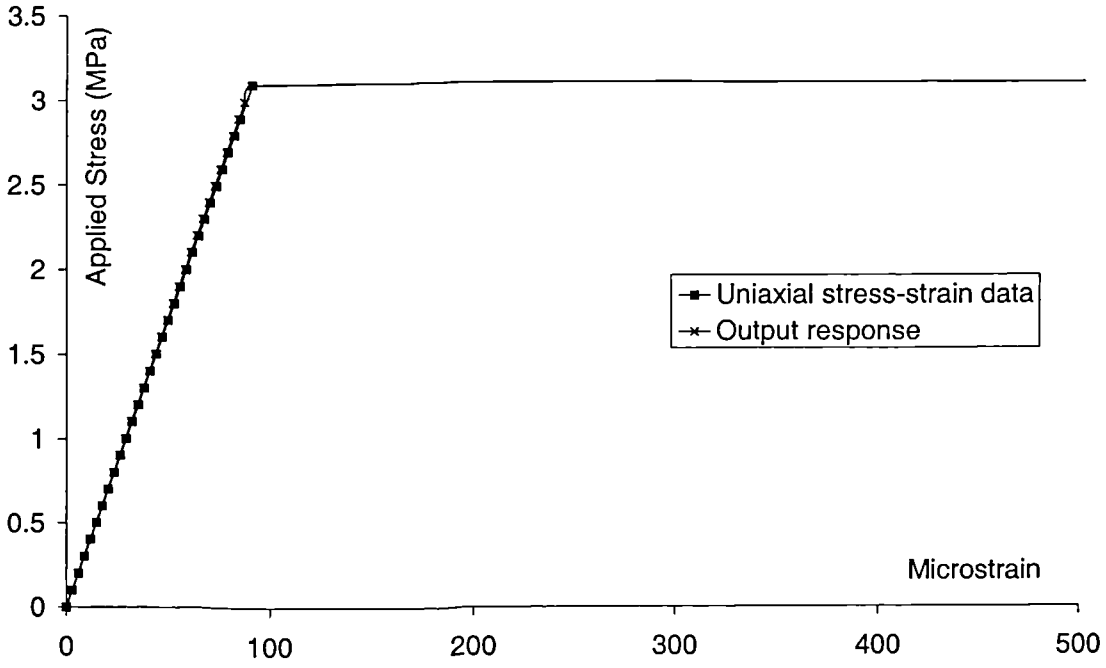

Figure 5.2.2.1.2.1 Cylinder in tension, load-strain response

5.2.2.2 Simply supported beam model

Figure 5.2.2.2.1 shows the dimensions of the reinforced concrete beam modelled in this example. Experimental data was not available for this case study but the flexural behaviour of reinforced concrete members is well researched and the failure load of the model was compared with that predicted by BS 8110 [3] (with all safety factors removed).

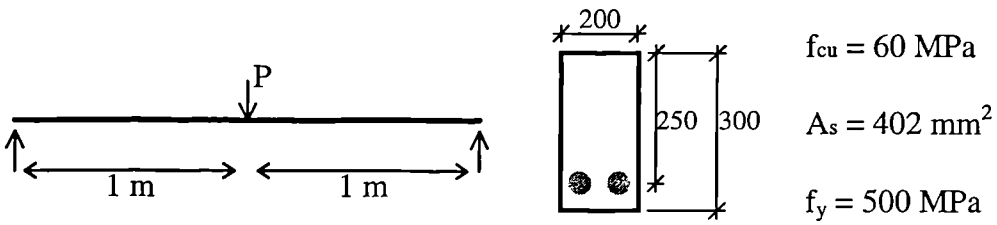

Figure 5.2.2.2.1 Simply supported beam

As the considered beam was expected to fail in flexure it was crucial that the elements in the compression zone at the top of the beam were refined to a size small enough to allow for the crushing of the concrete. For the models considered, the load was applied to the top face of the beam and the deflection was monitored from the middle node on the bottom face of the beam.

Three models were considered :

Figure 5.2.2.2.2 shows the model **R**einforced **C**oncrete **B**eam **A** (**RCBA**) which had no mesh refinement and used a relatively coarse global mesh. The load was applied to the middle node on the top face of the beam.

Figure 5.2.2.2.3 shows the model **RCBB** which had a refined mid-section of the beam with the smallest element size being 35 × 35 mm square. The loading over this area was distributed over the central four elements to eliminate local crushing due to the point load.

Figure 5.2.2.2.4 shows the model **RCBC** which had a highly refined upper mid-section of the beam with the smallest element size being 15 × 15 mm square. Again the loading was distributed over the central region to prevent local element crushing.

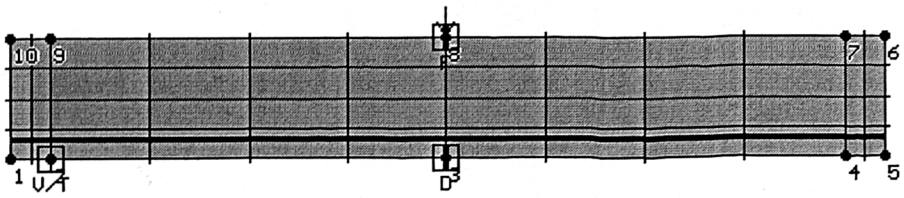

Figure 5.2.2.2.2 Model RCBA

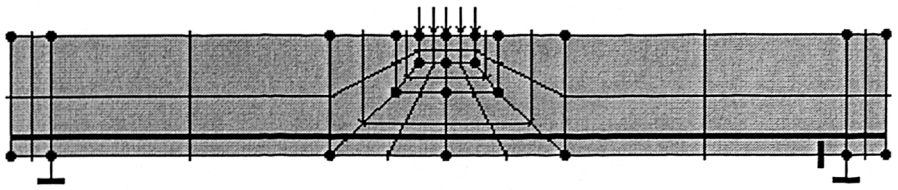

Figure 5.2.2.2.3 Model RCBB

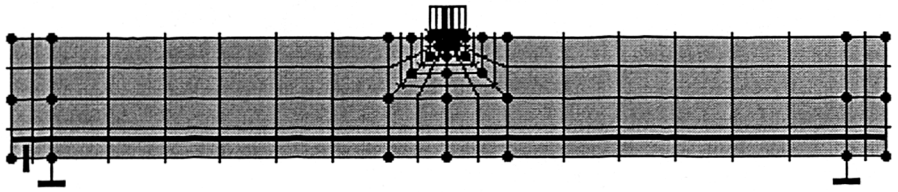

Figure 5.2.2.2.4 Model RCBC

Figure 5.2.2.2.5 shows the load deflection response from the three models. The predicted failure load from BS 8110 [3] is indicated by the dashed horizontal line.

Figure 5.2.2.2.5 shows that the performance of model RCBA was very poor as it continued to withstand an increasing load well in excess of the BS 8110 failure prediction. The model RCBB showed a much better response although it only contained 56 elements, 8 more than RCBA. The reason for the vast improvement in performance for approximately the same computing time highlights the importance

of mesh refinement. The model RCBC used 128 elements to produce a more refined compression zone and as a result displayed the best performance.

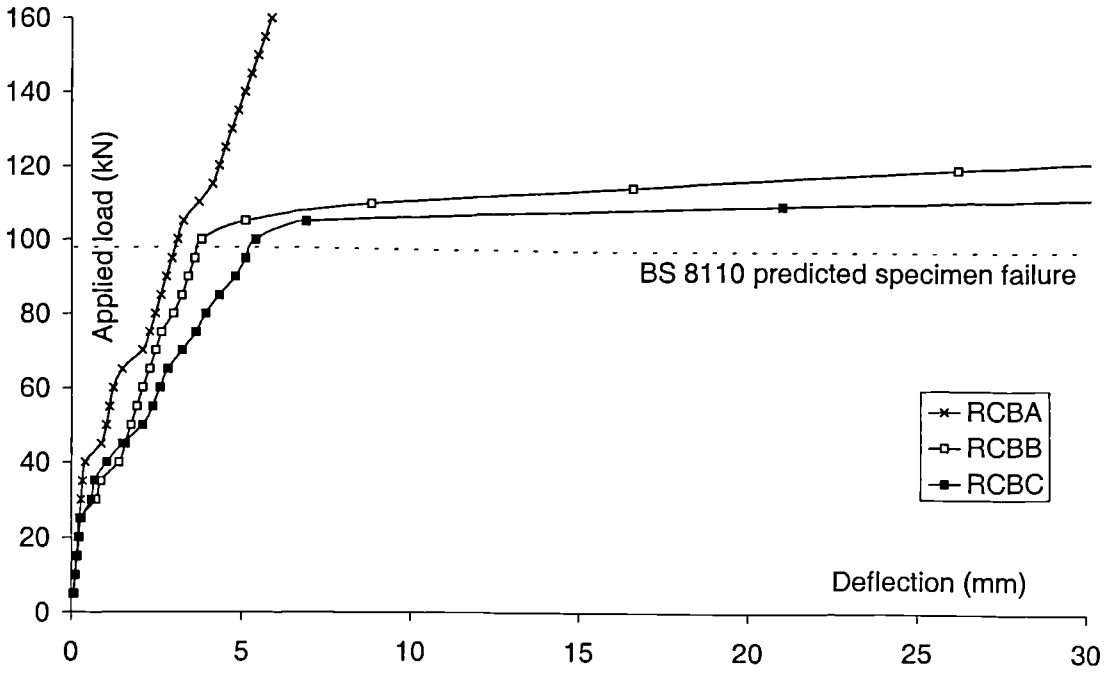

Figure 5.2.2.2.5 Load-deflection response of the models

5.2.2.3 Cantilever model

Using similar mesh refinement techniques developed in Section 5.2.2.2 the reinforced concrete cantilever shown in Figure 5.2.2.3.1 was modelled. The dimensions of the cantilever were the same as those for the beam for the experimental investigation.

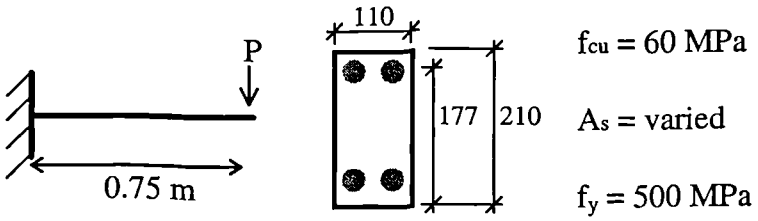

Figure 5.2.2.3.1 Simple cantilever

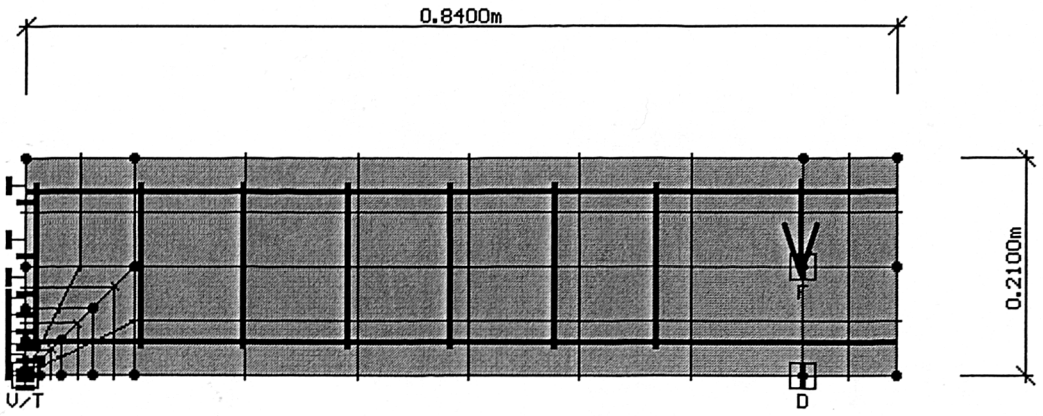

Figure 5.2.2.3.2 Modelled cantilever

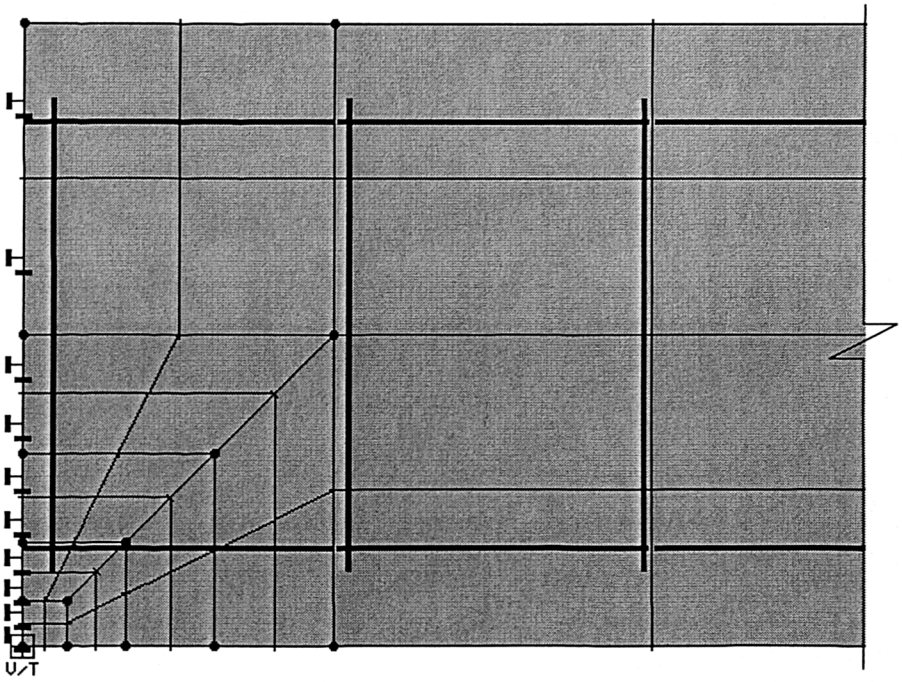

Figure 5.2.2.3.3 Modelled cantilever - mesh refinement

Figure 5.2.2.3.2 shows the mesh used to model the simple cantilever. Figure 5.2.2.3.3 shows a more detailed view of this same mesh. The same layout was used for two different steel percentages; for the model **CAN**tilever **A** (**CANA**) 2T16 mm bars were used for the main steel; model CANB used 2T12 mm bars. 6 mm beam stirrups were used for shear reinforcement in both specimens. Figure 5.2.2.3.4

displays the response from both models. The dashed horizontal lines again represent the BS 8110 [3] predicted failure loads.

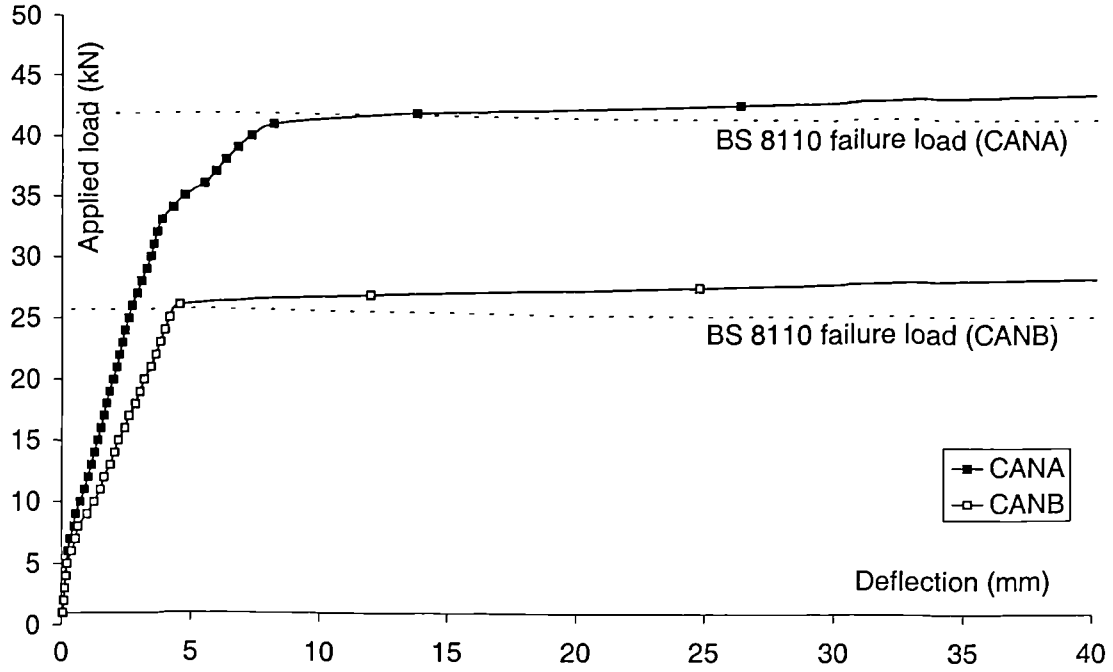

Figure 5.2.2.3.4 Load-deflection response - modelled cantilevers

Figure 5.2.2.3.4 shows that an ultimate capacity very similar to that predicted by BS 8110 [3] was achieved by the modelling. Comparisons can also be made from experimental specimens. Specimen C3 from Scott's [8] research failed in flexure at a beam load of 26 kN. This is a similar load to that which the cantilever model CANB failed at. The author's specimens C4ALN3C and C4ALN3D failed, in flexure, at beam loads of 41 kN. Similarly, the model CANA failed at a load near this value.

5.2.3 The beam-column connection model

The mesh refinement methods used for the beam model, RCBC, and the cantilever model, CANB, were developed further to produce a *standard* beam-column connection mesh. Figure 5.2.3.1 shows the **B**eam-**C**olumn **C**onnection model **A**, **BCCA**. The compression zones within the beam, the lower column and the upper column were all similarly refined. The mesh within the joint zone was also refined

in an attempt to model the shear and anchorage effects. The elements in the beam and column spans were left reasonably coarse to allow for flexibility and to minimise computational costs. **This final model contained 472 individual elements.** Figure 5.2.3.2 shows a magnified view of the joint area of BCCA.

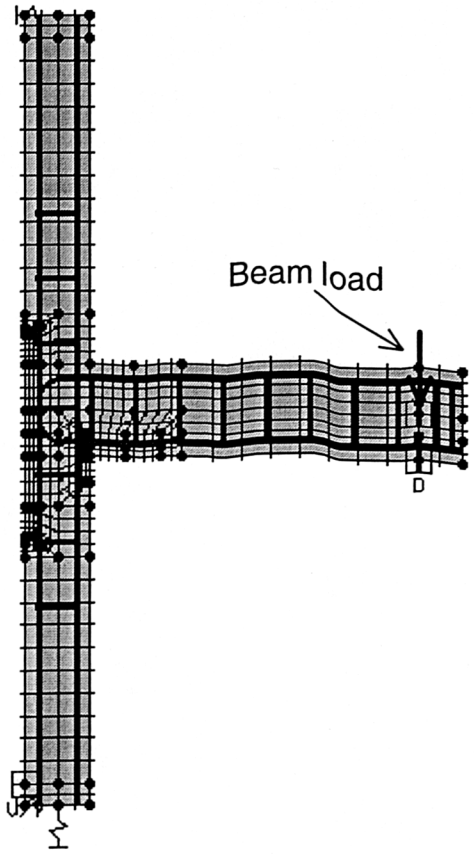

Figure 5.2.3.1 The model BCCA

The model used concrete with a compressive cube strength of 60 MPa and was based on the experimental specimen C6LN1. The experimental column load was expressed as a distributed load over the elements in the upper column. Beam loading was applied in increments of 1 kN at the point indicated in Figure 5.2.3.1.

The end restraints were modelled by the use of vertical and horizontal springs at the bottom of the column and a horizontal spring at the top of the column. Spring supports allowed a small amount of movement but full rotation and these displacements were later calibrated to the actual specimen response.

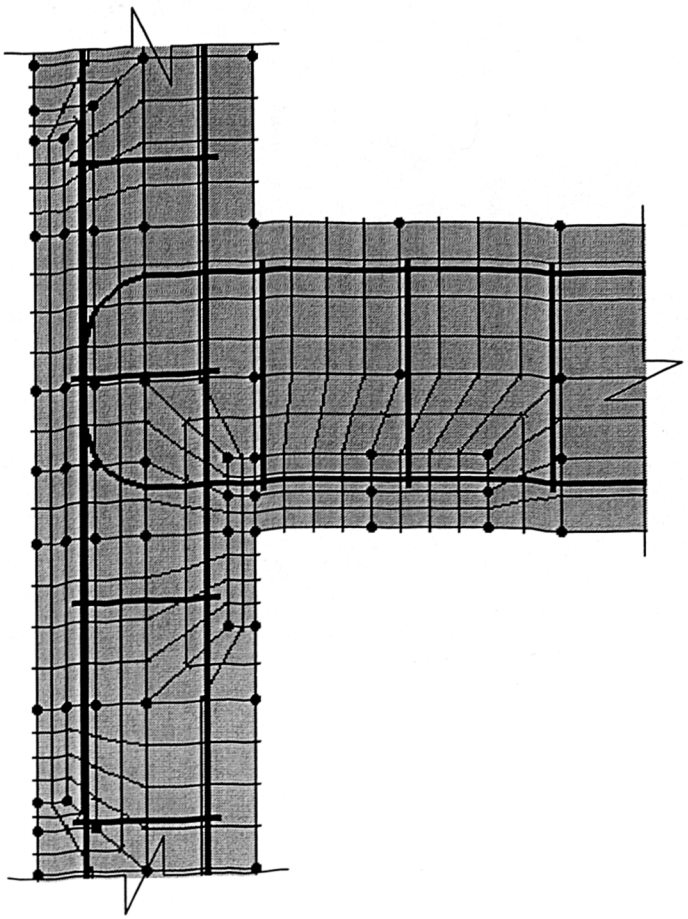

Figure 5.2.3.2 The joint zone of model BCCA

A comparison of the performance of model BCCA and experimental specimen C6LN1(r) is displayed in Figure 5.2.3.3.

Figure 5.2.3.3 shows that the load-deflection response of BCCA was initially very good and showed excellent correlation with the response from the experimental specimen. However, after joint cracking at 18 kN the behaviour became significantly different. The experimental response became much less stiff and failure occurred at 27 kN. The response of the model stayed very stiff, however, and failure did not occur until around 35 kN. This was an over prediction of around 35%.

It is suggested that this poor performance was due to the inability of SBETA to allow any independent movement of the reinforcing bars. The vertical section of the beam's U-bar, in model BCCA, overlapped the outer column reinforcement within

the joint. SBETA assumed a perfect bond between these two rebars. This delayed the onset of failure by restricting any independent movement between the bars.

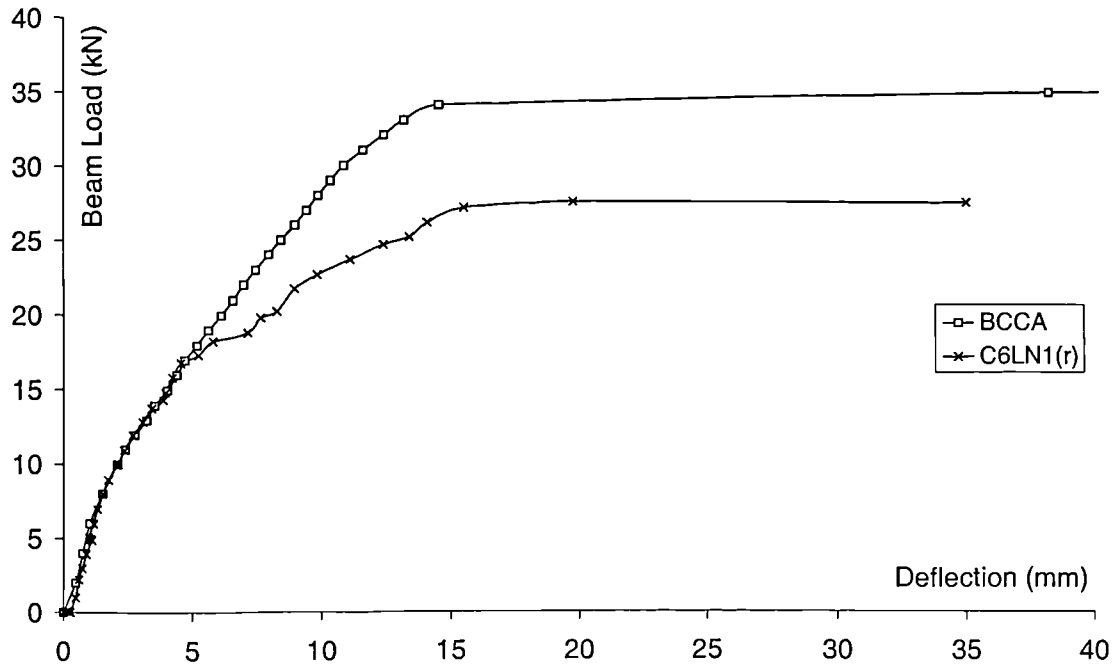

Figure 5.2.3.3 The load-deflection response of model BCCA

Figure 5.2.3.4 shows the model BCCB. This was different from the model BCCA as the U-bar and the outer column bar were moved slightly apart. A gap the size of one element was left between the two rebars to allow independent movement.

Figure 5.2.3.5 shows the load-deflection response of the improved model BCCB. Although the post-joint cracking stiffness was still not modelled perfectly it showed an improved correlation with the experimental response. The failure load was around 26 kN which compared with 25 and 27 kN for the specimens C6LN1 and C6LN1(r) respectively.

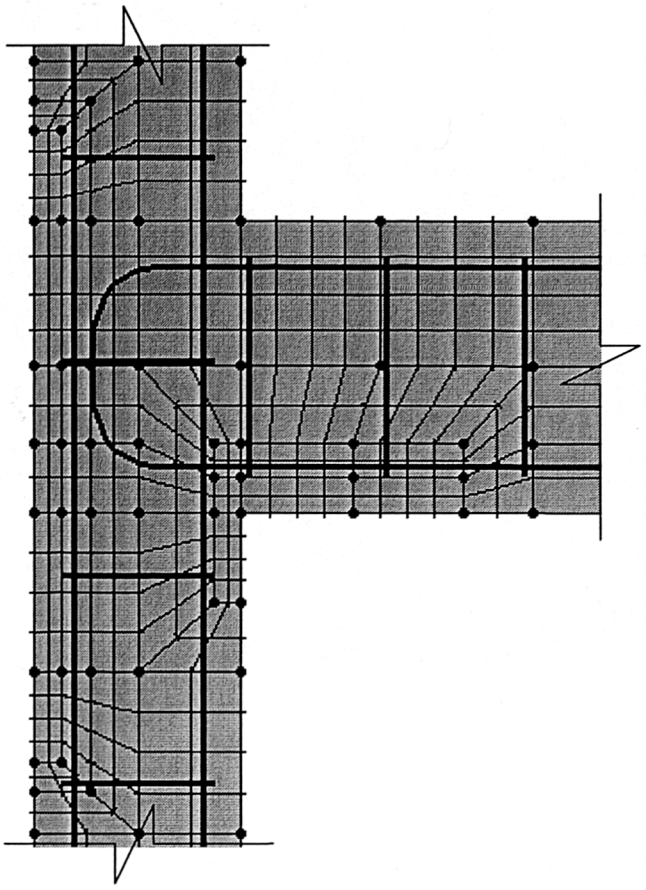

Figure 5.2.3.4 The joint zone of model BCCB

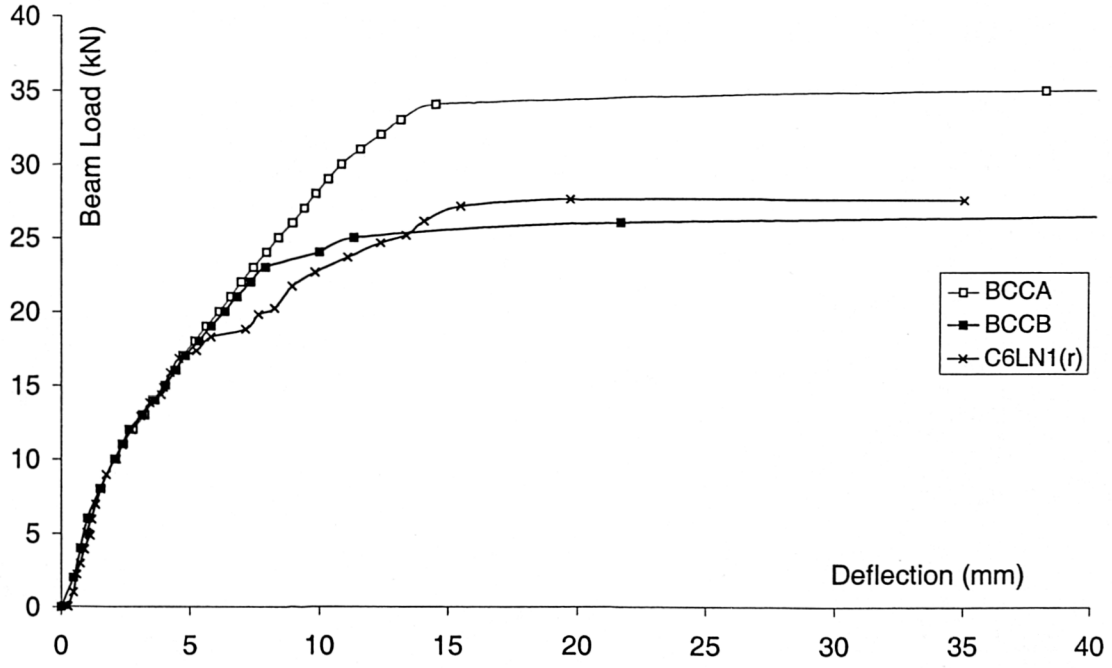

Figure 5.2.3.5 The load-deflection response of model BCCB

The specimens with beam steel bent down into the column were known to have better anchorage characteristics than the specimens using U-bars (Section 3.5). Figure 5.2.3.6 displays the steel layout for a typical model using bent down steel.

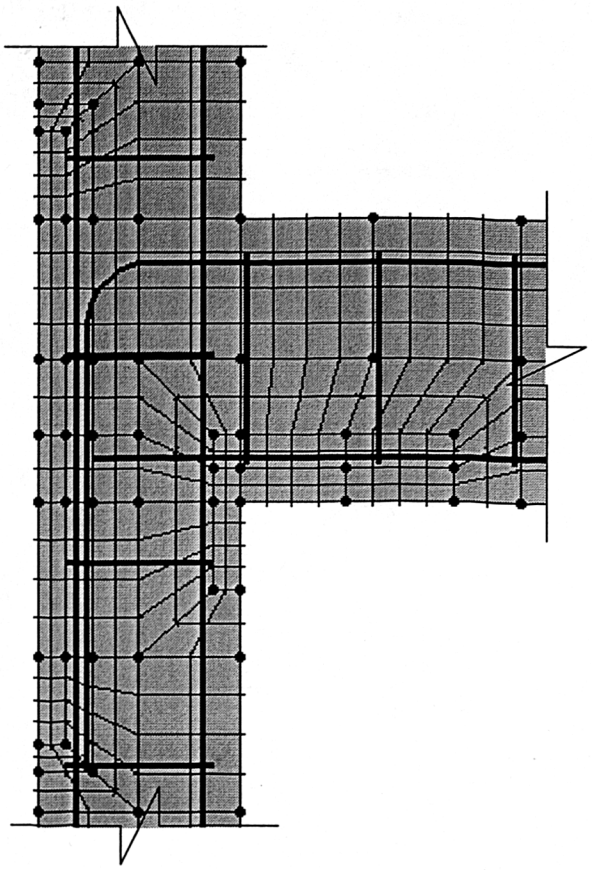

Figure 5.2.3.6 The mesh layout for a typical model using bent down beam steel

Figure 5.2.3.6 shows that the outer column bar and the bent down beam steel were positioned in adjacent elements. This gave an improved correlation with experimental strain results.

The concrete mesh design for specimen BCCB was chosen as the *standard* for beam-column connections within this finite element modelling program.

This *standard* concrete mesh design was consistent for all models. The individual steel reinforcement layout was chosen for each particular specimen and simply *positioned* onto the mesh.

5.2.3.1 Limitations of the model

The main limitation of the finite element package, SBETA, was its **inability to model independent movement of rebars** within the same concrete element.

The *discreet* reinforcement option (as outlined previously in 5.1.1) was considered better than the *smeared* reinforcement option. Smeared reinforcement was averaged over a complete macroelement. The concrete and the steel properties were then combined into the solution matrix for that whole macroelement. Discreet reinforcement, however, was a lot more precise. The reinforcement properties were only considered for the elements in which the rebar was placed. The option of using curved rebars also allowed the load transfer from the beam into the joint to be modelled.

However, as outlined previously, when two (or more) rebars overlapped in the same concrete element a perfect bond was assumed and no independent movement was allowed. This problem is believed to exist for all 2D finite element packages and was acknowledged as the main limitation within the model. Previously in Section 5.2.3 the method of approximating this bar slip by positioning the rebars in adjacent elements was highlighted.

Uncertainties also exist regarding how the joint zone models the tie behaviour. The mesh refinement within this standard model was reasonably coarse. This was in a deliberate attempt to keep computational costs low and to reduce stiffness. However, the complexity of joint behaviour, especially after initial cracking had occurred, was previously highlighted in Chapter 4. It was acknowledged that the chosen mesh design was a necessary compromise between mesh refinement and computational costs / stiffness.

5.3 Validation of the Failure Mechanisms

It was important that when using the *standard* mesh design that model failure was observed to follow the correct mechanism. Four models were therefore designed, each with a known weakness in a certain area. As the mode of failure and ultimate capacity were already known an assessment of model performance was possible. The following failure mechanisms were considered :

1. Flexural failure within the beam
2. Flexural failure within the column
3. Joint failure (no beam rebar slippage)
4. Joint failure (beam rebar slippage)

5.3.1 Flexural failure within the beam

Model BCC1 was designed to fail due to beam flexure. The weak point of this model was the beam as a pair of 12 mm rebars were used for the beam tension reinforcement. Sufficient strength was ensured in the column by providing 4T16 mm bars and in the joint through the presence of seven 8 mm ties. BS 8110 [3] indicated that this steel arrangement would result in flexural beam failure at an applied beam load of around 25 kN.

The data output from SBETA indicated which elements within the mesh had crushed and the elements in which the steel had yielded. Figure 5.3.1.1 shows a magnified view of the joint for BCC1 at failure. The elements which had failed are shaded whilst the darker shaded elements signify those that crushed earliest. The letter Y signifies that the steel within the element indicated had yielded.

The failure mechanism was typical of a flexural beam failure. The concrete had crushed on the underside of the beam and the tension steel had yielded along the top of the beam. Figure 5.3.1.2 shows that the load-deflection response from the model BCC1 demonstrates a good comparison with that predicted by BS 8110.

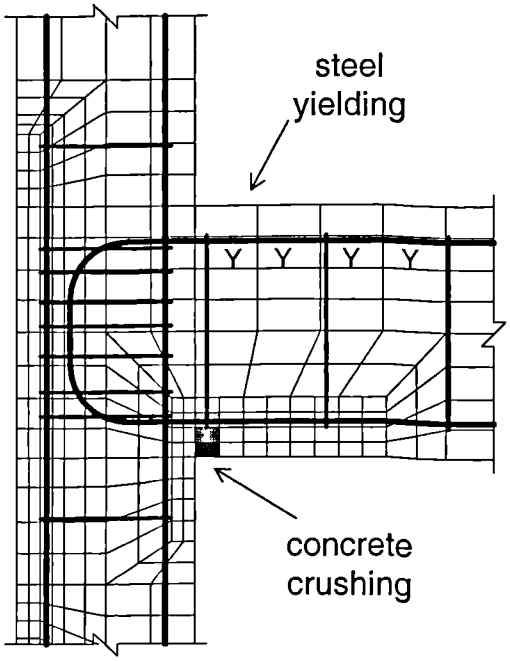

Figure 5.3.1.1 The beam flexural failure of model BCC1

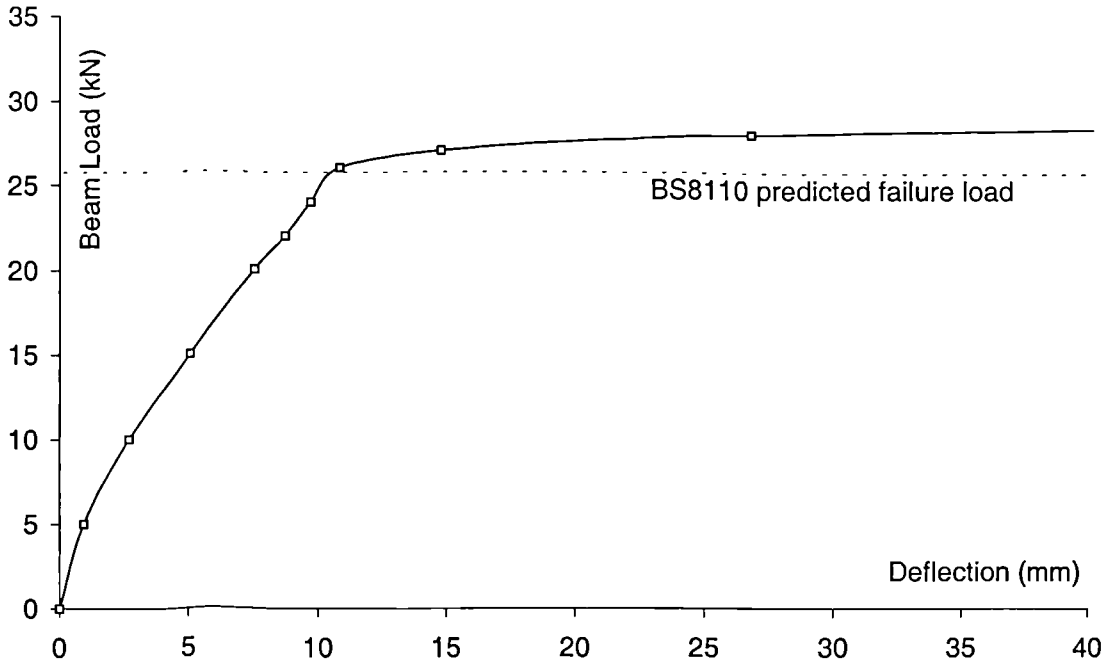

Figure 5.3.1.2 Model BCC1 - load-deflection response

5.3.2 Flexural failure within the column

Model BCC2 was designed to fail due to column flexure. Although this failure mechanism did not occur within the experimental programme the author believes it was necessary to demonstrate that SBETA could model this type of failure appropriately. The weak point of this model was the column with four 12 mm rebars used for this reinforcement. Sufficient strength was ensured in the beam by providing 2T16 mm tension bars and in the joint through the presence of seven 8 mm ties. BS 8110 [3] indicated that this steel arrangement would result in flexural column failure at an applied beam load of around 34 kN.

Figure 5.3.2.1 shows a magnified view of the joint from BCC2 approaching the end of the test. The failure mechanism was that of flexural failure of the column. The column bars can be seen to have yielded in the areas of greatest flexure. Crushing occurred within the column in the regions of greatest compression.

Figure 5.3.2.2 shows the load-deflection response from model BCC2 and again the failure load of the modelled specimen shows a good comparison with that predicted by BS 8110 [3].

5.3.3 Joint failure (no rebar slippage)

Model BCC3 was designed to fail within the joint. Sufficient strength was ensured in the beam through the presence of a pair of 16 mm rebars for the tension steel. The column was reinforced with 4T16 mm rebars. The weak point of this model was the joint as it contained no ties for shear protection. This model was based on the experimental specimen C4PLN0 which used beam rebars attached to an anchorage plate. This anchorage technique ensured that slippage of the beam tension bars did not occur.

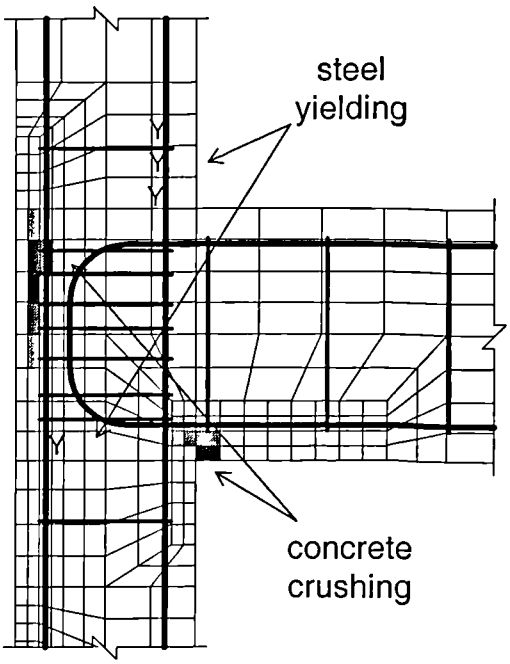

Figure 5.3.2.1 Approaching column flexural failure - BCC2

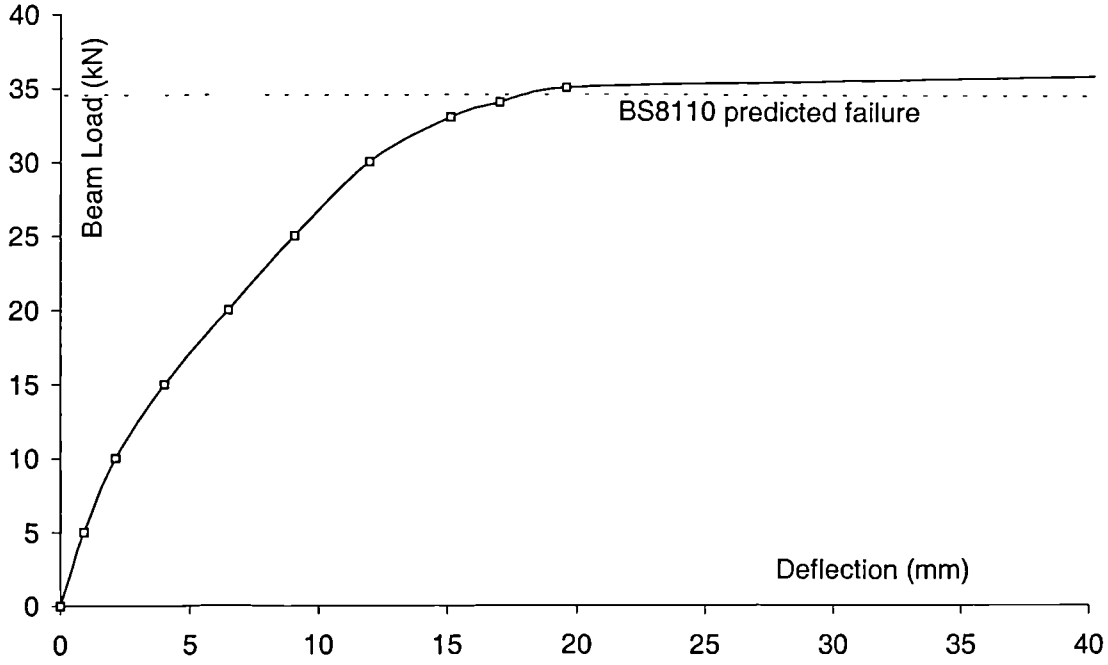

Figure 5.3.2.2 Model BCC2 - load-deflection response

Figure 5.3.3.1 shows a magnified view of the joint from model BCC3 at the end of the test. The failure mechanism was that of shear failure within the joint. The reinforcement bars within the beam and column had remained elastic. However crushing was evident, predominantly within the joint, which was due to the shear failure of these elements.

Figure 5.3.3.2 shows the load-deflection response of model BCC3 compared with the response from experimental specimen C4PLN0. The initial response of the model was excellent, but after joint cracking the SBETA model again failed to demonstrate the reduced stiffness as seen with the experimental model. The failure load of BCC3 was around 15% lower than that of C4PLN0.

5.3.4 Joint failure (beam rebar slippage)

Model BCC4 was again designed to fail within the joint. Identical steel percentages were used in the beam and column as with the previous model BCC3. In addition to no ties being present within the joint the beam steel was bent into a U-bar. As outlined in Section 5.2.3, a gap the width of one element was left between the outer column bars and the beam steel. The purpose of this gap was to give a more realistic bond and to allow relative displacements.

Figure 5.3.4.1 shows a magnified view of the joint from BCC4 approaching the end of the test. The failure mechanism was joint failure. The main difference between the behaviour of this model and BCC3 was that the initial crushing of the joint was of the elements between the beam steel and the outer column steel.

Figure 5.3.4.2 shows the load-deflection response from the model BCC4 compared with the response from the experimental specimen C6LN1B. (Specimen C6LN1B was believed to have exhibited behaviour very similar to C6LN0). Although the modelled response was again slightly stiffer than the experimental specimen, failure occurred at an applied load of a similar magnitude.

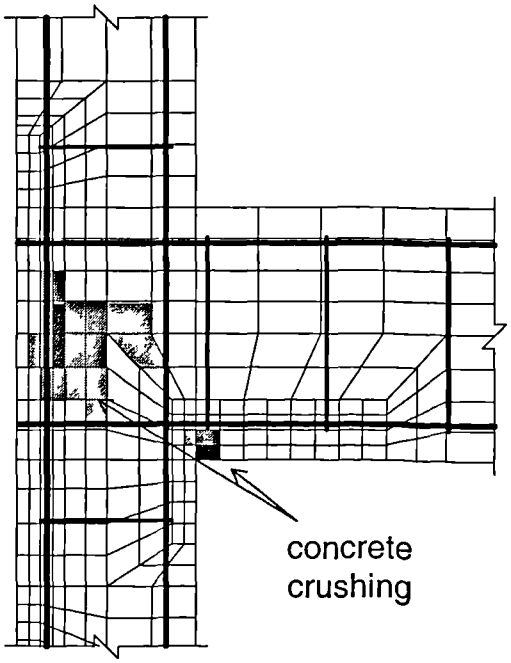

Figure 5.3.3.1 The shear failure of model BCC3

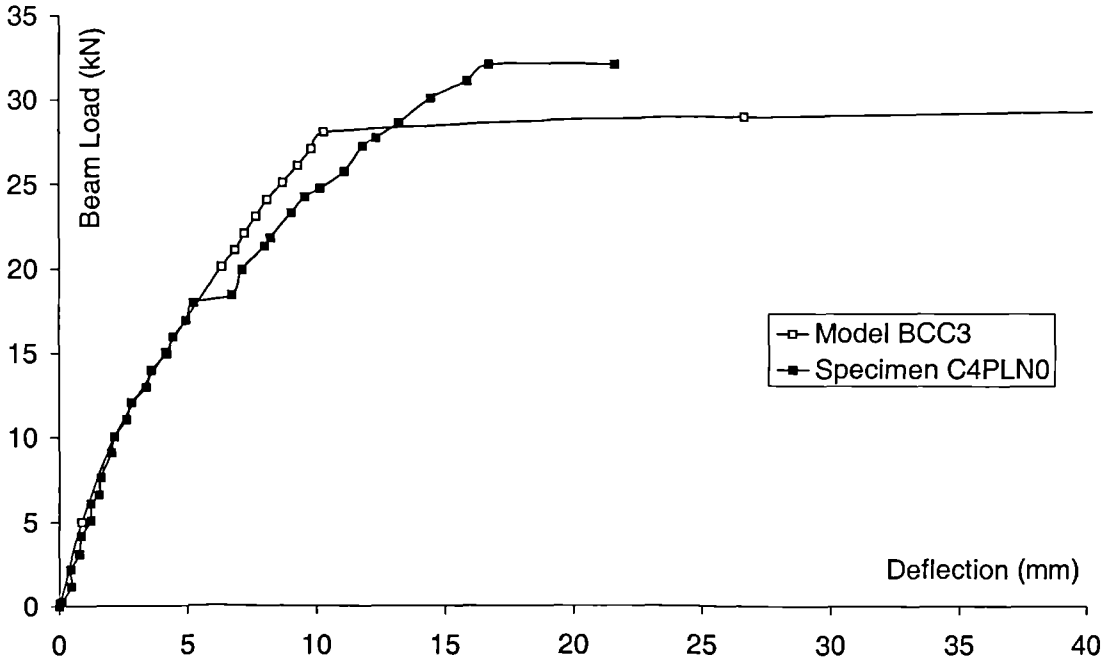

Figure 5.3.3.2 Model BCC3 - load-deflection response

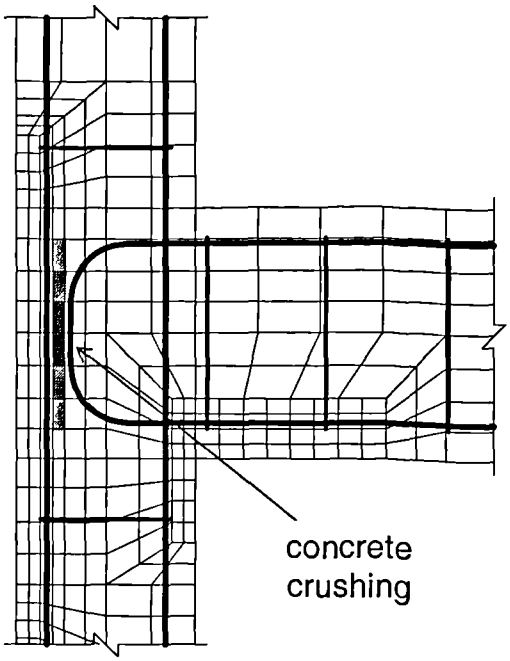

Figure 5.3.4.1 The bar slippage within model BCC4

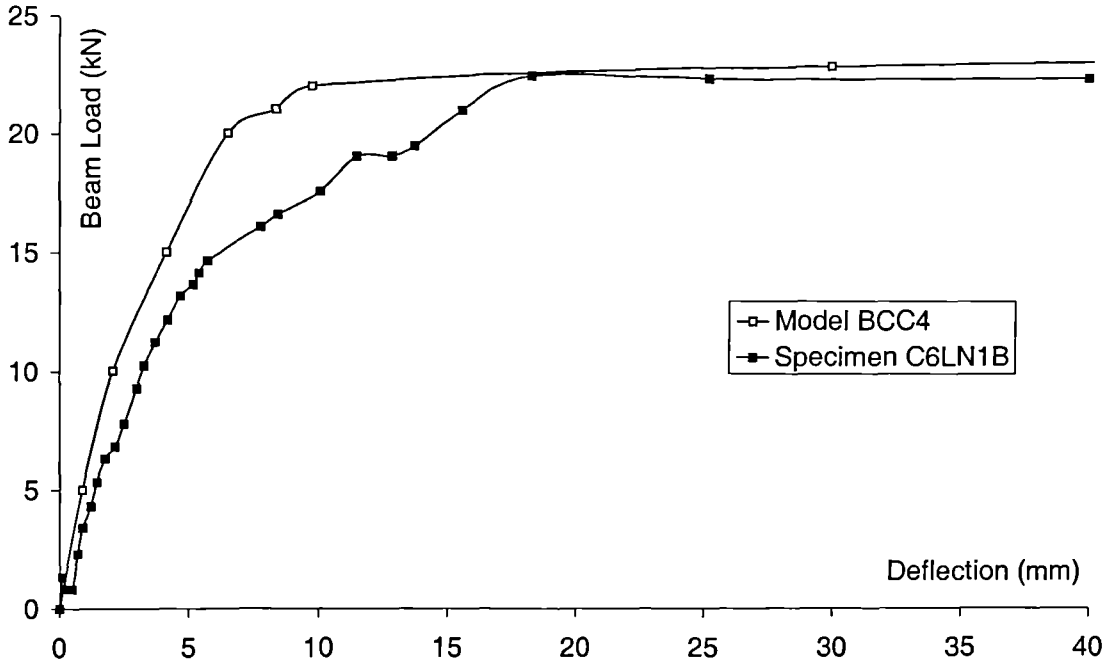

Figure 5.3.4.2 Model BCC4 - load-deflection response

5.3.5 Overall response

Table 5.3.5 shows that all four specimens exhibited the failure mechanisms that theory / experimental results suggested.

Table 5.3.5 Failure loads of the models

Model	Failure mechanism	Expected failure load (kN)	Modelled failure load (kN)
BCC1	Flexural beam	≈ 25	27.5
BCC2	Flexural column	≈ 34	35.3
BCC3	Joint	< 32	29.0
BCC4	Joint (slippage)	≈ 24	22.8

Note

1. Within the modelling the failure load was defined as the load which corresponded to a beam displacement of 25 mm. This was consistent with the experimental response.

The expected and modelled failure loads showed a good correlation. Although the expected failure loads were only approximate, the performance of the models gives good confidence regarding the validation of the *standard* mesh design.

5.4 Solution Criteria

The experimental specimen C6LN1 was modelled several times, varying the solution parameters, to give a comparison of the different time and computational costs. As outlined previously the majority of the modelling took place on a 200 MHz computer with 32 MB of RAM, which at the time of purchase was considered fast. Within this chapter all time considerations are based on modelling runs using a computer of this speed.

5.4.1 Loading increments

The SBETA solution requires the user to define a maximum number of iterations for each load increment. After this number of iterations the solution will continue to the next load step if the *out of balance* forces are within a prescribed limit. The control limit chosen for the modelling was 0.001 (0.1%), which was believed to give a good compromise between accuracy and computational costs.

The size of the load increments used within a solution also has an influence on the model's response. These increments must be small enough to allow the failure mechanism to develop but not so small that an unacceptable demand is put on time and computational costs.

Table 5.4.1 shows the results of using different sizes of load increments on five identical models. The different failure loads, the time (to the nearest 15 mins) and the required disk space are all displayed.

Figure 5.4.1(a) shows the load-deflection response from the models, Figure 5.4.1(b) shows the time cost and Figure 5.4.1(c) shows the computational cost (a maximum number of 30 iterations was used for each of the modelling runs).

Table 5.4.1 The variation of load step size

Load step size (kN)	No. of load steps	Failure load (kN)	Time (hrs/min)	Disk Space required (MB)
8	5	32.8	30 m	4.1
4	9	29.0	1 hr	5.1
2	14	26.4	1hr 15 m	6.5
1	25	24.2	2 hrs 15 m	9.3
0.5	48	23.4	5 hrs	15.4

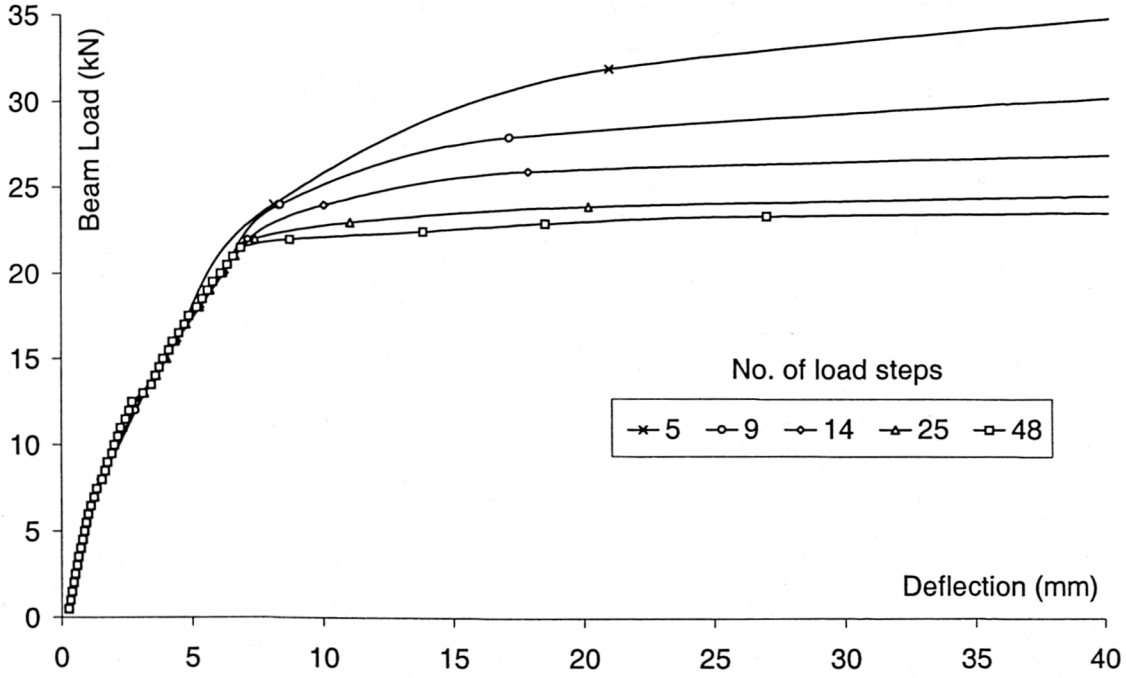

Figure 5.4.1(a) Load-deflection response - load step size

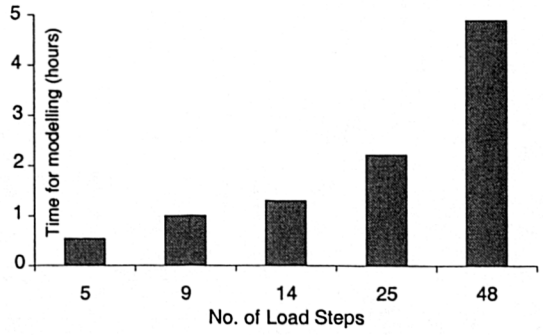

Figure 5.4.1(b) Time cost

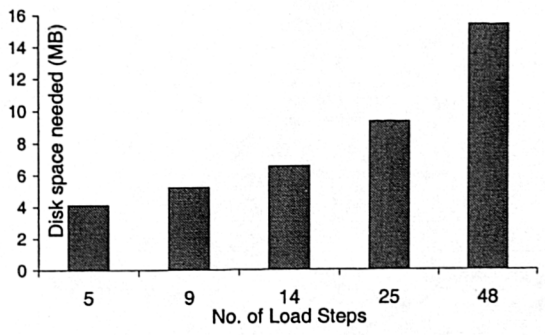

Figure 5.4.1(c) Computational cost

As a result of these tests the load increment size selected for the modelling was 2 kN for the first five steps and then 1 kN until failure occurred. Although steps of 0.5 kN gave a more pronounced failure point, a time of around five hours for an individual test was thought to be too excessive. Initial load steps of 2 kN were chosen as over the initial load stage the load-deflection response was essentially elastic.

5.4.2 Number of iterations

Ideally equilibrium should be achieved before proceeding to the next load step. However, to ease the time / computational costs SBETA allows an equilibrium control limit. Each load step is considered complete after a certain number of iterations **if** the solution is within the equilibrium control limit.

Table 5.4.2 shows the results using different values for the maximum number of iterations for five identical models. The different failure loads, the time (to the nearest 15 mins) and the required disk space are all displayed.

Figure 5.4.2(a) shows the load-deflection response from the models, Figure 5.4.2(b) shows the time cost and Figure 5.4.2(c) shows the computational cost. The *standard* load step size and the equilibrium controls previously defined were used.

Figure 5.4.2(a) shows that using 10 or less iterations per load step caused the solution to abort at a load approaching failure. This was because the *out of balance* forces at the end of the load step were greater than the prescribed control limit.

Table 5.4.2 shows that the free disk space required to run a model actually reduced with an increased number of iterations. The modelled failure load did not show much variation once the maximum number of iterations was greater than 20.

As a result of these tests the chosen maximum number of iterations for the *standard* model was 30. Again a compromise between computer time and precision was made.

Table 5.4.2 Variation of maximum number of iterations

Max. no. of iterations	Failure load (kN)	Time (hrs/min)	Disk Space required (MB)
5	-	30 m	8.8
10	-	45 m	8.8
20	25.2	1 hrs 30 m	8.5
40	24.8	2 hrs 45 m	8.3
60	24.2	4 hrs 45 m	8.1

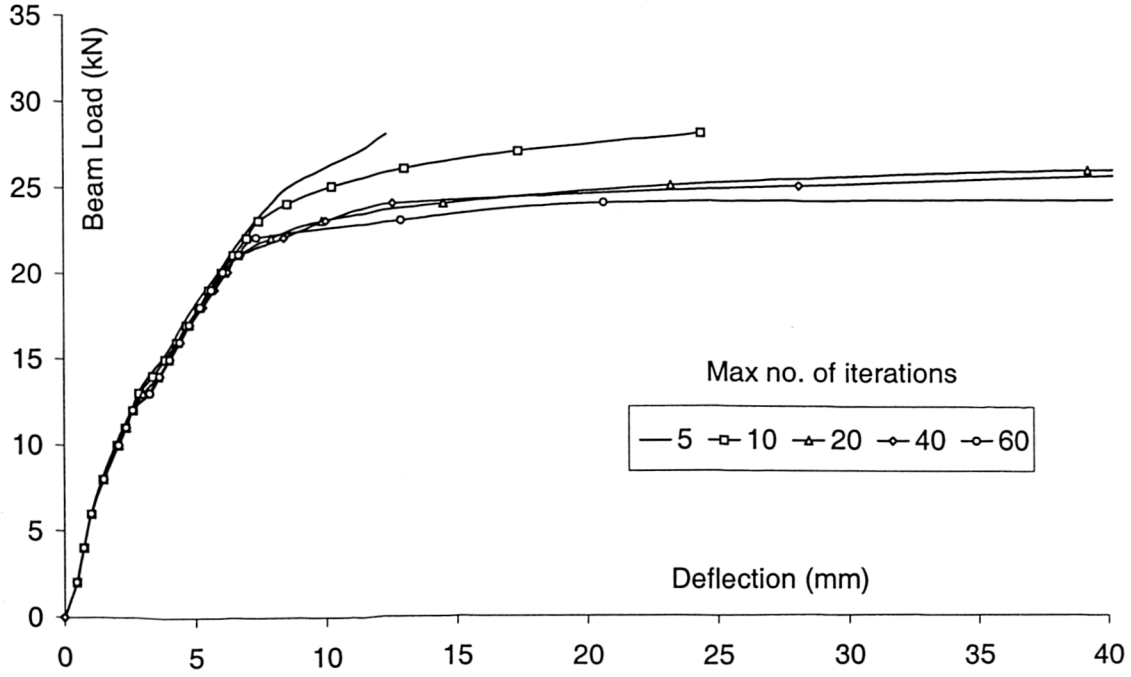

Figure 5.4.2(a) Load-deflection response - maximum number of iterations

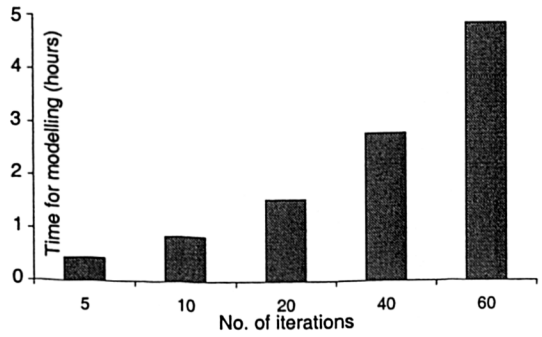

Figure 5.4.2(b) Time cost

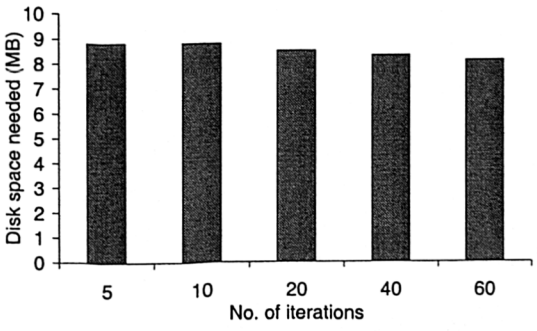

Figure 5.4.2(c) Computational cost

5.4.3 Mathematical solution method

The output response achieved using both the Newton-Raphson and the Arc-length method was investigated. Figure 5.4.3.1 shows the load-deflection response from the simply supported beam model RCBC (Section 5.2.2.2). This response was calculated using both of the mathematical solution methods available within SBETA. Figure 5.4.3.2 shows the load-deflection response of the beam-column connection model BCCB. The results from both solution methods are displayed.

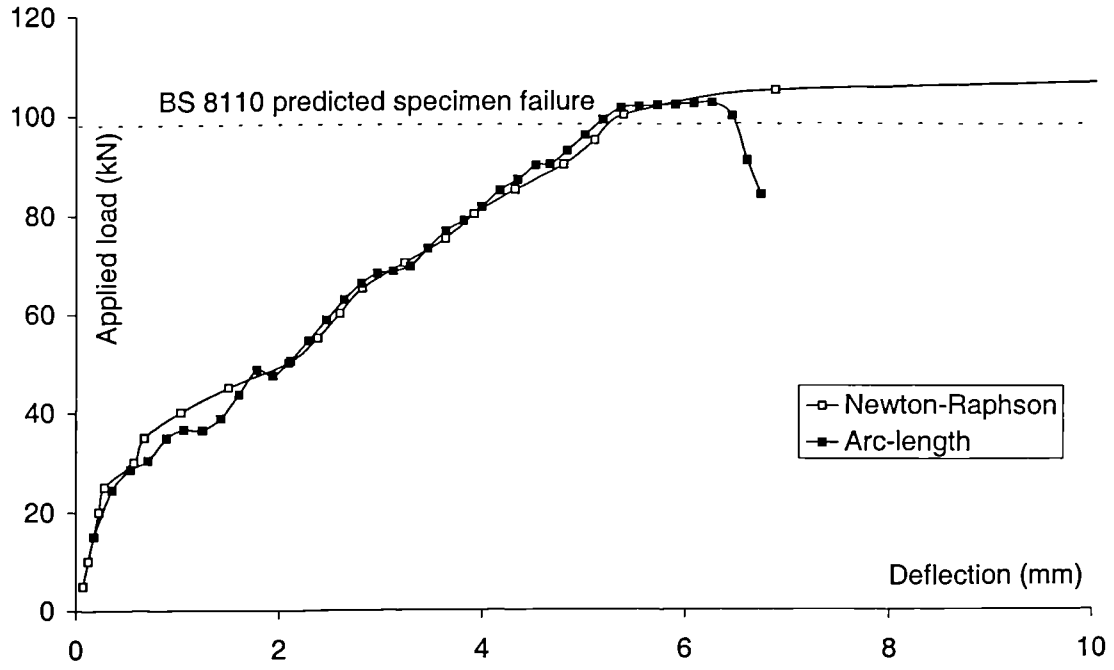

Figure 5.4.3.1 Comparison of solution methods - model RCBC

Figure 5.4.3.1 and 5.4.3.2 show that both solution methods gave a similar response. The advantage of using the Arc-length method was that a precise ultimate capacity was evaluated for the model. However, the main disadvantage using this method was that it is *displacement controlled.* When modelling a structure it is more difficult to predict what displacement the model will fail at as opposed to the load. Choosing displacement steps which are too small will result in too many steps being required before failure occurs. Choosing displacement steps which are too large will result in the specimen failing prematurely and yielding inaccurate results.

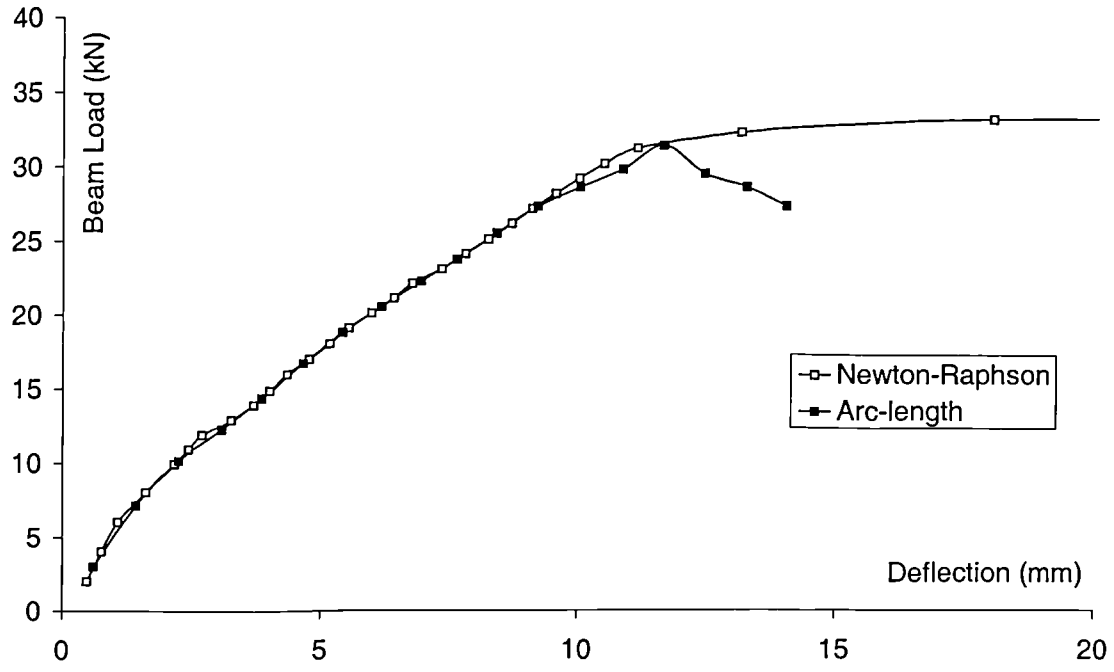

Figure 5.4.3.2 Comparison of solution methods - model BCCB

Ideally the Newton-Raphson method would be used for the initial loading of the specimen and then the Arc-length method would be used approaching failure. However as this combination was not possible using SBETA the author decided to use the Newton-Raphson method for all tests.

5.4.4 Prescribed solution criteria

The prescribed solution criteria were as follows :

Mathematical solution method	Newton-Raphson
Equilibrium control limit	0.001
Load step size	2 kN initially and then 1kN steps
Max. no. of iterations per load step	30

The time and computational costs depended on the number of load steps needed for model failure to occur. Typically, however, the free disk space required was around 15 MB and the time for each modelling run was around two and a half hours.

5.4.5 Confidence level

Due to uncertainty regarding the stability of the numerical solution it was important to establish how the output response varied with small changes in the material properties. An example of this would be what influence a small variation in the tensile strength of a model would have on the output response.

Four of the generated concrete properties are functions of the selected value of compressive cube strength (outlined in Section 5.2.1.2). These are the compressive and tensile cylinder strength, the Young's modulus and the crushing strain.

U-bar beam steel arrangement and concrete properties generated from a compressive cube strength of 60 MPa were used for this consideration of the confidence levels. To investigate the reliance of the numerical solution on each of the four properties each was independently varied while the other test constraints were kept constant.

Figure 5.4.5.1 shows the failure load as the compressive cylinder strength was varied from 24 to 56 MPa. The results from nine models are displayed and a second order polynomial, best fit curve, was evaluated from the data points.

The same process was then undertaken for the other three properties. This was also done for the user defined cube strength to investigate the overall numerical stability. The results from forty five models are displayed in Table 5.4.5.1.

Table 5.4.5.1 indicates that **all data produced from a SBETA solution contains a statistical error value of around 2.0%**. (Through correspondence with colleagues the author has been informed that this stability is actually better than some of the other more complex packages available).

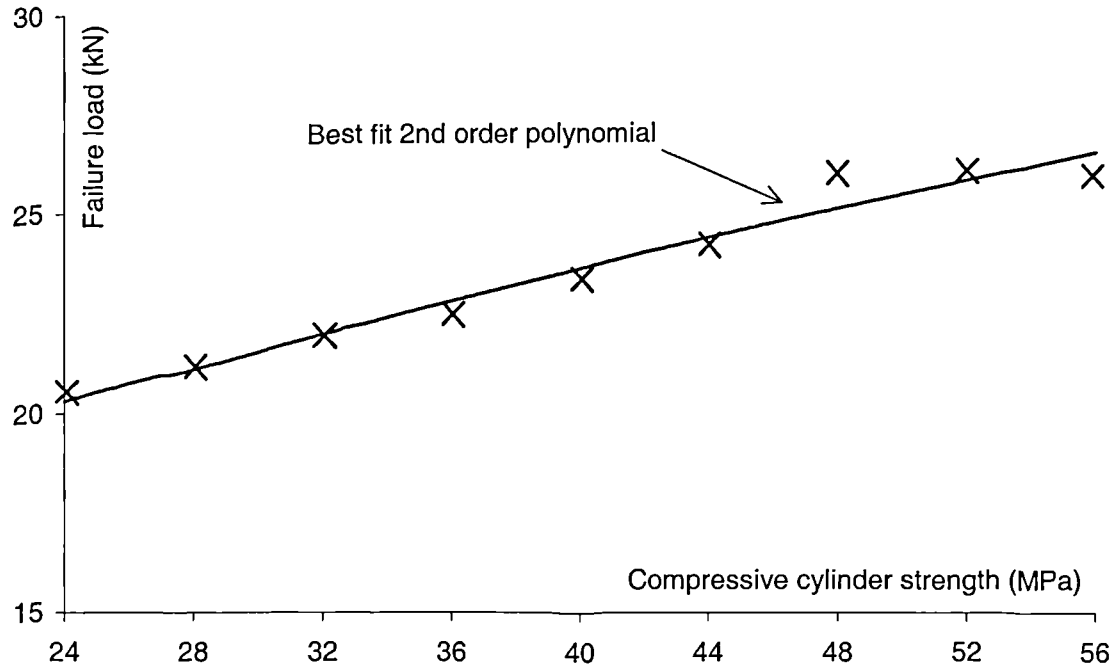

Figure 5.4.5.1 Failure load against the compressive cylinder strength

Table 5.4.5.1 Confidence levels when varying model parameters

Parameter		Range	No. of models	Var. (s.d./mean)
Compressive strength	R_c	24 to 56 MPa	9	1.7%
Tensile strength	R_t	1.5 to 5 MPa	9	2.7%
Young's modulus	E_c	2.8 to 3.6 × 10^4 MPa	9	2.0%
Crushing strain	e_c	2200 to 2400 με	9	1.1%
User input (cube strength)	f_{cu}	30 to 70 MPa	9	2.0%

Notes

1. The choice of range for each parameter was believed to be over the values expected for normal strength concrete,
2. Due to the results being relative to the best fit curve all mean averages were equal to 1.00 and as a consequence the standard deviation of each series of data was equal to the variation coefficient.

5.5 Modelling of the Test Specimens

The following section examines the performance of the *standard* mesh in predicting the response of experimental specimens within this investigation.

For each modelled specimen, concrete and steel properties were matched with the experimental values.

The file naming system used by SBETA allowed the use of only four characters. As a result the general notation given to the SBETA models was as follows :

Example notation -	**Part**	**1st**	**2nd**	**3rd**
	Name	S6	N	1

The first part of this notation refers to the beam tension steel detail :

S4 - Bent down beam steel within a 210 mm deep beam,
S6 - U-bar beam steel within a 210 mm deep beam,
S7 - Bent down beam steel within a 300 mm deep beam,
S9 - U-bar beam steel within a 300 mm deep beam.

The second part of this notation refers to the concrete strength :

N - Normal strength concrete with a typical cube strength of 60 MPa,
H - High strength concrete with a typical cube strength of 120 MPa.

The third part of this notation is equal to the number of joint ties.

All models using this notation were subjected to a low column load (as defined previously in Section 2.1.3) and all ties were positioned symmetrically about the joint's mid-height.

This notation is for the modelling of specimens from this investigation. Later within this chapter when specimens from previous research are modelled a different notation is used.

5.5.1 Standard specimens

5.5.1.1 Cracking loads

All normal strength SBETA models exhibited joint shear cracking at a load of around 13 kN. This value was reasonably constant regardless of the number of joint ties present and the method of beam steel anchorage used.

The load at which joint shear cracking first occurred for the experimental specimens ranged from 13 to 20 kN. Again this was seen to be irrespective of the number of joint ties present or the method of beam steel detailing used. Therefore, the predicted cracking load was seen to give a good *lower bound* for the experimental performance.

5.5.1.2 Failure loads

Table 5.5.1.2.1 shows the modelled failure loads and how they compared with the actual experimental values. As all of the specimen parameters were matched the conversion of the failure load into a failure shear stress was not necessary.

All eight of the models failed at loads which show good correlation with experimental results. The mean average of the accuracy was 1.01 and the variation coefficient was 8.1%.

Table 5.5.1.2.1 Modelled results - (anchorage detail / presence of joint ties)

Actual Specimen	SBETA Model	Cube strength f_{cu} (MPa)	Actual failure load (kN)	Modelled failure load (kN)	Accuracy (model/actual)
Bent down beam steel					
C4ALN0	**S4N0**	53	26.5	30.4	1.15
C4ALN1	**S4N1**	57	33.5	33.2	0.99
C4ALN3	**S4N3**	52	35.2	33.2	0.94
C4ALN5	**S4N5**	63	39.5	37.7	0.95
U-bar beam steel					
C6LN0	**S6N0**	64	23.9	26.1	1.09
C6LN1	**S6N1**	64	24.6	24.7	1.00
C6LN3	**S6N3**	61	28.7	29.3	1.02
C6LN5	**S6N5**	46	33.9	30.3	0.89
				Mean average	**1.01**
				Standard deviation	**0.08**
				Variation (s.d./mean)	**8.1%**

5.5.1.3 Modelled response

A comparison of the load-deflection response is displayed in Figure 5.5.1.3.1. The response from the experimental specimen C6LN1(r) is compared with that from model S6N1.

Figure 5.5.1.3.1 shows that over the initial load stages the modelled and experimental responses show a very good correlation. The compared response after joint cracking does not show such a close correlation. It would appear that SBETA does not allow the loss of specimen stiffness associated with joint cracking to fully occur.

A number of specimens contained strain gauged reinforcement (as outlined in Section 2.2.1). This allowed very detailed comparisons to be made between the response of the experimental specimens and that of the finite element models.

Comparisons were made for all *fully* strain gauged specimens at loads prior to joint cracking and specimen failure.

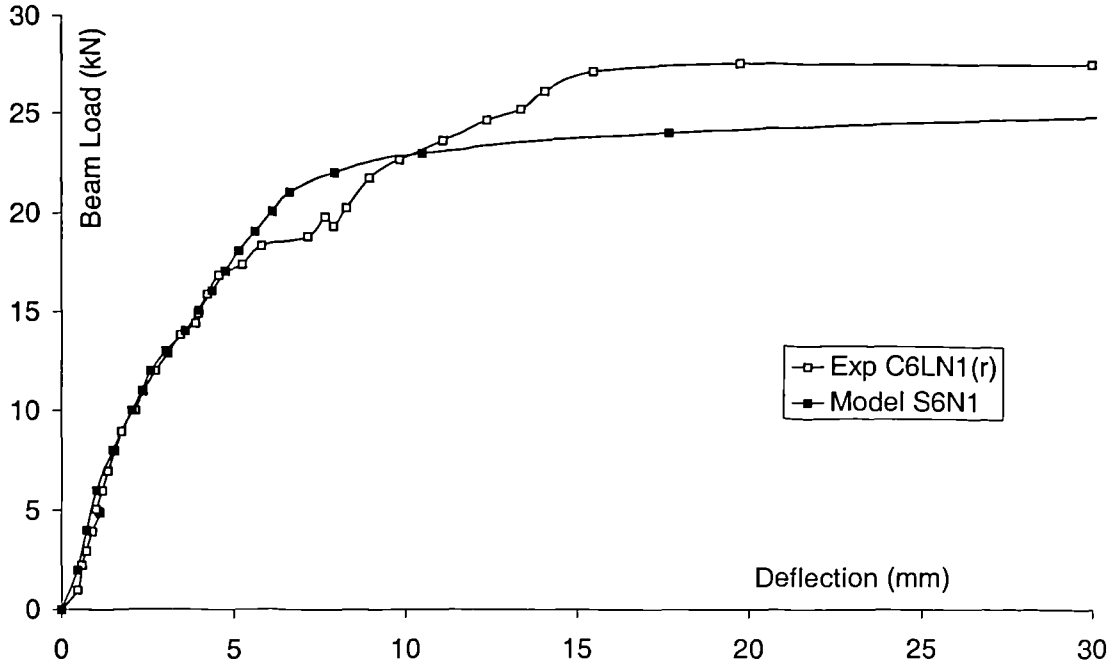

Figure 5.5.1.3.1 Load-deflection response comparison - normal strength model

Steel strains from the model were constant over each element. The strains were therefore most detailed in regions of the model where the mesh refinement was greatest.

Figures 5.5.1.3.2 to 5.5.1.3.7 show the comparisons of reinforcement strain distributions within the experimental specimen C6LN1 and the model S6N1. The reinforcement bars and load cases considered are indicated below :

Figure 5.5.1.3.2 Outer column bar - 15 kN beam load

Figure 5.5.1.3.3 Inner column bar - 15 kN beam load

Figure 5.5.1.3.4 Beam bars - 15 kN beam load

Figure 5.5.1.3.5 Outer column bar - load case prior to failure

Figure 5.5.1.3.6 Inner column bar - load case prior to failure

Figure 5.5.1.3.7 Beam bars - load case prior to failure

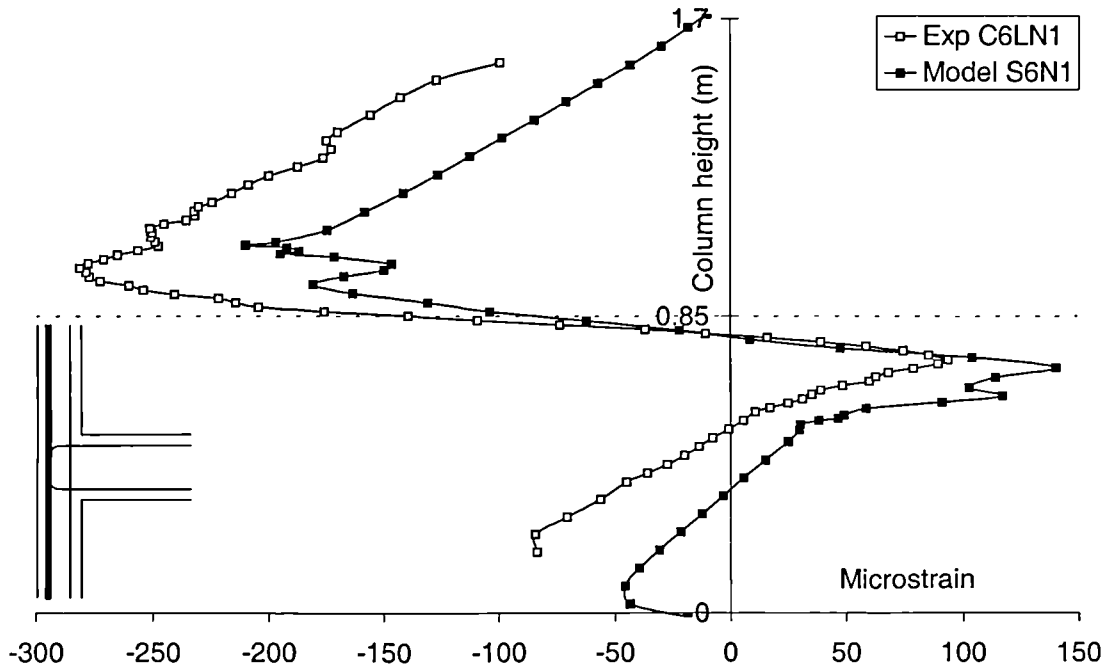

Figure 5.5.1.3.2 Strain comparisons at 15 kN - outer column bar

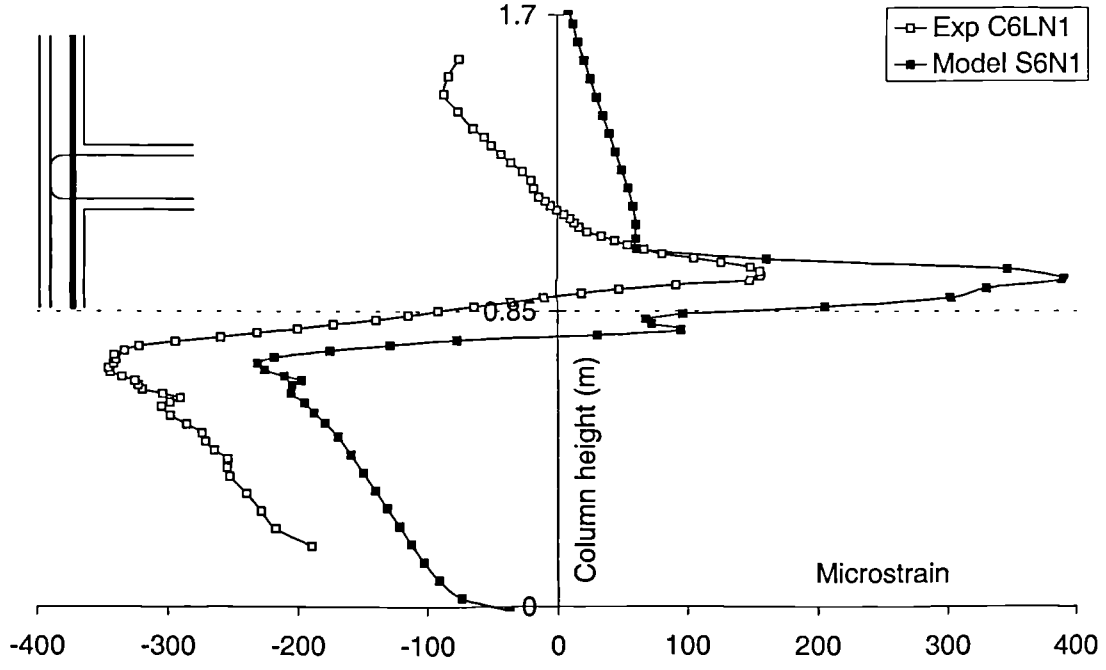

Figure 5.5.1.3.3 Strain comparisons at 15 kN - inner column bar

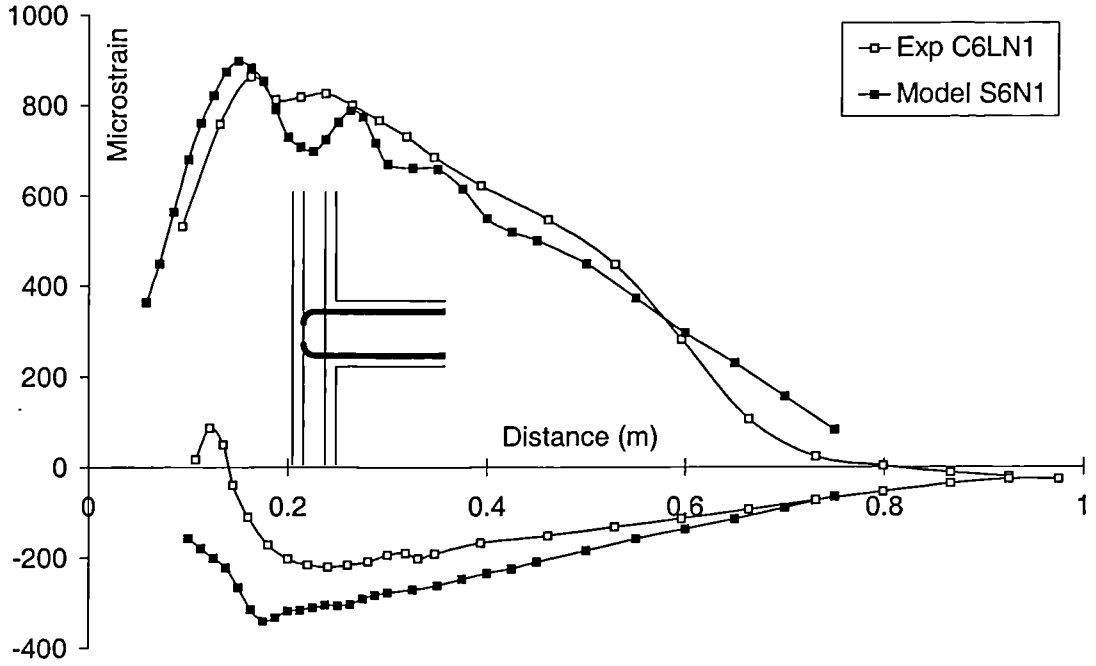

Figure 5.5.1.3.4 Strain comparisons at 15 kN - beam bars

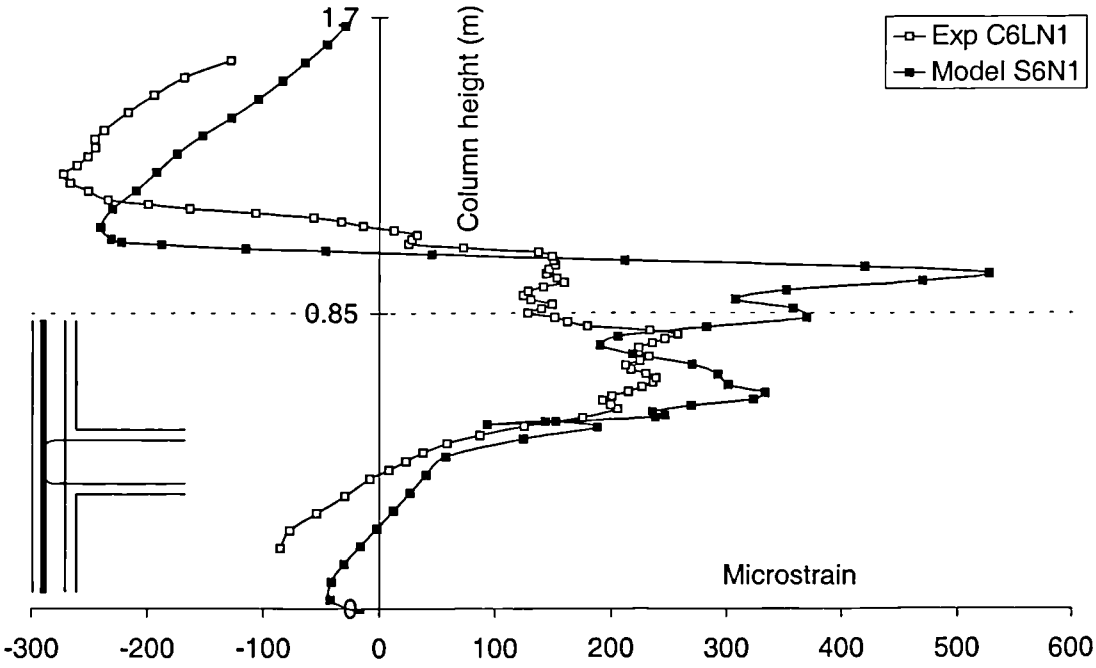

Figure 5.5.1.3.5 Strain comparisons prior to failure - outer column bar

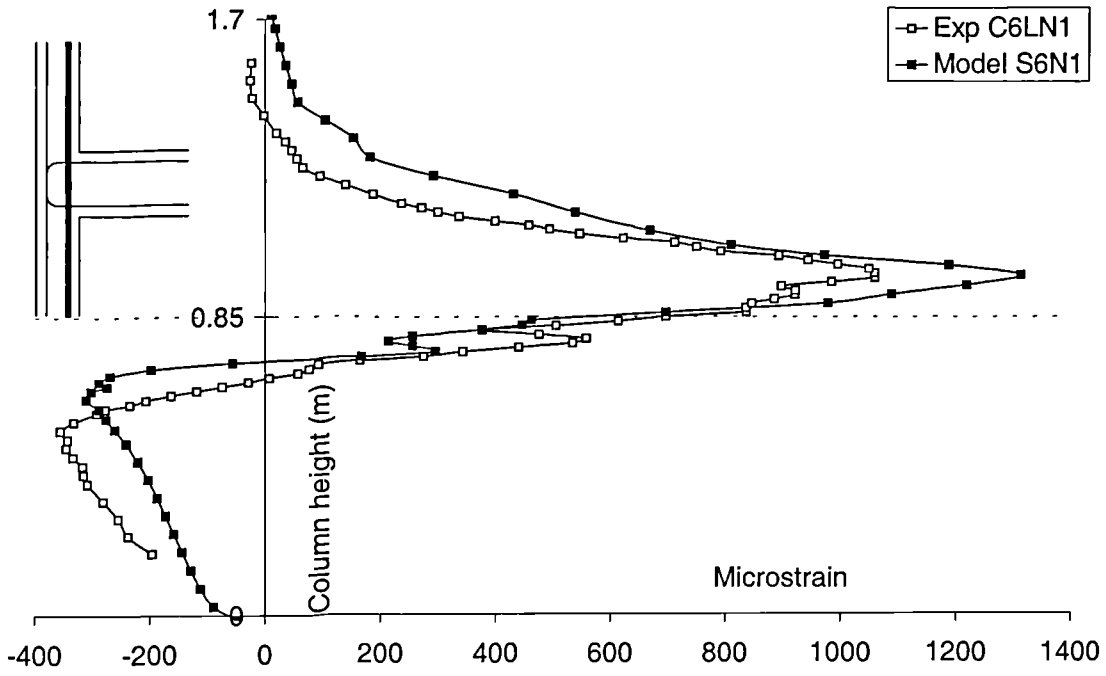

Figure 5.5.1.3.6 Strain comparisons prior to failure - inner column bar

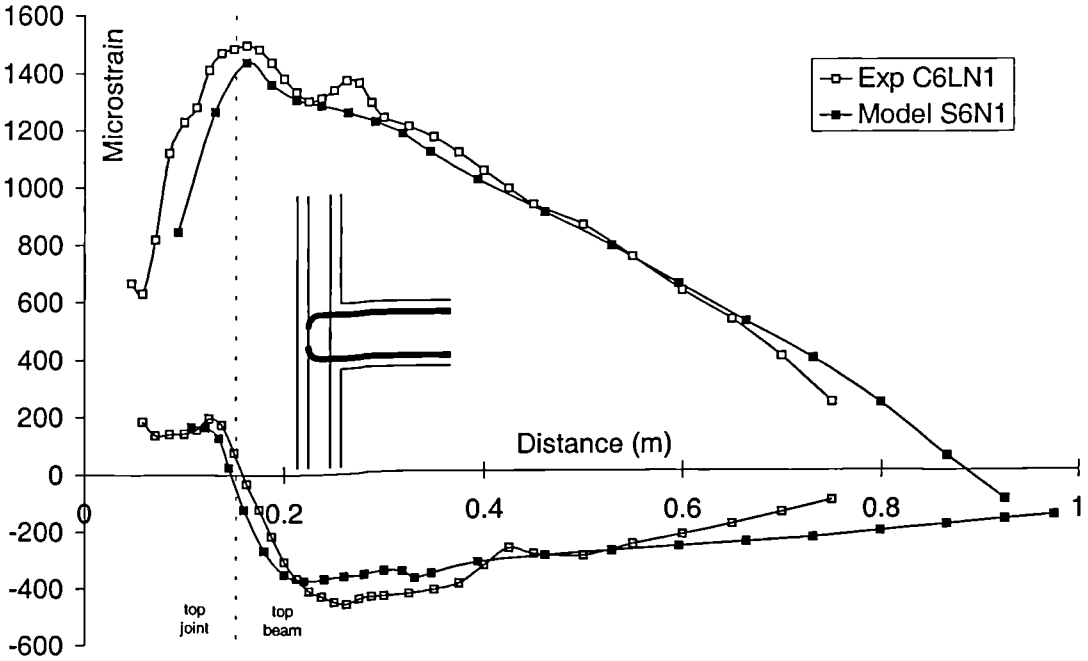

Figure 5.5.1.3.7 Strain comparisons prior to failure - beam bars

Figures 5.5.1.3.2 to 5.5.1.3.7 show that the reinforcement strains within the model, S6N1, are of a good comparison to those within the experimental specimen, C6LN1, throughout the load history.

Comparisons of the strain distributions are especially close for the inner column bar and the beam U-bar in tension. The region of the outer column bar within the joint showed the worst correlation of strain results. It is believed that this is due to the extensive crushing / splitting of the concrete elements within this region.

One limitation of the analysis was the modelling of the anchorage of the beam steel within the joint. Figure 5.5.1.3.8 displays the strains prior to failure within the beam tension bar for the experimental specimen C4ALN1 and the model S4N1.

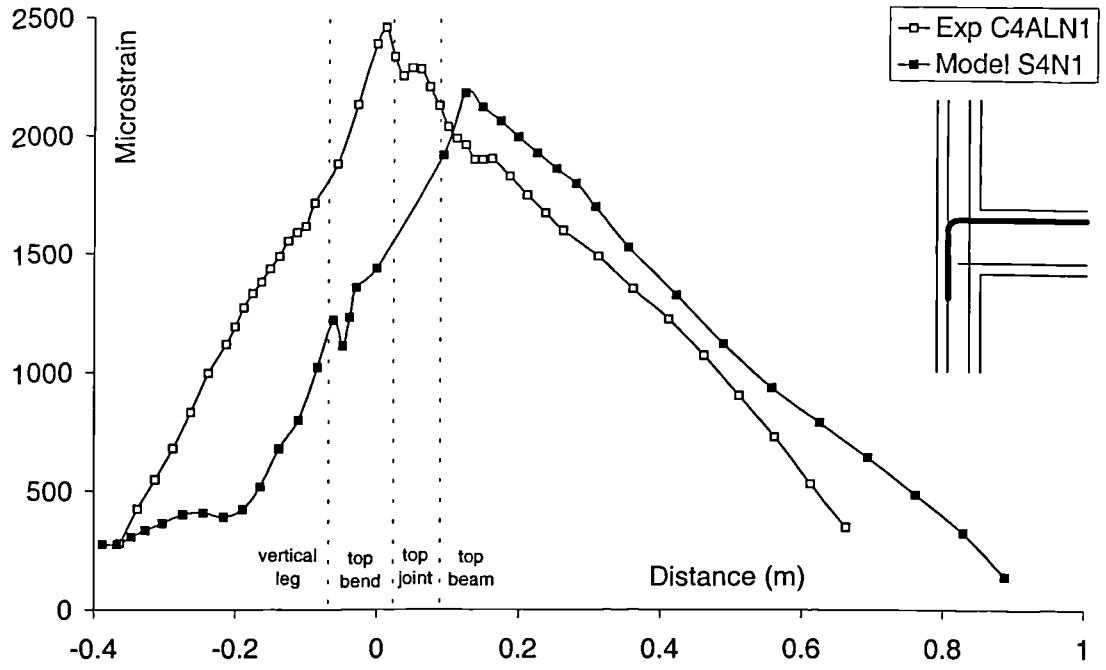

Figure 5.5.1.3.8 Strain comparisons prior to failure - bent down bar

Figure 5.5.1.3.8 shows that S4N1 models the strains in the reinforcement well for the top section of the beam tension bar. However, the strain peaked at the column face and then the bond was developed over the full anchorage length. The true strain response peaked at the start of the top bend due to bond failure across the top joint

region. This highlights the problems of modelling anchorage in a region of a structure as complex as a joint within a beam-column connection.

A comparison of average strains within the joint tie of experimental specimen C6LN1 and model S6N1 is given in Figure 5.5.1.3.9. The average strains for C6LN1 were calculated by taking the mean average of the ten strain gauges present within the joint tie. The average strains for S6N1 were calculated by taking the mean average of the strains present within the steel with the four central elements within the centre of the joint.

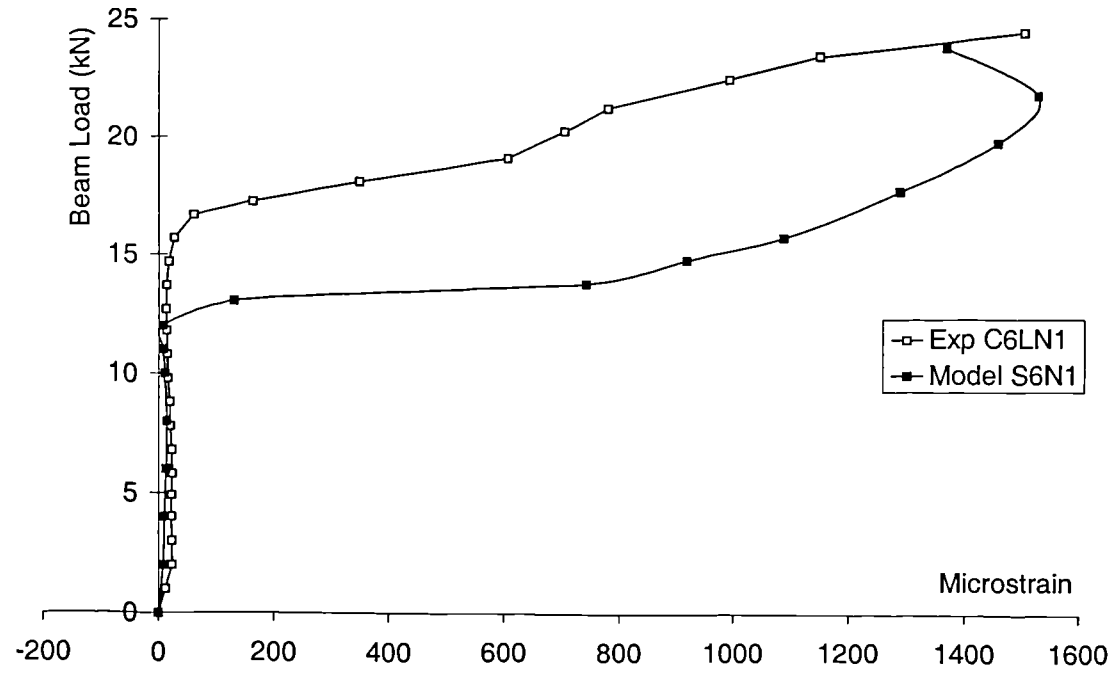

Figure 5.5.1.3.9 Comparison of joint tie strains

Figure 5.5.1.3.9 confirms that joint cracking occurred at a load of around 13 kN for the normal strength models. Over the initial load stages only a nominal amount of strain existed within the joint ties. After joint cracking the strain in both the model and the experimental specimen developed at a similar rate. Considering the amount of element crushing and splitting that occurred within the joint this modelled response was reasonable.

Table 5.5.1.3.1 shows the comparisons between the average strains within the ties of the experimental and modelled specimens. All strains displayed were from the load step prior to failure.

Table 5.5.1.3.1 Joint tie average strain comparisons

	Top	Middle	Bottom
C6LN1	-	1150	-
S6N1	-	1340	-
C6LN3	1690	1560	930
S6N3	1460	1400	1530
C4ALN1	-	990	-
S4N1	-	1980	-
C4ALN3	1460	1590	950
S4N3	1740	1820	230

Table 5.5.1.3.1 shows that the correlation of results is again reasonable. Due to the excessive element cracking and crushing at this stage of the modelling the tie behaviour should be taken with some caution.

SBETA's consideration of tie positioning within the joint is analysed in Section 5.5.4.

5.5.2 High strength specimens

High strength concrete has a wider range of constituents than normal concrete. As a result of this the properties of high strength concrete can not be generated using the same equations as those of normal strength concrete (see Section 5.2.1).

The equations shown in Table 5.5.2.1 were used in this section. They were taken from both the author's experimental data and previous research [25, 26].

Table 5.5.2.1 High strength concrete properties

Property		Value	Units
Uniaxial compressive cylinder strength	**Rc**	$0.8 \times f_{cu}$	MPa
Tensile strength	**Rt**	$0.4 \times f_{cu}^{0.5}$	MPa
Young's modulus	**Ec**	4.3×10^4	MPa
Crushing strain	$\mathbf{e_c}$	$(0.7R_c^{0.31})/1000$	-
Poisson's ratio	$\mathbf{n_u}$	0.20	-

Note

1. Properties not listed were taken to be the same as those for normal strength concrete.

5.5.2.1 Cracking loads

All high strength specimens exhibited joint shear cracking at a load of around 20 kN. This value was reasonably constant regardless of the number of joint ties present and the method of beam steel anchorage used.

The load at which joint shear cracking first occurred for the experimental specimens ranged from 20 to 27 kN. Again this was seen to be irrespective of the number of joint ties present or the method of beam steel detail used. Therefore the predicted cracking load was seen to give a good *lower bound* for the experimental performance.

5.5.2.2 Failure loads

Table 5.5.2.2 displays the modelled failure loads and how they compared with the actual experimental loads.

All modelled properties were generated from the experimental compressive cube strength using the equations in Table 5.5.2.1.

Table 5.5.2.2 Modelled results - (high strength concrete)

Actual Specimen	SBETA Model	Cube strength f_{cu} (MPa)	Actual failure load (kN)	Modelled failure load (kN)	Accuracy (model/actual)
Bent down beam steel					
C4ALH0	**S4H0**	130	$43.2_{(F)}$	$44.3_{(F)}$	1.03
C4ALH1	**S4N1**	119	$43.4_{(F)}$	$43.8_{(F)}$	1.01
C4ALH3	**S4H3**	132	$45.6_{(F)}$	$45.5_{(F)}$	1.00
C4ALH5	**S4H5**	123	$48.6_{(F)}$	$46.3_{(F)}$	0.95
U-bar beam steel					
C6LH0	**S6H0**	126	36.1	35.7	0.99
C6LH1	**S6H1**	127	37.1	38.4	1.04
C6LH3	**S6H3**	121	41.2	41.5	1.01
C6LH5	**S6H5**	125	$51.4_{(F)}$	$46.8_{(F)}$	0.91
				Mean average	**0.99**
				Standard deviation	**0.04**
				Variation (s.d./mean)	**4.3%**

Note

1. F - indicates flexural beam failure.

Table 5.5.2.2 shows that all eight models failed at loads which showed a good correlation with the experimental results. The mean average of the accuracy was 0.99 and the variation coefficient was 4.3%. This correlation was slightly better than that for the original eight normal strength specimens.

5.5.2.3 Modelled response

A comparison of the load-deflection behaviour is displayed in Figure 5.5.2.3.1. The response from the experimental specimen C6LH3 is compared with that from the model S6H3.

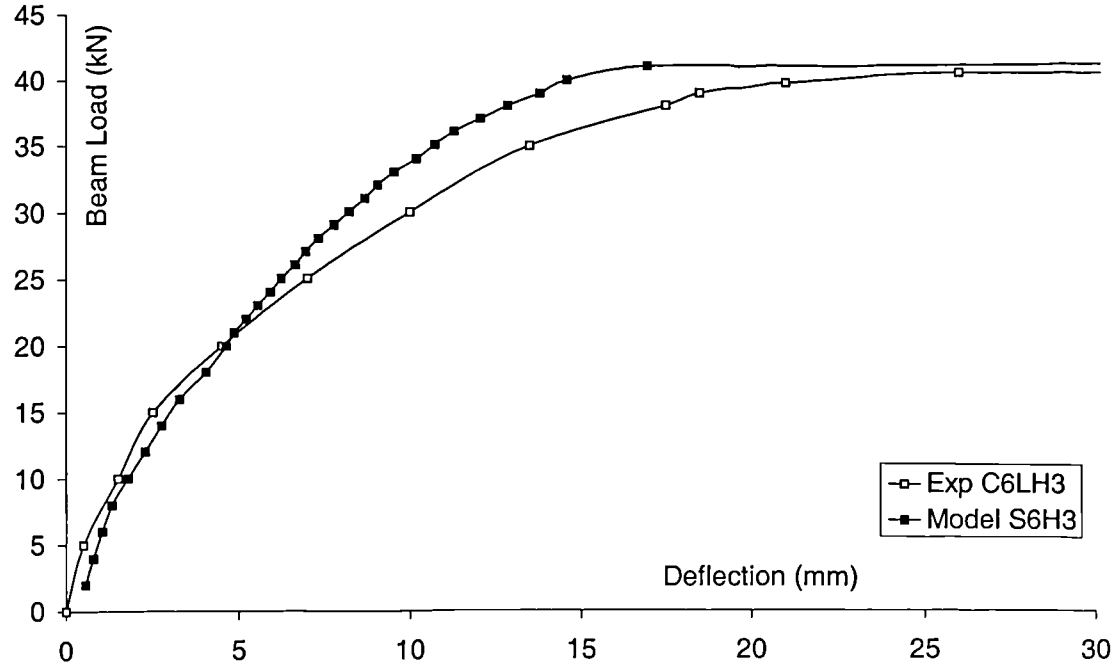

Figure 5.5.2.3.1 Load-deflection response comparison - high strength model

Figure 5.5.2.3.1 shows that the modelled and experimental response show a very good correlation over the initial load stages. Again, however, after joint cracking the modelled response was slightly stiff.

Similarly to the normal strength specimens, a number of high strength specimens contained strain gauged reinforcement (as outlined previously in Section 2.2.1). This allowed very detailed comparisons to be made between the response of the experimental specimens and the finite element models. Comparisons were made for all *fully* strain gauged specimens at loads prior to joint cracking and specimen failure.

Figure 5.5.2.3.2 to 5.5.1.3.4 show the comparisons in reinforcement strain distributions for the experimental specimen C6LH1 and the model S6H1. The rebars and load cases considered are indicated below :

Figure 5.5.2.3.2 Outer column bar - load case prior to failure

Figure 5.5.2.3.3 Inner column bar - load case prior to failure

Figure 5.5.2.3.4 Beam bars - load case prior to failure

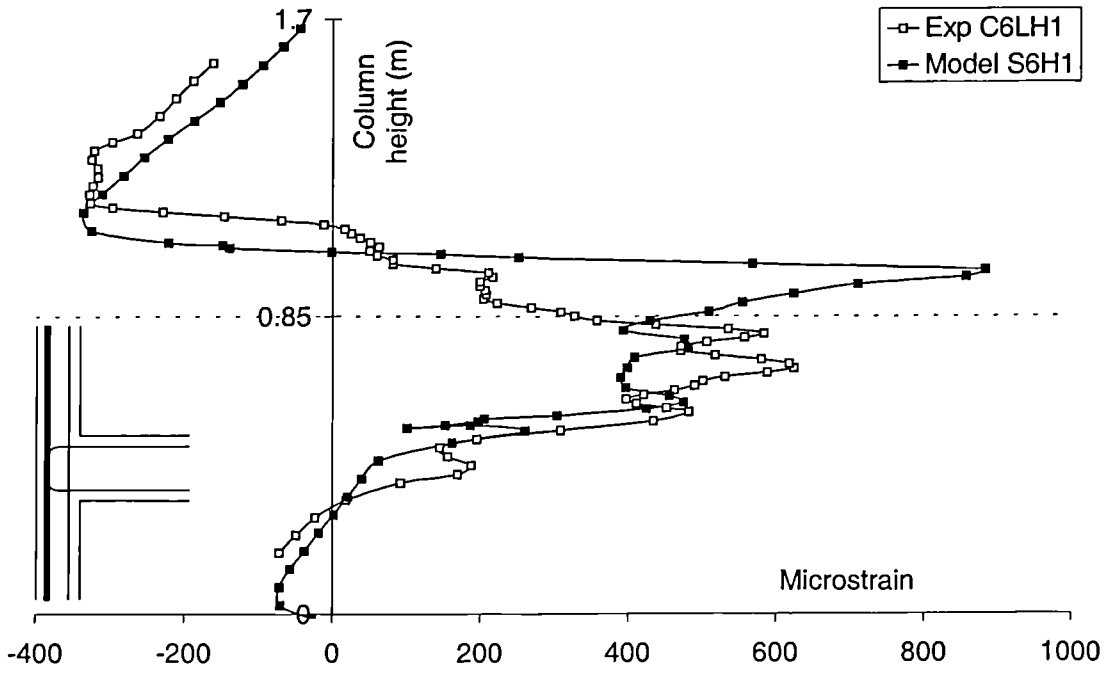

Figure 5.5.2.3.2 Strain comparisons prior to failure - outer column bar

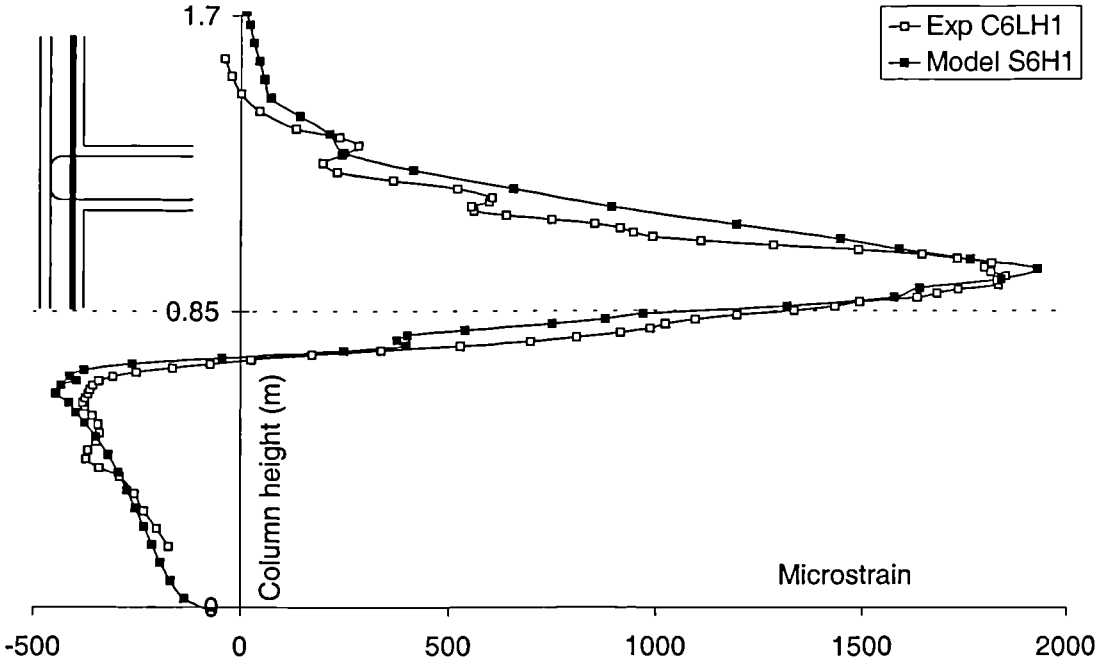

Figure 5.5.2.3.3 Strain comparisons prior to failure - inner column bar

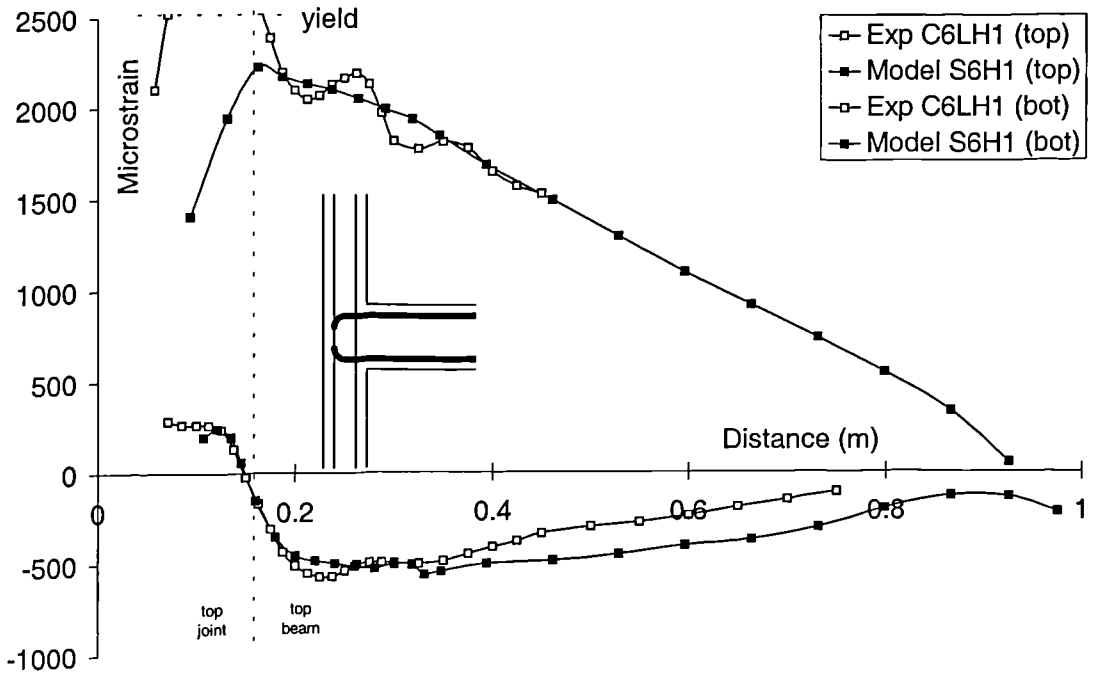

Figure 5.5.2.3.4 Strain comparisons prior to failure - beam bars

Figures 5.5.3.2.2 to 5.5.2.3.4 show that the reinforcement strains within the model S6H1 were similar to those from the experimental specimen C6LH1.

The modelling of the high strength specimens was seen to be very similar to the modelling of the normal strength specimens. Again, the comparisons of the strain distributions were especially close for the inner column bar and the U-bar. The strains in the outer column bar, particularly within the joint region, again showed the worst correlation.

Overall, the finite element analysis performed equally well for the high strength specimens as for the normal strength specimens.

5.5.3 Joint aspect ratio specimens

The eight specimens with an increased joint aspect ratio were modelled. The *standard* mesh design (with the same number of elements) was adapted as shown in Figure 5.5.3.1.

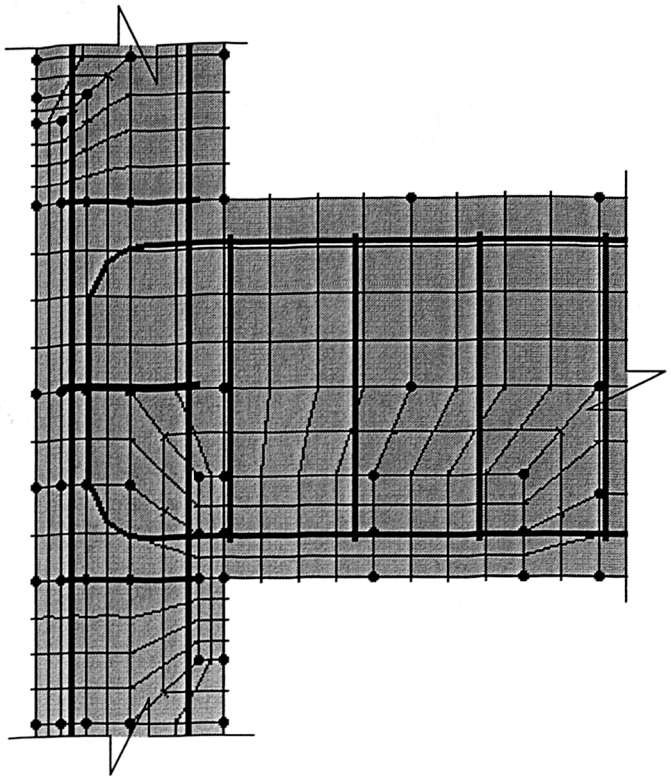

Figure 5.5.3.1 The mesh design for the models with increased joint aspect ratio

5.5.3.1 Cracking loads

All models exhibited joint shear cracking at a load of around 18 kN regardless of the number of joint ties present or the method of beam steel detail used. Similarly to the normal and high strength models this cracking load was at the lower end of the range of experimental values. The load at which joint cracking first occurred for the experimental specimens was from 18 to 30 kN.

5.5.3.2 Failure loads

Table 5.5.3.2.1 shows the modelled failure loads and how they compared with the actual experimental values. The modelled specimens generally underestimated the failure load of the experimental specimens. The mean average of this accuracy was 0.88, an underestimation of the strength by 12%. The correct trend was again seen, however with a variation coefficient of 7.1%.

Table 5.5.3.2.1 Modelled results - (joint aspect ratio)

Actual Specimen	SBETA Model	Cube strength f_{cu} (MPa)	Actual failure load (kN)	Modelled failure load (kN)	Accuracy (model/actual)
Bent down beam steel					
C7LN0	S7N0	48	35.7	33.5	0.94
C7LN1	S7N1	47	39.7	39.3	0.99
C7LN3	S7N3	50	47.5	39.6	0.83
C7LN5	S7N5	50	54.0	45.2	0.84
U-bar beam steel					
C9LN0	S9N0	51	33.3	27.2	0.82
C9LN1	S9N1	48	33.2	30.1	0.91
C9LN3	S9N3	46	37.9	32.1	0.85
C9LN5	S9N5	44	45.9	38.5	0.84
				Mean average	**0.88**
				Standard deviation	**0.06**
				Variation (s.d./mean)	**7.1%**

5.5.3.3 Modelled response

A comparison of the load-deflection response is displayed in Figure 5.5.3.3.1. The response from the experimental specimen C7LN1 is compared with that from the model S7N1.

Figure 5.5.3.3.1 shows that this load-deflection response is extremely close throughout the loading history. The loss of stiffness associated with previous models was not apparent.

Unfortunately none of the main reinforcement within the experimental specimens investigating joint aspect ratio was strain gauged. Detailed strain comparisons were therefore not possible.

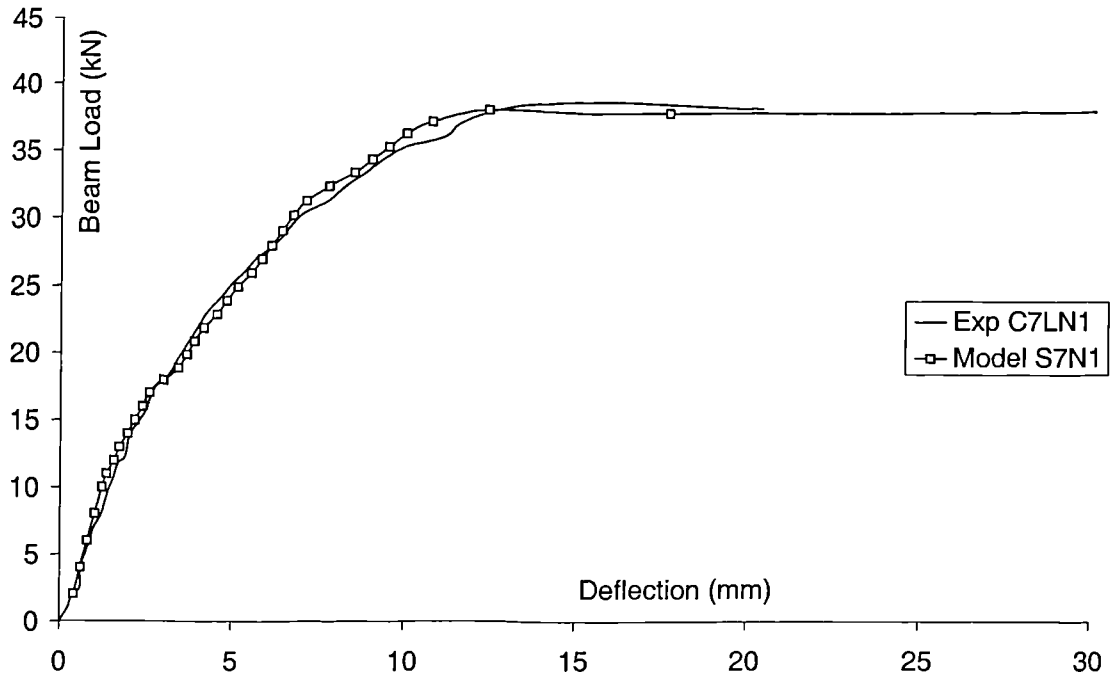

Figure 5.5.3.3.1 Load deflection response comparison - joint aspect ratio

5.5.4 Modelling of specimens from previous research

The experimental specimens from previous research were also modelled. The purpose of this was to confirm that the *standard* mesh design chosen was not only suitable for specimens used within this research.

The experimental specimens tested by both Reys de Ortiz [10] and Parker [11] were considered. Both investigations used specimens significantly larger than those tested by the author (see Section 1.2).

5.5.4.1 Reys de Ortiz [10]

The seven specimens tested by Reys de Ortiz were modelled. Figure 5.5.4.1.1 shows the joint zone of **OSB1** (**O**rtiz **S**BETA model **1**) used to model the experimental specimen BCJ1. The mesh design contains the same layout and number of elements that were used for the modelling of the author's experimental specimens. Similarly,

the beam steel and the outer column bar were placed in adjacent elements. This was believed to give a reasonable approximation of the true anchorage behaviour.

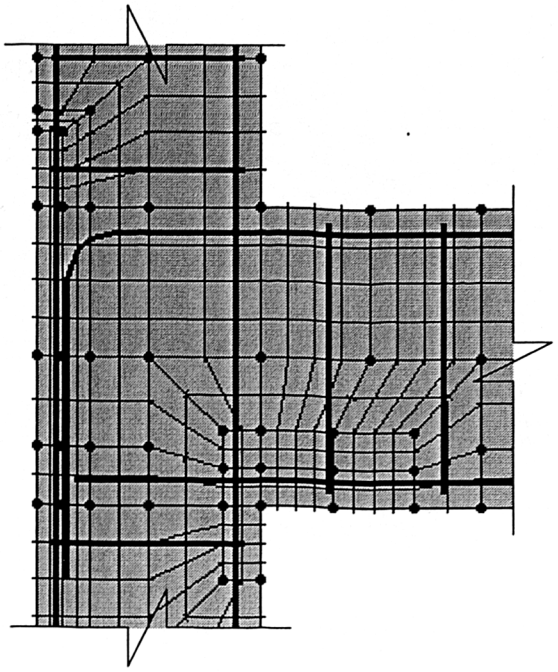

Figure 5.5.4.1.1 Mesh design - model OSB1

This mesh design selected was used to model all of the experimental specimens. Concrete and steel material properties were matched with those given in Reys de Ortiz's thesis. The specimen dimensions, the loading set up and the restraints were also matched with those from the experimental programme.

The column load was represented as a distributed load over the upper column elements. The loading criteria were selected to be as similar as possible to the previous modelling outlined within this chapter.

Table 5.5.4.1.1 displays the modelled failure loads and how they compared with the actual experimental loads. The models failed at values which showed a reasonable correlation with the experimental results. The mean average was 0.90 and the variation coefficient was 7.5%.

Table 5.5.4.1.1 Modelled failure loads - (Reys de Ortiz)

Actual Specimen	SBETA Model	Cube strength f_{cu} (MPa)	Actual failure load (kN)	Modelled failure load (kN)	Accuracy (model/actual)
BCJ1	**OSB1**	42	118	96	0.81
BCJ2	**OSB2**	47	125	115	0.92
BCJ3	**OSB3**	41	118	110	0.93
BCJ4	**OSB4**	42	130	121	0.93
BCJ5	**OSB5**	47	115	99	0.86
BCJ6	**OSB6**	44	115	117	1.02
BCJ7	**OSB7**	44	170 (F)	146 (F)	0.86
				Mean average	**0.90**
				Standard deviation	**0.07**
				Variation (s.d./mean)	**7.5%**

Note

1. F - indicates flexural failure of the beam.

As expected these were not as good a match as observed within the models within the author's investigation. However, considering the size of the specimens and the uncertainty about the anchorage conditions the results were very encouraging.

5.5.4.2 Parker [11]

The sixteen experimental tests by Parker were also modelled. Again, as with Reys de Ortiz [10], the experimental specimens were of a reasonably large scale. In addition there were concerns regarding the anchorage of Parker's specimens (Section 1.4.2).

Unfortunately, a 3-dimensional finite element package would have been required to accurately model an influence such as anchorage. Knowing the concerns regarding the anchorage of Parker's specimens in advance the modelling results were expected to be higher than the experimental values.

Again the mesh design used contained the same layout and number of elements that were used for the modelling of the author's experimental specimens. Similarly, the beam steel and the outer column bar were placed in adjacent elements. As mentioned previously this was (unfortunately) expected to give an enhanced representation of the true anchorage behaviour.

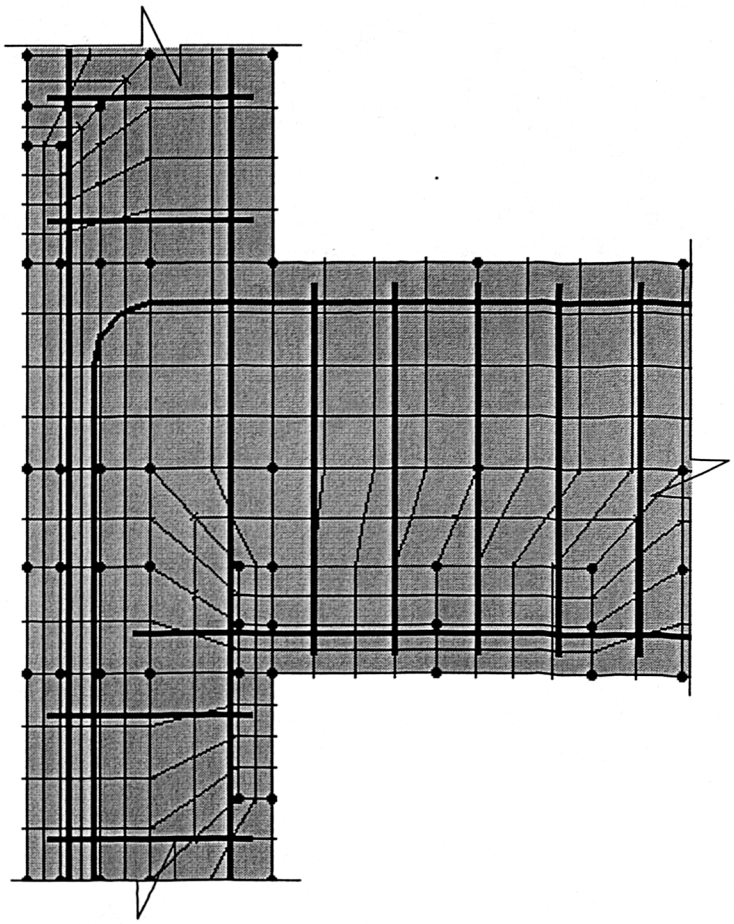

Figure 5.5.4.2.1 Mesh design - model PA4A

Table 5.5.4.2.1 displays the modelled failure loads and how they compared with the actual experimental loads. The models failed at values which showed a reasonable correlation with the experimental results. The mean average was slightly high at 1.12 and the variation coefficient was 7.4%.

However, these results were encouraging considering the scale of the specimens and the uncertainties regarding the beam steel anchorage.

Table 5.5.4.2.1 Modelled failure loads - (Parker)

Actual Specimen	SBETA Model	Cube strength f_{cu} (MPa)	Actual failure load (kN)	Modelled failure load (kN)	Accuracy (model/actual)
4a	**PA4A**	49	$118_{(FC)}$	$148_{(FC)}$	1.25
4b	**PA4B**	49	138	168	1.22
4c	**PA4C**	46	170	172	1.01
4d	**PA4D**	49	150	192	1.28
4e	**PA4E**	50	160	196	1.23
4f	**PA4F**	47	183	213	1.16
5a	**PA5A**	53	$213_{(FC)}$	$245_{(FC)}$	1.15
5b	**PA5B**	54	236	256	1.08
5c	**PA5C**	54	$242_{(FB)}$	$273_{(FB)}$	1.13
5d	**PA5D**	54	$226_{(FC)}$	$276_{(FC)}$	1.22
5e	**PA5E**	56	$295_{(FC)}$	$314_{(FC)}$	1.06
5f	**PA5F**	54	322	316	0.98
				Mean average	**1.15**
				Standard deviation	**0.10**
				Variation (s.d./mean)	**8.4%**

Note

1. FC - indicates flexural column failure, FB - indicates flexural beam failure.

5.5.5 Modelling accuracy

Table 5.5.5.1 displays a summary of the modelling results within this investigation.

Table 5.5.5.1 shows that the overall accuracy of the modelling was good and that the variation of the results was reasonable considering the number of parameters that were varied.

The author chose not to model his experimental fibre specimens. Only a limited amount of information on the *specific* fibre reinforced concrete properties was

available. In addition the number of specimens tested was not considered enough to allow valid modelling to take place.

Table 5.5.5.1 Modelled failure loads and accuracy

Test series	No. of specimens	Mean average	Variation (s.d./mean)
Normal strength	8	1.01	8.1%
High strength	8	0.99	4.3%
Joint aspect ratio	8	0.88	7.1%
Reys de Ortiz [10]	7	0.90	7.5%
Parker [11]	12	1.15	8.4%
All	**43**	**1.00**	**12.4%**

5.6 Parametric Study

Once the *standard* finite element model had been shown to display good results, it was then used to conduct a parametric study. A substantial new series of modelling was conducted to investigate the parameters outlined below :

Concrete strength

To confirm the relationship between joint strength and concrete compressive strength, sixty new modelling runs were conducted on different size models.

Column axial stress

Twenty seven new modelling runs were conducted on different size models. As outlined in Chapter 1 (*Literature Review*), previous research presents conflicting views on the influence of column stress on the joint strength. Axial stresses were considered to allow the comparison of different size specimens.

Joint ties

Fourteen new modelling runs were conducted in an attempt to establish the influence of **joint tie positioning**.

Detailing arrangement for the beam steel

The results presented in Section 5.5 were used to establish the influence of beam steel detail on the joint capacity.

Joint aspect ratio

The results presented in Section 5.5 were used to establish the influence of aspect ratio on the value of joint shear stress at failure.

5.6.1 The influence of concrete strength

Sixty models with concrete compressive cube strengths ranging from 30 to 130 MPa were analysed. The concrete properties were generated using *normal strength* considerations (Table 5.2.1.2) for cube strengths up to 70 MPa and *high strength* considerations (Table 5.5.2.1) for cube strengths of 80 MPa and above. Throughout the modelling all other parameters were maintained at their *standard* values defined below :

Beam steel percentage (A_{beam}) 2.06%
Column steel percentage (A_{col}) 2.29%
Joint steel percentage (A_{joint}) 0%
Column stress (N) 2.22 MPa

To eliminate the influence of any size effects, models of three different sizes were used; *small*, *medium* and *large*. The dimensions of these models are shown in Table 5.6.1. The column and beam lengths were based on the author's experimental specimens and the mesh was the *standard* design as outlined previously within this Chapter. Bent down steel anchorage was used.

Table 5.6.1 Model dimensions (units in mm)

Scale	Beam		Column	
	height	width	width	depth
Small	210	110	150	150
Medium	250	130	180	180
Large	290	150	210	210

Note

1. Cover to the centre of the reinforcement was 33 mm for the small scale specimens, 40 mm for the medium and 46 mm for the large scale specimens.

The results of the sixty models are displayed in Figure 5.6.1. To eliminate the influence of the size effects, the failure results were displayed as shear stresses. The chart displays failure shear stress against the square root of the concrete compressive cylinder strength (in compliance with EC2 [17]).

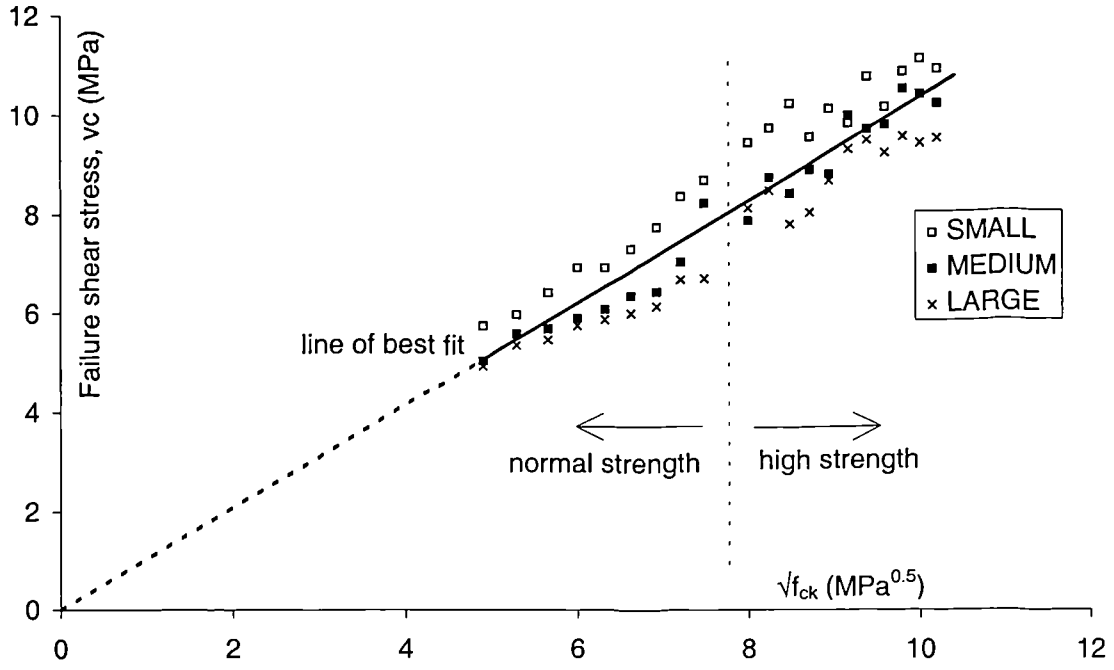

Figure 5.6.1 Failure shear stress against the concrete cylinder strength

Figure 5.6.1 shows how the SBETA finite element package related the failure shear stress to the concrete compressive cylinder strength. The general trend of the sixty modelling runs, on three different size specimens, indicates that :

$v_c = \sqrt{f_{ck}}$ .....eq. (5.6.1)

This was for an unreinforced joint under an axial stress of 2.22 MPa.

The mean average of the ratio $v_c/\sqrt{f_{ck}}$ was 1.04 with a variation coefficient of 8.1%.

5.6.2 The influence of column axial stress

Twenty seven models with column axial stress values ranging from 0 to 35.6 MPa were tested for the three sizes. Throughout the modelling series all other parameters were maintained at their *standard* values, with a concrete cube strength of 60 MPa.

Figure 5.6.2.1 shows the percentage enhancement in joint capacity against the column axial stress for these twenty seven models.

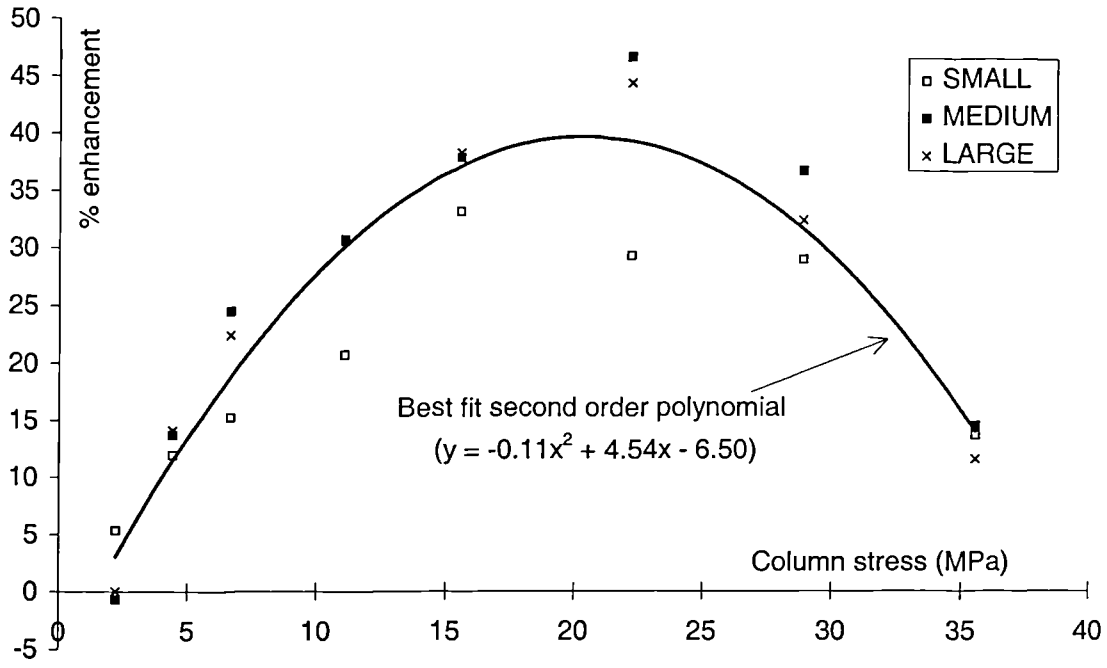

Figure 5.6.2.1 Percentage enhancement against column stress

Figure 5.6.2.1 shows that the results from SBETA indicate that a significant enhancement in joint capacity is achieved as the magnitude of the column stress increases. A best fit second order polynomial was added to the chart which indicated that the enhancement to the joint capacity reached a peak of around 40% approaching a column stress of 20 MPa. This enhancement then reduced as the column stress increased further. Although column stress was not investigated within this research it was discussed in detail in Section 1.4.3. *It should be noted that 20 MPa is around the design limit for the for a column using 60 MPa concrete.*

5.6.3 Influence of joint tie positioning

The influence of joint tie positioning within SBETA was investigated. The behaviour of specimens using both bent down and U-bar beam steel detail was considered. It was important that a significant enhancement was considered in order to establish the optimum position of the ties. It was decided that using a **pair** of closely spaced (*in adjacent elements*) **8 mm** ties would allow clear conclusions to be drawn.

5.6.3.1 Bent down steel detail

Figure 5.6.3.1.1 shows the joint tie positions for the eight considered models. The tie position is shown as the height above the centre line of the joint and the two ties were positioned closely either side of this. All models had the dimensions of a standard experimental specimen and used concrete with a compressive cube strength of 60 MPa.

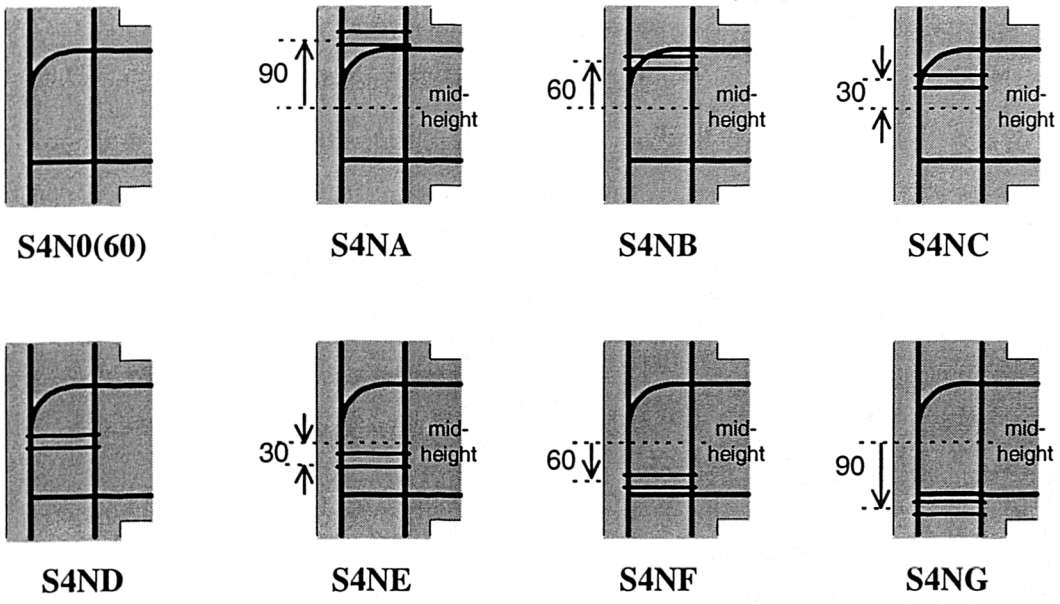

Figure 5.6.3.1.1 Joint tie positioning (dimensions in mm)

The results of this analysis are displayed in Table 5.6.3.1.1 and are represented as both a failure load and a percentage enhancement of the joint capacity (using the

unreinforced model as a base). Figure 5.6.3.1.2 gives a graphical representation of the percentage enhancement.

Table 5.6.3.1.1 Modelled results - (bent down bar / tie positioning)

SBETA model	Tie pos. (mm)	Failure load (kN)	Percentage enhancement
S4N0(60)	-	28.3	-
S4NA	90	29.1	2.8%
S4NB	60	32.6	15.2%
S4NC	30	35.2	24.4%
S4ND	0	35.3	24.7%
S4NE	-30	32.6	15.2%
S4NF	-60	29.6	4.6%
S4NG	-90	29.3	3.5%

Note

1. The tie positioning (Tie pos.) was indicated previously in Figure 5.6.3.1.1.

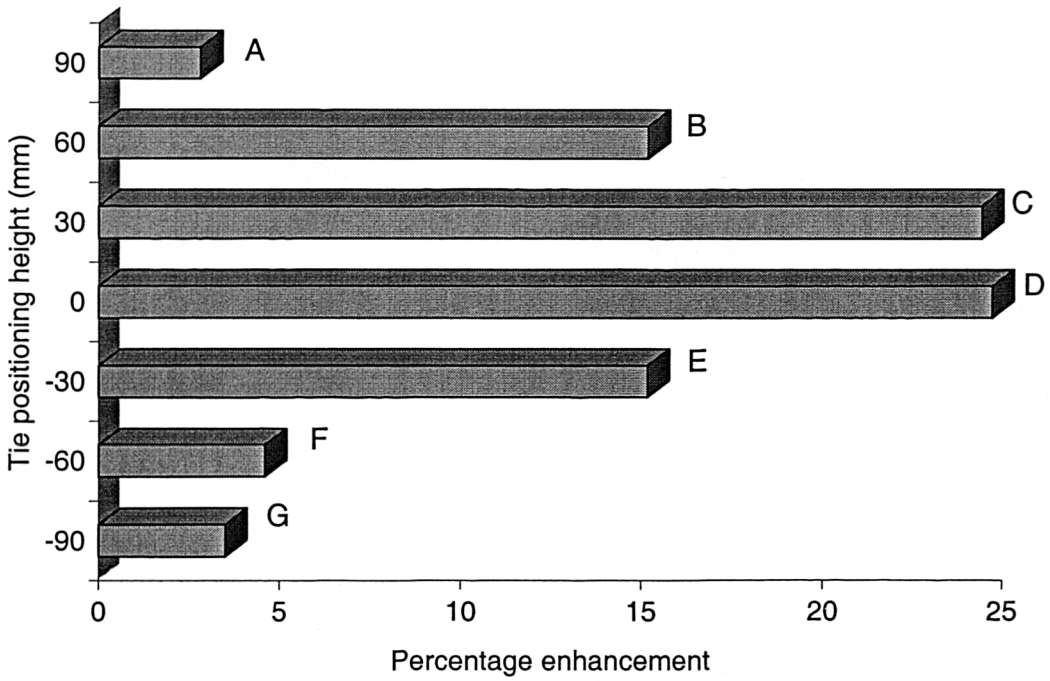

Figure 5.6.3.1.2 % enhancement from joint tie positioning

Figure 5.6.3.1.2 indicates that SBETA considers only ties within the upper three quarters of the joint to be of significant influence. For bent down beam steel detail the optimum position for ties within the joint was found to be just above the mid-height level of the joint.

5.6.3.2 U-bar steel detail

Tie positioning within a model using U-bar steel detail was also considered. Figure 5.6.3.2.1 displays the tie positioning within the joint for the eight models used.

Table 5.6.3.2.1 displays the results from the modelling and Figure 5.6.3.2.2 gives a graphical representation of the enhancement achieved by considering tie positioning. Again, the enhancement is calculated taking the model with an unreinforced joint as a base. All models had the dimensions of the standard experimental specimens and a 60 MPa cube strength was used throughout.

Figure 5.6.3.2.2 shows that SBETA considers the influence of tie positioning to be slightly less for specimens with U-bar beam steel. Again only ties in the upper three quarters of the joint produced a significant enhancement to the strength. The optimum position for the ties was again just above the mid-height.

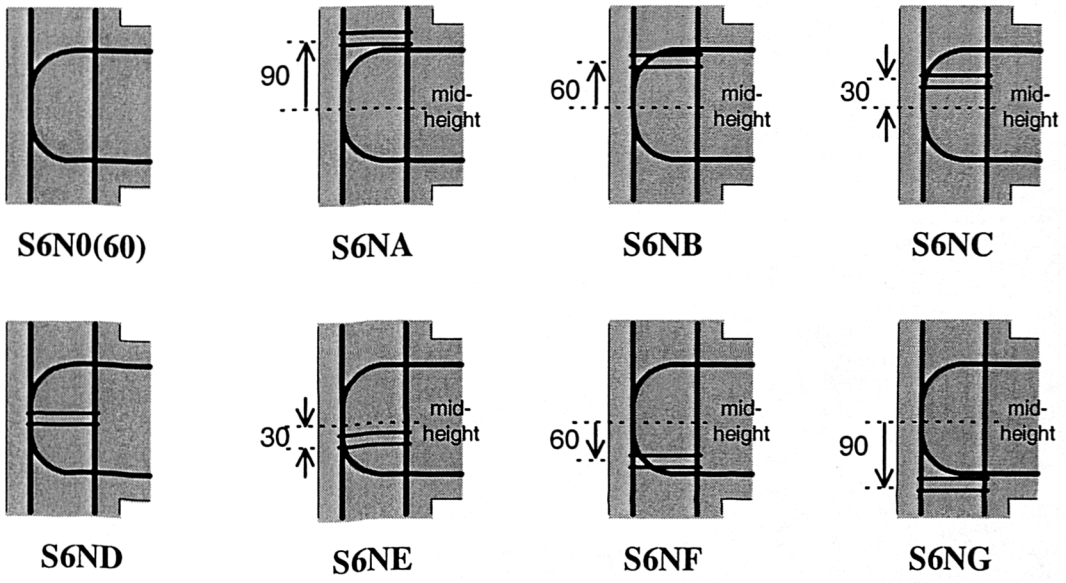

Figure 5.6.3.2.1 Joint tie positioning (dimensions in mm)

Table 5.6.3.2.1 Modelled results - (U-bar / tie positioning)

SBETA model	Tie pos. (mm)	Failure load (kN)	Percentage enhancement
S6N0(60)	-	23.6	-
S6NA	90	24.3	2.9%
S6NB	60	27.0	14.4%
S6NC	30	27.2	15.3%
S6ND	0	28.0	18.6%
S6NE	-30	27.4	16.1%
S6NF	-60	24.3	2.9%
S6NG	-90	23.4	-0.9%

Notes

1. The tie positioning (Tie pos.) was indicated previously in Figure 5.6.3.2.1.

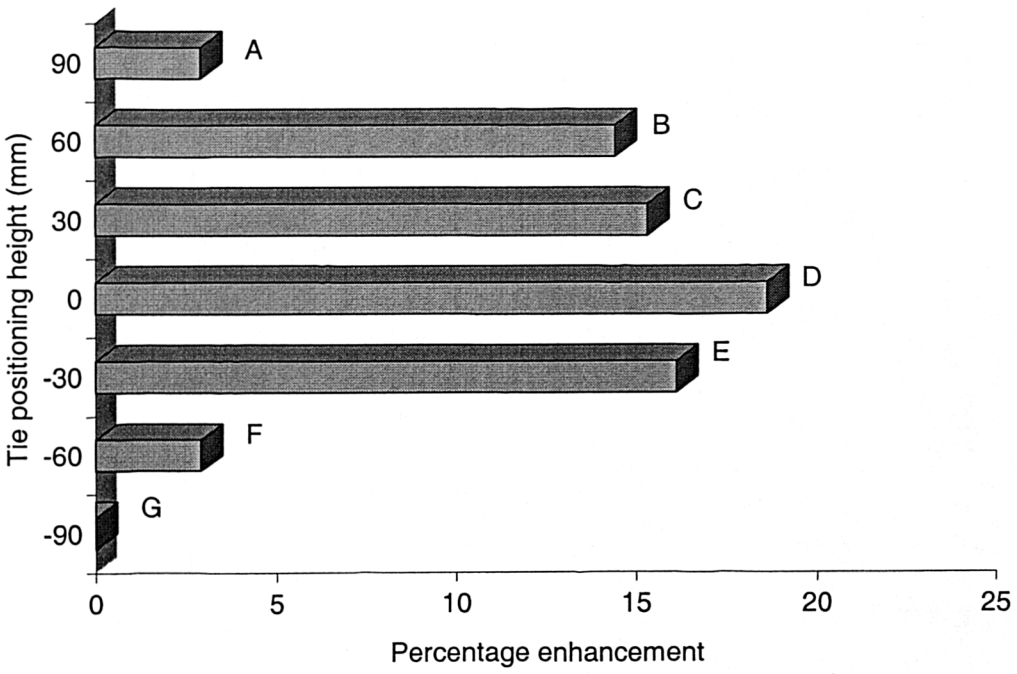

Figure 5.6.3.2.2 % enhancement from joint tie positioning

5.6.3.3 Tie positioning and experimental specimens

The results from the modelling confirm the experimental findings (Section 4.3.2) of ties within the upper section of the joint having the greatest influence on the joint strength.

The peak enhancement for models with bent down steel detail was around 25% at positions C and D. However, the peak enhancement for models with U-bar steel detail was less than 20%. This was in contrast with the experimental results in which the U-bar detail benefited most from additional joint ties due to its weaker anchorage.

The results from models S6NA and S4NA suggest that no suitable enhancement in joint capacity could be achieved by positioning ties above the level of the main beam tension steel. Experimental results indicate, however, that the strength of joints (particularly within specimens with U-bar beam steel) can be significantly strengthened by positioning ties above this level (Section 4.3.2). Experimental specimens C6LN1A and C6LN2A displayed an increase in capacity which was believed to be the result of improved anchorage of the beam tension steel.

The author would suggest that the joint zone from the *standard* mesh design was not capable of accurately modelling tie behaviour. The fact that the element size was still relatively large within the joint zone suggests that the tie may have had too small an influence within the element. As the mesh was only two dimensional and had a 150 mm depth, the concrete material properties had a much greater influence than those from the tie. This concern was highlighted previously in Section 5.2.3.1.

The model confirmed the following general experimental findings :

1. The addition of ties to the joints provided an enhancement to the joint strength.
2. The positioning of ties in the upper region of the joint was more beneficial than in the lower region of the joint.

5.6.4 Influence of beam steel detail

To investigate the influence of beam steel detail the results from previous modelling were used, as follows :

1. **Original normal strength specimens** - The eight models previously displayed in Table 5.5.1.2.1 were considered. Four of these had U-bar beam steel detail and four had bent down steel detail.
2. **Joint aspect ratio specimens** - The eight models previously displayed in Table 5.5.3.2.1 were considered. Four of these had U-bar beam steel detail and four had bent down steel detail.
3. **Tie positioning specimens** - The fourteen models previously displayed in Tables 5.6.3.1.1 and 5.6.3.2.1 were considered. Seven of these had U-bar beam steel detail and seven had bent down steel detail.

In order to eliminate the influence of concrete strength, the failure loads were normalised by dividing by the square root of the compressive strength (*Section 5.6.1 established that joint capacity was proportional to the square root of concrete strength. As f_{ck} is taken as equal to $0.8 \times f_{cu}$ then the use of either is equally valid*).

The average percentage reduction in joint capacity when using U-bar beam steel is displayed in Table 5.6.4.1.

Table 5.6.4.1 shows that using U-bar beam steel detail leads to a joint capacity reduction of around 18% (by modelling beam-column joints using the methods outlined within this chapter).

Table 5.6.4.1 Average percentage reduction in joint capacity

Model series	No. of specimens	Percentage reduction
Standard	8	18.8%
Joint aspect ratio	8	17.5%
Tie positioning	14	18.7%

The experimental specimens indicated that this reduction was around 18% for the standard specimens but only around 13% for the specimens investigating joint aspect ratio.

5.6.5 Influence of joint aspect ratio

To investigate the influence of joint aspect ratio the results from previous modelling were used, as follows :

1. **Original normal strength specimens** - The eight models previously displayed in Table 5.5.1.2.1 were used. These had a joint aspect ratio of 1.4.
2. **Joint aspect ratio specimens** - The eight models previously displayed in Table 5.5.3.2.1 were used. These had a joint aspect ratio of 2.0.

Failure loads were converted into normalised joint shear stresses to eliminate the influence of both concrete strength and joint dimensions. The values are displayed in Table 5.6.5.1.

Table 5.6.5.1 shows that a specimen's joint shear strength reduced by around 25% as the joint aspect ratio (h_b/h_c) increased from 1.4 to 2.0.

The experimental specimens indicated that this reduction was slightly less at around 15%.

Table 5.6.5.1 The influence of joint aspect ratio on shear stress values at failure

Aspect ratio 1.4	$v_{fail}/\sqrt{f_{ck}}$ ($MPa^{0.5}$)	Aspect ratio 2.0	$v_{fail}/\sqrt{f_{ck}}$ ($MPa^{0.5}$)	Percentage reduction
Bent down beam steel				
S4N0	1.30	**S7N0**	0.88	32%
S4N1	1.37	**S7N1**	1.06	23%
S4N3	1.46	**S7N3**	1.03	29%
S4N5	1.49	**S7N5**	1.19	20%
U-bar beam steel				
S6N0	0.98	**S9N0**	0.68	31%
S6N1	0.92	**S9N1**	0.79	14%
S6N3	1.14	**S9N3**	0.86	25%
S6N5	1.42	**S9N5**	1.08	24%
			Mean average	**24.7%**

Note

1. Aspect ratio is defined as h_b/h_c, where h_b is the height of the beam and h_c is the section depth of the column.

The following chapter of this thesis uses the experimental results, strengthened with the results from this finite element study, to develop a set of monotonic design guidelines.

The author believes that these guidelines should be considered when designing external beam-column joints within a reinforced concrete structure.

6. Monotonic Design Guidelines

This chapter summarises the findings from the monotonic experimental results (*Chapter 4*) and the finite element analysis (*Chapter 5*). These are presented in the form of *rule of thumb* guidelines for the design of reinforced concrete external beam-column joints.

As previously outlined in the *Literature Review*, this investigation was concerned with the design of external joints as they are subjected to the greatest shear force within a framed structure. A diagrammatic representation of an external beam-column joint and its location in a typical framed structure is shown in Figure 6.1.

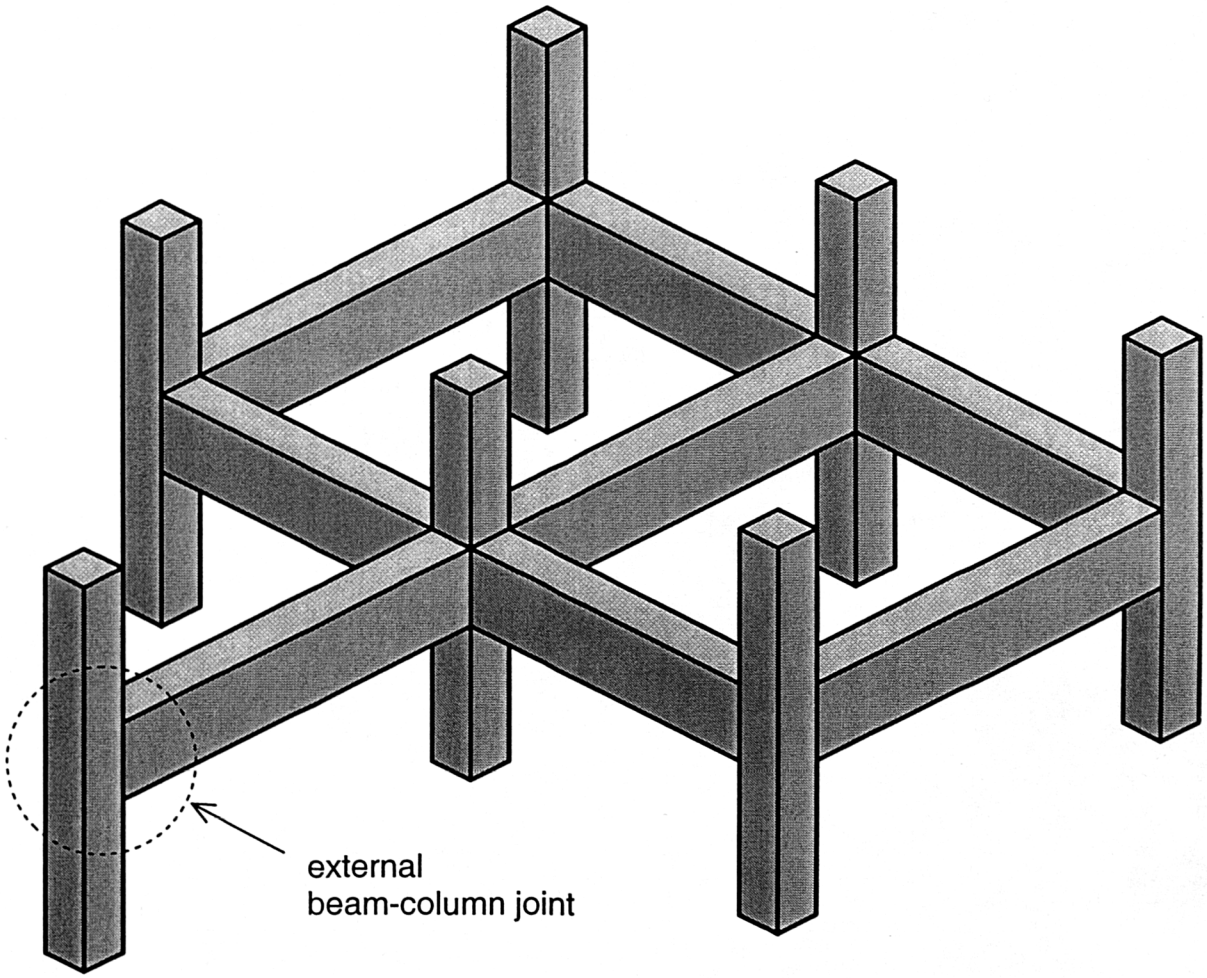

Figure 6.1 An external beam-column joint within a framed structure

6.1 Monotonic Design Guidelines

The author suggests that these guidelines should be considered in the design of external beam-column joints within a reinforced concrete structure.

6.1.1 Basic joint strength

Prior to joint design the beam and column members within a framed reinforced concrete structure should be designed using standard design methods such as BS 8110 [3] or EC2 [17].

The shear stress within the joint should be evaluated at the applied load equivalent to the beam's ultimate moment of resistance (with the design safety factors removed). The method used for this, within this thesis, was outlined previously in Section 1.3.

This equivalent shear stress, v_{umr}, should then be compared with the shear strength of the unreinforced joint, v_{ult}, where v_{ult} is evaluated by :

$$v_{ult} = \alpha\beta\sqrt{f_{ck}} = \alpha\beta\sqrt{(0.8\times f_{cu})} \quad \text{.....(eq. 6.1.1.1)}$$

where α is a reduction factor, ($\alpha = 1$ for bent down beam steel, $\alpha = 0.83$ for U-bar beam steel,)
(*beam anchorage*)

β is a reduction factor, $\beta = 0.25\left(5.4 - \frac{h_b}{h_c}\right)$,
(*joint aspect ratio*)

h_b is the total depth of the beam,
h_c is the total depth of the column,
for specimens where $1.4 < h_b/h_c < 2.0$.

If $v_{ult} > v_{umr}$ then the joint strength is sufficient.

If $v_{ult} \leq v_{umr}$ then the joint is weaker than the beam framing into it and thus requires strengthening.

6.1.2 Methods of joint strengthening

If the joint requires strengthening the value of v_{ult} may be increased using the following design guidelines.

Increasing the concrete strength

Joint strength is directly proportional to the square root of concrete strength. Therefore, the use of high strength concrete within the joint region can significantly enhance the joint capacity. This enhancement factor is given below :

$$\text{Concrete strength enhancement factor} = \sqrt{\left(\frac{f_{cu(joint)}}{f_{cu(basic)}}\right)} \quad \text{.....(eq. 6.1.2.1)}$$

where $f_{cu(joint)}$ is the compressive strength of the joint concrete,

$f_{cu(basic)}$ is the compressive strength of the concrete in the intersecting members.

An example of this is displayed in Table 6.1.2.1. The enhancement values are based on a basic compressive cube strength of 40 MPa within the intersecting members.

Table 6.1.2.1 Possible joint enhancement to 40 MPa concrete structure

f_{cu} (MPa), joint concrete only	60	80	100	120
Enhancement to v_{ult}	22%	41%	58%	73%

The addition of joint ties

Ties positioned within the joint give an increased capacity by providing both added resistance to crack propagation and increased confinement to the concrete core. Ties also reduce beam rebar slippage by providing additional confinement to the concrete below the beam rebar's top bend.

Results from both the experimental specimens and the finite element analysis found that ties positioned, in the top half of the joint, below the level of the beam rebar gave the most significant enhancement. This region of the joint is indicated in Figure 6.1.2.1.

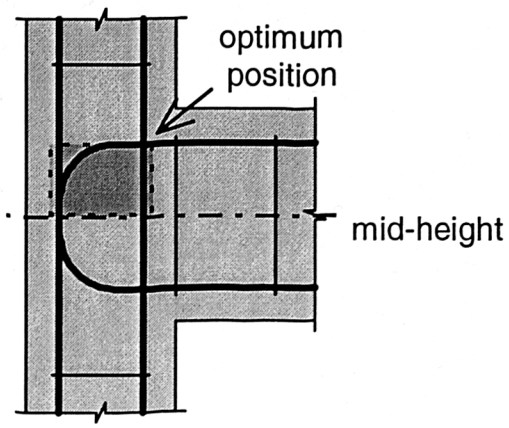

Figure 6.1.2.1 Optimum tie position within the joint

Table 6.1.2.2 displays the joint enhancement, achieved within this investigation, from the positioning of ties within the *optimum* region of the joint as shown in Figure 6.1.1.1.

Table 6.1.2.2 Possible enhancement from joint ties

Percentage of joint steel	0.37%	0.74%	1.12%
Enhancement to v_{ult}	25%	40%	55%

Notes

1. These are purely empirical enhancement factors based on the author's experimental results,
2. The percentage of joint steel is evaluated from $A_j/b_e d_{col}$; where Aj is the cross sectional area of both the tie's legs, b_e is the effective breadth of the column and d_{col} is the effective depth of the column,
3. The author used smooth joint ties with a characteristic strength of, f_y = 500 MPa.

The addition of steel fibres

Steel fibres enhance the joint strength as they provide the concrete with a greater tensile strength. Table 6.1.2.3 displays the joint enhancements achieved within this investigation from the addition of steel fibres to the joint zone.

Table 6.1.2.3 Possible joint enhancement from the addition of steel fibres

Volumetric fibre percentage	0.4%	1.5%	2.3%
Enhancement to v_{ult}	10%	40%	60%

Notes

1. These are purely empirical enhancements based on the author's experimental results,
2. These are based on the most conservative enhancements achieved from the tests specimens. Higher percentages were possible using longer fibres,
3. The author used fibres with properties outlined previously in Figure 2.2.2.

The addition of steel joint plates

Joint capacity may be substantially increased by the addition of a steel shear plate. The steel plate design used within this investigation was outlined previously in Section 4.6.4. This provided a joint enhancement of over 100%.

A summary of these enhancement factors is displayed in the following figures :

Figure 6.1.2.2 Joint enhancement from increased concrete strength

Figure 6.1.2.3 Joint enhancement from the addition of joint ties

Figure 6.1.2.4 Joint enhancement from the addition of steel fibres

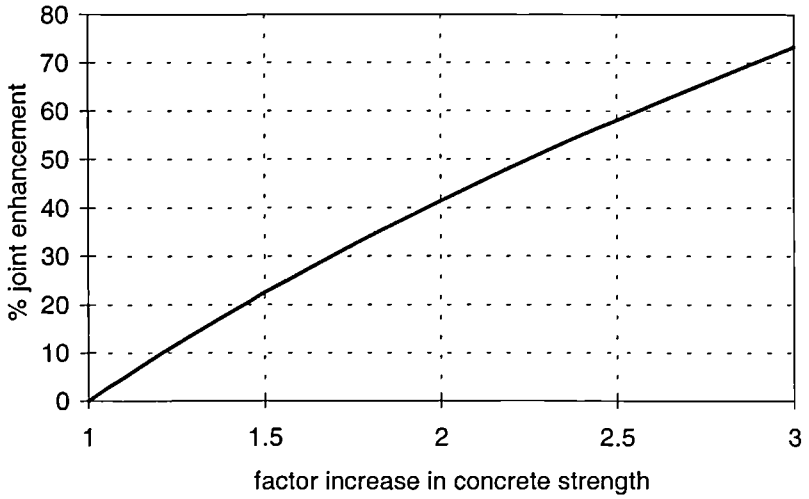

Figure 6.1.2.2 Joint enhancement from increased concrete strength

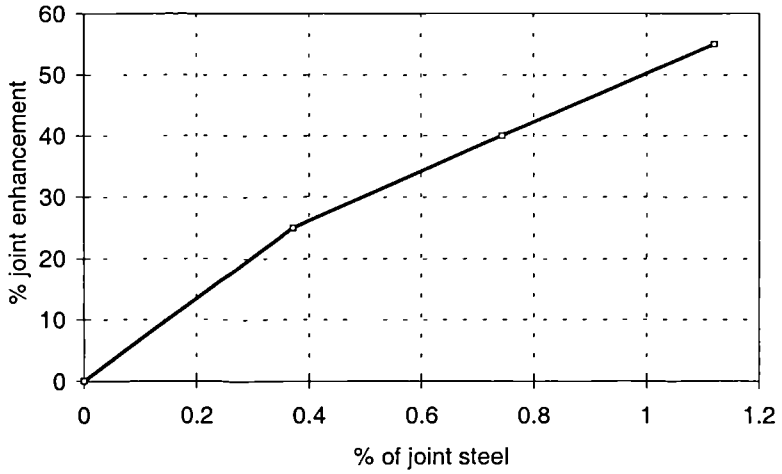

Figure 6.1.2.3 Joint enhancement from joint ties

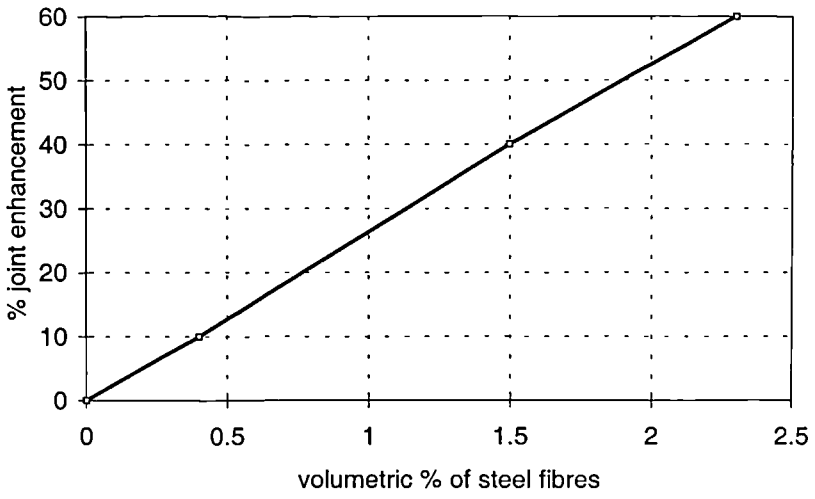

Figure 6.1.2.4 Joint enhancement from steel fibres

6.1.3 Design examples

The following examples evaluate the strength of external beam-column joints within a structure. The design stage considered is that after the steel layout and section dimensions have been selected.

Design example one

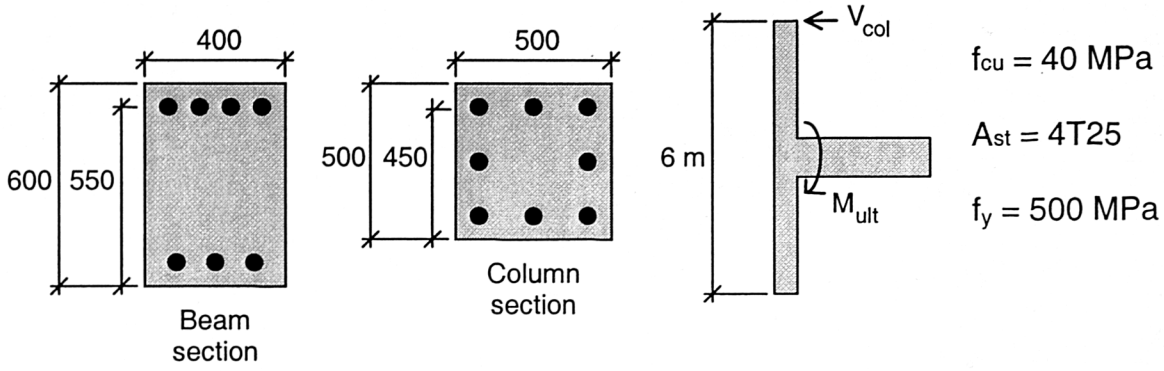

Figure 6.1.3.1 Design example one

The shear force within the joint at the ultimate moment of resistance of the beam is evaluated from the following expression :

$V_{umr} = T_{bm} - V_{col}$ .....(eq. 1.3.1)

where T_{bm} is the force in the beam tension steel,

V_{col} is the shear force within the upper column.

Using BS 8110 [3] to calculate the ultimate moment of resistance of the beam (with all safety factors removed) :

$M_{ult} = 503$ kNm

The maximum force in the beam tension reinforcement is at yield conditions :

$T_{bm} = A_{st} \times f_y = 1960\ mm^2 \times 500\ MPa = 980\ kN$

By taking moments, clockwise, about the base of the beam-column connection :

$M_{ult} - (V_{col} \times L_{col}) = 0$

$$V_{col} = \frac{503}{6} = 84\ kN$$

Thus the shear force in the joint at the ultimate moment of resistance of the beam is :

$V_{umr} = T_{bm} - V_{col} = 980 - 84 = 896\ kN$

The equivalent shear stress is :

$$v_{umr} = \frac{V_{umr}}{b_e d_{col}} = \frac{896000}{450 \times 450} = \underline{\mathbf{4.4\ MPa}}$$

To evaluate the shear capacity of the joint equation 6.1.1.1 is used :

$v_{ult} = \alpha\beta\sqrt{(0.8 \times f_{cu})}$

where $\alpha = 1$ (assume bent down steel design),

$\beta = 1$ (as the joint aspect ratio is less than 1.4).

thus $v_{ult} = \sqrt{(0.8 \times 40)} = \underline{\mathbf{5.7\ MPa}}$

as $v_{ult} > v_{umr}$ $(5.7 > 4.4)$ **further joint design is not necessary.**

(**note** : As the strength of joint is 30% greater than required the use of U-bar beam steel detail would be permitted).

Design example two

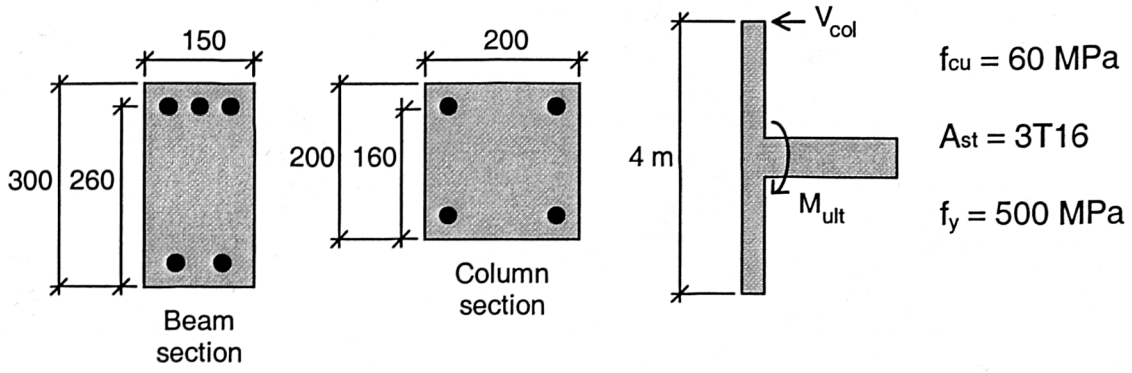

Figure 6.1.3.2 Design example two

Using BS 8110 [3] to calculate the UMR of the beam (with all safety factors removed) :

$M_{ult} = 72$ kNm

The maximum force in the beam tension steel is :

$T_{bm} = A_{st} \times f_y = 603 \text{ mm}^2 \times 500 \text{ MPa} = 302$ kN

By taking moments, clockwise, about the base of the beam-column connection :

$M_{ult} - (V_{col} \times L_{col}) = 0$

$$V_{col} = \frac{72}{4} = 18 \text{ kN}$$

Thus the shear force in the joint at the ultimate moment of resistance of the beam is :

$V_{umr} = T_{bm} - V_{col} = 302 - 18 = 284$ kN

The equivalent shear stress is :

$$v_{umr} = \frac{V_{umr}}{b_e d_{col}} = \frac{284000}{175 \times 160} = \underline{\mathbf{10.1\ MPa}}$$

To evaluate the shear capacity of the joint equation 6.1.1.1 is used :

$$v_{ult} = \alpha\beta\sqrt{(0.8 \times f_{cu})}$$

let $\alpha = 1$ (assume bent down steel design),

$$\beta = 0.25 \times \left(5.4 - \frac{h_b}{h_c}\right) = 0.25 \times \left(5.4 - \frac{300}{200}\right) = 0.975$$

thus $v_{ult} = 0.975 \times \sqrt{(0.8 \times 60)} = \underline{\mathbf{6.8\ MPa}}$

As $v_{umr} > v_{ult}$ (10.1 > 6.8) **further joint strengthening *is* required** - an enhancement of 49% is needed.

Using the design charts suggested in Section 6.1.2 either (or a combination) of the following methods may be used to achieve this enhancement :

Increasing the concrete strength - the use of high strength concrete with a cube strength of 140 MPa within the joint would give an enhancement of 53%.

The addition of joint ties - the use of three 8 mm diameter ties, ($A_j/b_e d_{col}$ = 1.1%), positioned in the *optimum region* of the joint would give an enhancement of around 50%.

The addition of steel fibres - the use of a volumetric percentage of 2.0% steel fibres would give a joint enhancement of around 52%.

7. Cyclic Testing (Background)

As stated previously in Chapter 1 (*Literature Review*) and Chapter 2 (*Monotonic Experimental Programme*) the monotonic test programme was extended to investigate the behaviour of **monotonically designed reinforced concrete beam-column connections subjected to cyclic loads.**

Previously within this thesis only the basic monotonic shear capacity of the joint has been considered. This section of the thesis, however, studies the way the joint capacity of a monotonic connection varies as the specimen is loaded cyclically to produce increasing displacements.

There is a growing need for knowledge regarding monotonically designed connection behaviour under cyclic loading conditions. An example of this problem is in developing countries where reinforced concrete structures have been built (and are being built), in seismic regions, without proper design considerations. This can be demonstrated by comparing the cost of the earthquake in Armenia in 1988 and that in the USA in 1989. Although the earthquake in the USA was far more severe in magnitude, the fatalities in Armenia, the developing country, were higher by a ratio of around 400 to 1.

There are also growing concerns in the USA regarding the behaviour of structures in regions of low to moderate seismicity [53, 54]. These structures were not built to guidelines as strict as those in regions of high seismicity.

A review of the previous *cyclic testing methods* of reinforced concrete beam-column connections is considered relevant and is presented here. This investigation was not concerned with the specific behaviour of seismically design reinforced concrete beam-column connections. A comprehensive review of the seismic literature is included elsewhere [18, 21].

7.1 Previous Cyclic Testing Methods

In 1961, a book by Blume *et al* [55] contained recommendations for the design of reinforced concrete structures in seismic regions. To withstand a major earthquake the beam-column joints within a structure must be both strong and ductile. Blume presented the following design recommendations :

1. Sufficient transverse shear reinforcement should be provided to ensure a shear strength greater than the flexural strength.
2. There should be limitations on the amount of tensile reinforcement, or required use of compression reinforcement, to ensure ductility and energy-absorbing capacity.
3. Confinement of the concrete should be provided by hoops or spirals (ties or stirrups) at critical sections, such as beam-column connections, to increase the ductility of columns under combined axial load and bending.
4. There should be special attention to details, such as splices in reinforcement and exclusions of planes of weakness that would result from bending or terminating all bars at the same section.

Blume *et al* commented that : "*A structure should resist a moderate earthquake without damage, and should survive the most severe earthquake reasonably predictable during the life of the building, without major structural damage. Furthermore, the structure should not collapse even when subjected to an earthquake of abnormal intensity*".

In 1967, Hanson and Connor [56] reported on the testing of seven external reinforced concrete beam-column connections subject to load reversals. This research was amongst the earliest investigations on the behaviour of reinforced concrete structures subjected to cyclic loading.

During earthquake motions a structure will be moved vertically up and down by ground waves and simultaneously moved from side to side by transverse ground vibrations. By similar triangles, Hanson and Connor showed that testing a specimen

by loading the column ends horizontally whilst restraining the beam was effectively the same as restraining the column ends and loading the beam vertically. This is demonstrated in Figure 7.1.1.

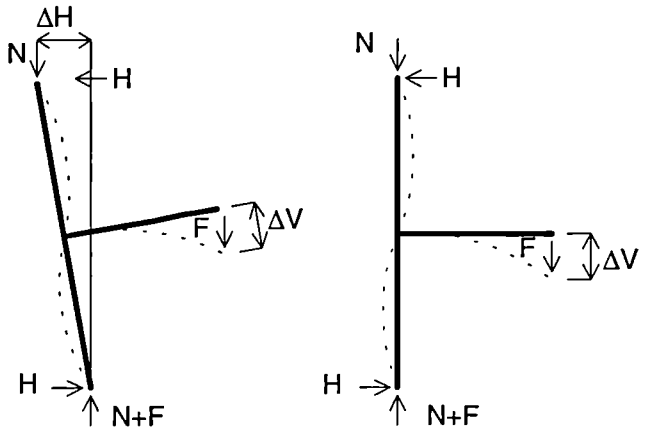

Figure 7.1.1 Equivalent cyclic loading techniques

Hanson and Connor also considered the speed of this cyclic loading. They commented that although earthquakes are dynamic in nature, the vibrations are relatively slow. Discussions by Blume *et al* [55] indicate that the strength and energy-absorption characteristics of reinforced concrete members are increased with increased speed of loading. Therefore slow cycling, as a basis of testing reinforced concrete members, would appear conservative.

A number of different cycling techniques have been used since the tests by Hanson and Connor. However, all consider the cycling in terms of a **ductility factor, μ**. The definition of this is the ratio of either the **rotation** at ultimate load to the rotation at yield load or the **displacement** at ultimate load to the displacement at yield load.

Hanson and Connor used the loading technique shown in Figure 7.1.2. This was chosen to represent the effect of two major earthquakes. The purpose of the first loading cycle was to establish the *elastic* behaviour of the connection. The next two cycles were to represent the first major earthquake. The next three *elastic* cycles were to establish the behaviour of the connection after a major earthquake and the

final three cycles were to simulate a second major earthquake. The so-called *elastic* cycles were to 75% of the yield load.

Figure 7.1.2 Loading technique used by Hanson and Connor [56]

Over the last thirty years, since Hanson and Connor's tests, the cyclic loading techniques adopted by various investigators were all to imposed ductility factors. More typically, these ductility factors steadily increased with the number of cycles. This was in contrast with Hanson and Connor who previously had subjected their connections to alternate large displacements and then elastic cycles.

Figure 7.1.3 shows the loading technique used by Burguieres *et al* [57] in 1979. The specimen was cycled three times to a ductility factor of one and then three times to a ductility factor of two, and so forth, up to the limit of the test apparatus.

Figure 7.1.4 shows the similar loading technique used by Bertero *et al* [58] in 1980. After a series of initial elastic cycles the specimen was cycled twice to a ductility factor of one and then twice to a ductility factor of two, and so forth, up to the limit of the test apparatus.

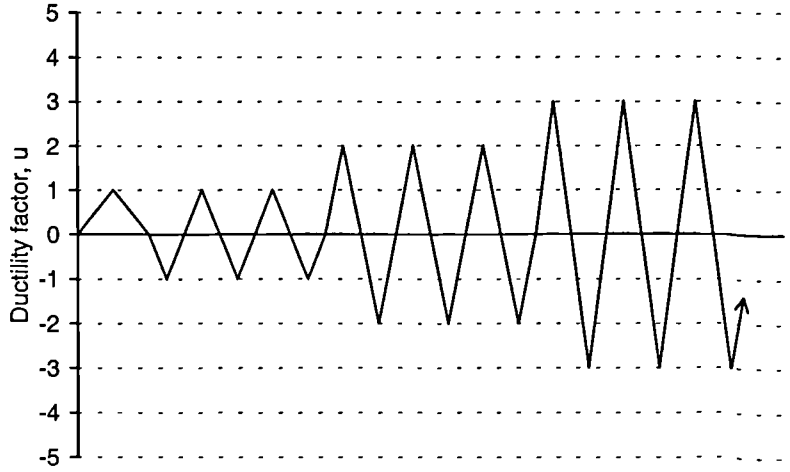

Figure 7.1.3 Loading technique used by Burguieres *et al* [57]

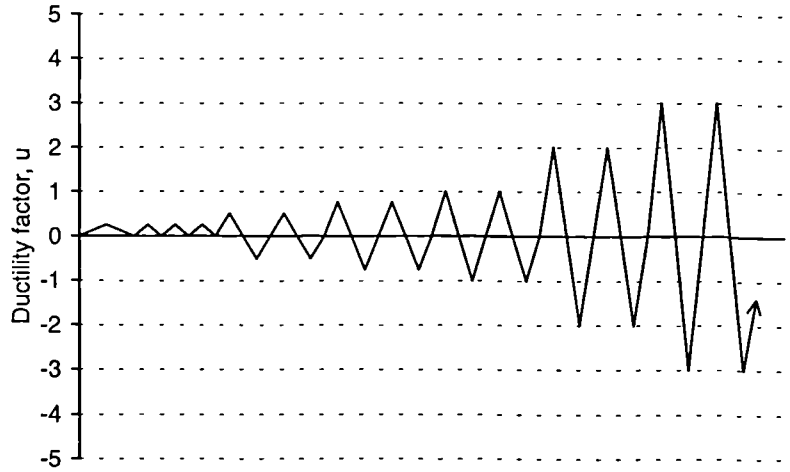

Figure 7.1.4 Loading technique used by Bertero *et al* [58]

Bonacci and Pantazopoulou [18] conducted an extensive parametric investigation on the seismic behaviour of beam-column joints in 1993. After the consideration of tests from 27 different investigations they commented that : *"...a variety of levels of displacement intensity and waveform have been used, thereby introducing another parameter in an already complicated problem. The diversity in the level and the history of displacements reflects the differences in acceptable performance criteria by the various investigators around the world."*

From the parametric study it was concluded that the majority of loading techniques had been to ductility factors of increasing amplitudes (similar to shown in Figures 7.1.3 and 7.1.4).

After carefully considering all of the previous cyclic loading techniques the author decided to use the method implemented by Durrani *et al* [59, 60, 61] at the University of Michigan, USA. This loading technique is displayed in Figure 7.1.5.

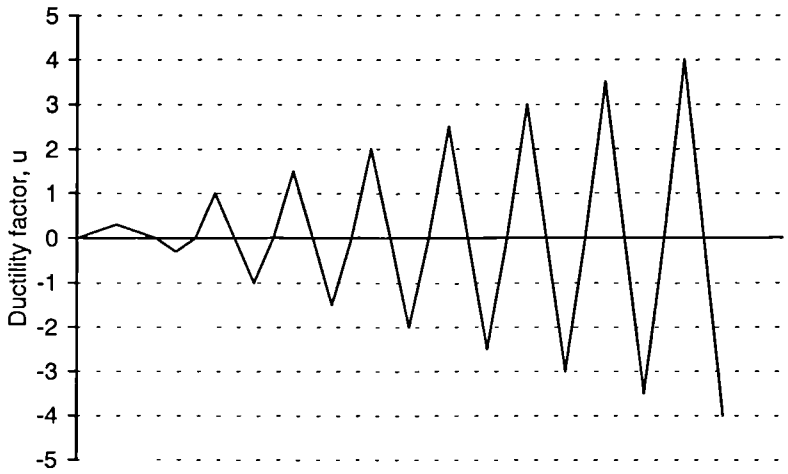

Figure 7.1.5 Loading technique used by Durrani *et al* [59, 60, 61]

The first cycle was to determine the specimen's *elastic* response. Subsequent cycles were to ductility factors of 1.0, 1.5, 2.0 and so forth until a ductility factor of 4.0. The majority of previous research agreed that a ductility factor of around 3.0 to 4.0 was equivalent to the effect of a major earthquake.

This loading technique was chosen as it was simple and gave a good indication of the joint deterioration with increasing factors of ductility. This method is considered in more detail in Section 7.3.

7.2 Cyclic Test Programme

The cyclic test programme set out to investigate the behaviour of a series of sixteen monotonically designed beam-column connection specimens. The parameters to be investigated were the influence of ties within the joint, the strength of the concrete and the detailing arrangement of the beam tension steel. Figure 7.2.1 shows how this original test programme of sixteen specimens developed into the complete cyclic test programme of twenty three specimens.

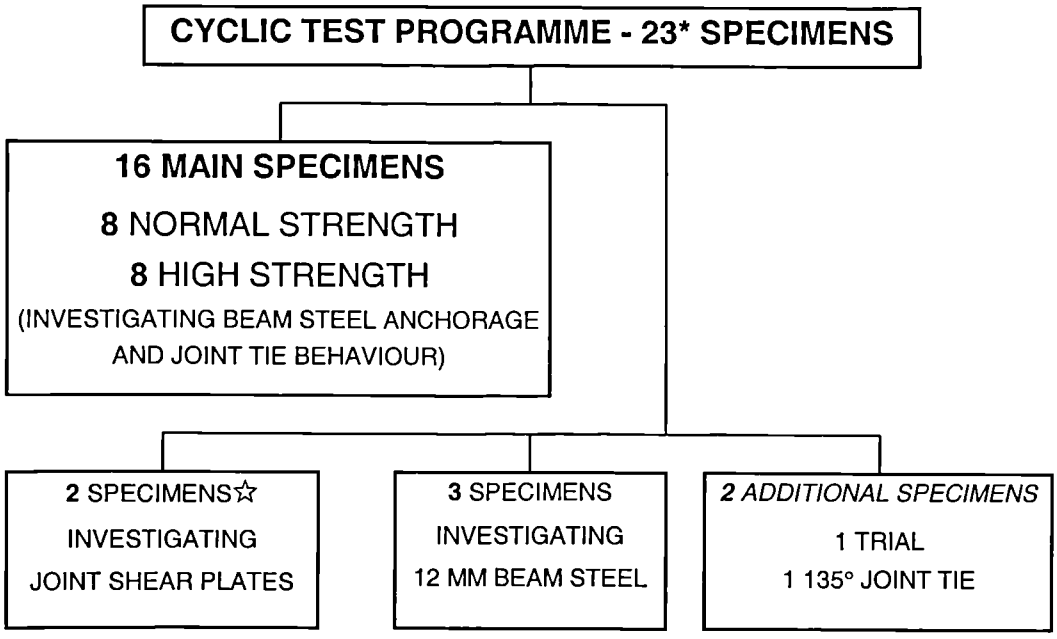

Figure 7.2.1 Breakdown of test programme

Notes 1 ☆ Baglin's specimens,

2 * the joint shear plate specimens were part of the monotonic programme.

The sixteen main specimens were divided into two test series; eight normal strength specimens (defined as the *standard* cyclic test series) and eight high strength specimens. As this investigation developed further, additional specimens were manufactured and tested. The two specimens containing joint shear plates were tested cyclically after their monotonic strength had been determined. Three specimens were tested using a reduced quantity of beam tension steel. Two additional specimens were also tested; a trial specimen to establish the correct loading techniques and positioning of instrumentation and a specimen investigating tie anchorage.

Diagrammatic representations of the individual joint zones are shown in the following tables :

Table 7.2.2 Standard cyclic specimens
Table 7.2.3 High strength cyclic specimens
Table 7.2.4 Specimens investigating 2T12 beam steel
Table 7.2.5 Additional specimens

Note
The two specimens containing shear plates were shown previously in Table 2.7.

7.2.1 Specimen details

The specimen dimensions and steel properties were identical to those outlined previously in Section 2.1. Similarly, the method of manufacture was identical to that outlined in Section 2.2.

7.2.2.1 Standard cyclic specimens

The strain gauge layout used for the main beam steel within specimen C4ALN3CY was shown previously in Figure 2.2.1.2.7. The strain gauge layout used for the main beam steel within specimen C6LN3CY was shown previously in Figure 2.2.1.2.6. Both specimens used the strain gauged tie layout shown previously in Figure 2.2.1.2.1.

7.2.2.2 High strength cyclic specimens

Specimens C4ALH3CY and C6LH3CY had exactly the same gauging layout as the normal strength specimens C4ALN3CY and C6LN3CY.

Table 7.2.2 Standard cyclic specimens

Specimen	Joint Layout	Gauging	Beam steel anchorage	No. of joint ties
C4ALN1CY	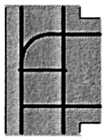	-	Bent down	1
C4ALN3CY	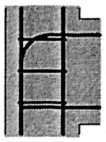	Joint ties, beam steel	Bent down	3
C4ALN5CY	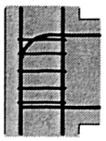	-	Bent down	5
C4ALN7CY	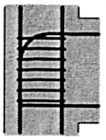	-	Bent down	7
C6LN1CY	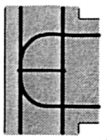	-	U-bar	1
C6LN3CY	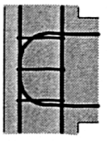	Joint ties, beam steel	U-bar	3
C6LN5CY	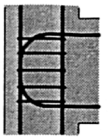	-	U-bar	5
C6LN7CY	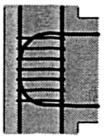	-	U-bar	7

Note

For gauging details see Section 7.2.1

Table 7.2.3 High strength cyclic specimens

Specimen	Joint Layout	Gauging	Beam steel anchorage	No. of joint ties
C4ALH1CY	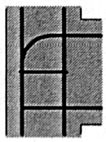	-	Bent down	1
C4ALH3CY	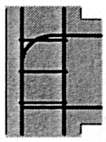	Joint ties, beam steel	Bent down	3
C4ALH5CY	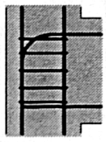	-	Bent down	5
C4ALH7CY	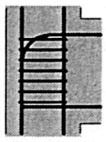	-	Bent down	7
C6LH1CY	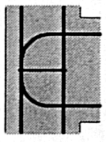	-	U-bar	1
C6LH3CY	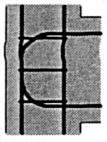	*Joint ties,* beam steel	*U-bar*	*3*
C6LH5CY	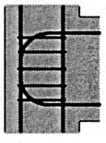	-	U-bar	5
C6LH7CY	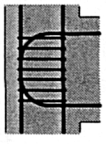	-	U-bar	7

Table 7.2.4 Specimens investigating 2T12 beam steel

Specimen	Joint Layout	Gauging	Beam steel anchorage	No. of joint ties
C3LN7CY	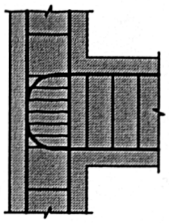	-	U-bar	7
C3XLN7CY	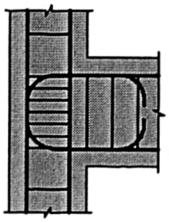	-	*Double* U-bar	7
C3HLN7CY	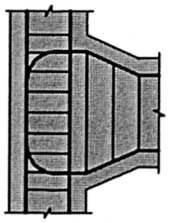	-	U-bar	7

Table 7.2.5 Additional specimens

Specimen	Joint Layout	Gauging	Beam steel anchorage	No. of joint ties
C6LN3CYT	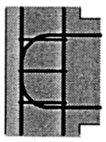	-	U-bar	3
C6LN3CYE	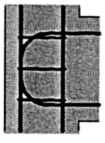	-	U-bar	3

7.2.2.3 Specimens investigating shear plates

These specimens were outlined previously in Section 2.1.3.

7.2.2.4 Specimens investigating 2T12 beam steel

Three specimens were tested using 12 mm rebars for the beam steel.

C3LN7CY

Figure 7.2.2.4.1 shows the details for specimen C3LN7CY. **C3** indicates that a pair of 12 mm U-bars was used for the beam reinforcement. Seven 6 mm ties were used for the joint reinforcement.

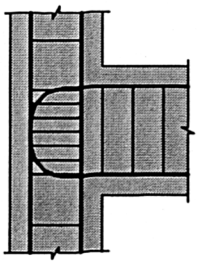

Figure 7.2.2.4.1 Specimen C3LN7CY

C3XLN7CY

Figure 7.2.2.4.2(a) shows the details for specimen C3XLN7CY. **C3X** indicates that extra beam steel was provided within the joint area. Two pairs of 12 mm U-bars were provided; one pair were standard U-bars which continued along the beam's length, one pair were anchored at a distance of 100 mm from the column face using 90° bends.

This technique was used in an attempt to force the beam to develop a plastic hinge at a distance 100 mm from the column face. Again seven 6 mm ties were used for the joint reinforcement.

C3HLN7CY

Figure 7.2.2.4.2(b) shows the details for specimen C3HLN7CY. **C3H** indicates that the beam was *haunched.* The beam had a depth of 300 mm at the column face and the main section of the beam had a depth of 210 mm. The haunched section of the beam had a horizontal length of 100 mm.

This technique was again used in an attempt to force the beam to develop a plastic hinge at a distance 100 mm from the column face. Seven 6 mm ties were present within the joint.

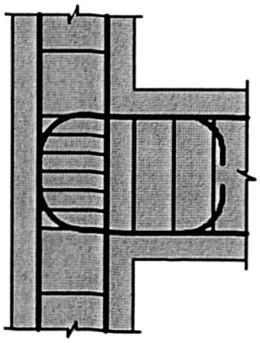

Figure 7.2.2.4.2(a)
Specimen C3XLN7CY

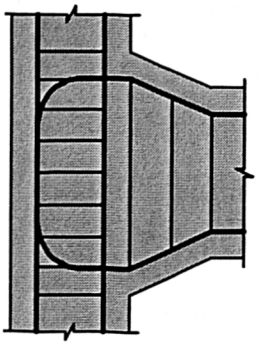

Figure 7.2.2.4.2(b)
Specimen C3HLN7CY

7.2.2.5 Additional specimens

C6LN3CYT

Prior to the cyclic programme, a trial specimen C6LN3CY**T,** was tested in an attempt to establish a suitable loading technique.

C6LN3CYE

Specimen C6LN3CY was repeated using joint ties with legs bent through 135° (see Section 2.1), which was specimen C6LN3CY**E**. Figure 7.2.2.4.1 shows the

specimen layout for C6LN3CYE. The ties indicated in bold had their legs bent through 135°. This additional anchorage is shown in Figure 7.2.2.4.2.

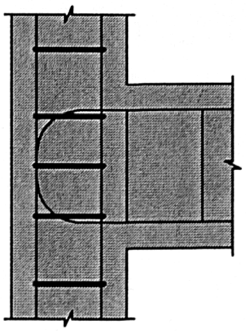

Figure 7.2.2.4.1 Specimen C6LN3CYE (bold ties indicate 135° anchorage)

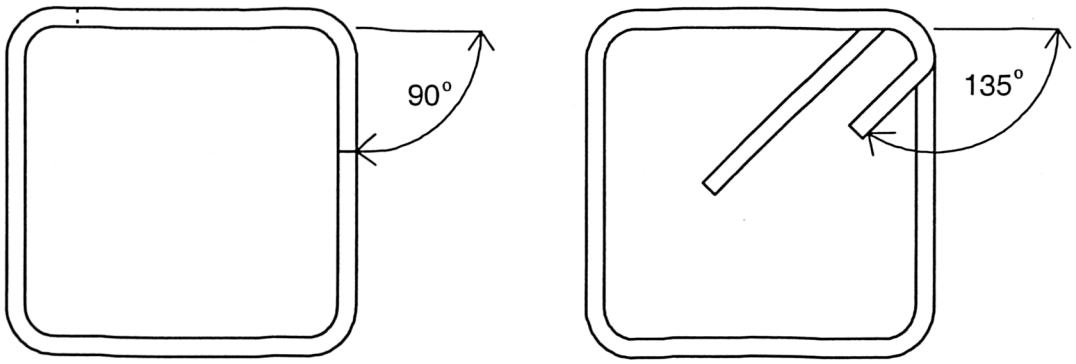

Figure 7.2.2.4.2 Joint tie anchorage

7.3 Specimen Testing

7.3.1 Instrumentation

Towards the end of the monotonic test programme three electronic tilt meters were purchased. These were to be used for rotation measurements as part of the cyclic test programme.

Figure 7.3.1.1 shows a consideration of rotations at three different locations. The symbols indicate the region of the specimen under consideration. It can be seen that the rotation measured at the position of the beam is actually the combination of the lower column, joint and beam rotation. Throughout this thesis the rotation measurement at this point is defined as the **overall rotation**.

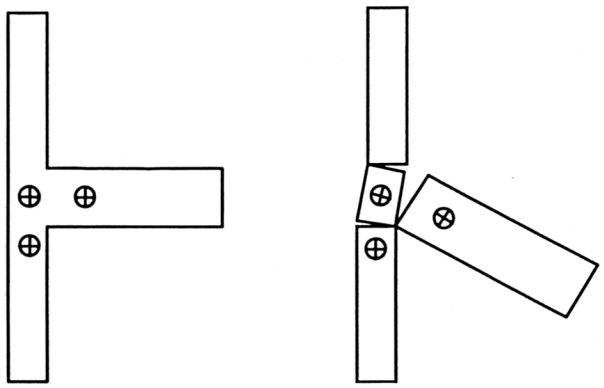

Figure 7.3.1.1 Rotation considerations

A tilt meter was mounted on the beam of four monotonic specimens to establish the relationship between rotation and failure load. Figure 7.3.1.2 shows this load-rotation response.

Figure 7.2.1.2 shows that for a typical monotonic specimen the *overall* rotation which corresponded to the yield load was around 1.4°. For each of these tests the beam tilt meter was positioned at the mid-height of the beam 150 mm from the column face.

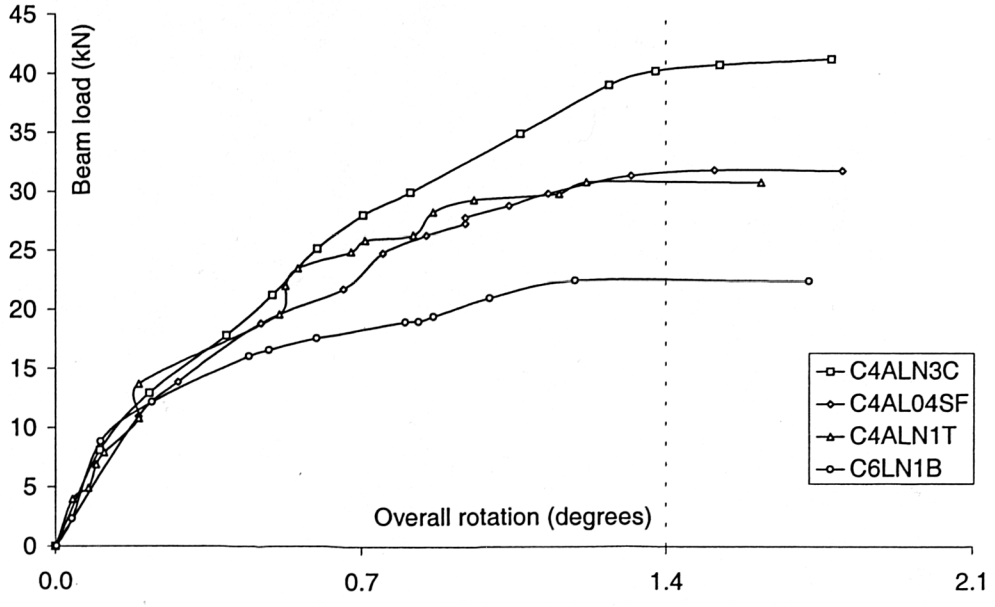

Figure 7.3.1.2 Load-rotation response

During the preliminary cyclic test, three tilt meters were positioned on the beam at distances 100, 200 and 300 mm from the column face. Figure 7.2.1.3 shows the rotation response from these tilt meters.

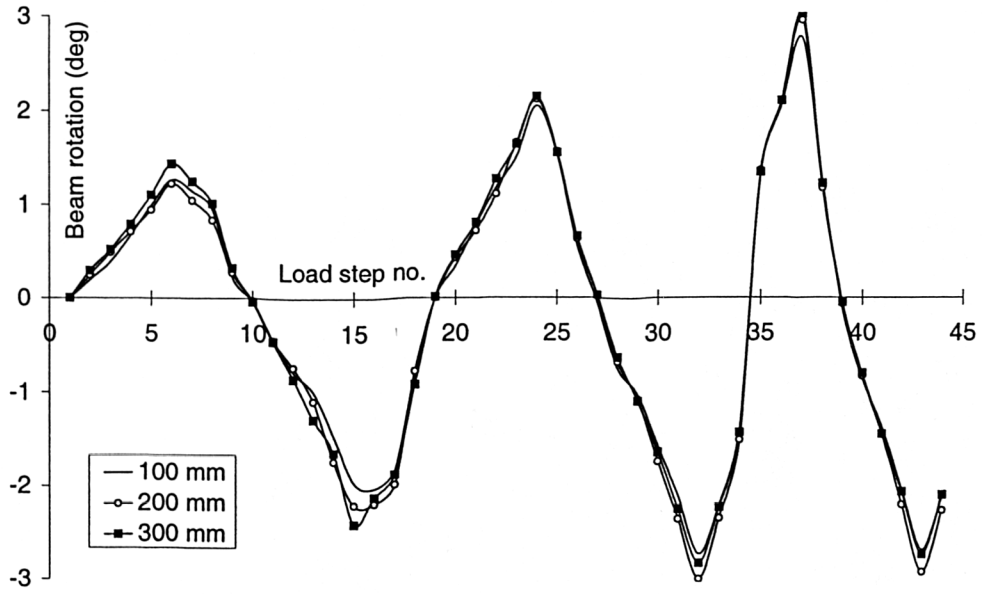

Figure 7.3.1.3 Beam rotation at three locations

Figure 7.3.1.3 shows that the rotation values were very similar over the first 300 mm of the beam length. As a result, a distance of 150 mm was selected for the beam tilt meter position. In previous monotonic tests, flexural cracking of the beam had been initiated at the location of the beam stirrups. A distance of 150 mm was exactly between the stirrup positions of 100 and 200 mm.

At this location a ductility factor of 1.0 was equivalent to an *overall* rotation of 1.4°.

In addition to the three tilt meters, five electronic displacement transducers were purchased. The location of this instrumentation is shown in Figure 7.3.1.4.

7.3.2 Loading technique

The loading technique used was based on that by Durrani *et al* [59, 60, 61] as outlined previously in Section 7.1. The first stage of this loading procedure was to load the column, in 25 kN steps, to 50 kN for normal strength specimens and 100 kN for high strength specimens. This column load was then maintained throughout the test while the beam was loaded incrementally at a point 750 mm from the column face.

The first cycle was to load the beam downwards and then upwards until joint cracking occurred in both directions. Figure 7.3.2.1(a) displays an example load rotation response corresponding to this first load cycle. The sign convention used was *positive* for downward loading and the corresponding beam rotation.

The loading then continued to increasing ductility factors in increments of 0.5. Figure 7.3.2.1(b) shows a typical load-rotation response at a ductility factor of 1.0. Figure 7.3.2.1(c) shows a typical response by the end of a test. Figure 7.3.2.1(d) displays a simplified version of the load history showing only the peak loads from each of the cycles.

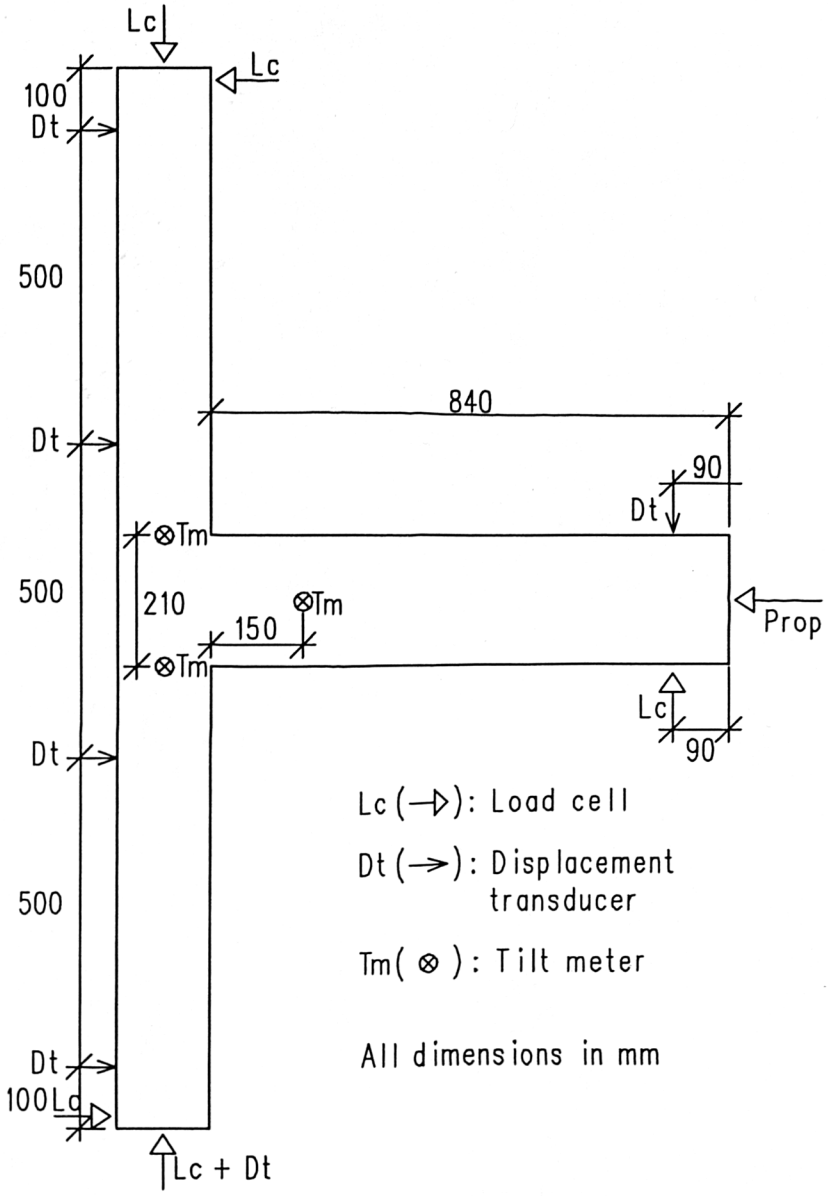

Figure 7.3.1.4 Instrumentation layout for the cyclic specimens

The energy absorption capacity for each cycle may be deduced from the area beneath the load-rotation curves. The example response shown in Figure 7.3.2.1(c) shows relatively sharp, thin curves. This would represent a poor energy absorption capacity. The cyclic strength of a specimen is dependent on the failure mode. The strength of a joint shear failure rapidly deteriorates with each cycle. The strength of a flexural beam failure remains reasonably constant through the load cycling due to the ductility of the plastic hinge.

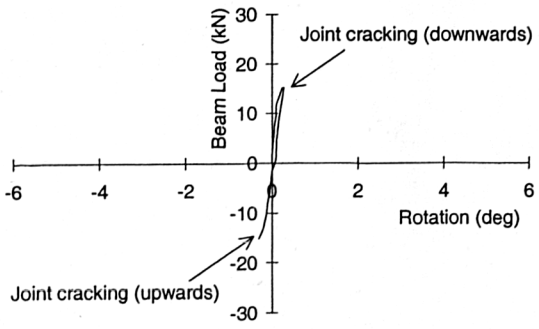

Figure 7.3.2.1(a) Joint cracking

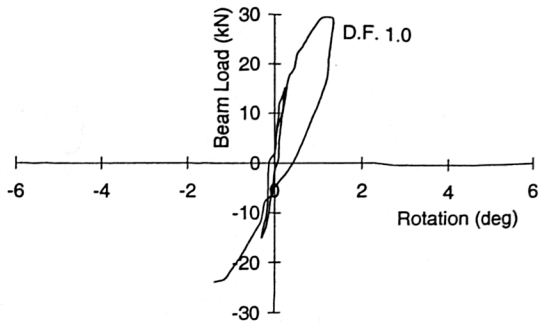

Figure 7.3.2.1(b) Ductility factor 1.0

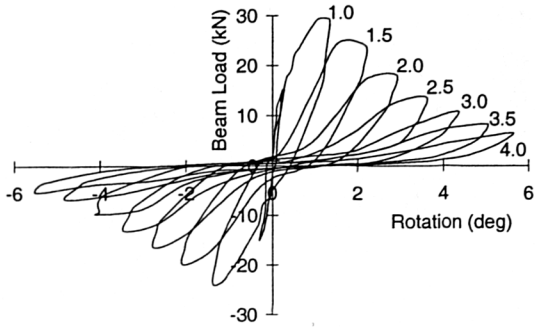

Figure 7.3.2.1(c) Full load history

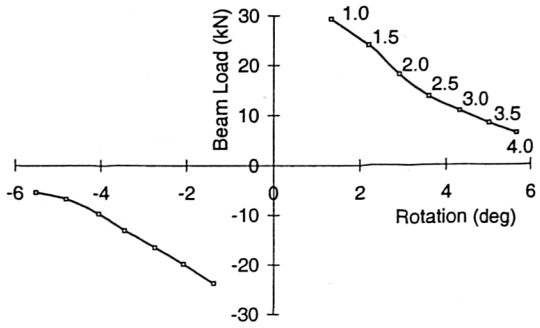

Figure 7.3.2.1(d) Peak load history

An example load-rotation response from a specimen with a good energy absorption capacity is shown in Figure 7.3.2.2(a). The curves are relatively wide and are less sharp in comparison to the previous example. The peak loads also remain high throughout the testing. This example is typical of a specimen which has its cycles controlled by the flexural strength of the beam. Figure 7.3.2.2(b) shows a simplified version of the load history displaying only the peak loads from each of the cycles.

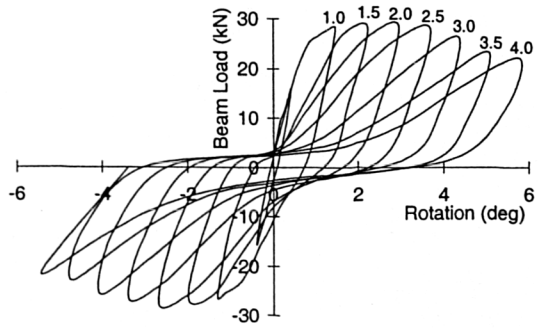

Figure 7.3.2.2(a) Full load history

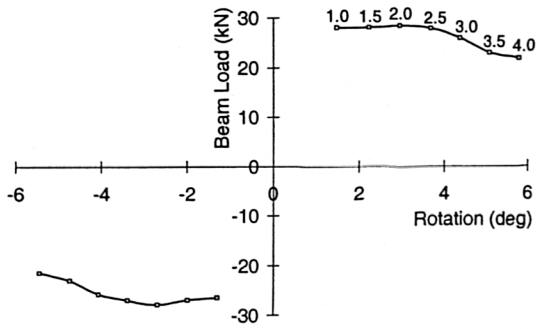

Figure 7.3.2.2(b) Peak load history

7.3.3 Cyclic performance definitions

Within this investigation approximate definitions were used to judge a specimen's cyclic performance. This was necessary as there has not been a universally accepted method for cyclically testing reinforced concrete members. Figure 7.3.3.1 displays these cyclic performance definitions.

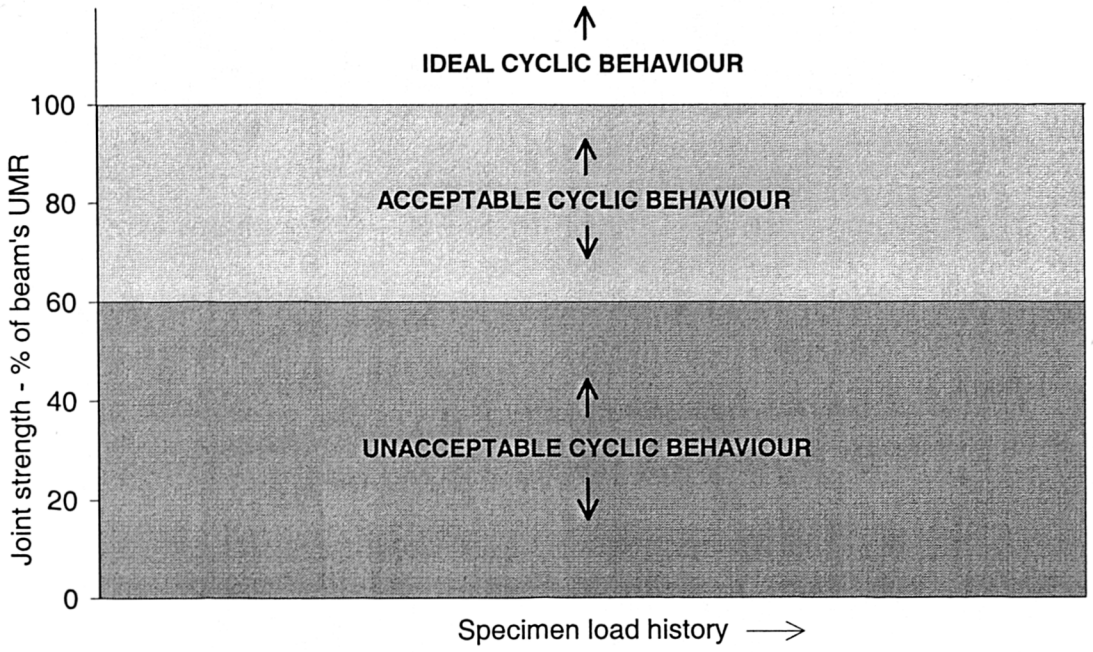

Figure 7.3.3.1 Cyclic performance definitions

Figure 7.3.3.1 shows that over a specimen's load history its joint capacity should **ideally** remain higher than that equivalent to its beam's ultimate moment of resistance. Under large cyclic displacements it would be **acceptable** for the joint capacity to remain above that equivalent to 60% of its beam's ultimate moment of resistance. However, if the capacity dropped below this 60% value then the behaviour would be classed as **unacceptable**.

This is the definition of cyclic performance used within this investigation. The two example specimen responses from the previous section are displayed in Figures 7.3.3.2 and 7.3.3.3 (both specimens are assumed to have flexural strengths equivalent

to a beam load of 30 kN. The equivalent 60% strength lines are marked on both figures).

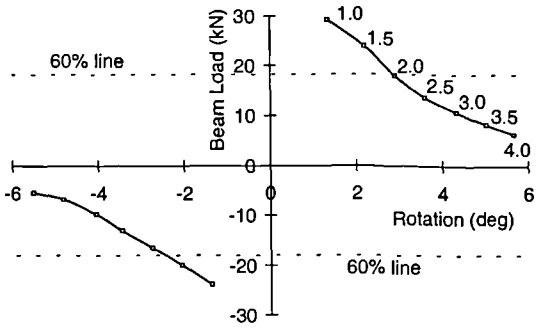

Figure 7.3.3.2 Peak load history (specimen 1 - unacceptable)

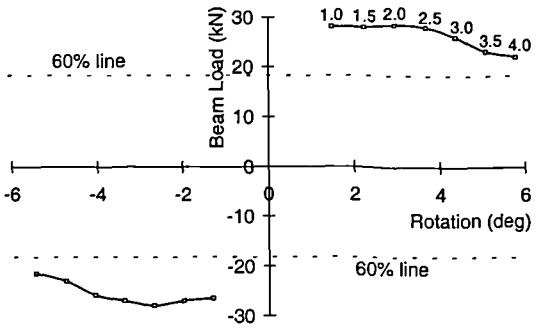

Figure 7.3.3.3 Peak load history (specimen 2 - acceptable)

Figure 7.3.3.2 shows that specimen 1 has an acceptable cyclic behaviour up to a ductility factor of 2.0. After this point in its load history the joint capacity falls below the 60% value and the behaviour is then classed as unacceptable.

Figure 7.3.3.3 has acceptable specimen behaviour throughout its load history. Even at a ductility factor of 4.0 the joint capacity is still higher than the 60% value.

8. Cyclic Results and Discussion (Overview)

The Cyclic Results and Discussion section of this thesis is split into two chapters; **Chapter 8** provides an overview of the results from the entire cyclic test programme, **Chapter 9** is a discussion of the results, in detail, from the individual test series within the cyclic programme.

Within the Cyclic Results and Discussion section of this thesis, the test programme is divided into the following five test series :

1. Standard specimens (cyclic)
2. High strength specimens (cyclic)
3. Specimens investigating shear plates
4. Specimens investigating 2T12 beam steel
5. Additional specimens

Tables 8.1 to 8.5 display the test results from these specimens. The concrete compressive strengths, obtained from the average of three cube tests, and indirect tensile strengths, obtained from an average of three cylinder splitting (Brazilian) tests are displayed. The peak beam loads corresponding to each load cycle are displayed. Although the loads are shown to one decimal place, the author suggests that they should be taken as no more accurate than to the nearest kN. The failure mode for each cycle was joint failure unless otherwise indicated. A letter *B* indicates flexural failure of the beam.

The loads are shown as *actual* loads in kN and **were not converted into a normalised shear stress**. This was because desirable cyclic behaviour is governed by flexural effects and not shear.

Table 8.1 Standard specimens (cyclic) results

Specimen	D.F.	Load (kN)↓	Load (kN)↑	Specimen	D.F.	Load (kN)↓	Load (kN)↑
C4ALN1CY	1.0	38.9	14.8	**C6LN1CY**	1.0	29.3	23.8
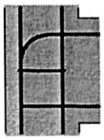	1.5	30.7	8.4	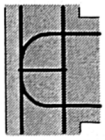	1.5	23.9	19.9
	2.0	17.0	5.4		2.0	18.1	16.5
	2.5	14.1	2.1		2.5	13.7	13.1
J.C. = 17.6 kN	3.0	10.8	3.5	**J.C. = 15.2 kN**	3.0	10.8	7.3
f_{cu} = 55 MPa	3.5	7.3	3.0	**f_{cu} = 56 MPa**	3.5	8.3	6.8
f_t = 3.0 MPa	4.0	5.8	2.5	**f_t = 3.0 MPa**	4.0	6.4	5.4
C4ALN3CY	1.0	37.3	16.2	**C6LN3CY**	1.0	30.0	25.9
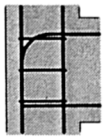	1.5	32.4	10.9	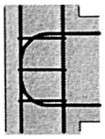	1.5	28.0	25.0
	2.0	22.4	5.4		2.0	23.1	19.5
	2.5	17.8	3.0		2.5	18.2	15.7
J.C. = 16.8 kN	3.0	14.3	2.5	**J.C. = 16.7 kN**	3.0	14.2	12.2
f_{cu} = 55 MPa	3.5	11.4	2.5	**f_{cu} = 52 MPa**	3.5	11.3	9.4
f_t = 3.3 MPa	4.0	7.4	-	**f_t = 3.3 MPa**	4.0	7.8	6.9
C4ALN5CY	1.0	$42.5_{(B)}$	17.1	**C6LN5CY**	1.0	35.1	27.8
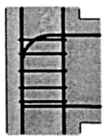	1.5	$42.0_{(B)}$	7.8	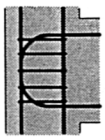	1.5	30.2	25.8
	2.0	36.1	3.5		2.0	24.4	22.4
	2.5	29.8	2.5		2.5	19.5	18.0
J.C. = 19.6 kN	3.0	23.9	1.5	**J.C. = 16.5 kN**	3.0	15.6	15.6
f_{cu} = 60 MPa	3.5	20.0	2.5	**f_{cu} = 56 MPa**	3.5	13.2	13.2
f_t = 3.0 MPa	4.0	17.1	1.0	**f_t = 2.5 MPa**	4.0	9.8	11.2
C4ALN7CY	1.0	$44.5_{(B)}$	18.9	**C6LN7CY**	1.0	39.5	36.1
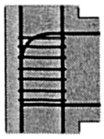	1.5	$45.0_{(B)}$	11.1	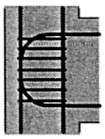	1.5	35.6	32.7
	2.0	$39.7_{(B)}$	4.2		2.0	28.3	26.4
	2.5	30.9	3.3		2.5	21.9	20.1
J.C. = 19.2 kN	3.0	24.0	2.8	**J.C. = 18.8 kN**	3.0	18.6	16.1
f_{cu} = 63 MPa	3.5	21.6	2.8	**f_{cu} = 59 MPa**	3.5	15.1	14.1
f_t = 3.5 MPa	4.0	17.7	3.4	**f_t = 3.3 MPa**	4.0	12.2	11.3

Table 8.2 High strength specimens (cyclic) results

Specimen	D.F.	Load (kN)↓	Load (kN)↑	Specimen	D.F.	Load (kN)↓	Load (kN)↑
C4ALH1CY	1.0	43.2$_{(B)}$	25.5	**C6LH1CY**	1.0	46.5$_{(B)}$	36.1
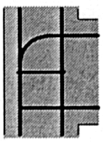	1.5	41.5$_{(B)}$	14.7	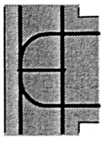	1.5	42.1$_{(B)}$	35.1
	2.0	29.7	4.0		2.0	31.3	27.8
	2.5	21.7	2.5		2.5	18.0	21.5
J.C. = 24.7 kN	3.0	16.3	2.5	**J.C. = 25.5 kN**	3.0	12.5	18.2
f_{cu} = 126 MPa	3.5	11.8	1.5	**f_{cu} = 117 MPa**	3.5	9.3	14.8
f_t = 4.1 MPa	4.0	7.4	3.0	**f_t = 5.1 MPa**	4.0	6.6	12.0
C4ALH3CY	1.0	46.4$_{(B)}$	23.0	**C6LH3CY**	1.0	43.0$_{(B)}$	37.1
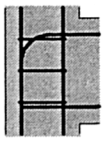	1.5	46.4$_{(B)}$	19.5	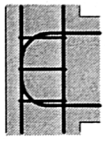	1.5	40.6$_{(B)}$	35.6
	2.0	44.4$_{(B)}$	4.4		2.0	34.7	28.3
	2.5	34.6	3.0		2.5	22.5	21.5
J.C. = 26.2 kN	3.0	29.6	2.5	**J.C. = 29.8 kN**	3.0	13.2	15.1
f_{cu} = 116 MPa	3.5	20.1	2.5	**f_{cu} = 119 MPa**	3.5	8.3	12.7
f_t = 5.4 MPa	4.0	14.2	2.5	**f_t = 5.1 MPa**	4.0	5.4	9.8
C4ALH5CY	1.0	47.9$_{(B)}$	23.5$_{(B)}$	**C6LH5CY**	1.0	45.5$_{(B)}$	39.5$_{(B)}$
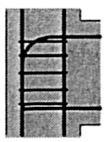	1.5	44.9$_{(B)}$	25.0$_{(B)}$	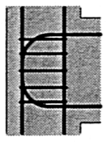	1.5	41.1$_{(B)}$	38.0$_{(B)}$
	2.0	45.4$_{(B)}$	25.0$_{(B)}$		2.0	41.1$_{(B)}$	40.5$_{(B)}$
	2.5	42.0$_{(B)}$	24.5$_{(B)}$		2.5	40.6$_{(B)}$	42.0$_{(B)}$
J.C. = 31.6 kN	3.0	23.2	22.0	**J.C. = 31.7 kN**	3.0	37.2$_{(B)}$	24.9
f_{cu} = 128 MPa	3.5	20.7	18.1	**f_{cu} = 131 MPa**	3.5	22.0	12.7
f_t = 5.0 MPa	4.0	12.8	19.6	**f_t = 5.5 MPa**	4.0	-	-
C4ALH7CY	1.0	44.4$_{(B)}$	25.5$_{(B)}$	**C6LH7CY**	1.0	50$_{(B)}$	41$_{(B)}$
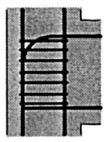	1.5	42.5$_{(B)}$	25.5$_{(B)}$	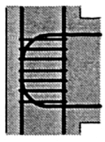	1.5	45$_{(B)}$	41$_{(B)}$
	2.0	43.5$_{(B)}$	25.3$_{(B)}$		2.0	44$_{(B)}$	40$_{(B)}$
	2.5	38.5$_{(B)}$	25.5$_{(B)}$		2.5	43$_{(B)}$	39$_{(B)}$
J.C. = 30.1 kN	3.0	26.7	24.5$_{(B)}$	**J.C. = -**	3.0	40$_{(B)}$	37$_{(B)}$
f_{cu} = 114 MPa	3.5	26.2	22.5	**f_{cu} = 127 MPa**	3.5	26	17
f_t = 4.6 MPa	4.0	18.2	22.5	**f_t = 4.9 MPa**	4.0	11	12

Table 8.3 Specimens investigating shear plates - results

Specimen	D.F.	Load (kN)↓	Load (kN)↑	Specimen	D.F.	Load (kN)↓	Load (kN)↑
C6LNP4	1.0	38.2	33.5	**C6PLNP4**	1.0	47.8	45.3
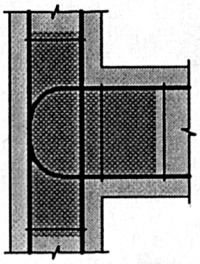	1.5	33.4	32.0	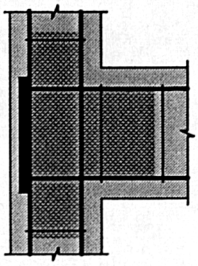	1.5	46.4	45.3
	2.0	28.0	27.0		2.0	43.4	40.5
	2.5	23.4	23.2		2.5	36.1	32.2
	3.0	17.3	17.9		3.0	26.4	21.0
	3.5	13.4	13.0		3.5	15.2	12.7
J.C. = 19.8 kN	4.0	10.5	10.0	**J.C. = 17.6 kN**	4.0	10.3	9.3
f_{cu} = 58 MPa				**f_{cu} = 51 MPa**			
f_t = 3.0 MPa				**f_t = 3.2 MPa**			

Table 8.4 Specimens investigating 2T12 beam steel - results

Specimen	D.F.	Load (kN)↓	Load (kN)↑	Specimen	D.F.	Load (kN)↓	Load (kN)↑
C3LN7CY	1.0	$28.1_{(B)}$	$26.5_{(B)}$	**C3XLN7CY**	1.0	$29.6_{(B)}$	$28.3_{(B)}$
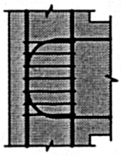	1.5	$28.1_{(B)}$	$26.9_{(B)}$	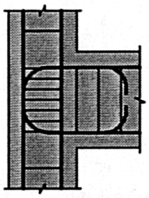	1.5	$30.0_{(B)}$	$28.8_{(B)}$
	2.0	$28.6_{(B)}$	$27.9_{(B)}$		2.0	$30.0_{(B)}$	$28.4_{(B)}$
	2.5	$28.0_{(B)}$	$27.0_{(B)}$		2.5	$28.5_{(B)}$	$26.9_{(B)}$
J.C. = 15.8 kN	3.0	$26.1_{(B)}$	$25.7_{(B)}$	**J.C. = 17.2 kN**	3.0	$27.1_{(B)}$	$25.9_{(B)}$
f_{cu} = 54 MPa	3.5	$23.2_{(B)}$	$23.0_{(B)}$	**f_{cu} = 55 MPa**	3.5	$25.6_{(B)}$	$26.5_{(B)}$
f_t = 3.3 MPa	4.0	$22.1_{(B)}$	$21.5_{(B)}$	**f_t = 3.0 MPa**	4.0	19.7	$23.9_{(B)}$
C3HLN7CY	1.0	$24.9_{(B)}$	$24.6_{(B)}$				
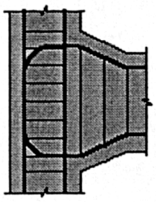	1.5	$24.4_{(B)}$	$26.2_{(B)}$				
	2.0	$25.9_{(B)}$	$27.1_{(B)}$				
	2.5	$27.0_{(B)}$	$29.0_{(B)}$				
	3.0	$28.0_{(B)}$	$29.5_{(B)}$				
J.C. = -	3.5	$27.6_{(B)}$	$30.9_{(B)}$				
f_{cu} = 61 MPa	4.0	$27.6_{(B)}$	$31.8_{(B)}$				
f_t = 3.4 MPa							

Table 8.5 Additional specimen results

Specimen	D.F.	Load (kN)↓	Load (kN)↑
C6LN3CYE	1.0	32.9	26.3
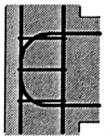	1.5	30.4	25.8
	2.0	25.6	21.4
	2.5	21.6	16.5
J.C. = 15.3 kN	3.0	16.7	13.6
f_{cu} = 55 MPa	3.5	13.3	11.6
f_t = 3.0 MPa	4.0	10.4	9.7

Notes (for Tables 8.1 to 8.5)

1. J.C. - is the abbreviation for the joint cracking load,
2. D.F. - is the abbreviation for the ductility factor,
3. The data logger crashed towards the end of testing for specimen C6LH7CY. As a result, only the peak loads, recorded by hand, were available from this test. However, the author is still confident that these results are accurate to the nearest kN.

9. Cyclic Results and Discussion (Detailed)

As outlined previously in Tables 9.1 to 9.5, the cyclic test programme was divided into five test series. The results from these test series are reviewed in detail within this chapter.

Each test series is considered in the following categories :

1. **Specimen behaviour** - General comments are made regarding specimen performance. For certain tests a selection of photographs is presented to demonstrate their behaviour.
2. **Load-rotation response** - Both the cyclic behaviour and the strength decay rates of the specimens are considered. All load-rotation plots consider the *overall rotation* as defined previously in Section 7.3.1.
3. **Strain distributions** - A number of specimens contained internally strain gauged reinforcement allowing both strain distributions and bond stresses to be analysed.

9.1 Standard Cyclic Specimens

This section considers the results from the eight standard cyclic specimens. The parameters investigated were the **number of ties present within the joint** and the **beam tension steel anchorage detail**. The specimen details are given in Table 9.1.

9.1.1 Specimen behaviour

Photographs within this section are of the specimens at ductility factors of 1.0 and 2.0 in the downwards direction and 3.0 in both directions. The specimens with one and seven joint ties are considered as these are the specimens with the least and most joint reinforcement respectively.

Table 9.1 ***Standard cyclic specimens*** **- details**

Specimen	Gauging	Beam steel anchorage	No. of joint ties
C4ALN1CY	-	Bent down	1
C4ALN3CY	*Full*	Bent down	3
C4ALN5CY	-	Bent down	5
C4ALN7CY	-	Bent down	7
C6LN1CY	-	U-bar	1
C6LN3CY	*Full*	U-bar	3
C6LN5CY	-	U-bar	5
C6LN7CY	-	U-bar	7

Note

1. *Full* gauging of a cyclic specimen was defined as the gauging of the main beam steel and joint ties.

C4ALN1CY

Figure 9.1.1.1(a) shows a photograph of specimen C4ALN1CY at a ductility factor of 1.0. The ultimate joint capacity of the specimen corresponded to an applied beam load of 39 kN. Two clear diagonal cracks were visible within the joint zone.

Figure 9.1.1.1(b) shows a photograph of specimen C4ALN1CY at a ductility factor of 2.0. The joint capacity had reduced by more than 50% and signs of extensive deterioration were now apparent. In addition to the diagonal cracking in both directions, a large crack believed to be due to slippage effects was evident. This is indicated on Figure 9.1.1.1(b).

Figure 9.1.1.1(c) shows a photograph of specimen C4ALN1CY at a ductility factor of 3.0. The joint strength at this stage of the test was less than 30% of its original capacity. A section of concrete in the lower joint had broken free due to the lack of anchorage of the straight 12 mm beam bar.

Figure 9.1.1.1(d) shows a photograph of specimen C4ALN1CY at a ductility factor of 3.0 loaded in the upwards direction. The cracking was similar to that previously visible in Figure 9.1.1.1(c). The beam load required for this ductility factor was only 4 kN as the straight lower beam rebar had lost nearly all of its effective anchorage.

C4ALN7CY

Figure 9.1.1.2(a) shows a photograph of specimen C4ALN7CY at a ductility factor of 1.0. This specimen failed in beam flexure and thus did not achieve its ultimate joint capacity. Only slight cracking of the joint zone was visible, the seven joint ties had contained the width of the cracks. The beam's ultimate moment of resistance corresponded to an applied beam load of 45 kN.

Figure 9.1.1.2(b) shows a photograph of specimen C4ALN7CY at a ductility factor of 2.0. Although the joint cracks were more prominent at this stage of the test the strength was still controlled by the yielding of the beam steel. The main flexural crack within the beam's plastic hinge region is indicated on Figure 9.1.1.2(b). The deterioration of the compression zone of the beam was apparent and this resulted in a shorter beam lever arm and thus a lower flexural strength.

Figure 9.1.1.2(c) shows a photograph of specimen C4ALN7CY at a ductility factor of 3.0. At this stage of the test the diagonal cracking of the joint zone was quite extensive. A large volume of concrete had also broken away from the compression zone of the beam. It was not clear if it was joint or beam effects which were influencing the ultimate strength of the specimen. The strength was slightly higher than 50% of the beam's ultimate moment of resistance.

Figure 9.1.1.2(d) shows a photograph of specimen C4ALN7CY at a ductility factor of 3.0 loaded in the upwards direction. The cracking pattern was similar to that seen previously in Figure 9.1.1.2(c). The beam load required for this ductility factor was only 3 kN as the straight lower beam rebar had lost nearly all of its effective anchorage.

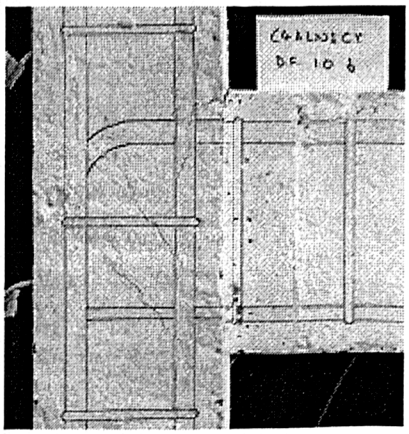

Figure 9.1.1.1(a) D.F. 1.0 ↓ (39 kN)

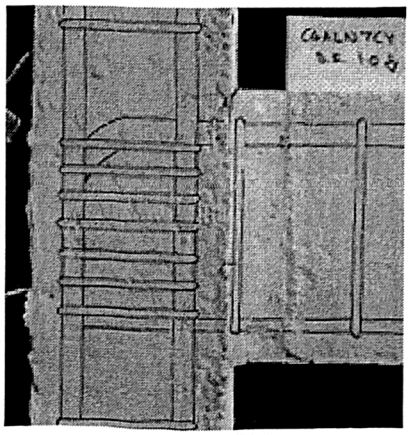

Figure 9.1.1.2(a) D.F. 1.0 ↓ (45 kN)

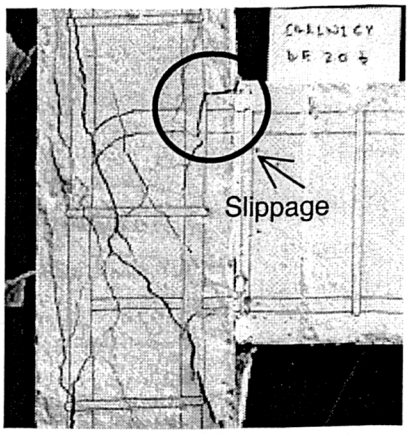

Figure 9.1.1.1(b) D.F. 2.0 ↓ (17 kN)

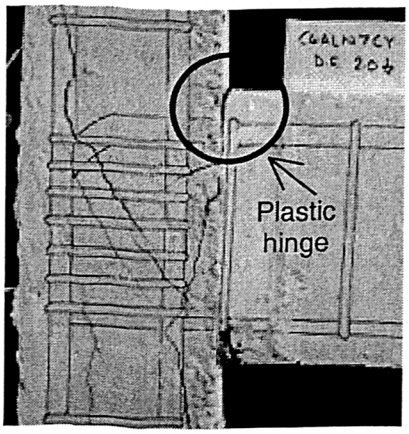

Figure 9.1.1.2(b) D.F. 2.0 ↓ (40 kN)

Figure 9.1.1.1(c) D.F. 3.0 ↓ (11 kN)

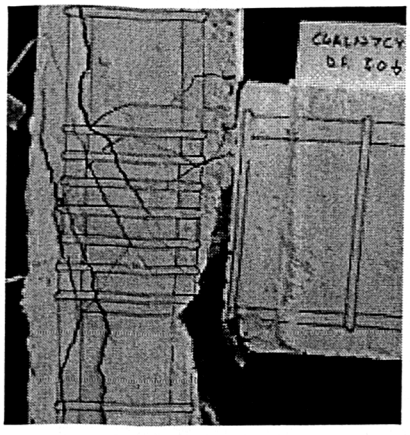

Figure 9.1.1.2(c) D.F. 3.0 ↓ (24 kN)

Figures 9.1.1.1(a-c) - C4ALN1CY and Figures 9.1.1.2(a-c) - C4ALN7CY

Figure 9.1.1.1(d) D.F. 3.0 ↑ (4 kN)

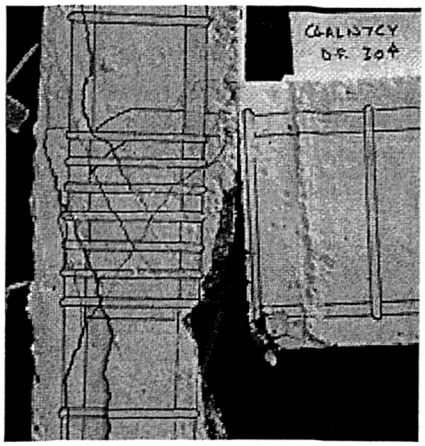

Figure 9.1.1.2(d) D.F. 3.0 ↑ (3 kN)

Figures 9.1.1.1(d) - C4ALN1CY and Figures 9.1.1.2(d) - C4ALN7CY

C6LN1CY

Figure 9.1.1.3(a) shows a photograph of specimen C6LN1CY at a ductility factor of 1.0. The ultimate joint capacity of the specimen corresponded to an applied beam load of 29 kN. Diagonal cracking typical of a joint failure was clearly visible. A horizontal crack level with the beam tension steel height was evidence of bond failure of the straight section of the beam steel within the joint.

Figure 9.1.1.3(b) shows a photograph of specimen C6LN1CY at a ductility factor of 2.0. Extensive cracking of the joint was apparent across both diagonals. As the initial failure capacity was well below the beam's ultimate moment of resistance there was no significant flexural cracking of the beam.

Figure 9.1.1.3(c) shows a photograph of specimen C6LN1CY at a ductility factor of 3.0. At this stage of the loading almost all of the joint's concrete cover had broken off leaving the steel within the joint core clearly visible. The strength of the joint was comparable to specimen C4ALN1CY at the same ductility factor.

Figure 9.1.1.3(d) shows a photograph of specimen C6LN1CY at a ductility factor of 3.0 loaded in the upwards direction. The cracking pattern was similar to that previously visible in Figure 9.1.1.3(c). At this stage of the test the joint capacity had been greatly reduced and the U-bar was rotating within the joint causing little further damage. By this stage of the test this joint capacity had reduced to a value corresponding to an applied beam load of 7 kN.

C6LN7CY

Figure 9.1.1.4(a) shows a photograph of specimen C6LN7CY at a ductility factor of 1.0 (specimen failure). Although the joint was reinforced with seven ties, the beam's ultimate moment of resistance was still not reached. The ultimate capacity of the joint corresponded to an applied beam load of 40 kN.

Figure 9.1.1.4(b) shows a photograph of specimen C6LN7CY at a ductility factor of 2.0. More cracking was visible within the joint and the cracking previously visible in Figure 9.1.1.4(a) had worsened. By this stage of the test this joint capacity had reduced to a value corresponding to an applied beam load of 28 kN.

Figure 9.1.1.4(c) shows a photograph of specimen C6LN7CY at a ductility factor of 3.0. As with specimen C6LN1CY the joint's concrete cover had broken off by this stage leaving the steel within the joint core clearly visible. By this stage of the test the joint's strength was less than 50% of its original capacity.

Figure 9.1.1.4(d) shows a photograph of specimen C6LN7CY at a ductility factor of 3.0 loaded in the upwards direction. The cracking pattern was similar to that previously visible in Figure 9.1.1.4(c). By this stage of the test this joint capacity had reduced to a value corresponding to an applied beam load of 16 kN. More core concrete was present than with specimen C6LN1CY, shown in Figure 9.1.1.3(d), at the same stage of testing.

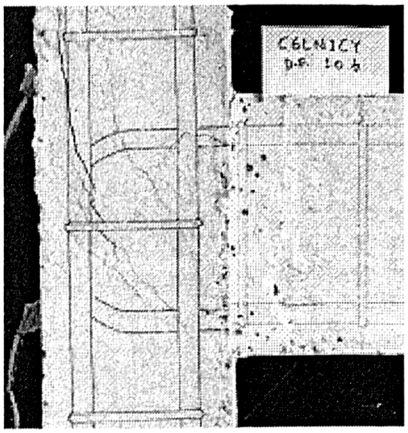

Figure 9.1.1.3(a) D.F. 1.0 ↓ (29 kN)

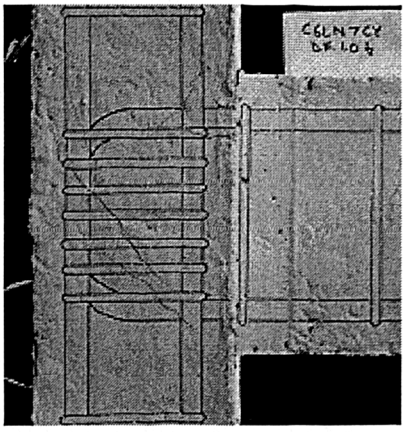

Figure 9.1.1.4(a) D.F. 1.0 ↓ (40 kN)

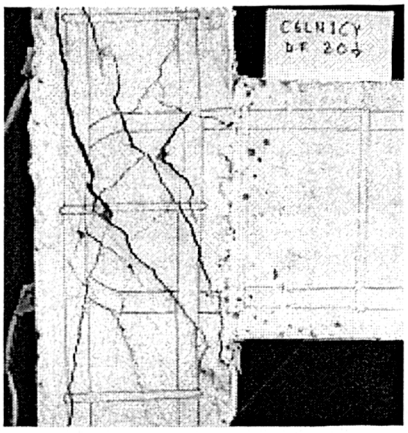

Figure 9.1.1.3(b) D.F. 2.0 ↓ (18 kN)

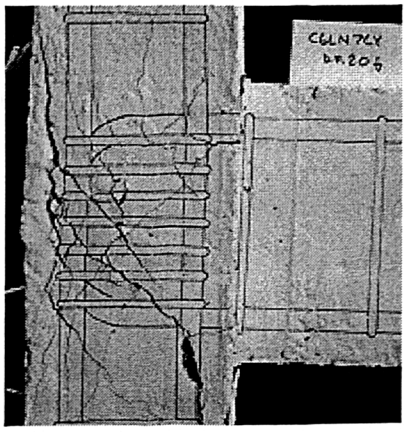

Figure 9.1.1.4(b) D.F. 2.0 ↓ (28 kN)

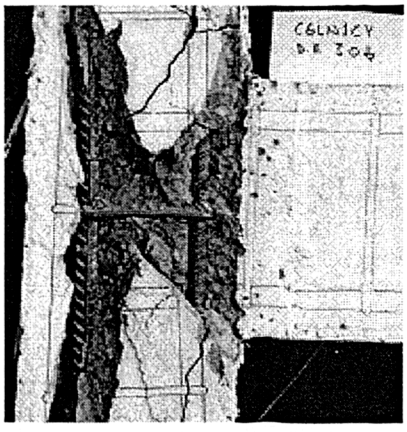

Figure 9.1.1.3(c) D.F. 3.0 ↓ (11 kN)

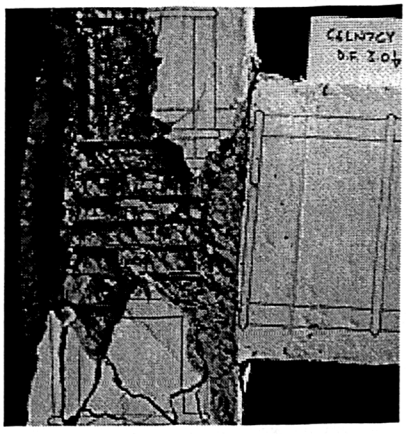

Figure 9.1.1.4(c) D.F. 3.0 ↓ (19 kN)

Figures 9.1.1.3(a-c) - C6LN1CY and Figures 9.1.1.4(a-c) - C6LN7CY

Figure 9.1.1.1(d) D.F. 3.0 ↑ (7 kN)

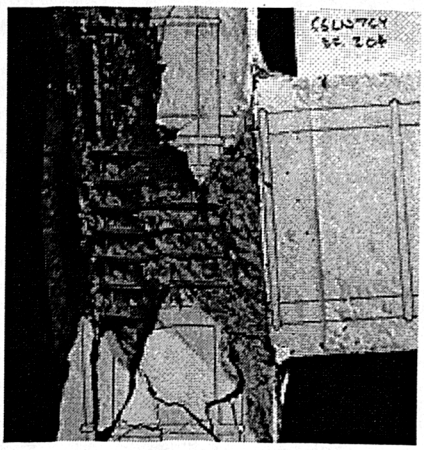

Figure 9.1.1.2(d) D.F. 3.0 ↑ (16 kN)

Figures 9.1.1.1(a-c) - C6LN1CY and Figures 9.1.1.2(a-c) - C6LN7CY

9.1.2 Load-rotation response

Figures 9.1.2.1(a)-(d) display the load-rotation response for the specimens with bent down beam steel detail. Figures 9.1.2.2(a)-(d) display the load-rotation response for the specimens with U-bar beam steel detail (the rotation considered is the overall specimen rotation as previously defined in Section 7.3.1).

The peak load history of the specimens, as previously defined in Figure 7.2.1.3(d), is indicated on all the figures. However, this was not included for the upward cycles for specimens with bent down steel. The 12 mm straight rebar within these beams had very poor anchorage characteristics and thus the strength in the upward direction was quickly lost.

The peak loads from each cycle are displayed in Figures 9.1.2.3(a) and 9.1.2.3(b) for specimens with bent down and U-bar beam steel respectively. The ultimate moment of resistance (U.M.R.) of the beam corresponded to an applied load of around 45 kN. This value and the value 60% of this are indicated on both charts, for the downward cycles, by dashed horizontal lines (a joint capacity less than this 60% value is defined as unacceptable within this investigation).

D.F.	↓ (kN)	↑ (kN)
1.0	39	15
1.5	31	8
2.0	17	5
2.5	14	2
3.0	11	3
3.5	7	3
4.0	6	2

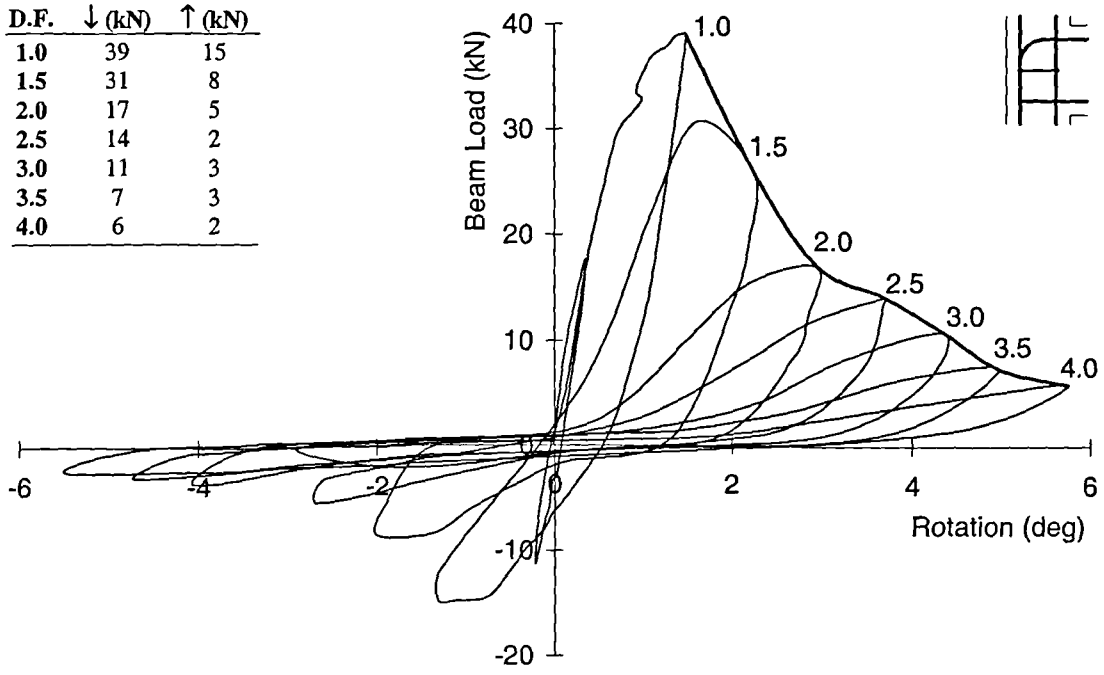

Figure 9.1.2.1(a) Load-rotation response - C4ALN1CY

D.F.	↓ (kN)	↑ (kN)
1.0	37	16
1.5	32	11
2.0	22	5
2.5	18	3
3.0	14	3
3.5	11	3
4.0	7	-

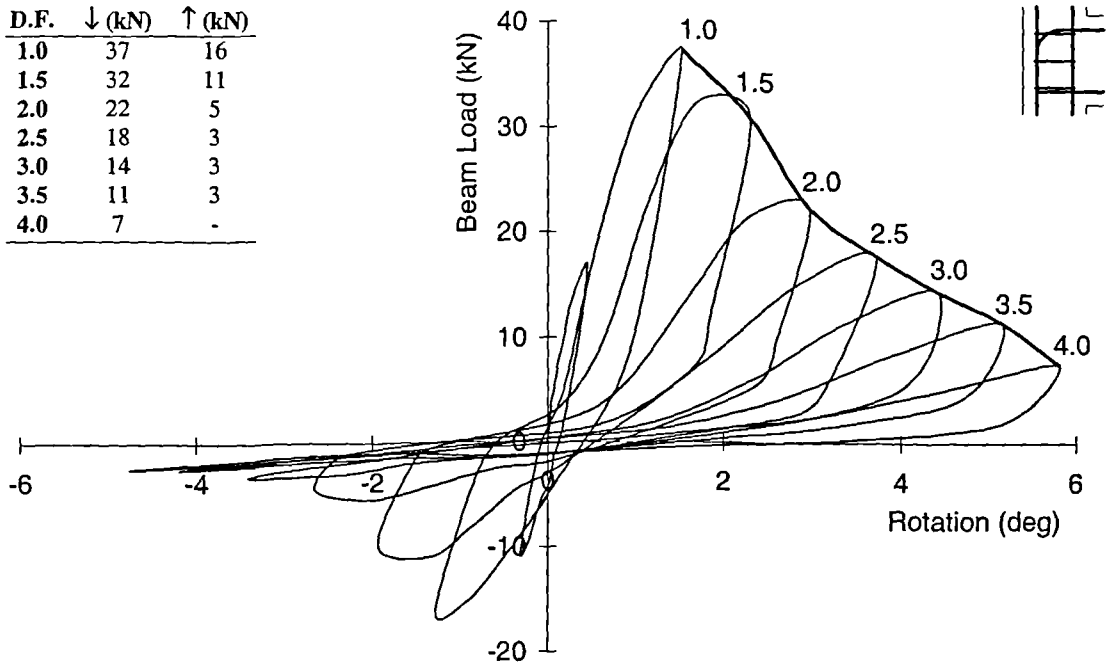

Figure 9.1.2.1(b) Load-rotation response - C4ALN3CY

D.F.	↓ (kN)	↑ (kN)
1.0	42	17
1.5	42	8
2.0	36	3
2.5	30	2
3.0	24	2
3.5	20	2
4.0	17	1

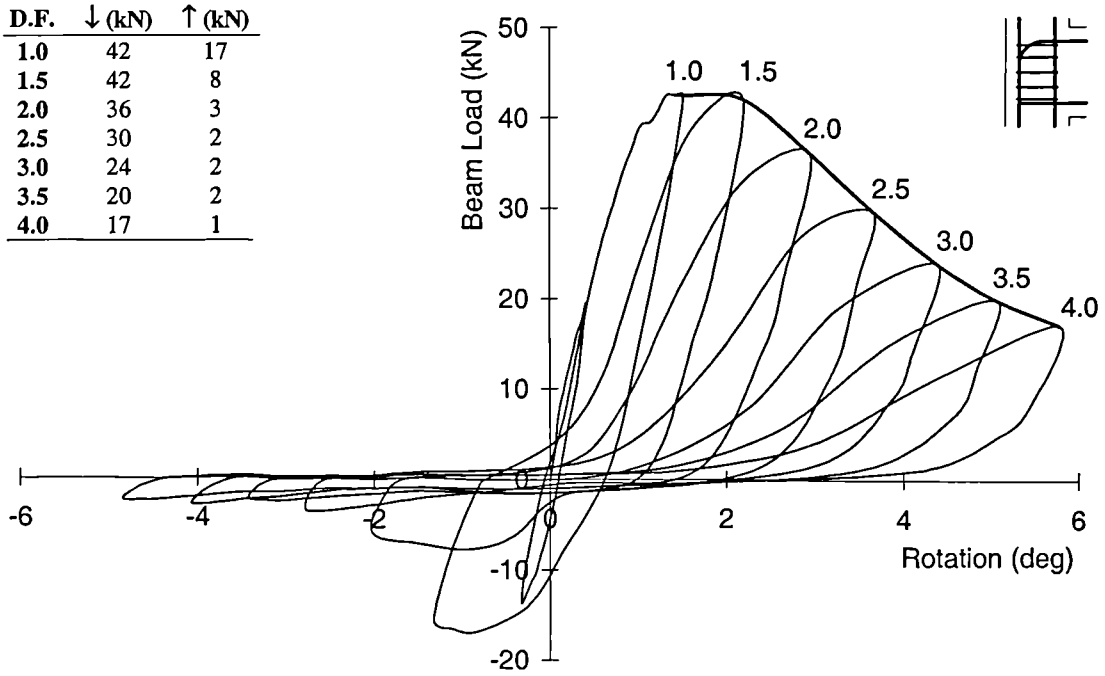

Figure 9.1.2.1(c) Load-rotation response - C4ALN5CY

D.F.	↓ (kN)	↑ (kN)
1.0	45	19
1.5	45	11
2.0	40	4
2.5	31	3
3.0	24	3
3.5	22	3
4.0	18	3

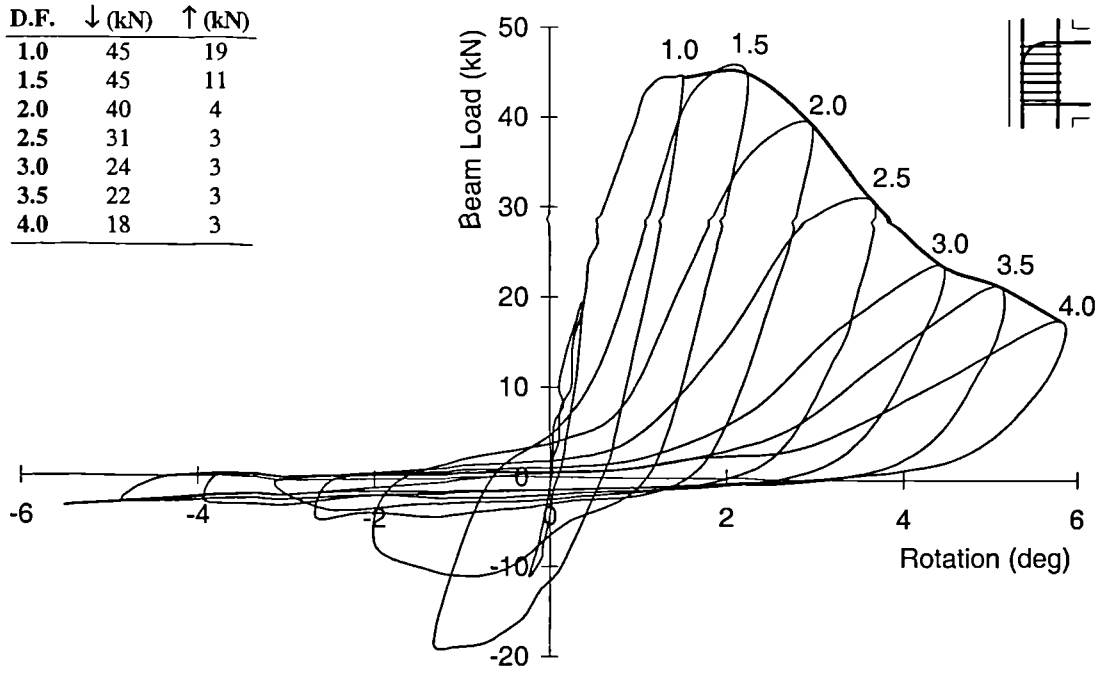

Figure 9.1.2.1(d) Load-rotation response - C4ALN7CY

D.F.	↓ (kN)	↑ (kN)
1.0	29	24
1.5	24	20
2.0	18	17
2.5	14	13
3.0	11	7
3.5	8	7
4.0	6	5

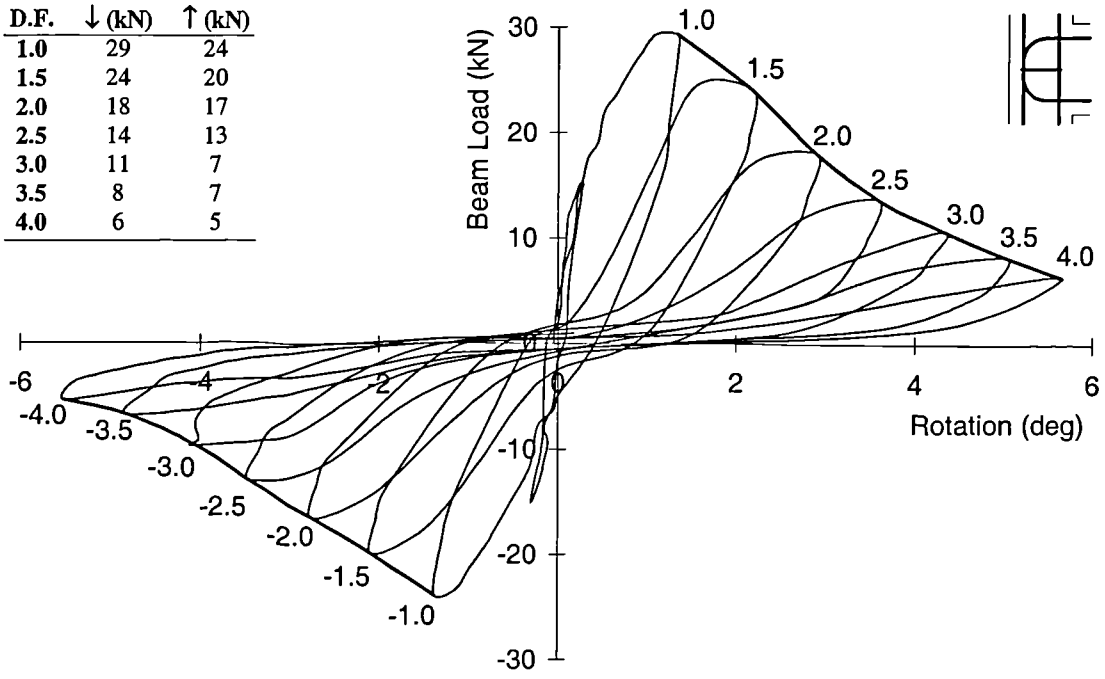

Figure 9.1.2.2(a) Load-rotation response - C6LN1CY

D.F.	↓ (kN)	↑ (kN)
1.0	30	26
1.5	28	25
2.0	23	20
2.5	18	16
3.0	14	12
3.5	11	9
4.0	8	7

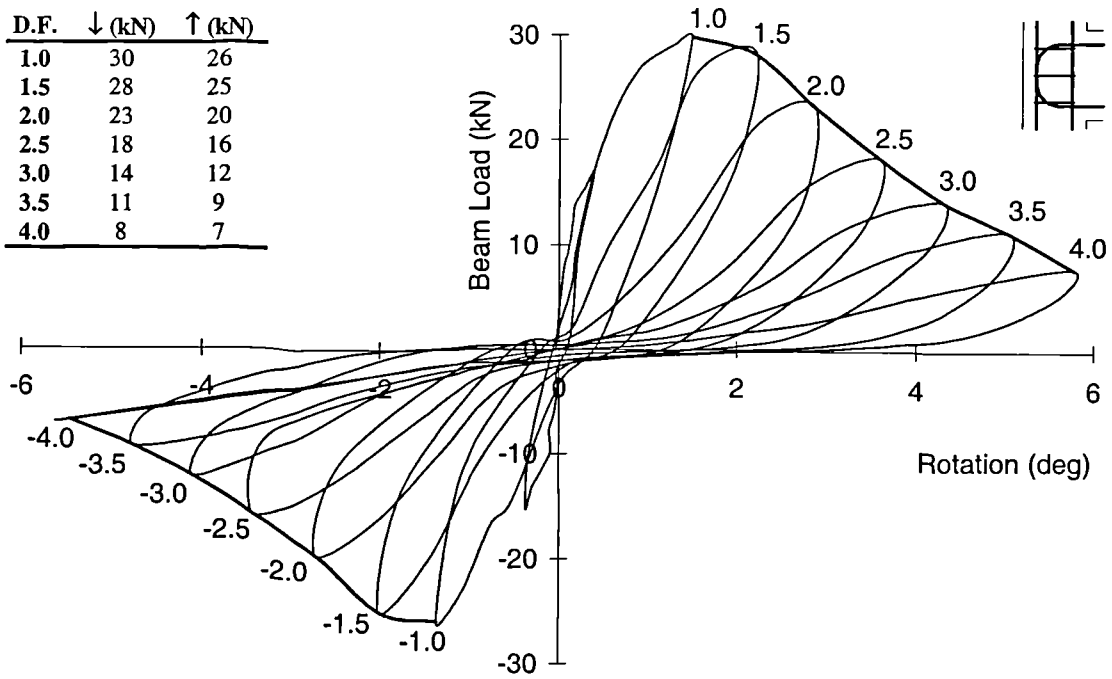

Figure 9.1.2.2(b) Load-rotation response - C6LN3CY

D.F.	↓ (kN)	↑ (kN)
1.0	35	28
1.5	30	26
2.0	24	22
2.5	20	18
3.0	16	16
3.5	13	13
4.0	10	11

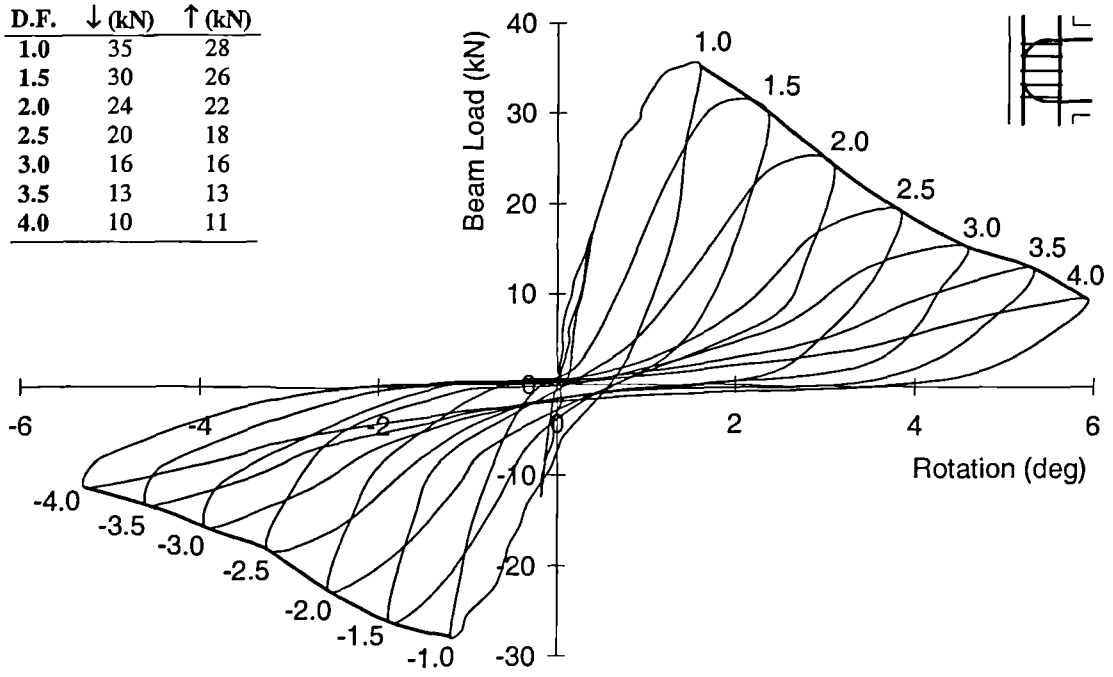

Figure 9.1.2.2(c) Load-rotation response - C6LN5CY

D.F.	↓ (kN)	↑ (kN)
1.0	40	36
1.5	36	33
2.0	28	26
2.5	22	20
3.0	19	16
3.5	15	14
4.0	12	11

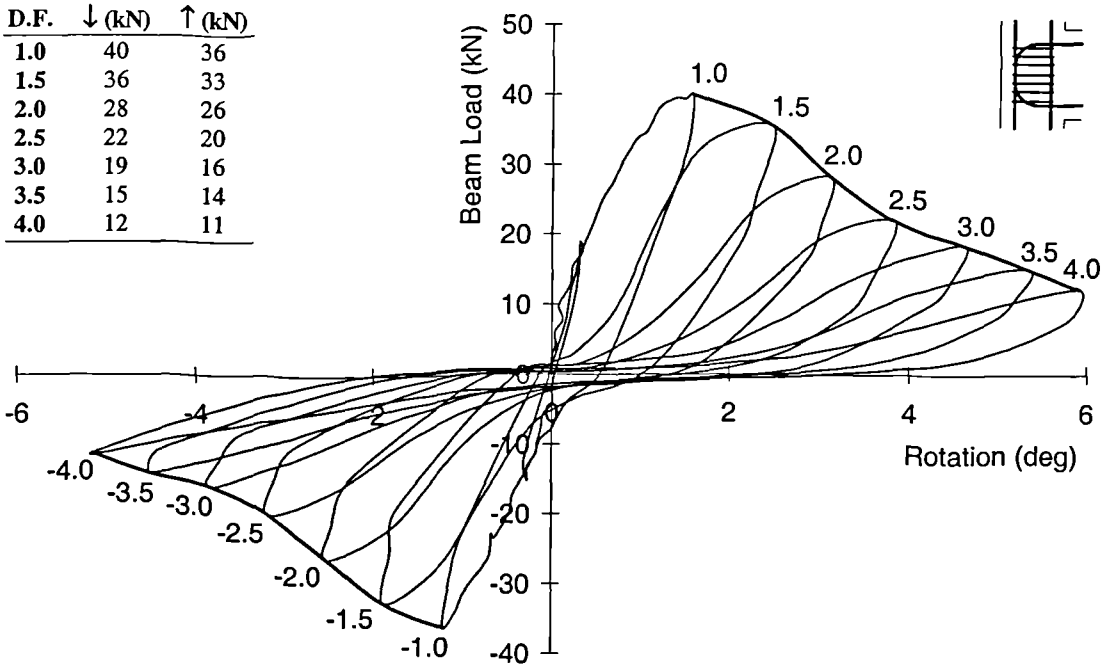

Figure 9.1.2.2(d) Load-rotation response - C6LN7CY

Specimens with bent down beam steel detail

Figure 9.1.2.3(a) shows that specimens C4ALN1CY and C4ALN3CY performed poorly. They could not resist a load higher than 60% of the beam's U.M.R. after two load cycles (D.F. of 1.5). Specimens C4ALN5CY and C4ALN7CY performed better and resisted four load cycles (D.F. of 2.5) before their cyclic strength dropped below 60% of the beam's U.M.R.

The first two cycles of specimens C4ALN5CY and C4ALN7CY were controlled by the flexural capacity of their beams. This allowed their cyclic strength to remain high at a value corresponding to an applied load of around 45 kN. By the third load cycle, once joint cracking had occurred, both specimens lost strength rapidly.

The presence of ties only influenced the initial joint capacity. **The rate of decay, once joint cracking had occurred, was the same for all specimens.**

Specimens with U-bar beam steel detail

Figure 9.1.2.3(a) shows the performance of the four specimens with U-bar beam steel detail. None of these specimens had joints strong enough to allow the beam's U.M.R. to be reached. Again, as with the bent down specimens, the presence of ties influenced only the initial joint capacity. The rate of decay, once joint cracking had occurred, was constant for each test.

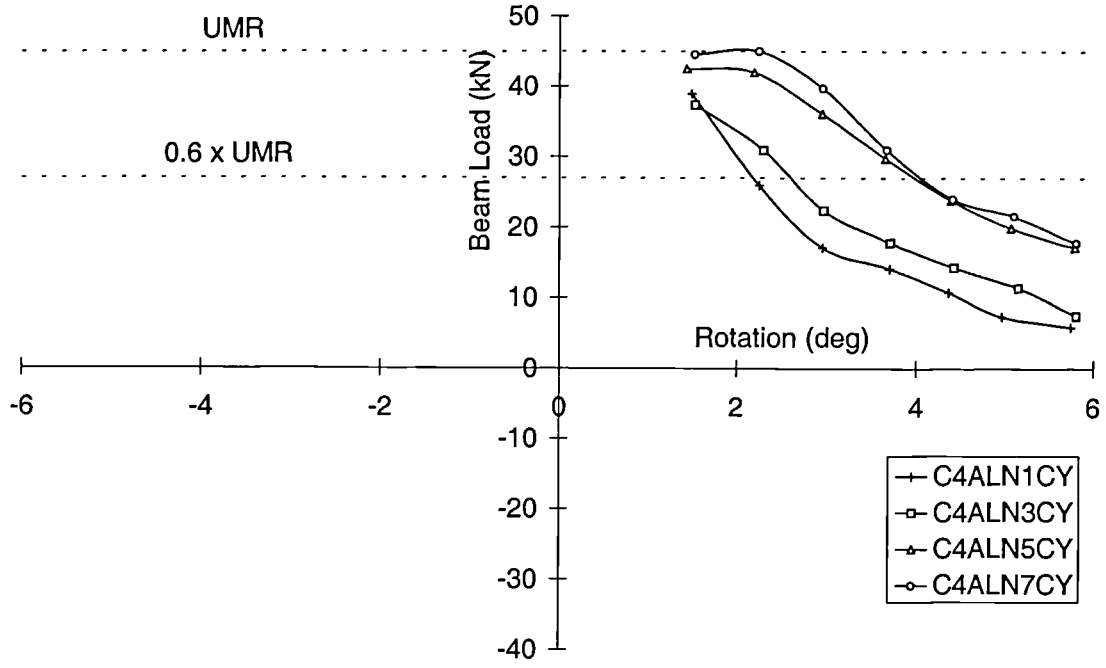

Figure 9.1.2.3(a) Peak loads - bent down beam steel detail

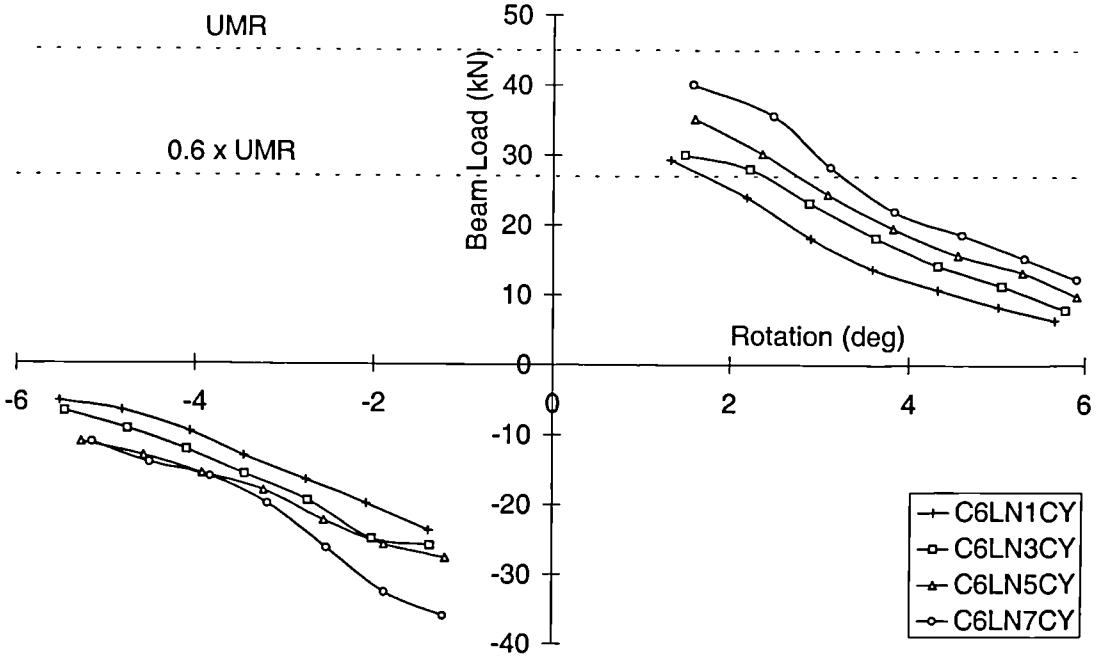

Figure 9.1.2.3(b) Peak loads - U-bar beam steel detail

9.1.3 Strain distributions

This section considers the strain distributions in the beam's main steel and the joint ties. The beam steel is considered in the regions previously defined in Section 4.1.3.3. As previously indicated in Table 9.1 specimens C4ALN3CY and C6LN3CY contained *fully* strain gauged reinforcement.

9.1.3.1 Beam steel

C4ALN3CY

Figures 9.1.3.1.1 to 9.1.3.1.4 display the reinforcement strains present in the beam steel from specimen C4ALN3CY. The considered rebar and the direction of loading are indicated below :

Figure 9.1.3.1.1 Bent down bar - downward load cycles
Figure 9.1.3.1.2 Bent down bar - upward load cycles
Figure 9.1.3.1.3 12 mm straight bar - downward load cycles
Figure 9.1.3.1.4 12 mm straight bar - upward load cycles

The ductility factors are indicated in the respective *legends* within the figures. The peak loads and the rate of strength decay for specimen C4ALN3CY were displayed previously in Figure 9.1.2.1(b).

Figure 9.1.3.1.1 shows that at a ductility factor of 1.0 the strain in the bent down bar at the beam-column interface was approaching yield. As seen previously, for similar monotonic specimens, this strain dropped to zero around the *top bend* and *vertical leg* region of the rebar. The maximum strain recorded was at a ductility factor of 2.0 and was 3780 $\mu\varepsilon$. The applied beam load was transferred into the joint and lower column by use of this large section of rebar. As a result of this, the average bond stress over this region was relatively low.

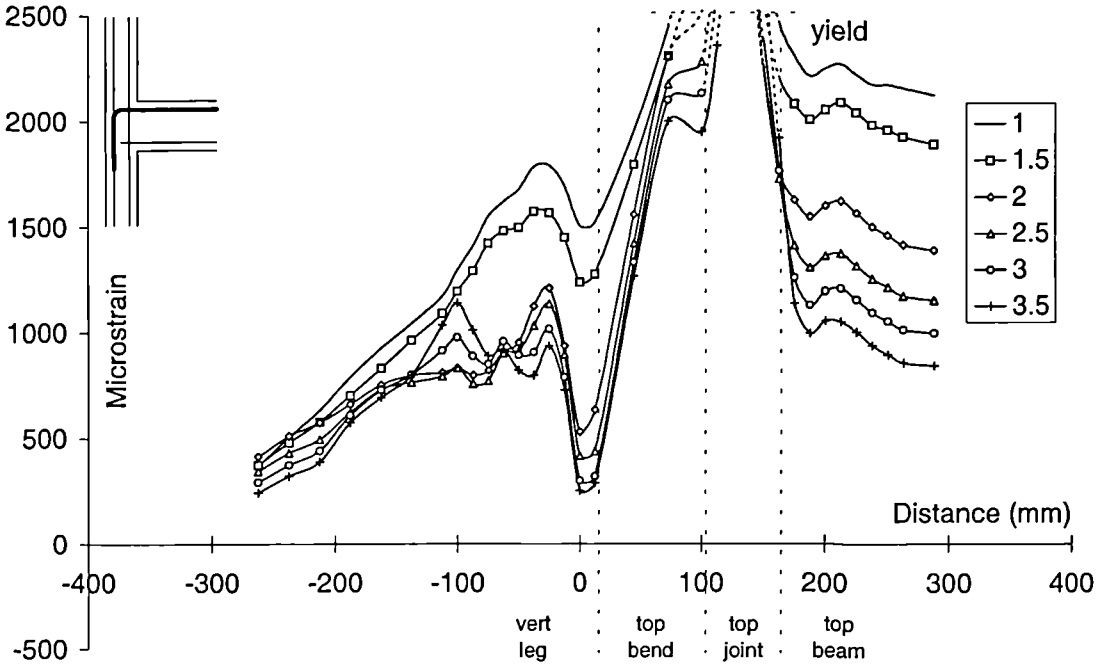

Figure 9.1.3.1.1 Top rebar strains - downward load cycles - C4ALN3CY

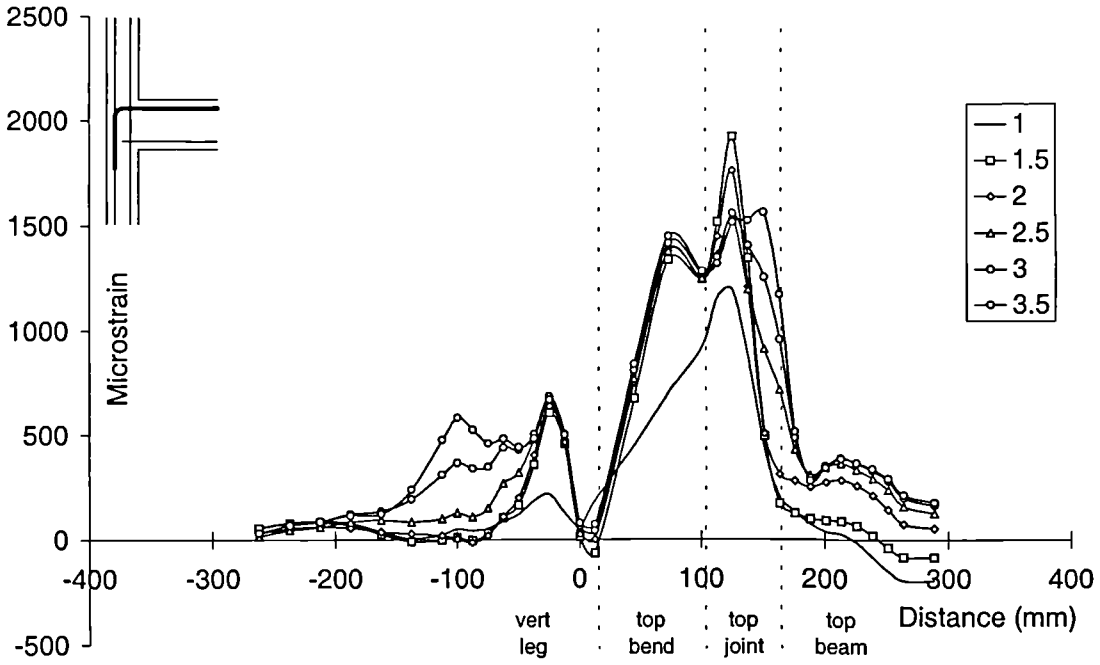

Figure 9.1.3.1.2 Top rebar strains - upward load cycles - C4ALN3CY

The concrete-steel bond was lost in regions where extensive joint cracking occurred. After the initial load cycle, the ability to develop bond stress at the start of the *top bend* and the start of the *vertical leg* was lost. Due to this loss of bond the load capacity reduced with each cycle. The strains in the beam at the column face were directly related to the applied load. This can be seen to decrease with each load cycle.

Figure 9.1.3.1.2 shows that the bent down bar was not subject to any major compressive strain during the test. As the applied beam loads corresponding to the upward load cycles were small, the compressive strains in the bent down bar were also small. In addition, residual tensile strains remained in the *top bend* and *top joint* regions from the downward cycles.

Figure 9.1.3.1.3 displays the reinforcement strains present in the straight 12 mm beam steel within specimen C4ALN3CY for the downward load cycles. The straight bar was in compression along its *beam* region for all of the downward cycles. The region of the bar within the joint gave varied strain readings due to the extensive joint cracking. The strains within the joint peaked at a ductility factor of 2.5 with a maximum tensile strain value of 2650 με and a maximum compressive strain value of -3820 με.

Figure 9.1.3.1.4 displays the reinforcement strains present in the straight 12 mm beam steel within specimen C4ALN3CY for the upward load cycles. The straight bar was in tension along its *beam* region for all of the upward cycles. This strain was highest for the first load cycle with a peak of around 1800 με at the beam column interface. By a ductility factor of 2.0, the strain within the beam region had fallen to a peak of around 700 με. Again the region of the bar within the joint gave varied strain readings due to the extensive joint cracking. The strains within the joint peaked at a ductility factor of 2.5 with a maximum tensile strain value of 8350 με and a maximum compressive strain value of -6090 με.

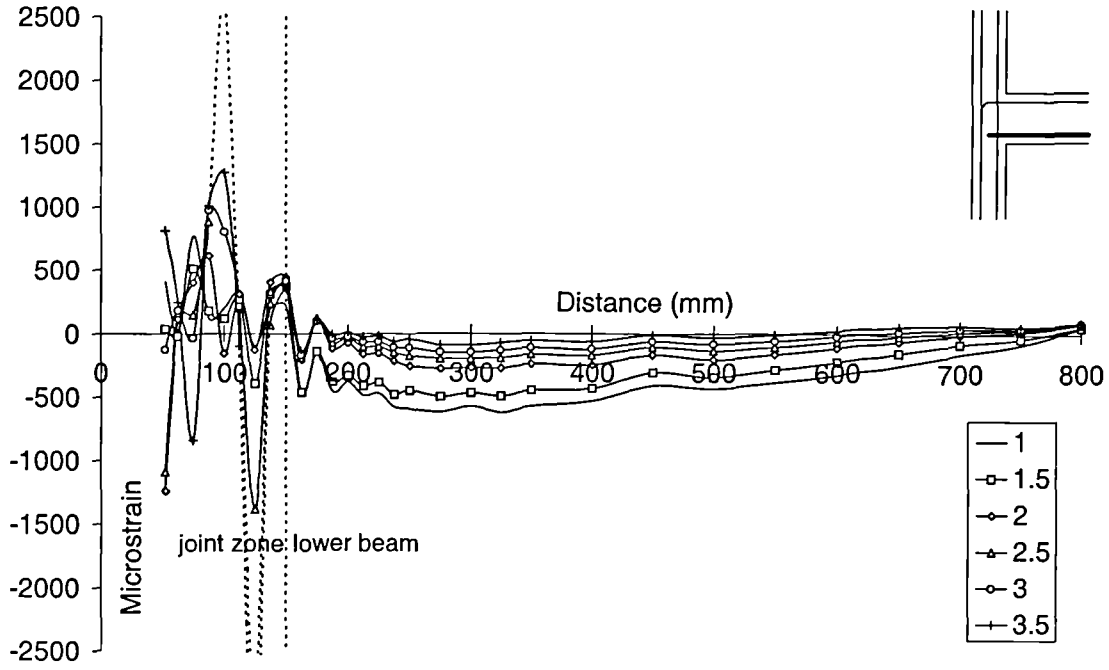

Figure 9.1.3.1.3 Bottom rebar strains - downward load cycles - C4ALN3CY

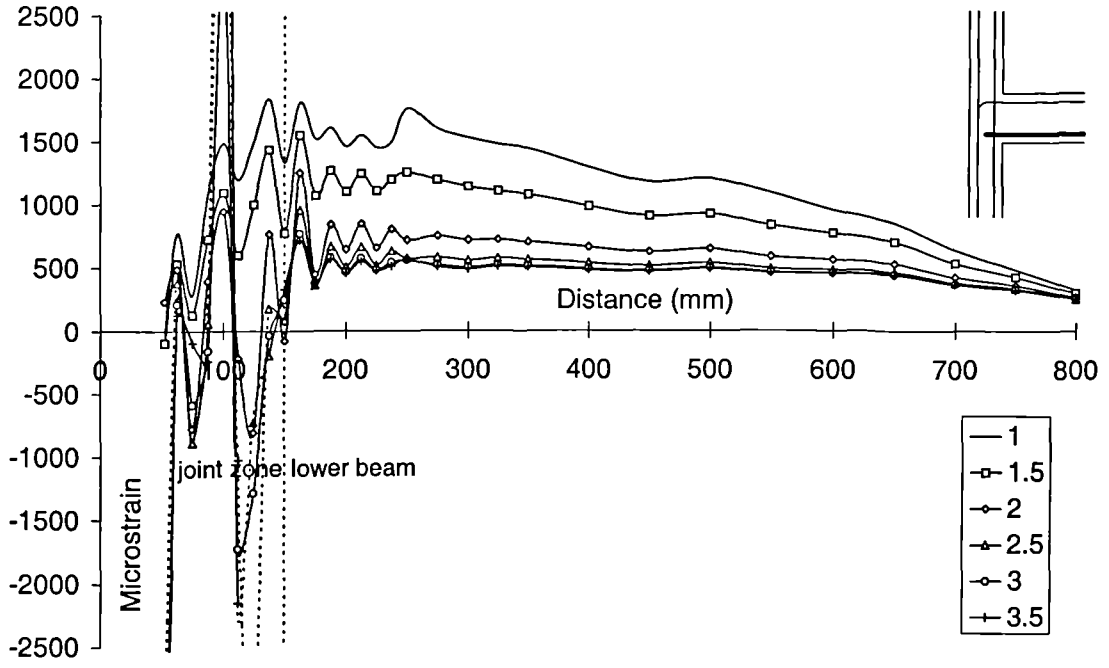

Figure 9.1.3.1.4 Bottom rebar strains - upward load cycles - C4ALN3CY

C6LN3CY

Figure 9.1.3.1.5 displays the reinforcement strains present in the U-bar beam steel within specimen C6LN3CY for the downward cycles. Figure 9.1.3.1.6 displays the reinforcement strains present in the U-bar beam steel within specimen C6LN3CY for the upward cycles. The ductility factors are indicated in the *legends* within the figures.

The strain distributions in Figures 9.1.3.1.5 and 9.1.3.1.6 are almost a mirror image about the mid-point of the U-bar. As a result of this, only Figure 9.1.3.1.5 is considered.

Figure 9.1.3.1.5 shows that after joint cracking the *bottom bend* could no longer develop bond stress for the downwards cycles. Clear residual strains from the upward cycles are visible within this region.

All of the load transfer from the beam into the joint occurred around the *top bend* and *vert* regions. As the joint became more extensively cracked the bond capacity of this region decreased and thus the overall load capacity of the joint reduced. The strain values within the beam at the column face reduced with each load cycle.

9.1.3.2 Joint ties

A huge amount of joint tie strain data was generated by the cyclic tests. It was decided that the most effective way to display this would be to consider the **average stress** values within each tie. This was the mean value of stress from the ten gauges evaluated using the stress-strain relationship displayed previously in Figure 2.1.2.1.

Average values were considered due to the huge amount of data. Stress values were considered as strain values greater than yield are non-linear and would therefore give a misleading average value.

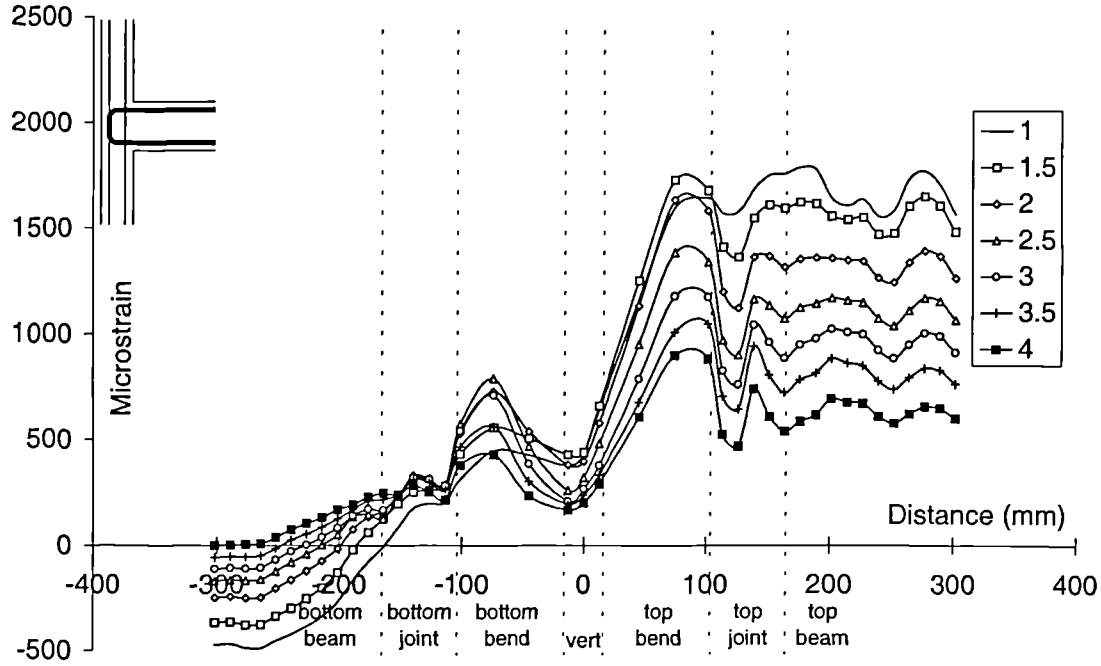

Figure 9.1.3.1.5 Reinforcement strains - downward load cycles - C6LN3CY

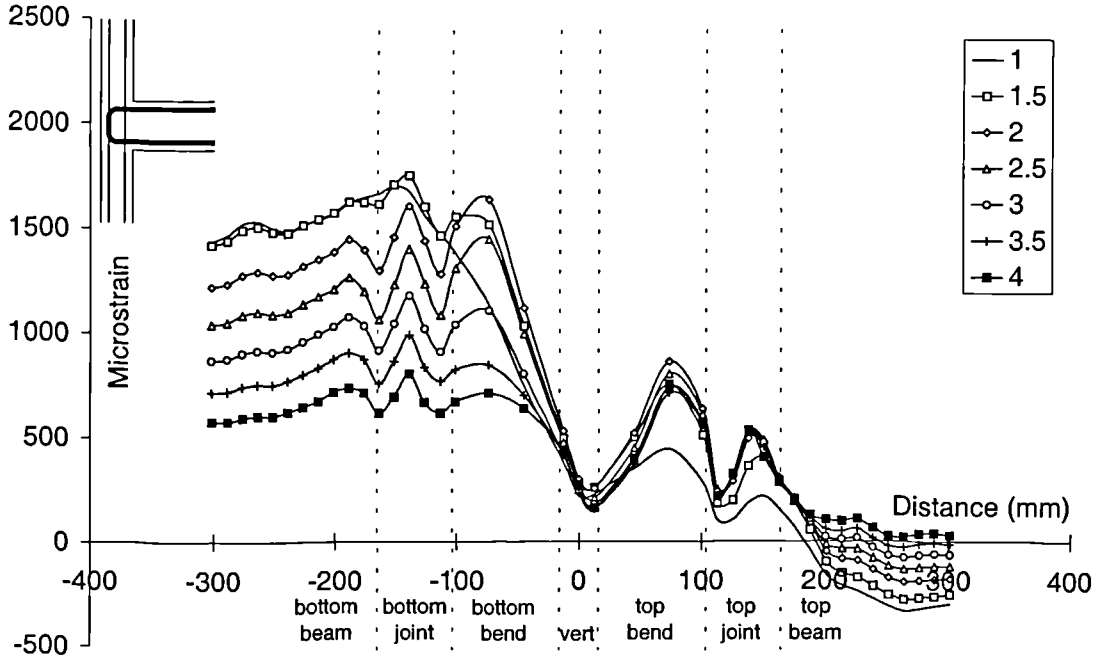

Figure 9.1.3.1.6 Reinforcement strains - upward load cycles - C6LN3CY

C4ALN3CY

Figure 9.1.3.2.1(a) displays the average stress present in the upper tie within specimen C4ALN3CY. The peak average stress, for the downward cycles, was around 280 MPa at a ductility factor of 1.0 and this reduced slightly throughout the test to around 180 MPa at a ductility factor of 4.0. The influence of upward cycling on this tie was minimal. The residual stress between cycles, when loading ceased, was around 80 MPa. This was consistent with the value at initial joint cracking and this trend was apparent for all three ties.

Figure 9.1.3.2.1(b) displays the average stress present in the middle tie within specimen C4ALN3CY. The peak average stress, for the downward cycles, was around 280 MPa at a ductility factor of 1.0 and this reduced slightly throughout the test to around 120 MPa at a ductility factor of 4.0. The influence of upward cycling on this tie was apparent for the first two load cycles but was then minimal throughout the remainder of the test.

Figure 9.1.3.2.1(c) displays the average stress present in the lower tie within specimen C4ALN3CY. As this tie was in the lower region of the joint the stress recorded as a result of downward cycling was not as significant. This effect of tie positioning within the joint was considered previously in Section 4.3. The influence of upward cycling on this lower tie was significant for the first full load cycle and an average stress of around 360 MPa was recorded. This value of stress reduced throughout the test as the bond developed by the beam's straight bar was lost.

Throughout the test, the extent of the joint cracking and thus the physical expansion of the joint became increasingly significant. However, the peak stresses within all three joint ties, for both downward and upward cycles, generally decreased. It is suggested that this was because full anchorage of the tie's legs was not achieved.

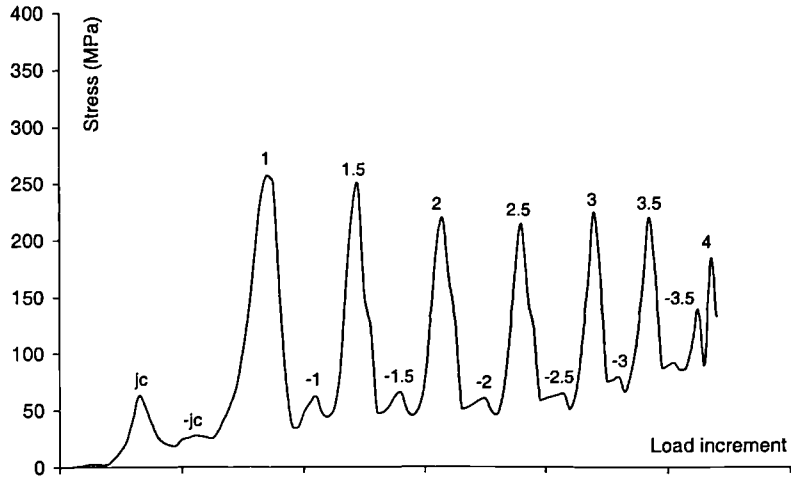

Figure 9.1.3.2.1(a) Average tie stresses - C4ALN3CY (upper tie)

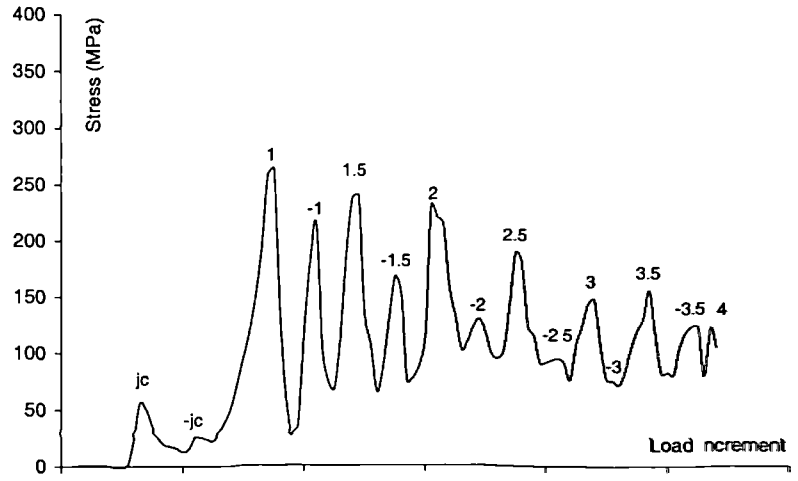

Figure 9.1.3.2.1(b) Average tie stresses - C4ALN3CY (middle tie)

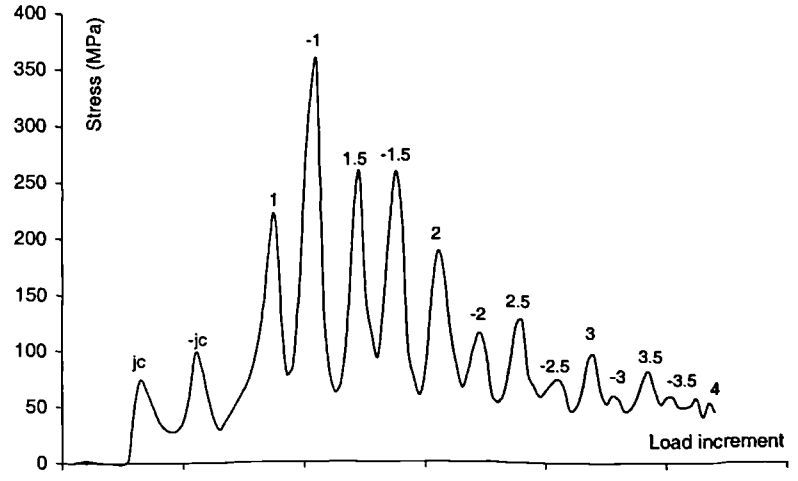

Figure 9.1.3.2.1(c) Average tie stresses - C4ALN3CY (lower tie)

C6LN3CY

Figure 9.1.3.2.2(a) displays the average stress present in the upper tie within specimen C6LN3CY. The peak average stress, for the downward cycles, was very similar to that seen within the same tie in specimen C4ALN3CY. The effect of upward cycling on this tie however was more significant. The U-bar beam steel detail resisted the load cycling in both directions and as a result stress of around 160 MPa was recorded in this upper tie. The residual stress between cycles was around 100 MPa. This was consistent with the stress value at initial joint cracking. This trend was observed for all three ties, although the largest value of stress was in this upper tie.

Figure 9.1.3.2.2(b) displays the average stress present in the middle tie within specimen C6LN3CY. The peak average stress for the downward cycles was initially large with stresses of around 400 MPa being recorded. This value had reduced to around 160 MPa by the end of the test. The stresses for the upward cycles ranged from around 280 MPa at a ductility factor of 1.0 to 140 MPa at a ductility factor of 4.0.

Figure 9.1.3.2.2(c) displays the average stress present in the lower tie within specimen C6LN3CY. The stress value for the upward cycles was more significant for this tie. Again this was due to effects outlined previously in Section 4.3. The stress within the downward cycles was almost negligible by the end of the test.

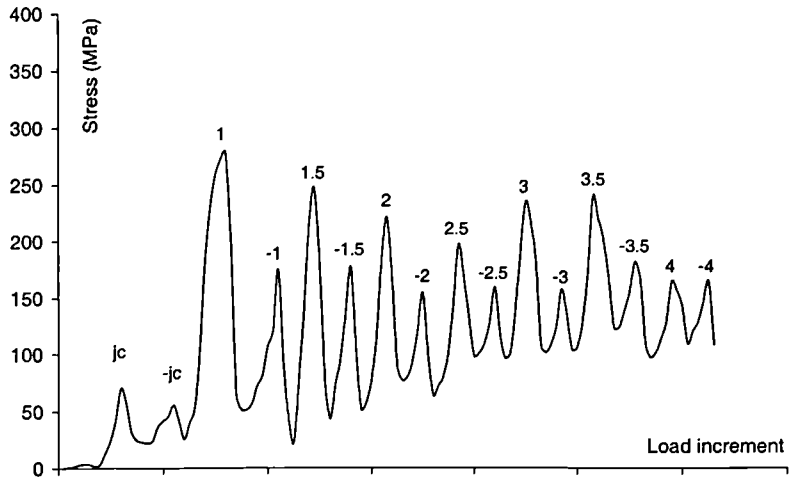

Figure 9.1.3.2.2(a) Average tie stresses - C6LN3CY (upper tie)

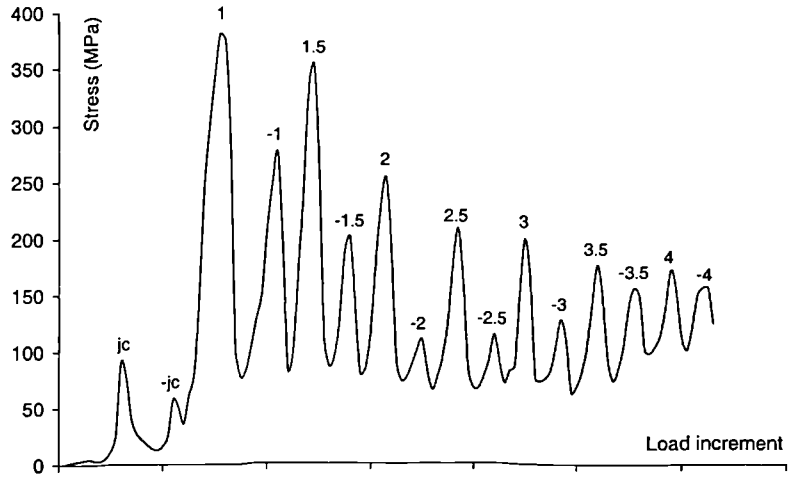

Figure 9.1.3.2.2(b) Average tie stresses - C6LN3CY (middle tie)

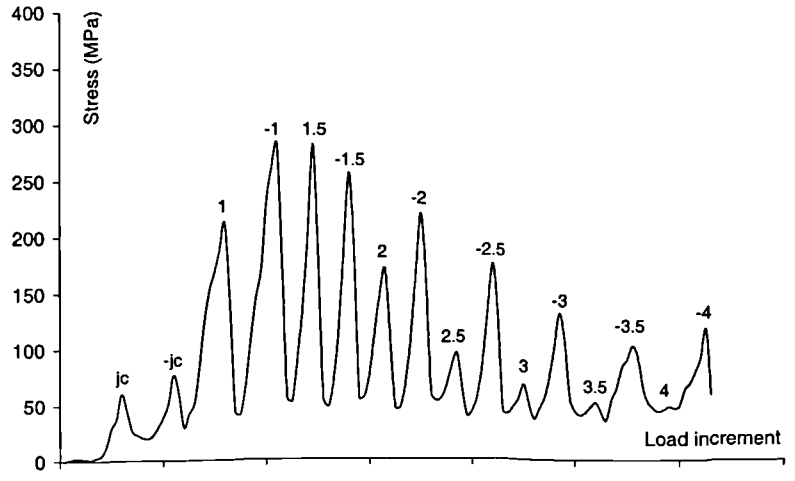

Figure 9.1.3.2.2(c) Average tie stresses - C6LN3CY (lower tie)

9.2 High Strength Cyclic Specimens

This section considers the results from the eight high strength cyclic specimens. The concrete used had a typical compressive cube strength of 120 MPa. The parameters investigated were the number of ties present within the joint and the beam tension steel anchorage detail. The specimen details are given in Table 9.2.

Table 9.2 ***High strength cyclic specimens*** **- details**

Specimen	Gauging	Beam steel anchorage	No. of joint ties	f_{cu} (MPa)
C4ALH1CY	-	Bent down	1	126
C4ALH3CY	Full	Bent down	3	116
C4ALH5CY	-	Bent down	5	128
C4ALH7CY	-	Bent down	7	114
C6LH1CY	-	U-bar	1	117
C6LH3CY	Full	U-bar	3	119
C6LH5CY	-	U-bar	5	131
C6LH7CY	-	U-bar	7	127

Note

1. Full gauging of a cyclic specimen was defined as the gauging of the main beam steel and joint ties.

9.2.1 Load-rotation response

Figures 9.2.1.1(a)-(d) display the load-rotation response for the high strength cyclic specimens with bent down beam steel detail. Figures 9.2.1.2(a)-(d) display the load-rotation response for the high strength specimens with U-bar beam steel detail. The peak load history, as defined previously in Figure 7.2.1.3(d), is indicated on all the figures.

D.F.	↓ (kN)	↑ (kN)
1.0	$43_{(B)}$	25
1.5	$42_{(B)}$	15
2.0	30	4
2.5	22	2
3.0	16	2
3.5	12	1
4.0	7	3

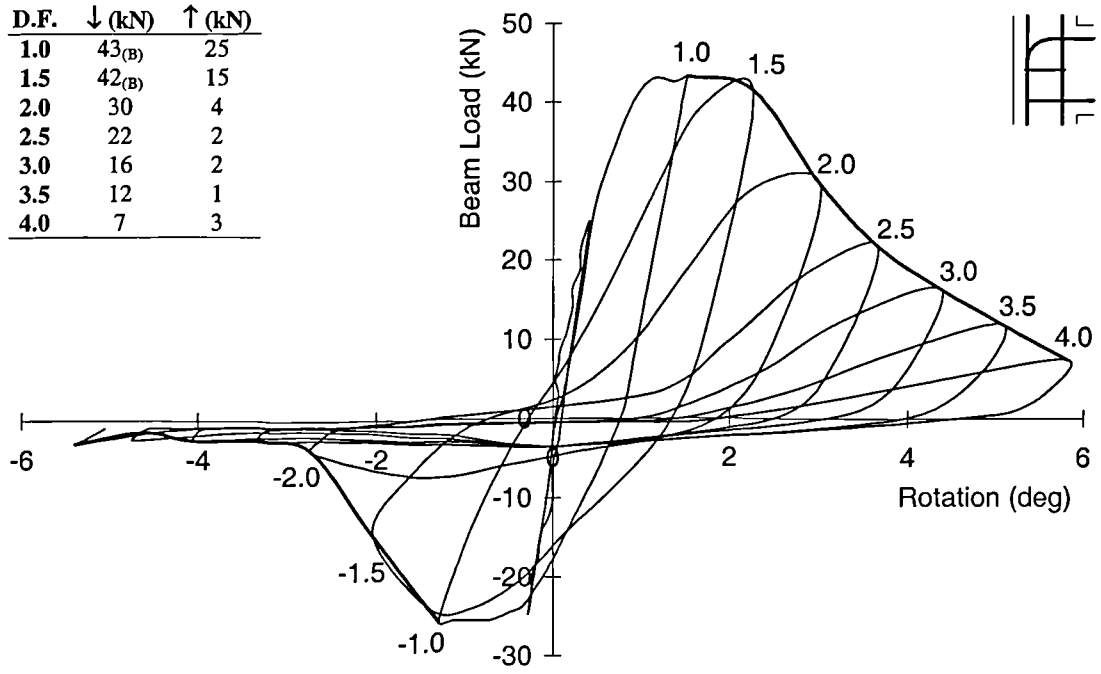

Figure 9.2.1.1(a) Load-rotation response - C4ALH1CY

D.F.	↓ (kN)	↑ (kN)
1.0	$46_{(B)}$	23
1.5	$46_{(B)}$	20
2.0	$44_{(B)}$	4
2.5	35	3
3.0	30	3
3.5	20	3
4.0	14	3

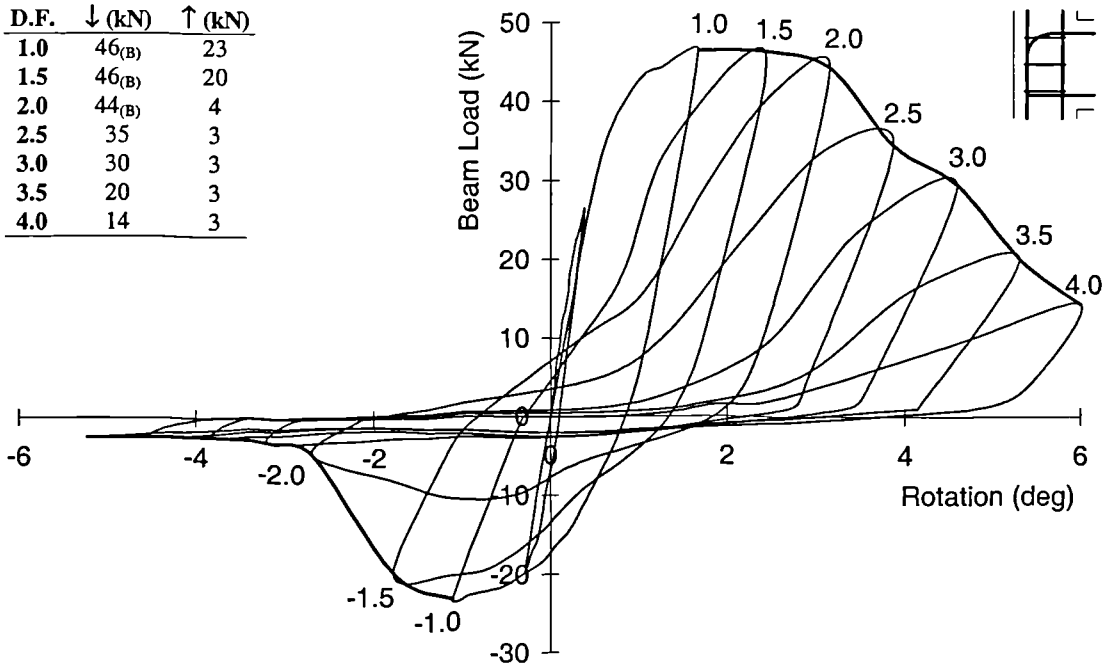

Figure 9.2.1.1(b) Load-rotation response - C4ALH3CY

D.F.	↓ (kN)	↑ (kN)
1.0	$48_{(B)}$	$24_{(B)}$
1.5	$45_{(B)}$	$25_{(B)}$
2.0	$45_{(B)}$	$25_{(B)}$
2.5	$42_{(B)}$	$25_{(B)}$
3.0	23	22
3.5	21	18
4.0	13	20

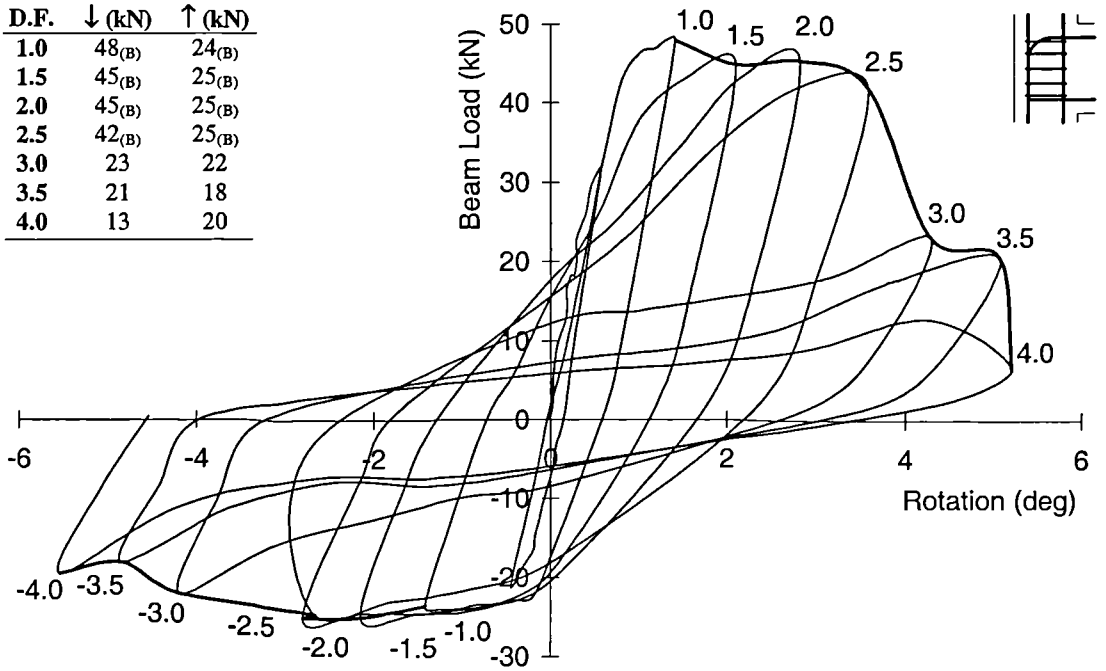

Figure 9.2.1.1(c) Load-rotation response - C4ALH5CY

D.F.	↓ (kN)	↑ (kN)
1.0	$44_{(B)}$	$25_{(B)}$
1.5	$42_{(B)}$	$25_{(B)}$
2.0	$44_{(B)}$	$25_{(B)}$
2.5	$38_{(B)}$	$25_{(B)}$
3.0	27	$25_{(B)}$
3.5	26	23
4.0	18	22

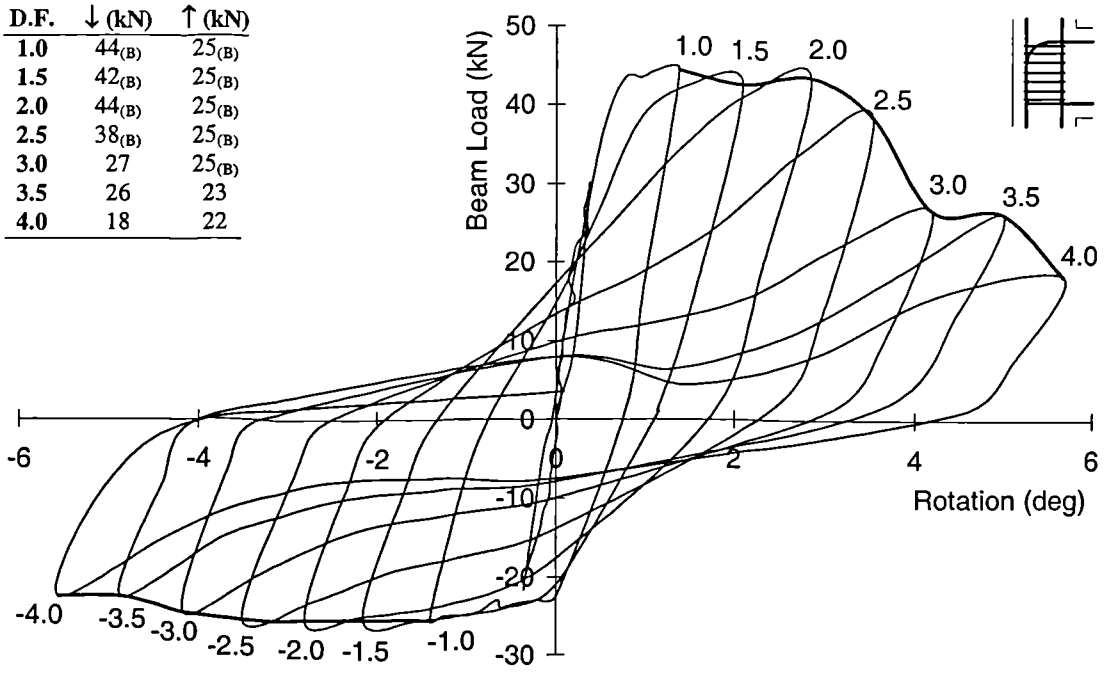

Figure 9.2.1.1(d) Load-rotation response - C4ALH7CY

D.F.	↓ (kN)	↑ (kN)
1.0	$47_{(B)}$	36
1.5	$42_{(B)}$	35
2.0	31	28
2.5	18	22
3.0	13	18
3.5	9	15
4.0	7	12

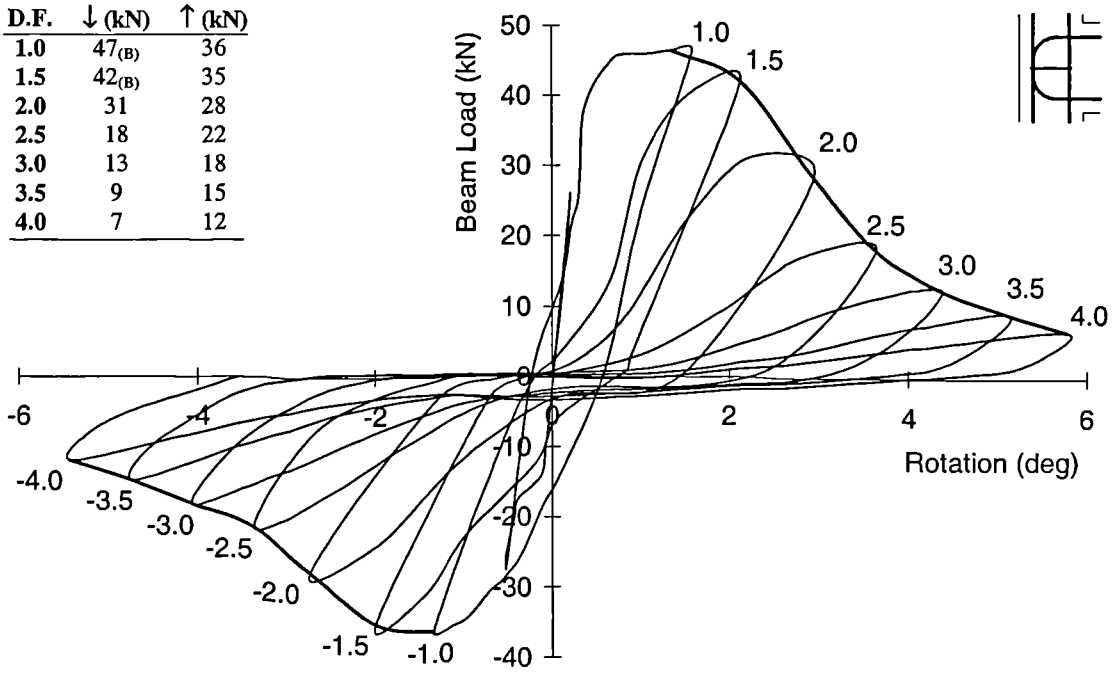

Figure 9.2.1.2(a) Load-rotation response - C6LH1CY

D.F.	↓ (kN)	↑ (kN)
1.0	$43_{(B)}$	37
1.5	$41_{(B)}$	36
2.0	35	28
2.5	22	21
3.0	13	15
3.5	8	13
4.0	5	10

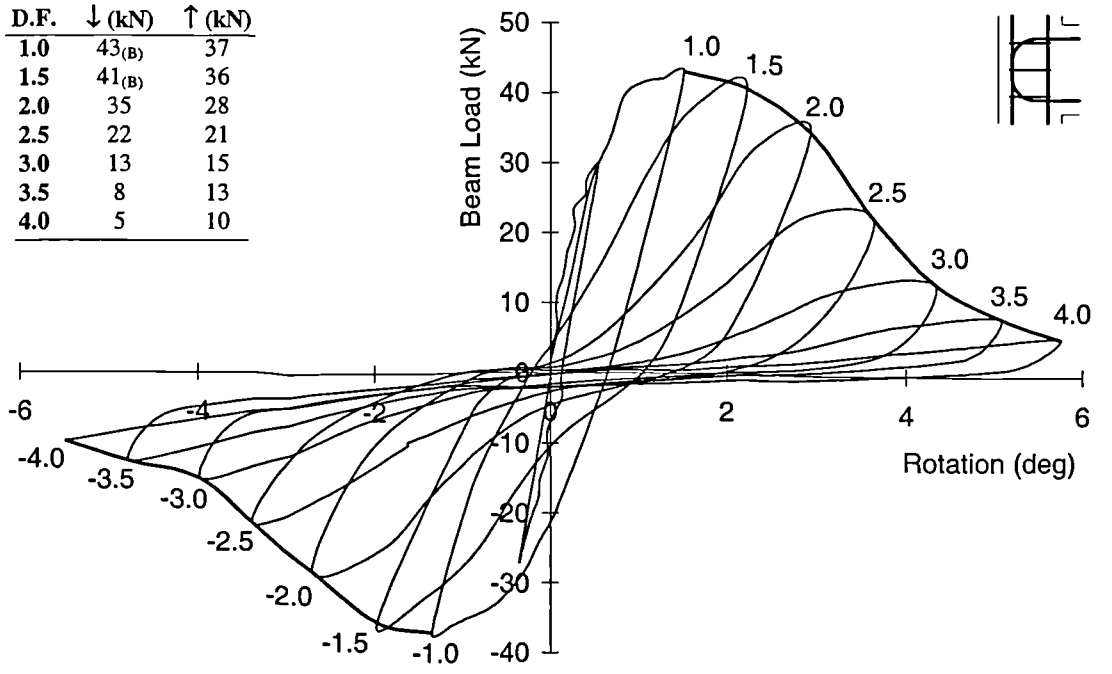

Figure 9.2.1.2(b) Load-rotation response - C6LH3CY

D.F.	↓ (kN)	↑ (kN)
1.0	$46_{(B)}$	$40_{(B)}$
1.5	$41_{(B)}$	$38_{(B)}$
2.0	$41_{(B)}$	$41_{(B)}$
2.5	$41_{(B)}$	$42_{(B)}$
3.0	$37_{(B)}$	25
3.5	22	13
4.0	-	-

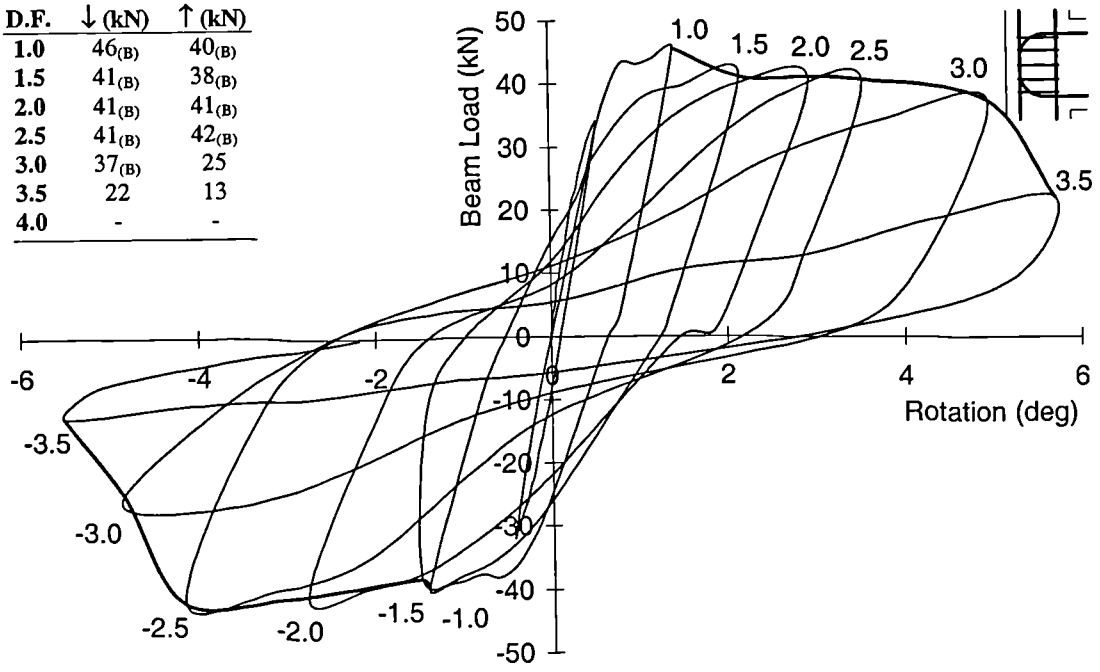

Figure 9.2.1.2(c) Load-rotation response - C6LH5CY

D.F.	↓ (kN)	↑ (kN)
1.0	$50_{(B)}$	$41_{(B)}$
1.5	$45_{(B)}$	$41_{(B)}$
2.0	$44_{(B)}$	$40_{(B)}$
2.5	$43_{(B)}$	$39_{(B)}$
3.0	$40_{(B)}$	$37_{(B)}$
3.5	26	17
4.0	11	12

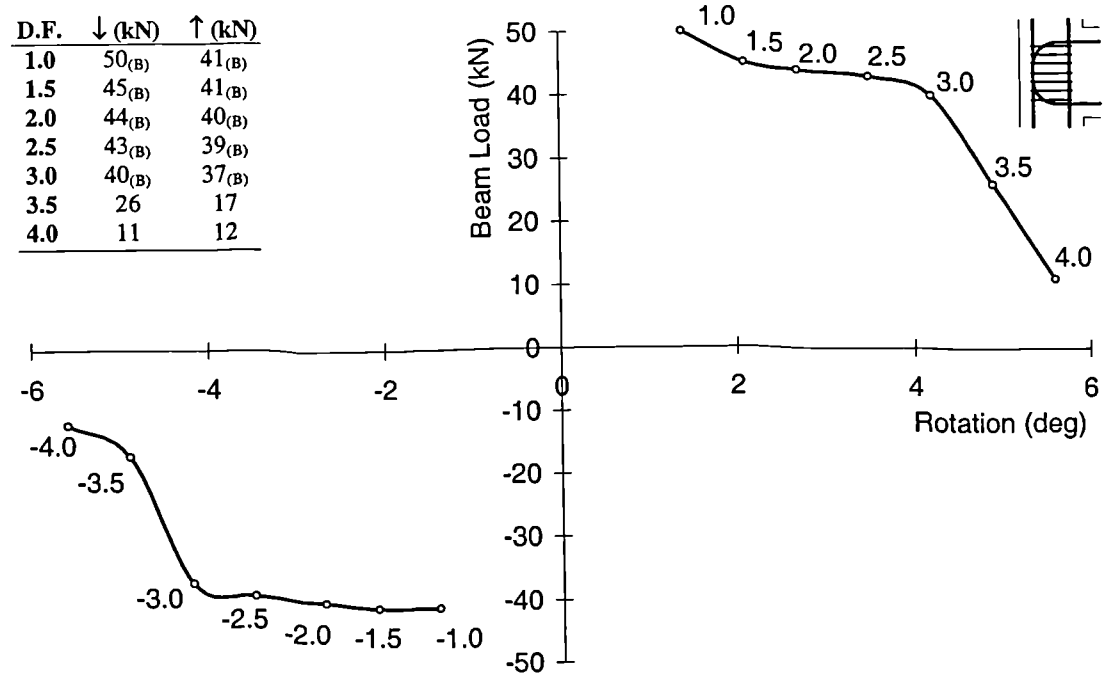

Figure 9.2.1.2(d) Load-rotation response - C6LH7CY

The peak loads from each cycle are displayed, in Figures 9.2.1.3(a) and 9.2.1.3(b), for specimens with bent down and U-bar beam steel respectively. As with the normal strength specimens the ultimate moment of resistance (U.M.R.) of the beam was around 45 kN. This value and the value 60% of this are indicated on both figures for the downward load cycles by dashed horizontal lines. Again a joint strength lower than this 60% value is unacceptable within this investigation.

Specimens with bent down beam steel detail

Figure 9.2.1.3(a) shows that specimen C4ALH1CY did not perform very well and by three load cycles (D.F. of 2.0) could not resist a load higher than 60% of the beam's U.M.R. The specimens with a greater number of joint ties, C4ALH3CY, C4ALH5CY and C4ALH7CY, all performed better. These specimens withstood a load higher than 60% of the beam's U.M.R. by five load cycles (D.F. of 3.0).

The cyclic strength depended on the joint's ability to withstand shear failure and for the cycles to be controlled by the beam's flexural strength. Once joint failure occurred the strength of all specimens rapidly decreased.

All specimens with bent down beam steel detail exhibited beam flexural failure for their initial **upward** cycles. The increased concrete-steel bond achieved using high strength concrete allowed the straight bars to yield. This flexural behaviour was apparent throughout the test for specimens C4ALH5CY and C4ALH7CY.

Specimens with U-bar beam steel detail

Figure 9.2.1.3(b) shows the performance of the four specimens with U-bar beam steel detail. Specimens C6LH1CY and C6LH3CY both exhibited joint failure by a ductility factor of 2.0. Once joint failure occurred the strength of the specimens fell below 60% of their beam's U.M.R. Specimens C6LH5CY and C6LH7CY withstood six full cycles (D.F. of 3.5) before their strength fell below this 60% value.

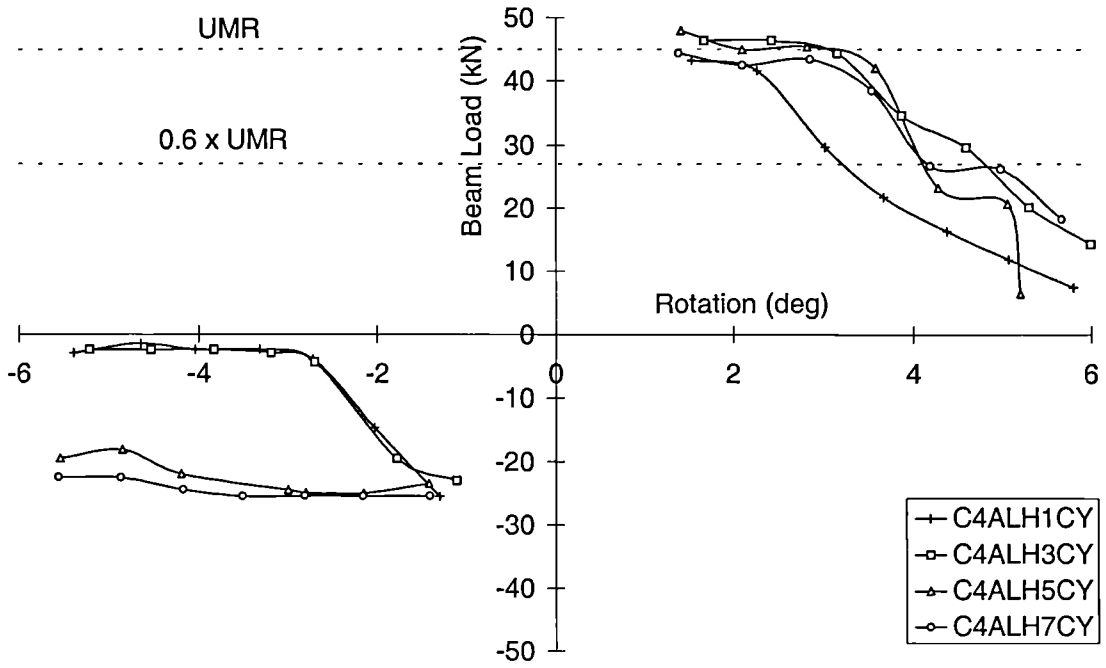

Figure 9.2.1.3(a) Peak loads - Bent down beam steel detail

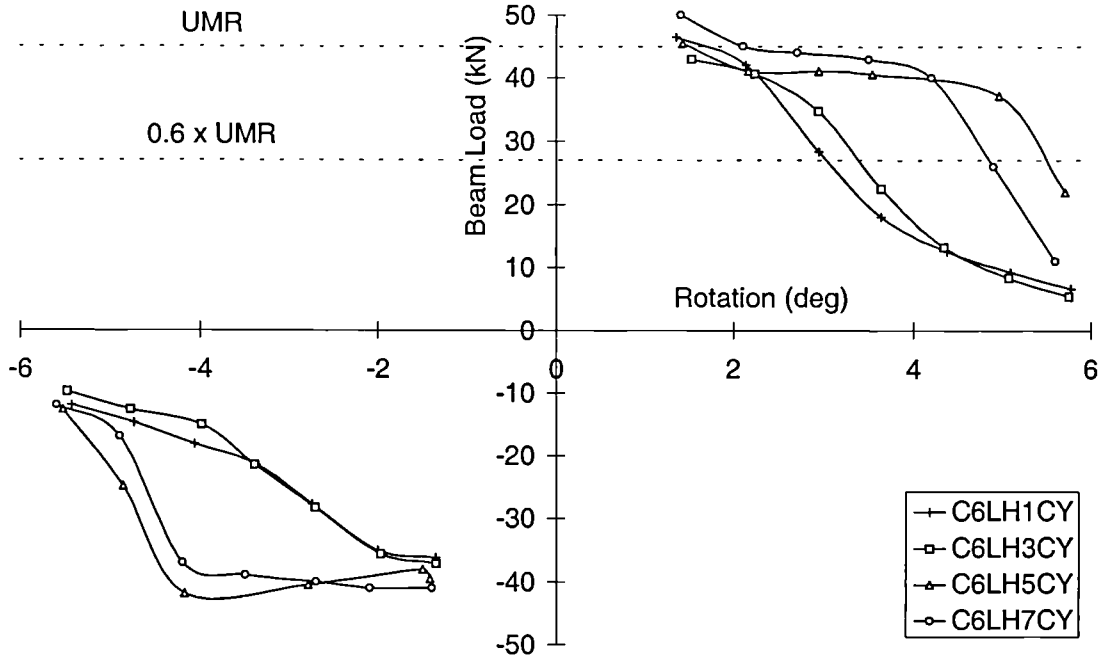

Figure 9.2.1.3(b) Peak loads - U-bar beam steel detail

Again the cyclic capacity remained high providing the strength of the specimens was controlled by the beam's flexural strength. Once shear failure occurred the specimen's strength reduced quite rapidly.

9.2.1.1 Normal strength comparisons

Figure 9.2.1.1.1 compares the cyclic performance of the normal strength specimens C6LN1CY and C6LN3CY with the high strength specimens C6LH1CY and C6LH3CY. These four specimens were selected as they all exhibited joint failure early in their cyclic history. The cyclic peak loads were normalised by dividing by the value of their ultimate capacity (at a D.F. of 1.0).

Figure 9.2.1.1.1 shows that the gradient of the strength decay lines for the high strength specimens was steeper than for the normal strength specimens. After shear failure the deterioration of the joint occurred more rapidly for specimens using high strength concrete. **This would suggest that although the use of high strength concrete increased the joint capacity of the specimen, once joint failure occurred the cyclic strength was lost more rapidly.**

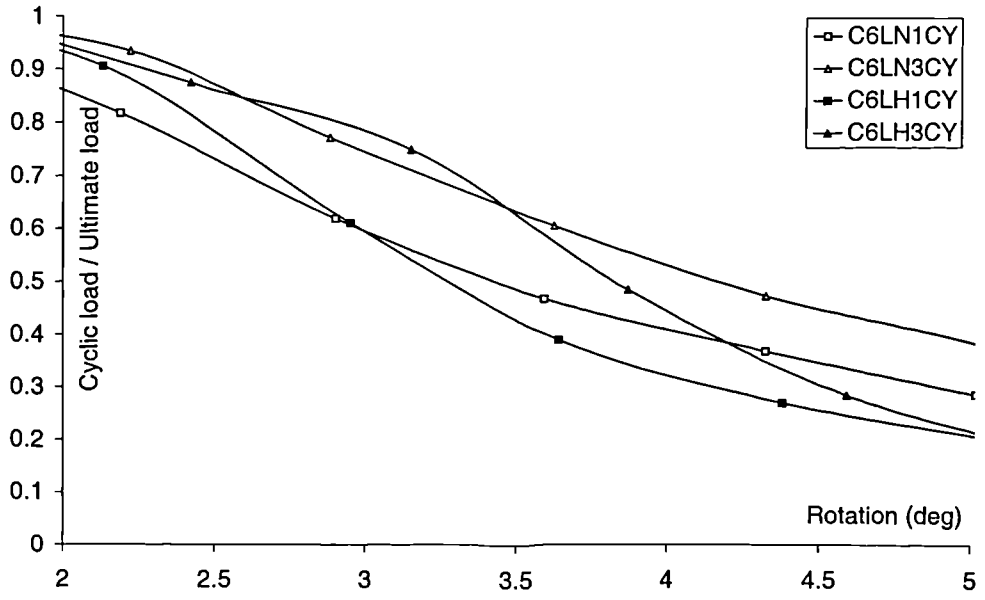

Figure 9.2.1.1.1 Strength decay line comparisons

9.2.2 Strain distributions

This section considers the strain distributions in the beam's main steel and the joint ties. The beam steel is considered in the regions previously defined in Section 4.1.3.3. As previously indicated in Table 9.2, specimens C4ALH3CY and C6LH3CY contained *fully* strain gauged reinforcement.

Both of the considered specimens had their initial cycles controlled by beam flexural effects. Gross yielding occurred within the beam steel and as a result very high strain values were recorded. Previous strain plots within this thesis have only considered strain values up to yield (2500 με). However, for these high strength specimens strains up to a maximum value of 30 000 με are considered.

In certain cases the strain in the bar exceeded the strain gauge capacity - these readings are excluded from the strain distribution plots.

9.2.2.1 Beam steel

C4ALH3CY

Figures 9.2.2.1.1 to 9.2.2.1.4 display the reinforcement strains present in the beam steel from specimen C4ALH3CY. The considered rebar and the direction of loading are indicated below :

Figure 9.2.2.1.1 Bent down bar - downward load cycles
Figure 9.2.2.1.2 Bent down bar - upward load cycles
Figure 9.2.2.1.3 12 mm straight bar - downward load cycles
Figure 9.2.2.1.4 12 mm straight bar - upward load cycles

The ductility factors are indicated in the respective *legends* within the figures. The peak loads and the rate of strength decay for specimen C4ALH3CY were displayed previously in Figure 9.2.1.1(b).

Figure 9.2.2.1.1 shows the extent of the yielding within the bent down bar. For the first full downward cycle the steel had yielded from a position 150 mm from the column face to mid-way around the *top bend* region of the rebar. The steel-concrete bond was generated around this *top bend* region and along the length of the *vertical leg*. By the first load cycle, one gauge within the beam had failed due to excessive strain. As the downward cycles continued, the strain propagated around the *top bend* region of the bar. At a ductility factor of 2.0 the excessive cracking within the joint region began to weaken the connection and the *vertical leg* region of the bar within the joint had also yielded. A maximum strain value of 24 800 με was recorded in the *top joint* region.

Figure 9.2.2.1.2 shows that for the upward cycles huge residual tensile strains remained. The only significant compressive strain present was at a ductility factor of 1.0 at the beam face. The maximum strain value recorded was 21 500 με which was a residual strain in the *top joint* region of the bar. The region of the vertical leg outside of the joint was under no significant strain.

Figure 9.2.2.1.3 displays the reinforcement strains present in the straight 12 mm beam steel within specimen C4ALH3CY for the downward load cycles. The straight bar was in compression along its beam region for all of the downward cycles. The region of the bar within the joint was in residual tension due to yielding from the upward cycles. A maximum tensile strain of 5100 με was recorded at the beam-column interface.

Figure 9.2.2.1.4 displays the reinforcement strains present in the straight 12 mm beam steel within specimen C4ALH3CY for the upward load cycles. The strain readings confirm that the bar had yielded at the beam-column interface for the first full load cycle. A maximum strain of 9900 με was recorded at this location. The strain within the bar in the beam was high for the first two cycles but by a ductility factor of 2.0 the bar anchorage had failed and thus the strain value decreased.

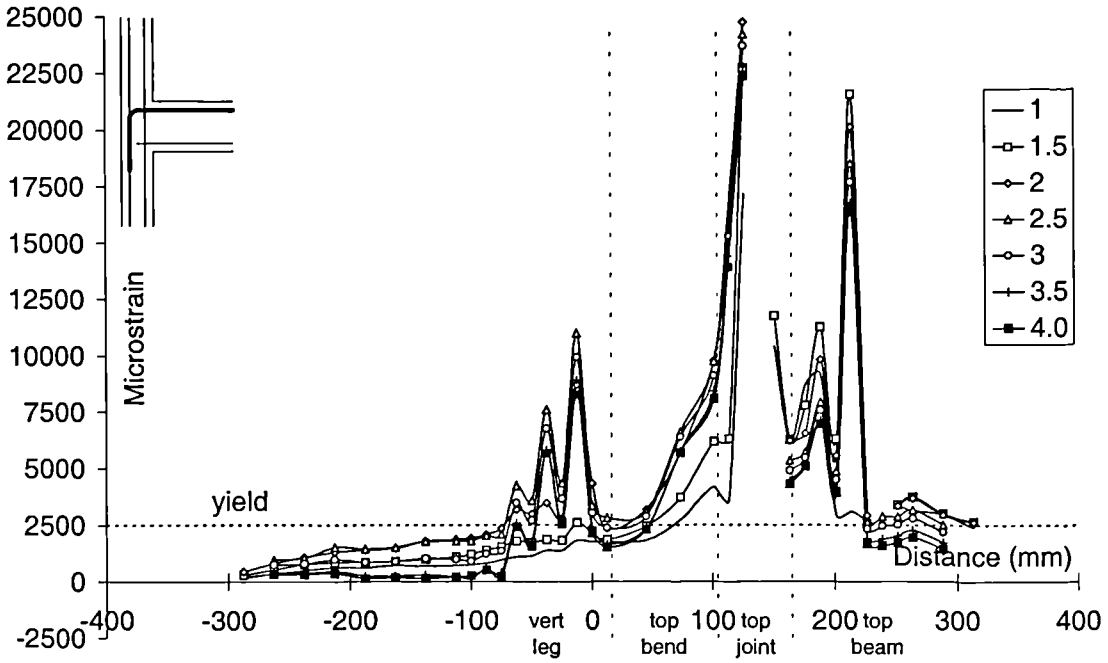

Figure 9.2.2.1.1 Top rebar strains - downward cycles - C4ALH3CY

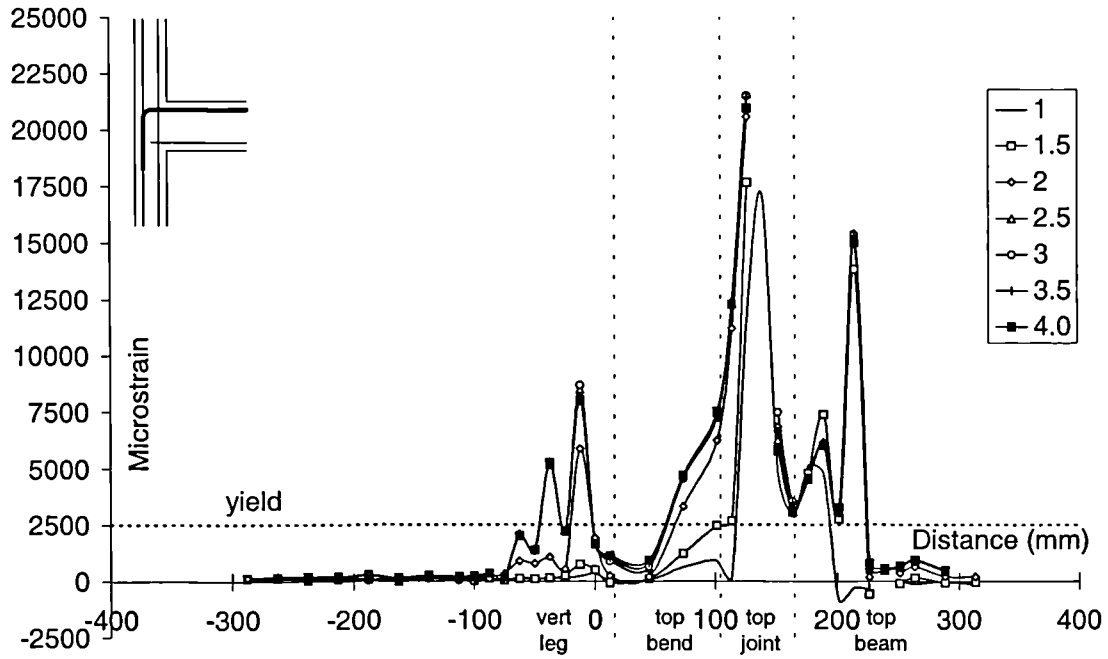

Figure 9.2.2.1.2 Top rebar strains - upward cycles - C4ALH3CY

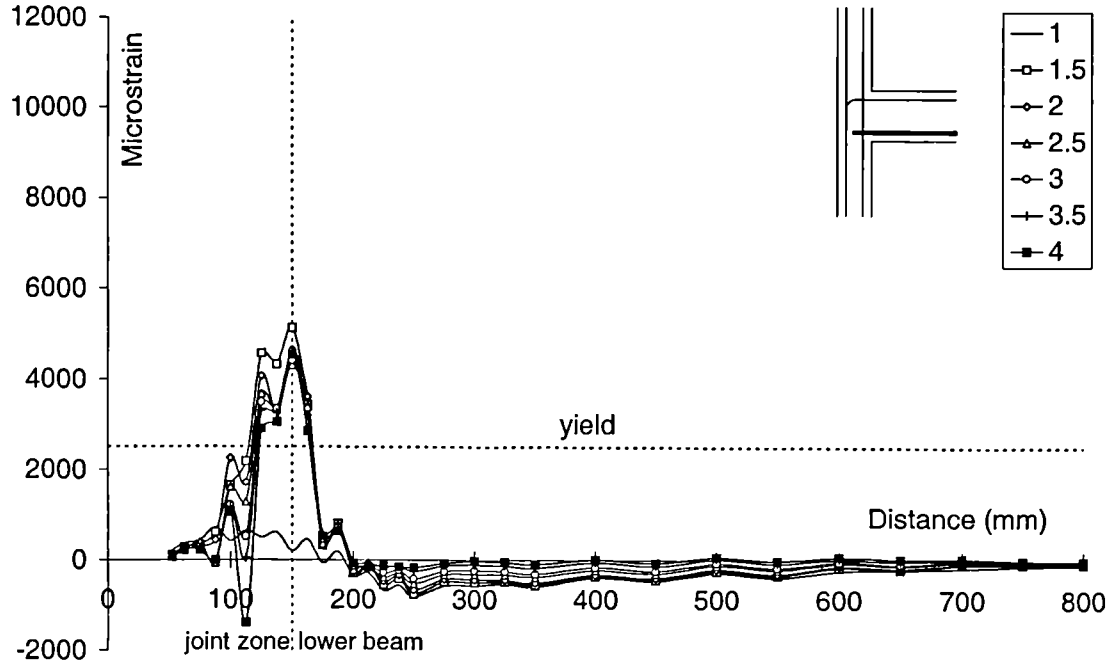

Figure 9.2.2.1.3 Bottom rebar strains - downward cycles - C4ALH3CY

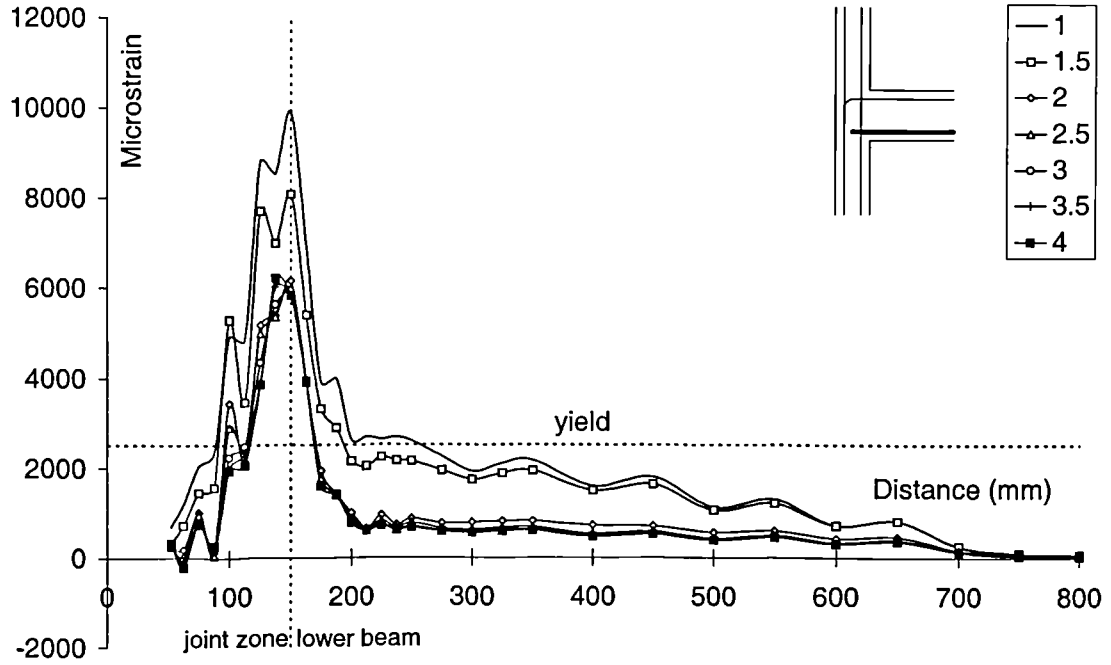

Figure 9.2.2.1.4 Bottom rebar strains - upward cycles - C4ALH3CY

C6LH3CY

Figure 9.2.2.1.5 displays the reinforcement strains present within the U-bar beam steel within specimen C6LH3CY for the downward cycles. Figure 9.2.2.1.6 displays the reinforcement strains present within the U-bar beam steel within specimen C6LH3CY for the downward cycles. The ductility factors are indicated in the *legends* within the figures.

Again, as with the equivalent normal strength specimen C4ALN3CY, the strain distributions in the two figures were almost a mirror image about the mid-point of the U-bar. As a result of this, only Figure 9.2.2.1.5 is considered.

Figure 9.2.2.1.5 shows that the strain at the beam-column interface exceeded the strain gauge capacity. The highest recorded value of strain was around 28 500 $\mu\varepsilon$ (this was the highest value recorded during the investigation). During the initial load cycles, the bond stress developed around the *top bend* region of the bar. This bond was significantly reduced at a ductility factor of 2.0 due to extensive joint cracking.

9.2.2.2 Joint ties

As previously outlined in Section 9.1.3.2, the joint tie behaviour was analysed by considering the average stress values.

C4ALH3CY

Figure 9.2.2.2.1(a) displays the average stress present in the upper tie within specimen C4ALH3CY. The peak average stress, for the downward cycles, was around 460 MPa at a ductility factor of 1.5. This peak corresponded to the final cycle to be controlled by the flexural strength of the beam. The cracking of the joint throughout the remainder of the test resulted in slippage of the legs and thus a loss of stress in the tie. The influence of the upward cycling on this upper tie was minimal.

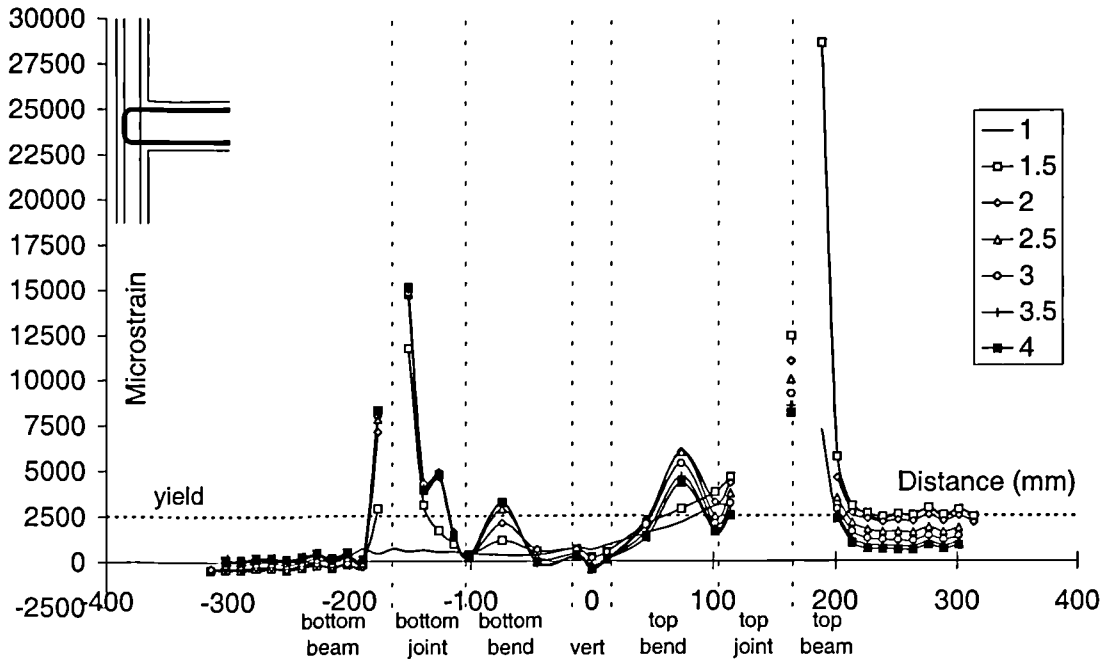

Figure 9.2.2.1.5 Reinforcement strains - downward cycles - C6LH3CY

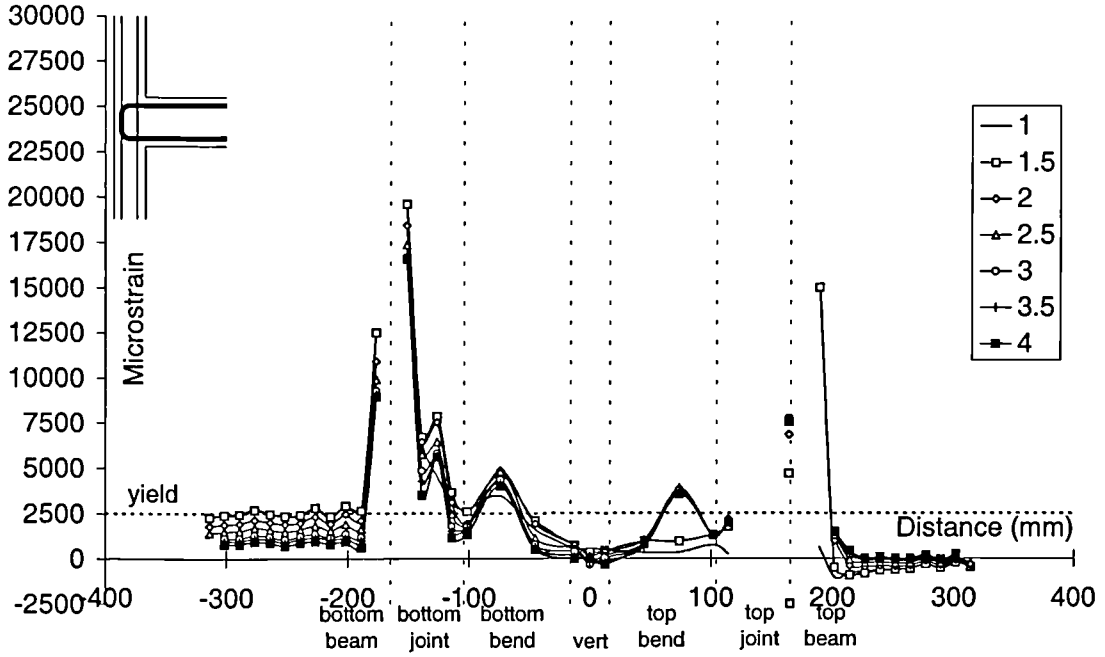

Figure 9.2.2.1.6 Reinforcement strains - upward cycles - C6LH3CY

Figure 9.2.2.2.1(b) displays the average stress present in the middle tie within specimen C4ALH3CY. At a ductility factor of 1.5 all ten of the strain gauges had yielded and the corresponding average stress was 500 MPa. The value recorded for the downward cycles was slightly less at around 470 MPa. By the end of the test this average stress had reduced to around 400 MPa.

Figure 9.2.2.2.1(c) displays the average stress present in the lower tie within specimen C4ALH3CY. As this tie was in the lower region of the joint the stress recorded as a result of downward cycling was not very significant. For the first two upward cycles the peak stress within the tie was 500 MPa. However, by a ductility factor of 2.0 this value had reduced steadily to around 300 MPa.

C6LH3CY

Figure 9.2.2.2.2(a) displays the average stress present in the upper tie within specimen C6LH3CY. As the tie was positioned in the upper region of the joint the stresses were highest for the downward load cycles. Similarly to C4ALH3CY the peak stress was recorded at a ductility factor of 1.5. This corresponded to the last cycle which was controlled by beam flexural effects. The maximum stress was around 370 MPa which reduced to 50 MPa by the end of the test. This low value was due to the extensive cracking of the joint at this stage of the test.

Figure 9.2.2.2.2(b) displays the average stress present in the middle tie within specimen C6LH3CY. Again as, this tie was in the middle of the joint the stress values were similar for both the upward and the downward cycles. The maximum stress was around 450 MPa which reduced to less than 200 MPa by the end of the test.

Figure 9.2.2.2.2(c) displays the average stress present in the lower tie within specimen C6LH3CY. The peak stresses for this tie were for the upward load cycles due to its position in the lower joint. The maximum average stress was around 400 MPa at a ductility factor of 1.0. This had reduced to less than 150 MPa by the end of the test.

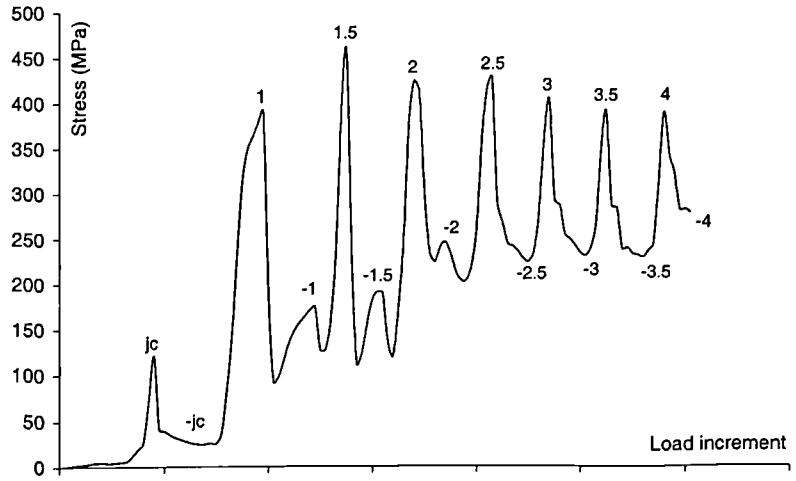

Figure 9.2.2.2.1(a) Average tie stresses - C4ALH3CY (upper tie)

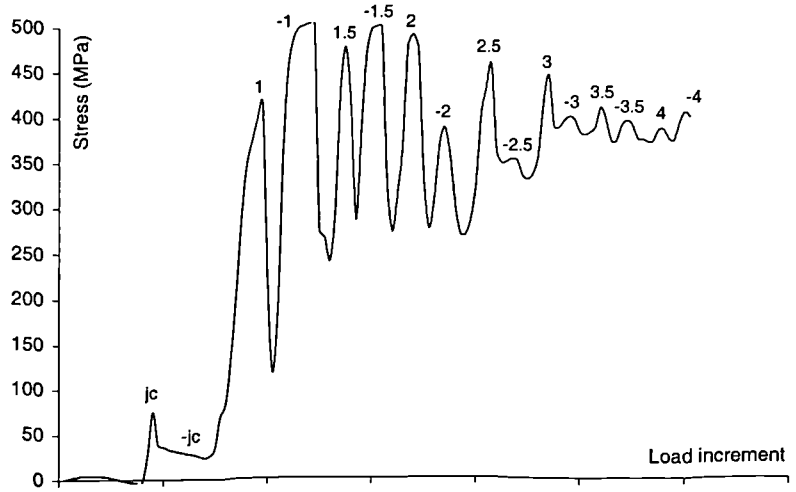

Figure 9.2.2.2.1(b) Average tie stresses - C4ALH3CY (middle tie)

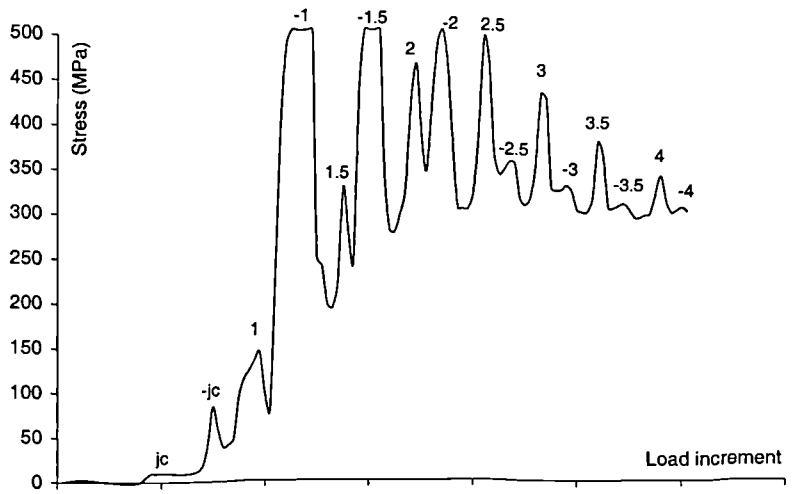

Figure 9.2.2.2.1(c) Average tie stresses - C4ALH3CY (lower tie)

The strain distributions followed a similar trend for both specimen C4ALH3CY and C6LH3CY. The magnitude of the stress continued to rise if the cycles were controlled by beam flexural behaviour. This was because the joint was still reasonably intact and the concrete-steel bond was therefore still good. Once joint failure had occurred then extensive cracking of the concrete led to this bond being lost.

Throughout the cyclic tests joint ties in the upper joint underwent greater stress during the downward cycles, joint ties in the lower joint underwent greater stress during the upward cycles.

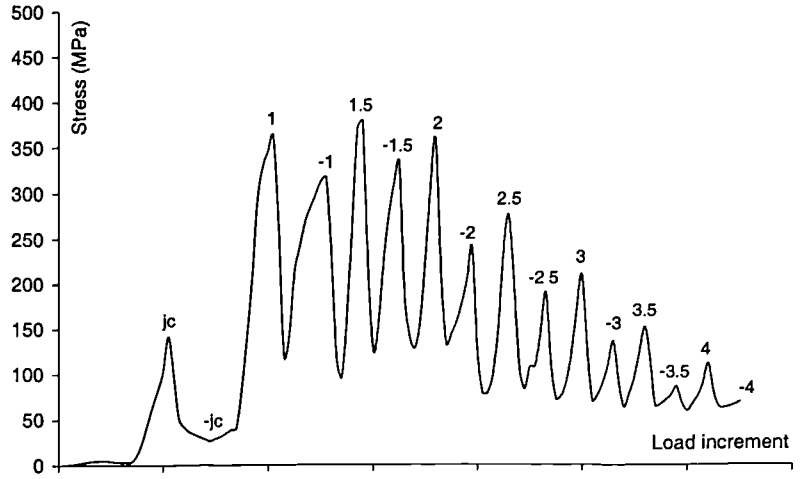

Figure 9.2.2.2.2(a) Average tie stresses - C6LH3CY (upper tie)

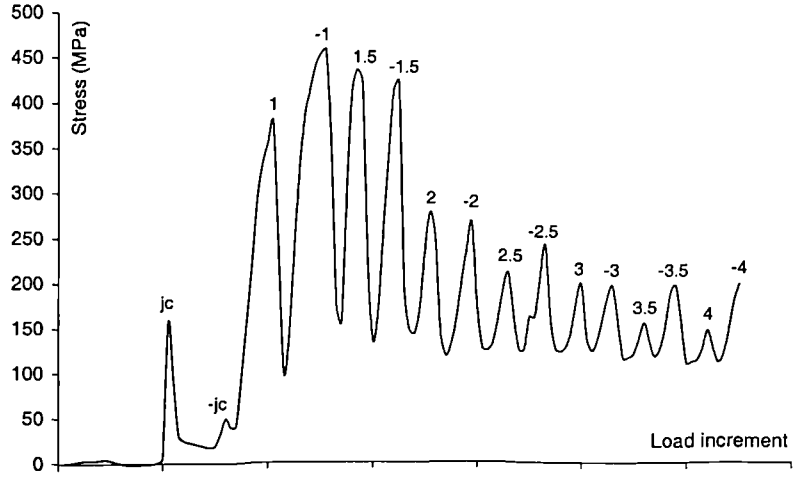

Figure 9.2.2.2.2(b) Average tie stresses - C6LH3CY (middle tie)

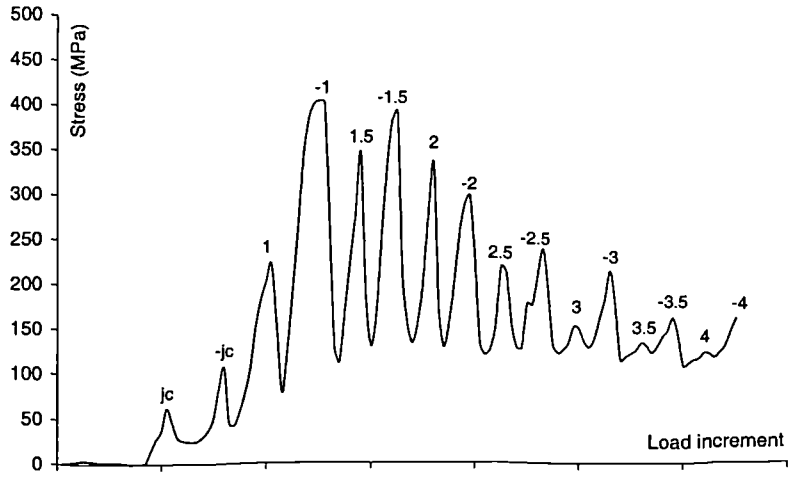

Figure 9.2.2.2.2(c) Average tie stresses - C6LH3CY (lower tie)

9.3 Specimens Investigating Shear Plates

This section considers the cyclic performance of both specimens containing joint shear plates. The monotonic performance of these specimens was discussed previously in Section 4.6.4. After monotonic testing these specimens were then cyclically tested. Diagrammatic representations of both specimens were displayed previously in Figures 2.1.3.3(a)-(b).

9.3.1 Specimen behaviour

Photographs within this section are of the specimens at ductility factors of 1.0, 2.0 and 3.0. Due to the symmetrical nature of the specimens loading in the downward direction only is considered.

C6LNP4

Figure 9.3.1.1(a) shows a photograph of specimen C6LNP4 at a ductility factor of 1.0. The ultimate joint capacity of this specimen corresponded to an applied load of 38 kN. Diagonal cracking was clearly visible within the joint but the beam was relatively uncracked.

Figure 9.3.1.1(b) shows a photograph of specimen C6LNP4 at a ductility factor of 2.0. The cracking of the joint was more extensive by this stage. A horizontal crack due to bond failure of the top region of the U-bar was clearly visible. The joint capacity had reduced by around 30%.

Figure 9.3.1.1(c) shows a photograph of specimen C6LNP4 at a ductility factor of 3.0. A significant amount of concrete cover from the joint region had broken off by this stage of the test. The joint capacity had reduced to less than 50% of its original strength.

C6PLNP4

Figure 9.3.1.2(a) shows a photograph of specimen C6PLNP4 at a ductility factor of 1.0. This specimen had failed due to a large diagonal crack within its joint. Although the failure load was 48 kN the beam was still relatively uncracked. Beam flexural failure had not occurred because the shear plate extended a distance of 100 mm into the beam giving an increased flexural strength.

Figure 9.3.1.2(b) shows a photograph of specimen C6PLNP4 at a ductility factor of 2.0. Several large shear cracks were visible by this stage. A large horizontal crack at the level of the upper beam rebar was evidence of bond failure. The load capacity of the joint was still high at a value corresponding to an applied beam load of 43 kN. This high value was believed to be due to the cycles being controlled by the yielding of the shear plate along its diagonal and not the brittle failure of the concrete.

Figure 9.3.1.2(c) shows a photograph of specimen C6PLNP4 at a ductility factor of 3.0. The majority of the concrete cover had now broken away from the joint exposing the column steel and the bearing plate. The load capacity by this stage of the test was now significantly reduced. This failure was believed to be due to the edge of the shear plate destroying the concrete in the upper and lower column above and below the joint.

Figure 9.3.1.3 displays evidence of this failure within C6PLNP4. By the end of the test, the concrete cover from the joint had broken off but the joint concrete in contact with the steel plate was still intact. The plate ends within the upper and lower column were visible and the deterioration of the concrete in these regions was apparent.

The initial failure loads of both specimens, C6LNP4 and C6PLNP4, show that shear plates clearly can be used to increase the joint capacity of reinforced concrete

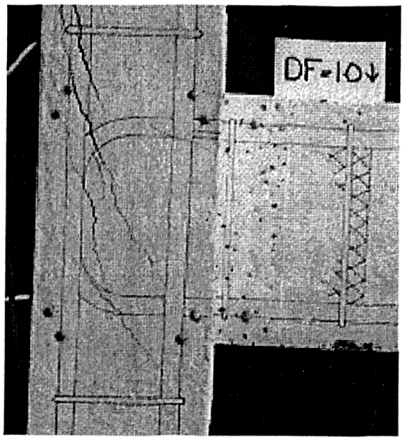

Figure 9.3.1.1(a) D.F. 1.0 ↓ (38 kN)

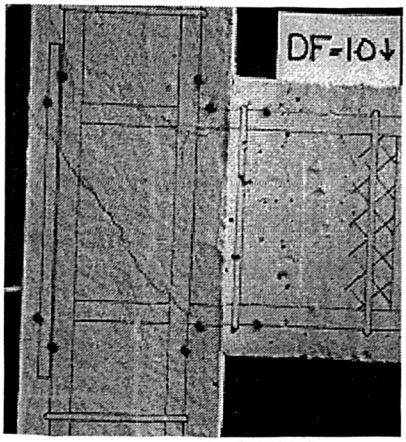

Figure 9.3.1.2(a) D.F. 1.0 ↓ (48 kN)

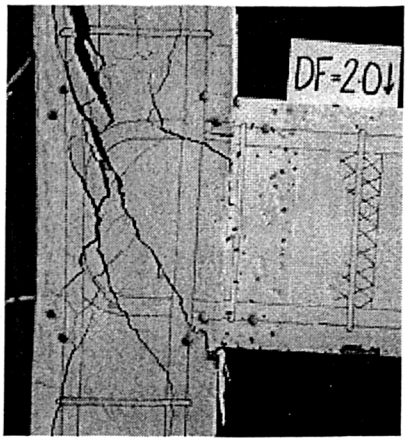

Figure 9.3.1.1(b) D.F. 2.0 ↓ (28 kN)

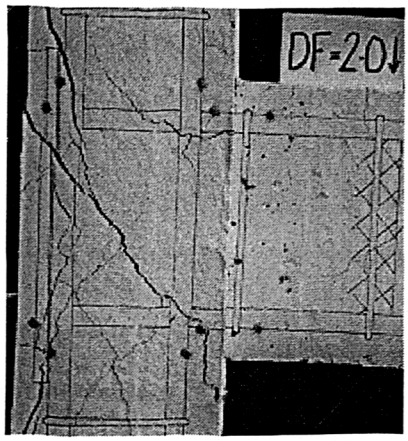

Figure 9.3.1.2(b) D.F. 2.0 ↓ (43 kN)

Figure 9.3.1.1(c) D.F. 3.0 ↓ (17 kN)

Figure 9.3.1.2(c) D.F. 3.0 ↓ (26 kN)

Figures 9.3.1.1(a-c) - C6LNP4 and Figures 9.3.1.2(a-c) - C6PLNP4

beam-column connections. The cyclic response of both test specimens however, suggests that further consideration is necessary to establish the best way of utilising this method.

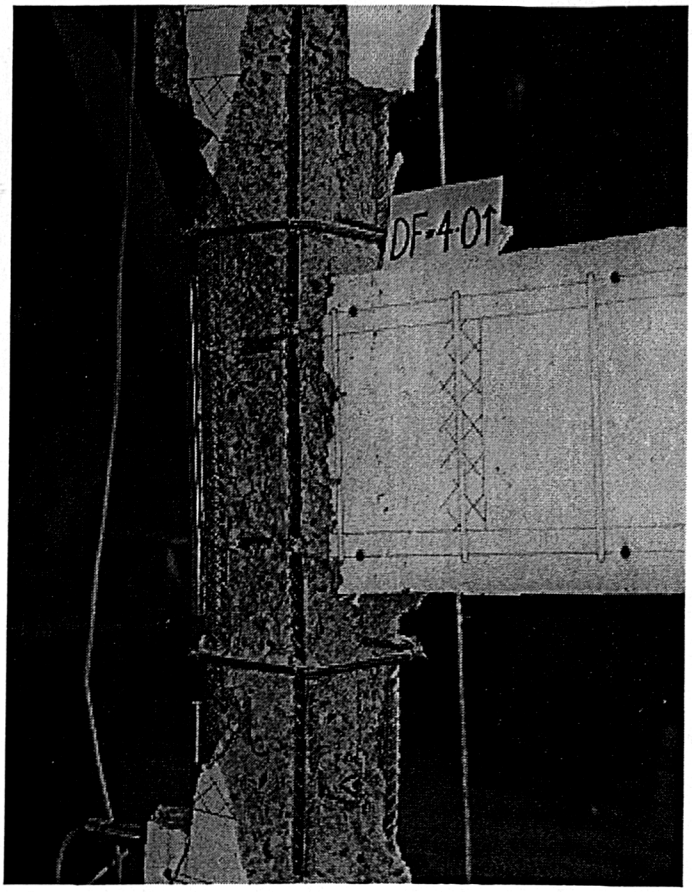

Figure 9.3.1.3 Specimen C6PLNP4 at the end of the test

9.3.2 Load-rotation response

Figure 9.3.2.1(a) displays the load-rotation response for specimen C6LNP4. Figure 9.3.2.1(b) displays the load-rotation response for specimen C6PLNP4. The peak loads for both specimens are displayed in Figure 9.3.2.2. This performance is compared with specimen C6LN7CY from the normal strength cyclic test series and specimen C6LH7CY from the high strength cyclic test series.

D.F.	↓ (kN)	↑ (kN)
1.0	38	34
1.5	33	32
2.0	28	27
2.5	23	23
3.0	17	18
3.5	13	13
4.0	11	10

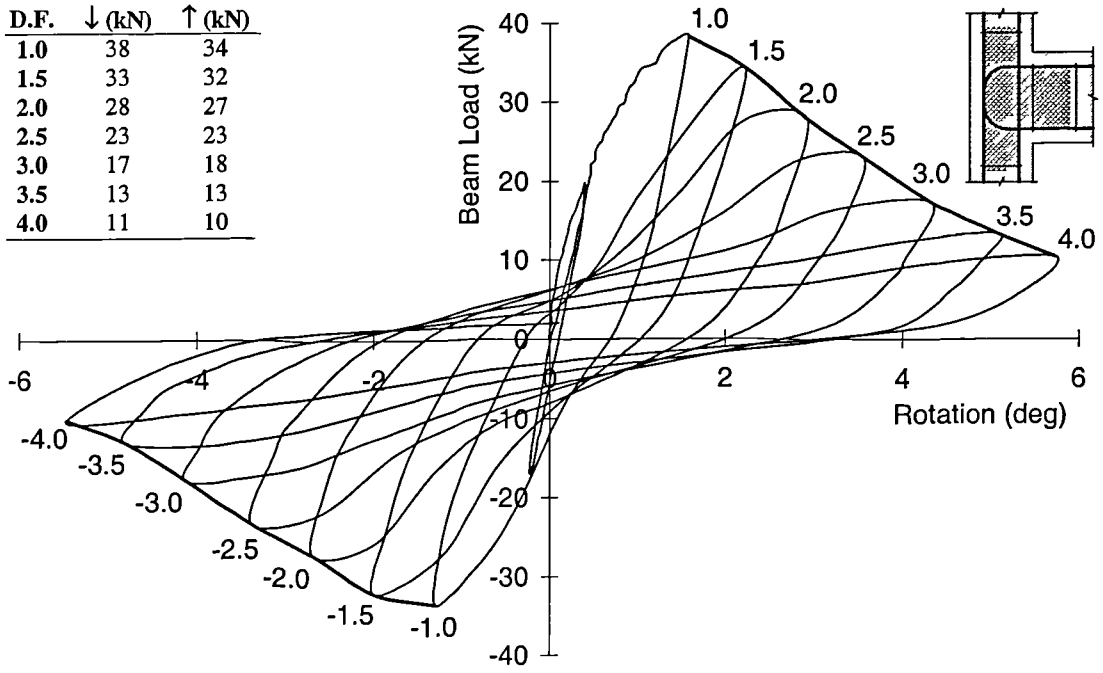

Figure 9.3.2.1(a) Load-rotation response - C6LNP4

D.F.	↓ (kN)	↑ (kN)
1.0	48	45
1.5	46	45
2.0	43	41
2.5	36	32
3.0	24	21
3.5	15	13
4.0	10	9

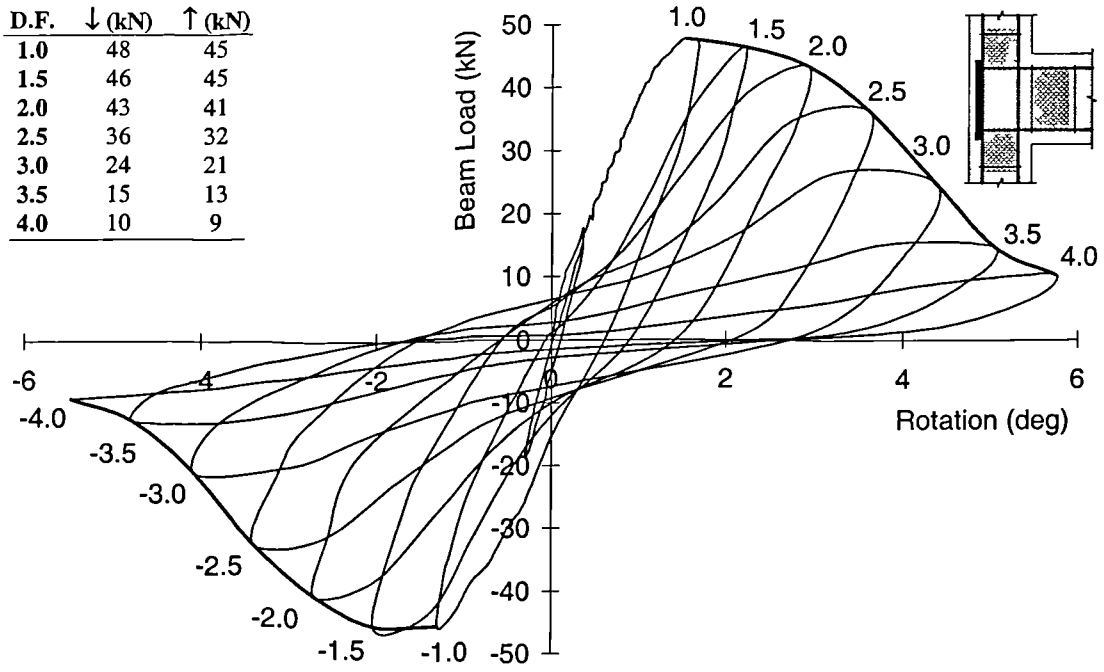

Figure 9.3.2.1(b) Load-rotation response - C6PLNP4

Figure 9.3.2.2 shows that C6LNP4 behaves very similarly to C6LN7CY. Both specimens exhibited joint failure during their first load cycle and then the rate of strength loss was of the same rate.

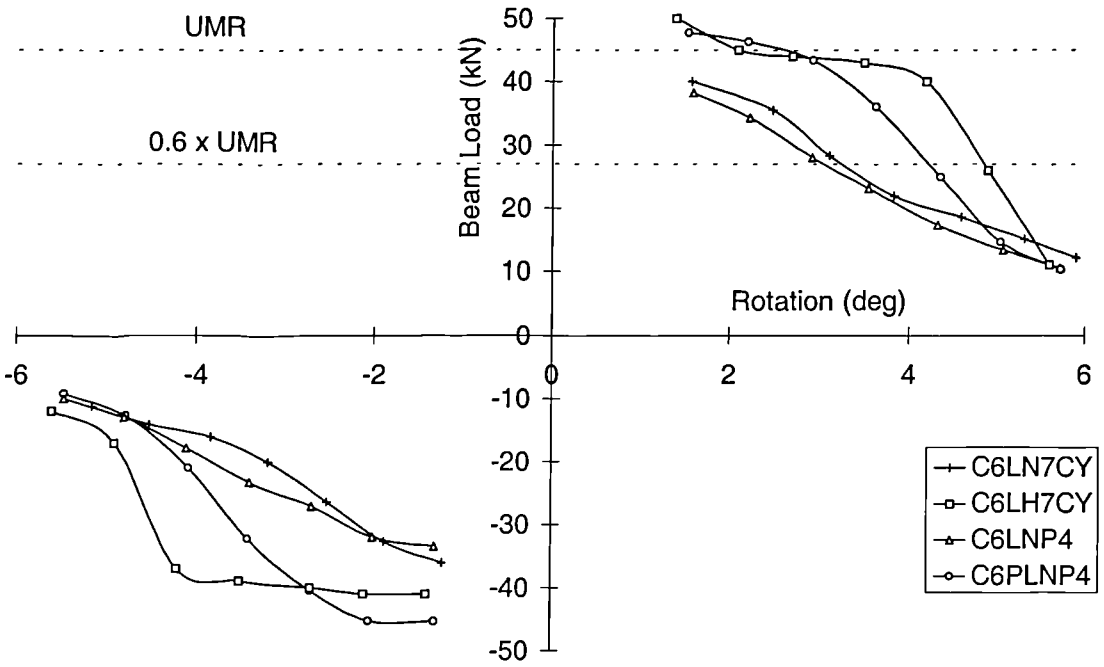

Figure 9.3.2.2 Peak loads and comparisons - plate reinforced joints

Figure 9.3.2.2 shows specimen C6PLNP4 initially behaved similarly to C6LH7CY. During the first three cycles both specimens showed very little reduction in strength. The cyclic capacity of C6LH7CY was controlled by the beam's flexural strength whereas the plate's strength controlled the behaviour of C6PLNP4. However, once the plate edges caused column failure to occur, at a D.F. of 3.0, then C6PLNP4's cyclic strength decayed rapidly.

9.4 Specimens Investigating 2T12 Beam Steel

This section considers the results from the three specimens which had a pair of 12 mm rebars for the beam steel. Diagrammatic representations of these specimens were displayed previously in Section 7.2.2.4.

9.4.1 Specimen behaviour

Photographs within this section are of the specimens at ductility factors of 2.0, 3.0 and 4.0. Due to the symmetrical nature of the specimens loading in the downward direction only is considered.

C3LN7CY

This section compares the behaviour of specimen C3LN7CY with specimen C6LN7CY from the *standard* test series. Specimen C3LN7CY had a pair of 12 mm U-bars for the beam steel whereas specimen C6LN7CY had a pair of 16 mm U-bars. This was the only difference between the two specimen details.

The pairs of photographs considered are at ductility factors of 2.0, 3.0 and 4.0. These values were selected in order to show the specimen behaviour towards the end of the test.

Figures 9.4.1.1(a) and 9.4.1.2(a) show photographs of specimens C3LN7CY and C6LN7CY respectively at a ductility factor of 2.0. By this stage of the test specimen C3LN7CY had a slightly higher cyclic strength than C6LN7CY. This was because of the difference in specimen behaviour. C3LN7CY had a joint which was relatively uncracked and had its cycles controlled by the flexural strength of the beam. The joint region of C6LN7CY had failed in shear and thus the relatively higher flexural strength of its beam could not be reached. As outlined previously within this chapter, it is crucial that cyclically designed specimens exhibit flexural behaviour.
Figures 9.4.1.1(b) and 9.4.1.2(b) show photographs of specimens C3LN7CY and C6LN7CY, respectively, at a ductility factors of 3.0. At this late stage of the test

(after five load cycles) the joint region of C3LN7CY was cracked but still intact whereas the same region of C6LN7CY was broken apart. The cyclic capacity of C3LN7CY had dropped slightly but was still over 90% of its original strength. The cyclic capacity of C6LN7CY had dropped significantly and was now less than 50% of its original strength.

Figures 9.4.1.1(c) and 9.4.1.2(c) show photographs of specimens C3LN7CY and C6LN7CY respectively at a ductility factor of 4.0. C3LN7CY, the specimen with reduced beam steel, still had a cyclic capacity nearly 80% of its original strength. The cyclic capacity of C6LN7CY had now dropped to around 30% of its original strength.

This comparison clearly shows that the joint strength of an external connection should be significantly greater than the beam's flexural strength for seismic design. The fact that specimen C6LN7CY performed worse than specimen C3LN7CY even though it had a significantly higher initial monotonic strength shows the importance of proper seismic design.

The joint of specimen C3LN7CY was clearly starting to show extensive cracking by the end of the test. Previous research [62] had suggested that a beam's plastic hinge at a column face may induce cracking within the joint due to its close proximity.

In an attempt to shift this plastic hinge away from the joint two further specimens were tested. Specimen C3XLN7CY contained an extra pair of U-bars within the beam which were terminated at a distance 100 mm from the column face. Specimen C3HLN7CY was designed with a haunched beam with the same aim of initiating a plastic hinge in the beam 100 mm from the column. The details of both specimens were previously described in Section 7.2.2.4.

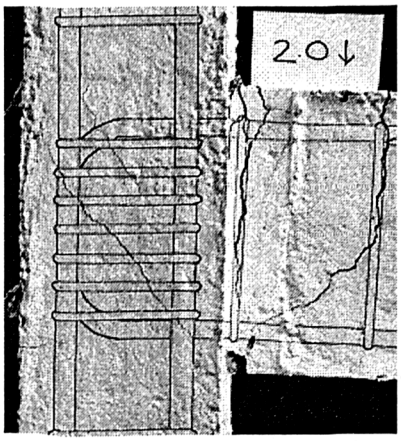

Figure 9.4.1.1(a) D.F. 2.0 ↓ (29 kN)

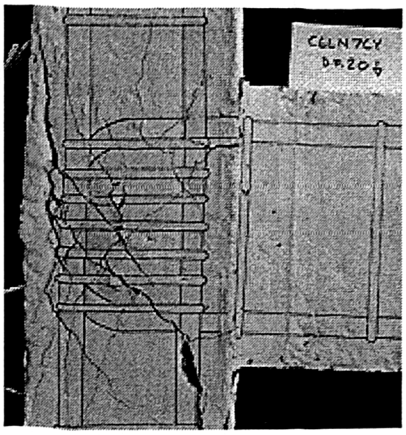

Figure 9.4.1.2(a) D.F. 2.0 ↓ (28 kN)

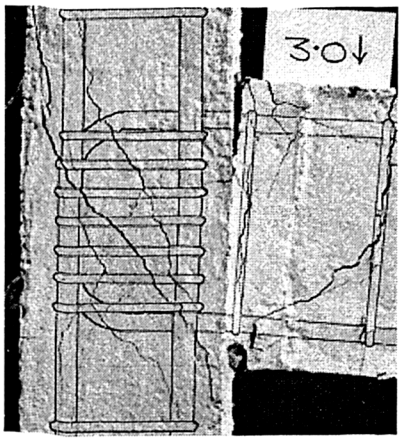

Figure 9.4.1.1(b) D.F. 3.0 ↓ (26 kN)

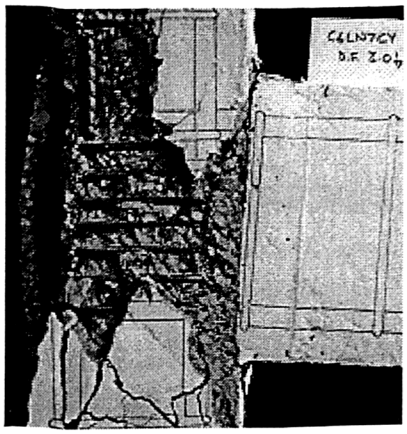

Figure 9.4.1.2(b) D.F. 3.0 ↓ (19 kN)

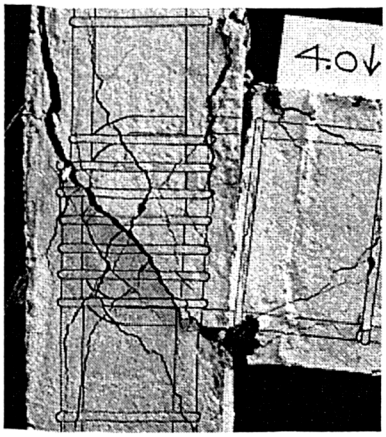

Figure 9.4.1.1(c) D.F. 4.0 ↓ (22 kN)

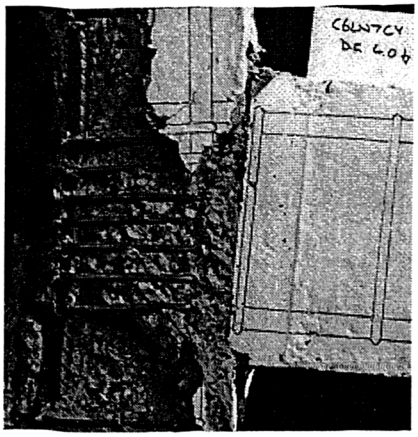

Figure 9.4.1.2(c) D.F. 4.0 ↓ (12 kN)

Figures 9.4.1.1(a-c) - C3LN7CY and Figures 9.4.1.2(a-c) - C6LN7CY

C3XLN7CY

Figure 9.4.1.3(a) shows a photograph of specimen C3XLN7CY at a ductility factor of 2.0. The beam had yielded 100 mm from the column face at the position the additional steel had been terminated. The joint region of C3XLN7CY exhibited one clear shear crack but was still intact.

Figure 9.4.1.3(b) shows a photograph of specimen C3XLN7CY at a ductility factor of 3.0. The plastic hinge region of the beam was severely cracked by this late stage of the test. However, as it was located away from the column face the cracking had not propagated into the joint. The drop in cyclic capacity was still less than 10% after five complete load cycles.

Figure 9.4.1.3(c) shows a photograph of specimen C3XLN7CY at a ductility factor of 4.0. A reasonably large drop in cyclic capacity occurred during this last load cycle. It was believed that the percentage of steel was too high in the first 100 mm of the beam which caused a large amount of the concrete to break away. However, the strength of the specimen was still nearly 70% of its original capacity.

C3HLN7CY

Figure 9.4.1.4(a) shows a photograph of specimen C3HLN7CY at a ductility factor of 2.0. Similarly to C3XLN7CY, specimen C3HLN7CY developed a plastic hinge in its beam at a distance 100 mm from the column face. An advantage of the large joint aspect ratio of this specimen was that no cracking was visible in the joint.

Figure 9.4.1.4(b) shows a photograph of specimen C3HLN7CY at a ductility factor of 3.0. There was more cracking within the hinge area of the beam by this stage of the test but the joint had still not shown any signs of cracking. The cyclic capacity of the specimen was actually higher than the initial strength of the specimen.

Figure 9.4.1.4(c) shows a photograph of specimen C3HLN7CY at a ductility factor

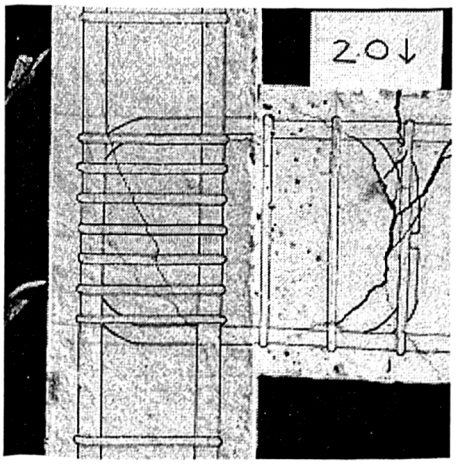

Figure 9.4.1.3(a) D.F. 2.0 ↓ (30 kN)

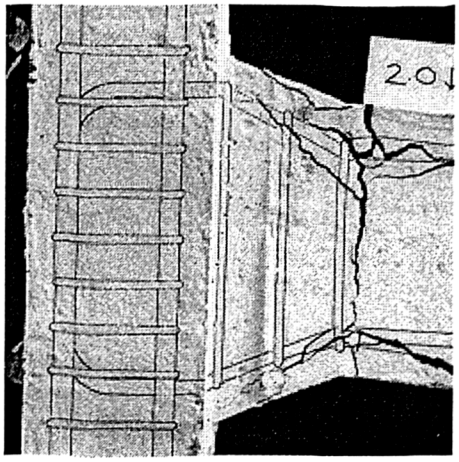

Figure 9.4.1.4(a) D.F. 2.0 ↓ (26 kN)

Figure 9.4.1.3(b) D.F. 3.0 ↓ (27 kN)

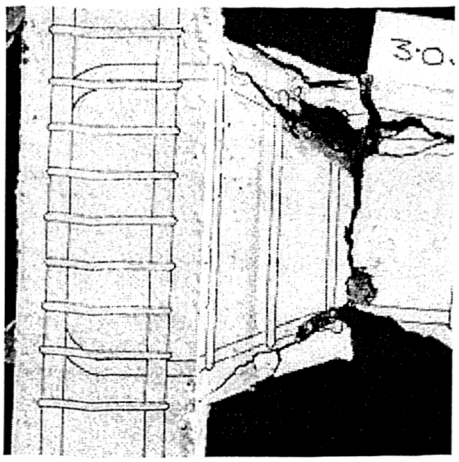

Figure 9.4.1.4(b) D.F. 3.0 ↓ (28 kN)

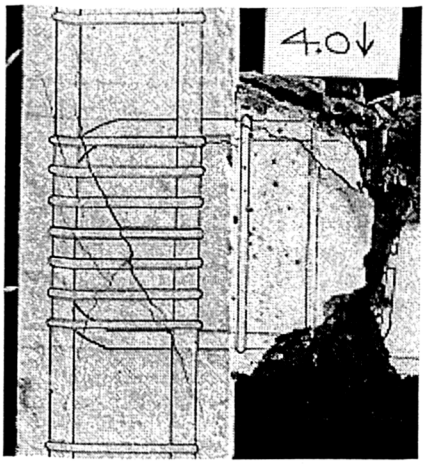

Figure 9.4.1.3(c) D.F. 4.0 ↓ (20 kN)

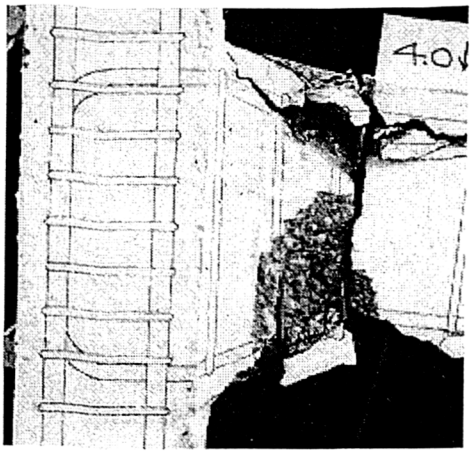

Figure 9.4.1.4(c) D.F. 4.0 ↓ (28 kN)

Figures 9.4.1.3(a-c) - C3XLN7CY and Figures 9.4.1.4(a-c) - C3HLN7CY

of 3.0. By the end of the test the joint was still intact and there were no signs of shear cracking. Although the beam was extensively cracked the specimen's strength was in fact 10% higher than its original capacity. It is believed that, due to the haunch design, the beam lever arm depth actually increased with increasing beam rotations. This allowed the specimen to actually get stronger as the testing progressed.

9.4.2 Load rotation response

The following figures display the load-rotation response from the three specimens using 2T12 beam steel :

Figure 9.4.2.1(a) Specimen C3LN7CY - load-rotation response
Figure 9.4.2.1(b) Specimen C3XLN7CY - load-rotation response
Figure 9.4.2.1(c) Specimen C3HLN7CY - load-rotation response

The peak loads from all three specimens are combined in Figure 9.4.2.2.

Figure 9.4.2.2 shows that all of the specimens which had a pair of 12 mm U-bars for their beam reinforcement performed very well. After seven full load cycles all three specimens had cyclic strengths considerably higher than 60% of their beam's U.M.R.

Specimen C3XLN7CY performed slightly better than C3LN7CY. The ability of C3XLN7CY to develop a plastic hinge away from the joint zone allowed a higher strength to be achieved during the test.

Specimen C3HLN7CY gave the best cyclic performance. The combination of the large joint aspect ratio with the plastic hinge away from the joint allowed no reduction in strength to be seen during the test.

D.F.	↓ (kN)	↑ (kN)
1.0	28	27
1.5	28	27
2.0	29	28
2.5	28	27
3.0	26	26
3.5	23	23
4.0	22	22

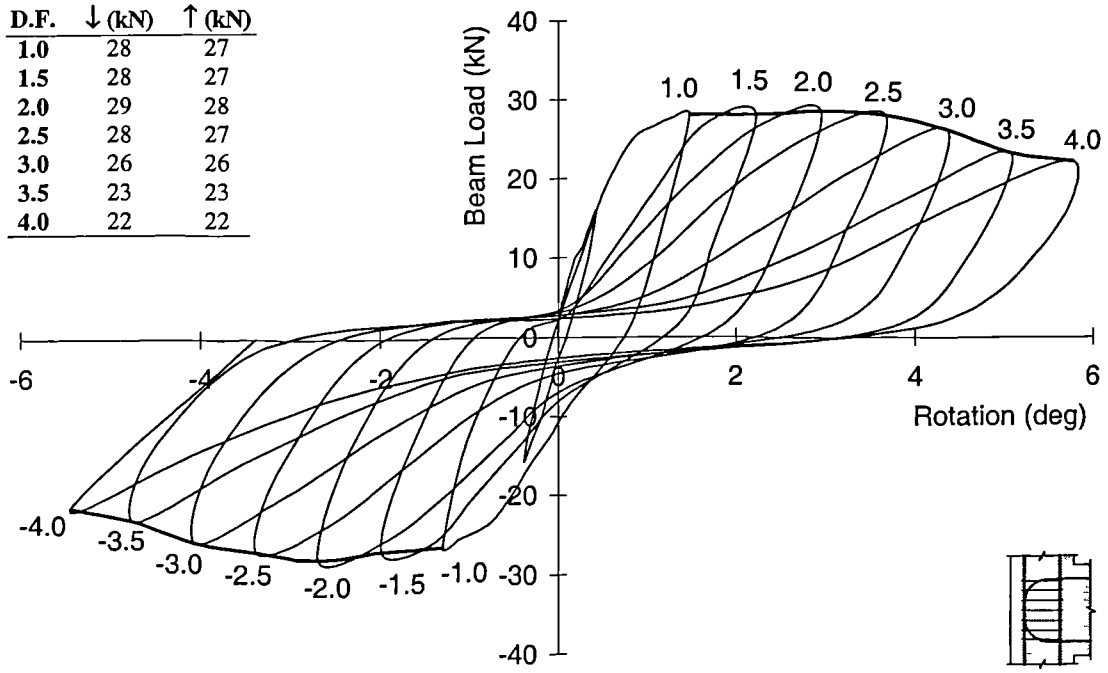

Figure 9.4.2.1(a) Load-rotation response - C3LN7CY

D.F.	↓ (kN)	↑ (kN)
1.0	30	28
1.5	30	29
2.0	30	28
2.5	29	27
3.0	27	26
3.5	26	27
4.0	20	24

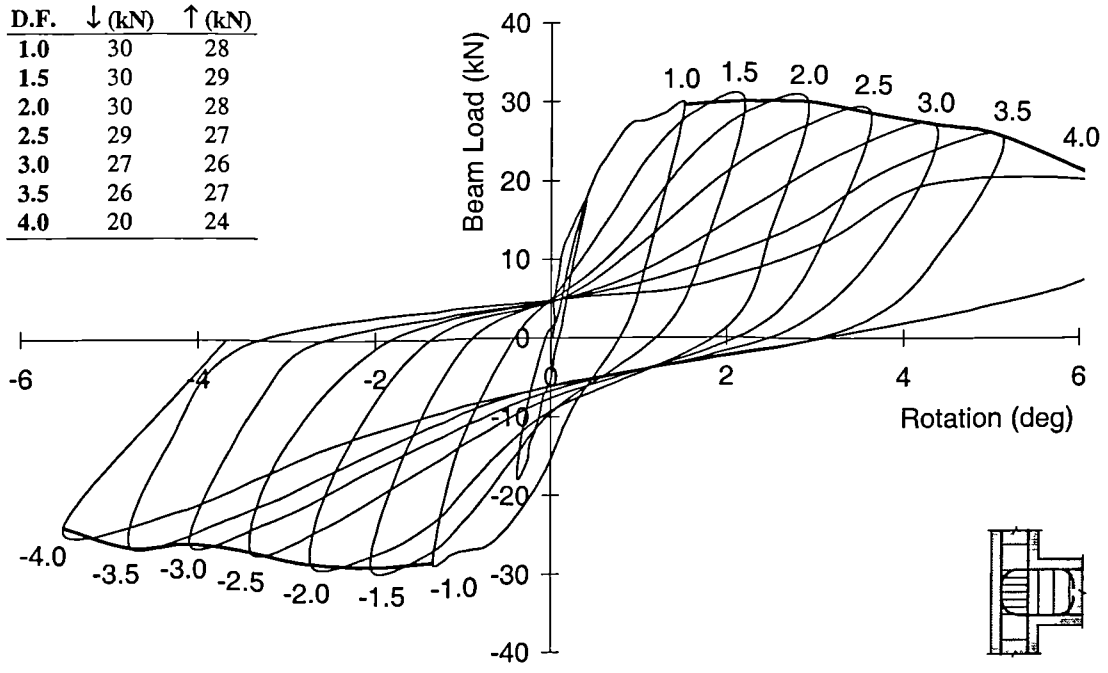

Figure 9.4.2.1(b) Load-rotation response - C3XLN7CY

D.F.	↓ (kN)	↑ (kN)
1.0	25	25
1.5	24	26
2.0	26	27
2.5	27	29
3.0	28	30
3.5	28	31
4.0	28	32

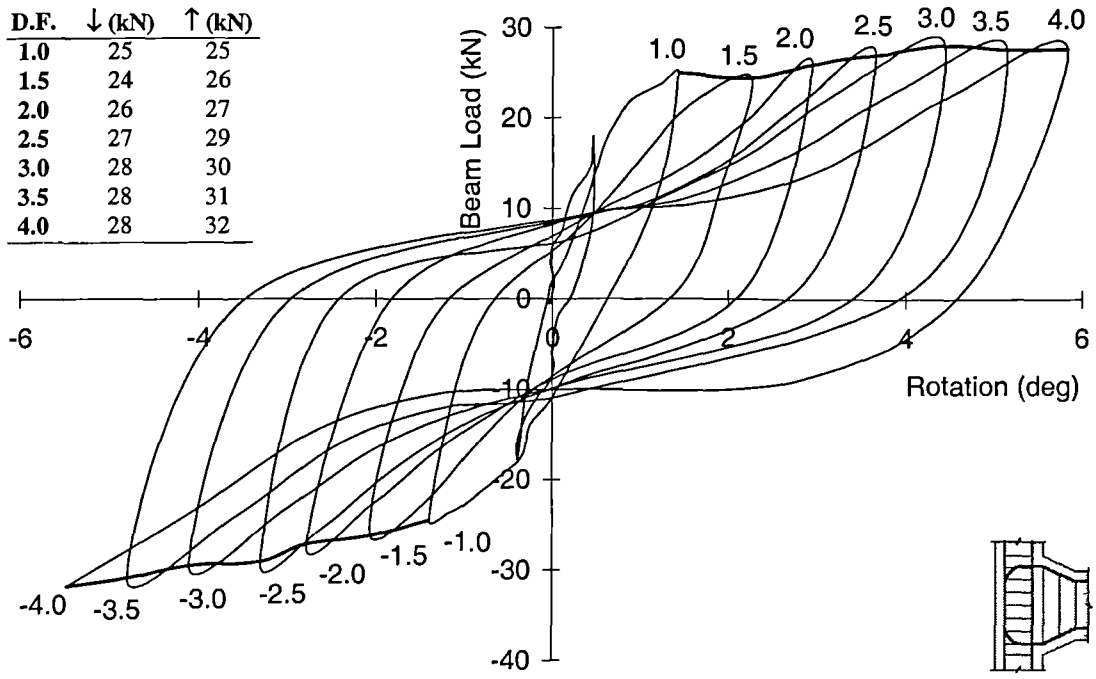

Figure 9.4.2.1(c) Load-rotation response - C3HLN7CY

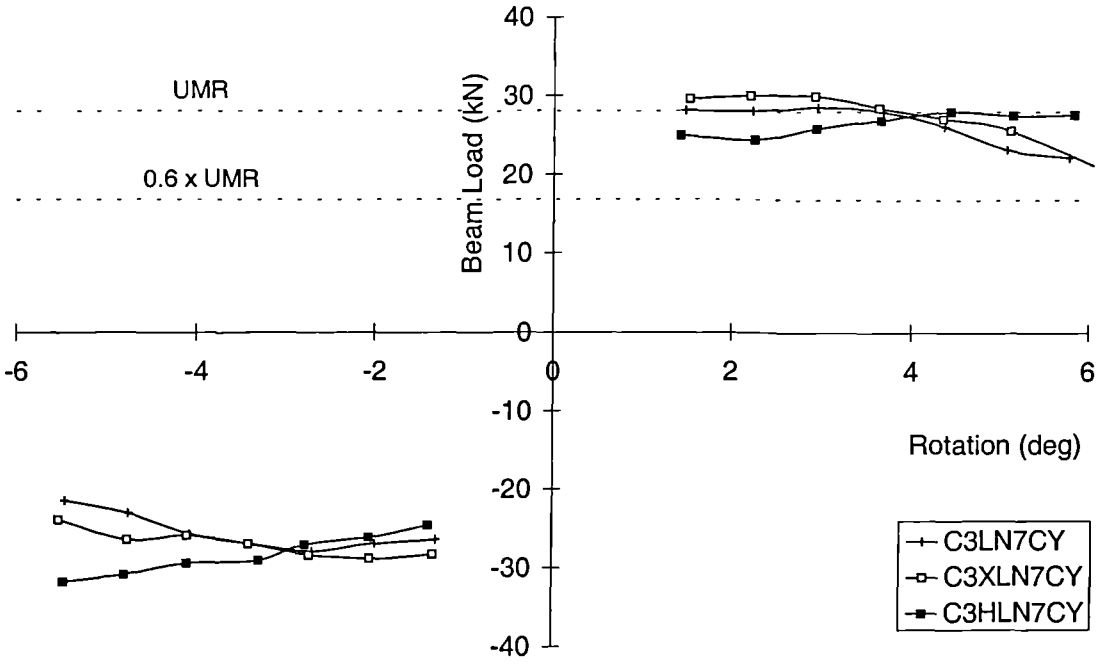

Figure 9.4.2.2 Peak loads - 12 mm beam tension steel

9.5 Additional Specimens

C6LN3CYE

Specimen C6LN3CYE was a repeat of C6LN3CY using joint ties bent through 135° (as shown previously in Figure 7.2.2.4.1). As outlined previously, the three ties within C6LN3CYE's joint all had this improved anchorage.

Within this section, applied loads from both C6LN3CYE and C6LN3CY were converted into normalised shear stresses. This is because both specimens failed in the joint and not in the beam. This allows the influence of concrete strength to be eliminated.

Figure 9.5.1 displays the normalised shear stress-rotation response of specimen C6LN3CYE. Figure 9.5.2 compares the peak shear stresses from both specimen C6LN3CYE and C6LN3CY.

Figure 9.5.2 shows that using ties with legs bent through 135° as opposed to 90° produced an improved cyclic performance. However, the improvement in performance from the use of such ties was small. An enhancement of around 10% was achieved for the downward cycles and only around 5% for the upward cycles.

Section 4.5.5.2 previously demonstrated that an enhancement of 13% in the monotonic capacity of a specimen was possible by using a single tie with these improved anchorage characteristics. This 10% improvement to the cyclic capacity was therefore slightly low considering that five ties had their legs bent through 135°.

The author would suggest that anchoring the tie's legs does not enhance the specimens performance. It is, however, suggested that failure to anchor the legs may weaken the joint due to slippage effects.

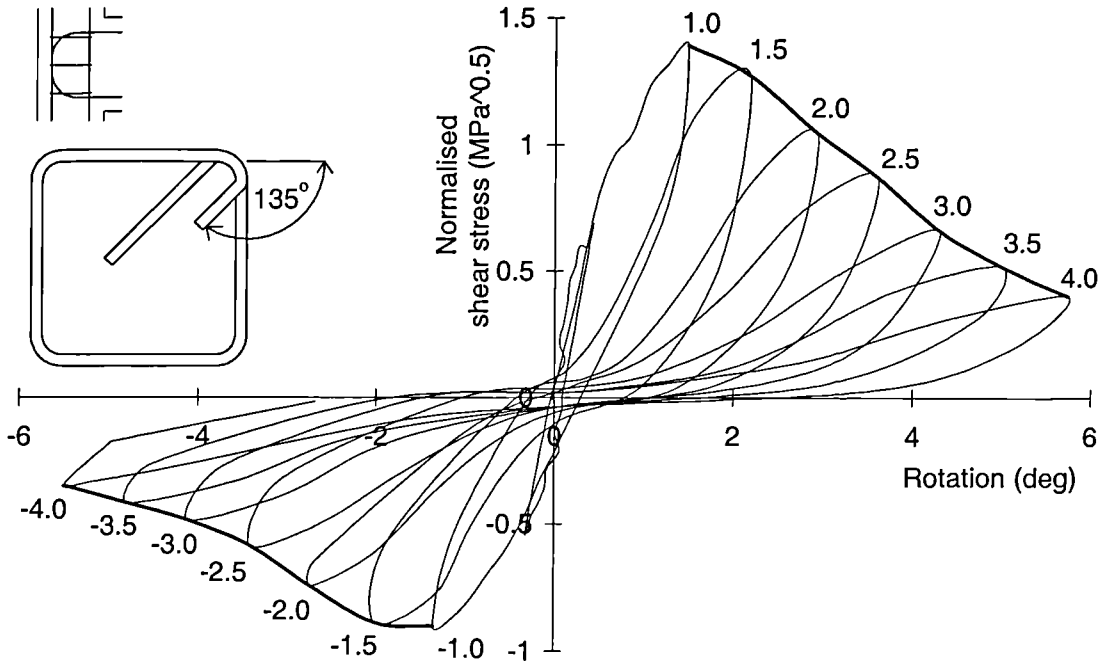

Figure 9.5.1 Load-rotation response - C6LN3CYE

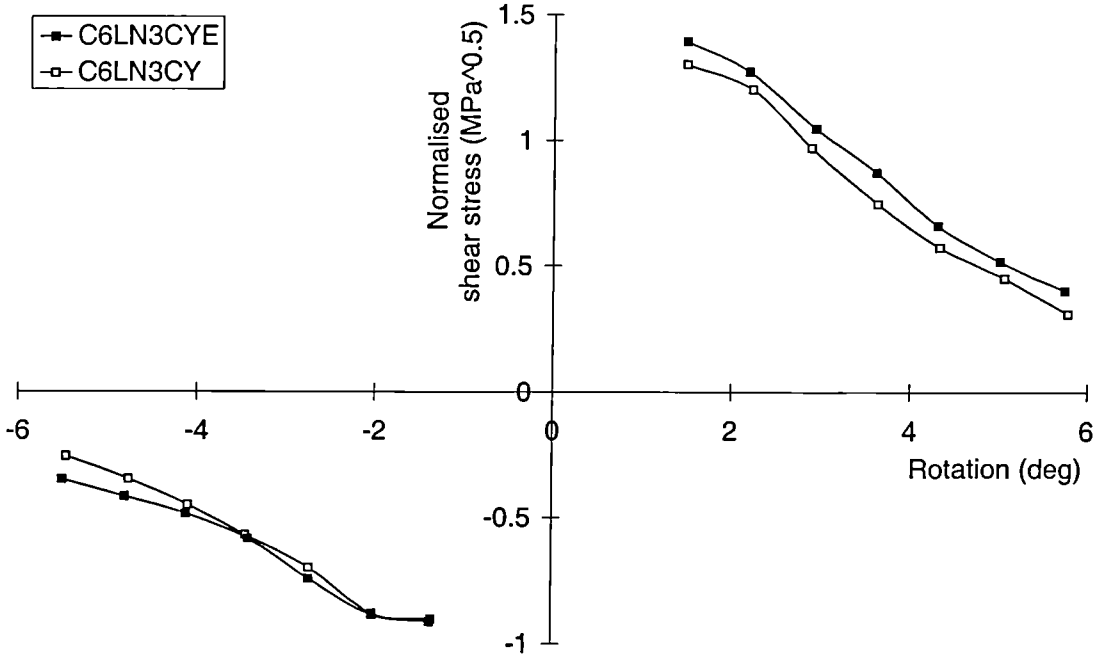

Figure 9.5.2 Peak load comparisons - C6LN3CYE / C6LN3CY

9.6 Review of Cyclic Performance

Table 9.6.1 displays a review of all of the cyclic test results. **The results are displayed in terms of the *cyclic performance criteria* defined previously in Section 7.3.3.**

The test results showing *acceptable* cyclic behaviour are indicated by light grey shading. The test results showing *ideal* cyclic behaviour are indicated by dark grey shading. The test results showing *unacceptable* behaviour are not shaded.

Results are displayed at two stages for each test :

1. **Ductility factor of 2.0** - This was the third full cycle. The overall tilt of the beam, at this stage, was 2.8° to the horizontal.
2. **Ductility factor of 4.0** - This was the seventh, and final, full cycle. The overall tilt of the beam, at this stage, was 5.6° to the horizontal. This was a considerable displacement of the structure.

The results show that, by a ductility factor of 2.0, the **standard specimens** were not, generally, displaying an acceptable cyclic performance. In addition to this, the specimens with beam steel bent down into the column had effectively no strength in the upwards direction.

By a ductility factor of 4.0, all standard specimens were displaying unacceptable cyclic behaviour.

By a ductility factor of 2.0, the **high strength specimens** were, generally, still displaying an acceptable cyclic performance. Again, however, the specimens with beam steel bent down into the column were not displaying acceptable behaviour when loaded in the upward direction.

Table 9.6.1 Review of all cyclic test results (as a percentage of beam UMR)

	D.F. = 2.0		D.F. = 4.0	
	Down ↓	Up ↑	Down ↓	Up ↑
Standard specimens (cyclic)				
C4ALN1CY	38	12	13	6
C4ALN3CY	50	12	16	-
C4ALN5CY	80	8	38	2
C4ALN7CY	88	9	39	8
C6LN1CY	40	37	14	12
C6LN3CY	51	43	17	15
C6LN5CY	54	50	22	25
C6LN7CY	63	59	27	25
High strength specimens (cyclic)				
C4ALH1CY	66	9	16	7
C4ALH3CY	99	10	32	6
C4ALH5CY	101	56	28	44
C4ALH7CY	97	56	40	50
C6LH1CY	70	62	15	27
C6LH3CY	77	63	12	22
C6LH5CY	91	90	-	-
C6LH7CY	98	89	24	27
Specimens investigating shear plates				
C6LNP4	62	60	23	22
C6PLNP4	96	90	23	21
Specimens investigating 2T12 beam steel				
C3LN7CY	102	100	79	77
C3XLN7CY	107	101	70	85
C3HLN7CY	93	97	99	114

Notes

over 100 - Ideal specimen performance

60 to 100 - Acceptable specimen performance

less than 60 - Unacceptable specimen performance

By a ductility factor of 4.0, all high strength specimens were displaying unacceptable cyclic behaviour.

By a ductility factor of 2.0, the **specimens investigating shear plates** were all still displaying an acceptable cyclic performance. However, by a ductility factor of 4.0, the cyclic behaviour had become unacceptable.

The **specimens using 2T12 beam steel** performed best. By a ductility factor of 2.0, all were still displaying almost ideal cyclic performance. By a ductility factor of 4.0, the cyclic performance was still acceptable.

This review of the cyclic tests strengthens the following findings :

1. Increasing the amount of steel within the joint zone (by the use of joint ties or shear plates) improves a connection's cyclic performance.

2. Limiting the amount of tension steel within the beam improves the connection's cyclic performance.

3. When considering the cyclic performance of a connection, anchorage of the steel in the upper beam and lower beam is crucial. Within this investigation, all specimens with bent down bars in the upper beam and straight bars in the lower beam displayed an unacceptable cyclic performance.

It should be noted that a beam-column connection may exhibit excellent behaviour when loaded in the downward direction but rapidly deteriorate if loaded in the upward direction. This is of relevance to a monotonically designed building as it may display an unacceptable performance in the event of an earthquake. There are particular worries regarding this on both the East Coast of the USA and in developing countries around the world.

10. Conclusions

The following conclusions are taken from the results presented within this thesis. Seventy reinforced concrete external beam-column connection specimens were tested and over three hundred finite element modelling runs took place.

The conclusions are split into three main sections :

10.1 Conclusions from the Monotonic Test Programme
10.2 Conclusions from the Finite Element Analysis
10.3 Conclusions from the Cyclic Test Programme

Joint shear stresses are referred to throughout these conclusions. These were calculated using the methods outlined previously in Section 1.3. The influence of concrete strength on the joint shear stress was *normalised* by dividing the value of joint shear stress by the square root of the compressive cylinder strength.

10.1 Conclusions from the Monotonic Test Programme

10.1.1 INITIAL JOINT CRACKING CAPACITY

10.1.1.1 The value of normalised shear stress at initial joint cracking was not influenced by the quantity or positioning of joint ties.

10.1.1.2 The value of normalised shear stress at initial joint cracking was not influenced by the use of high strength concrete.

10.1.1.3 The value of normalised shear stress at initial joint cracking was not influenced by the joint aspect ratio.

10.1.1.4 The author recommends the use of BS 8110 equation 6b [3] when it is necessary to avoid shear cracking prior to the ultimate limit state :

$$v_c' = v_c \sqrt{\left(1 + \frac{N}{b_c h_c v_c}\right)} \quad \text{.....(eq. 10.1.1.4 / BS 8110 6b)}$$

where v_c is the design concrete shear stress for a reinforced concrete section (BS 8110 Table 3.9),

N is the column load,

b_c and h_c are the column breadth and height respectively.

10.1.1.1 Increasing the joint capacity at initial cracking

10.1.1.1.1 The value of shear stress at initial joint cracking was increased by the use of fibre reinforced concrete. Using 2.3% of short or long fibres (as defined previously in Section 2.2.2) gave an enhancement of around 50% to the joint capacity.

10.1.1.1.2 The value of shear stress at initial joint cracking was increased by the use of steel shear plates within the joint. The use of a 4 mm steel deformed plate (as defined previously in Section 2.1) gave an enhancement of around 25% to the joint capacity.

10.1.2 ULTIMATE JOINT CAPACITY

10.1.2.1 The ultimate shear capacity of a joint, without shear reinforcement, under a *low column load**, was found to be directly proportional to the square root of its compressive cylinder strength.

$$v_{ult} = \sqrt{f_{ck}} \quad \text{.....(eq. 10.1.2.1)}$$

where the compressive cylinder strength is related to the compressive cube strength by the following expression, $f_{ck} = 0.8 \times f_{cu}$ [17],

* the *low column load* within this investigation produced an axial stress in the column of 2.2 MPa or less.

This expression was also valid for high strength concrete (up to f_{ck} = 100 MPa).

10.1.2.2 The use of U-bar beam steel anchorage was found to reduce the ultimate shear capacity by a value of up to 17%. This was due to the U-bar transferring all of the beam's load into the joint region. The maximum bond stress at failure was located around the top bend of the U-bar. This value was an average of around 8 MPa for normal strength concrete. An average bond stress of over 12 MPa was achieved over this same region for high strength specimens.

10.1.2.3 Using bent down steel detail for the beam tension steel allowed the full capacity of the joint to be reached. The anchor leg transferred a large proportion of the beam's load into the lower column region. This value of bond stress at failure was significantly lower than for the U-bar steel at around 3 MPa.

10.1.2.4 The experimental specimens with a joint aspect ratio of 2.0 failed at a shear stress 15% lower than the value predicted by equation 10.1.2.1. This was believed to be due to slenderness effects within the joint core.

10.1.2.5 The two reduction effects highlighted in 10.1.2.2 and 10.1.2.4 should be incorporated into equation 10.1.2.1. This gives the following empirical expression for the evaluation of the ultimate joint capacity.

$$v_{ult} = \alpha\beta\sqrt{f_{ck}} \quad \text{.....(eq. 10.1.2.4)}$$

where α is a reduction factor, $\alpha = 1$ for bent down beam steel,

$\alpha = 0.83$ for U-bar beam steel,

β is a reduction factor, $\beta = 0.25\left(5.4 - \frac{h_b}{h_c}\right)$,

h_b is the total depth of the beam,

h_c is the total depth of the column,

for specimens where $1.4 < h_b/h_c < 2.0$.

10.1.2.1 Increasing the ultimate joint capacity

10.1.2.1.1 The ultimate joint capacity was significantly enhanced through the use of joint ties. The placement of joint ties around the centre of the joint was found to increase the shear capacity of the concrete.

10.1.2.1.2 The placement of joint ties around the level of beam tension steel reduced the risk of anchorage induced joint failure by giving confinement to the concrete beneath the top bend of this rebar.

10.1.2.1.3 Within this investigation the placement of a single tie ($Aj/d_cb_c = 0.4\%$), in the top half of the joint below the level of beam tension steel, gave a joint enhancement of around 25%. The placement of three ties ($Aj/d_cb_c = 1.1\%$), in the top half of the joint below the level of beam tension steel, gave a joint enhancement of around 50%.

(where Aj is the joint steel cross sectional area,

d_c is the depth of the column and b_c is the width of the column).

10.1.2.1.4 Using joint ties which were not fully anchored resulted in a reduction in joint shear capacity of 10% due to slippage of the tie legs. To allow the full capacity of the joint to develop it was necessary to bend the free ends of the tie legs through at least 135°.

10.1.2.1.5 The ultimate joint capacity was significantly increased through the use of fibre reinforced concrete. Using 1.5% of short or long fibres (as defined previously in Section 2.2.2) gave an enhancement of over 40% to the joint capacity. Using 2.3% of short or long fibres gave an enhancement of over 65% to the joint capacity.

10.1.2.1.6 The ultimate joint capacity was significantly increased through the use of steel shear plates. Using a 4 mm steel deformed plate (as defined previously in Section 2.1) within a U-bar beam steel arrangement gave an enhancement of around 100% to the joint capacity.

10.2 Conclusions from the Finite Element Analysis

10.2.1 General modelling

10.2.1.1 A standard finite element mesh was proposed for use in beam-column connection design. Guidance was also proposed for the generation of the concrete and steel properties. Both normal and high strength concrete (as defined previously in Section 2.2.2) were considered. Guidance was also given on the placement of the steel layout for optimum performance.

10.2.1.2 The viability of both the finite element package and the mesh refinement technique was demonstrated by the successful modelling of simple problems with known solutions.

10.2.1.3 The standard finite element mesh design was shown to demonstrate four different failure mechanisms : flexural failure of both the beam and the column; and joint failure due to both shear effects and also those induced by beam anchorage slippage.

10.2.1.4 The eight standard, normal strength specimens from the experimental test series were modelled. The modelled failure loads showed excellent correlation with the experimental results. The mean average of the accuracy ($failure_{model}/failure_{test}$) was 1.01 and the variation coefficient was 8.1%.

10.2.1.5 The eight standard, high strength, specimens from the experimental test series were modelled. The modelled failure loads showed excellent correlation with the experimental results. The mean average of the accuracy was 0.99 and the variation coefficient was 4.3%.

10.2.1.6 Strain values from the reinforcing bars within the experimental specimens were modelled for both the normal and high strength specimens. The correlation was excellent for the main column and beam steel.

10.2.1.7 The modelling of the tie strains and the beam steel anchorage approaching failure was less accurate. This was due to the extensive crushing and cracking of the concrete elements within the joint.

10.2.1.8 The eight specimens investigating joint aspect ratio from the experimental test series were modelled. The modelled failure loads showed good correlation with the experimental results. The mean average of the accuracy was 0.88 and the variation coefficient was 7.1%.

10.2.1.9 Load-deflection comparisons were generally good for all of the modelled test series. However, the modelled response after initial joint cracking was slightly stiff.

10.2.1.10 The standard mesh design gave a good *lower bound* prediction for the initial joint cracking capacity for all of the modelled test series.

10.2.1.11 The same mesh design was adapted to model the seven test specimens by Reys de Ortiz [10] and the twelve test specimens by Parker [11]. Both modelled failure loads showed good correlation with the experimental results. For Reys de Ortiz's specimens the mean average of the accuracy was 0.90 and the variation coefficient was 7.5%. For Parker's specimens the mean average of the accuracy was 1.15 and the variation coefficient was 8.4%.

10.2.2 Parametric study

10.2.2.1 The influence of concrete strength on a beam-column joint was considered using sixty models of three different sizes. The ultimate shear capacity of a joint was found to be equal to the square root of its compressive cylinder strength.

$$v_{ult} = \sqrt{f_{ck}} \quad \text{.....(eq. 10.2.2.1)}$$

where the same conditions applied as previously with equation 10.1.2.1

10.2.2.2 The influence of column axial stress on a beam-column joint was considered using twenty seven models and three different scale factors. The ultimate shear capacity was found to be enhanced by around 40% when subjected to an axial stress of 20 MPa. Prior to a stress of 20 MPa

this relationship was reasonably linear, but this enhancement rapidly reduced with any further increase in axial stress.

10.2.2.3 The influence of joint tie positioning was investigated using seven models with bent down steel detail and seven models with U-bar beam steel detail. The optimum position for joint ties was found to be in the upper two thirds of the joint below the level of the beam tension steel.

10.2.2.4 The influence of beam steel anchorage was investigated using thirty models with two different joint aspect ratios. The use of U-bar beam steel anchorage was found to reduce the ultimate shear capacity by an average value of 18%.

10.2.2.5 The influence of joint aspect ratio was investigated using the results of sixteen models with two different beam steel details. The shear stress at failure reduced by around 25% as the joint aspect ratio increased from 1.4 to 2.0.

10.2.2.6 These enhancement / reduction factors may be incorporated into equation 10.2.2.1. This gives the following empirical expression for the evaluation of the ultimate shear capacity.

$$v_{ult} = \alpha\beta\gamma\sqrt{f_{ck}} \quad \text{.....(eq. 10.2.2.6)}$$

where α is a reduction factor, *(beam anchorage)*

$\alpha = 1$, for bent down beam steel,

$\alpha = 0.82$, for U-bar beam steel,

β is a reduction factor, *(joint aspect ratio)*

$$\beta = 0.42\left(3.8 - \frac{h_b}{h_c}\right),$$

h_b is the total depth of the beam,

h_c is the total depth of the column,

for specimens where $1.4 < h_b/h_c < 2.0$,

γ is an enhancement factor *(column axial stress)*

$$\gamma = 0.02(50 + f_c),$$

f_c is column axial stress,

$f_c < 20$ MPa or $0.4f_{ck}$ whichever is lowest.

Note

The enhancement factor for column axial stress was taken from the results of the modelling study. There have been no experimental tests within this thesis investigating the influence of column axial stress. Doubts were expressed in the Literature Review (Section 1.4.3) over whether column axial stress has any influence over the ultimate joint capacity.

10.3 Conclusions from the Cyclic Test Programme

The following conclusions are based on the cyclic testing methods outlined previously in Section 7.2.1.

10.3.1 Joint failure is undesirable during cyclic loading. Specimens which exhibited joint failure rapidly lost their strength. This behaviour under actual earthquake motions may result in structural collapse.

10.3.2 Joint failure was accompanied by excessive shear cracking of the joint concrete. This resulted in a reduction in bond of the beam tension steel and thus a lower joint capacity. With each subsequent cycle this bond loss increased as the specimen rapidly lost its strength.

10.3.3 The presence of ties raised the ultimate shear capacity of a joint. However, once joint failure occurred the presence of ties did not influence the deterioration rate of its strength.

10.3.4 The use of high strength concrete raised the ultimate shear capacity of a joint. However, once failure occurred the high strength specimens lost their strength more rapidly than their corresponding normal strength specimens.

10.3.5 The 4 mm shear plate within a U-bar steel arrangement (as defined previously in Section 2.1.3) raised the ultimate shear capacity of specimen C6LNP4. However, once failure occurred the presence of this shear plate did not influence the deterioration rate of its strength.

10.3.6 The 4 mm shear plate within the welded steel / anchor plate arrangement (as defined previously in Section 2.1.3) significantly raised the ultimate shear capacity of specimen C6PLNP4.

10.3.7 Specimens which had joints strong enough to allow beam flexural failure to occur exhibited the best behaviour. The yielding of the beam steel allowed the joint to remain largely intact. This allowed the full bond to be developed within the joint for each cycle.

10.3.8 Specimens were observed which failed initially due to beam flexure but then after subsequent cycles failed in the joint due to shear. Once joint failure occurred these specimens lost their strength rapidly.

10.3.9 Specimens designed to initiate beam flexural failure away from the joint face (as outlined previously in Section 7.2.2.4) had reduced deterioration of the joint during cycling. Within this investigation a specimen with a haunched beam was manufactured and tested and this was successful in keeping the joint intact. A specimen with additional beam steel within the joint, terminated 100 mm from the column face, was also manufactured and tested and this was successful in keeping the joint intact.

10.3.10 Structures which may have to resist earthquake motions, very high winds or blast effects should be designed to provide a joint shear strength substantially higher than the beam's flexural strength. Considerations regarding initiating beam flexural failure away from the joint face should also be made.

10.3.11 Structures which may have to resist earthquake motions, very high winds or blast effects should have sufficient steel anchorage for large displacements of the beam in both directions. A beam-column connection may exhibit excellent behaviour when loaded in the downward direction but rapidly deteriorate if loaded in the upward direction. Straight compression bars do not provide an acceptable anchorage length for large displacements in the upwards direction.

11. Recommendations for Further Work

There is a clear need for further tests on monotonically loaded reinforced concrete beam-column connections. It is the author's opinion that further work should be carried out to determine the following :

11.1 ***The influence of column load.*** The literature review proved inconclusive on this issue. The majority of previous research agreed that initial joint cracking strength was enhanced by an increased column load. However, contradictory information exists regarding the influence of column load on the ultimate joint capacity.

11.2 ***The influence of joint aspect ratio.*** Test results have been presented within this investigation and also by Scott [8]. However, the available data on specimens with varying joint aspect ratio is limited.

11.3 ***Beam tension steel behaviour.*** Parker's [11] and Reys de Ortiz's [10] specimens were reasonably similar, however, Parker's specimens failed at a low joint shear strength. Suggestions have been made by Vollum [12] that this may have been due to Parker using large diameter bars at relatively large spacings.

11.4 ***Column longitudinal reinforcement.*** Previous research clearly indicated that the joint capacity at initial cracking was enhanced with an increasing percentage of column longitudinal reinforcement. However, equations presented in previous research do not take this into consideration

11.5 ***Joint shear strengthening techniques.*** A number of techniques were used within this investigation to strengthen the ultimate shear capacity of the joint. Further work is clearly needed to establish recommendations for the use of steel fibres and shear plates within beam-column connections.

11.6 ***The influence of superplasticiser.*** Test results within this investigation have shown that the ultimate joint capacity was increased by over 10% through the addition of superplasticiser to the concrete mix. This increase in strength was not in accordance with the respective concrete compressive or tensile strengths. As a result it may be inferred that the superplasticiser influenced the concrete-steel bond.

11.7 ***Three-dimensional finite element analysis.*** The author believes that a 3-D finite element package should be used to produce an improved beam-column connection model. The inability of a 2-D finite element package to model independent steel movement of rebars within the same concrete element provided limitations. For similar reasons a 3-D package may also improve the accuracy of modelling of joint tie positioning.

References

1. **Taylor, H.P.J.** : 'The behaviour of in situ beam-column joints', Technical Report 42.492, Cement & Concrete Association, May 1974
2. **British Standards Institution. CP 110 : 1972** : The structural use of concrete
3. **BS 8110 Structural use of concrete** : Part 1 : Code of practice for design and construction, London, British Standard Institution, 1985
4. **Ryan, J.** : 'Reinforced concrete beam-column connections', Concrete Magazine, pages 37-39, March 1977
5. **Meinheit D.F. and Jirsa J.O.** : 'The shear strength of reinforced concrete beam-column joints', Austin, University of Texas at Austin, Dept. of Civ Eng., 1977, Report 77-1
6. **Kordina K.** : 'Bewehrungsführung in ecken und rahmenendknoten', Deutscher Ausschuss fur Stahlbeton, Heft 354, 1984, 93pp
7. **Sarsam K.F. and Phipps M.E.** : 'The shear design of in situ reinforced concrete beam-column joints subjected to monotonic loading', Magazine of Concrete Research, Vol 37, No 130, March 1985
8. **Scott R.H.** : 'The effects of detailing on RC beam/column connection behaviour', The Structural Engineer, Vol 70, No 18, 15 September1992, pages 318-324
9. **Scott R.H.** ***et al*** : 'Reinforced concrete beam-column connections and BS 8110', The Structural Engineer, Vol 72, No 4, 15 February 1994, pages 55-60
10. **Reys de Ortiz I.** : 'Strut and tie modelling of reinforced concrete short beams and beam-column joints', PhD thesis, University of Westminster, 1993
11. **Parker D.E.** : 'Shear strength within reinforced concrete beam-column joints', PhD thesis, Bolton Institute of Higher Education, 1997
12. **Vollum R.L.** : 'Design and analysis of reinforced concrete beam-column joints', PhD thesis, Imperial College, London, 1998
13. **Vollum R.L. and Newman J.B.** : 'The design of external, reinforced concrete beam-column joints', The Structural Engineer, Volume 77, Numbers 23 & 24, 7 December 1999, pages 21-27
14. **Abrams D.P.** : 'Scale relations for reinforced concrete beam-column joints', ACI Structural Journal, November-December 1987, pages 502-512

15. **ACI** : 'ACI-318-89 (revised 1992) : Building code requirements for reinforced concrete', American Concrete Institute, Detroit, 1992
16. **CEB-FIP** : 'Model code for concrete structures', CEB-FIP international recommendations, 1990
17. **EC2** : 'Design of concrete structures, Part 1, General rules and rules for buildings', DD ENV 1992-1-1 : 1992
18. **Bonacci, J. and Pantazopoulou, S.** : 'Parametric investigation of joint mechanics', ACI Structural Journal, January-February 1993, pages 61-71
19. **I. Struct. E. / ICE Joint Committee** : 'Manual for the design of concrete building structures', Institution of Structural Engineers, London, 1985
20. **ACI-ASCE Committee 352** : 'Recommendations for the design of beam-column joints in monolithic reinforced concrete structures', ACI Journal, Proceedings V. 82, No. 3, May-June 1985, pages 266-283
21. **Architectural Institute of Japan** : 'Design guidelines for earthquake resistant reinforced concrete buildings based on ultimate strength concept and commentary', October 1988, page 337
22. **New Zealand Standard. NZS 3101** : Part 1 : 1995 : 'Concrete Structures Standard', Standards New Zealand, 1995
23. **Eurocode 8** : 'Design provisions for earthquake resistance of structures', 1995
24. **Iravani, S.** : 'Mechanical properties of high-performance concrete', ACI Materials Journal, September-October 1996, pages 416-426
25. **Sabir, B.B.** : 'High strength condensed silica fume concrete', Magazine of Concrete Research, September 1995, Vol. 47, No. 172, pages 219-226
26. **Van Gysel, A. and Taerwe, L.** : 'Analytical formulation of the complete stress-strain curve for high strength concrete', Materials and Structures, Vol. 29, November 1996, pages 529-533
27. **Ehsani, M.R. and Alameddine, F.** : 'Design recommendations for type 2 high strength reinforced concrete connections', ACI Structural Journal, May-June 1991
28. **Mphonde, A.G. and Frantz, G.C.** : 'Shear tests of high and low strength concrete beams without stirrups', ACI Structural Journal, Proceedings, V. 81, No. 4, July-Aug 1984, pages 350-357

29. **Ahmad, S.H.** ***et al*** : 'Shear capacity of reinforced high strength concrete beams', ACI Journal, Proceedings, V. 83, No. 2, March-April 1986, pages 297-305
30. **Elzanaty, A.H.** ***et al*** : 'Shear capacity of reinforced concrete beams using high strength concrete', ACI Journal, Proceedings, V. 83, No. 2, March-April 1986, pages 290-296
31. **Ha** ***et al*** : 'Response of reinforced high strength beam-column joints under load reversals', Magazine of Concrete Research, September 1992, Vol. 44, No. 160, pages 175-184
32. **Maidl, B.R.** : 'Steel fibre reinforced concrete', Ernst & Sohn, 1995
33. **ACI Committee 506 (Hrsg.)** : 'State of the art report on fibre reinforced shotcrete', Report No. ACI 506.1 R-84, Concrete International, December 1984
34. **Spang, J.** : 'Beitrag zur Geschichte der Spritzverfahren für Mortel und Beton, der Spritzmaschinen und des Spritzbetons', Bautechnik 63 (1986), Heft 3, S. 87-92
35. **Tan, K.H.** ***et al*** : 'Shear behaviour of steel fibre reinforced concrete beams', ACI Structural Journal, January-February 1993, pages 3-11
36. **Adebar, P** ***et al*** : 'Shear tests of fiber concrete beams without stirrups', ACI Structural Journal, January-February 1997, pages 68-76
37. **Olariu** ***et al*** **:** 'Steel fibre reinforced ductile joints', Proceedings of the ninth world conference on earthquake engineering, August 2-9, 1988, Toky-Kyoto, Japan
38. **Gefken P.R. and Ramey M.R.** : 'Increasing hoop spacing in type 2 seismic joints using fibre reinforced concrete', ACI Journal, March-April 1989, pages 168-172
39. **Henager, C.H.** : 'Steel fibrous, ductile concrete joints for seismic resistant structures', SP 53-14, Battelle Memorial Institute Pacific North West Laboratories.
40. **Baglin P.S.** : 'Plate reinforcement for shear-The analysis, design and detailing of plate reinforced concrete beams', PhD thesis, University of Dundee, 1998
41. **Berander, K.G.** : 'An investigation of bond by means of strain measurements in high tensile bars embedded in long cylindrical pull-out specimens', in RILEM Symposium on bond and crack formation in reinforced concrete, Vol 1, Stockholm, 1957, pages 203-210

42. **Mains, R.M.** : 'Measurement of the distribution of tensile and bond stresses along reinforcing bars', Journal of the American Concrete Institute, Proc Vol 48, No 11, November 1951, pages 225-252
43. **Perry, E.S. and Thompson, J.N.** : 'Bond stress distribution of tensile and bond stresses along reinforcing bars', Journal of the American Concrete Institute, Proc Vol 63, No 8, August 1966, pages 865-874
44. **Nilson, A.H.** : 'Internal measurement of bond slip', Journal of the American Concrete Institute, proc Vol 69, No 7, July 1972, pages 439-441
45. **Jiang, D.H., Andonian, A.T. and Shah, S.P.** : 'A new type of bond test specimens', Bond in concrete: Proceedings of an international conference', Paisley College of Technology, June 1982, (ed Bartos, P.), Applied Science Publishers, London, 1982, pages 127-139
46. **Scott, R.H. and Gill, P.A.T.** : 'Developments in the measurement of reinforcement strain distributions in reinforced concrete members', Strain, Vol 18, No 2, May 1982, pages 61,63, 79
47. **Scott, R.H. and Gill, P.A.T.** : 'Techniques in experimental stress analysis for reinforced concrete structures', Experimental stress analysis : Proceedings of an international conference, Amsterdam, May 1986, (ed Wieringa, H.), Martinus Nijhoff Publishers, The Netherlands, 1986, pages 87-96
48. **Fibre Technology Ltd**, Brokhill Road, Pinxton, Nottingham NG16 6NT
49. **DIANA** finite element package, webpage : http://www.diana.nl
50. **SBETA** finite element package, webpage : http://www.cervenka.cz
51. **Segerlind, L. J.** : 'Applied finite element analysis', New York : Wiley, c1976
52. **SBETA user's manual**, Cervenka Consulting, Predvoje 22, 162 00 Prague 6, Czech Republic
53. **Kunnath, S.K.** ***et al***, 'Gravity-load-designed reinforced concrete buildings - Part I : Seismic evaluation of existing structures', ACI Structural Journal, May-June 1995, pages 343-354
54. **Kunnath, S.K.** ***et al***, 'Gravity-load-designed reinforced concrete buildings - Part II : Evaluation of detailing enhancements', ACI Structural Journal, July-August 1995, pages 470-478
55. **Blume, J.A.** ***et al*** : 'Design of multi-story reinforced concrete buildings for earthquake motions', Portland Cement Association, Skokie Ill, 1961

56. **Hanson, N.W. and Connor H.W.** : 'Seismic resistance of reinforced concrete beam-column joints', Proceedings ASCE, Vol 93, ST5, October 1967, pages 533-560

57. **Burguieres, S.T.** ***et al*** : 'The behaviour of beam-column joints under bi-directional load reversals', Atti Delle, Giornate Aicap 1979, Roma, pages 4-8

58. **Bertero, V.V.** ***et al*** : 'Seismic behaviour of lightweight concrete beam-column subassemblages', ACI Journal, January-February 1980, pages 44-52

59. **Durrani, A.J. and Wight, J.K.** : 'Behaviour of interior beam-to-column connections under earthquake-type loading', ACI Journal, May-June 1985, pages 343-349

60. **Durrani, A.J. and Zerbe, H.E.** : Seismic resistance of R/C exterior connections with floor slabs', Journal of Structural Engineering, Vol 113, No 8, August 1987, pages 1850-1864

61. **Durrani, A.J. and Wight, J.K.** : 'Earthquake resistance of reinforced concrete interior connections including a floor slab', ACI Structural Journal, September-October 1987, pages 400-406

62. **Abdel-Fattah, B. and Wight, J.K.** : 'Study of moving plastic hinging zones for earthquake-resistant design of r/c buildings', ACI Structural Journal, January-February 1987, pages 31-39

63. **Collins, M.P. and Mitchel, D.** : 'Prestressed concrete structures', Prentice Hall, Englewood Cliffs, New Jersey 07362, 1991, 766 pp.

Appendix A - Strut-Tie Methods

This Appendix presents the strut-tie methods of analysis presented by Reys de Ortiz [10], Parker [11] and Vollum [12]. The author does not comment on these methods; they are simply presented to complete the review of monotonic beam-column connection literature.

All three methods are for the design of exterior beam-column connections both with and without joint ties.

A1. Reys de Ortiz [10]

The CEB-FIP [16] concrete compressive stress block (with a maximum value of $0.85f_{ck}$) and a bi-linear stress-strain relationship for the reinforcement are used.

The joint shear force is evaluated using the following relationship :

$V_j = T_{beam} - V_{col}$ .....(eq. A1.1)

Where T_{beam} is the tensile force in the beam steel,

V_{col} is the shear force in the upper column.

By resolving forces in the vertical direction, the vertical forces F_v which act on the internal and external faces of the column at the joint boundary are :

$F_{ve} = N + T_{ci} + T_{ce}$ .....(eq. A1.2)

$F_{vi} = N + P + T_{ci} + T_{ce}$ .....(eq. A1.3)

where N is the column load,

P is the beam load,

T_c is the tensile force in the column bars,

The subscripts i and e indicate the words internal and external.

The concrete strut within the joint is shown in Figure A1.

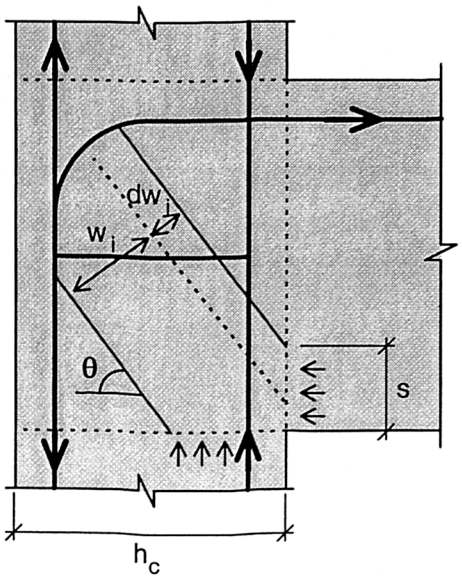

Figure A1 Strut dimensions

The following equilibrium equations apply :

$D.\sin\theta = F_{ve}$ .....(eq. A1.4)

$D.\cos\theta = V_j$ .....(eq. A1.5)

Where D is the axial force present within the inclined strut.

Dividing equation A1.4 by A1.5 gives the following expression :

$$\theta = \tan^{-1}\left(\frac{F_{ve}}{V_j}\right) \quad \text{.....(eq. A1.6)}$$

For the maximum compressive concrete strength at failure the design strength for the cracked concrete, f_{cd2}, proposed by the CEB-FIP Code [16] is used :

$f_{cd2} = 0.6f_{ck}(1-(f_{ck}/250))$ .....(eq. A1.7)

A maximum allowable width for the strut is defined as :

$W = h_c.\sin\theta + s.\cos\theta$ .....(eq. A1.8)

where h_c is the column width,

s is the distance from the compression face of the beam to the neutral axis.

However, the width of the strut is not necessarily the maximum width as defined in equation A1.8. The effective width of the strut is defined as follows :

Unreinforced joint strength

The capacity of the inclined strut is given by :

$D = f_{cd2}bw_i$ .....(eq. A1.9)

where b is the joint breadth.

w_i is defined as the effective strut width. This was Reys de Ortiz's method of model calibration. The following empirical relationship was used to evaluate the effective strut width :

$w_i = 0.45W$ .....(eq. A1.10)

Influence of joint ties

When joint ties are provided the strut's width rises by a value δw_i, where the maximum value of $w_i + \delta w_i$ may not exceed W. The ties are assumed to have yielded at failure and thus give an enhanced joint strength of δV_j :

$$\delta V_j = A_{sv} f_{yv} = \delta D.\cos\theta \quad \text{.....(A1.11)}$$

where A_{sv} is the area of the tie legs,

f_y is the tie's yield strength.

Thus the increase in strut capacity is:

$$D + \delta D = f_{cd2} b(w_i + \delta w_i) \quad \text{.....(eq. A1.12)}$$

and δw_i is evaluated using :

$$\delta w_i = \left(\frac{A_{sv} f_y}{\cos\theta}\right)\left(\frac{1}{f_{cd2} b}\right) \quad \text{.....(eq. A1.13)}$$

A2. Parker [11]

Parker initially reviewed the strength of a rectangular reinforced concrete beam. The arrangement is displayed in Figure A2.1.

The concrete strut, shown in Figure A2.1, resists the shear forces and is at an angle θ to the horizontal. The maximum axial force in the strut is given by :

$$C_v = \nu f_{cu} by.\cos\theta \quad \text{.....(eq. A2.1)}$$

where ν is the concrete effectiveness factor (taken from EC2 [17]),

f_{cu} is the concrete compressive cube strength,

b is the beam breadth,

$y = (h-a_v.\tan\theta)$,

h is the beam height,

a_v is the shear span.

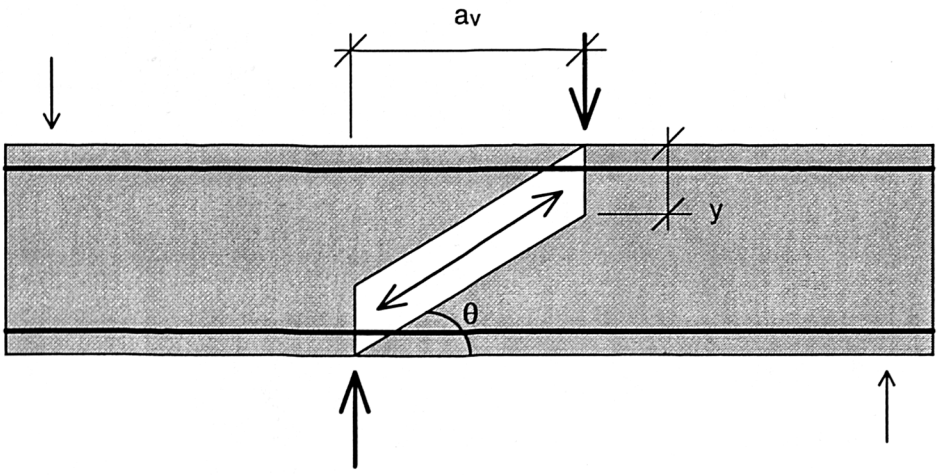

Figure A2.1 Model beam arrangement

The shear force is the vertical component of this force :

$V = C_v.\sin\theta \propto \nu f_{cu} bh$ .....(eq. A2.2)

Substituting equation A2.1 into A2.2 and introducing a constant, K, gives :

$K = [1-(a_v/h).\tan\theta].\sin\theta.\cos\theta$ .....(eq. A2.3)

The shear capacity is given by the critical angle, θ_{crit}, which leads to the maximum value of K.

Differentiating K with respect to $\tan\theta$ gives :

$\tan\theta_{crit} = \sqrt{[(a_v/h)^2 + 1]} - \{a_v/h)$ .....(eq. A2.4)

and

$$K_{max} = \left(\frac{\tan\theta_{crit}}{2} \right) \quad \text{.....(eq. A2.5)}$$

This method was extended to consider **beam-column joints without shear reinforcement**. The shear force in the joint was taken as :

$$V_j = T_{beam} - V_{col} \quad \text{.....(eq. A2.6)}$$

where T_{beam} is the tensile force in the beam steel,

V_{col} is the shear force in the upper joint.

Figure A2.2 displays the shear span and the strut within a beam-column joint.

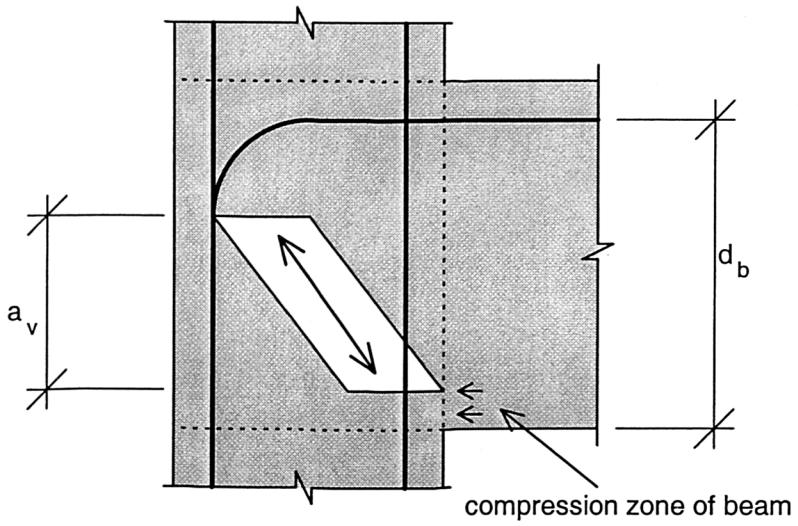

Figure A2.2 Strut dimensions

Parker defined the length of the shear span as :

$$a_v = 0.8d_b - 0.8R \quad \text{.....(eq. A2.7)}$$

where d_b is the effective depth of the beam,

R is the centreline radius of the beam bars.

(***Note*** : This value of R was taken as *negative* for bent up beam steel)

This value of shear span is used to evaluate the critical value on inclination, θ_{crit}. Applying Newton's iterative method solutions to equation A2.3 gives the following, (where γ is equal to a_v/h) :

For $\gamma < 0.5$, $\tan\theta_{crit} = 1 - \frac{\gamma}{2}$ .....(eq. A2.8)

For $\gamma > 0.5$, $\tan\theta_{crit} = \frac{1}{2\gamma} + \left(\frac{\gamma^2 - 0.75}{6\gamma^3 + 2.5\gamma} \right)$ .....(eq. A2.9)

The shear strength of the joint is evaluated using the following techniques :

Longitudinal steel

For a column with symmetrical reinforcement and an axial load, N, the shear capacity is :

$V_1 = (A_{sc}f_y + N).\tan\theta_{crit}$ .....(eq. A2.10)

where A_{sc} is the total area of reinforcement in the column

Concrete strut

With the concrete strut extending over the effective depth of the column the shear capacity is :

$V_2 = \alpha\upsilon f_{cu}bd$ .....(eq. A2.11)

where $\alpha = (1-\gamma.\tan\theta_{crit})/(\tan\theta_{crit} + 1/\tan\theta_{crit})$,

$\upsilon = 0.56 - f_{cu}/310 > 0.40$ (EC2 [17]),

$\gamma = a_v/d$.

Beam-column joints with ties

The strength of a joint with ties is given by :

$V_3 = V_2 + A_{sv}f_{yv}(a_v/s_v - 1)$ .....(eq. A2.12)

where A_{sv} is the area of the ties,

f_{yv} is the yield stress of the ties,

s_v is the spacing of the ties.

The concrete strength cannot exceed a maximum value based on the strength of the concrete struts between the ties, defined as :

$V_4 = \beta V_2$ .....(eq. A2.13)

where $\beta = (d_v - s_v.\tan\theta)/(d-a_v\tan\theta)$, where $d_v = 0.9d$

To conclude :

For beam-column joints without shear reinforcement, the lower of the two values V_1 and V_2 gives the ultimate joint capacity.

For beam-column joints with shear reinforcement, the lower of the three values, V_1, V_3 and V_4 gives the ultimate joint capacity.

A3. Vollum [13]

Vollum presented a strut-tie model considerably more detailed than either Reys de Ortiz's [11] or Parker's [12]. Due to the detail of Vollum's model it is not presented in full here and the author recommends referral to Vollum's thesis [13]. However, an overview of the model taken from Section 5.10 of Vollum's thesis is presented here.

General

1. The concrete strength can be predicted within the joint using Collins and Mitchell's strain softening model [63].

2. The redistribution of column bar forces at joint boundaries can have a significant effect on the predicted failure load if no joint stirrups are provided or the upper column load is low. Vollum considered it essential to take account of the effects of redistribution in either of these cases. The test data suggests that the tensile force in the inner column bars increases over and above that calculated assuming that plane sections remain plane if the column load is low. The effect of this is that a hinge can form in the upper column at a lower load than predicted by conventional analysis.

No joint ties

3. The width of the direct strut is related to the width of the stress blocks at the joint boundaries. The tensile force in the inner column bars is adjusted to give a minimum strut width of $0.4h_c/\sin\theta$ at the top node. The coefficient of 0.4 was found by calibrating the model to predict the failure load of Reys de Ortiz's [10] specimens without joint ties and is assumed to be independent of joint aspect ratio and concrete strength. The strut width increases above the minimum width of $0.4h_c/\sin\theta$ when the column load is increased above a critical value that depends on concrete strength and joint aspect ratio. Failure is assumed to occur when the stress at the top node reaches the concrete strength.

Joint ties

4. The width of the struts is related to the width of the stress blocks at the joint boundaries.

5. Joint ties are considered to have potential for increasing the joint shear strength if positioned between the top of the flexural compressive zone of the beam and the

underside of the beam tensile reinforcement. Analysis of test results suggest that the depth of the flexural compression zone can be taken as $h_b/3$ in the calculation of the effective number of ties.

6. The force in the ties is calculated by a stiffness analysis. The width of the direct strut is taken as $0.349h_c/\sin\theta$ at the bottom node in the stiffness model. The coefficient of 0.349 was found by calibrating the model to predict the failure load of Reys de Ortiz's [10] specimen BCJ4. The factor of 0.349 is assumed to be independent of joint aspect ratio and concrete strength.

7. Through the use of the strut-tie model the value at which joint failure occurs may be calculated. The model is calibrated to predict joint failure of specimens using bent down beam tension steel. The joint strength should be reduced by a factor of 0.8 if U-bars are to be used for the beam reinforcement.

Appendix B - Computer Coding

Both of these programs were written, by the author, using the Microsoft QuickC Compiler, Version 2.50.

B1. RCBCC - Coding

```
/*********************************************************************
*********************************************************************
***                          RCBCC.C                                ***
***                                                                 ***
***                       S J Hamil 11/98                           ***
***                                                                 ***
***          This program reads in the logger data file             ***
***          and then converts it into a user friendly              ***
***          table in .TXT format.                                  ***
***                                                                 ***
***          See help for more information                          ***
***                                                                 ***
*********************************************************************
*********************************************************************/

#include <stdio.h>
#include <math.h>
#include <graph.h>

#define MAXNUM 50

FILE *filep;
FILE *fileq;

int i, n, m, datchan = 1, st = 1, scans = 200;
int dat[50] ;
float a[MAXNUM], b[MAXNUM] , con[50];
char filein[50], fileout[50];


void defpar(void), checkpar(void);
void runprog(void), help(void);

/***
a menu page is created
this uses a switch statement which calls a particular function
on the users request
***/

main ()
{
      int ii;

      while(1)
      {
            _clearscreen(_GCLEARSCREEN);
            _setbkcolor(_BLACK);

            printf("\n\tResults organiser - SJH - Nov 98\n\n");
            printf("\tMENU\n\n");
            printf("\t1\tDefine Parameters\n\n");
            printf("\t2\tCheck Parameters\n\n");
            printf("\t3\tRun Program\n\n");
            printf("\t4\tHelp\n\n");
            printf("\t5\tExit\n\n\t");
```

```
                scanf("%d",&ii);

                switch(ii)
                {
                        case 1 : defpar();
                        scanf("%c");
                        break;

                        case 2 : checkpar();
                        scanf("%c");
                        break;

                        case 3 : runprog();
                        scanf("%c");
                        break;

                        case 4 : help();
                        scanf("%c");
                        break;

                        case 5 : exit();
                }
        }
}

/***
this first function defines the parameters
the conversion factors and the amount of data
are kept in two separate arrays
***/

void defpar(void)

{

        _clearscreen(_GCLEARSCREEN);
        _setbkcolor(_BLACK);

        printf("How many data channels are they : ");
        scanf("%d",&datchan);
        printf("\n");

        for(i = 0 ; i < datchan ; i++)
        {
                printf("Enter con factor and amount of data for channel %d :
                ",i+1);
                scanf("%f%d",&con[i],&dat[i]);
        }
        printf("Press return to continue");
}

/***
this function displays the parameters
***/

void checkpar(void)

{

        _clearscreen(_GCLEARSCREEN) ;
        _setbkcolor(_BLACK) ;

        if(con[0] == 0)

        {
                printf("\n\tYou must define some parameters first\n\n");
                printf("\tPress return to continue");
                scanf("%c");
                main();
        }
```

```
        printf("       group no. , conversion factor , number of
        channels\n\n");

        for(i = 0 ; i < datchan ; i++)
        {
                printf("\t%2d\t%12.4f\t\t%6d\n", i+1 , con[i] , dat[i]);
        }
        printf("\n\tPress return to continue");
}


/***
two files are opened - the input file to read the data off
and a new file to write the new data to

note that the zero error is taken out by the use of the b[n] array
***/

void runprog(void)
{
        printf("\nEnter the filename to open : ");
        scanf("%s",filein);
        printf("\n");

        filep = fopen( filein , "r" );

        if(filep == NULL)
        {
                printf("Error opening file %s for reading\n", filein);
                exit();
        }

        printf("\nEnter the filename to write to : ");
        scanf("%s",fileout);
        printf("\n");

        fileq = fopen( fileout , "w" );

        if(fileq == NULL)
        {
                printf("Error opening file %s for writing\n", fileout);
                exit();
        }

        for(n=0 ; n < datchan ; n++)
        {
                fscanf ( filep , "%c%c\n" );
                fscanf (filep , "%d\n" , &st );
                fscanf ( filep , "%f%f%f%f%f%f\n" );

                for (m=0 ; m < dat[n] ; m++)
                {
                        fscanf( filep , "%f\n" , &a[n] );
                        a[n] = a[n] * con[n];
                        b[n] = a[n];
                        fprintf(fileq , "%8.2f ",a[n] - b[n]);
                        printf("%8.2f ",a[n]-b[n]);
                }
        }

        printf("\n");
        fprintf( fileq ,"\n");

        for( i=0 ; i < scans ; i++)
        {
                for (n=0 ; n < datchan ; n++)
                {
                        fscanf ( filep , "%c%c\n" ) ;
                        fscanf (filep , "%d\n" , &st ) ;
                        if (st == 0)
                        {
```

```
                        printf("\n\tFile %s is succesfully written\n",
                        fileout);
                        printf("\tThere were %d load steps\n", i);
                        printf("\tPress return to continue");
                        scanf("%c");
                        main();
                }

                fscanf ( filep , "%f%f%f%f%f%f\n" );

                for (m=0 ; m < dat[n] ; m++)
                {
                        fscanf( filep , "%f\n" , &a[n] );
                        a[n] = a[n] * con[n];
                        fprintf(fileq , "%8.2f ",a[n]-b[n]);
                        printf("%8.2f ",a[n]-b[n]);
                }
        }
        printf("\n");
        fprintf( fileq ,"\n");
    }

    fclose (filep);
    fclose (fileq);
}

/***
help function - as it reads
***/

void help(void)
{

    _clearscreen(_GCLEARSCREEN) ;
    _setbkcolor(_BLACK) ;

    printf("\n\t\t\t\tHELP\n\n");
    printf("This program reads an input file (from the data logger\n");
    printf("used in the beam-column connection experiments) and
    then\n");
    printf("converts the data into a user friendly output file.\n\n");
    printf("Before using this program it is important that the  following
steps are taken:\n\n");
    printf("1.\tMake a note of all of the groups used,\n");
    printf("\tthe conversion factors and the no. of channels\n\n");
    printf("2.\tEdit the input file so that it's in its simplest
    form\n");
    printf("\ti.e. no messages or setting up information\n\n");
    printf("3.\tAfter the *F command at the end of the input file\n");
    printf("\tinsert a 0 (zero) on the line below\n\n");
    printf("4.\tMake sure that the input file is in the user
    directory\n\n");
    printf("The author recommends using Microsoft Excel to open the
    output files\n");
    printf("The file is space delimited (1 space between each bit of
    data)\n");
    printf("Any problems please contact Stephen Hamil on:\n");
    printf("internal 4234 or 3832 / S.J.Hamil@dur.ac.uk\n\n");
    printf("Press return to continue");

}
```

B2. AVBON - Coding

```
/*********************************************************************
*********************************************************************
***                            AVBON.C                            ***
***                                                               ***
***                        S J Hamil 2/99                         ***
***                                                               ***
***          This program calculates the bond stresses            ***
***         and average bond stresses from the strain             ***
***          data.  This is written in a user friendly            ***
***          table in .TXT format.                                ***
***                                                               ***
***          See help for more information                        ***
***                                                               ***
*********************************************************************
*********************************************************************/

#include <stdio.h>
#include <math.h>
#include <graph.h>

FILE *filep;
FILE *fileq;

int i, n, m, datchan = 7, scans = 200;

float area = 201.0, E = 2.0, diameter = 16.0, avbon, grad;

float sumx, sumy, sumb, sums;

int dat[50];
float x[50], y[50];
char filein[50], fileout[50];


void par(void), checkpar(void);
void runprog(void), help(void);

/***
a menu page is created
this uses a switch statement which calls a particular function
on the users request
***/

main ()
{
       int ii;

       while(1)
       {

              _clearscreen(_GCLEARSCREEN);
              _setbkcolor(_BLACK);

              printf("\n\tAverage bond stress generator - SJH - Feb
              99\n\n");
              printf("\tMENU\n\n");
              printf("\t1\tEnter parameters\n\n");
              printf("\t2\tCheck parameters\n\n");
              printf("\t3\tRun Program\n\n");
              printf("\t4\tHelp\n\n");
              printf("\t5\tExit\n\n\t");
              scanf("%d",&ii);

              switch (ii)
              {
                     case 1 : par();
                     scanf("%c");
```

```
                    break;

                    case 2 : checkpar();
                    scanf("%c");
                    break;

                    case 3 : runprog();
                    scanf("%c");
                    break;

                    case 4 : help();
                    scanf("%c");
                    break;

                    case 5 : exit();
            }
        }
}

/***
par function - reads in user parameters
***/

void par(void)

{
        _clearscreen(_GCLEARSCREEN);
        _setbkcolor(_BLACK);

        printf("      No. of strain gauges : ");
        scanf("%d",&datchan);
        printf("\n");

        printf("              bar diameter : ");
        scanf("%f",&diameter);
        printf("\n");

        printf("                  bar area : ");
        scanf("%f",&area);
        printf("\n");

        printf(" Young's Modulus (x 10^11) : ");
        scanf("%f",&E);
        printf("\n\n");

        printf("Press return to continue\n");
}

/***
checkpar function - user defined values are displayed
***/

void checkpar(void)

{
        _clearscreen(_GCLEARSCREEN);
        _setbkcolor(_BLACK);

        printf("DEFINED PARAMETERS\n\n");
        printf("Number of channels =            %d\n", datchan);
        printf("      Bar diameter =           %2.0f mm\n", diameter);
        printf("          Bar area =       %5.2f mm^2\n", area);
        printf("    Youngs modulus = %3.2f x 10^11 Pa\n", E);

        printf("\n\tPress return to continue");
}


/***
runprog function - The mathematics section
data is read from an input file and then converted
into average bond stresses these values are then
```

```
written into an output file
***/

void runprog (void)
{
       printf("\nEnter the filename to open : ");
       scanf("%s",filein);
       printf("\n");

       filep = fopen( filein , "r" );

       if (filep == NULL)
       {
              printf("Error opening file %s for reading\n", filein);
              exit();
       }

       printf("\nEnter the filename to write to : ");
       scanf("%s",fileout);
       printf("\n");

       fileq = fopen( fileout , "w" );

       if(fileq == NULL)
       {
              printf("Error opening file %s for writing\n", fileout);
              exit();
       }

       for (n=0 ; n < datchan ; n++)
       {
              fscanf ( filep , "%f" , &x[n]);
       }

       fscanf (filep , "\n") ;

       for ( i=0 ; i < scans ; i++)
       {
              for (n=0 ; n < datchan ; n++)
              {
                     fscanf ( filep , "%f" , &y[n] ) ;

                     if (y[n] == -10000)
                     {
                            printf("\n\tFile %s is succesfully written\n",
                            fileout);
                            printf("\tThere were %d load steps\n", i);
                            printf("\tPress return to continue");
                            scanf("%c");
                            main();
                     }
              }

              sumx = 0;
              sumy = 0;
              sumb = 0;
              sums = 0;

              for (n=0 ; n < datchan ; n++)
              {
                     sumx = sumx + x[n];
                     sumy = sumy + y[n];
                     sums = sums + (x[n]*x[n]);
                     sumb = sumb + (x[n]*y[n]);
              }

              grad = ((datchan*sumb)-(sumx*sumy))/((datchan*sums)-
              (sumx*sumx)) ;
              avbon = (E*area*grad)/(10*3.142*diameter);

              printf("%d  %5.2f  %5.2f\n", i, grad , avbon);
              printf("\n") ;
```

```
                fprintf(fileq , "%3d  %5.2f  %5.2f" , i ,grad , avbon);
                fprintf( fileq ,"\n");
        }

        fclose (filep);
        fclose (fileq);
}

/***
help function - as it reads
***/

void help(void)
{
        _clearscreen(_GCLEARSCREEN) ;
        _setbkcolor(_BLACK) ;

        printf("\n\t\t\t\tHELP\n\n");
        printf("This program reads in a set of strain values over a certain
        length\n");
        printf("of bar.\n\n");
        printf("The input data should be in the following format :\n");
        printf("(The xn data is the displacement data,\n");
        printf("the strain data is an,bn,cn etc...)\n\n");
        printf("For 6 rod channels\n\n");
        printf("\tx1\tx2\tx3\tx4\tx5\tx6\n");
        printf("\ta1\ta2\ta3\ta4\ta5\ta6\n");
        printf("\tb1\tb2\tb3\tb4\tb5\tb6\n");
        printf("\tc1\tc2\tc3\tc4\tc5\tc6\n");
        printf("\tz1n\tz2\tz3\tz4\tz5\tz6\n\n");
        printf("The user should input the value -10000 at the end of the
        input file\n");
        printf("This tells the computer when to return to the menu
        page\n\n");
        printf("Any problems please contact Stephen Hamil on :\n");
        printf("internal 4234 or 3832 / S.J.Hamil@dur.ac.uk\n\n");
        printf("Press return to continue");
}
```

Appendix C - Finite Element Methods

This Appendix presents the finite element method used by Taylor [1] and Vollum [12]. The author does not comment on these methods; they are simply presented to complete the review of monotonic beam-column connection literature.

It should be noted that both Taylor and Vollum performed these finite element methods as additional analysis within their research. Neither, however, continued their finite element studies further than an initial investigation.

C1. Taylor [1]

Taylor did not report on his finite element analysis in great detail. However, an outline of the technique used is given here.

The joint zone was modelled using an elastic finite element program. The mesh design used is shown in Figure C1. Six noded triangular elements were used and the loads were applied to the three continuous faces of the joint.

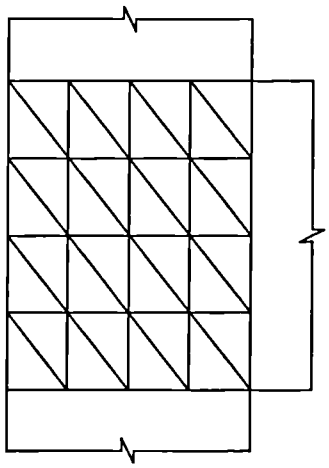

Figure C1 Finite element mesh

As this finite element analysis was elastic only joint behaviour prior to cracking was considered. Taylor did find that the diagonal stress field gave stresses of magnitude similar to the indirect tensile strength of the concrete.

This analysis was very time-consuming (considering the computing power available in the 1970's) and, once it had been shown that it gave good results, was discontinued.